Advanced Ceramics for Dentistry
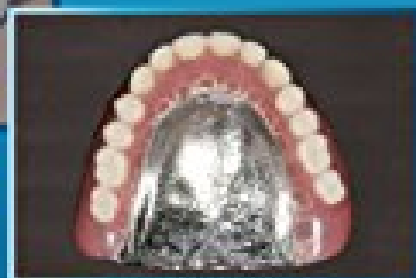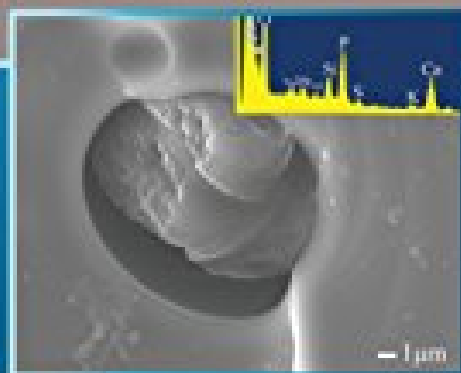
Editors:
James Zhijian Shen
and Tomaž Kosmač

Advanced Ceramics for Dentistry

Advanced Ceramics for Dentistry

James Zhijian Shen and Tomaž Kosmač

Notice
No responsibility is assumed by the publisher for any injury and/or damage to persons or property as a matter of products liability, negligence or otherwise, or from any use or operation of any methods, products, instructions or ideas contained in the material herein. Because of rapid advances in the medical sciences, in particular, independent verification of diagnoses and drug dosages should be made.

For information on all Butterworth-Heinemann publications
visit our website at books.elsevier.com

Working together
to grow libraries in
developing countries

ELSEVIER   Book Aid
            International

www.elsevier.com • www.bookaid.org

List of Contributors

Erik Adolfsson Ceramic Materials, Swerea IVF, Box 104, SE-431 22 Mölndal, Sweden

Matts Andersson Chalmers University of Technology, SE-412 96 Göteborg, Sweden

Thomas Beikler Department of Operative and Preventive Dentistry and Periodontics, Heinrich-Heine-Universität Düsseldorf, Moorenstraße 5, 40225 Düsseldorf, Germany

Dag Henrik Bergsjö Chalmers University of Technology, SE-412 96 Göteborg, Sweden

Johan Carlson Fraunhofer-Chalmers Research Centre for Industrial Mathematics, Chalmers Science Park, SE-412 88 Göteborg, Sweden

Haifeng Chen Department of Biomedical Engineering, College of Engineering, Peking University, Beijing, China

Saverio Giovanni Condo Department of Clinical Sciences and Translational Medicine, University of Rome Tor Vergata, Rome, Italy

Robert Danzer Institut für Struktur- und Funktionskeramik, Montanuniversität Leoben, 8700 Leoben, Austria

Jenny Fäldt Nobel Biocare AB, P.O. Box 5190, SE-402 26 Göteborg, Sweden

Boštjan Jančar Jožef Stefan Institute, Jamova cesta 39, SI-1000 Ljubljana, Slovenia

Tomaž Kosmač Jožef Stefan Institute, Jamova cesta 39, SI-1000 Ljubljana, Slovenia

Danjela Kuscer Jožef Stefan Institute, Jamova cesta 39, SI-1000 Ljubljana, Slovenia

Yihong Liu Peking University School and Hospital of Stomatology, National Engineering Laboratory for Digital and Material Technology of Stomatology, Beijing 100081, China

Tanja Lube Institut für Struktur- und Funktionskeramik, Montanuniversität Leoben, 8700 Leoben, Austria

Karel Maca Department of Ceramics and Polymers, Brno University of Technology, Czech Republic

Corrado Piconi Orthopedics Institute, Sacred Heart Catholic University, Rome, Italy

Belinda Reinhardt Department of Operative and Preventive Dentistry and Periodontics, Heinrich-Heine-Universität Düsseldorf, Moorenstraße 5, 40225 Düsseldorf, Germany

Simon Jegou Saint-Jean

David Salamon CEITEC-Central European Institute of Technology, Brno University of Technology, Technická 3058/10, 61600 Brno, Czech Republic

Rikard Söderberg Chalmers University of Technology, SE-412 96 Göteborg, Sweden

Peter Schüpbach Schupbach Ltd, Service and Research Laboratory, Zugerstraße 64, CH-8810 Horgen, Switzerland

James Zhijian Shen Berzelii Center EXSELENT on Porous Materials, and Department of Materials and Environmental Chemistry, Arrhenius Laboratory, Stockholm University, SE-106 91, Stockholm, Sweden

Martin Stefanic Jožef Stefan Institute, Jamova cesta 39, SI-1000 Ljubljana, Slovenia

Saso Sturm Jožef Stefan Institute, Jamova cesta 39, SI-1000 Ljubljana, Slovenia

Martin Trunec Department of Ceramics and Polymers, Brno University of Technology, Czech Republic

Xinzhi Wang Department of Prosthedontics, Peking University School and Hospital of Stomatology, 100081 Beijing, China

Jing Zhao Department of Prosthedontics, Peking University School and Hospital of Stomatology, 100081 Beijing, China; Department of Materials and Environmental Chemistry, Arrhenius Laboratory, Stockholm University, Stockholm SE-106 91, Sweden

Nowadays, you are likely to find references to the topics covered in this book, in two types of publication: reference books about bioceramics or dental ceramics; or about dental materials. However, whilst books covering the subject of bioceramics might provide indepth coverage of the topic, books in the latter category will more likely present ceramics in an over simplified manner. In a way, neither type reflects the current status of the field, particularly the actions that are rapidly being taken for future developments. This is because the majority of ceramics currently in use in restorative dentistry are regarded neither as bio-oriented nor as being developed for dental purposes only, at least not at the moment of introduction into the field of dentistry.

It was during close collaboration with dental practitioners and the dental industry that the editors of this book recognized a dissymmetry of knowledge concerning ceramics and the demands for ceramics. They felt a similar knowledge gap existed between ceramics and, in general, the practical demands of ceramics, in the fields of materials science and engineering. Advanced ceramics for dentistry appears to be such a topic. The original motivation for this book was to integrate two topics (advanced ceramics and the demand for advanced ceramics in restorative dentistry) into a single, comprehensive resource. We were encouraged by the favorable responses received during a successful symposium on "Advanced Ceramics and Ceramic Processes for Dentistry," which we organized together with Horst Fisher, Leif Hermansson, and Jenny Fäldt in association with the 12th Conference of the European Ceramic Society that was held in Stockholm in June 2011.

This book is still materials-oriented, but with a strong focus on the latest applications of advanced ceramics for solving the problems encountered in restorative dentistry. By highlighting existing problems and emphasizing new needs, we hope this book can, besides facilitating a better understanding of state-of-the-art solutions in both ceramics and dentistry, encourage interdisciplinary efforts for developing new concepts, materials, and technologies for the future. We realized the challenge at the very beginning of this initiative, when selecting activities across disciplines. Accordingly, efforts were made to create a balance between dental demands and materials demands, between fundamentals and practice, between coverage and depth, and between the current status of the field and future development.

It would not have been possible to write a book with such broad coverage without the understanding and collaboration of all the individual authors involved. We sincerely appreciate the time and effort they have dedicated to this work. We would like to acknowledge the JECS Trust for the financial support that made it possible to arrange the topical symposium "Advanced

Ceramics and Ceramic Processes for Dentistry." It was during this multidisciplinary symposium that most of the topics in this book were discussed. We would also like to thank Professor Daniel van Steenberghe for encouraging discussions and for suggesting topics, particularly those that relate to dental implants. One of us (Shen) would like to take this opportunity to acknowledge Professor Matts Andersson (the inventor of Procera®) and Professor Hailan Feng (School and Hospital of Stomatology, Peking University) for their inspiring discussions and close collaborations over the years.

James Zhijian Shen
Tomaž Kosmač

Introduction

James Zhijian Shen* **and Tomaž Kosmač†**
**Berzelii Center EXSELENT on Porous Materials; and Department of Materials and
Environmental Chemistry, Arrhenius Laboratory, Stockholm University,
Sweden; †Jožef Stefan Institute, Ljubljana, Slovenia*

Ceramic materials are currently used in two categories of application for restorative dentistry, namely, all-ceramic fixed-partial dentures (FPDs) and implantable components. While the former mainly demand integrated and balanced properties of mechanical and aesthetic origins, the latter also rely a great deal on the bio-oriented properties of materials. Innovations in ceramics and ceramic processes are vital to ensure reliable and affordable dental-restoration solutions with aesthetically pleasing outcomes.

A broad range of issues is challenging researchers and engineers in the ceramics community. These include developing bioactive surfaces on otherwise inert but load-bearing ceramics for implants; combining inherently chemically stable and physically stiff ceramics into highly coherent laminate composites for prosthetic crowns and bridges; improving the optical translucency of load-bearing ceramics for the manufacture of fully anatomic restorations (without the need for aesthetic veneering porcelain); and integrating feasible techniques for producing (in cost-effective and material-saving ways) long-lasting, individualized ceramic components with biocompatibility, complexity, and high precision.

The development of advanced ceramics for dentistry is a topic of practice-motivated science that requires a multidisciplinary approach, and calls for collaborations across the disciplines of materials science, product design, mechanical engineering, imaging technologies, biology, chemistry, and clinical technologies for the development of new concepts, new materials, and new technologies. This is a never-ending journey, pursuing optimized clinical solutions through better understanding, better materials, and better processes to satisfy the increasing demands of patients, dentists, and social and environmental concerns. In general, patients are looking for affordable treatments by applying long-lasting prostheses that can restore or enhance their natural appearance and fulfill all the necessary functions. Dentists would prefer to achieve the above goals through less invasive, less painful, more comfortable, and quicker procedures. In addition, social and environmental concerns place strong demands on green and material-saving approaches.

1

The purpose of this book is to provide an overview of the recent progress made in this multidisciplinary field with a focus on the challenges presented to future concepts as well as current and emerging technologies. It is not our intention to provide a history of the application of ceramics in dentistry, or to an in-depth review of the ceramic materials and processes currently in use in dentistry, although we will cover most of the ceramics and ceramic components used for today's dental restorations. This is why the book is entitled Advanced Ceramics for Dentistry rather than Advanced Ceramics in Dentistry. It is our aim to cover the topics of current focus and those of future interest. We hope that in this way the developers and manufacturers of ceramics will gain a better understanding of the exact demands of dental practices, while dentists and dental technicians will become more aware of the limitations and the potential of ceramics and ceramic processes in this field. In other words, by emphasizing the needs and exposing the problems, we hope this book will inspire a new way of thinking and encourage interdisciplinary efforts, rather than just be used as one more reference source.

Because we had in mind potential readers from two different disciplines: materials science and dentistry (who have essentially different educational backgrounds), the first thing we did was to balance the selected topics and optimize their presentation. Efforts were made to establish a good structure for the sequence of covered topics in order to avoid the obvious risks of disordering and disintegration that can easily happen when handling a broad range of interdisciplinary topics. The book's topics can thus be divided into seven groups:

1. Teeth as natural materials (Chapter 2).

   In this chapter, we look at teeth as natural materials. The development; formation; composition; microstructure; optical and mechanical properties; common defects; and damage to human teeth are reviewed. This knowledge set forms the basis of restorative dentistry for designing preventive treatments in order to maintain tissue integrity and to replace damaged tissues with synthetic materials (e.g. ceramics that mimic the natural appearance and performance of teeth).

2. Dental prostheses and dental implants and their clinical failures (Chapter 3–5).

   In these chapters, the common problems and difficulties encountered in restorative dentistry are described, including tooth defects and edentulism, as well as the clinical failures of dental prostheses. Despite the fact that there are no omnipotent prostheses, some general guidelines for prostheses selection are given. This is essential for readers with a materials background, and is designed to help them get an understanding of the real-world problems that can be encountered. We hope it will also refresh the existing knowledge of readers with a dental background, and also present problems in such a way that their counterparts in another field can easily understand them.

3. Advanced ceramics, their processes and mechanical properties (Chapters 6–9).

    In these chapters, detailed descriptions are given to answer the general questions that readers with a dental background might have about advanced ceramics. How are they prepared? What are the relationships between their properties and microstructures? How can their microstructures and properties be characterized? The main focus is on their mechanical properties. This is essential materials knowledge used for dealing with ceramics, and is presented in a way that is easy to follow for readers with a dental background, but is still of interest to readers with a materials background when linked to clear application demands.

4. Interfaces between tissues and ceramics (Chapter 10).

    This chapter stands alone. The information presented here is about the interface between tissues and ceramics, and is also the interface of two disciplines: dentistry and materials. In order to understand this chapter, knowledge and skills from both disciplines are required.

5. Advanced ceramics currently in use in dentistry (Chapters 11–14).

    These chapters review the ceramics currently used in dentistry. An effort is made to not only describe where and how these ceramics are used, but also to explain why certain ceramics are chosen for specific purposes and what problems are typically encountered. Accordingly, the means of improving the mechanical, bio-, and aesthetic properties of ceramics as bulk, porous bodies, or surface-active layers are presented. We hope the knowledge and philosophy presented in this part will pave the way towards ceramics by design.

6. Industrial-scale production of customized ceramic prostheses (Chapter 15).

    The current, highly flexible production processes used for customized dental prostheses are reviewed in this chapter. These include digitalization, computer-aided design, and milling. Quality issues are also addressed, including prospects for further improvements: adapting new ceramic materials, and using new materials processes and highly digital treatment processes.

7. Concepts for the future (Chapters 16–18).

    These chapters address material and process demands for solving the problems encountered in current practice that indicate the direction of future development. In the near future, minimization of processing defects will continuously appear as a major task for improving the performance and reliability of dental prostheses. In the longer-term, biomimetic materials and related processes will be topics of general importance. Current subtractive manufacturing processes, which generate huge material waste, have encouraged the development of more sustainable, material-saving, and cost-effective concepts (e.g. rapid additive manufacturing processes).

It is worth mentioning that R&D of advanced ceramics, as part of the field of materials science and engineering, is full of cases of phantom innovations. Many current applications of advanced ceramics are far beyond the original aims of their development. The zirconia family of ceramics is one such example. Although today dentistry has become the second-largest consumer of zirconia, the initial development of zirconia ceramics was motivated by the demands of thermally insulating engine components. Alumina is another example; it was made optically translucent as early as the 1960s. Glass ceramics are a third example: they were initially developed for low-thermal-expansion applications. Therefore, we strongly believe that while advanced ceramics by design and the development of advanced ceramics for dentistry are good aims, identifying, integrating, and synergizing available materials and technologies is equally important for meeting the demands of restorative dentistry.

By closing the link between the development of ceramic materials and their rapidly increasing uses in restorative dentistry, we hope this book will be of interest to a broad audience that covers dentists, dental technicians, and dental students, as well as ceramicists and students in the fields of materials science and engineering. With a description of the materials problems faced in restorative dentistry, this book may be used as a textbook and reference literature for ceramics researchers and students to plan their needs-driven activities. With a solutions-based presentation of ceramic materials, this book can be used as both a textbook and as reference literature for dental specialists and students to gain an understanding of ceramics and ceramic processes. By highlighting the importance of ceramic processes and future demands, this book may also attract the interest of ceramics manufacturers, developers and users.

Teeth

Haifeng Chen[*] **and Yihong Liu**[†]

[*]*Department of Biomedical Engineering, College of Engineering, Peking University, Beijing, China;* [†]*Peking University School and Hospital of Stomatology, National Engineering Laboratory for Digital and Material Technology of Stomatology, Beijing 100081, China*

Contents

2.1 INTRODUCTION

Teeth are vital organs in vertebrates whose main function is to bite and chew food into pieces small enough to swallow, thus making it possible for digestive enzymes to react more effectively with the food granules.[1] Some species use their teeth in the pursuit of prey and as a means of defense. Whereas human teeth are not only functional, but also play a great part in the appearance and beauty of a human face. Human teeth are also important for word pronunciation and the protection of support organs. The right anatomical shape and arrangement of teeth is necessary so that they can perform these functions.

Humans develop two sets of teeth during the course of their lives.[2] Primary (deciduous) teeth will begin to erupt 7–8 months after birth, and all twenty should have developed by 2–4 years of age. Secondary (permanent) teeth usually begin to appear between 6–7 years and are completed by 12–13 years of age. Deciduous teeth gradually fall out during this time. The complete set consisting

of thirty two permanent teeth may not finish developing until the third molars appear between the ages of 17 and 25 years of age. Before eruption, teeth in the jaw have experienced a long and complex process of dental germ development and dental tissue differentiation. The enamel organ, dental papilla, and dental sac constitute the dental germ which is formed from the interaction of the oral epithelial and ectomesenchyme of the stomodeum. Finally, the enamel organ develops into enamel, the dental papilla develops into dentin and pulp, and the dental sac develops into cementum and periodontal tissue. Periodontal tissue consists of four parts, including gums, alveolar bone, root cementum, and the periodontal ligament, which together support tooth function.

2.2   MICROSTRUCTURE OF TEETH

Each tooth consists of three parts: the crown, which projects beyond the gum; the root that is buried in the alveolar bone; and the neck, which is at the junction of crown and root.[3] The dental pulp cavity is located at the center of the tooth, which contains blood vessels and nerves and is connected with the periodontal tissue by a narrow root canal. Each tooth has two types of tissue, hard calcified tissue that includes enamel, dentin, and cementum, and soft tissue (pulp). Figure 2.1 provides a sectional view of a human tooth.

2.2.1   Enamel

Dental enamel is the outermost layer of the human tooth, covers the crown surface, and is exposed directly to the oral cavity. It varies in thickness up to 2.5 mm.[3] Dental enamel is the most extreme case of mammalian biomineralization and is the hardest substance in the body. The color of enamel is milky white or light yellow, depending on its thickness and the degree of mineralization. A higher level of mineralization leads to a more transparent enamel that reflects the yellowish color of the dentin below. Deciduous enamel appears more milky white because the degree of mineralization is much lower than that of permanent teeth.

As development proceeds, the enamel organ assumes a bell-shaped structure with a well-defined dental papilla along its concave internal. It can be divided
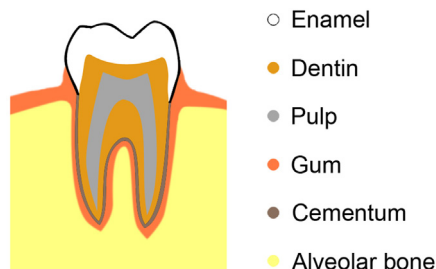

○ Enamel
● Dentin
● Pulp
● Gum
● Cementum
○ Alveolar bone

FIGURE 2.1   Sectional view of a human tooth.

into four regions: the outer enamel epithelium, the stellate reticulum, the stratum intermedium, and the inner enamel epithelium.[4] The inner enamel epithelium further differentiates into ameloblasts. The ameloblasts make and secrete the enamel organic matrix, and are then calcified with calcium phosphates to form the enamel. Unlike other calcified tissues, such as dentin and bone, there are no living cells in mature enamel. Ameloblasts are no longer present when enamel is formed. Thus, when enamel is damaged, there are no cells to carry out the repair. Mature enamel is made up of pure chemicals and can be seen as a natural nanodevice with a unique hierarchical structure comprised of a highly organized keyhole-shaped microarchitectural unit, known as enamel prisms or rods that are about 4–6 μm.[5,6] This structure spans the entire enamel thickness and is likely to play an important role in determining the extraordinary mechanical and anti-abrasion properties of enamel. Ninety-five percent (by volume) of human enamel is comprised of nanorod-like carbonated hydroxyapatite crystals which have a rough cross section of 25–100 nm and a length of 100 nm–100 μm or longer along the c-axis.[7–9] There is evidence that during enamel development these crystal rods project into the enamel matrix from the enamel/dentin junction and are separated by nanospheres of amelogenin; the major enamel protein constitutes approximately 90% of all organic matrix material in developing enamel.[7–11] The amelogenin is believed to play a vital role in developing enamel by stabilizing newly formed enamel crystals and influencing their subsequent growth. Figure 2.2 shows a transmission electron microscopic (TEM) image of nanorod-like hydroxyapatite crystals formed in the presence of recombinant rat amelogenin. In amelogenin knockout mice the enamel is hypoplastic and the characteristic prism pattern is completely absent. Amelogenins are synthesized
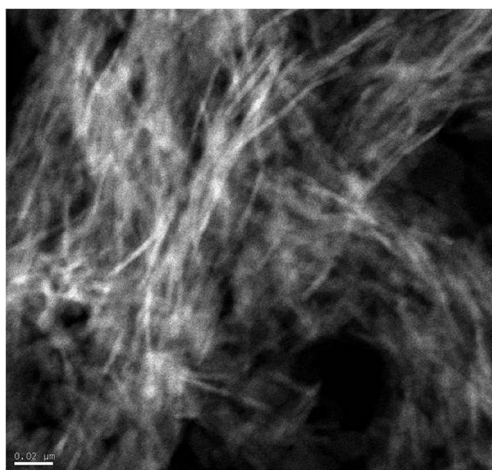

0.02 μm

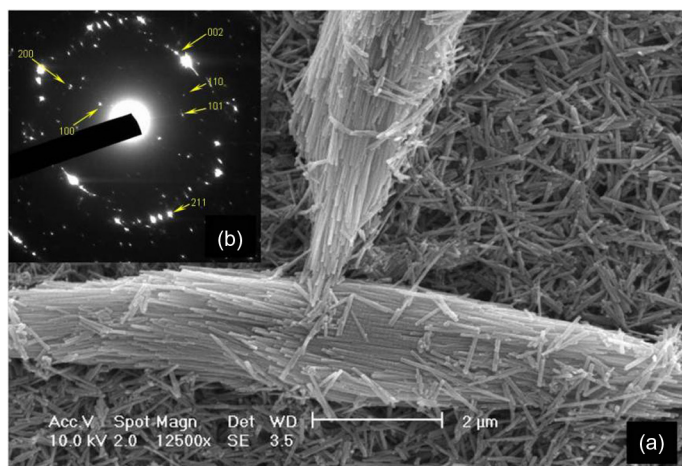**FIGURE 2.2** TEM image of nanorod-like hydroxyapatite crystals formed in the presence of recombinant rat amelogenin.

FIGURE 2.3 (a) SEM image of enamel prisms and enamel crystals; and (b) SAED pattern of enamel crystals. Lattice planes are indicated by arrows.[7]

and secreted by ameloblast cells. The only hydrophilic part of the nascent amelogenin molecule is comprised of a carboxy-terminated teleopeptide of 12 amino acid residues. The cleavage of this C-terminated motif would decrease its apatite binding ability and lower the inhibitory potential of the molecule to apatite growth. It has been proposed that the amelogenin can self-assemble into nanosphere structures approximately 20 nm in diameter with the hydrophilic C-terminals externalized and form a negatively charged surface. These nanospheres would then interact electrostatically with the enamel hydroxyapatite crystal faces parallel to the c-axis and prevent crystal–crystal fusions. Enzymes (proteinase-1) eventually digest away the charged surface of the nanospheres to produce hydrophobic nanospheres that further assemble and stabilize the growing crystallites to form well-organized prism patterns.

Figure 2.3a shows the scanning electron microscopic (SEM) image of rat enamel prisms and enamel crystals. TEM images and selected area electron diffraction (SAED) patterns (Figure 2.3b) show that these crystals are single crystals with a hydroxyapatite crystalline structure. Electron-dispersive X-ray spectroscopy (EDS) data show that the Ca/P ratio is approximately 1.6, which approaches that of the ideal HA (Ca/P of 1.67). Although the main mineral of enamel is a hydroxyapatite, $[Ca_{10}(PO_4)_6(OH)_2]$, natural tooth enamel always contains many other inorganic anions and cations (e.g. HCO_3^-, F^-, CO_3^{2-}, SO_4^{2-}, Na^+, Mg^{2+}, K^+, Cl^-) and form a relatively complex apatite structure.[11,12] But X-ray diffraction (XRD) usually shows the typical diffraction pattern of apatite (Figure 2.4a). These inorganic ions are believed to have a close relationship with dental health. For instance, fluorapatite $[Ca_{10}(PO_4)_6F_2$, FA] is hexagonal and has the highest symmetry found among the apatite minerals. The crystal structure can be considered as Ca^{2+} and PO_4^{3-} arranged around the central column of fluoride
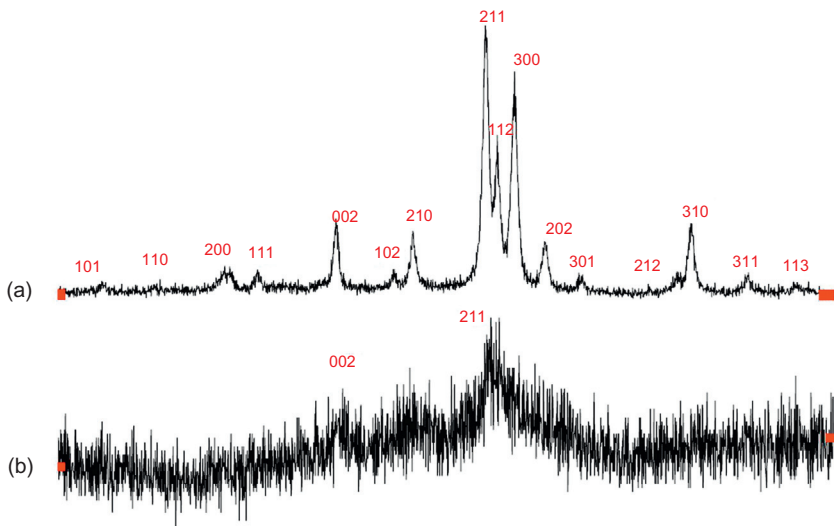
FIGURE 2.4   XRD spectra of (a) Human enamel; and (b) Dentin.

ions, which extends throughout the crystals in the [001] direction (c-axis). The substitution of OH^-, Cl^-, CO_3^{2-}, or other ions for the F^- usually leads to atomic displacements and lower symmetry, therefore compromising its chemical stability. Fluorapatite is chemically stable but is known to release fluoride as the pH in the oral cavity falls. It is believed that fluoride's anti-caries effect is due to its ability to partly transform the carbonated hydroxyapatite (HA) in enamel to thermodynamically more stable fluorapatite (FA) or fluorhydroxyapatite (FHA). During the caries process the fluoride is released, which changes the dynamics of the demineralization/remineralization process.[12]

Mature enamel is an acellular calcified tissue with the highest mineral level.[4] The overall composition is about 96% mineral by weight, with only 1–1.5% being organic matter, and the remainder being water. The organic portion of mature enamel is mainly composed of proteins and lipids. Besides the main protein, amelogenin (described previously), other proteins like enamelin, ameloblastin and tuftelin (all of which have a strong affinity for hydroxyapatite) play important roles in crystal nucleation and morphology development. They may also play a key role in bonding crystals together and forming the enamel rod structure. Other proteinases such as matrix metallopeptidase 20 (MMP20) and serine proteinase are important for degradation of the enamel proteins and promote maturation of the enamel crystals.

Enamel has a highly ordered multilevel hierarchical structure.[13,14] Besides the main component of enamel—enamel prisms described above, there are two other important structural components, interprismatic or interrod enamel, and the aprismatic enamel. The difference between the prism and the interprism is the orientation of hydroxyapatite crystals; the rod contains aligned crystallites,
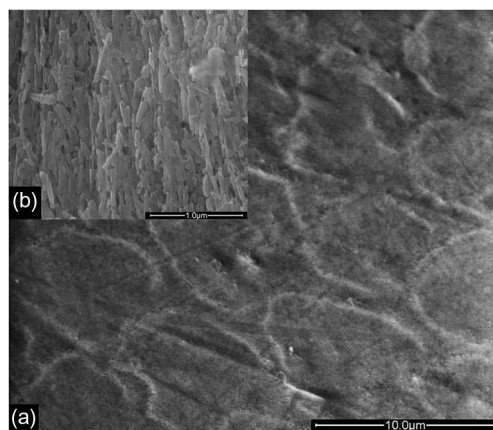
FIGURE 2.5   SEM images of natural human enamel surface. Scale bars: (a) 10.0 μm; and (b) 1.0 μm.

whereas the crystals in the interrod have a different orientation, less ordered and containing more organic components. The aprismatic enamel refers to the structures containing HA crystals without the prism-like structure. These aprismatic areas are located adjacent to the dentino-enamel junction (DEJ) and at the outer surfaces of both deciduous and permanent human enamel. The Tomes' process, a unique structure present at the secretory pole of the ameloblast, is responsible for aligned mineral formation in the prismatic enamel. The absence of this process may give rise to the aprismatic zone in the tooth. It should be noted that the human enamel rods do not simply run straight from the DEJ towards the enamel surface. In the cuspal areas the rods twist and form gnarled enamel, which may increase fracture resistance. Figure 2.5 is a surface microstructure SEM image of the natural human enamel. The arrangement of enamel rods is different among species. For instance, the adjacent two layers of rat enamel rods cross each other at a certain angle as shown in Figure 2.6.

2.2.2   Dentin

Dentin constitutes the bulk of the tooth, which is covered by enamel on the crown surface, cementum on the root, and pulp in the center.[3,4] The formation of dentin (dentinogenesis) is initiated by odontoblasts, which develop from dental papilla contact with the enamel organ. Unlike enamel, dentin continues to form throughout life and can be initiated in response to stimuli, such as tooth decay or abrasion.

With progressive deposition of dentin matrix, the odontoblastic process lengthens and becomes embedded in mineralized tissue. The space occupied by the odontoblastic process is known as the dentinal tubule. The dentinal tubule extends from the DEJ or cementum at the root to the predentin at the
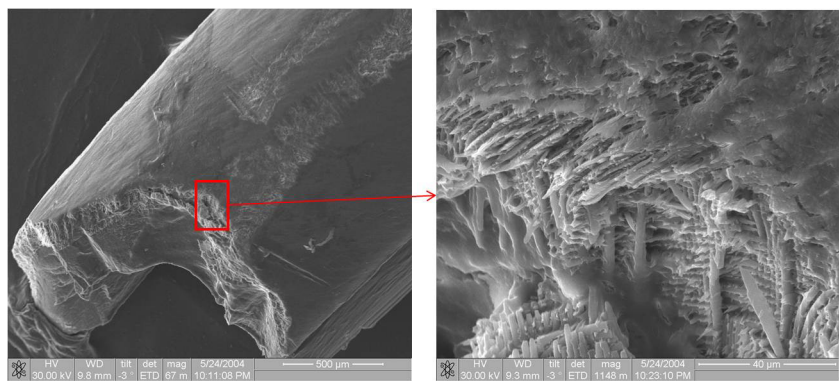
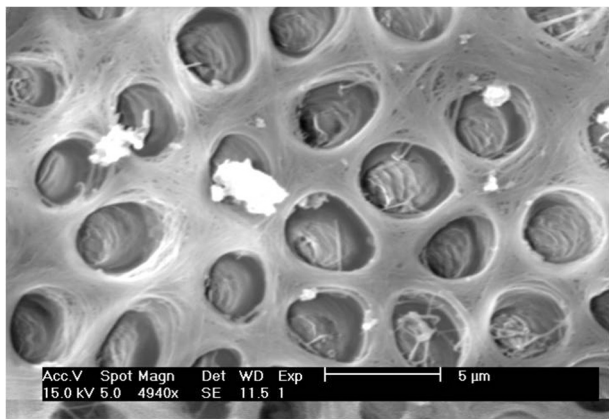**FIGURE 2.6**   SEM images of rat enamel.

FIGURE 2.7   SEM image of human dentin.

junction to the pulp chamber, where the odontoblastic cell bodies lie in nearly a close-packed array. Figure 2.7 shows the typical SEM image of dentin. Most of the collagen fibers arrange vertically to the dentinal tubules and interweave into a mesh. In the interstitial dentin, due to different degrees of mineralization, they can be divided into the following areas: peritubular dentin, intertubular dentin, incremental line, Tomes' granular layer, and predentin.

The overall composition of dentin is about 70% mineral by weight, about 20% organic matter, and 10% water.[4] The mineral of dentin is also comprised of crystals of a substituted carbonated hydroxyapatite with an organic matrix. However, unlike the long crystals in enamel, the crystals in dentin are much smaller and irregular. Figure 2.8 shows the atomic force microscopic (AFM) images of isolated dentin crystals.

It is widely accepted that these nanometer-sized crystals are needle or plate-like in morphology, based on studies using TEM and AFM. Figure 2.4b shows
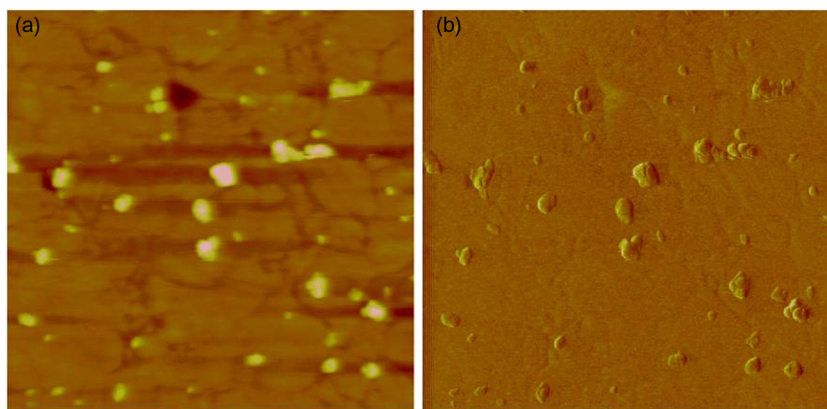
FIGURE 2.8 AFM images of dentin crystals isolated from human tooth crown. (a) Topography image; and (b) Lateral force image.

the XRD pattern of human dentin, which has a different crystallinity as compared to enamel crystals. Dentin crystals are only partially crystalline, while the enamel crystals are completely crystalline. The dentin mineralization process involves the formation and growth of hydroxyapatite crystals in an extracellular matrix.[15,16] Type I collagen accounts for 90% of the extracellular matrix of dentin. The collagen fibers provide the framework for HA deposition and the subsequent crystal growth to form a mineralized matrix. This biomineralization process is highly regulated by a set of matrix proteins that are secreted by odontoblasts. The function of these dentin matrix proteins in dentin mineralization has been widely discussed. Of these dentin matrix proteins, phosphophoryn (PP) is the most abundant noncollagenous protein.

More than 80% of this protein's amino acid composition is aspartic acid and serine, and 85–90% of the serine residues are phosphorylated.[15] These unique characteristics make PP a very acidic protein. Early studies have suggested that PP is a mineral nucleator and may have the ability to regulate HA formation.[16] Later studies have shown that PP affects in vitro mineralization in various ways. It was reported that mineral formation could be induced at low supersaturation by covalently binding rat PP to agarose beads and, conversely, that mineral formation could be inhibited when PP was free in the solution.[15,16]

Another important acidic extracellular matrix protein, dentin matrix protein 1 (DMP-1), was shown to be expressed in the early stages of dentin mineralization. Expression decreased after the appearance of mineral formation. Thus, it is postulated that DMP-1 has a regulatory role in dentin mineralization. The amino acid composition of DMP-1 is 28% glutamic acid and aspartic acid, which suggests that DMP-1 should have a great capacity for binding divalent cations such as calcium.[15] In an in vitro Ca-binding assay and nucleating test, recombinant DMP-1 showed not only strong Ca-binding ability, but also the capability to assemble calcium and phosphate ions to facilitate HA crystal

formation. An in vitro study of apatite growth in a gelatin gel system showed that the length and degree of phosphorylation of DMP-1 affected the initiation and regulation of mineral formation. DMP-1 initiates mineralization when it is dephosphorylated or cleaved, but inhibits mineralization when it is in its native form. Phosphorylation of acidic dentin matrix proteins such as DMP-1 and PP has been reported to affect crystal nucleation and subsequent mineral formation. More direct evidence using AFM revealed that PP had a stronger capacity for binding to enamel crystals than dephosphorylated PP.[16]

Dentin sialoprotein (DSP) is another extracellular matrix protein that has been widely investigated. DSP and PP are the cleavage products from a large transcript encoded by the gene dentin sialophosphoprotein (DSPP), but the amount of DSP found in dentin is much less than in DPP. The DSP transcript is expressed in odontoblasts and transiently expressed in preameloblasts. Immunohistochemical studies of DSP have shown that it is present in dentin and predentin. These results indicate a role for DSP in dentin mineralization, but as yet this role has not been defined.[15]

2.2.3   Cementum

Cementum covers the root surface and is an important tissue to maintain dental and periodontal attachment.[2–4] Light yellow in appearance, cementum is thinner near the tooth neck, about 20 to 50 microns thick, and about 150 to 200 microns thick at the root apex. Cementum is excreted by cells called cementoblasts, which develop from undifferentiated mesenchymal cells in the connective tissue of the dental sac. Cementum is slightly softer than dentin and consists of about 45–50% inorganic mineral (mainly the apatite crystals) by weight and 50–55% organic matter (mainly collagen and glycoproteins) and water by weight. Sharpey's fibers (perforating fibers) are portions of the principal collagenous fibers of the periodontal ligament embedded in the cementum and alveolar bone that attach the tooth to the alveolus. Cementum is formed continuously throughout life because a new layer of cementum is deposited to keep the attachment intact as the superficial layer of cementum ages, but unlike bone tissue that can be constantly rebuilt and remodeled, cementum has a stronger anti-absorption capacity compared to the alveolar bone and is only capable of repairing itself to a limited degree.

The structure of cementum is similar to the compact bone. Both are composed of cells and mineralized extracellular matrix. But unlike bone, there are no Haversian canals, blood vessels, and nerves in the cementum. Two kinds of cementum are formed, acellular and cellular, and fibers can be intrinsic or extrinsic, which results in four possible permutations.

2.2.4   Pulp

Pulp is found within the pulp cavity and is surrounded by hard dentin and connected by apical foramen to the periodontal tissue.[2–4] Developing from the same dental papilla as dentin, pulp is a soft and loose connective tissue which contains

cells, fibers, nerves, blood vessels, lymphatic vessels, and other extracellular matrix.

Fibroblasts (also known as dental pulp cells) are the main cells in the dental pulp, and contain an active collagen synthesis function.[4] The odontoblasts that line the walls of the pulp cavity form dentin. The pulp contains more defensive cells, such as histiocytes and undifferentiated mesenchymal cells. Pulp organic matrix principally consists of type I and III collagens. In addition, ground materials such as glycosaminoglycans, glycoproteins, and water comprise a supporting medium for cells and also for transportation of nutrients and other metabolites between the cells and vasculature.

The primary function of the dental pulp is to form dentin by the odontoblasts.[2,4] As dentin and pulp are embryologically, histologically, and functionally the same tissue, the two together are known as the dentin–pulp complex, which is responsible for dentin formation and protection of the tooth. Pulp is rich in blood vessels that keep the organic components of the surrounding mineralized tissue supplied with nutrients. Most of the nerves in the pulp are myelinated nerves that conduct pain. The other few unmyelinated nerves are part of the sympathetic nervous system that can regulate the contraction and relaxation of blood vessels. When the nerve in the pulp is stimulated, the reaction is pain, but it can't distinguish between the sensations of cold, heat, pressure, or chemical stimulation. This may be related to the lack of specific receptors in the pulp.

2.3 OPTICAL PROPERTIES OF TEETH

The appearance of natural teeth is mainly determined by their optical properties. Color is always considered the most crucial property. Besides color, opacity and translucence; fluorescence; opalescence; and metamerism, etc. also play important roles in the optical characteristics of teeth. All these optical properties are attributed to the special compositions or construction of natural teeth, when exposed to light and as seen by the human eye.

2.3.1 Color

The perception of the color of an object is the result of a physiological response to a physical stimulus.[17] The crown of natural teeth is a multilayered structure. The inner dental pulp is directly covered by dentin, and enamel is located on the outermost layer, as shown in Figure 2.9. When light hits the surface of natural teeth, reflection, absorption, and transmission occurs in each layer at different degrees. The reflective light perceptible by human eyes determines the color of the teeth. Dentin, which contains a large number of organic compounds, effectively reflects the longer wavelengths of light and appears yellow. The crucial influence of dentin on tooth color has been confirmed by Ten Bosch et al.[18] In their study, the color of dentin is correlated strongly with the color of the complete tooth. In other words, enamel plays only a minor role in the origination of tooth color.

FIGURE 2.9 The crown of natural teeth is a multilayered structure. The inner dental pulp is directly covered by dentin, and enamel is located on the outermost layer.

Since the tooth crown in different positions does not have the same construction, tooth color varies.[19] In the anterior area, the maxillary teeth are more yellow than the mandibular teeth. The central incisor has a similar color to the lateral incisor, while the canine is redder, yellower, and more saturated. Due to the inhomogeneous distribution of three dental tissues, even for an individual tooth there is a color gradient.[20] Along the long axis of a natural tooth, lightness increases from incisor, middle, to cervical part, and the tooth looks redder and yellower. Color differences are reported among persons of different race, gender, region, etc.

Tooth discoloration always occurs, and influences individual appearance. There are three categories of tooth discoloration: intrinsic, extrinsic, and internalized.[21] Intrinsic discoloration is the result of a structural change in the dental hard tissues. It is caused by numerous metabolic diseases, local, and systemic factors. Extrinsic discoloration, both metallic and non-metallic stain, originates from the deposition of calcium phosphate and other pigments onto the tooth surface or inside the acquired pellicle. Internalized discoloration is a complementary category of extrinsic discoloration. It highlights the procedure of extrinsic stain inflating into the interior of the tooth. Defective enamel or a porous surface of exposed dentin is the pre-requisite of internalized discoloration. Either can be induced by developmental defects or acquired during daily life through tooth wear, gingival recession, dental caries, and application of restorative materials.

Sometimes, tooth discoloration is the result of several factors. For example, with an increase in age, the tooth looks yellower, redder, and darker due to the shrinkage of dental pulp cavity and an increase of secondary dentin. Meanwhile, abrasion of enamel leads to the exposure of dentin directly to the outermost surface. Calcium phosphate may deposit in the enamel or peritubular dentin, and food pigments lie on both the surface and the DEJ through the dentin tubules.

Scientific description of tooth color is important for measuring tooth color in order to reproduce it with restorative materials. Nowadays, the Munsell color system, the CIE XYZ tristimulus system, and the CIELab* color system are commonly used.[22] Numerous shade guides and shade-taking devices have been developed based on these systems. The Vitapan Classical shade guide, for example, includes 16 tabs arranged in four groups representing brown–yellow (A), orange–yellow (B), grey–yellow (C) and red–yellow (D), respectively. As one example, A2 is the most popular color for Chinese people's teeth.[23]

2.3.2   Opacity and Translucency

Opacity and translucency represent the ability of an object to prevent or permit the passage of light, respectively.[17] Natural tooth is translucent due to the comprehensive effect of dental tissues. Enamel is more translucent than dentin. One reason for this is the relatively small difference in refractive index between air (~1) and enamel (~1.7).[24] No serious refraction occurs in the enamel during light transmission. However, dentin contains ~70% inorganic compounds and various kinds of organic compounds. The differences in refractive indexes among them are obvious, and increases the refraction and absorption of light and generates lower translucency than enamel. Furthermore, the homogeneous and densely packed enamel prisms are helpful in letting more light penetrate the enamel.[25]

Similar to a gradation of color, translucency also varies within an individual tooth.[25] The incisor region is always the most translucent, while the middle region exhibits poorer translucency than the other regions. This is because enamel with high translucency occupies most of the incisor region, while the dental pulp cavity reaches the central region of the tooth crown; the pulp tissues absorb more light, which reduces translucency. In addition, as the negative relationship between thickness and translucency has been confirmed, the translucency of the middle region is also expected to be lower than the other two regions.

There is also an age-related effect on translucency.[25] Translucency of a tooth increases as a person gets older. Three possible reasons are considered: aged and shrunken pulp tissue absorbs less light than fresh pulp; abrasion causes degeneration of the process of the odontoblast; and dentinal tubules are sealed by minerals. These changes can reduce the difference of the refractive index between the dentinal tubules and their surrounding compounds. Furthermore, the reduction of tooth thickness during abrasion improves translucency.

2.3.3   Fluorescence

Fluorescence is the emission of luminous energy by a material when a beam of light is shone on it.[17] Natural teeth are fluorescent. By absorbing ultraviolet light (365 nm), blue or white visible light is emitted. Particularly in the blue region (450 nm) of the spectrum, fluorescence becomes polychromatic with

great intensity. It gives natural teeth a blue and white appearance under fluorescent light, which is complementary to the yellow color observed under visible light. Fluorescence of natural teeth originates from the fluorescent substances contained in dental tissues. Dickson et al. first reported that dentin was more fluorescent than enamel.[26] When ultraviolet radiation (365 nm) hits dentin, fluorescent light with a 440±10 nm wavelength is emitted, the intensity of which is four times that emitted by enamel under the same conditions. The main fluorescent substances in dentin and enamel are dentinal tubules and enamel lamellae and tufts, respectively. The positive correlation between the intensity of fluorescence and the degree of mineralization of the tissue has been confirmed.[27] Increases in fluorescence intensity are also caused by structural arrangements such as those found in the Hunter-Schreger bands of enamel. Opinions on the effect of fluorescence on tooth color are controversial.[28] Some researchers consider that the fluorescent light emitted by both dentin and enamel could increase the lightness and whiteness of natural teeth without obvious changes in translucency, while others believe that the influence of fluorescence on tooth color is too small to be detected under daily lighting conditions.

2.3.4   Opalescence

Opalescence can be defined as the milky, iridescent appearance of a dense, transparent medium or colloidal system when illuminated by visible light. When visible light is shone on natural teeth, a blue–grey incisal halo will appear at the incisal margin. This phenomenon is mainly caused by enamel, in which lots of hydroxyapatite crystals are organized into enamel prisms surrounded by small amounts of organic compounds. This special construction could give enamel the ability to reflect the shorter wavelengths of light (blue color), transmit the longer wavelengths (yellow–orange), and absorb the medium wavelengths (green color). The opalescence parameter of natural human teeth is in the range of 19.8 to 27.6.[29]

2.3.5   Metamerism

Metamerism is a phenomenon where the color of two objects appear the same under a particular light source, but actually have different spectral energy distributions.[24] When a different kind of light source is used, the color difference between them is revealed. The reason for metamerism is that some crossing points exist in these distinct spectrums. Metamerism creates a challenge for reproducing the color of natural teeth accurately. Since there is a tight correlation between the light source and metamerism, the quality and intensity of light should be taken into account during color matching. Some researchers suggest that for best color matching, it should be done in the natural light from a large window with a northern exposure; that is what is most typically used for artificial crowns. Meanwhile, matching the color under color-correct fluorescent

lighting is also recommended. A full-spectrum light source can also eliminate the occurrence of metamerism.

2.4   MECHANICAL PROPERTIES OF TEETH

Teeth are the major component of human chewing organs.[1] The sharp-edged incisors cut food and the pointed canines tear it.[2–4] The flat surfaces of the pre-molars and molars are well adapted to grinding and crushing food. Human teeth must be able to repeatedly withstand occlusion pressure from various directions over a lifelong term. It is estimated that the combination of enamel and dentin must withstand about a 20 MPa occlusion pressure 3000 times per day. However, it is clinically rare to see a complete fracture of teeth. This is partly due to the hardness and rigidity of enamel and the toughness and flexibility of dentin. Enamel is the hardest tissue in the human body with a Knoop Hardness of about 343–431 KHN, equivalent to 5 times that of dentin (68–80 KHN). Enamel is brittle and easily broken if it loses the support of the flexible dentin below.

Enamel is highly patterned and consists of organized interweaving bundles of enamel rods.[13,14] It has a higher reported toughness than that of crystalline HA, indicating that the organization of the crystallites is essential for enamel function. Because of the high mineral and low organic content, enamel is brittle. Interestingly, the architecture of enamel crystallites can deflect a propagating crack, preventing it from reaching the DEJ, which has also been shown to resist delamination of the tissues, despite differences in composition. The mechanical properties of enamel, dentin, and the DEJ are not completely understood and are a significant area of research. Understanding the properties of these tissues could serve to motivate further engineering of more robust dental materials as well as to inspire fabrication of nonbiological materials. Details on the mechanical properties of the tooth are summarized in Table 2.1.[13]

2.5   COMMON DEFECTS AND DAMAGE

Common defects and damage of teeth include imperfections caused by abnormal development, chronic injury of hard tissue, traumatic injuries, and tooth diseases such as pulp disease, periapical disease, and dental caries.[30,31]

Dental caries are an infectious microbiologic disease of the teeth that results in localized dissolution and destruction of the calcified tissues (Figure 2.10a). The characteristics of a carious lesion vary with the nature of the surface on which the lesion develops. Trauma implies a reasonably severe, non-physiological lesion to any part of the body. Any thermal, chemical, or mechanical lesion that affects the dentition should be analyzed as a dental trauma, and its effect as a traumatic dental injury. Erosion is chemical wear as a result of extrinsic or intrinsic acids or chelators acting on plaque-free tooth surfaces. Abrasion is physical wear as a result of mechanical processes involving foreign substances or objects. Enamel hypoplasia is qualitatively defective enamel in which normal amounts of enamel

TABLE 2.1 Properties of Enamel and Dentin[13]

Property	Enamel	Dentin
Density	2.96 g/cm^3	2.1 g/cm^3
Compressive		
Modulus of elasticity	60–120 GPa	18–24 GPa
Proportional limit	70–353 MPa	100–190 MPa
Strength	94–450 MPa	230–370 MPa
Tensile		
Modulus of elasticity		11–19 GPa
Strength	8–35 MPa	30–65 GPa
Shear strength	90 MPa	138 MPa
Flexural strength	60–90 MPa	245–280 MPa
Hardness	3–6 GPa	0.13–0.51 GPa

FIGURE 2.10   Common defects and damages of tooth.

are produced but are hypomineralized (Figure 2.10b). Various preparations of the antibiotic drug tetracycline can cause the most distracting, generalized type of intrinsic discoloration (Figure 2.10d). The severity of staining depends on the dose, duration of exposure to the drug, and type of tetracycline analogue used. Different types of tetracyclines induce different types of discoloration, varying

from yellow–orange to dark blue–gray. Dark blue–gray, tetracycline-stained teeth are considerably more difficult to treat than teeth with mild yellow-orange discolorations. Staining from tetracycline-type drugs most frequently occurs at an early age and is caused by ingestion of the drug concomitant with the development of permanent teeth. Drinking water that contains fluoride at levels greater than one part per million ingested during the time when crowns are being formed may result in enamel hypoplasia or hypocalcification, known as fluorosis (Figure 2.10c). Fluoride appears to create significant enamel defects through retention of the amelogenin proteins in the enamel structure, which leads to the formation of hypomineralized enamel. These alterations create a permanent hypomaturation of the enamel in which an increased surface and subsurface porosity of the enamel is observed. This enamel structure alters the light reflection and creates the appearance of white, chalky areas. Most of the problems associated with dental fluorosis are aesthetic and concern the appearance of the anterior teeth.

ACKNOWLEDGMENTS

REFERENCES

1. Johnson MD. Human biology: concepts and current issues, 6th ed. Upper Saddle River: Pearson Education; 2012.
2. Avery JK. Oral development and histology, 3rd ed. New York: Theme; 2002.
3. Woelfel JB, Scheid RC. Dental anatomy, 6th ed. Baltimore: Lippincott Williams & Wilkins; 2002.
4. Garant PR. Oral cells and tissues. Chicago: Quintessence; 2003.
5. Yin Y, Yun S, Fang J, Chen H. Chemical regeneration of human tooth enamel under near-physiological conditions. Chem Commun 2009;39:5892–4.
6. Wang X, Xia C, Zhang Z, Deng X, Wei S, Zheng G, et al. Direct growth of human enamel-like calcium phosphate microstructures on human tooth. J Nanosci Nanotechnol 2009;9: (Sp. Iss.) 1361–4.
7. Chen H, Clarkson BH, Sun K, Mansfield JF. Self-assembly of synthetic hydroxyapatite nanorods into an enamel prism-like structure. J Colloid Interface Sci 2005;288:97–103.
8. Chen H, Chen Y, Orr BG, Banaszak-Holl MM, Majoros I, Clarkson BH. Nanoscale probing of enamel nanorod surface using polyamidoamine dendrimer. Langmuir 2004;20(10):4168–71.
9. Chen H, Banaszak-Holl MM, Orr BG, Majoros I, Clarkson BH. Interaction of dendrimers (Artificial Proteins) with biological hydroxyapatite crystals. J Dent Res 2003;82(6):443–8.
10. Chen H, Tang Z, Liu J, Sun K, Chang SR, Peters MC, et al. Acellular synthesis of a human enamel-like microstructure. Adv Mater 2006;18:1846–51.
11. Chen H, Czajka-Jakubowska A, Spencer NJ, Mansfield JF, Robinson C, Clarkson BH. Effects of systemic fluoride and in vitro fluoride treatment on enamel crystals. J Dent Res 2006;85:1042–5.

12. Chen H, Sun K, Tang Z, Law RV, Mansfield JF, Czajka-Jakubowska A, et al. Synthesis of fluorapatite nanorods and nanowires by direct precipitation from solution. Cryst Growth Des 2006;6:1504–8.
13. Sakaguchi RL, Powers JM. Craig's restorative dental materials 13th ed. Philadelphia: Elsevier; 2012.
14. Palmer LC, Newcomb CJ, Kaltz SR, Spoerke ED, Stupp SI. Biomimetic systems for hydroxyapatite mineralization inspired by bone and enamel. Chem Rev 2008;108:4754–83.
15. Chang S, Chen H, Liu J, Wood D, Bentley P, Clarkson B. Synthesis of a bioactive, hydroxy-apaptite nucleating molecule. Calcif Tissue Int 2006;78:55–61.
16. Wallwork ML, Kirkham J, Chen H, Chang SR, Robinson C, Clarkson BH. Imaging dentin proteins on enamel crystal using atomic force microscopy. Calcif Tissue Int 2002;71:249–55.
17. Powers JM. Optical, thermal and electrical properties. In Craig RG, Powers JM, editors. Restorative dental materials 11th ed. St. Louis: Mosby; 2002. p. 67–142.
18. Ten Bosch JJ, Coops JC. Tooth color and reflectance as related to light scattering and enamel hardness. J Dent Res 1995;74(1):374–80.
19. Goodkind RJ, Schwabacher WB. Use of a fiber-optic colorimeter for in vivo color measure-ments of 2830 anterior teeth. J Prosthet Dent 1987;58(5):535–42.
20. Zhang L, Wang XZ, Gao CZ. Measurement and analysis on dentin color of 129 Chinese teeth. J Jpn Acad Color Dent 1999;6(1):13–17.
21. Watts A, Addy M. Tooth discolouration and staining: a review of the literature. Br Dent J 2001;190(6):309–16.
22. Anusavice KJ. Color and color perception. In Anusavice KJ, editor. Phillips' science of dental materials 11th ed. London: Elsevier Science Health Science; 2003. p. 46–51.
23. Wu HW, Wang XZ, Gao CZ. Differences in shading between dentists and patients. J Pract Stomatol 2003;19(6):627–9.
24. Houwink B. The index of refraction of dental enamel apatite. Br Dent J 1974;137(12):472–5.
25. Xiong F, Chao Y, Zhu Z. Translucency of newly extracted maxillary central incisors at nine locations. J Prosthet Dent 2008;100(1):11–17.
26. Dickson G, Forziati AF, Lawson ME, et al. Fluorescence of teeth; a means of investigating their structure. J Am Dent Assoc 1952;45(6):661–7.
27. Foreman PC. Fluorescent microstructure of mineralized dental tissues. Int Endod J 1988;21(4):251–6.
28. Joiner A. Tooth colour: a review of the literature. J Dent 2004;32 Suppl. 1:3–12.
29. Lee YK, Yu B. Measurement of opalescence of tooth enamel. J Dent 2007;35(8):690–4.
30. Feliciano KMPC, Caldas AF. A systematic review of the diagnostic classifications of trau-matic dental injuries. Dent Traumatol 2006;22(2):71–6.
31. Regezi JA, Sciubba JJ, Jordan RCK. Oral pathology: clinical pathologic correlations, 5th ed. Philadelphia: Elsevier; 2008.

Dental Prostheses

Jing Zhao[*,†] and Xinzhi Wang[*]

[*]*Department of Prosthodontics, Peking University School and Hospital of Stomatology, Beijing, China;* [†]*Department of Materials and Environmental Chemistry, Arrhenius Laboratory, Stockholm University, Stockholm, Sweden*

Contents

3.1 INTRODUCTION OF PROSTHODONTICS AND DENTAL PROSTHESES

The health of a tooth is vulnerable for numerous reasons, and cumulative effects are detrimental, as was illustrated in Chapter 2. Once a tooth or dentition suffers from a structural defect, oral health is threatened because the defect is unable to self-regenerate. Therefore, artificial appliances known as dental prostheses are needed to restore the damaged, unaesthetic, or dysfunctional tooth, or to replace one or more missing natural teeth. This section is a general introduction to prosthodontics and dental prostheses is given in the present section. Commonly used dental prostheses for the restoration of various tooth defects, partial edentulism, and complete edentulism are introduced

in Sections 3.2, 3.3, and 3.4, respectively. The dental implant, a major component in modern prosthodontics, is presented in detail in Chapter 4.

Prosthodontics is the branch of dentistry that pertains to the diagnosis, treatment planning, rehabilitation, and maintenance of oral function, comfort, appearance, and health of patients with clinical conditions associated with missing or deficient teeth, and/or maxillofacial tissues using biocompatible substitutes.[1] The subject highlighted in this chapter is special prostheses for tooth and dentition.

The general requirements of dental prostheses are obvious from the goal of prosthodontics. Thus, the most important aim of restoration is to rehabilitate oral function, especially the masticatory function. It means that the individual geometry of the dental prostheses is needed to establish appropriate and efficient occlusal contacts. For example, the detailed characteristics of the cusps of the posterior artificial tooth, like the cuspal inclination, height, and geometry, should match those of the opposite fossa. Then, the two opposite posterior teeth should form a pestle-and-mortar-like structure that is efficient for grinding food.

Crucial factors to a good long-life performance of dental prostheses are strength, intraoral ageing resistance and fatigue resistance, etc. Observed signs of pulposus or other negative symptoms of the natural tooth must be considered before treatment. Furthermore, dental prostheses should take into account the wear resistance and abrasion of the opposing natural teeth. Excessive abrasion of tooth tissue (more than 29 μm per year) caused by the dental prostheses should be avoided since it jeopardizes the health and function of the juxtapose natural teeth.

Patient comfort is one important parameter used to evaluate the success of the dental prostheses. From this point of view, fixed prostheses are favored over removable prostheses. Fixed prostheses are tooth- and/or implant-supported and are fixed through adhesion or mechanical locks. In contrast, removable prostheses are tooth and mucosa co-supported; therefore, a denture base and connectors are unavoidable. Foreign body sensation becomes more obvious when a larger denture base and more connectors are applied. A metal base and connectors also decrease the visual aesthetics. These negative effects are the main reasons why fixed treatments are favored over removable prostheses in prosthodontic dentistry.

Besides restoring oral function and appearance, dental prostheses should maintain or improve the general health of the patient. Firstly, restorative materials must have a good biocompatibility, which is the ability of enthetic materials or appliances to be used without any toxic or injurious effects on patients' biological systems. Secondly, dental prostheses should protect the remaining tooth structure or teeth. A systematic review has stressed the positive effects of good dental prostheses on prolonging the durability of abutments and remaining teeth.[2] Prosthodontic treatments promote the '8020 movement' which was proposed by the World Health Organization (WHO) in 2001, by aiming for

the retention of 20 natural teeth at the age of 80. Finally, there is a close relationship between oral health and general health. For example, effective mastication reduces the burden on the digestive system. Therefore, improving oral health is expected to improve general health.

Prosthodontic design and treatment should always strive for optimization of the following principles: function, longevity, aesthetics, comfort, biocompatibility, and protection. One point should be stressed, however, that no absolutely perfect or omnipotent prostheses exists for every individual patient. Individual oral condition, a patient's willingness to use prostheses, and other affecting factors should be considered carefully by prosthodontists. Commonly used dental prostheses are presented in the following sections.

3.2   RESTORATION OF TOOTH DEFECTS

The type of restoration chosen to repair a tooth defect depends on the characteristics of its lesion, such as position, geometry, or range. Therefore, it is helpful to understand the principle of prosthodontic design by considering the typical characteristics of lesions. The most widely accepted classification of tooth defects or cavities was put forth by Dr. G. V. Black over one hundred years ago. It is based on the specific location of the lesion as illustrated in Figure 3.1.[3]

G. V. Black's Classification:

Class I: Cavities involve the pits and fissures of the teeth, including the lesions that occur on the occlusal areas of molars and premolars or in the lingual pits of incisors and canines. All other classifications (II-VI) involve smooth surfaces of the teeth.

Class II: Cavities involve the proximal and occlusal surfaces of premolars and molars.

Class III: Cavities involve the proximal surfaces of incisors and canines that do not involve the incisal angle.

Class IV: Cavities are located on the proximal surface of incisors and canines and do involve the incisal angle.

Class V: Cavities are located on the facial or lingual surfaces of the cervical one-third of all teeth that do not involve a pit or fissure.

Class VI: Cavities are on the incisal edges of anterior teeth or on the occlusal cusp heights of posterior teeth (not included in the original classification by G.V. Black).

The general principle of prosthetic design is that no matter which kind of tooth defect exists, if sufficient coronal tooth structure exists, an *intracoronal restoration* can be employed. Coronal tooth tissue must be strong enough to retain and protect a restoration under the anticipated stresses of mastication and the rebuilt integral structure. Intracoronal restoration is more suitable to the vital tooth than to the non-vital tooth, regardless of whether the root canal
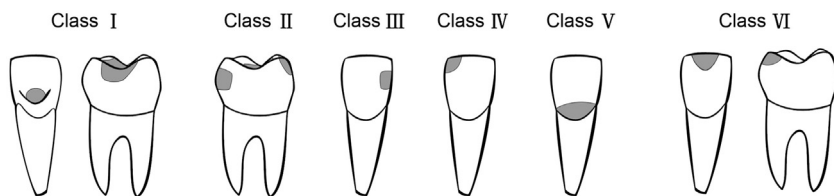
FIGURE 3.1 According to the G.V. Black Classification, various tooth defects are categorized into six classes based on the specific location of the lesions.

treatment (RCT) has been done or not. Since the RCT-ed (root canal treated) non-vital tooth might not have enough remaining tooth tissue, it is prone to brittleness. Common intracoronal restorations include *direct fillings*; *inlays* and *onlays*; and *laminate veneers*.

An *extracoronal restoration* is needed when insufficient coronal tooth structure remains to keep the restoration within the crown of the tooth. It will reproduce the morphology and contours of the damaged crown and allow normal oral function. It could also protect the remaining tooth structure from further damage. In addition, extracoronal restoration may be used if there are extensive areas of defective axial tooth structure, or if there is a need to modify contours to refine occlusion and improve aesthetics. According to whether a partial or whole crown is needed, the extracoronal restoration is classified as *partial crown* or *full crown*, respectively. When further support and retention are needed, *posts and cores* are recommended.

Besides the distinct indications of intracoronal restorations or extracoronal restorations, good oral hygiene is the common prerequisite for their application. The oral cavity is a warm, moist, and sub-acidic environment that contains symbiotic bacteria. If poor oral hygiene causes severe periodontitis, potential abutments cannot provide support and retention for the restorations. Meanwhile, abutments are more vulnerable to secondary caries and can lead to unexpected failure since the margins of dental restorations are always exposed directly to the oral environment.

3.2.1 Direct Fillings

If the lesions are not so severe and the biting force is not too high, no matter which kind of lesion exists, they are always directly filled by dentists using fictile materials. After shaping and curing, the fillings become hard and the restorations are formed. This chair-side treatment can be completed during a single clinic visit. An example of the restoration of occlusal and buccal-occlusal carious lesions in the maxillary first and second molar, respectively, is illustrated in Figure 3.2. By using direct fillings, healthy hard tooth tissues are protected, although some tooth preparation is always needed for removing all lesions and providing the necessary retention.

FIGURE 3.2 (a) Two carious lesions were detected in the maxillary first and second molar. (b) After removing all caries and tooth preparation, (c) the cavities were filled by tooth-color composite resin to rebuild the individual geometry and aesthetic appearance of the crowns.

Direct filling is good for shaping pits and fissures; and forming smooth and flat surfaces. However, rebuilding a curved convex structure, like cusps, marginal ridges, and incisal edges, is not so easy due to the soft status of materials during application. Also, direct filling fictile materials have neither the high strength nor the good wearability of metal alloy materials or ceramics. Therefore, fictile materials are not applied in those cases related to the cusps, tips, and edges where strong materials are needed, like Class IV and VI lesions.

In terms of material selection, great improvements have been made recently. Silver amalgam fillings have been widely used since the 1800s due to their low cost, ease of application, strength, and durability, especially for Class I lesions. However, mercury has gotten negative attention for both its harmfulness to the environment and to a patient's general health. In addition, poor aesthetics and poor longevity have diminished the popularity of silver amalgams, and they are often avoided.[4]

Composite fillings have become a feasible alternative to silver amalgams. With the development of novel composite resins, overall properties have been improved (especially aesthetics and strength) and their usage has increased.[5] An aesthetic restorative example is shown in Figure 3.3 where the lesion is restored by a tooth-colored composite resin. However, the potential disadvantages of composite fillings should always be considered, including polymerization shrinkage, wearability, strength, and discoloration. The leakage of
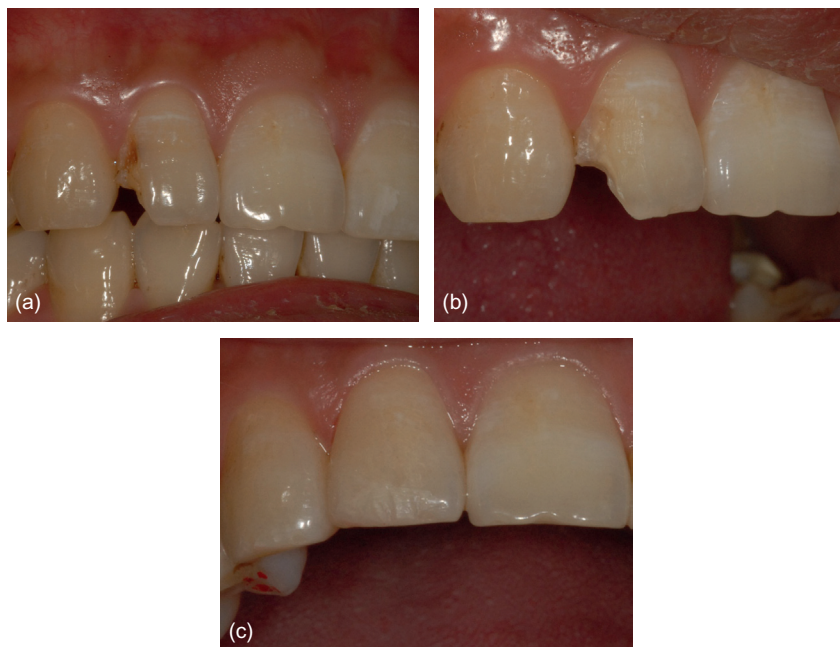
FIGURE 3.3   Aesthetic composite resin is applied to restore the Class IV lesion on the right maxillary lateral incisor. The pictures show the buccal view: (a) Initial lesion; (b) Cavity preparation; and (c) Final appearance after restoration.

composite fillings allows bacteria, viruses, toxins, and infectious agents to penetrate the tooth and harm its health.

3.2.2   Inlays and Onlays

As mentioned before, direct fillings might not be the best choice for Class IV/VI lesions or for the other lesions with more extensive defects. Indirect restorations, like inlays and onlays, are recommended instead.

Inlay is a restoration that fits within the anatomic contours of the clinical crown of a tooth. Onlay is useful for restoring a more extensively damaged tooth, especially where cuspal fracture has occurred but there is still enough remaining tooth structure to work with. A schematic diagram showing inlay and onlay can be found in Figure 3.4. Commonly used processing methods are casting, milling, and pressing of the industrial prefabricated blocks. Thereby, the individual and precise geometry of restorations are easy to obtain.

Due to their ability to restore convex structures, inlays and onlays are also preferred in the following four cases: a serious tooth defect with bad proximal relation, a food impaction needing proximal contact recovery, an abutment with caries, or an attachment with an inlay as retainer. An example of the use
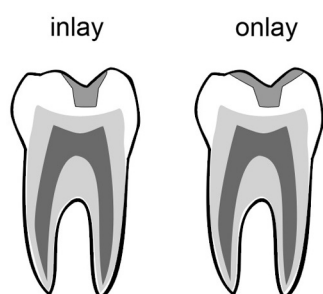
inlay

onlay

FIGURE 3.4 Diagram showing indirect intracoronal restorations.
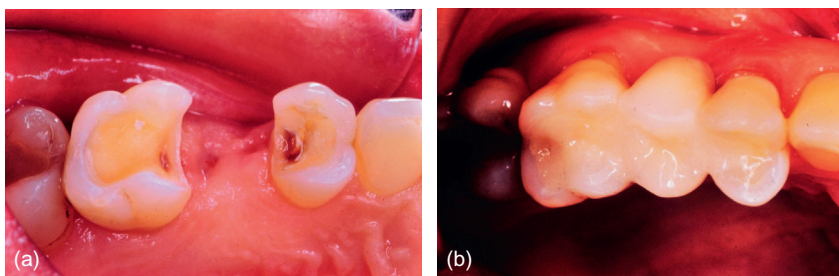

(a)

(b)

FIGURE 3.5 The missing second premolar and the defective abutments (a) were restored by an inlay-supported prosthesis (b).

of inlay-supported prostheses is shown in Figure 3.5. The ideal inlay preparation design was proposed by Thompson et al.[6]

There are some limitations, however.[7] Compared to direct fillings, more tooth preparation is needed for inlays/onlays. The tooth preparation must allow enough retention of restorations and the tooth structure must be thick enough to resist fracture. This means that young permanent or deciduous teeth, which have high pulp horn, are contraindications. Moreover, neither a small and superficial occlusal surface defect nor a proximal and labial surface defect with an uninvolved incisal angle is suitable for restoration by inlays/onlays. Inlays only replace lost tooth structure and do not protect the remaining part of the tooth. Therefore, an inlay cannot be used in cases where there is a serious defect; poor resistance or retention shape; or where there are high requirements for aesthetics and long-term stability.

A lot of different materials are available for the fabrication of inlays and onlays, comprising composite resins, metal alloys, and ceramics.[8] The material selection always depends on the individual application. Ceramic inlays and onlays have become popular in the anterior area due to their excellent natural appearance and biocompatibility. On the contrary, the application of metal fillings is limited to the posterior area. Ceramic onlays, especially mesial-occlusal-distal (MOD) onlays, should be fabricated carefully because without generous occlusal thickness, these restorations are susceptible to fracture.[9]

FIGURE 3.6 Microdontia of the maxillary lateral incisors with an unaesthetic appearance was the complaint (a and b). After a small amount of tooth preparation within tooth enamel (c), laminate veneers made from porcelain (d) were attached to the teeth's surface. A better aesthetic appearance was immediately created (e and f).

3.2.3 Laminate Veneers

Laminate veneers are important cosmetic dentistry appliances that were invented as early as 1937 for aesthetic purposes. By affixing a thin veneer onto a tooth's facial surface, the visual appearance can be improved. It can also protect the remaining tooth structure to a high degree and simplify treatment. Therefore, the most obvious advantage of this technique is the improvement of aesthetic properties with minimum requirements for tooth preparation. This factor is attractive to the patient and dentist alike.[10] Nowadays, laminate veneers are widely used to restore limited defects within the enamel on the facial surface, and to improve the appearance of discolored or malformed teeth (Figure 3.6).
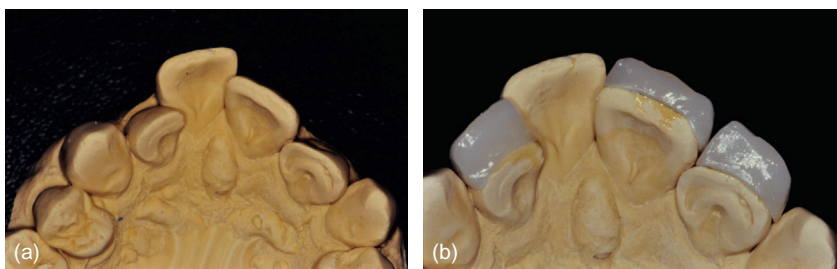
FIGURE 3.7 The dislocated teeth in the anterior area (a) were restored with laminate veneers (b) to improve the general appearance of the patient's teeth.

Besides these applications, laminate veneers are useful for slightly dislocated teeth and diastema in the anterior area where the patient would not accept an orthodontic treatment. An illustrative example of dislocated anterior teeth that have been restored by laminate veneer to improve appearance is shown in Figure 3.7. Finally, laminate veneers are suitable for restoration of a too-short natural tooth or an exceptionally worn tooth with a new protective coating.

Follow-up reports indicate that the clinical acceptance rate for porcelain veneers is around 64%. The main reasons for failure are fractures of the porcelain and large marginal defects, like discoloration and the recurrence of caries. Fortunately, most of these problems are repairable and do not require replacement.[11] Therefore, laminate veneers are wished to be thin with a smooth surface, precise shape and perfect margins. The laminate should not irritate the gingiva and should hide any discoloration. In addition, the ideal laminate has good wear-resistance, fracture-resistance, durability, coloration-resistance, micro-leakage resistance, and is easy to fabricate and repair.[12] These properties are always desired at a low cost, but in reality require a compromise by both dentist and patient.

Although several kinds of materials are available, like composite veneers, acrylic veneers, porcelain veneers, and ceramic veneers, none of them fulfill the combination of requests listed above. For example, the most frequently used low-cost porcelain veneers are so brittle that they are prone to fracture and are difficult to repair. A severely discolored tooth cannot be restored to its natural color using only laminate due to the limited space for hiding a pronounced color.

Contraindications for the use of laminate veneers must be considered from the following conditions.[12] Firstly, no space for laminate veneers is available in maxillary tooth labioversion. Secondly, neither sufficient nor effective adhesive areas are available due to severe enamel dysplasia or fluorosis. Thirdly, unsuitable occlusion, like anti-jaw teeth and mandibular teeth with severe deep malocclusion, would undermine the retention and resistance of laminate veneers. Finally, a laminate veneer is not recommended for patients with bad oral habits, such as bruxism and the habit of biting abnormal objects.

3.2.4   Partial Crowns

When there is a less healthy tooth structure present, but the tooth destruction is not too excessive, a partial crown might be designed.[13] The partial crown is an extracoronal restoration that restores a tooth with one or more intact axial surfaces and some of the remaining coronal tooth structure. Depending on the tooth coverage area, the partial veneer crown can be described as a half crown, 3/4 crown, 7/8 crown, etc. For instance, when a mesially tilted mandible molar is chosen as the abutment of the fixed partial denture, a modified 3/4 crown, without coverage on the distal surface of the tilted molar, would be helpful for gaining a common path of insertion with another abutment. Moreover, a partial crown can be applied to re-establish anterior guidance and to splint teeth.

The intact area of a partial crown with gingiva is shorter and has smaller stimulation on the gingival tissue than a full crown. The requirements of tooth preparation are not as large as that of a full crown, and more tooth tissues can be preserved. With carefully finished margins, a partial crown can satisfy moderate aesthetic demands in the maxillary arch, although not as satisfactorily as the veneered full crown.

The retention and resistance of a partial crown, however, is still relatively low. This limits its application for restoring tooth with a short clinical crown, RCT-ed teeth, or using as retainers for a long-span fixed partial denture.[14] Since some surfaces of the tooth will not be covered by the partial crown, it cannot be used for patients with active caries or periodontal disease. These drawbacks have decreased the partial crown's popularity. Above all, the partial crown is mostly used to restore moderate tooth defects, which is the restoration level between an intracoronal restoration and a full crown.

3.2.5   Full Crowns

The full or complete crown, is used to restore a tooth with multiple defective axial surfaces and to reproduce the clinical crown of a natural tooth. It provides the maximum retention possible in any given situation. One important issue should be reiterated here: enough healthy tooth structure is required for application of a full crown. Otherwise, tooth fracture or crown de-bonding may occur.

According to the structure and the restorative material used, full crowns can be classified into three major groups with different indications.[13] They are: the full metal crown, the porcelain fused to metal crown (PFM), and the non-metal full crown (Figures 3.8a, b, and c respectively).

Full metal crown. This crown requires less removal of tooth tissue than the crowns with a ceramic component. Full metal crowns are strong, but use must be restricted to situations where neither aesthetic expectations nor metal allergy reactions exist. Of utmost importance for all metal-based restorations is the careful consideration of the selected metal alloy.[15] Nowadays in dentistry, casting alloys are more popular than wrought alloys because casting
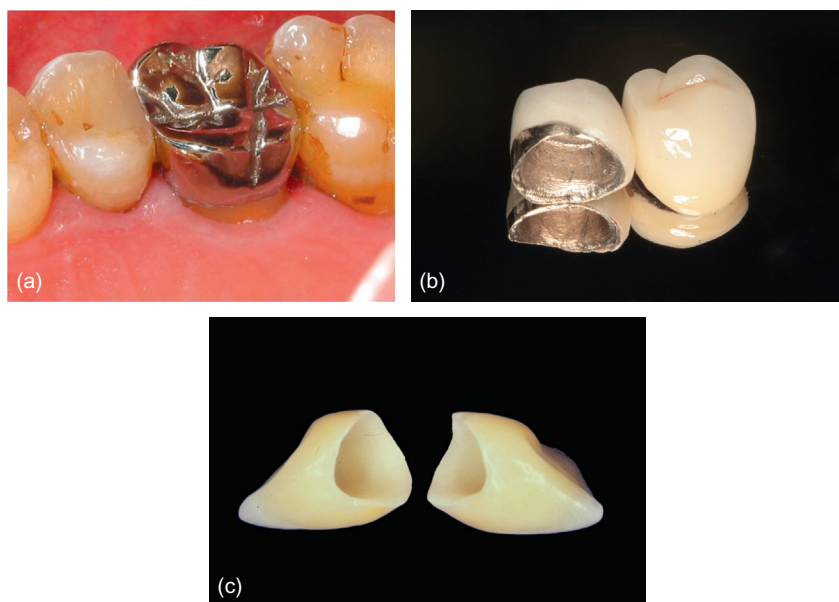
FIGURE 3.8 Three commonly used complete crowns: (a) Full metal crown; (b) Porcelain fused to metal crown; and (c) Non-metal full crown (all-ceramic crown).

technology gives a more homogeneous metal structure. The benefits of this are higher precision and longer-lasting performance. Based on their compositions, casting alloys can be classified into high-noble metal alloys, noble metal alloys, and non-noble metal alloys. High-noble metal content generally improves bio-acceptance, but the alloys are softer. From a strength point of view, these are acceptable for a restoration that has lower strength requirements. In some cases, when high occlusal forces occur, or for the support of a long-span FPD, metal components should be selected that make the alloy hard and strong. In summary, the selection of alloy metals should be based on biocompatibility, strength requirements, and the economic considerations of the patient.

Porcelain fused to metal crown (PFM). The PFM innovation comes from a desire to combine strength and aesthetics in one complete crown (Figure 3.8b). A strong metal cope and porcelain veneers are joined together for this purpose. Due to its natural appearance, good wearability, and good resistance to fracture and corrosion, PFM crown is always thought to be a permanent prosthesis.[16]

The fabrication procedure is complex and the success of a PFM crown is determined by numerous factors. Firstly, a thick, homogenous porcelain layer is expected to lower the risk of brittleness failures. Thus, a careful preparation with considerable tooth structure loss is required. Secondly, an opaque metal

cope can seriously decrease the translucency of the restorations, and sometimes its golden color will create a negative visual effect for the final appearance. Another key factor for the restorative success of PFM crowns is the metal-porcelain bond strength. Thermal expansion mismatch, for example, can cause residual stresses to build up between the two materials, which results in partial delamination or fracture of porcelain veneers.

In some cases, this technique cannot be applied. Since relatively significant tooth preparation is necessary to provide enough space for aesthetic porcelain veneers and sufficient retention and resistance, it cannot be used to restore young permanent teeth with a large pulp cavity or teeth that are too small. Moreover, porcelain is a brittle material. PFM crowns cannot be used for patients with a severe, deep overbite or for patients who bite too tightly. In addition, PFM crowns cannot be finished in a single visit, so patients who cannot undergo repeated treatments (based on physical/mental status) should be excluded.

Non-metal full crowns. There are two basic categories of non-metal full crowns: composite resin crowns and all-ceramic crowns (Figure 3.8c). These are good alternatives to metal-based crowns for patients who are allergic to metal or require high aesthetics. For the composite resin crown, the obvious advantages are the low-cost, good aesthetics, and easy fabrication. Aging of resin materials, however, is a serious problem for the durability of resin crowns, so this kind of crown is used only for temporary restorations.

Presently, all-ceramic crowns generate more interest due to their high strength, appropriate hardness, low thermal conductivity, wear-resistance, color stability, and biocompatibility.[17] Numerous ceramic materials are available, but they differ in properties. Examples of ceramics used for reinforcement in dental porcelains are feldspathic, sanidine, leucite, and lithium disilicate, but due to their brittle behavior they cannot withstand large occlusal forces or unsuitable occlusions. The strongest and most popular all-ceramic crowns are made of alumina- or zirconia-based ceramics, nowadays. Conventional tooth preparation for an all-ceramic restoration is relatively extensive so this restoration is not suitable for small teeth, deciduous teeth with a vivid pulp, or young permanent teeth with a severe defect.

3.2.6   Post-and-core

Crowns can't be used in some cases because they are unable to gain enough retention. A typical example of this is where a tooth suffered extensive damage and lost large parts of its hard tooth tissue, sometimes with the defect even extending into the sub-gingival area. Fortunately, a remaining root canal can provide the foundation for a special crown. This technique is called post-and-core.

A post is inserted into the pre-treated root canal for enhanced retention. Core is the superstructure of the root and provides retention and resistance for the artificial crown. Therefore, the final restoration consists of three parts: the

FIGURE 3.9 Restorative treatment of the second mandibular lateral incisor was obtained with a post-and-core crown: (a) Non-vital tooth with excessive tooth defect; (b) Final view of the restored tooth; (c) prepared abutment tooth; and (d) Metal post-and-core inserted and adhered into the root canal.

post, the core, and the crown. Post-and-core are fabricated to fit as a unified arrangement. When first introduced, the crown was also joined with the post-and-core unit and the set-up was called a dowel crown. Richmond crown is one typical example of the dowel crown. It has an artificial crown consisting of a metal base that fits the prepared abutment tooth.[1]

Nowadays, almost all post-and-core and crown units are fabricated separately and referred to as post-and-core crowns (Figure 3.9). This non-integrative restoration has better edge fitness than the integrative dowel crown. It can slightly change the direction of the tooth and help the fitting of a malposition or torsiversion tooth. In addition, the crown that's being fabricated separately can be changed if requirements are altered. This can be done without touching the post-and-core.

Several kinds of post-and-core units are commercially available (Figure 3.10), and are fabricated through different procedures. One process is by metal casting or milling of ceramic blocks, which results in post-and-core assemblies with individual geometries. Liu et al. proposed a novel CAD/CAM fabricated glass fiber post-and-core which has good aesthetics and is strong enough to restore the fractured anterior tooth.[18] Another process uses prefabricated standard posts that are delivered to the dentist, who then builds the individual resin composite core onsite. This technique promises the post-and-core will be constructed chairside and all at once, which reduces the frequency of visits but increases operating
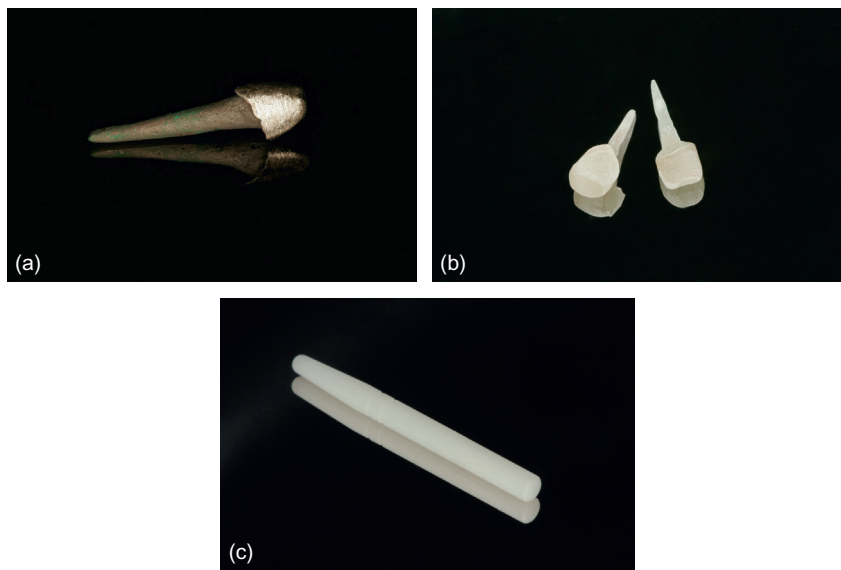
FIGURE 3.10 The three common post-and-core systems fabricated through different procedures: (a) Monoclinic post-and-core made by metal casting; (b) Monoclinic post-and-core made by composite milling; and (c) Prefabricated post on which the dentist will build up a core using composites.

time. The selection of post-and-core materials mainly depends on their characteristics. Meanwhile, the inter-reaction of both post-and-core and crown should be taken into consideration. For instance, if a metal post-and-core is chosen, the crown material should have the ability to mask its metal color and rebuild the natural appearance of the tooth at the same time.[19]

The characteristics of the patient's tooth root canal are the crucial factors for judging the proper use of the post-and-core. In some special situations this application must be prohibited. Contraindications are a too-short root or curved, tiny root canal that will not provide the needed space for the post. In addition, a too-brittle root without strong enough bone support cannot be chosen (e.g. severe bone absorption of greater than 1/3 of the root). Neither patients with a profound bite nor teeth with compact occlusions are suitable for post-and-core technique.[12]

3.3   RESTORATION OF PARTIAL EDENTULISM

Partial edentulism refers to cases where some, but not all teeth are lost, resulting in an incomplete dentition. Similar to G.V. Black's Classification of tooth defects, there is a Kennedy Classification system of partial edentulism originally introduced by Dr. Edward Kennedy in New York in 1923.[20] This classification system has a very close relationship with the prosthodontic design,
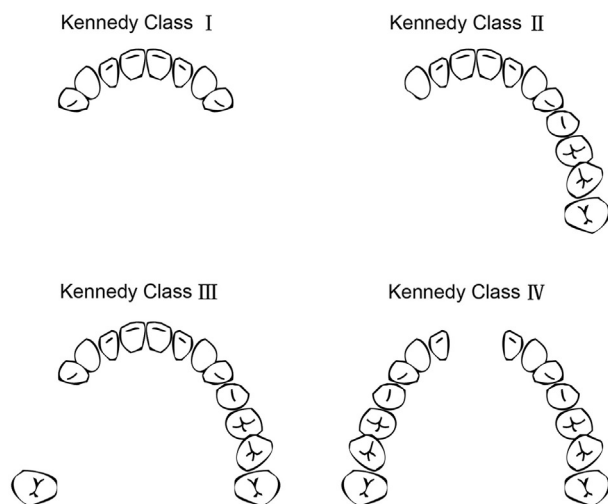
FIGURE 3.11   Diagram illustrating the Kennedy Classification of various defect dentitions.

since partial edentulism has been divided into four basic classes based on the position of the missing teeth. An overview diagram of the Kennedy Classification is shown in Figure 3.11.

Kennedy Classification:

Class I: Bilateral distal edentulous area located posterior to existing teeth.
Class II: Unilateral distal edentulous area located posterior to existing teeth.
Class III: Unilateral edentulous area with remaining teeth located mesial and distal to the edentulous area.
Class IV: Bilateral anterior edentulous area with remaining teeth located distal to the edentulous area (i.e. crossing the midline).

To restore a partial edentulism, either a fixed partial denture or a removable partial denture is commonly used. A bonded bridge is one special application of fixed partial dentures. Precise attachments broaden the indications of removable partial dentures and improve prosthetic effect. But besides these dentures, another solution exists. Implants combined with a superstructure can be used to restore a single missing tooth or several teeth without support from adjacent teeth. (Implants are introduced in the following chapter.)

3.3.1   Fixed Partial Dentures

The fixed partial denture (FPD) is a dental restoration used to replace missing teeth and that is permanently attached to adjacent teeth or dental implants.[21] It is like a 'bridge' fixed on the 'stages.' Here, the adjacent teeth or dental
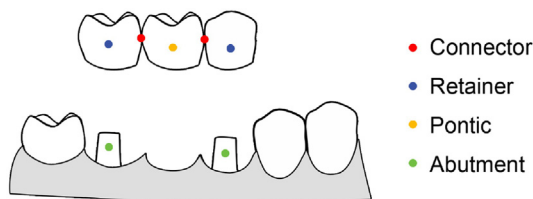
FIGURE 3.12   Diagram showing all components of a three-unit FPD.

implants, called abutments, act as the stages to support the FPD bridge. Three main components are locked together in one FPD unit: pontic, retainer, and connector (Figure 3.12).

A Pontic is the artificial tooth on an FPD that replaces the missing natural tooth and restores its function. [The *retainer* is an important appliance that unites the abutment teeth with the suspended portion of the bridge. Both intracoronal and extracoronal restorations can be used as retainers and are fixed by adhesion. A *connector* is another important appliance that unites the retainer(s) and pontic(s). There are two kinds of connectors, either a rigid (locked) connector or a non-rigid connector (that works like a hinge). When an occlusal force is applied to the pontic, it is delivered to the connector, retainer, and finally to the abutments and the surrounding bone structure by connecting the FPD and abutments together.

The quality of the abutments and surrounding bone play a very important role in the success of the FPD. The general principle is that the rigid support provided by abutments should overcome any stress levels applied on the pontics. In other words, the prerequisite is that there are enough healthy abutments to compensate for the missing tooth/teeth. Based on Robert's Law and Ante's Law, biting forces and the periodontal membrane area must be considered when selecting the abutment tooth.[22] Figure 3.13 illustrates a successful 8-unit FPD of a damaged mandibular dentition.

It's recommended that FPDs always have two rigid ends of abutments. Partial edentulism of Kennedy Classification III and IV are therefore suitable for restoration with FPDs. In some special cases, when replacing only one tooth, a cantilever FPD can be used. A cantilever FPD has the abutment at one end only, with the other end of the pontic remaining unattached. When it is engaged in a bite, the forces generated at the pontic create a large load on the abutment tooth as the pontic acts as a lever. The abutment tooth will be depressed by a force with a strong occlusal vector and must be selected with careful consideration of this extraordinary situation. Thus, the cantilever FPD abutment must have lengthy roots and a favorable root configuration. Long clinical crowns with good crown–root ratios should be used, and require a healthy periodontium. For Kennedy I and II Classifications, where only the second molar is lost, a cantilever FPD can be used for restoration (Figure 3.14).

FIGURE 3.13   Four missing mandibular incisors (a) were restored by FPDs with the first premolars as abutments (a) An 8-unit long span FPD was fabricated; (b) and fixed onto the abutments to establish the comprehensive dentition (c).
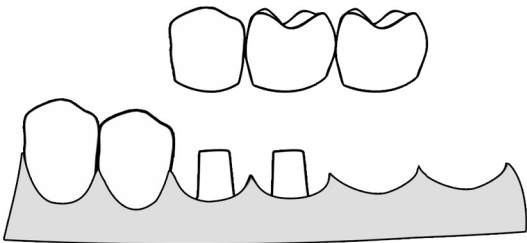

FIGURE 3.14   A missing second mandibular molar was replaced by a cantilever FPD supported by two neighboring abutments, the second premolar and the first molar.

Likewise, a cantilever FPD can be used to restore a lateral incisor with no occlusal contact on the pontic in either centric or lateral excursions. It can also be used to restore a missing first premolar tooth with the cantilever FPD supported by the second premolar/first molar simultaneously.

3.3.2   Bonded Bridges

One drawback of the conventional FPD is that a large amount of tooth tissue from the abutment teeth must be removed to provide the appropriate retention and resistance shape. For example, an approximately 2 mm-thick occlusal space
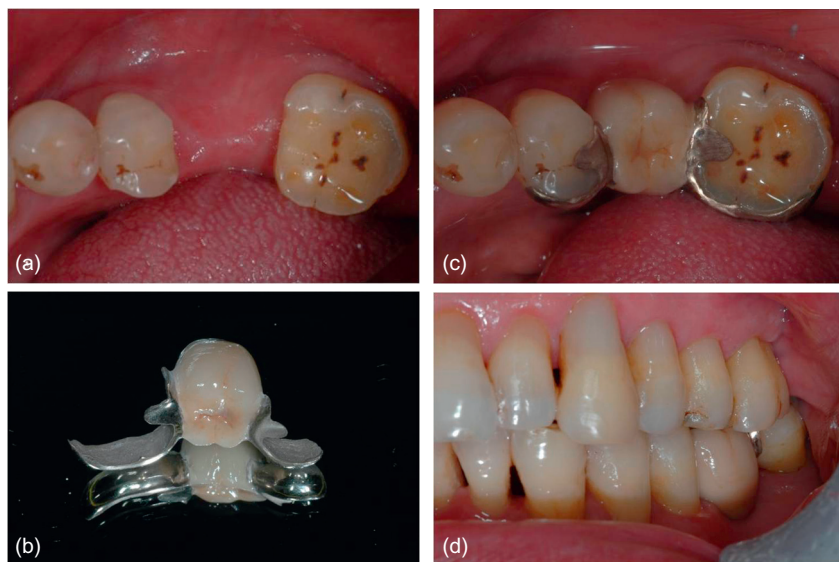
FIGURE 3.15 A missing mandibular first molar (a) was restored by a Maryland Bridge (b). After the bridge was affixed to the prepared second premolar and second molar, the defective dentition was repaired. Figures (c) and (d) show the occlusal and buccal view, respectively.

is needed for posterior abutments. This might not be in consensus with the thoughts of conservative dentistry and might even risk an endodontic-free tooth.

A bonded bridge where much of the tooth reduction is restricted to enamel is a feasible alternative for sparing the tooth structure.[23] The well-known bonded bridge was developed at the University of Maryland. The conventional Maryland Bridge consists of two porous metal wings that adhere to the adjacent abutments (Figure 3.15). Most of the retention/resistance comes from the adhesion to long, well-defined grooves made in the abutments; only minor preparation is required. Furthermore, since the metal wings are located at the lingual side of the abutments, aesthetics are not significantly compromised.

Nowadays, metal wings of the traditional Maryland Bridge are replaced by fiber-reinforced resin composites. All-ceramic bonding bridges have also been applied. Better aesthetics are also obtainable with this novel bonding bridge (Figure 3.16).

Bonded bridges are useful for younger patients because their immature teeth have large pulps. Tilted abutments can be accommodated if the mesio-distal difference in abutment inclination is not too great, and there is enough tooth structure to allow a change in the normal alignment of axial reduction. There can be little or no difference in the inclination of the abutments facio-lingually.[12]

Bonded bridges cannot be used for replacing a missing anterior tooth where there is a deep vertical overlap. Although this type of prosthesis has
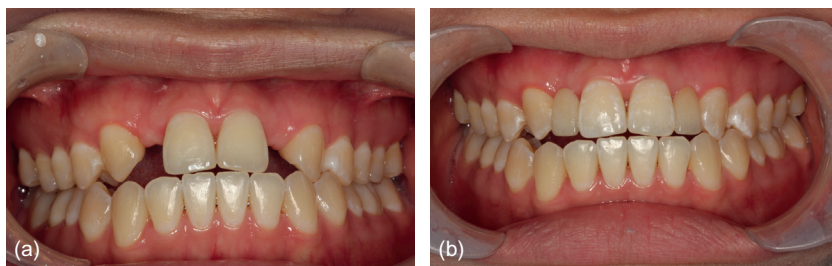
FIGURE 3.16   The missing maxillary lateral incisors (a) were restored by two bonding bridges (b) with little tooth preparation.

been described for periodontal splints, it should be used with extreme care in these situations. Abutment mobility has been shown to be a serious hazard in the successful use of this type of restoration.

3.3.3   Removable Partial Dentures

Removable partial denture (RPDs) as the names suggests, is not fixed permanently in the patient's oral cavity and can be easily removed by the patient. As with FPDs, the RPD can also restore an incomplete dentition, but with broader indications because of not-so-strict prerequisites. Sometimes patients do not like the long FPD preparation time, so an RPD is a good alternative. Besides being an immediate/temporary denture, the RPD also has many other applications, such as for partial edentulous individuals with an absence of alveolar bone, jaw, or soft tissue. In addition, an RPD can be used for occlusal reconstruction, as a removable periodontal splint, as an immediate surgical obturator (cleft of palate obturator), or as a food impaction appliance.

The four basic components involved in an RPD are the artificial teeth, the denture base, retainers, and connectors (Figure 3.17).

Artificial teeth are used to replace missing teeth and restore their function. They are fixed inside the dental base and distribute force from each tooth to the base. Many materials are available for fabrication of artificial teeth (e.g. resin, porcelain, and metal). Resin teeth are widely used due to their strong chemical bonding with the denture base and low weight; they are not too brittle and can be easily adjusted or repaired. For anterior teeth, re-establishing aesthetics is important, so the shape, size, and color of the artificial teeth should be considered carefully. For posterior teeth, the individual matching of occlusal geometry (anatomic teeth) always guarantees effective mastication. Nevertheless, general rules cannot always be applied since artificial teeth with various cuspal inclines (such as 30° and 20°) are sometimes used due to uneven loss of bone tissue or local biting force.[6]

The denture base is a supporting base for artificial teeth; it also connects to other parts. Some of the occlusal force distributed from artificial teeth is

FIGURE 3.17   A mandibular RPD was made to restore a Kennedy II defect dentition.

FIGURE 3.18   A patient suffering from partial edentulism along with periodontal disease was treated using RPDs. The occlusal view of the restored dentitions is displayed in (a) and (b), respectively, and a buccal appearance is shown in (c).

transferred to the edentulous ridge directly through the denture base. Since there is some surface adhesion and friction between the denture base and oral mucosa, this assists the retention and stability of partial dentures. The ideal base is strong enough to avoid fractures and deformation, is easy to repair, and has the proper size and thickness for comfort. So far, the resin base, the metal base, and the metal-resin base can be chosen depending on the individual case, with the latter combining advantages of the former two.

The direct retainer is used to retain and prevent dislodgment. It consists of a clasp assembly or precision attachment that directly attaches to the abutments for retention and stability. Connectors are fixed onto the denture base and conduct the partial occlusal force to the abutments and oral mucosa. There are two kinds of connectors, major and minor connectors. The major connector connects the components on one side of the arch to the components on the other side. It should be strong enough to provide support and distribute the force without fracture or deformation displacement; therefore, it is very rigid. The major connector includes the palatal/lingual bar/plate and the buccal (labial) bar and will not irritate the tongue or trap food particles. Minor connectors are any components that serve as stress distributors or connecting links between the major connector and other components of the prosthesis. They include clasp assembly, indirect retainers, occlusal rests, or cingulum rests. The dentist must be careful when using these connectors so as to prevent the formation of secondary caries beneath the clasps.[24] A case restored by RPDs is shown in Figure 3.18.

3.3.4   Precise Attachment Dentures

A precision attachment denture is a kind of RPD that contains precision attachment(s) to lock the denture onto the natural teeth. Precision attachment dentures are made up of two components. The 'male' part is fixed to the natural teeth and the corresponding 'female' section is incorporated into the denture. The female and male pieces lock together to yield a very stable prosthesis that gives the patient maximum comfort and ease of use. These locking effects hold the denture securely in place and give the patient confidence to socialize and smile.[25] Commonly used precise attachments include keyway attachments, bar attachments, stud-snap attachments, ball-socket attachments, and magnetic attachments. In the magnetic attachment, for example (Figure 3.19), the magnets are placed in the denture. When paired with a magnetizable alloy keeper on the abutment roots, a closed field magnetic retention is generated.[26] The amount of retention can be adjusted to suit the patient's needs, and this magnetic attachment denture can be inserted and removed by the patient.

3.4   RESTORATION OF COMPLETE EDENTULISM

When all the teeth in the oral cavity are lost, it is called complete edentulism.[7] The patient will look old, suffer from dysphonia, and the masticatory function will be lost completely. All potentially harmful effects will influence the patient's general health. Although oral health has improved during recent years, complete edentulism is still prevalent in elderly populations. For restoration of a totally edentulous jaw, *complete dentures* are necessary (Figure 3.20). If only one jaw suffers, a *single complete denture* should be used opposite the natural dentition which possibly combined with partial dentures. Any
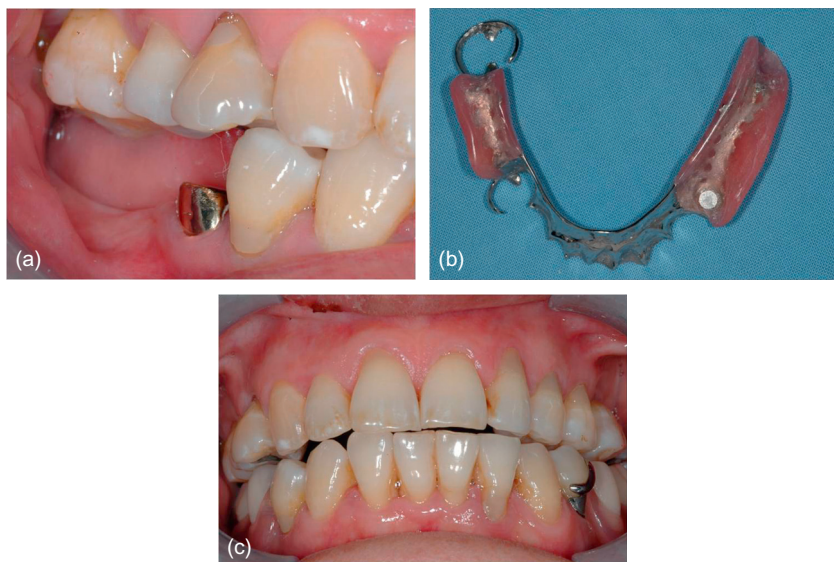
FIGURE 3.19 A Kennedy class II defect dentine was restored by a magnetic attachment-supported RPD.

FIGURE 3.20 Complete edentulism is shown in (a) and (b). By applying complete dentures for both jaws, oral functions was re-established (c).
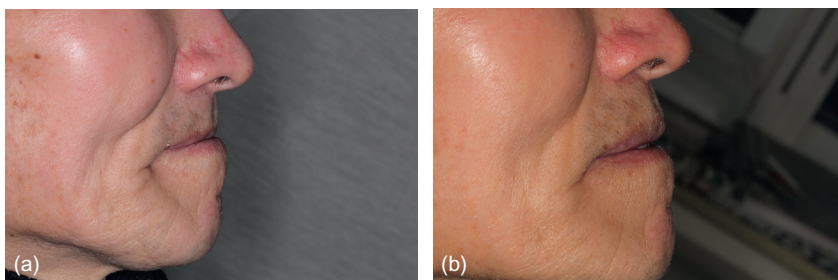
FIGURE 3.21   Side facial pictures show the change of the edentulous patient (a) before and (b) after prosthetic treatment.

dental implants or natural roots existing in the jaw can be applied to enhance retention. These are called ***overdentures***. After restoration an obvious change in the patient's appearance and an improvement of oral functions will take place, as illustrated in Figure 3.21.

3.4.1   Complete Dentures

Complete dentures consist of two main parts, namely the artificial teeth and the denture base. As described previously, an artificial tooth is used to restore the appearance of the natural tooth, its occlusion, oral function, and to assist in word pronunciation. The dental base is the foundation of the artificial tooth and can be used to restore the defective soft and hard tissues. Biting force is distributed from the artificial tooth through the denture base to the oral mucosa and bone tissues. Since tooth support cannot be obtained, the denture base of complete dentures covers a larger area of oral mucosa than that of RPDs complete dentures can fulfill all of these functions. Unlike RPD's, with complete dentures connectors are not used as there is no need for space to install a major connector onto the complete denture, and minor connectors cannot be used since no healthy abutment is available.

Retention of a complete denture benefits from both sub-pressure and adherence to the underlying tissue.[12] Sub-pressure will occur between the denture base and oral mucosa if they are attached close to each other and a good peripheral seal is applied. A peripheral seal is the tight contact formed by the marginal surface of the denture with the oral mucosa. The posterior edge of the upper denture (postdam area) is of vital importance during speech. The atmospheric pressure outside the dental base presses it firmly onto the oral mucosa. Good adsorption is mainly ascribed to a thin sticky layer of saliva between the dental base and oral mucosa that contributes greatly to retention. Thus, the large dental base area is important to guarantee retention of the complete dentures. Of course, it should not disturb normal oral function or reduce comfort.
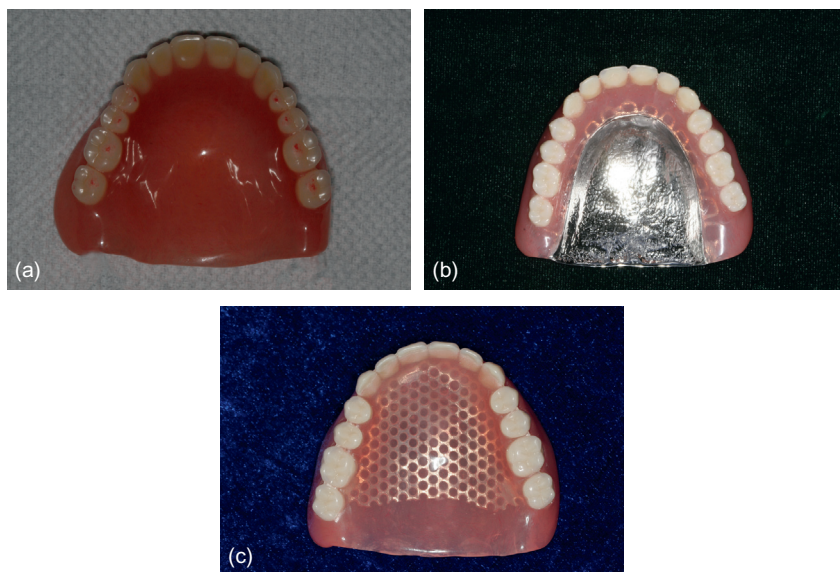
FIGURE 3.22   Three common denture bases are made from different materials for different purposes: (a) Resin base; (b) Metal base; and (c) Metal mesh embedded resin base.

When the prosthetic plan is made, the effects of oral hard and soft tissues on necessary retention should be considered carefully. If there is large tuberosity, sharp bone apexes, or hyperplastic oral mucosa, the denture cannot remain stable. Sometimes a special oral operation is needed to resolve these problems before prosthetic treatment, as retention of complete dentures would otherwise be dramatically decreased. If the jaw bone, especially the residual alveolar ridge, has been seriously absorbed and becomes narrow and flat, or if the oral mucosa has lost its initial elasticity and thickness, retention is dramatically decreased. In these cases, additional affiliations, like implants, may become necessary.

The stability and longevity of complete dentures are crucial. Commonly used complete dentures are made from composite resins (Figure 3.22a). The obvious advantages of these kinds of materials are that they are low-cost, easy to fabricate, and repair. However, low strength and poor aging properties always reduce the longevity of complete dentures made of resins. Alternatives with improved properties can be found among metal materials, especially pure titanium or titanium alloy denture bases (Figure 3.22b). Compared to conventional composites, titanium-based denture bases are not as popular. This is mainly due to high price, the complex process of installation, and difficulties with repair. A dental base made from a composite resin strengthened by prefabricated metal meshes or metal wires embedded inside the resin as reinforcement is a good compromise (Figure 3.22c).

FIGURE 3.23   An overdenture was used to restore a mandibular partial edentulism with three seriously defective but stable teeth. Pictures from before and after treatment are shown in (a) and (b). First the defected crowns of three teeth were removed (c) and two metal caps were fixed on the root surfaces of the canines (d). An overdenture, which contains the corresponding magnetic appliances, was then fabricated (e and f).

Abrasions of artificial teeth occur and the alveolar ridge will change over time. Therefore, regular re-examination is very important for edentulous patients. Complete dentures should be adjusted to fit any new oral settings and to keep them in good condition with continued good oral functions.

3.4.2   Overdentures

Conventional overdentures are complete or partial removable dentures supported by retained roots. Precise attachments can be fixed on the roots and provide more support and stability.[26] This precise attachment-supported

overdenture can also increase the tactile and proprioceptive feeling and reduce ridge resorption (Figure 3.23).

There are two important prerequisites for overdentures. One of these is good oral hygiene. The root surface of the overdenture is directly exposed in the oral environment and is prone to suffer from caries and periodontal disease. Poor oral hygiene is thus harmful for the health of the natural roots. The second requirement is that every natural root left in the oral cavity should accept the complete RCT. An open root canal provides a way for bacteria and other deleterious matters to pass. If these factors are not considered in advance, the success of prosthetic treatment with overdentures will be compromised.[12]

ACKNOWLEDGMENTS

REFERENCES

1. The glossary of prosthodontic terms. J Prosthet Dent 2005;94(1):10–92.
2. Yatani H. 8020 and prosthetic treatments: a review of literature. J Jpn Prosthodont Soc 2005;49:190–8.
3. Black GV. A work on operative dentistry: the technical procedures in filling teeth. Chicago: Medico-Dental Publishing; 1917.
4. O'Brien WJ. Dental materials and their selection. Chicago: Quintessence Publishing Co, Inc; 2002. p. 175–91.
5. García AH, Lozano MAM, Vila JC, et al. Composite resins. A review of the materials and clinical indications. Med Oral Patol Oral Cir Bucal 2006;11(2):E215–20.
6. Thompson MC, Thompson KM, Swain M. The all-ceramic, inlay supported fixed partial denture. Part 1. Ceramic inlay preparation design: a literature review. Aust Dent J 2010;55(2):120–7. quiz 231.
7. Bernard T, Paul M, Dan N. Chapter 3 Ceramic laminate veneers. Esthetic dentistry and ceramic restorations. London: Martin Dunitz Ltd; 1999. p. 262–6.
8. Bergman MA. The clinical performance of ceramic inlays: a review. Aust Dent J 1999;44(3):157–68.
9. Smales RJ, Etemadi S. Survival of ceramic onlays placed with and without metal reinforcement. J Prosthet Dent 2004;91(6):548–53.
10. Peumans M, Van Meerbeek B, Lambrechts P, et al. Porcelain veneers: a review of the literature. J Dent 2000;28(3):163–77.
11. Peumans M, De Munck J, Fieuws S, et al. A prospective ten-year clinical trial of porcelain veneers. J Adhes Dent 2004;6(1):65–76.
12. Feng HL, Xu J. Prosthodontics. Beijing: Peking University Medical Press; 2005.
13. Shillingburg HT, Hobo S, Whitsett LD, et al. Chapter 6 Treatment planning for single-tooth restorations. Fundamentals of fixed prosthodontics. Chicago: Quintessence Publishing CO; 1997. p. 73–83.

14. Krifka S, Anthofer T, Fritzsch M, et al. Ceramic inlays and partial ceramic crowns: influence of remaining cusp wall thickness on the marginal integrity and enamel crack formation in vitro. Oper Dent 2009;34(1):32–42.

15. O'Brien WI. Chicago: Quintessence Publishing Co, Inc.; 2002.

16. Weinstein M, Katz S, Weinstein AB. Permanent manufacturing corporation, assignee. Fused porcelain-to-metal teeth. U.S. Patnet No. 3,052,982,1962.

17. Rosenblum MA, Schulman A. A review of all-ceramic restorations. J Am Dent Assoc 1997;128(3):297–307.

18. Liu P, Deng XL, Wang XZ. Use of a CAD/CAM-fabricated glass fiber post and core to restore fractured anterior teeth: a clinical report. J Prosthet Dent 2010;103(6):330–3.

19. Ge J, Wang XZ, Feng HL. Influence of different post core materials on the color of empress 2 full ceramic crowns. Chin Med J (Engl) 2006;119(20):1715–20.

20. Cummer WE. Possible combinations of teeth present and missing in partial restorations. Oral Health 1920;10:421–30.

21. Shillingburg HT, Hobo S, Whitsett LD, et al. Chapter 7 Treatment planning for the replacement of missing teeth. Fundamentals of fixed prosthodontics. Chicago: Quintessence Publishing Co; 1997. p. 84–103.

22. Rosenstiel SF, Land MF, Fujimoto J. Section 1 planning and preparation. Contemporary fixed prosthodontics. St. Louis: Mosby, Inc.; 2002. p. 65–74.

23. Saunders WP. Resin bonded bridgework: a review. J Dent 1989;17(6):255–65.

24. Stratton RJ, Wiebelt FJ. An atlas of removable partial denture design: Quintessence Publishing Company; 1988.

25. Preiskel HW, Preiskel A. Precision attachments for the 21st century. Dent Update 2009;36(4):221–4. 6–7.

26. Preiskel HW. Overdentures made easy: a guide to implant and root supported prostheses: Quintessence; 1996.

Dental Implants

Belinda Reinhardt and Thomas Beikler

Department of Operative and Preventive Dentistry and Periodontics, Heinrich-Heine-Universität Düsseldorf, Düsseldorf, Germany

Contents

4.1   PRINCIPLE STRUCTURE OF DENTAL IMPLANTS

A dental implant is an artificial tooth that is inserted into the jawbone of the patient (Figure 4.1). This synthetic pier anchors dentures and orthodontic appliances, performing the function of the natural tooth root. Implants are screwed or simply plugged into the jawbone. Within three to six month they combine with the surrounding bone to form a solid, load-bearing, ultimate support unit. The bone range is one of the most important requirements for the success of implant insertion. Furthermore, all implants must possess a certification from the health authorities as safe medical devices (CE- or FDA-approved).

A successful implantation is characterized by a clinical, solid, pain- and inflammation-free implant without any signs of peri-implant osteolysis. The most frequently used criteria for determining success at the implant level are mobility, pain, radiolucency, and peri-implant bone loss (>1.5 mm); those for peri-implants at the soft-tissue level are suppuration, bleeding, and probing
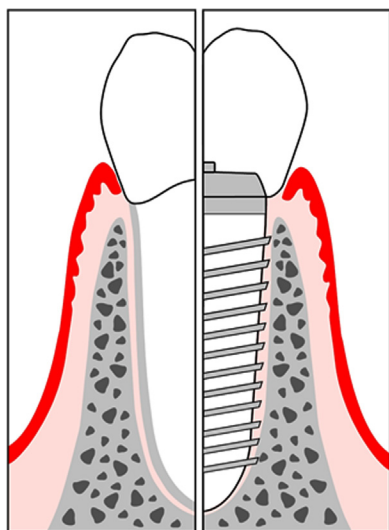
FIGURE 4.1   Dental implant.

pocket depth. The criteria used to assess success at the prosthetic level are the occurrence of technical complications/prosthetic maintenance, adequate function, and aesthetics over a five-year period. The criteria reported to assess patient satisfaction levels are discomfort, satisfaction with appearance, and the ability to function and chew.[1] However, a clear definition of implant success and implant failure is still missing, thus hampering the development of a causal treatment strategy.

4.1.1 Classification of Implantation and Loading Mode

Implants can be divided into monophasic or biphasic healing implants. Monophasic healing implants are immediately fitted with a prosthesis and burdened after insertion and care of the mucous wound. As a consequence of this insertion technique the implants heal transmucosally. Very important is a primary blocking of the inserted implants through a suprastructure. A precondition for this type of implant is that the patient has a qualitatively and quantitatively sufficient bone supply, so that primary stability is guaranteed.[2]

For biphasic healing implants, a second exposure to surgery is necessary. The advantage of this is that the implant can heal unstressed, which reduces the risk of postoperative complications. For the upper jaw the healing period takes an average of five to six months and for the lower jaw three to four months. After the healing period, the implants can be loaded.[2]

4.1.2 Classification by Time of Implantation After Tooth Loss

There are three different time periods when implants can be fitted: immediate implantation, delayed immediate implantation, and late implantation.[2] Immediate implantations can be conducted up to seven days after tooth extraction by inserting the implant into the extraction socket. The major disadvantage with this technique is that the implant may not always be covered by mucosa, increasing the risk of infection. One advantage of this system is the trans-alveolar implant insertion, which eliminates the need for incision, flap preparation, and suturing; and can also prevent alveolar bone atrophy.

The delayed immediate implantation involves the insertion of the implant six to eight weeks after tooth extraction. In this time, the alveolar bone is not fully regenerated, but the mucosal wound is completely closed. This allows for mucosal coverage and a clean wound, greatly reducing the risk of infection.

The late implantation takes place at least 3 to 4 months after extraction, allowing full regeneration of the alveolar bone and complete healing of the mucosal wound. One downside of this process, is that the long healing period can cause the alveolar bone to atrophy. On the plus side, insertion of the implant can be accomplished without having to orient onto the extraction socket and a mucosal coverage of the implant is possible.

4.1.3   Indications

Today, nearly all patients can be treated with implants. There exist, however, some health alterations and conditions that might increase the risk of implant failure.[3] Irrespective of any implant endangering systemic and local conditions, infection control is the most important issue in preventing serious complications (peri-implantitis) which can lead to bone and or/implant loss, thus stressing not only the meticulous planning of dental implant treatment but also the importance of implant maintenance. If the surrounding bone support is limited, additional surgical interventions may be needed to allow dental implants to be inserted.

Generally, patients with the following indications are most suitable for implants:

- Patients where the functionality of the dentition cannot be restored with conventional restorative means (i.e. extreme atrophy of the jaw, bone defects due to congenital or accidental aspects, or after tumor resection).
- Patients who have a functional advantage and/or less damage of remaining dental hard tissue compared to conventional treatment (i.e. edentulous jaws, single tooth replacement with a fixed partial denture, or orthodontic treatment).
- Patients who have had comparable functional results with a conventional replacement. Also, local and subjective findings can lead to the insertion of an implant.

4.1.4   Indication Limitation

The implant outcome can be influenced by systemic and local factors. Those factors do not exclude an implant placement *a priori*, but require certain preparatory actions. Poor patient compliance or inadequate oral hygiene is a limitation to insertion of an implant directly. An implant has to be cleaned even more thoroughly than the natural tooth. Since there is a direct connection from the oral cavity to the gap between the implant and bone, infection risk (peri-implantitis) is higher. Therefore, oral hygiene instructions are necessary and the clinician should only insert the implant when he is sure the patient has an appropriate oral hygiene regimen and will be compliant with a strict recall program.

Another potential limitation is an insufficient bone supply. In the case of an otherwise healthy patient this is, however, not considered to be a strict contraindication anymore because of the availability of safe and predictive bone regeneration, sinus lift, and bone augmentation strategies. As with any surgical operation there is a potential risk of injuring important anatomical structures like the N. alveolaris inferior or A. palatina. To reduce this hazard a suitable pre-surgical planning and implantation technique is assumed. The surgeon is committed to inform the patient about possible intra- or post-operative complications before surgery. The informed consent should take place at least one day before surgery, so that the patient has the chance to consider the risks before he opts for surgery.

Specific diseases of the bone, oral mucosa, or periodontal tissues can interfere with healing and the outcome of dental implant placement. The treatment of these diseases and/or conditions prior to implant placement is mandatory to allow uneventful healing and long-term success. Many people suffer from bruxism or other adverse occlusal disorders. This can limit the success of an implant because of the weight the teeth and the newly inserted implant must endure. Bruxism can induce complications during the healing period of the implant, therefore splint therapy might be needed. Other systemic problems like xerostomia and macroglossia can also be a limitation. Exogenous factors like smoking or alcohol dependence affect the short- and long-term outcome of implant therapy and need to be controlled prior to implant placement.

4.1.5   Contraindications

Even today there are still some medical or local conditions that, at least temporarily, do not allow implant placement. Patients who have undergone chemotherapy not only have a compromised immune system, but also a limited capacity to heal. Such patients would have to wait several months, at least, before having an implant. Patients who take bisphosphonates need to be carefully evaluated prior to implant insertion. After surgical treatment there is a high risk that bone will degenerate in the surrounding area. Additionally, one cannot estimate how long it takes until these drugs lose their effect once they have left deposits in the bone. Similar to tetracycline, bisphosphonates attach themselves to bone where they can remain for 5 to 10 years.

Other intraoral contraindications:

- Unfavorable jaw condition.
- Radiotherapy.
- State before or after tumor resection.

  General medical contraindications:

- Decompensated or strongly pronounced metabolism; heart and circulation; liver; kidney; lung; bone; or connective tissue diseases.
- Impaired immune and hematological system.

  Other contraindications:

- Mental contraindications like neuroses or psychoses.
- Incomplete jaw growth.
- Not satisfying aesthetic demands of the patient.

4.1.6   Advantages of Implants

In comparison to conventional restoration therapy with crowns or bridges, implants have some considerable advantages:

- Mastication and aesthetics as the own teeth (fixed dentures).
- Safe and fixed denture retention.

- Preservation of bone.
- In case of single-tooth gaps, adjacent teeth do not need to be harmed by additional preparation to anchor fixed dental prostheses (FDP).
- Good to very good prognosis.
- Long durability.

4.1.7   Disadvantages of Implants

An appreciable disadvantage of implants is the need for surgery to insert the implant into the jawbone. This includes anesthesia, incision, implant bed preparation, and suturing. This treatment can be followed by intra- or post-surgical complications as listed below. In biphasic healing implants there is also the need for a second operation.

4.1.8   Implant Materials: Titanium vs. Zirconia

Most implants today are made of titanium or zirconium. Because of their good mechanical and biological properties they are particularly suitable for the replacement of natural teeth. Both are chemical elements that are transformed through chemical reactions into biocompatible materials that can be inserted into the jawbone.

Titanium is a so-called transition metal and in the same group of the periodic table as chrome, nickel, and cobalt. Titanium atoms are arranged in a metal lattice that is characterized by the presence of free electrons and a certain 'mobility' at the atomic level. That is where titanium gets its typical metallic properties, such as electric and thermal conductivity, metallic luster, and elasticity.[4] It also has superior corrosion resistance, due to the characteristic oxide layer that is built by dense oxides on its surface. This is the reason for the high biocompatibility of titanium. However, accumulation of titanium in the inner organs and lymph nodes after implantation has been reported. Galvanic side effects after contact with saliva and fluoride have also been described. Although allergic reactions to titanium are rare, cellular sensitization has been demonstrated.[5] Furthermore, titanium has several other drawbacks that may compromise the long-term success of endosseous implants. These inherent weaknesses include an unnatural grayish color and the possible accumulation of titanium particles in adjacent tissues. The unnatural dark, grayish color can compromise implant aesthetics, especially in cases of visible titanium or thin overlying of soft tissue.[6]

For dental use, ceramic is used in a modified molecular form. The zirconium dioxide (zirconia) ceramic is made from the mineral zircon, a silicate with the chemical formula $ZrSiO_4$. In this form it loses its initial metallic properties because it is not arranged in a metal lattice anymore but is embedded into a very stable and inert inorganic nonmetallic crystal lattice.[4] Zirconia is a bioinert and nonresorbable metal oxide that offers mechanical properties that

FIGURE 4.2   Zirconia dental implant (ZV3 Implantat).

are superior to other ceramic biomaterials (e.g. high fracture toughness and bending strength).[7] It is a polymorphic crystal that can be found in three crystallographic forms: monoclinic (M), cubic (C), and tetragonal (T). Zirconium is monoclinic at room temperature, being stable up to 1170°C. Above this temperature it becomes tetragonal, and over 2370°C it passes into the cubic phase, where it is stable until it reaches its melting point at 2380°C. During cooling, a T–M transformation takes place in a temperature range about 100°C below 1070°C. This transformation phase is associated with a volume expansion of about 3–4%. The stress generated in the expansion causes microfractures that after sinterization (between 1500–1700°C) may result in disintegration of the material at room temperature. The attraction of stabilizing doping agents like CaO, MgO, CeO, and Y_2O_3 to pure zirconia allows the production of multiphase materials known as partially stabilized zirconia (PSZ). PSZ's monostructure consists at room temperature of a cubic zirconia matrix with minor tetragonal and monoclinic zirconia precipitates. Garvie et al. described in 1975 the optimization of the phase transformation in PSZ, thus improving zirconia's mechanical strength and toughness. They observed that tetragonal metastable precipitates that are finely dispersed within the cubic matrix are transformed into the monoclinic phase when the constraint exerted on them by the matrix was relieved, thus causing a reduced risk for fractures.[8] This optimization made zirconia a very interesting material for dental implants. Figure 4.2 shows a dental implant made of zirconia ceramics. For more detailed information about zirconia, readers are encouraged to read Chapter 11.

4.1.9 History of Ceramic Implants

Zirconium (Zr) was originally discovered by the chemist Martin Heinrich Klaproth in Berlin (Germany) in 1789, as an end product of a gem-heating reaction. It was isolated in 1824 by the Swedish chemist Jöns Jacob Berzelius. The major end-uses of $ZrSiO_4$ are refractories, foundry sands, and ceramic opacification.[9] The first reference concerning the application of zirconia in medicine appeared in the late sixties with Helmer and Driskell's (1969) work. This was followed 20 years later by the first publication referring to its use in orthopedic surgery, particularly in total hip replacements to solve the problem of alumina brittleness and potential implant failures.

In the 1970s, the first ceramic implants had been performed in the United States and Germany, initially as medical joint substitutes. For dental endosseous implantation, the Tübingen implant, made from Al_2O_3, was introduced in 1974. Frequent fracture incidences, however, led to the substitution of this material by titanium; this was despite excellent biocompatibility and plaque adhesion properties. The introduction of zirconia decreased the fracture rates of ceramic materials and therefore made it a good alternative to titanium.[10]

From 1998 until 2000, Dr. Ulrich Volz, a dentist, developed the first licensed and certificated metal-free ceramic implant system (Z-system) made of zirconium oxide. The third generation of Z-system has been in use since 2001.

The first ceramic abutments were CerAdapt™ (Nobel Biocare, Göteborg, Sweden) made of alumina and designed to fit the extern hexagonal Branemark implant type. In 1995, Andersson et al. evaluated the short- and long-term clinical function of CerAdapt abutments. In all cases the peri-implant mucosa was stable. Nevertheless, there was a higher loss of marginal bone around the titanium abutments than around the ceramic ones. In five years there was a cumulative success rate of 97.2%.[8]

4.1.10 Properties of Ceramics

Zirconia's impressive physical, mechanical, and chemical properties make it a material of interest for dental and orthopedic surgery. These abilities include:[6,9,10]

- High biocompatibility.
- Great flexural strength (900–1200 MPa).
- Hardness (1200 Vickers).
- High modulus of elasticity.
- High fracture resistance.
- Lower bacterial adhesion than titanium.
- Minimal reaction with adjacent living tissue.
- Very low thermal and electrical conductivity.
- Chemical inertness.

FIGURE 4.3   ZV3 Implanate.

FIGURE 4.4   ZV3 Implanate.

- Minimal biodegradation.
- Ability to transmit light.
- No allergic abilities.

4.1.11   Advantages of Ceramic Implants

Compared to titanium, zirconia has a lot of advantages that make it suitable for use in dental implants due to its attractive material properties and excellent aesthetic characteristics. A very important difference between the two elements is the less mucosal discoloration of zirconia. It has the ability to transmit light, which gives the material a more natural aesthetic appearance (see Figures 4.3 and 4.4). This is very important in cases of visible implant segments or thin overlying soft tissue. It also has a lower rate of adhesion of bacteria and a lower plaque affinity.[11] Due to those abilities and its smooth surface, fewer inflammatory infiltrates are found in soft tissue around zirconia, compared to titanium implants and only minimal ion release is detected. Additionally, zirconia is impressive because of its minimal cytotoxicity, optimal tissue compatibility, and sufficient mucosal attachment.[12] It also has high corrosion stability. As such, the material is considered to be highly biocompatible, which contributes to the absence of incompatibilities or allergies.

A new type of ceramic material based on zirconium dioxide, yttria-stabilized tetragonal zirconia polycrystal (Y-TZP), has a unique ability to resist crack propagation by being able to transform from one crystalline phase to another; the resultant volume increase stops cracks and prevents them from propagating. This material has the potential to be used for larger restorations in the molar area.[13]

Since ceramic implants are mostly made of one piece, no gaps between abutment and implant are found. One-piece zirconia dental implants also demonstrate good stability in vitro and in vivo.[14] In multi-piece systems, new studies demonstrate smaller microgaps between implant and ceramic abutment compared to those described in the literature for titanium abutments. The precise fit of these abutments could lead to better biologic and biomechanical behavior.[15]

Another study indicates that zirconia implants generated the lowest stresses in cortical bone, and the zirconia abutment resulted in lower vM and compressive stresses than titanium abutments in implants and cortical bone.[16]

Due to the biocompatible characteristics of the material, the aesthetic aspects like tooth color, the good scientific results in the comparable osseointegration to titanium implants, and its ability to be machined, zirconia is a good alternative to the conventionally used titanium.[14]

4.1.12   Disadvantages of Ceramic Implants

The most important disadvantage in ceramic implant use is that there exists only a limited number of long-term studies on the outcome of dental implant therapy using zirconia implants. This hampers any definite conclusions regarding its long-term success (greater than 10 years) in dental implantology.[14]

Older ceramics such as alumina do not withstand tensile forces as well as metals and are susceptible to brittle fractures; the connector area is especially prone to fracture.[13] That is why the use of newer ceramic materials such as zirconia is required. The costs of ceramic implants are expected to be higher than for conventional metal-based implants but this is likely to change with increased usage and production.

4.2   IMPLANTS

4.2.1   Implant Types

There are different types of implant that can be used in dental treatments, however, only the enossal implants are in use today because of the increased risk for infections seen in other implant types. Submucous implants lay epiperiostal in specially prepared mucosal pockets, and were formally used to stabilize the position of total dentures, although they are no longer in use. Subperiostal implants were anchored directly onto the bone in a large area lying beneath the oral mucosa. They were used in cases where there was a high risk of bone

loss where the jawbone was too shallow for cylindrical or extension implants. The simple superposition of the flat implant under the periosteum often led to widespread inflammation, sometimes with severe bone loss due to the lack of protection against infection by a high bacteria density. Another type of implant is the extension implant. These are flat, leaf-shaped implants which are inserted along the curve of the jaw into a 1 mm wide prepared slot with a length of 4–14 mm. The indication of this implant was to protect the mandibular nerve. Disc implants were inserted laterally into the jaw. A stop is achieved in the hard and well-vascularized outer wall. Because of their special form they can also provide stable healing in cases of low bone height and advanced bone loss. The most popular type of implant in use today is the enossal implant. It is screwed directly into the jawbone and anchors dental restorations.

4.2.2   Implant Forms

The three-dimensional structure of the implant, with all the elements and characteristics that compose it, is referred to as the implant design. The type of prosthetic interface, the presence or absence of threads, additional macro-irregularities, and the shape/outline of the implant are considered some of the most important aspects of implant design.

Dental implants can be categorized into threaded and non-threaded, cylindric, or press-fit designs. Implant companies have been using a plethora of additional features to accentuate or replace the effect of threads including vents, grooves, flutes, indentations, and perforations of various shapes. Implants can be hollow or solid, with a parallel, tapered/conical, or stepped shape/outline, and a flat, round, or pointed apical end.

The most important implant forms are cylindrical or conical. Cylindrical implants have the same diameter in the upper and lower section of the implant. Conical implants have a different diameter in the various sections of the implant. The diameter decreases from the upper to the lower section and therefore imitates the shape of a tooth root. Both implant forms are usually produced as screw implants.[2]

4.2.3   One-piece and Multi-part Systems

Today, multi-piece implant systems are mainly madeup of two parts. There used to be a neck piece located separately in the oral mucosa, but since more pieces produce more gaps and more gaps increase the risk of bacterial accumulation and therefore the risk of wound infection, this construction is no longer used. Today's two-piece implant systems consist of a bone-anchored body part and a headpiece that accommodates the superstructure. These parts of the implant are mostly screwed together. The superstructures (crowns, bridges, or prostheses) are screwed, cemented, or bonded onto the implant

system. Two-part systems have the advantage that they are not prone to stress during the healing period.

One-piece dental implants are, as the name implies, manufactured from one piece. After insertion, the head of the implant is not covered from the oral mucosa and pokes into the oral cavity. It heals non-submerged. In non-submerged healing, a precondition for adequate bone formation at the implant surface is a close adaption of the soft tissue around the implant neck.[17]

Zirconia implants are mostly one-piece implant systems because fine-scale structures are more difficult to manufacture. The advantages of single-piece zirconia implants are that there is no need for a second exposing surgery, there is no gap (as seen in multi-piece implant systems), and late complications such as the loosening or breaking of the connecting screw between implant and abutment (also seen in multi-piece systems) is out of the question.

4.2.4 Survival Rates

As mentioned previously, there are few evaluations of the long-term success of ceramic implants. Still, the short-term results (up to five years) from various studies are promising. Several studies have demonstrated that truly anatomic, root-analog zirconia implants showed no complications during the healing period. After one year of insertion, one study demonstrated a 95.4% survival rate with almost no loss of attachment and no significant difference in parameter bleeding (Table 4.1). Also, a good functional and aesthetic result was achieved with minimal bone resorption and soft tissue recession after 30 months.[18] Another 3-year follow-up study supported this outcome by presenting good stability of soft tissues and bone level.[19]

However, conflicting observations have also been published. In one study the clinical and radiographic outcome of a one-piece zirconia oral implant after one year was assessed.[20] The cumulative survival rate of the studied ceramic implant was comparable to the reported survival rate of titanium implants. However, the frequency of increased radiographic bone loss (>2 mm) after one year was considerably higher compared to conventional two-piece titanium implants.[18] Since there was no control group to compare titanium with zirconia in the study, the evaluation was in conclusive.

4.3 ABUTMENTS

An abutment is a component that anchors superstructures to an implant. It supports and provides retention for a fixed or removable dental prosthesis. Since the abutment is the connecting link between implant and superstructure, it has to able to withstand great force. Therefore, the strength values of the abutments have to be superior to the registered maximum values for the anterior sector that can fluctuate between 90–370 N.[8]

TABLE 4.1 Peri-implant Soft Tissue Conditions at Crown Insertion and 1-year Follow-up[20]

Parameters				
Bleeding				
Prosthesis insertion	Mean (SD)	0.36 (0.50)	0.23 (0.36)	p = 0.196
	n	63	114	
1-year follow-up	Mean (SD)	0.23 (0.32)	0.20 (0.24)	p = 0.866
	n	62	111	
Significance test		p = 0.626	p = 0.902	
Plaque				
Prosthesis insertion	Mean (SD)	0.26 (0.35)	0.43 (0.48)	p = 0.022
	n	63	114	
1-year follow-up	Mean (SD)	0.11 (0.23)	0.30 (0.40)	p = 0.001
	n	62	111	
Significance test		p = 0.012	p = 0.013	
Probing depth		**Implants**	**Ref. teeth**	**Significance test***
Prosthesis insertion	Mean (SD)	2.75 (0.75)	2.07 (0.57)	p < 0.001
	n	63	113	
1-year follow-up	Mean (SD)	2.34 (0.66)	1.94 (0.49)	p < 0.001
	n	62	111	
Significance test		p<0.001	p = 0.014	
CAL				
Prosthesis insertion	Mean (SD)	2.84 (1.19)	2.40 (0.99)	p = 0.009
	n	63	112	
1-year follow-up	Mean (SD)	2.71 (0.75)	2.45 (0.72)	p = 0.020
	n	62	111	
Significance test		p = 0.271	p = 0.436	

The abutment can be made from many different materials, such as alumina, titanium, or zirconia. For this reason, the question arises: Which material is the best for the patient? The most important considerations are fracture resistance, strength value, and aesthetic aspects.

In 2003, Yildrim et al. studied the fracture resistance of different abutment materials when subjected to statistic loads. The values obtained for zirconia abutments were more than twice those for alumina. Still, both materials revealed an ability to bear incisal forces, documented in the literature. Zirconia abutments even registered strength values at least 15% higher than anterior bite force. It was also checked that the abutment preparation did not adversely affect their resistance to fracture. The flexion strength of zirconia abutments

is greater or similar to those of titanium. If there is failure, the majority of the studies indicate that the ceramic abutment failure is more frequent in the cervical region, very close to the interface implant/abutment.[8]

In patients with thin peri-implant soft tissues, zirconia abutments and all-ceramic crowns should be used in combination. In cases with thick mucosa, titanium can also be used as the abutment material, in combination with metal-ceramic crowns.[21]

In the past, there was a widespread hypothesis that ceramic abutments should only be used in anterior regions because of stronger bite forces in the molar region. Today, further material developments make the usage of ceramic abutments even in the posterior region possible. This new type of ceramic material that is based on zirconium dioxide, yttria-stabilized tetragonal zirconia polycrystal (Y-TZP), has a unique ability to resist crack propagation by being able to transform from one crystalline phase to another, and the resultant volume increases stop cracks and prevent them from propagating. Therefore, this material has the potential for use both in extended restorations and in the molar area.[13]

4.3.1   Abutment Design: Individually Produced vs. Prefabricated

Prefabricated abutments can be used or they can be individually produced according to the shape of the tooth. Most studies concerning these two abutment designs have established that both custom-made and prefabricated zirconia abutments have comparable failure loads.[22] In another study, crowns were cemented onto tooth-like abutments in one group, and in another group, onto implant-like titanium abutments. They presented significantly higher loads at fracture and less severe fractures for crowns with anatomically shaped cores compared to simple cores of even thickness.[13]

In pronounced angulations of the teeth, an individually produced abutment is advisable. These specially designed abutments simulate the geometry of a ground-down tooth and are therefore advantageous for an anatomically correct skeleton design. Those customized abutments can also be individually prepared according to anatomic needs, thus allowing an individual placement of the margin of the crown.[12] The preparation of an abutment is seen as critical because excessive heat during preparation may compromise osseointegration.

A study that looked at heat transfer in the implant–bone interface during preparation of a zirconia abutment emphasized that preparation caused an increase in temperature within the implant, but this temperature increase did not reach the critical level described in implant literature.[23]

4.3.2   Survival Rates of Ceramic Abutments

The outcome of custom-made zirconia abutments for implant-supported single-tooth restorations up to five years after insertion has been investigated in several studies. The overall conclusion of one study was that zirconia

TABLE 4.2 Parameters for Zirconia and Titanium Abutments and Control Teeth at 5 years

	mPCR	mBOP	mMM/MG	mPmes	mPdist
ZrO$_2$ abutments	0.1 ± 0.3	0.5 ± 0.3	0.1 ± 1.0	2.3 ± 0.6	2.1 ± 0.8
Control teeth	0.2 ± 0.3	0.3 ± 0.2	−0.6 ± 1.0		
Ti abutments	0.3 ± 0.2	0.6 ± 0.3	0.3 ± 0.7	2.2 ± 0.8	1.9 ± 0.9
Control teeth	0.2 ± 0.2	0.4 ± 0.3	−0.6 ± 0.6		
Significance ZrO$_2$ vs. Ti	p = 0.96	p = 0.96	p = 0.86	p = 0.72	p = 0.52

Abbreviations: mPCR, mean plaque control record; mBOP, bleeding on probing; MM, marginal mucosa; MG, marginal gingiva; mPmes, mesial papilla index; mPdist, distal papilla index.

TABLE 4.3 Mean Pocket Probing Depth (mPPD)

		Baseline	1 year	3 years	5 years
ZrO$_2$ abutments	mPPD	2.9 ± 0.9	3.5 ± 0.7	3.2 ± 1.0	3.3 ± 0.6
Control teeth	mPPD	2.4 ± 0.5	2.5 ± 0.7	2.1 ± 0.7	2.5 ± 0.7
Ti abutments	mPPD	3.1 ± 0.8	3.3 ± 0.6	3.4 ± 0.5	3.6 ± 1.1
Control teeth	mPPD	2.5 ± 0.3	2.6 ± 0.4	2.1 ± 0.4	2.6 ± 0.4

MPPD (in mm) with standard deviation at different timepoints at zirconia and titanium abutments and their corresponding control teeth. There were no significant differences at any timepoint (p = 0.85).

abutments performed well with a survival rate of 100% over 3–4 years. The rates of both technical and biological complications were low, and the patients were generally extremely satisfied. No all-ceramic crowns fractured, and only two abutments (out of 185, about 1%) fractured after five years. There were no significant differences in changes in any of the soft tissue registrations or peri-implant marginal bone levels between the conventional two-piece abutment-crown restoration and the one-piece restoration.[12] Also, there were no statistical differences between zirconia and titanium abutments related to parameters like plaque index and bleeding on probing (Tables 4.2–4.4).[24]

4.4 SUPRASTRUCTURE

There are two options available for anchoring implants, either fixed or removable prostheses. Fixed dentures like crowns or bridges can be screwed or cemented onto the abutment.[25] Since screwing the superstructure into the implant has more disadvantages, cementation is the more popular method of

TABLE 4.4 Mean Marginal Bone Levels

		Baseline	1 year	3 years	5 years
ZrO$_2$ abutments	mMBL	1.5 ± 0.7	1.4 ± 0.7	1.7 ± 1.0	1.8 ± 0.5
	mDBL	1.5 ± 0.9	1.5 ± 0.9	1.6 ± 1.0	2.0 ± 0.8
Ti abutments	mMBL	2.0 ± 0.7	2.2 ± 1.0	2.0 ± 1.0	2.0 ± 0.8
	mDBL	2.0 ± 0.7	2.3 ± 1.0	2.1 ± 1.0	1.9 ± 0.8

Abbreviations: mMBL, marginal bone levels, mesially; mDBL, marginal bone levels, distally. Measurements are in mm. There were no significant differences at any timepoint (global P-value MBL: $P = 0.95$; DBL: $P = 0.99$) at zirconia and titanium abutments.

affixing the dentures to the implant. Possible complications with the removable, screw-in dentures are the loss of the cover of metal-composite, metal-ceramic crowns or prostheses; or the chipping of ceramics. While these do not affect the function of the prosthesis, they can be an aesthetic detraction for the patient. Also, the screw can fracture or get lost. Screw-loosening incidents range from 6 to 38%. Therefore, cementation of the superstructure should be considered as the superior method of fixing dentures onto the implant. At first, the prostheses should be cemented temporarily if alterations are foreseeable, then if the implant has successfully integrated and no soft tissue inflammation is visible, the dentures can be fixed permanently.

4.5 CLINICAL PROCEDURES

4.5.1 Surgical Procedure

The surgical procedure includes pre-surgical planning, the intra-operative procedure, and the post-surgical education of the patient.

4.5.1.1 Pre-Surgical Planning

At first, the determination of any contraindications, such as certain systemic or genetic diseases or insufficient bone quality and quantity (i.e. after tumor resection) is necessary. Therefore, the clinician has to thoroughly examine the patient and familiarize himself with the patient's anamnesis and any other influencing factors.

Once the case history and examination has taken place, the number, lengths, and diameter of the implants to be inserted have to be determined, and for this reason, thorough pre-surgical planning is obligatory. Pre-surgical planning includes clinical examination, functional analysis, and evaluation of the hard and soft tissue. The clinical examination will include extra- and intraoral inspection and palpation; and the determination of the distance of the

alveolar crest at the implantation site to the antagonistic occlusal surface, the tooth space width, and the latitude of the fixed gingiva and the alveolar ridge. Functional analysis determines whether there are any disorders of the mandibular joint, the occlusion, or the articulation, and will help the clinician to determine whether implant prosthetic rehabilitation is possible or not.

To determine the implant position and produce a measurement or operation template, plaster models of the upper and lower jaw and an X-ray to show bone volume are required. Basic documentation should include an OPTG, and can be supplemented with periapical radiographs, lateral radiographs, occlusal X-rays, and DVTs. It is important to evaluate the distance to critical anatomical structures (e.g. the N. alveolaris inferior).

According to the dental situation, one distinguishes between single- and multi-tooth replacement and implantation in the edentulous mandible. In general, removable implant-supported dentures in the toothless mandible should be supported on four implants. Fixed implant-supported dentures should be supported on six implants.

4.5.1.2   Intra-operative Behavior

Shortly before surgery, the patient should rinse with 2% chlorhexidine for two minutes in order to disinfect the oral cavity. The implant insertion surgery starts with local anesthesia of the operation area. The incision used is mostly crestal with vestibular relief cuts while preserving the adjacent gingival papilla. The goal of the incision is to have a good overview of the implantation area with the option to extend the area if needed and to avoid a traumatization of adjacent structures. It is followed by flap preparation with detachment of the gingiva and periosteum from the bone. Contact of the periosteum with the bone in the surrounding area should be maintained. The anatomical structures close to the implantation point, such as the mental foramen, should be displayed. Implant bed preparation starts by using a round bur to make a small indentation into the alveolar bone in the position where the implant is supposed to be inserted. It is followed by a gradual preparation of the implant site ready for the intended implant diameter and length. All rotating instruments are used at low engine speeds (800–1200 U/min). After rinsing the bone cavity with physiological saline, the implant is inserted and the interior space of the implant is closed with a cover screw. This is followed by repeated wound debridement with saline and suturing. Sutures are removed 7 to 10 days after surgery. Subsequently, the patient needs to be carefully instructed regarding post-surgical behavior. Since implant insertion is biphasic, a second exposure surgery follows after a healing period of three to six months, depending on the localization of the implant (maxillar or mandibular).

4.5.1.3   Post-surgical Behavior and Education

Since zirconia implants are mostly one-piece implants it is important that they are protected from burdening during the healing period. After insertion into the

bone, the zirconia implants protrude through the gum and into the oral cavity. Protection against loading is accomplished by wearing a metal-free protective splint or prosthesis.

The infection prophylaxis in the first 48 hours after surgery is most important. Although direct and intensive cleaning of the surgical area with a hard toothbrush should be avoided in the first few days, the rest of the teeth should be cleaned thoroughly.

It is recommended that an antiseptic mouth-rinse, such as chlorhexidinedigluconate is used. If a patient wears a removable prosthesis, it is important that it doesn't irritate the surgical area. Dental implants have to be controlled at regular intervals because of the infection risk.

4.5.2   Complications

4.5.2.1   Intra-operative Complications

Intra-operative complications can occur due to complex jaw conditions, insufficient pre-surgical planning, or incorrect work carried out by the clinician. Every patient should be informed of possible operation risks before surgery, such as:

- Injury of nerves lying close to the operation area, such as the N. alveolaris inferior.
- Violation of the roots of neighboring teeth.
- Soft tissue injury.
- Massive bleeding (from A. palatina).
- Violation of the maxillary sinus.
- Insufficient primary stability of the implant.
- Perforation of the lower jaw.
- Thermal damage to the bone due to insufficient cooling or too much pressure during preparation.

4.5.2.2   Post-operative Complications

Post-operative complications can arise either immediately after surgery, or during or after the healing period, and can lead to a high level of patient discomfort and clinical problems such as bone loss.[14] To prevent early post-operative complications, some precautions can be taken. The clinician should use antimicrobial substances such as saline to prevent wound infections, and daily use of chlorhexidine at home is also recommended. To prevent swelling, the patient can take prednisolone before surgery, and two days after. In spite of this, early post-operative complications can still arise, and therefore the patient must be informed about them.

Late post-operative complications can arise due to insufficient cleaning of the implant by the patient at home, or from other systemic problems of the patient. Therefore, a thorough medical history must be conducted, and patient instructions must be given.

Early post-operative complications that can occur are:

- Pain.
- Hematoma.
- Wound healing disturbances.
- Wound infection.
- Swelling.
- Bleeding.
- Dehiscence.
- Flap necrosis.

Late post-operative complications that can occur are:

- Peri-mucositis.
- Peri-implantitis.
- Implant loss.
- Osteolysis.
- Implant fracture.

4.6   FITTING AND BITE FORCE

4.6.1   Fitting of Ceramic Implants

A precise fit of the implant is crucial since microgaps at the implant–abutment interface allow for microbial colonization, which can lead to peri-implant tissue inflammation.[26] An exact fit of these abutments can lead to better biologic and biomechanical behavior.[15] Therefore, the microgap between implant and abutment should be as small as possible. The best option is to have no microgap at all, which can be achieved with one-piece abutments, such as zirconia implants.

Another factor is that the adjustment between implants and the implant-supported prosthesis has been described as a relevant factor in stress transference and in complications of the prosthetic restoration. The adjustment between the external hexagon of the implant and the internal hexagon of the abutment must allow less than 5° of rotation to maintain screw union stability. (This value was established by Binon in 1996 and reviewed by Garine et al.) Vertical or horizontal misalignment can apply extra load to the different restoration components, to the implant, and to the bone, which causes several possible complications, such as loosening of the prosthesis retention, abutment fractures, bone microfractures, loss of crestal bone, and osseointegration loss.[8]

There are different thoughts in the literature about the fitting qualities of titanium and zirconia abutments. One study says the implant–titanium abutment connection shows significantly better fit than all zirconia abutment configurations, which demonstrated mean gaps that were approximately three to seven times larger than those in the titanium abutment system.[26] However, another study that evaluated microgaps in different zirconia and titanium implants

found that the mean microgap was less than 2 μm in zirconia implants. The microgap decreased quickly from the outer region to the inner. In this study it was demonstrated that smaller microgaps were found in zirconia abutments compared to those described in the literature for titanium abutments.[15] Despite these conflicting reports, both materials are biocompatible, have good mechanical properties, and therefore seem to be suitable for use as abutment materials.

4.6.2 Bite Force and Fracture Risk of Implants

The human jaw can exert a surprising amount of force while biting dependent on sex, age, and the strength of the individual's jaw muscles. The average bite force value of incisors is 25 kg (55 lb) and 90 kg (200 lb) for molars. Occlusal overloading is the primary cause of biochemical implant complications, which include fracturing and loosening of the implant fixture or prosthetic components. It may also disrupt the intricate bond between the implant surface and bone, leading to peri-implant failure.[27] Therefore, the prevention of occlusal overloading is as important as the right stress-bearing implant material.

Preventing occlusal overloading involves conducting comprehensive examinations, treatment planning, precise surgical and prosthetic treatment, and regular maintenance. If occlusal overloading occurs, management of biomechanical implant complications and the prevention and treatment of peri-implant bone loss involves surgical and prosthetic treatment modalities. They include occlusal treatment; repair and replacement of defective prosthetic components; and surgical treatment of bony craters.[27]

For a long time, the only material that was load- and stress-bearing enough to withstand an implant insertion and the expected bite force, was titanium. A new material was then introduced that was able to endure bite forces and stress at the same level as titanium-zirconia. Several studies demonstrated that titanium and zirconia restorations were functioning and had no complete fractures, after one year. However, fractures of the veneering material were noted. At the five-year follow-up all restorations were still functioning without complete fractures, but there was an increase in veneer fractures.[13]

Another study that compared compressive and tensile stress occurring on implants, abutments, and surrounding bone using a single titanium implant with a titanium abutment, a single titanium implant with a zirconia abutment, and a single one-piece zirconia implant, even found that lower stresses occurred on the zirconia implant (except in the case of tensile stress under oblique loading). The zirconia implant generated the lowest stresses in cortical bone, and the zirconia abutment resulted in lower vM and compressive stresses than the titanium abutment in implant and cortical bone.[16]

Since the bite force in the molar region is a lot higher compared to the incisor region, the implant material used in this position has to be extremely stable and load-bearing. Therefore, a new type of ceramic material, based on zirconium dioxide, yttria-stabilized tetragonal zirconia polycrystal (Y-TZP), was

developed. Y-TZP has the unique ability to resist crack propagation by being able to transform from one crystalline phase to another, and the resultant volume stops cracks and prevents crack propagation. Which is why this material has the potential to be used for larger restorations, and in the molar area.[13]

However, there is still a small percentage of fractured implants despite the use of the right implant materials. Failure analysis of fractured dental zirconia implants found that many fractured implants were located in the anterior side (bending loads directed from palatal, respectively, lingual towards buccal, as the cause of damage) of the maxilla and mandibula. In all cases, mechanical overloading caused the fracture of the implants (i.e. strong bruxism).[14] That is why prevention or treatment of occlusal overloading (as mentioned earlier) is necessary. Another study on one-piece implants published by Andreiotelli and Kohal[28] reports that in vitro preparation of these implants leads to a statistically significant negative influence on the fracture strength of the implant.[14,28] The preparation, as well as cyclic loading can decrease the fracture strength of zirconia implants. Nevertheless, even the lowest values of mean fracture strength of the implants, used in one study, seemed to withstand average occlusal forces after an extended interval of artificial loading.[29]

4.7   INFECTION MANAGEMENT

Implants have a higher susceptibility to infection than the natural tooth due to their open connection to the oral cavity. The mouth being a humid milieu, with a practically constant temperature of 36.6°C, offers a multitude of ecological niches for buccal flora. This flora is essentially composed of commensal microorganisms whose abundance and virulence are individually dependent and in constant evolution from birth to death. Different factors influence the buccal flora, which is rich with more than 500 species. The adhesion capacity of bacteria that are able to secrete a layer of slime or glycocalix mainly composed of extracellular insoluble polysaccharides is of major importance.[9] Thus, the oral flora should be considered as a dynamic complex ecosystem in dynamic equilibrium between adhesion capacity of the microorganisms and the removal forces active in the mouth. Tooth crowns, fixed partial dentures, and endosseous implants provide non-shedding surfaces that facilitate the formation of thick biofilms that are generally in equilibrium with the host. However, loss of control of these biofilms on such surfaces is the main source of dental pathologies (i.e. gingivitis, periodontitis, peri-implantitis, or stomatitis) and failure in implantology.[9] Adhesion, proliferation, and colonization of cells and microorganisms are dependent upon surface properties, including biocompatibility, surface topography (i.e. roughness), and surface free-energy.[30] Bacterial colonization of abutments starts directly after exposure to the oral environment and within weeks the subgingival microbiota are similar to those found around teeth in the same mouth. Strategies aimed at reducing bacterial adhesion and biofilm formation on implant abutment surfaces are of

pertinent clinical interest and can be used for the maintenance of soft tissue health or possibly in the treatment of peri-implantitis.[30]

Compared to titanium, zirconia surfaces accumulated significantly fewer bacteria and had a reduced plaque affinity, which decreased the risk of inflammatory changes in the adjacent soft tissue.[9,31] This is a major advantage of zirconia, and can be attributed to the smoother surface of this highly biocompatible material.

Therefore, educating the patient in the correct post-operative treatment and hygiene regime for the newly inserted implant is of great importance. The patient must take even more care of his oral hygiene than usual. In addition to conventional oral hygiene products such as a toothbrush, toothpaste, and floss, the patient should use dental aids like interdental brushes and antiseptic mouthwash to keep the area around the implant clean.

4.8   OSSEOINTEGRATION

The term osseointegration can be defined as a direct, functional linkage of the implant surface and the surrounding bone.[10] It is crucial for the long-term success of dental implants and depends on tissue reaction at the tissue–implant interface.[5] Additionally, crestal bone stability and healthy soft tissues are necessary for the long-term success of implant-supported restorations.[32] One prerequisite for successful osseointegration is preparation of the implant site to keep the bone around the implant vital.

In the early stage of osseous healing a coagulum on the implant surface is formed. Fibrin is the conducting tissue for regeneration cells (pre-osteoblasts), capillaries, and collagen fibers. Within the coagulum a cell differentiation from pre-osteoblasts to osteoblasts takes place and the bone formation on the implant surface begins. Depending on the gap between implant and the surrounding bone, different types of bone are formed. In narrow gaps (up to 0.2 mm) lamellar bone is formed, and in gaps larger than 0.2 mm, woven bone is formed. Within the following two months the oven bone is converted into lamellar bone. Bone remodeling takes place at a speed of 1 μm/day.

Surface roughness and topography influence osseointegration of zirconia implants to a great extent.[33] The smooth surface of zirconia means that longer healing periods are needed to accomplish osseointegration compared to roughened titanium surfaces. Surface modifications can be used to increase the roughness of zirconia. Therefore, many different methods of roughening the surface have been developed. These range from coated to uncoated, all the way up to acid-etched surfaces. The success rate of acid-etched surfaces is significantly better than the other two methods.[34] Nanoporous, selective infiltration-etched zirconia implant surfaces improved osseous healing and bone apposition at the bone-implant interface; this should improve clinical performance of zirconia implants.[35] During the first days of culture, zirconia improves cell proliferation significantly, but it does not improve attachment and adhesion strength.[5]

Various studies have revealed that there were no statistically significant differences in bone apposition between zirconia and titanium implants, and observed comparable rates of bone apposition in the surfaces after the 6th and 12th week of healing.[10,36] All implants had areas of tight bone to implant contact (BIC). The trabecular architecture of bone around the zirconia implants was classified as lamellar bone due to the circular apposition of bone lamellae around the Canals of Havers. All implants showed few signs of natural bone remodeling, apposition of osteoid, osteoblasts, or lacunae of osteoclasts. Mature bone structure was observed with osteoblasts within the mineralized bone and tight alignments of osteoblasts surrounding the osseous trabeculae. Polymorphonuclear cells as signs of an inflammation reaction to a foreign body were not observed.[10] Both titanium- and zirconium-based implants revealed a periostal and endostal callous in close proximity to the implant. A clear demarcation was noted between the original cortical bone and the new bone growing in between the threads. The original cortical bone was clearly defined by its compact, lamellar appearance, and by the presence of osteons, whereas the bone growing into threads appeared to be less organized, less lamellar, and appeared consistent with woven bone.[6]

REFERENCES

1. Papaspyridakos P, Chen CJ, Singh M, et al. Success criteria in implant dentistry: a systematic review. J Dent Res 2012;91:242–8.
2. Reichart P, Hausamen JE, Becker J, Schliephake H, Schmelzeisen R. Zahnärtliche Chirurgie Band I. Berlin: Quintessenz Verlag; 2002.
3. Beikler T, Flemmig TF. Implants in the medically compromised patient. Crit Rev Oral Biol Med 2003;14:305–16.
4. Lambrich M. Metallfreie dentale Implantation. CO MED: CO MED Verlags GmbH, 2008.
5. Depprich R, Ommerborn M, Zipprich H, et al. Behavior of osteoblastic cells cultured on titanium and structured zirconia. Head Face Med 2008;4:29.
6. Shin D, Blanchard S, Ito M, et al. Peripheral quantitative computer tomographic, histomorphometric, and removal. Clin Oral Implants Res 2011;22:242–50.
7. Depprich R, Zipprich H, Ommerborn M, et al. Osseointegration of zirconia implants compared with titanium: an in vivo study. Head Face Med 2008;4:30.
8. Gomes A, Montero J. Zirconia implant abutments: a review. Med Oral Patol Oral Cir Bucal 2011;16:e50–5.
9. Hisbergues M, Vendeville S, Vendeville P. Zirconia: established facts and perspectives for a biomaterial in dental. J Biomed Mater Res B Appl Biomater 2009;88:519–29.
10. Koch F, Weng D, Kramer S, et al. Osseointegration of one-piece zirconia implants compared with a titanium implant. Clin Oral Implants Res 2010;21:350–6.
11. Ozkurt Z, Kazazoglu E. Zirconia dental implants: a literature review. J Oral Implantol 2011;37:367–76.
12. Ekfeldt A, Furst B, Carlsson G. Zirconia abutments for single-tooth implant restorations: a retrospective and. Clin Oral Implants Res 2011;22:1308–14.
13. Larsson C. Zirconium dioxide based dental restorations. Studies on clinical performance and fracture behaviour. Swed Dent J Suppl 2011;213:9–84.

14. Gahlert M, Burtscher D, Grunert I, et al. Failure analysis of fractured dental zirconia implants. Clin Oral Implants Res 2012;23:287–93.

15. Baixe S, Fauxpoint G, Arntz Y, et al. Microgap between zirconia abutments and titanium implants. Int J Oral Maxillofac Implants 2010;25:455–60.

16. Caglar A, Bal B, Karakoca S, et al. Three-dimensional finite element analysis of titanium and yttrium-stabilized. Int J Oral Maxillofac Implants 2011;26:961–9.

17. Stadlinger B, Hennig M, Eckelt U, et al. Comparison of zirconia and titanium implants after a short healing period. A pilot study in minipigs. Int J Oral Maxillofac Surg 2010;39:585–92.

18. Pirker W, Wiedemann D, Lidauer A, et al. Immediate, single stage, truly anatomic zirconia implant in lower molar. Int J Oral Maxillofac Surg 2011;40:212–6.

19. Oliva X, Oliva J, Oliva JD. Full-mouth oral rehabilitation in a titanium allergy patient using zirconium. Eur J Esthet Dent 2010;5:190–203.

20. Kohal R, Knauf M, Larsson B, et al. One-piece zirconia oral implants: one-year results from a prospective cohort. J Clin Periodontol 2012;39:590–7.

21. Sailer I, Zembic A, Jung R, et al. Single-tooth implant reconstructions: aesthetic factors influencing the decision. Eur J Esthet Dent 2007;2:296–310.

22. Hjerppe J, Lassila L, Rakkolainen T, et al. Load-bearing capacity of custom-made versus prefabricated commercially available zirconia abutments. Int J Oral Maxillofac Implants 2011;26:132–8.

23. Huh J, Eckert S, Ko S, et al. Heat transfer to the implant-bone interface during preparation of a zirconia/alumina abutment. Int J Oral Maxillofac Implants 2009;24:679–83.

24. Zembic A, Bosch A, Jung RE, et al. Five-year results of a randomized controlled clinical trial comparing zirconia and titanium abutments supporting single-implant crowns in canine and posterior regions. Clin Oral Implants Res 2012;24:384–90.

25. Kern M, Kohal RJ, Mehl A, et al. Vollkeramik auf einen Blick-Leitfaden zur Indikation, Werkstoffauswahl, Vorbereitung und Eingliederung von vollkeramischen Restaurationen. Ettlingen: Arbeitsgemeinschaft für Keramik in der Zahnheilkunde e.V; 2012.

26. Baldassarri M, Hjerppe J, Romeo D, et al. Marginal accuracy of three-implant ceramic abutment configurations. Int J Oral Maxillofac Implants 2012;27:537–43.

27. Fu J, Hsu Y, Wang H. Identifying occlusal overload and how to deal with it to avoid marginal bone loss around implants. Eur J Oral Implantol 2012;5:S91–S103.

28. Andreiotelli M, Kohal R. Fracture strength of zirconia implants after artificial aging. Clin Implant Dent Relat Res 2009;11:158–66.

29. Kohal R, Wolkewitz M, Tsakona A. The effects of cyclic loading and preparation on the fracture strength of zirconium-dioxide implants: an in vitro investigation. Clin Oral Implants Res 2011;22:808–14.

30. Van Brakel R, Cune M, van Winkelhoff A, et al. Early bacterial colonization and soft tissue health around zirconia and titanium abutments: an in vivo study in man. Clin Oral Implants Res 2011;22:571–7.

31. Gahlert M, Rohling S, Wieland M, et al. Osseointegration of zirconia and titanium dental implants: a histological and histomorphometrical study in the maxilla of pigs. Clin Oral Implants Res 2009;20:1247–53.

32. Nothdurft F, Pospiech P. Zirconium dioxide implant abutments for posterior single-tooth replacement: first results. J Periodontol 2009;80:2065–72.

33. Gahlert M, Rohling S, Wieland M, et al. A comparison study of the osseointegration of zirconia and titanium dental implants. A biomechanical evaluation in the maxilla of pigs. Clin Implant Dent Relat Res 2010;12:297–305.

34. Oliva J, Oliva X, Oliva JD. Five-year success rate of 831 consecutively placed Zirconia dental implants in humans: a comparison of three different rough surfaces. Int J Oral Maxillofac Implants 2010;25:336–44.
35. Aboushelib M, Salem N, Abotaleb A, et al. Influence of surface nano-roughness on osseointegration of zirconia implants in rabbit femur heads using selective infiltration etching technique. J Oral Implantol 2011;9:9.
36. Hoffmann O, Angelov N, Zafiropoulos G, et al. Osseointegration of zirconia implants with different surface characteristics: an evaluation in rabbits. Int J Oral Maxillofac Implants 2012;27:352–8.

Clinical Failures of Ceramic Dental Prostheses

Yihong Liu[*] **and James Zhijian Shen**[†]

[*]*Peking University School and Hospital of Stomatology, National Engineering Laboratory for Digital and Material Technology of Stomatology, Beijing 100081, China;* [†]*Berzelii Center EXSELENT on Porous Materials; and Department of Materials and Environmental Chemistry, Arrhenius Laboratory, Stockholm University, Stockholm, Sweden*

Contents

5.1   FRACTOGRAPHIC ANALYSIS OF CERAMICS AND GLASSES

Ceramics and glasses are known for their strength under compressive load, but they are brittle under tensile stress or heavy impact. Thus, upon failure, brittle fractures commonly occur with very little or no plastic deformation of the materials microstructure. This gives rise to typical fracture patterns, and direct observation of the fractured surfaces provides rich information. Indeed, analysis of failed ceramics and glasses are easier to interpret than similar analysis of ductile metals or polymers. In the former, fractographic analysis produces reliable facts about the cause of the fracture. A lot of information can be gathered just by visual examination of the sizes, shapes, and failure history of the fragments. Thus, the overall breaking pattern of brittle materials can give enough information for a first assessment of fracture origin, lessening the need for a more detailed microscopic examination. In other cases, however, a careful microscopic investigation of the fracture surfaces and the related crack patterns is needed to identify the fracture initiation point. The origin is always at the point that has the highest tensile stress level and/or a critical fault. Optical stereomicroscopy or scanning electron microscopy (SEM) are useful because brittle materials leave explicit markings on fracture surfaces that can be interpreted with confidence. Fracture surface appearance is a direct consequence of crack propagation stresses; pattern recognition is important for the fracture analysis. Fracture types can be further confirmed by looking at the breakage history and shapes of the fragments. The ideal fractographer should have a broad knowledge of materials science and mechanics–in particular, the fracture mechanics of brittle solids – plus a skill for problem solving. They should also be comfortable with the use of microscopy, since some of the features to be studied will be indistinguishable to the naked eye. In summary, for a correct assessment of fracture surface analyses, integration of knowledge from a variety of scientific disciplines is necessary.

5.1.1   Tools and Equipment

The analysis of any fractured piece always begins with a visual examination with the naked eye or simple magnification glass. It is often practical to photograph the entire component for documentation. An overall photo-view also provides an essential context for subsequent close-up photos. Scales or rulers should be set alongside the component in order to show the size or scale. Many camera types can be used to photograph the component and the fractured fragments, but digital cameras are the most popular. Also, digital data is convenient for computer evaluations.

In many cases, higher magnification will be needed to observe the fracture surfaces. The two most important tools are the binocular stereo-optical microscope and the SEM. It is best to inspect the fractured specimens with an optical microscope to obtain valuable optical information such as color, reflectivity, and internal flaws in translucent or transparent materials. Fracture origins or flaws in ceramics and glasses can often be found with a stereo-optical microscope that gives a magnified, naturally appearing and three-dimensional view of the fracture surface. The view is right-side up and laterally correct and can therefore be correlated to a specimen held by hand or on a stage. Most stereomicroscopes can be equipped with a camera port for a video or digital camera registration.

Even higher magnifications are sometimes needed to see flaws more clearly, and SEM is a versatile tool that enables the observation of large portions of a specimen at low magnifications. In addition, it is possible to instantly zoom into regions of interest for high-resolution close-ups with high depth of field. Note that SEM images often appear 'flatter' so it can be difficult to interpret whether a minor topographic feature is above a surface or a depression below. A great advantage of using SEM equipment is that elemental compositional analysis can be done with an attached detector that is sensitive to the emission of each element's characteristic X-ray radiation. Elemental analysis can be done from a selected point on the specimen or a scanned surface area by controlling the electron beam position. This analysis is called energy-dispersive X-ray spectroscopy (EDS or EDXS). Elemental analysis is particularly useful for detecting strength-limiting flaws such as inclusions, secondary phase variations, or compositional inhomogeneities.

Other exclusive tools can play support roles in careful scientific studies. Field emission scanning electron microscopes (FESEM) offer dramatic increases in magnifications (600,000X) and improved resolutions down to 1 nm. FESEM can achieve the same resolution and contrast as with transmission electron microscopy (TEM). The environmental scanning electron microscope (ESEM) is designed to function in either high or low vacuums and can operate in gas environments that contain water vapor or other inert gases. The ESEM is primarily used for biological materials or for materials without a carbon coating. The atomic force microscope (AFM) is a powerful microscope that is used for high-resolution, sensitive examinations of surface roughness down to the atomic level.

The dramatic advancements in digital camera and computer technology have revolutionized imaging technology. They open up new capabilities and some shortcomings of conventional optical microscopes or SEM can be overcome or moderated (e.g. limited depth of field and flatter-appearing images, respectively). Virtual three-dimensional images can be constructed with automatically restoring optical microscope views or by analysis of multiple SEM images taken with slightly different specimen tilts. Pseudo-three-dimensional images can be displayed, tilted, and rotated to present different

perspectives. Various quantitative numerical analyses of surface topography can be performed at almost no extra effort since the surface topography has been recorded digitally (e.g. surface roughness or even fractal dimensional analysis). Low-cost software programs are now available that can overcome the depth of field limitations of virtually any optical microscope. A series of photos is taken at the same magnification while slightly readjusting the focus in sequential steps. The software interprets the regions that are in focus and stitches these together to create a single image with an infinite depth of field.[1]

5.1.2 Fracture Patterns and Origins

The general examination often begins with a reassembly of the component and all fragments. The entire part and all of the components should be well documented by photographs and/or sketches. The overall fracture pattern reveals information about the fracture event and the component stress state at the failure.

The fracture origin is the source from which brittle fracture begins. Therefore, it is essential to find this primary object. Normally, for brittle fractures, like in ceramics and glass, the cracks radiate outward from this fracture origin. Note that severe thermal stresses or strong impact loads may create multiple fracture origin sites. In an instant of time, several sites might have extreme combinations of tensile stresses and/or critical flaw concentrations. A majority of origins in brittle materials are from surface- or edge-located flaws. Crack branch patterns are valuable aids in diagnosing the propagation direction and they indicate fracture stress conditions and magnitudes. A crack propagates normal to the direction of the local principal tension stress. As the crack propagates, minor changes in the direction of local principal tension can modify the plane of cracking. These minor perturbations can create revealing markings. Internal stresses or inhomogeneities can also cause local crack direction deviations. Cracks that have reached their terminal velocity (normally about 50–60% of the shear wave velocity) may split into two cracks with an angle between them.

A general quantitative assessment of the stresses in a failed component can be made from the number of fragments, as fragmentation is related to the stress magnitudes. The radiating pattern intuitively leads the observer back to the origin, which is usually in the middle. At low stress levels, the low available energy creates minimal crack branching and hence fewer fragments. In contrast, high-energy stress levels yield fractures with extensive fragmentation.[1,2]

5.1.3 Fracture Surface Examination

Stereo-optical microscopes and SEM are ideal tools for the examination of details. Crack propagation markings on fracture surfaces allow one to estimate the state of stress, the crack velocities, and to follow crack paths back to an origin, as described above.
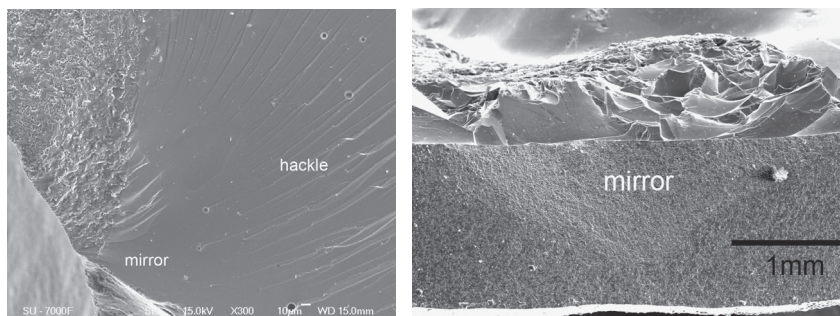
FIGURE 5.1   Mirrors found in porcelain and ceramics. (a) The SEM view of a fracture mirror in the porcelain veneer of a broken bi-layer alumina all-ceramic crown. The view of the mirror is incomplete since it was large relative to the veneer cross-section size. The advancing crack propagated into a decreasing stress field in the interior and did not have sufficient energy to form the mirror and hackle in a complete circle. The incomplete mirror in the direction of the interior is a sign indicative of bending stress. (b) The SEM view of a fracture mirror in an alumina core of a broken alumina bi-layer all-ceramic crown.

Fracture mirrors are relatively smooth regions surrounding the fracture origin. The fracture mirror is the region where a crack radiates rapidly outwards from the fracture origin. The crack accelerates in microseconds from near zero velocity to terminal velocity over a very short distance where the mirror is formed. The term 'mirror' came into use with early optical microscopic examinations of broken glasses, where the mirror region was so smooth that it reflected light like a mirror (Figure 5.1). In polycrystalline ceramics or composites, an inherent roughness from the microstructure may appear in the mirror area. This 'mist-mirror' zone has a slightly frosty appearance, such as when water condenses on a reflecting mirror. The misty appearance depends on the size and arrangement of the inherent microstructure components, is easy to see in glassy composites, but may be difficult or impossible to discern in dense fine-grained ceramics. It is important to find the location of any mirror since it will draw attention to the fracture origin and its size will reflect the stress level at the moment of fracture. The smaller the mirror is, the larger the stress at the origin site. Therefore, a small mirror is proof that the structure part was strong and/or had a small strength-limiting flaw. On the contrary, a large mirror demonstrates that the failure stress was lower and implies a weaker microstructure and/or a large defect.

A *hackle* is a line on the fracture surface that runs in the local direction of cracking. It separates parallel, but non-coplanar portions of the crack surface (Figure 5.1a). Hackles are very useful for establishing the direction of crack propagation and for tracing cracks back to their origin.

Coarse hackles are large, broad hackle lines that form in ceramics, most likely depending on variations in the microstructure. Ceramics may develop coarse hackle lines even in the absence of a mirror or other well defined fracture surface markings. This occurs particularly in low strength or porous
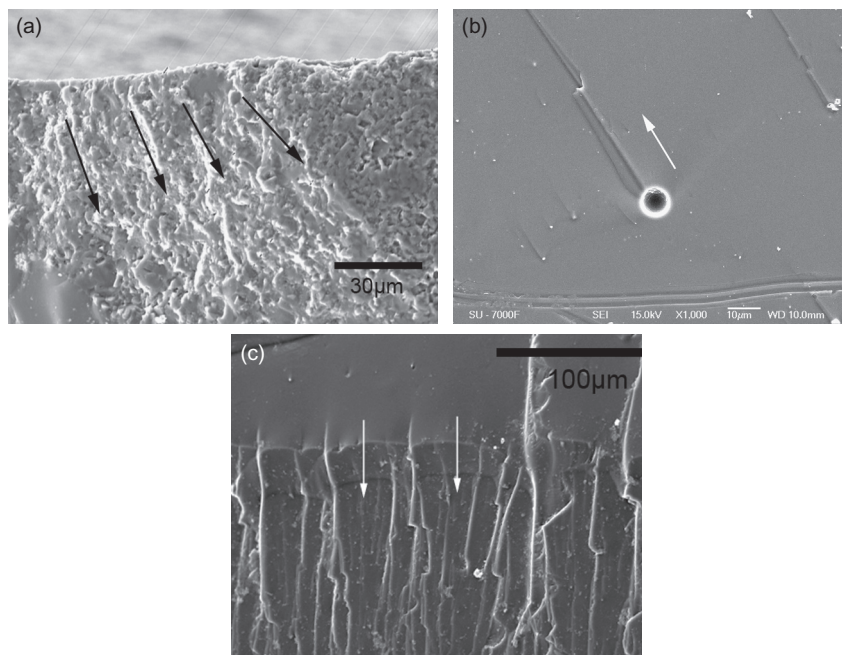
FIGURE 5.2 SEM micrographs show hackles in alumina ceramics and veneer porcelain. (a) The fracture surface of a broken alumina ceramic crown has a very rough bulky appearance. The coarse hackle lines (black arrows) in this alumina ceramic guide the observer back to the origin. (b) The fracture surface of a broken porcelain veneer shows wake hackles initiated at the bubbles. The crack was running in the direction of the white arrow. (c) The fracture surface of broken porcelain veneer shows twist hackles and the crack was running in the direction of the white arrows.

ceramics and is often the only feature that indicates the direction of crack propagation. A typical example of coarse hackles in an alumina ceramic is shown in Figure 5.2a.

A *wake hackle* is a hackle mark extending from a singularity at the crack front in the direction of propagation. When an advancing crack encounters an elastic singularity, such as an inclusion or a pore, the crack front may split at the object and sweep past it on both sides. As the two fronts pass the obstacle they often continue on slightly different microstructural planes and create a step or 'trail' between them. The trail may fade away quickly or persist for long distances. These markings are very recognizable and can be either large or small, but they show the direction of local crack propagation. In some dental ceramics, like glass or porcelain veneers, the wake hackle is often the only recognizable fracture trace, as illustrated in Figure 5.2b.

A *twist hackle* is a hackle that separates portions of the crack surface, each of which has rotated from the original crack plane in response to a lateral rotation or twist in the axis of principal tension. Twist hackles are very revealing
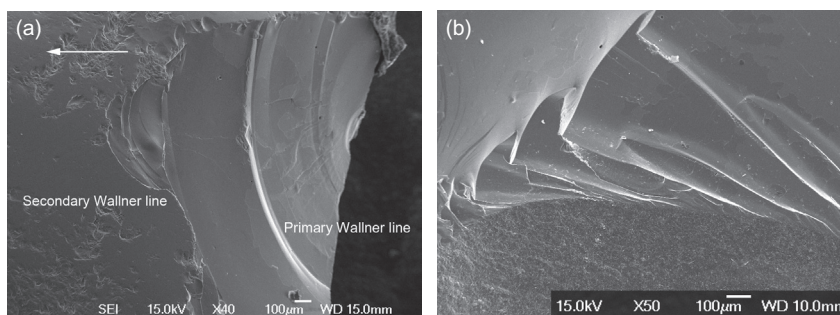
FIGURE 5.3   SEM images show Wallner lines and compression curls. (a) Two types of Wallner line are presented in the fractured porcelain surface of a broken bi-layer zirconia all-ceramic crown. The image shows the primary Wallner line starting from the sides of a fracture origin. The crack was running in the direction of the white arrow. The primary Wallner line appeared as a well-formed arch, whereas the secondary Wallner line was formed by the crack itself. (b) The compression curls are shown on the fractured surface of porcelain veneer of a broken bi-layer alumina all-ceramic crown.

markings and the roughly parallel segments point in the direction of local crack propagation. Twist hackles can be generated by the primary crack as it travels directly through the body, especially if it goes around corners or geometric irregularities, or if the stress conditions have otherwise markedly changed. In polycrystalline ceramics, twist hackle markings within coarse grains can serve as helpful markers. An illustrative twist hackle is shown in Figure 5.2c.

A ***Wallner line*** is a rib-shaped mark with a wave-like contour caused by a temporary excursion of the crack front out of plane in response to a tilt in the axis of principal tension. It may also form from passage of the crack front through a region with a locally shifted stress field, as at an inclusion, pore, or surface discontinuity. The Wallner line is the locus of the elastic wave and the crack front intersections. The elastic wave momentarily causes the crack to ripple out of plane like a wave on a pond surface. Wallner lines are indispensable in determining the direction of crack propagation. They are usually curved (arched) in the direction of crack propagation. Wallner lines are easy to see optically on fracture surfaces once the lighting is adjusted, but they are difficult to see by SEM as they are shallow and produce almost no contrast. Primary Wallner lines are commonly generated by surface imperfections and irregularities such as scratches, pits, or edge chips. Unlike primary Wallner lines that form as a result of a crack encountering an external feature, secondary Wallner lines occur from interactions the crack generates itself (Figure 5.3a).

An ***arrest line*** is a sharp line on the fracture surface that defines the crack front shape of an arrested or momentarily hesitated crack prior to resumption of crack propagation under a more or less altered stress configuration. Arrest lines are different than Wallner lines in two key respects: arrest lines are sharp,
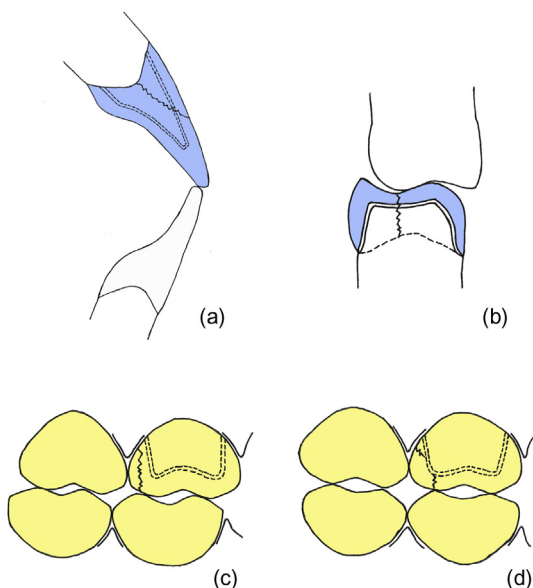
FIGURE 5.4 Schematic illustrations of the fracture circumstances upon occlusal contact and the subsequent fracture trajectories of clinically failed bi-layer all-ceramic crowns: (a) An incisor crown broken into two pieces on the labial surface under the bite load. The crack is initiated at the margin from where it propagates though the labial surface and through both inner core and outer silicate porcelain layer. (b) A molar crown, broken into two pieces where the crack is initiated on an occlusal contact from which it propagates through both inner core and outer porcelain layer under the bite load on the central fossa. (c) A molar crown that failed by porcelain chipping-off in the axial wall as a result of the bite load on the marginal ridge. (d) A molar crown that failed by porcelain delamination in the axial wall caused by the bite load on the cusp.

and, unlike most Wallner profiles, arrest lines show the crack front profile at an instant in time. The sharp line usually corresponds to where a crack hesitates or stops. Therefore, a series of parallel arrest lines usually indicate that a fatigue-initiated crack is present.

A *compression curl* results from failure caused by bending stress, and is also known as a cantilever curl. It is the curved lip just before the total fracture of a ceramic body that failed by bending. It is a sign that the specimen was either loaded primarily in bending or had a strong bending stress component at the moment of failure (Figure 5.3b).[1–4]

5.2　FAILURES OF CERAMIC DENTAL PROSTHESES

5.2.1　Fracture Features

The overall fracture circumstances and crack features of failed bi-layer ceramic crowns are illustrated as three major types according to the schematic drawings in Figures 5.4a, b, c, and d.[4]
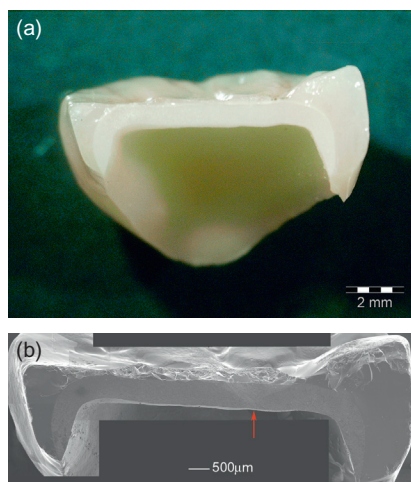
FIGURE 5.5   The lingual part of a broken upper molar alumina crown is shown by optical microscopy (a). The same object is illustrated by merging 11 SEM images (b). The white arrow indicates the position of the fracture origin being typically located at the interface surface of the alumina core. In addition, the porcelain shell is very thin on this dental crown and extensive porcelain chipping-off damage with several different initiation points are obvious on the occlusal side.

5.2.1.1   Cracking Initiated at the Margin

Clinically failed crowns are typically entirely broken into two pieces by faults found at the margin area. The margin area is always the thinnest part of the whole crown in both anterior and posterior teeth. In addition, the proximal margins of crowns are always under highest tensile stress upon bite load in anterior teeth. Therefore, this type of fracture is found in failed anterior ceramic crowns for both bi-layer and single-layer cases. A typical fracture feature is exemplified by an anterior alumina crown that is entirely broken into two pieces on the incisal 1/3 of the labial surface (see fig.5.19b, or details in Section 5.2.5.2).

Finally, it was noted that the cracks often initiated at the restoration areas, where the core materials were thinnest. This shows the need for careful scrutiny of restoration margin areas to reduce all-ceramic crown failures.

5.2.1.2   Cracking Initiated at Occlusal Contacts

These fracture types are found both in anterior incisor and posterior molar, all-ceramic crowns. When failure occurs in incisor crowns, the fracture always begins on the lingual side of the teeth. The restoration is entirely broken into two or more pieces and fracture is initiated on the inner surface of the restorations by the occlusal contacts. High tensile stress easily builds up in this area on bite load, and a crack will initiate at the weakest point, such as a surface flaw. Total fracture can be found both for bi-layer all-ceramic restorations (e.g. an alumina/porcelain crown), and for single-layer all-ceramic restorations, such as e.max,

Vitamark®, or glass ceramic crowns. An illustrative example is a posterior molar alumina crown entirely broken into two pieces under the occlusal contacts (Figure 5.5). A high tensile stress built up on bite load, and crown cracking was initiated on the inner surface of the core ceramic. The critical defect of the failed molar alumina crown could be identified using the same analytical approach described above (i.e. follow the arrest and hackle lines). The origin is indicated at the posterior crown by a white arrow in Figure 5.5b. The primary defect that leads to cracking is located inside the ceramic core close to the inner surface.[2–10]

5.2.1.3 Porcelain Chipping and Delamination

Porcelain chipping and delamination are observed only in bi-layer restorations made of a strong inner coping and an outer porcelain shell for aesthetics, and for adjusting the anatomy contour of individual teeth. The materials that produce the coping could be either metals or ceramics (e.g. zirconia). With this construction the failure of the restorations often happens within the weaker porcelain veneers and seldom in the stronger copings. Cone cracks originate from defects at the veneering porcelain surface caused by high cyclic compressive stresses at the occlusal contacts due to bite force. These cyclic loads initiate local tensile stresses in the veneer, and initiate micro-cracks by fatigue. Once formed, these micro-cracks will grow and propagate until one of them penetrates the porcelain shell, resulting in porcelain chipping. Therefore, chipping of porcelain is found at the bite contact of opposite teeth. Such chipping areas are at the proximal marginal ridge, or lingual cusp of the upper teeth/labial cusp of lower teeth, and also at the incisial corner of anterior crowns. Sometimes, chipping located at the cervical area could be found at the labial side of lower molar crowns; cervical chipping also happens at the upper incisor crowns. Cervical chipping is not caused by the impact of compressive bite force directly, as this failure is initiated by the tensile stresses formed at the underside of the veneers. Sometimes the chipping is small and does not affect the proximal contact area with the adjacent teeth or change the contour of the teeth. In this case, the dental restoration could still perform as normal and did not fail. In another instance, however, the restoration can ultimately fail and need to be taken out and replaced, especially when the chipping damage of the proximal margin ridge results in the loss of the normal contact area with adjacent teeth.

When a crack penetrates the porcelain layer towards the porcelain–core interface it is often deflected along this interface. The relatively weak bond at the porcelain–core interface compared to the mechanically strong inner core material results in partial porcelain delamination. Porcelain chipping is observed in association with thicker porcelain layers, while delamination is often a result associated with thinner porcelains. This behavior is comparable to the situation observed by finite element analysis (FEA) in bending test simulations, where it is clearly predicted from the material's intrinsic properties. The interfacial delamination has been ascribed either to the large mismatch of the fracture toughness alone, or to both the fracture toughness and elastic modulus mismatches. In an FEA simulation, the differences of the elastic modulus are dominant and to a lesser extent
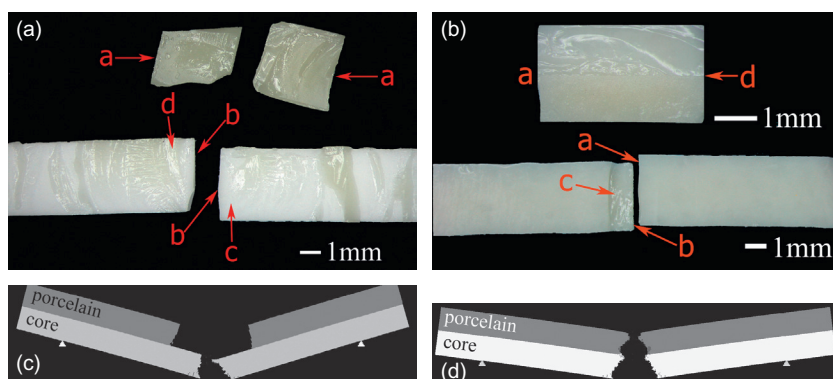
FIGURE 5.6   The optical microscope views of the surface perpendicular to the fracture surface of a zirconia (a) and an alumina (b) bi-layer specimen after a 3-point bending test in comparison with the FEA simulated fracture of zirconia (c), and alumina (d). The observed experimental fracture modes agree with the FEA simulations. In bending of zirconia bi-layer composites, severe interfacial delamination was observed (a). The 'a' arrows in this image indicate pieces of veneer porcelain completely peeled away from the zirconia core; 'b' arrows indicate the location of fracture surfaces of the specimen; arrow 'c' indicates the zirconia core surface after interfacial delamination; and arrow 'd' indicates the veneer porcelain remaining on core interface. In the case of alumina bi-layer composites it is obvious that interfacial delamination was very low, see image (b). The 'a' and 'b' arrows indicate the location of fracture surfaces; arrow 'c' indicates a tiny delamination zone; and arrow 'd' indicates the location of the veneer/core interface. (From Liu YH, Feng HL, Bao YW, Qiu Y, Xing N, Shen ZJ. Fracture and interfacial delamination origins of bilayer ceramic composites for dental restorations. J Euro Ceram Soc, 2010;30(6):1927-1305. Reproduced with permission of Elsevier Limited.)

affected by the fracture toughness. Yet, the effect of fracture toughness is acting indirectly, as bending strength is proportional to toughness and relates also to the critical defect size. The FEA simulation reveals that the frequent interfacial delamination observed in zirconia bi-layer composites compared to alumina composites is initiated by higher shear stresses building up along the zirconia interface due to the mechanical property differences of these two constitutional ceramic components. This suggests that the delamination observed for zirconia copings might be reduced by increasing the bending strength of the veneer porcelain. The FEA simulations discussed above were carried out under the condition of one loading cycle and the results are illustrated in Figure 5.6. Bearing in mind that interfacial delamination starts well before any crack propagates through the zirconia coping, one can understand that veneer flaking may occur and that no critical damage to the zirconia core itself has taken place. This is consistent with the fact that veneer flaking of zirconia crowns and bridges is frequently observed in the clinic.

Failed ceramic crowns have been observed in the clinic with porcelain chipping-off the distal axial wall that was initiated from the distal marginal ridge on the occlusal surface of the upper molar zirconia crown. Fracture failures are observed only near the top surface on the proximal marginal ridge, especially when a thick veneering porcelain shell is present. For further details see Section 5.2.5, Figure 5.19 and Figure 5.20.[2–10]
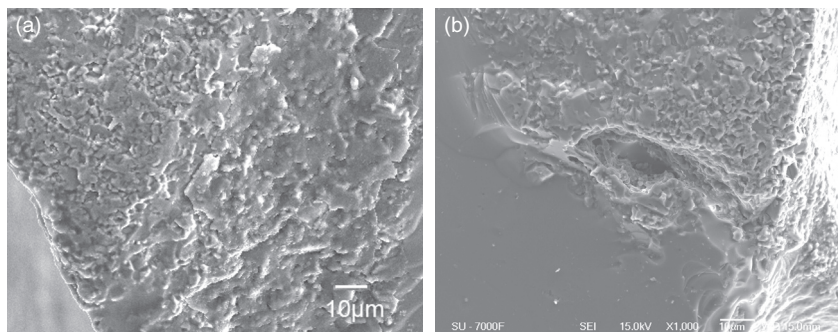
FIGURE 5.7   Example of a fracture origin observed in both corresponding halves of the alumina core of a broken bi-layer alumina all-ceramic crown. (a) The area of fracture origin in one of the two broken parts, without any obvious flaws. (b) The fracture surface of the other part, where a large void area is easily identified.

5.2.2   Analysis of Failure Origin

The observed fracture of a clinical restoration is always a failure of the weakest component. Analysis of the fracture origin and crack propagations can be done using a photograph of the entire structure and close-up photographs of various critical features. Start with the overall image of the component and then add images at progressively higher magnification at key locations. At each step, the relationship of the images to each other should be clear. The characterization of the fault origin should be based upon the object rather than how it appears, since the latter may depend upon the mode of viewing. For this purpose, the fault often needs to be observed by SEM to detect the exact intrinsic quality, as the shape's appearance in an optical microscope is not enough. Whenever possible, both halves of the fracture surface should be examined since each contains information about the fracture origin. This is exemplified in a case where a large void was strength limiting (Figure 5.7). If only the half seen in (a) had been examined, the analyst may have ignored the flaw clearly visible in (b).

5.2.2.1   Failure Origins as Defects or Flaws

The fracture origin is always found near the spot where the highest tensile stress concentration is built up under bite load. Microscopic defects/flaws located close to this spot are often the origin of initial cracks that lead to fracture failure when the stress exceeds a critical level. The primary defect (of critical size) causing the original crack and other, minor structural defects or pre-existing micro-cracks, will then interact with the stress field extending out in front of the crack. This will accelerate and steer crack propagation in a certain direction.

Cracks originating at defects/flaws in the ceramic cores of alumina ceramic crowns, zirconia ceramic crowns, or single-layer glass ceramic crowns, such as e.max and Vitamark®, always result in total failure of the of bi-layer all-ceramic restorations. A typical example is a failed anterior alumina crown
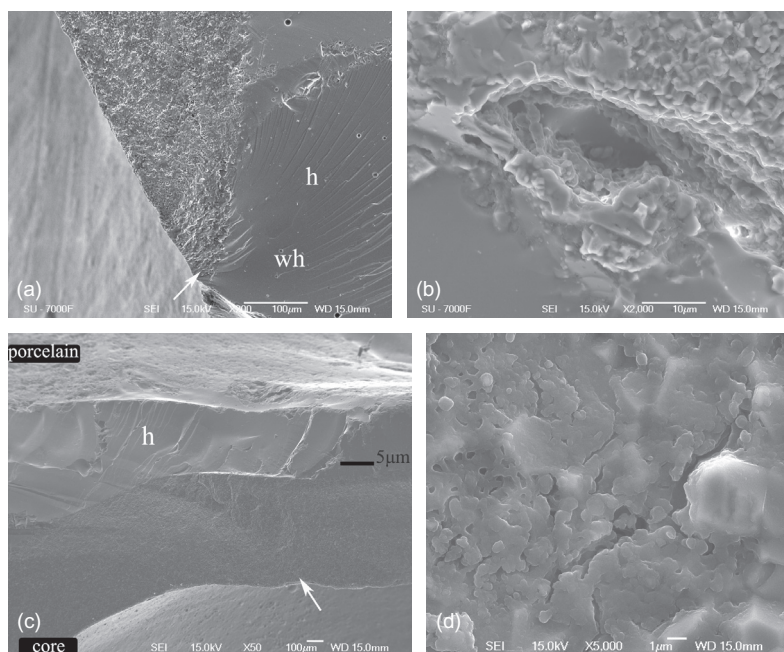
FIGURE 5.8   High magnification SEM images of the regions around the fracture origins of failed ceramic dental crowns by following the indications of hackle lines (h) and wake hackles (wh). (a) The fracture origin of a failed incisor bi-layer alumina all-ceramic crown is indicated by an arrow. (b) The high magnification image of the fracture origin in "a" reveals a 30-40 μm large void in the alumina core very close to the alumina-porcelain surface. This void is a processing artefact and clearly identified to be responsible for the crown fracture. The inserted image is taken from another direction of the fracture surface. (c) Micrographs of the fractured molar bi-layer alumina all-ceramic crown from the area indicated by the arrow. (d) The high magnification image of the fracture origin in "c" reveal a substantial grain inhomogeneity and local micro-cracks which reduce strength.

where wake hackles are seen inside the porcelain shell and these hackles are seen progressing away from the inner core (Figure 5.8). The fracture features indicated that the primary crack initiated near the proximal margin inside the core ceramics (Figure 5.8a). High magnification SEM images of this area revealed a 30–40 μm void inside the alumina core (Figure 5.8b). Another example of a failed molar alumina crown is found in Figure 5.8c. Using the same analytical approach to follow surface indications like arrest and hackle lines, the primary defect was found to be located inside the ceramic core close to the inner surface. A high magnification SEM image of the region near the fracture origin reveals the presence of 20 μm long micro-cracks (Figure 5.8d).

5.2.2.2   Hertzian Cone Cracks Under Compressive Stress

Hertzian cone cracks result from blunt contact forces applied to a relatively flat surface. To model contact stresses during chewing, a test was done involving a steel ball cyclically loaded onto dental restoration materials. The results
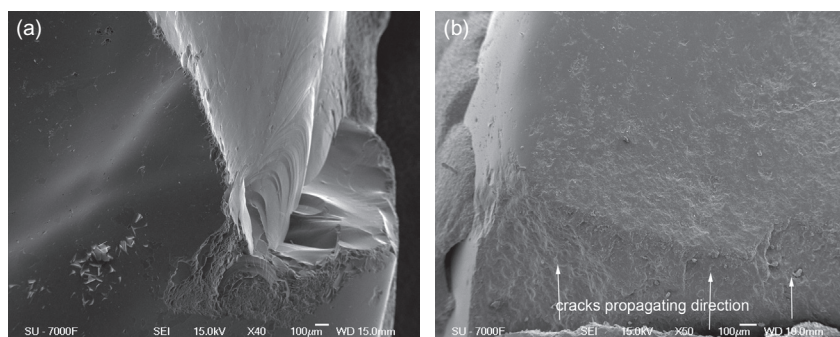
FIGURE 5.9 SEM images showing the fracture patterns of porcelain veneer in bi-layer ceramic crowns after repeated bite loads. (a) Typical Hertzian cone cracks observed on the occlusal porcelain surface of a failed bi-layer zirconia all-ceramic crown. The cone crack initiated at the occlusal contact of the opposite tooth cusp. (b) The porcelain fracture area of a failed galvano-gold bi-layer crown showing cracks and chipping. The crack propagating direction is marked by white arrows and the crack starts from the origin at the core metal/porcelain interface moving towards the porcelain surface of the crown.

from such tests show frequent Hertzian cone cracks, also simply referred to as 'cone cracks' or 'Hertzian cracks.'

Hertzian cracks initiated on the surface of porcelain shells under repetitive compressive bite loads can lead to veneer porcelain chipping off or veneer delamination in bi-layer ceramic restorations. Damage in the veneer does not always result in further ceramic core cracking. Thus, many observed occlusal porcelains in the clinic contain some visual Hertzian cracks, but they do not initiate catastrophic failure. Sometimes, the Hertzian cone crack looks like an oval instead of a circle. This crack can be described as a multi-origin cone crack. There are no obvious marks at an early stage of cone cracking that predict the exact failure-initiating flaw where fracture might later originate.

Hertzian cone cracks reflect fatigue damage of porcelain under repeated/cyclic compressive bite loads as micro-cracks are initiated in the veneering porcelain at the contact zone of the opposite natural tooth cusp. Thus, contact at the same place during every mastication cycle can generate fatigue cone cracks. An example of this can be seen in Figure 5.9a. In other cases, multi-origin oval cracks are observed, implying that the occlusal contact points between the opposite natural tooth cusp and the porcelain surface move around during different mastication cycles. Thus, Hertzian cracks propagate progressively under repetitive bite loads until cracks appear in the porcelain-core interface. Cracks do not penetrate into the strong ceramic core and are deflected along the interface and yield porcelain delamination. See Figure 5.9a for the SEM image.

5.2.2.3 Cracks at Interface Under Tensile Stress

In the case of failed bi-layer metal-ceramic crowns with porcelain shells, the fracture origin could be detected at the core metal/porcelain interface as

micro-cracks initiated by a momentary high tensile stress. When the cracks spread along the interface, the failure of the porcelain shell is unavoidable. The tension stress established in the porcelain layer at the interface is due to the plastic deformation of the core metal under the bite force. The resistance to such plastic deformation is related to the mechanical properties of the relatively soft metal, as well as the thickness of the coping. A failed upper incisor gold–ceramic crown is illustrated in Figure 5.9b. The arrest line has the concave side pointing towards the core metal/porcelain interface, which shows that the fracture is initiated at this interface.[2–10]

5.2.3   Flaws and Defects

5.2.3.1   Flaws/Defects and Failure Origins

In the parlance of the engineer or scientist, irregularities that initiate fracture are termed flaws or defects. Virtually all brittle materials are imperfect and contain small irregularities that can potentially behave as flaws. That the material contains flaws or defects below the critical size does not necessarily mean that the material has been prepared improperly or is somehow faulty. However, there are instances where larger defects or flaws do indicate defective material. Flaws are either surface- or volume-distributed, whilst inclusions are almost always volume-distributed. Glass usually, but not always, breaks from surface-distributed flaws. Finally, ceramics can fracture from either surface or internal flaws/defects.

5.2.3.2   Defects in Porcelain

Gas Bubbles

Gas bubbles are among the most common defects found in the porcelain shells of fractured crown samples. The diameter of the bubbles ranges from 10 to 100 μm, with a large population of bubbles of smaller sizes. Most gas bubbles are found near the surface area distributed in a ~20 μm thick surface zone (Figure 5.10).

Inclusions

Some gas bubbles in porcelain demonstrate unusual microstructural features, such as that shown in Figures 5.11a and b. The bubbles contain a solid core of agglomerated small particles composed of a high concentration of the elements calcium, phosphorous, and sulphur as revealed by EDS. These impurities are taken up during the veneering process, most likely gypsum or other materials that are widely found in dental laboratories. Some voids observed on the top surface indicate that a part of these gas bubbles are open (Fig.5.11a). This implies that a high gas pressure has built-up inside the bubble/void during processing, probably due to the partial decomposition of impurities. This hypothesis is confirmed by EDS, which reveals a high concentration of calcium and phosphorous inside the voids of broken bubbles.
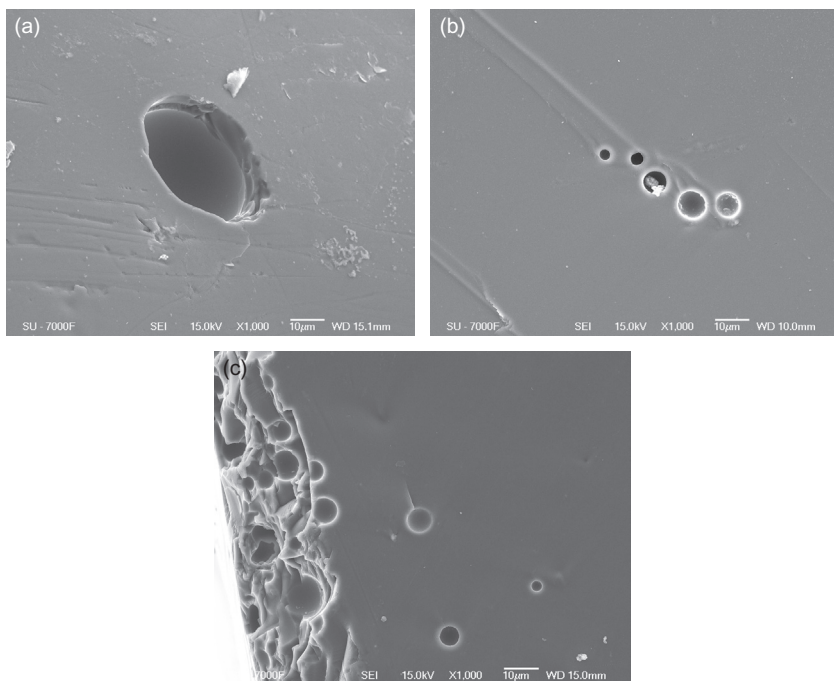
FIGURE 5.10 High magnification SEM images of gas bubbles found in veneering porcelain. (a) A large gas bubble observed on the outer surface of porcelain veneer. (b) Single gas bubbles observed on the fracture surface of the veneering porcelain of a failed bi-layer alumina all ceramic crown. (c) The gas bubbles observed on the fracture surface of the porcelain veneer. Note the high population formed closer to the surface at left.
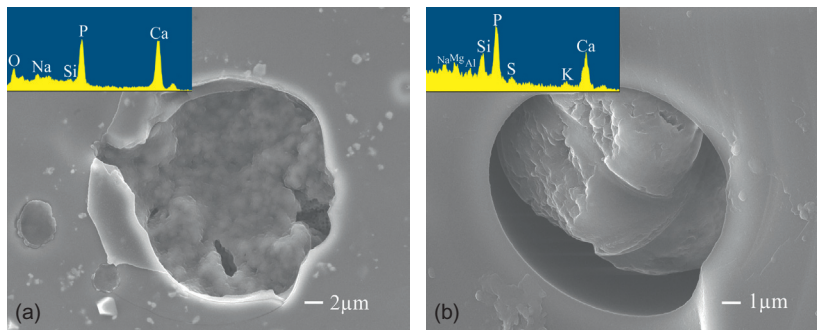
FIGURE 5.11 The SEM micrographs show inclusions in veneering porcelain. (a) Gas bubble containing a solid particle with a high concentration of calcium, phosphorous, and sulfur, observed in porcelain veneer. (b) An approximately 30 μm, open gas bubble; inside impurities are found that are enriched in calcium and phosphor as detected by EDS analysis. This image is a fracture surface of the porcelain veneer.
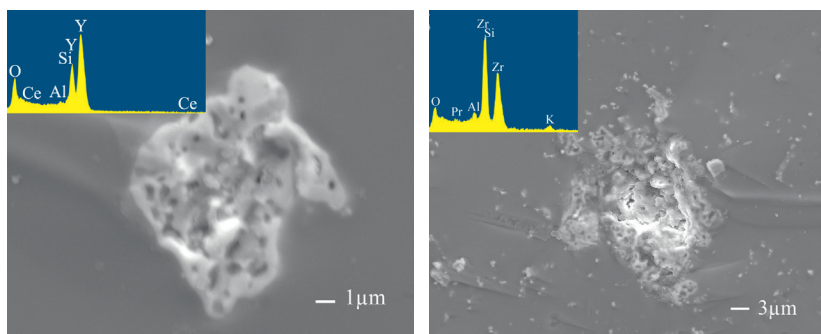
FIGURE 5.12   SEM images of the fracture surface of porcelain veneer that reveal a large particle agglomerate inside. (a) A large agglomerate of particles enriched in yttrium observed in the enamel porcelain layer. (b) A 20–30 μm agglomerate of particles enriched in zirconium observed in the porcelain layer.

Agglomerates

Agglomerates of small crystals up to 10–30 μm in size are occasionally observed on the fracture surface of the porcelain veneer, as demonstrated in the SEM images shown in Figure 5.12. EDS analysis confirms that these agglomerates consist of small yttria or zirconia particles pre-added as porcelain constituents. Micro-cracks are often found inside these types of particle agglomerates.

Compositional Inhomogeneities

Compositional inhomogeneities are microstructural irregularities related to the non-uniform distribution of primary constituents or the presence of a secondary phase. Porcelains are found to essentially be composites of silicate glasses and crystalline particles. Crystallization of glass is not a common process observed for these silicate glasses. However, local crystallization is occasionally observed and characterized as 'compositional inhomogeneities.' Typical examples are shown in Figures 5.13a, b and c. Local crystallization is often found on the top surface of the porcelain shell or in the bulk, accompanied by gas bubbles, which suggests heterogeneous nucleation of crystals at the gas or air–glass interface (Figure 5.13c).

5.2.3.3   Defects in Ceramics
Voids

Voids are the easiest flaws to find and identify. In ceramics they are often equiaxed, but can easily assume a myriad of odd shapes, as shown in pores in zirconia in Figure 5.14. Large voids of up to 20–30 μm diameter are often observed in dental core ceramics (Figures 5.14a, b, and c). Another example is observed in the fracture origin region of a molar alumina crown (Figure 5.14f). Other pores are formed due to the inhomogeneous packing of powder granules (Figure 5.14h).
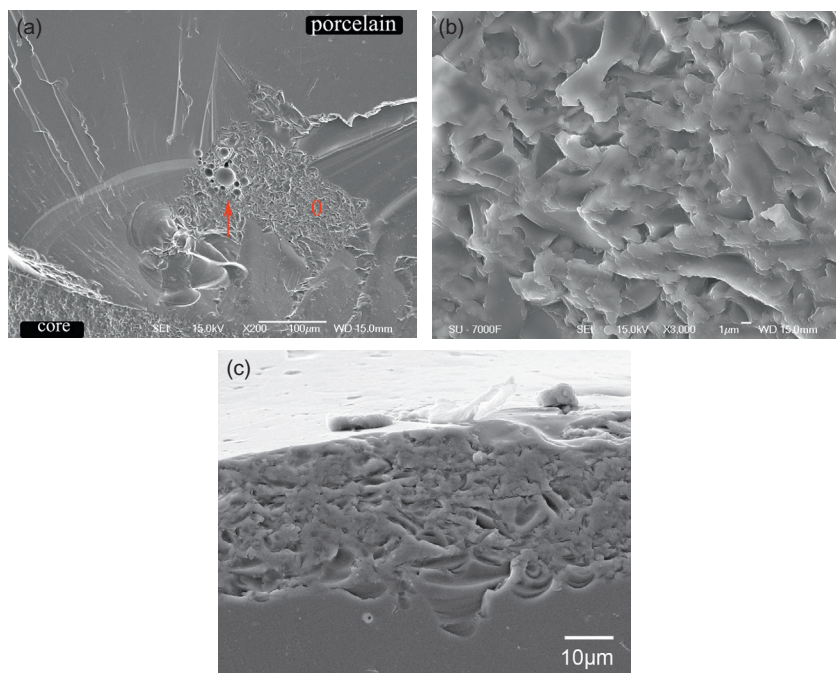
FIGURE 5.13   SEM images of compositional inhomogeneities found in porcelain veneer. (a) Image of the fracture surface of porcelain veneer of a bi-layer alumina all-ceramic crown. The local inhomogeneous crystallization associated with the gas bubble cluster is seen, marked by a arrow. (b) The high magnification image of 'a' is an enlarged view of the crystalline region marked by red "0". (c) The fracture surface of porcelain veneer revealed inhomogeneous crystallization distributed in a 30–50 μm thick surface zone.

Porous Regions and Seams

Porous regions are volume-distributed flaws that consist of three-dimensional zones of micro-porosity regions (Figures 5.14f and g). These can be obvious or very subtle, and optical microscopy may not be effective since the color and contrast at the fault origin match the surrounding material. SEM microscopy is usually needed to identify these flaws. An example of a porous region being the fracture origin is illustrated in Figure 5.14f. Porous seams are similar to porous regions, but are more planar or two-dimensional. If the material separates completely between these seams, the flaw might be more aptly described as a processing crack (Figure 5.14g).

Agglomerates

Agglomerates are volume-distributed flaws that consist of a cluster of grains, particles, platelets, or whiskers, or a combination thereof. They are observed as a commonly occurring flaw in sintered ceramics made from powder granules that are prepared by spray drying. Spray-dried agglomerates are often
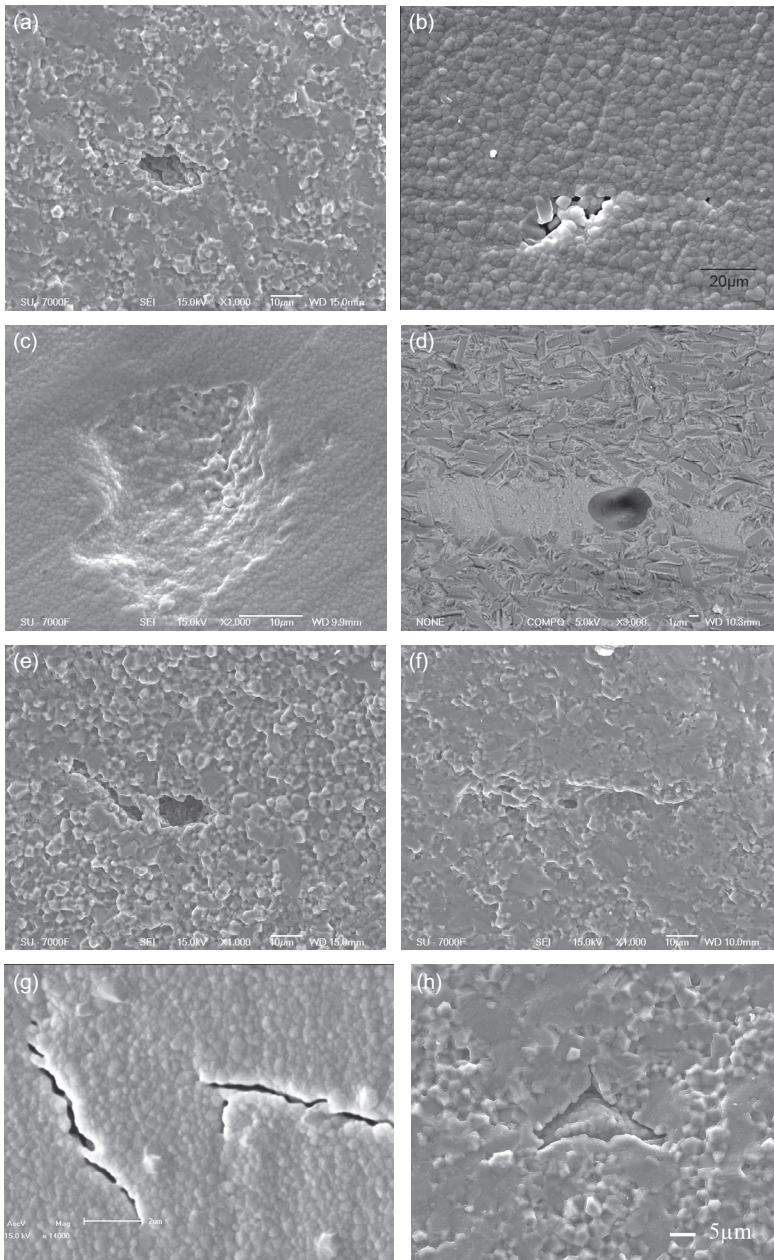
FIGURE 5.14 SEM micrographs showing pores, voids, and other flaws found in ceramics. (a) A large pore in alumina is seen in the middle of the SEM image, with a size of 20μm. (b) A large pore present on the fracture surface of a zirconia ceramic bar, with size around 20–30μm. Electron charging created the bright contrast at the pore edge. (c) The SEM image shows a pore at the surface of a zirconia disc. (d) A pore present on the fracture surface of lithium disilicate glass ceramic bar. (e) The fracture surface of a broken alumina core shows an irregular pore. (f) Examples of the porous region on the fracture surface of a failed alumina core. (g) Seams present on the surface of a tetragonal zirconia poly-crystal zirconia (3Y-TZP) disc. (h) A triangle-shaped void observed near the fracture origin of the fractured alumina core and formed due to inadequate packing of powder granules. Agglomerates consolidate faster than the poorly packed matrix leaving an empty void-like crack.
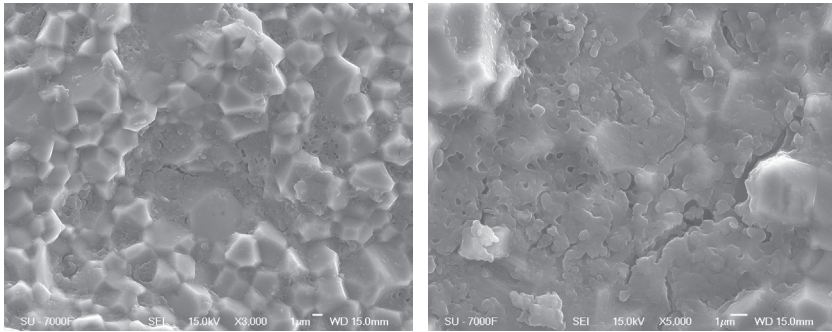
FIGURE 5.15   SEM micrographs illustrating alumina ceramics microstructure that contain small areas with substantial grain-size inhomogeneity. The presence of local micro-cracks that reduce strength are easily seen in the SEM images.

hollow with a dense shell. Inadequate packing before sintering of such agglomerates often results in a shell-like void at the agglomerate intersections. The color and reflectivity of this void are almost identical to the matrix. An example is shown in Figure 5.14h.

Compositional Inhomogeneities

Compositional inhomogeneities are microstructural irregularities related to the non-uniform distribution of the primary constituents, an additive, or a secondary phase. They may have a color or reflectivity difference compared to the matrix. Sometimes they stimulate grain growth or leave small pockets of glass in the ceramic structure. Figure 5.15 shows the microstructure of alumina ceramics containing small areas with a substantial grain-size inhomogeneity. Micro-cracks may coexist with poorly densified regions that have unusually small grains in the ceramic microstructure. This feature is rarely seen in densely sintered alumina ceramics, but an example is shown in Figure 5.15b. Elemental analysis by EDS reveals high calcium content in the small-grain region illustrated in this image, which indicates a possible contamination during the alumina core manufacture.

Large Grains

Large grains can be either a single grain or a cluster of grains that have significantly greater size than the normal grain size distribution. Large grains occur due to local exaggerated grain growth that might be triggered by a fluxing impurity during ceramic sintering. Subsequent EDS analysis can confirm the presence of any remaining elemental impurity in the area. Large grains are typical fracture origins as they often exceed the critical size for fracture of the sintered ceramics. The crack path may circumvent or pass straight through the large grains. Examples of large grains present at the fracture surface of a broken alumina ceramic core can be seen in Figure 5.16.
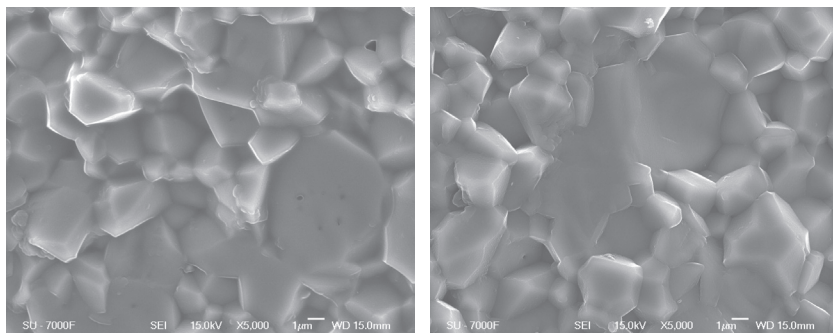
FIGURE 5.16   Examples of large grains found at the fractured surface of a broken alumina core. Trans-granular fracture of a cluster of large grains is easily seen in the first image.

5.2.3.4   Classification of Flaws/Defects

The flaws/defects/irregularities that act as fracture origins in advanced ceramics can develop during or after fabrication of the material. Large irregularities (relative to the average size of the ceramics microstructure) such as voids, agglomerates, and some inclusions are typically introduced during processing.

The manufacture of ceramic cores usually involves three processing steps, namely, green body formation by cold isostatic pressing of powder granules; machining of either green cold pressed, or partially sintered bodies, to form the required geometries; and final sintering. The large voids found in alumina cores are formed due to the inhomogeneous packing of powder granules. Once a large void has formed in the sintered microstructure it is hard to refill it by diffusion during normal pressure-less sintering. These voids are often found in alumina ceramics, but are rarely seen in zirconia ceramics. This can reflect the characteristics of the initial powder processing (i.e. particle size; inside distribution of sintering aids and binders; granule formation; and their packing flexibility). In general, by using softer granules or by applying a wet-forming process, it is possible to avoid packing voids.

One may consider inclusions and other irregularities as extrinsic flaws in a material, but due to the fact that they occur naturally during fabrication and cannot be avoided, they could also be considered intrinsic. For example, if a material customarily has a ball-milling step in the process, mill fragments can flake off and become inclusions in every batch.

The local formation of micro-cracks at the surface of the alumina-sintered cores can be a consequence of the contamination of the alumina green-body surface by the surrounding dust. A calcium-rich compound seems to hinder the densification of alumina at a small spot during sintering, as shown in Figure 5.15. Thus, special caution is always needed to maintain a clean working environment.

Still other flaws can be introduced during further processing as a result of machining, handling, impact, wear, and/or corrosion. Usually these can
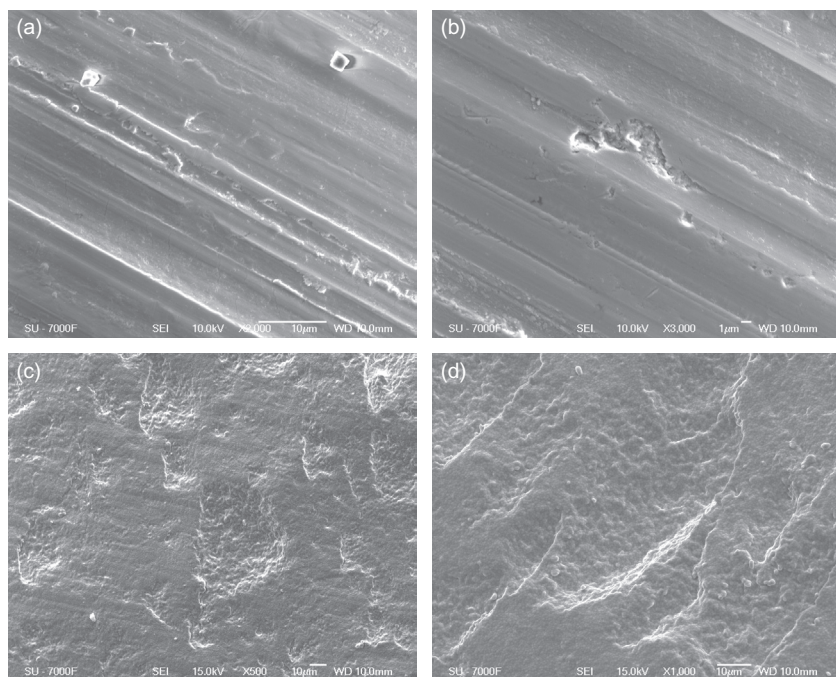
FIGURE 5.17 Examples of damage-handling in zirconia ceramics illustrated by SEM images. Defects after grinding and polishing are presented in (a) and (b), and defects after CAM milling are presented in SEM images (c) and (d).

be considered as having extrinsic origins. computer-aided design/computer-added manufacturing (CAD/CAM) processing is the main method for shaping a ceramic block into copings for dental crowns. During this process, machining defects such as cracks or scratches are introduced. Handling damage can include scratches, chipping, or other impact flaws. Scratch damage from machining, for example, varies widely depending upon the ceramic material and milling parameters. Such damage can be reduced by adjusting the process accordingly. Sometimes grooves with severe cracking may be generated by using high loads with abusive tools/conditions; a few of these examples can be seen in Figures 5.17a–d.

5.2.4   Wear

The wear between ceramic dental restorations and the adjacent tooth enamel generates another type of defect on the surface of restorations that can be well characterized by SEM. Wear is mainly determined by the friction properties and the micro-topography of the restoration porcelain. Commonly, the worn surface of the porcelain veneer shows parallel
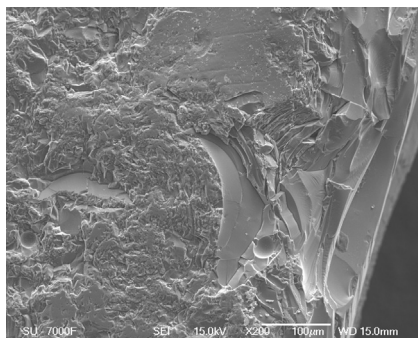
FIGURE 5.18 Illustration of wear scars (after long use) upon the porcelain surface of a bi-layer molar alumina all-ceramic crown.

grooves, micro-cracks, local mass loss, or increased overall roughness (Figure 5.18). The wear defects can be ascribed to the circular frictional movement between the porcelain and natural tooth cusps. The wear performance of dental crowns is especially affected by the surface finishing. In general, the frictional coefficient between enamel and polished restorations is smaller than that of rough restorations.[1,3,4,10]

5.2.5 Fractographic Case Studies

5.2.5.1 Zirconia/Porcelain Bi-layer All-ceramic Crown

A failed posterior zirconia bi-layer ceramic crown was removed in the clinic by carefully drill-cutting into two parts without destroying the chipping area. Water was used to cool the crown and abutment tooth. The broken crown was fabricated using commercially available products and individually produced in a central production line following CAD/CAM principles. The crown was assembled by building up the porcelain shell according to a well-established, dental laboratory, multi-step, layer-by-layer routine procedure.

Porcelain chipping-off was observed in the distal axial wall initiated from the distal marginal ridge on the occlusal surface of the upper molar zirconia crown where a high compressive stress concentration always builds up under bite force (Figure 5.19a). A thick veneering porcelain shell can be seen here that demonstrates porcelain chipping-off. When a crack originating at the veneering porcelain surface reaches the porcelain–core interface, it is deflected along this interface, thus causing delamination. Crown cracking is avoided since the zirconia core possesses a high bending strength. Veneer surface flaking is observed near the proximal marginal ridge.

A fractured occlusal surface that illustrates chipping-off is shown in Figure 5.20a. It is obvious that the fracture is initiated at the occlusal contact on the distal marginal ridge with cracks propagating towards the axial wall. Closer
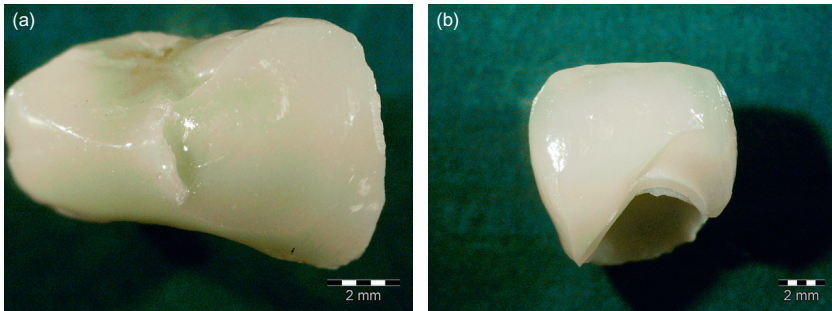
FIGURE 5.19 Pictures of clinical failure of bi-layer, all-ceramic crowns by stereo-microscopy. (a) An upper molar bi-layer zirconia crown, which failed by porcelain chipping-off in the distal axial wall as a result of the bite load on the distal marginal ridge. (b) An incisor bi-layer alumina crown broken into two pieces on the incisal 1/3 of the labial surface as a result of a strong bite load. The crack is initiated at the mesial margin from where it propagates to the distal margin through the labial surface and through both inner alumina core and outer silicate porcelain layer.
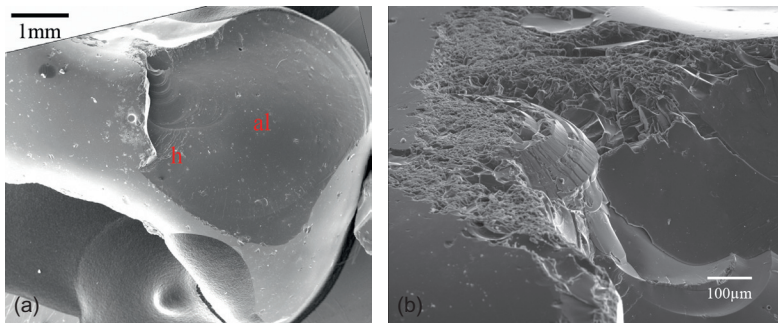
FIGURE 5.20 SEM micrographs that illustrate porcelain chipping-off damage. An all-ceramic crown with a zirconia core was failed clinically. (a) The porcelain chipping-off damage on occlusal surface observed in the upper molar zirconia crown. The black arrow indicates the origin of a surface Hertzian cone crack yielding the subsequent porcelain chipping-off and crown failure. Note that large gas bubbles from the veneering process leave visible tracks on the porcelain shell surface. (b) A Hertzian cone crack observed in the porcelain layer of the upper molar zirconia crown.

SEM inspection revealed Hertzian cone cracks on the occlusal surface of the porcelain shells (Figure 5.20b). Surface Hertzian cracks are formed and propagate progressively under repetitive bite load, resulting in massive porcelain damage/flaking. Porcelain delamination occurs on the interface leaving the zirconia core unharmed.[4]

5.2.5.2 Alumina/Porcelain Crown

An anterior alumina crown installed on the right central incisor was broken catastrophically into two pieces. The inner alumina ceramic core was made of a commercial product and individually produced in a central production line
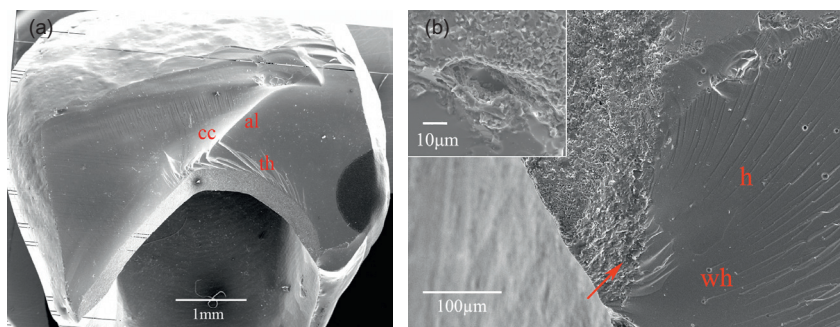
FIGURE 5.21   SEM micrographs of a clinical failed bi-layer alumina all-ceramic crown. (a) Overview by low magnification SEM of a broken incisor bi-layer all-ceramic crown. The lingual part is illustrated by merging 22 individual SEM images. Following the indications given by arrest lines (al), wake hackles (wh), and compression curl (cc), the fracture origin is located at the mesial margin area, as indicated by the arrow. (b) High magnification SEM image of the region around the fracture origin and the indications of hackle lines (h) and wake hackles (wh). The red arrow indicates the fracture origin of the incisor alumina crown. It reveals a 30–40 µm void in the alumina core very close to the alumina–porcelain interface. This void is a processing fault that is responsible for the crown failure. The inserted image of the void is taken from another direction of the fracture surface.

following CAD/CAM principles. The silicate-based porcelain veneer is also a standard product tailored to fit the alumina. The crown was assembled by building-up the porcelain shell according to a well-established, dental laboratory, multi-step, layer-by-layer routine procedure.

The anterior alumina crown is entirely broken into two pieces on the incisal 1/3 of the labial surface (Fig.5.19b). The margin area is always the thinnest part of the whole incisor crown, with the proximal margins under highest tensile stress upon bite load. A clear major arrest line is visible inside the porcelain shell of the fracture surface of an anterior alumina crown (Figure 5.21a). The arrest line has its concave side pointing towards the proximal margin and both hackle and twist hackle lines are observed. Wake hackles are seen in association with gas bubbles inside the porcelain shell, with hackles observed on the side away from the inner core. Two major compression curls can be observed, one close to the fracture origin and another in the center of the fracture surface. The primary crack that leads to failure is initiated near the proximal margin inside the core ceramics, as indicated by a white arrow to the lower right in Figure 5.21a. Higher magnification SEM images of this area reveal a 30–40 µm void inside the alumina ceramics (Figure 5.21b). In addition, a possible secondary fracture origin was observed close to the incisal edge with the crack propagation direction towards the top surface; this resulted in only local porcelain chipping-off.

In general, cracks initiated on the inner surface of the ceramic core under tensile stress result in the fracture and failure of the entire crown.[4]

ACKNOWLEDGMENTS

REFERENCES

1. Quinn GD. Fractography of ceramics and glasses: US Department of Commerce, Technology Administration, National Institute of Standards and Technology; 2007.
2. Quinn GD, Hoffman K, Quinn JB. Strength and fracture origins of a feldspathic porcelain. Dent Mater 2012;28(5):502–11.
3. Wang L, Liu Y, Si W, et al. Friction and wear behaviors of dental ceramics against natural tooth enamel. J Eur Ceram Soc 2012
4. Liu YH, LGH, Grüner D, Feng HL, Shen ZJ. A pilot fractographic study of clinically failed ceramic dental restorations. The First P-I Brånemark Scientific Symposium; 2010 2009; Gothenburg: Quintessence Publishing; 2010.
5. Quinn GD, Studart AR, Hebert C, et al. Fatigue of zirconia and dental bridge geometry: design implications. Dent Mater 2010;26(12):1133–6.
6. Quinn JB, Sundar V, Parry EE, et al. Comparison of edge chipping resistance of PFM and veneered zirconia specimens. Dent Mater 2010;26(1):13–20.
7. Quinn JB, Quinn GD, Kelly JR, et al. Fractographic analyses of three ceramic whole crown restoration failures. Dent Mater 2005;21(10):920–9.
8. Scherrer SS, Quinn JB, Quinn GD, et al. Fractographic ceramic failure analysis using the replica technique. Dent Mater 2007;23(11):1397–404.
9. Scherrer SS, Quinn GD, Quinn JB. Fractographic failure analysis of a Procera AllCeram crown using stereo and scanning electron microscopy. Dent Mater 2008;24(8):1107–13.
10. Liu Y, Feng H, Bao Y, et al. Fracture and interfacial delamination origins of bilayer ceramic composites for dental restorations. J Eur Ceram Soc 2010;30(6):1297–305.

Advanced Ceramics

David Salamon

CEITEC BUT – Central European Institute of Technology, Brno University of Technology, Brno, Czech Republic

Contents

6.1   INTRODUCTION

For the general public, the term ceramics is connected with pottery (representing the materials class), brittleness (representing the most characteristic property), and household and construction (representing typical applications). However, as a materials definition, the term ceramics is much broader and encompasses a variety of mainly polycrystalline inorganic non-metallic materials that are commonly formed into engineering shapes from powders at room temperature. They gain their typical physical properties through a high-temperature firing process. It is worth mentioning here that the Anglo-Saxon term ceramics often includes glass, enamel, and glass-ceramic items that are mainly amorphous and can be formed from melts. It also includes inorganic cementitious materials (cement, plaster, and lime) that do not require firing to acquire their final properties.

6.1.1   Classification

Traditionally, ceramics are made entirely by natural silicate and aluminosilicate minerals composed of aluminum, silicon, and oxygen, plus countercations (Ca, Mg, Na, K, etc.), with clay as a major constituent that allows shaping due to its plasticity. These materials are now classified as traditional ceramics. They are characterized by their poorly defined properties, poor reproducibility, and inferior reliability. Traditional ceramics are processed through a conventional procedure starting from the preparation of ceramic suspensions, and ending with sintering, as summarized in Figure 6.1.

Advanced ceramics are referred to as a new family of ceramics made by synthetic chemicals of high purity. Organic binders are often added to assist shaping. These ceramics are targeted at various industrial applications that demand high performance. Chemically, advanced ceramics are most frequently composed of oxides, nitrides, and carbides, though diamond and graphite, by definition, also belong to this category. Therefore, advanced ceramics are often classified based on their compositions as oxide or non-oxide ceramics. Oxide ceramics include binary oxides, aluminates, ferrites, titanites, niobates, zirconates etc.; non-oxide ceramics cover carbides, nitrides, borides, carbon etc.; and ceramic composites (i.e. combinations of oxides and non-oxides).

At the beginning, advanced ceramics were developed to optimize a single primary property for a single targeted application. In recent decades, novel advanced ceramics with tailor-made multi-functionalities have been developed that may integrate even naturally conflicting properties. Conventionally, multi-functionality has been achieved either at the expense of high performance, by diminishing one property in order to obtain acceptable values of other properties, or by combining different materials, as in composite structures. Those are relatively simple tasks for large components produced on a large scale. However, as the sizes of ceramic components diminish, designs must become

	Traditional ceramic	Advanced ceramic
Materials preparation	Raw materials Clay Silica	Precipitation Spray drying Freeze-drying Sol-gel Vapor phase
Shaping	Slip casting Pressure casting Potters' wheels	Slip casting Injection molding Hot pressing Hot isostatic pressing Rapid prototyping
High-temperature processing	Flame kiln	Electric furnace Hot press Vapor depositions Microwave furnace Plasma spraying
Finishing	Erosion Glazing	Laser machining Plasma coating Polishing Erosion
Characterization	Visible examination Light microscopy	Light microscopy X-ray diffraction Electron microscopy Surface analytical methods

FIGURE 6.1   The complexity is increased in processing advanced ceramics compared to traditional ceramics.

more efficient so that the materials must be capable of a greater range of properties than is currently available, and properties that naturally conflict must be developed in alternative ways. Therefore, new ceramic structures with intriguing properties are being developed for a variety of structural, functional, and bio-medical applications. In this way, advanced ceramics were also referred to in the literature as 'special,' 'fine,' 'technical,' 'high-tech,' or 'high-performance' ceramics. Based on the intended application, advanced ceramics can be further divided into three categories, namely, structural or engineering ceramics; functional ceramics; and nuclear ceramics.

Structural ceramics are known for their superior mechanical behaviors (e.g. mechanical strength, hardness, and wear resistance), particularly in corrosive environments and at high temperatures. These ceramics are usually selected to replace existing materials, normally metals. The majority of ceramics used in restorative dentistry today, such as zirconia, alumina, and glass-ceramics, belong to this category. Functional ceramics are characterized by their usual

functions, due to their tailor-made structures and properties. Ceramics are normally known as electrical insulators, but by manipulating their composition and microstructure, they can be turned into semiconductors and even superconductors. Many other properties/functions generated in functional ceramics, such as dielectric, ferroelectric, piezoelectric, thermoelectric, and multiferroic properties, are unique and can rarely be achieved in any other types of materials. Functional ceramics are thus selected as they provide unique functions. The application of functional ceramics in restorative dentistry is, up until now, rather rare, although in the future, piezoelectric ceramics may be used for sensing bite force.

Uranium oxide and nitride are used as nuclear fuels in the forming of ceramics and are referred to as nuclear ceramics.

The preparation of advanced ceramics usually involves more sophisticated processing steps. Figure 6.1 compares the processing technologies commonly involved in the preparation of advanced and traditional ceramics. More details about advanced ceramic processes are provided in the next chapter. In short, processes become rather complex and can differ for various applications during the development of advanced ceramics.

6.1.2   Historical Development

While traditional ceramics have been used for over 25,000 years, advanced ceramics have only been developed within the last 120. The history of sintering chemically defined powders started between 1879 and 1911 during the battle between electric and gas lighting, and between two rival methods of electric lighting. In Austria, Baron Carl Auer von Welsbach (1858–1929), discovered how to improve light produced by applying a flame to certain rare-earth oxides, specifically incandescent light by heating with a Bunsen burner. He patented a mixture of yttria/lanthana with magnesia/zirconia. The Welsbach mantle, marketed in 1890, was probably the first sintered oxide ceramic based on chemically prepared raw materials. The ionic conduction used in Nernst lamps (Walther Nernst, 1864–1941) was in response to the limitations of the filament lamp in 1890 and its limitations such as poor vacuum pumps. Modern analysis has shown that the lamps contained mainly zirconia with the addition of yttria-group rare earths. (Nernst's lamps were steadily improved, but eventually capitulated to the tungsten filament lamp after 1911.)

The development of *functional ceramics* quickly sped with the burgeoning radio and television broadcasting industry in the 20th century. The need for special heat-resistant materials that could withstand high-frequency electromagnetic fields resulted in the development of materials such as steatite (magnesium silicate). Subsequently, other electro-ceramics such as magnetic ceramics (ferrites) were developed, followed by capacitor ceramics (titanates), and electromechanical ceramics (piezoelectric ceramics). The boom in the electronics industry drove the need for protecting tiny transistors and

integrated circuits from ambient conditions and led to the development of ceramic packaging materials that facilitated further miniaturization of devices.

Together with the discovery of new materials, there was also an increase in the understanding of their structure and behaviors, which led to new applications for electro-ceramics. Today, more than half of the market for advanced ceramics is electrical and electronic ceramics and packages. In the 1960s, new functional properties of ceramic materials were implemented, such as solid-oxide fuel cells, which use a solid zirconia electrolyte. The complexity of functional ceramic materials is still growing and the discovery of high-temperature superconductivity in a family of oxide ceramics with complex chemical compositions in 1986 opened up enormous possibilities. The original promises have not yet been fulfilled, but the general possibilities of ceramic functionality are still to be fully explored and many ground breaking discoveries are expected in the future.

S*tructural ceramics* started as composites. In 1925, Krupp introduced a tough cermet (ceramic–metal composite) in which very hard tungsten carbide crystalline grains are held together by a soft matrix of metallic cobalt. This material was originally used to make wire-drawing dies to replace costly diamond, and was later used for metal-cutting tools. It was the first of many different cermets with impressive mechanical properties. Further understanding of the sintering process led to dense ceramic materials prepared from defined single phases. In the early stages of development, all such ceramics are porous after firing and are therefore opaque. Robert Coble found that the addition of a small amount of MgO inhibited discontinuous grain growth in Al_2O_3 and allowed it to be sintered to a theoretical density to yield a translucent product. Dense alumina (Al_2O_3) doped with magnesia (MgO) exhibits such optical translucency and stability and is suitable for use as the envelops for high-pressure Na-vapor lamps. Operating at high temperatures, Na-vapor lamps have the highest luminous efficiency and are dominant in outdoor lighting even now.

An entirely new structural ceramic material, silicon nitride, was introduced to the market in the early 1950s. Its unique, high-temperature properties were beyond those of the existing nickel-based superalloys. The feasibility of components made from silicon nitride-based ceramics has been demonstrated in the production of ceramic gas turbines. Nevertheless, the materials applications have not yet reached their full potential due to the lack of low-cost commercial processes for manufacturing such complex silicon nitride parts. The breakthrough discovery of ceramic steel in 1975 demonstrated that ceramics were not always inherently brittle or with low toughness.[1] This finding highlighted the potential of zirconia (ZrO_2)-based or added ceramics for gaining improved strength and toughness by utilizing stress-induced phase transformation from tetragonal to monoclinic zirconia.

The 20th century saw the greatest advancements in human history in ceramics and materials technology. The potential of advanced ceramics has been realized due to advances in the understanding of ceramic chemistry,

crystallography, and the extensive knowledge gained in regard to their production. Significant improvements in the fracture toughness, ductility, and impact resistance of ceramics has been achieved, thus, the gap in physical properties between ceramics and metals has started to close. The space shuttle is a typical example that demonstrates the capability and potential of advanced ceramics.

6.2   HIERARCHICAL STRUCTURES

6.2.1   Atomic Bonding and Atomic Level Defects

Most ceramics materials are polycrystalline with generally more complex crystal structures than those of metals. Such complexities have several origins. First, the constituent crystals of ceramics consist of atoms with significantly different sizes. Second, the charges of atoms are often diverse. Both of these factors are responsible for a more complicated arrangement of atoms in crystalline structures.

The type of inter-atomic bond affects the crystal structure that a material adopts. Ionic bonds have strong attraction forces to hold the solid together, no preferred bonding direction, and charge neutrality. Covalent bonds have bond direction, but the highest atomic packing density is sacrificed for the direction of the bonds. A simplified determination of bond character can be done based on electronegativity, which is listed in the periodic table of elements. Electronegativity is the measure of an atom's strength to attract electrons. Both electronegativity differences and average electronegativities are used to mainly classify binary compounds, where F_2, CsF, and Cs, are extreme examples of covalent, ionic, and metallic compounds, respectively. The suggested (Figure 6.2a) covalent compounds are characterized by low electronegativity differences and also by high average electronegativity. This is in contrast to (Figure 6.2b) ionic compounds, which are characterized by high electronegativity differences and require intermediate average electronegativities. (Figure 6.2c) Metals and metallic compounds have low electronegativity differences and low average electronegativities.[2] Figure 6.2 illustrates the difference between bond types.

Many physical attributes of crystalline solids are determined by the geometric arrangement of their constituent atoms. Visualization of atomic packing in crystalline solids takes each atom as a 'hard sphere' (Figure 6.3a), and then identifies the smallest repeating cluster of atoms, the unit cell. The unit cell is defined in conventional crystallography by the following rules: (1) The unit cell should have the same symmetry as the crystal (Figure 6.3b), where the base vectors are parallel to symmetry axes or perpendicular to symmetry planes; (2) The origin of the unit cell is usually a center of symmetry; (3) The base vectors should be short, and the cell volume minimized. Exceptions arise only when the symmetry is increased by enlargement of the cell; (4) The angle between the axis should be 90° and eventually >90°.
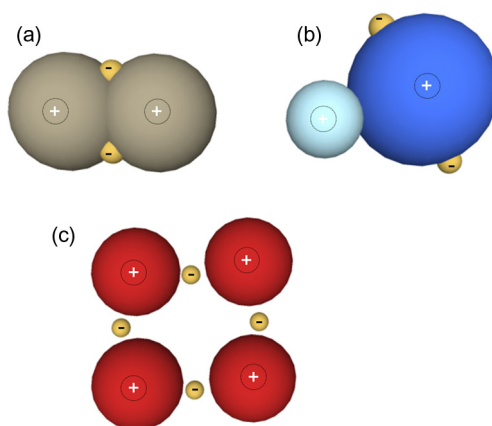
FIGURE 6.2   Schematic illustrations of the three basic types of primary bonds: (a) Covalent bond, valence electrons are shared; (b) Ionic bond, valence electrons are dominantly attracted by anion; (c) Metallic bond, valence electrons are delocalized.
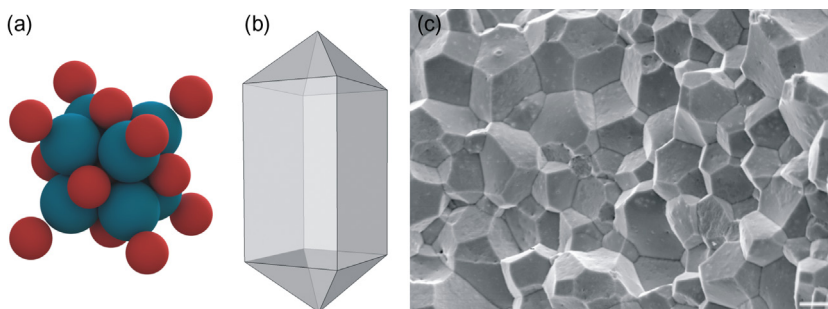
FIGURE 6.3   Tetragonal structure of ZrO_2: (a) The arrangement of zircon (red) and oxygen (blue) atoms in crystalline structure; (b) Ditetragonal dipyramidal crystal structure; (c) Polycrystalline tetragonal zirconia microstructure (SEM, bar 10 µm).

Crystalline materials have imperfections or irregularities in their atomic arrangement even when they are well prepared. The most common imperfections in atomic arrangements are vacancies, interstitials, impure (solute) atoms, and dislocations. Furthermore, as crystal size is not infinite, the imperfections introduced into polycrystalline ceramics (e.g. surfaces, interfaces, and grain boundaries) influence their physical and mechanical properties. Figure 6.4 demonstrates the types of defects in crystalline solids: the missing atom forms a vacancy and the dislodged atom forms self-interstitial defects after moving from its normal side. Vacancies exist in solids at all temperatures, and their concentration increases exponentially with temperature (Boltzmann distribution function). Vacancies also increase the disorder (entropy) in the crystal. Impurity atoms can be placed in interstitial or substitutional positions, and the
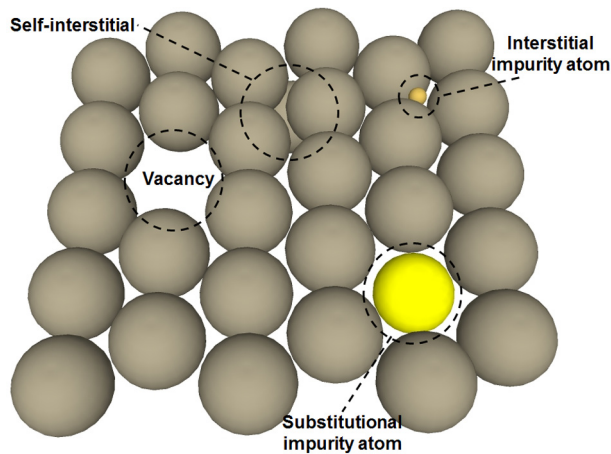
FIGURE 6.4 Illustration of the two types of point defects (vacancy, self-interstitial) and impurities (substitutional and interstitial impurity atoms) in crystalline solids.

solubility of impurities is favored when Hume-Romery criteria are satisfied (small difference in atomic radii, similar crystal structure, small difference in electronegativity, higher valence dissolves more readily than lower valence). In contrast to substitutional solid solutions determined by Hume-Romey criteria, interstitial solid solutions need small atomic radii to fit into the interstices of the host lattice. Even small amounts of solute can affect the electrical and physical properties of the solvent. Strengthening and hardening of materials uses the formed lattice strain to increase strength and hardness.

Besides single atom defects, dislocations are linear defects in crystals that are formed in a region where a plane of atoms terminates abruptly in the lattice. Due to disturbances in the periodicity of the lattice, distortions (stresses) are formed around atomic planes. All crystalline materials contain dislocations that influence the physical and mechanical behavior of the material, such as plastic deformation, phase transformation, and thermal stresses. Dislocations can be mobile under applied stress, and obstacles lead to strengthening of the material. Grain boundaries, secondary precipitates, inclusions, and other dislocations that form tangles and impede one another, are used for such strengthening.

Surfaces and interfaces are discontinuities in the atoms' ordered arrangement and can be interpreted as crystal defects. The free surface has broken atomic bonds associated with surface energy (or surface tension) of solids. This excess energy is the driving force for minimizing the free surface of solids. In reality, a solid-free surface is usually a multiphase interface between the solid and surrounding gas. Grain boundaries in crystalline materials also separate grains having various crystallographic orientations. This atomic mismatch (lattice strain) is also associated with excess energy. Small or low-angle grain

boundaries are formed when the mismatch is small and can be absorbed by an array or dislocations.

6.2.2 Microstructure

Generally, the microstructure of advance ceramics has many features (Figure 6.5). Three critical components of ceramic microstructure are phase boundaries, grains, and pores. Examples of phase boundaries in dense ceramics are interfaces among crystalline grains and between crystalline grain and a glassy phase. Often, it is difficult to distinguish if the grain boundary is also a phase boundary; for example, oxides have inter-granular film at the grain boundary or in a triple junction. If such film is over ~10 nm thick, it is already defined as a second phase.

Pores are very important for development of ceramic microstructure, because ceramic process deals with pores from the beginning and it is difficult to prepare truly pore-free ceramics. Porosity and pore size are two main parameters for the description of a porous solid. Porosity is defined as the ratio of the total pore volume to the apparent volume of the particle or powder (excluding interparticle voids). Porosity can be closed or open, which is determined by accessibility of the pore's volume by a given probe molecule (usually nitrogen or helium). Pore size is generally the distance between two opposite walls of the pore (diameter of cylindrical pores, width of slip-shaped pores). Three main categories are defined by IUPAC[3]: *micropores* have widths smaller than 2 nm, *mesopores* have widths between 2 and 50 nm, and *macropores* have widths larger than 50 nm. However, this classification is not always used properly in practice, especially due to a wide range of pore sizes over 50 nm. The terms pore and void are often used interchangeably. Generally, the term void refers to the empty pore (vacuum inside), however, sometimes big pores in foams are also referred to as voids.

Particles are distinct secondary phase distributions in a ceramic matrix, and some can dissolve at elevated temperatures, and some may never be able to dissolve in the crystalline matrix. Precipitates are interchangeable with the particles, but particles in ceramics, contrary to metals, are less likely to be formed by precipitation. Moderate heat treatments can be used for metal precipitation or cleaning. In ceramics it is difficult to use such procedures, and except for pure semiconductors, impurities are common. Heat treatment can change the oxidation state of constituent ions, which can have a positive or negative effect on mechanical behavior. Volume change of big impurities may support crack propagation, and contrarily, small particles on the grain boundary become useful in preventing crack movement; instead, they help toughen the ceramic. Similarly, a different crystalline (platelets) can improve damage resistance, one example is the addition of alumina platelets (Figure 6.5, crystalline phase 1) inside the ordinary alumina microstructure (Figure 6.5, crystalline phase 2).
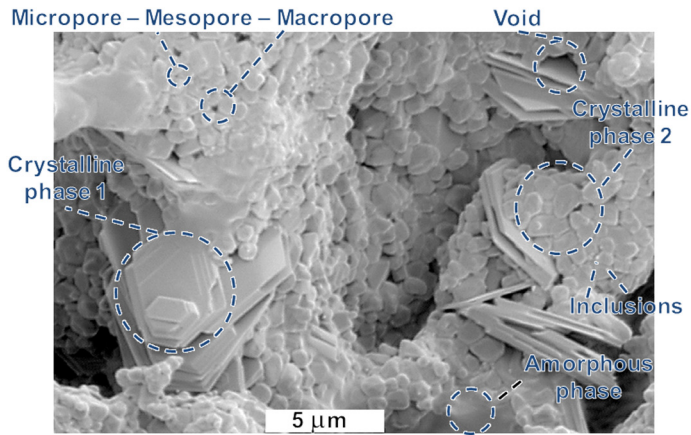
FIGURE 6.5 Illustration of various microstructure features present in advanced ceramic materials.
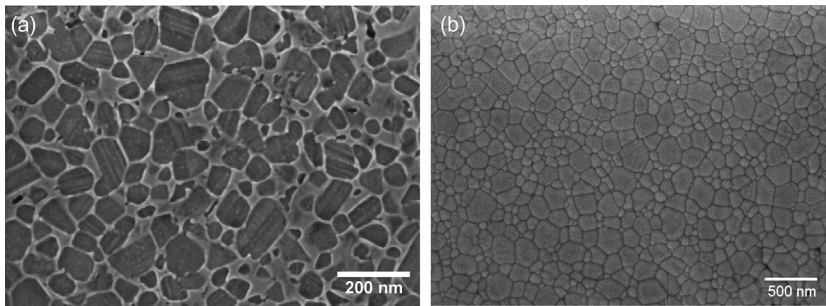
FIGURE 6.6 SEM micrographs taken on (a) Liquid-phase sintered silicon carbide; and (b) Solid-state sintered 3Y-TZP ceramic samples.

Structural integrity of ceramics is achieved by sintering in the solid state or with the involvement of a gaseous or liquid phase. A low melting glassy phase is usually used for non-oxide ceramics when liquid-phase sintering is neces-sary to achieve densification at reasonably low temperatures. Oxide ceramics are sintered via solid-state sintering and with a minimum of non-crystalline phase present. Figure 6.6 shows the scanning electron micrographs of two ceramics sintered (a) with, and (b) without the addition of a glassy phase.

6.3   STRUCTURE–PROPERTY RELATIONS

In the following sections, we link essential properties to hierarchical structures from atomic onwards. Examples are selected to give an overview of advanced

ceramics with a focus on structure-dependent properties, which has implications for restorative dentistry.

6.3.1   Intrinsic Physical and Chemical Properties of Individual Crystalline Grains

6.3.1.1   Optical Properties

Optical properties are determined to a large extent by atomic structure and the band gap structure of crystalline grains, with optical transparency also being influenced strongly by the density and existing grain boundaries in polycrystalline bodies. These are essential properties that influence the aesthetic appearance of ceramic dental prostheses, and are discussed at the end of this chapter.

6.3.1.2   Mechanical Strength

Mechanical properties such as theoretical fracture strength and Young's modulus can be predicted from an analysis of the strength of the ionic and covalent bonds. Young's modulus is related to inter-atomic bonding forces, when it is the measure of small changes in the separation of adjacent atoms (the same for both tension and compression).

Though oxide ceramics such as zirconia and alumina commonly used in restorative dentistry are strong, even stronger atomic bonding can be found in the group of non-oxide ceramics that comprises carbides, nitrides, and borides. These chemical compounds have covalent bonding (e.g. SiC, AlN, B_4C) or covalent-metallic bonding (e.g. TiB_2, TiC, WC); their bonding types determine general properties such as high melting points, high chemical resistance, high hardness, and high stiffness. To achieve fundamental mechanical strength, the covalent bonding has to be arranged in a symmetric crystalline structure. The crystal lattice of the hexagonal α-SiC, for instance, can be derived from the diamond lattice by replacing half of the carbon atoms with silicon, thus forming the SiC_3 and CSi_3 tetrahedral units that are arranged in layers. The various stacking sequences of these layers give rise to an enormous number of polytypes that are structurally different but maintain an identical chemical composition. Crystal structure defines the main characteristics of SiC, such as extreme hardness and strength, with no significant decrease in strength up to 1600 °C (at 1000 °C, SiC is 7.5 times stronger than Al_2O_3).[4] Another covalent carbide, boron carbide, is also an extremely hard material among mass-applied materials, and is second only to diamond. The general formula of boron carbide is $B_{12-x}C_x$ (0.06 ≤ x ≤ 1.7), and the structure accommodates a large variation in carbon content without any basic structural changes to the rhombohedral unit cell. All groups of materials such as metal borides (magnesium boride, zirconium boride, and titanium diboride) exhibit similar trends in their physical and chemical properties because they possess the same hexagonal crystal structure. Most majority of boride ceramics have very high melting

temperatures (2000–3250 °C), high mechanical strength, low mass density, very low coefficients of thermal expansion, high resistance to oxidation, and often also electrical conductivity.

6.3.1.3 Chemical (Biological) and Thermal Stability

Melting temperature is also an indicator of atomic bonding strength and there is relationship with Young's modulus. The general trend is that a higher melting temperature indicates a higher modulus and vice versa. Ordering of the crystalline lattice is energetically favorable and that means that crystalline structures are generally more stable (thermally and chemically) than amorphous (glasses). A good example is alumina, where the corundum structure is hexagonal, closely packed, and stable at high temperatures of up to 1925 °C in both oxidizing and reducing atmospheres. Its chemical stability is also excellent; only wet fluorine gases, hydrofluoric acid, hot orthophosphoric acid, and alkali metal vapor can attack the alumina structure. Chemical resistivity is dependent on the purity of the alumina, especially low-purity alumina compositions that contain glassy and secondary crystalline phases that are vulnerable to corrosion.

6.3.1.4 Functional Properties

Atom substitutions or vacancies in crystalline structures can radically change functional properties of advanced ceramics. A typical example is the ionic conductivity of zirconia at high temperatures, which is the result of the presence of oxygen vacancies in the crystalline structure. These 'defects' are introduced by stabilizing cations with valencies lower than that of the zirconium matrix cation. Similarly, oxygen vacancies are as important to titania ceramics. Stoichiometric titania is an electrical insulator at room temperature. However, the electrical resistance of titania ceramics in practice is sensitive to the gaseous environment due to the easy introduction of oxygen vacancies. The presence of oxygen vacancies strongly influences the surface characters of titania ceramics, particularly when it is porous, as in the case of titania porous coating on dental implants. The outstanding photocatalytic activity of titania is also related to the presence of this type of oxygen vacancy and also to the crystalline structure, which can be used for electrolytic splitting of water into hydrogen and oxygen; or self-cleaning and self-sterilizing surfaces; anti-fogging surfaces; anticorrosion systems; photocatalytic lithography; and photochromics.[5] Ionic bonds inside the crystalline structure are important in modern technical applications such as sensors, actuators, capacitors, thermistors, varistors etc. Inside this structure the oxygen anions pull valence electrons away from the metal cations, which results in strong electrical fields at the inter-atomic scale. This gives rise to electron correlation effects that underlie ferroelectricity and ferromagnetism; metal–insulator transition; superconductivity; electro- and photocatalysis; and other fascinating phenomena. Furthermore, defects in the crystal lattice originated from the exchange of oxygen with the surrounding

atmosphere, resulting in cation or anion vacancies. These defects add up to impurities; are responsible for electron and hole formation; and perturb the electronic structure of the materials. This has a profound impact on electrical, optical, magnetic, ferroelectric, piezoelectric, photocatalytic, and other functional properties.[6]

6.3.2　Properties Determined by Microstructure

Microstructure parameters such as the amount and character of porosity, grain size, grain morphology, and phase assembly (as well as their interrelationships) significantly affect a wide range of properties, from the electrical and magnetic to the mechanical.[7]

6.3.2.1　Properties Determined by Particle-packing Defects

Most powders contain agglomerates, which are weakly bonded groups of particles; some powders also contain aggregates (hard agglomerates), which are strongly bonded groups of particles. Agglomerates and aggregates often yield heterogeneities in particle packing during the shaping process; this results in differential shrinkage during sintering and the formation of residual pores. High specific surface area indicates small particles and high reactivity during sintering, but also the tendency to form agglomerates and absorb impurities on the surface. Particle packing during the shaping stage determines the microstructure and consequently the final properties of sintered ceramics. Methods have therefore been developed to minimize the negative influence of flaw formation superficially and internally (see following chapters for more details).

6.3.2.2　Properties Determined by Grain Boundaries

Grain boundaries are characteristic microstructure features of the polycrystalline ceramics that modify and/or introduce additional properties in ceramics, compared to their constituent crystalline phase(s). Inside the grain boundaries, atoms are less well-ordered in conjunction with the segregation of impurities and the formation of the secondary glassy phase. The grain boundaries can thus be regarded as structural-disorder weak interfaces. Properties sensitive to such weak interfaces are accordingly influenced. Relevant to restorative dentistry are the optical transparency, fracture toughness, low-temperature degradation of TZP ceramics, and dissolution of hydroxyapatite (HAp) and phosphate-based ceramics. Other properties less relevant to dental applications, such as transport properties (electrical or thermal conductivity) are also sensitive to the nature of such inter-granular barriers.

6.3.2.3　Properties Determined by Porosity and Pore Size

The mechanical properties (strength, hardness, elastic modulus) of ceramics are sensitive to porosity. Generally, strength and hardness exponentially

decrease with the increase of porosity. The decrease of strength with porosity is described by the Ryshkewitch equation (Eq. 6.1):

$$\sigma = \sigma_o e^{-cp} \tag{6.1}$$

The σ_o is strength at zero porosity, c is constant, and p is porosity. Experimental data usually shows a precipitous decrease of flexural strength at low levels of porosity; a similar drop is observed in the hardness of ceramics as a function of the porosity. Similarly, the elastic modulus of ceramics also decreases with the increase of porosity. For example Young's modulus of 3Y-TZP decreases from 210 GPa to 100 GPa and 50 GPa with decrease of theoretical density from 100% to 80% and 60%, respectively.[8]

Porosity and pore size of advanced ceramics also influence their chemical resistivity and bioactivity. Generally, chemical and biological activities increase with increasing porosity. Ceramics with open porosity and high surface area are especially vulnerable. Advanced ceramics aiming for bioactive applications usually require designed porosity. Not only are micro, meso, and macro porosities are present, but also voids and microchannels are introduced to achieve the required long-term bioactivity (Figure 6.7).

6.3.2.4   Properties Determined by Grain Size

The fracture failure of ceramics is controlled by the size of the microscopic cracks, which is in the same order as the size of the grains when the ceramics are well-prepared (i.e. when large processing voids are avoided). This implies that fine grain structure is preferable for ceramics with high mechanical strength for load-bearing prostheses. An extreme example is the development of nanoceramics, defined as ceramics composed of crystalline grains less than 100 nm. The
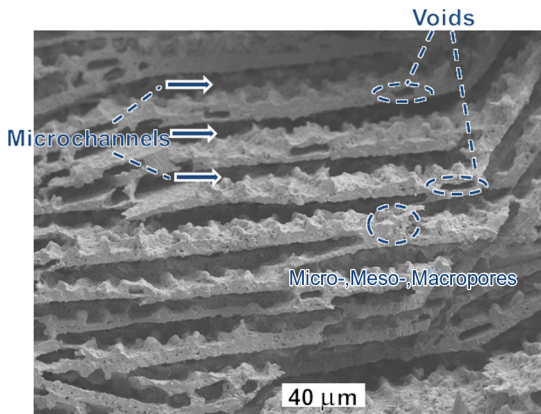
FIGURE 6.7   SEM micrograph of a porous hydroxyapatite containing microstructural features of various dimensions.

phase transformation behavior of partially stabilized zirconia also depends on grain size. When the grain size of tetragonal zirconia is too small ($< 0.3 \mu m$ for 3Y-TZP), the tetragonal zirconia appears very stable and can hardly transform to monoclinic zirconia under cracking stress. On the other hand, when the grain size of tetragonal zirconia is too large ($\geq 1 \mu m$ for 3Y-TZP), the tetragonal zirconia grains may spontaneously destabilize towards the monoclinical form. Grain size is also crucial for functional ceramics. In addition, grain size influences the surface friction and wear behavior of advanced ceramics.

6.3.2.5 Properties Determined by Grain Morphology

A good way to understand the influence of grain morphology on ceramic properties is to compare the hierarchical structure and properties of the synthetic and natural materials with similar overall chemical and phase composition. For example, HAp is mechanically weak as a synthetic ceramic material, and is unable to sustain even moderate tensile, shear, or compressive forces. The main reason is that despite its chemical similarity to bone mineral, synthetic HAp differs significantly in terms of its microstructure and macrostructure as compared to its nearest biological equivalent, cortical bone. Cortical bone is the composite material with a fiber-reinforced lamellar structure, and synthetic HAp is simply a fine-grained polycrystalline ceramic. This large difference in structure is responsible for huge variations in fracture toughness, $0.6–1.5 \, MPa \cdot m^{-1}$ for HAp, and $2–12 \, MPa \cdot m^{-1}$ for bone.[9] Materials engineering uses bio-inspired materials to achieve outstanding properties by mimicking the morphology of grains and internal structures of natural materials.[10] This bio-inspired approach combines grains elongated in one dimension (whiskers, roads) or two dimensions (platelets) with isotropic shape, and organizes them to achieve tailored properties.

6.3.2.6 Properties Determined by Phase Transformation

Phase transformation is an issue that must be considered during the ceramic process, but it can also be applied for further improvement of structural and functional properties. For example, the crystalline structure of alumina is temperature-dependent and several metastable structures exist; however, they all irreversibly transform to the hexagonal α-alumina (corundum) beyond $1150 \, °C$.[11] This transformation is connected with a big volume change, and metastable alumina can be used for preparation of strong porous α-alumina. One possibility is to use metastable alumina as the binder for α-alumina grains, or to directly prepare a strong porous body by coalescence of nanocrystals stimulated by phase transformation.[12]

The crystalline structure of pure zirconia is monoclinic (m-ZrO_2) up to $1170 \, °C$, at which point it transforms to the tetragonal phase (t-ZrO_2) and remains stable up to $2370 \, °C$, when cubic zirconia is formed (c-ZrO_2). Phase transformation of t-ZrO_2 to m-ZrO_2 is accompanied by considerable

dimensional changes. This causes stress that results in fragmentation of the material. Zirconia parts are usually sintered at temperatures above 1200°C, so pure zirconia (without stabilizing additives) can be used only in powder form. Before 1975, massive zirconia pieces were prepared by stabilization of c-ZrO_2 via the addition of other oxides ($MxOy$; mainly CaO, MgO, and Y_2O_3). Stabilized zirconia is free from phase transformation over the entire required temperature range, mainly from the sintering temperature to room temperature.

The crystalline structure of titanium dioxide exists in three polymorphic phases: tetragonal rutile, tetragonal anatase, and orthorhombic brookite. The metastable anatase and brookite phases convert to rutile upon heating at temperatures between 550 and around 1000 °C. The temperature of this transformation strongly depends on the impurities or dopants present in the material, as well as on the morphology of the sample.

6.4 OPTICAL PROPERTIES

Optical properties are governed by composition, crystal structure, and also by interferences (in the case of polycrystalline ceramics). Ceramics can interact with electromagnetic fields and exhibit changes in fluorescence, phosphorescence, color tone, photoconductivity, polarization, infrared activation, and birefringence. Many ceramic materials have interesting functional properties based on interactions with an electromagnetic field and show good transparency for infrared radiation. Nevertheless, due to the focus of this book we concentrate on the interactions of ceramics with visible light.

The pure form of the most dielectric ceramic single crystals are transparent to visible light due to the absence of free electron gas present in metals.[13] One particular ceramic material can be transparent, translucent, or opaque depending on its microstructure, in particular the features that diffuse light and make it difficult to pass through.

Three phenomena are important for the optical transparency of advanced ceramics: refraction, deflection, and transmission of light. These are wavelength dependent. Refraction is related to the velocity of light, which can be characterized by the refractive index (n). This is the ratio of the velocity of light in a vacuum to that in any other medium. Mathematically, n is given by the simple equation (Eq. 6.2):

$$n = \frac{c}{c_m} \tag{6.2}$$

The velocity of light in the material is c_m. Values of n range from 1.003 (air) to approximately 3 (dense solids), and change depending on material and wavelength (λ). The variation of n with λ is produced by dispersion of the light. Dispersion is then defined as $dn/d\lambda$, and the ability of the material to refract (bend) light is described as refringence. The non-symmetric crystalline structure of advanced

ceramics often results in the dependence of n on the crystallographic axis. Crystals with one unique axis along which the refractive index is different from the index along the other axis are known as uniaxial birefringent crystals. All crystalline ceramic materials without cubic structure are birefringent. In contrast, the glass phase has no birefringence due to its isotropic character.

Reflection is generally the change in direction of light at an interface between two different media. The amount of light reflected from surface of material to medium (air) is determined by the reflective index of the reflecting medium. Reflection of light may occur whenever light travels from media of a given refractive index into media with a different refractive index. In the most general case, a certain fraction of light is reflected from the interface and the remainder is refracted. The Fresnel equation can be used to predict how much of the light is reflected and how much is refracted in a given situation (Eq. 6.3):

$$R = \frac{(n_m - n_a)^2}{(n_m + n_a)^2} \qquad (6.3)$$

The refractive index of the ceramic material is represented by n_m, and n_a is the refractive index of air or another medium. Thickness of the films and the nature of the reflecting surface are also important. If the surface is not a smooth plane, some of the light will be scattered diffusely rather than reflected in a single direction.

Transmission of light (transparency) through dielectric advanced ceramics is generally good and the basic requirement is minimal interaction of the electromagnetic wave with the material. This is true for most single crystalline ceramics. Point defects of the crystal lattice can give rise to absorption in visible parts of the spectrum when energy states are added within the band gap. These levels allow electron transmissions to occur within the visible part of the electromagnetic spectrum. Examples of this are the red color of ruby (single crystalline Al_2O_3 with Cr) or the gray darkening of oxides sintered in reducing atmospheres (oxygen vacancies).

Polycrystalline ceramics have several limitations compared with their monocrystals. Beyond the presence of defects, optical transparency in polycrystalline materials is limited by the amount of light that is scattered by their microstructural features. Since visible light has a wavelength scale in the order of hundreds of nanometers, scattering centers will have dimensions on a similar spatial scale or bigger. Clear transparency requires high in-line transmission, otherwise the resulting material is translucent (opaque). The loss of transparency is due to scattering of the incident beam, which can occur because of several reasons (often combinations of these reasons). Figure 6.8 shows how incoming light can interfere with polycrystalline ceramics.

The first 'obstacle' for the incident beam is reflection by a surface. Then microstructural features such as residual porosity, precipitates, intergranular films, and grain boundaries cause incoherent scattering of light.
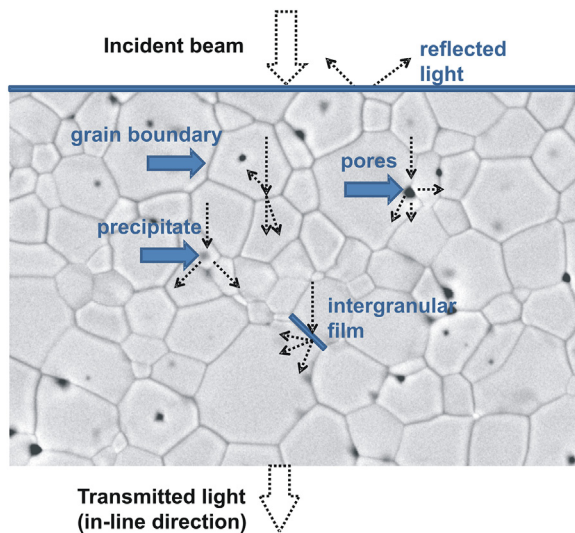
FIGURE 6.8 Mechanism of the loss of optical transparency due to light scattering at the surface and various microstructural features.

Transmission decreases rapidly with small increases in porosity (0.1% is significant). Furthermore, if pore size is close to the wavelength of the light, scattering is maximized. This scattering can be engineered by controlling green body preparation, sintering conditions, and by selection of processing methods.

Grain boundaries can scatter light when refractive indexes are discontinuous, and is caused by birefringence, precipitates, or intergranular film. Matching refractive indexes between different phases can reduce scattering losses. This is why symmetric cubic crystal structure is easily transparent. When the size of the scattering center (or grain boundary) is reduced well below the size of the wavelength of the light being scattered, there is no longer significant light scattering. Grain size is also an important parameter. Scattering is at a maximum when particle diameter is close to wavelength (λ). The reason is that small grain sizes have scattering centers that are too small, and big grains have reduced numbers of scattering centers (grain boundaries). Most oxide ceramics, such as alumina and associated compounds, are formed from fine powders. This yields a fine-grained polycrystalline microstructure that is filled with scattering centers comparable to the wavelength of visible light. The solution for transparency is preparation of nanoceramics with grain sizes below wavelength. Fabrication of transparent non-oxide ceramics has proven to be more difficult because of their low sinterability and their high level of intergranular films and precipitates in the polycrystalline sintered bodies.

The color of many ceramics can be changed by small additions of dopants or point defects. The most common way to color ceramics is by adding transition metal and rare earth cations; explanation of the color appearance is based on ligand field theory. The most common ligand in ceramics is oxygen, and placement of a transition metal into the crystal structure influences the ligands. These changes in energy are associated with electronic transitions that allow absorption of light; the situation is more complicated for distorted structures (corundum). Similarly, the addition of rare earth elements with different kinds of orbitals (f) allows absorption. Rare earth ions tend to color ceramic or glass less strongly than transition metal ions. Other possible sources of color in ceramics include electrons and holes in ionic materials (alkaline halides), defects produced by X-ray or neutron irradiation, and defects produced as the result of non-stoichiometry (TiO_2, ZrO_2).

ACKNOWLEDGMENTS

REFERENCES

 1. Garvie RC, Hannink RH, Pascoe RT. Ceramic steel. Nature 1975;258:703–4.
 2. Sproul GD. Electronegativity and bond type: I. Tripartate separation. J Chem Educ 1993;70:531–4.
 3. Rouquerol J, Avnir D, Fairbridge CW, Everett DH, Haynes JH, Pernicone N, et al. Recommendations for the characterization of porous solids. Pure Appl Chem 1994;66:1739–58.
 4. Charles AH. Handbook of ceramics glasses, and diamonds. The McGraw-Hill Companies, Inc.; 2001.
 5. Heimann, RB. Classic and Advanced Ceramics: From Fundamentals to Applications; 2010.
 6. Newnham RE, Ruschau GR. Smart electroceramics. J Am Ceramic Soc 1991;74:463–80.
 7. Rice RW. Ceramic processing: An overview. AIChE J 1990;36:481–510.
 8. Luo J, Stevens R. Porosity-dependence of elastic moduli and hardness of 3Y-TZP ceramics. Ceramics Int. 1999;25:281–6.
 9. Ruys AJ, Wei M, Sorrell CC, Dickson MR, Brandwood A, Milthorpe BK. Sintering effects on the strength of hydroxyapatite. Biomaterials 1995;16:409–15.
10. Munch E, Launey ME, Alsem DH, Saiz E, Tomsia AP, Ritchie RO. Tough, bio-inspired hybrid materials. Science 2008;322:1516–20.
11. Shelleman R, Messing G, Kumagai M. Alpha alumina transformation in seeded boehmite gels. J Non-Crystalline Solids 1986;82:277–85.
12. Shen Z, Xiong Y, Höche T, Salamon D, Fu Z, Belova L. Ordered coalescence of nanocrystals: a path to strong macroporous nanoceramics. Nanotechnology 2010:21.
13. Krell A, Klimke J, Hutzler T. Transparent compact ceramics: inherent physical issues. Opt Mater 2009;31:1144–50.

FURTHER READING

Barry Carter C, Grant Norton M. Ceramic materials-science and engineering. New York, USA: Springer Science + Business Media; 2007.

Britannica E. 2012. Advanced ceramics [Online]. Available: <http://www.britannica.com/EBchecked/topic/6657/advanced-ceramics>.

Ellingham HJT. Reducibility of oxides and sulfides in metallurgical processes. J Soc Chem Ind 1944;63:125–33.

Hench LL. Bioceramics: from concept to clinic. J Am Ceramic Soc 1991;74:1487–510.

Karageorgiou V, Kaplan D. Porosity of 3D biomaterial scaffolds and osteogenesis. Biomaterials 2005;26:5474–91.

Murray PE, García Godoy C, García Godoy F. How is the biocompatibilty of dental biomaterials evaluated? Med Oral Patol Oral Cir Bucal 2007;12:E258–66.

Organization, I. S. ISO 7405 Dentistry-Preclinical evaluation of biocompatibility of medical devices used in dentistry. Test methods for dental materials. International Standards Organization; 1996.

Verstraeten SV, Aimo L, Oteiza PI. Aluminium and lead: molecular mechanisms of brain toxicity. Arch Toxicol 2008;82:789–802.

Williams D. Revisiting the definition of biocompatibility. Med Device Technol 2003;14:10.

Wintermantel E, Ha SW. Medizintechnik mit biokompatiblen Werkstoffen und Verfahren. Springer DE; 2002.

Advanced Ceramic Processes

Martin Trunec and Karel Maca

Dept. of Ceramics and Polymers, Brno University of Technology, Czech Republic

Contents

123

7.1   INTRODUCTION

This chapter deals with the processing of bulk advanced ceramics. A general overview of ceramic processes is presented with a focus on the processes relevant to ceramics in dentistry. Because most advanced ceramics are produced by forming and sintering fine ceramic powders, only ceramic processes that start from fine powders are described here. In this chapter we are not concerned with powder synthesis, and powder is regarded as a raw material for processing ceramics. The basic steps of advanced ceramic processing can be specified as follows:

1. Powder treatment.
2. Shaping of ceramic green body.
3. Drying and binder removal.
4. Sintering.

In the first step, ceramic powders can be milled, mixed, fractionated, deagglomerated, surface-coated by additives, and granulated. All these procedures should improve the particle packing in the second step, where the particles are formed into the desired shape and consolidated. Regular particle packing is a key factor for the success of advanced ceramic processing.[1] Additives, solvents, and binders used to form and consolidate the ceramic powder into a shaped body must be removed during the next step to produce the porous particle body. Such a powder compact is densified by sintering at high temperatures, which results in a final, dense ceramic product. Ceramic components requiring close tolerances and low surface roughness must be additionally machined and/or polished after sintering.

7.2   POWDER TREATMENT

Ceramic powders often do not exhibit suitable characteristics for the fabrication of advanced ceramic components. These characteristics include particle size, particle size distribution, particle shape, particle structure, and homogeneity of multiphase powder mixtures. To meet the desired characteristics, the powders are treated prior to shaping and consolidation. During the powder treatment, surfactants, dispersants, binders, and other additives are usually applied to ensure particle dispersion and proper particle packing in the shaping step.

Most of the ceramic submicrometer- and nanometer-sized powders used in advanced ceramic processing are not produced with separate single-crystal particles, but consist of agglomerates or aggregates. In aggregates and agglomerates the primary dense particles, mostly crystallites, are bonded together to form large units. The difference between aggregates and agglomerates is not strictly defined, but generally the crystallites in an aggregate are more densely and strongly bonded together with less inter-crystallite porosity than crystallites in an agglomerate.[2] A schematic illustration of aggregates and
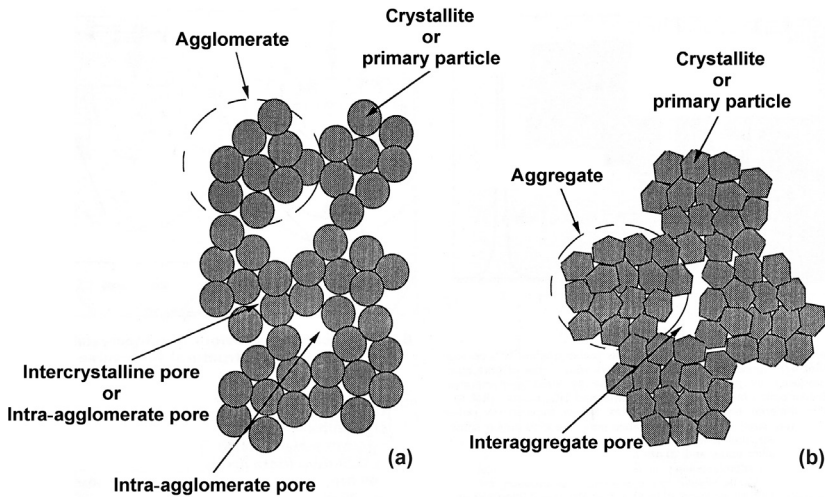
FIGURE 7.1   Schematic illustration of powder types: (a) Agglomerated; and (b) Aggregated. *(From Mayo MJ. Processing of nanocrystalline ceramics from ultrafine particles. Int Mater Rev 1996; 41(3):85–115, Fig. 6. Reproduced with permission of Maney Publishing.)*

agglomerates is shown in Figure 7.1. However, many authors use these two terms interchangeably.

Agglomerated or aggregated powders tend to provide powder compacts with non-uniform particle packing, which results in defective ceramics with exaggerated grain growth, porous structure, warpage, or even flaws and cracks. The causes of powder agglomeration and aggregation can be summarized as follows:

1. Van der Waals forces.
2. Moisture (hydrogen bonds).
3. Capillary forces.
4. Adsorbed foreign species.
5. Particle pre-sintering (during particle syntheses).

All the causes can be eliminated by an appropriate synthesis adjustment, except for van der Waals (vdW) forces. VdW forces are ubiquitous and always attractive between like particles. For spherical particles in close contact, the attractive vdW forces (F_{vdW}) can be calculated according to Eq. 7.1:[3]

$$F_{vdW} = \frac{AR}{12D^2} \qquad (7.1)$$

A is the Hamaker constant (describes dielectric properties of the materials), R is the particle radius, and D is the distance between particle surfaces. It can

be shown that the vdW forces between two particles in contact with a diameter of 1 μm are about 5–7 orders of magnitude higher than their weight. Thus, to prevent fine particles from agglomerating, the close contact between particles must be avoided. This can be accomplished by adsorption of dispersants on the particle surface. The dispersants give rise to repulsion forces when the particles approach each other and prevent the particles from coming into close contact and agglomerating.

Deagglomeration of the agglomerated particles to fine powders is the most important task in the first processing step. Ball milling and attrition milling have proved to be the most successful techniques for the elimination of agglomerates and for particle dispersion. Moreover, together with particle dispersion, other processes can be performed during the powder treatment step. Ball and attrition milling can be used for the following processes:

1. Particle size adjustment.
2. Disintegration of agglomerates.
3. Coating the particle surface with surface-active additives.
4. Mixing of multiphase powders.
5. Mixing the powder with a binder and/or other processing additives.
6. Particle dispersion and stabilization in a solvent.

The milling and mixing effect is realized through intensive movement and the impacts of grinding media (usually ceramic balls, short cylinders, or rods). In a ball mill the grinding bodies tumble in a rotating cylindrical powder container. In an attrition mill the grinding bodies are agitated by stirring arms mounted on an axial shaft. The schema of the attrition mill is shown in Figure 7.2. The milling can be dry (without liquid solvent) or wet (with liquid solvent) according to the subsequent processing steps.

7.3   SHAPE-FORMING PROCESSES

The general goal of all shaping methods is the fabrication of a body consisting of ceramic powder consolidated into the required shape, the so-called green body. The ceramic powder can be formed into the desired shape by many different shaping methods. The demands placed on shaping methods can be generalized and described by the following requirements, and should guarantee:

1. Homogeneous structure of the ceramic green body.
2. Minimal defect size in the green body (bubbles, cracks, warpage, impurities, etc.).
3. Minimal requirements on the machining of the final sintered body.

There are also other requirements on shaping methods that are not dictated by the ceramic component quality but concern the commercial and industrial utilization of shaping methods. They include automation capability and the use of environmentally harmless additives and procedures. Table 7.1 summarizes
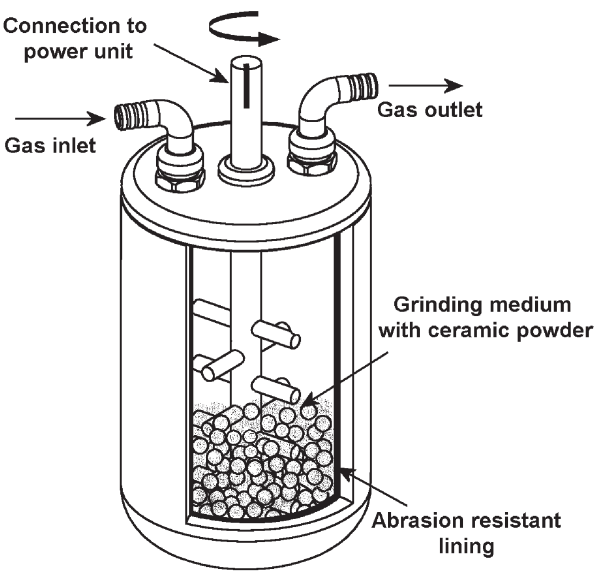
FIGURE 7.2   Cutaway illustration of an attrition mill.

TABLE 7.1 Shaping Methods Used for Fabrication of Bulk Advanced Ceramics

Methods		
Dry shaping	⟹	Uniaxial pressing
		Isostatic pressing
Wet shaping	⟹	Slip casting and related methods
		Direct casting methods
		Tape casting
Plastic shaping	⟹	Injection molding
		Extrusion
Solid free-form fabrication	⟹	3D printing
		Direct ink-jet printing
		Stereolithography
		Robocasting
		Fused deposition
		Selective laser sintering

the major methods for shaping and consolidation of ceramic powders. Shaping methods can be divided into three groups according to the nature of the consolidated ceramic mass. Dry shaping methods deal with loose powder and include the most frequently used shaping methods in advanced ceramic processing: uniaxial and isostatic pressing. Wet shaping methods work with suspensions of ceramic powders in low-molecular solvents. They provide the most regular particle packing in green bodies. These ceramics result in products with small processing defects and high reliability, and can be utilized in the most demanding applications. The wet shaping methods include slip casting and related methods, direct casting, and tape casting. Plastic shaping uses a plastic mixture of ceramic powders with binders and other additives. Many plastic shaping methods have been derived from the plastics industry and adapted to ceramic processing. The most important methods of this group are injection molding and extrusion. Solid free-form fabrication represents a special group of methods that is distinct from the previous methods. The previous methods use a mold, die, or other shaping tool to form the ceramic body. On the other hand, the methods used in the solid free-form fabrication group form the green bodies layer by layer, without the need for shaping tools. Because they work with computer-aided design (CAD) data and do not require shaping tools, the methods belong to the group known as rapid prototyping methods.

7.3.1   Dry Shaping Methods

7.3.1.1   Uniaxial Pressing

Uniaxial pressing is the most common method for the fabrication of ceramic bodies. During uniaxial pressing the powder is compacted in a rigid die by applying pressure along a single axial direction using a punch or piston. The process is easily automated, and the method is thus especially suitable for mass production. Uniaxial pressing is primarily suitable for low-height or tabular bodies. Pressing high bodies usually results in inhomogeneous packing of ceramic particles due to the die (wall and particle) particle friction.[4] Figure 7.3 shows the changes in packing pressure for different die geometries. During sintering, the lower-density areas will either not be densified completely or will shrink more than the surrounding areas. Both can result in deformations or even cracks in the sintered body. The density variation will decrease if the pressure is applied from both sides in double-acting presses. The homogeneity of particle packing in complex-shaped powder compacts or compacts with irregular height can be improved by pressing with segmented punches. Further improvement can be obtained if the pressure of each punch segment is independently controlled. A schematic example of pressing with segmented punches is shown in Figure 7.4.

7.3.1.2   Isostatic Pressing

Some limitations of uniaxial pressing that concern regular particle packing can be overcome by isostatic pressing (i.e. by applying pressure from all directions).
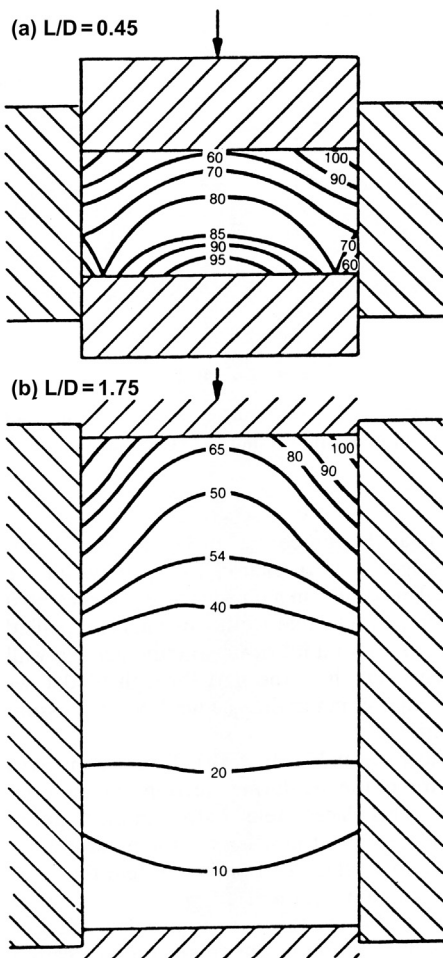
FIGURE 7.3   Pressure variations in the powder compact during uniaxial pressing for two ratios of height-to-diameter of the compact. *(From Richerson DW. Shape-forming processes. In: Modern ceramic engineering: properties, processing, and use in design, 2nd edition. New York: Marcel Dekker; 1992, p. 436, Fig. 10.14. Reproduced with permission of TAYLOR & FRANCIS GROUP LLC–BOOKS.)*

In isostatic pressing a uniform hydrostatic pressure is applied to the powder closed in a flexible rubber or plastic mold. Because of the flexible mold, isostatic pressing is not able to provide green bodies with the accurate dimensions that uniaxial pressing does. There are two types of isostatic pressing commonly used: wet-bag and dry-bag. Wet-bag pressing is illustrated in Figure 7.5. The powder is filled in a shaped and flexible mold, sealed, and immersed in liquid in a high-pressure vessel. The liquid is pressurized and the pressure is transmitted
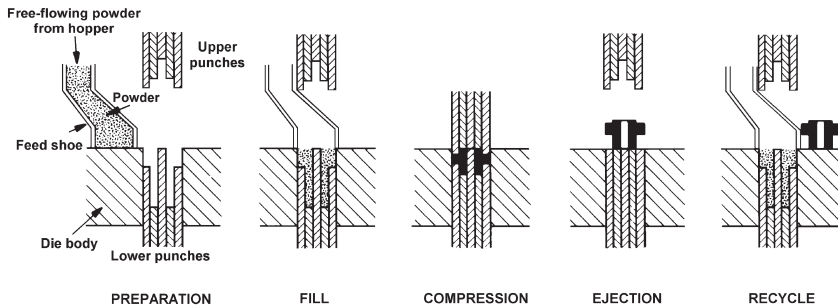
FIGURE 7.4 Schematic presentation of uniaxial pressing with segmented punches. *(From Richerson DW. Shape-forming processes. In: Modern ceramic engineering: properties, processing, and use in design, 2nd edition. New York: Marcel Dekker; 1992, p. 430, Fig. 10.10. Reproduced with permission of TAYLOR & FRANCIS GROUP LLC–BOOKS.)*
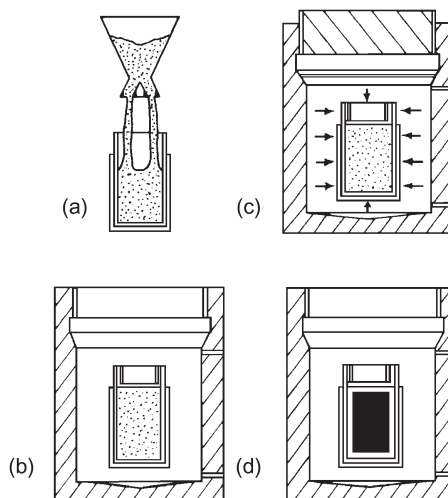
FIGURE 7.5 Schematic illustration of wet-bag isostatic pressing. (a) Filling; (b) Loading; (c) Pressing; and (d) Decompression prior to removing part. *(From Reed JS. Pressing. In: Principles of ceramics processing. New York: John Wiley & Sons; 1995, p. 443, Fig. 22.25. Reproduced with permission of John Wiley & Sons, Inc.)*

through the flexible wall of the mold to the powder, which results in compaction. After compaction, the pressure in the vessel is released and the compacted powder body is removed from the mold. The main advantage of wet-bag isopressing is higher packing uniformity than in uniaxial pressing. Pressures of up to 1000 GPa can be used, although the most common production units operate up to 200–300 MPa. Wet-bag isostatic pressing coupled with 3D green machining is
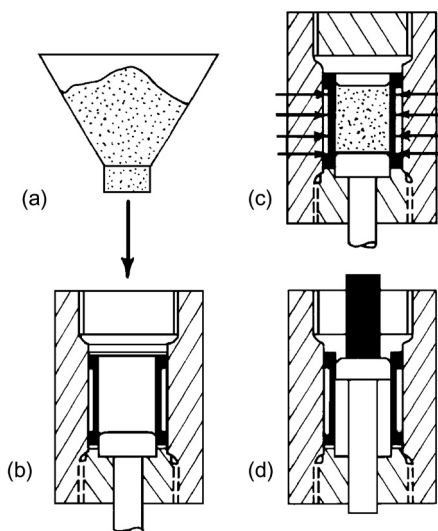
FIGURE 7.6   Schematic illustration of dry-bag isostatic pressing. (a) and (b) Loading of powder into the die; (c) Pressing; and (d) Ejection of pressed part through top or bottom of die. *(From Reed JS. Pressing. In: Principles of ceramics processing. New York: John Wiley & Sons; 1995, p. 443, Fig. 22.26. Reproduced with permission of John Wiley & Sons, Inc.)*

used to fabricate complex ceramic parts at very high quality. Dry-bag isopressing is easier to automate than the wet-bag process. It has a rubber mold tightly connected with the pressure vessel. This results in the pressurized liquid not acting from all directions, and the mold must be carefully designed to ensure homogeneous particle packing in the powder compact. Dry-bag isopressing can be automated as shown in Figure 7.6.

7.3.1.3   Powder Granulation

Due to the reason discussed above, fine powders agglomerate and do not flow easily. It is difficult to fill the die or mold with such powders and compact them homogeneously. Fine powders are therefore usually granulated, most commonly by spray-drying a well-dispersed ceramic slurry. The slurry is sprayed into a drying chamber with a stream of hot air. Small slurry droplets dry and produce spherical powder granules of 20–250 µm in size. Figure 7.7 shows a commercial spray-dried zirconia powder. The granules flow easily and regularly fill the die or mold. During compaction the granules must deform to fully eliminate the intergranulate pores while keeping the intragranular homogeneity (Figure 7.8). The organic additives present in the granules (3–5 wt.%) ensure the required plasticity of the granules and sufficient handling strength of the pressed compacts.
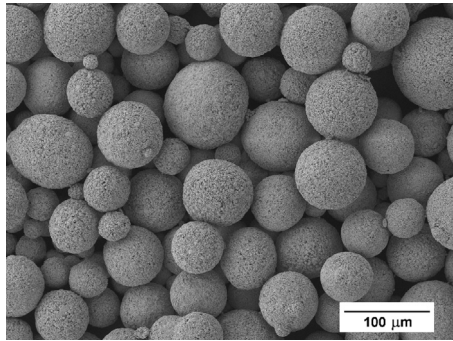
FIGURE 7.7   SEM microphotograph of spray-dried zirconia powder.
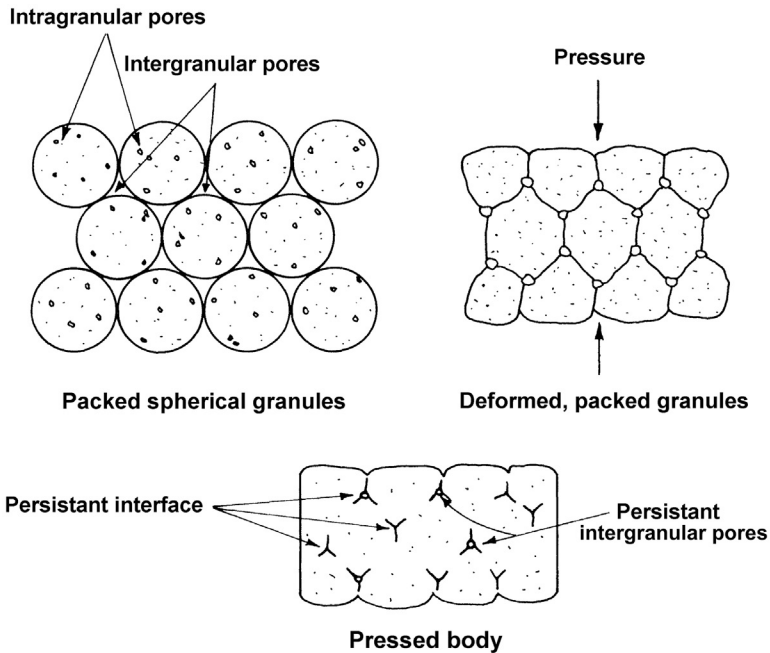
FIGURE 7.8   Illustration of change in shape and change of bimodal pore size distribution during compaction granulated powder. *(From Reed JS. Pressing. In: Principles of ceramics processing. New York: John Wiley & Sons; 1995, p. 428, Fig. 22.9. Reproduced with permission of John Wiley & Sons, Inc.)*

7.3.2   Wet Shaping Methods

7.3.2.1   Colloidal Suspensions

Wet shaping methods use suspensions of ceramic powders dispersed in low-molecular-weight solvents. With well-dispersed and stable suspensions, these
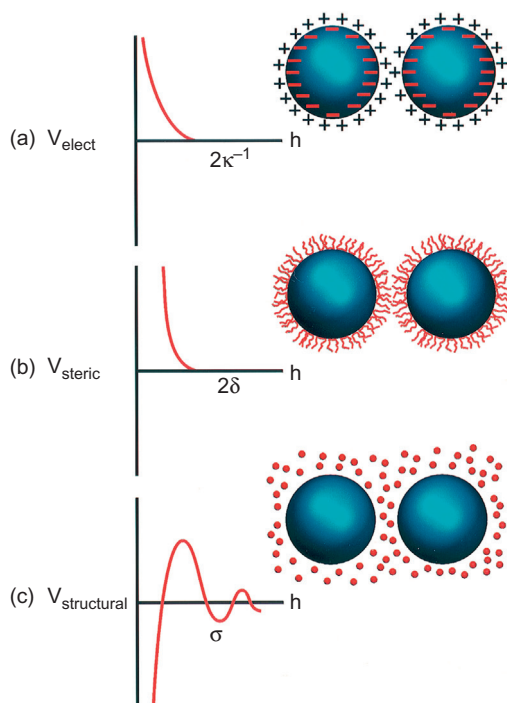
FIGURE 7.9 Schematic illustration of the interaction potential energy and relevant scales for (a) Electrostatic; (b) Steric; and (c) Structural contributions, where κ^{-1} is the effective double-layer thickness, δ is the polymer layer thickness, and σ is the depletant diameter. *(From Lewis JL. Colloidal processing of ceramics. J Am Ceram Soc 2000; 83(10):2341–59, Fig. 3. Reproduced with permission of John Wiley & Sons, Inc.)*

methods can provide highly regular particle packing in consolidated bodies, which results in ceramics for the most demanding applications.[5] Because the particle size of powders utilized in advanced ceramic processing is mostly well below 1 μm, colloidal approaches can be advantageously applied to prepare dispersed and stable suspensions. The colloidal processing of suspensions is based on a careful control of interparticle forces.[6] The attractive VdW forces must be eliminated by establishing repulsive forces between particles to achieve the desired degree of suspension stability. Potential interparticle repulsion can involve electrostatic, steric, or depletion interactions (Figure 7.9).[7] Electrostatic repulsion arises from interaction between particles with the same electrostatic surface charge. However, the repulsion is not a simple case of repulsion between charged particles. An electrical double layer of ions present in the solvent is formed around charged particles and the repulsion occurs as a result of the interaction of these double layers. The steric repulsion arises from the interaction between uncharged polymer chains adsorbed onto the particle surface. Polyelectrolyte species (macromolecules with dissociable groups)
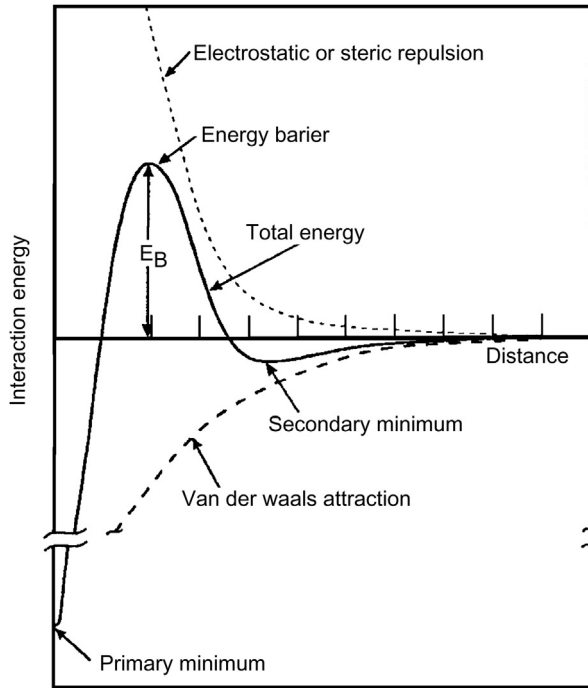
FIGURE 7.10 Schematic illustration of attractive, repulsive, and total potential energy curves for two particles in a suspension. *(From Sigmund WM, Bell NS, Bergström L. Novel powder-processing methods for advanced ceramics. J Am Ceram Soc 2000; 83(7):1557–74, Fig. 4. Reproduced with permission of John Wiley & Sons, Inc.)*

can provide both electrostatic and steric repulsion, the so-called electrosteric repulsion. Depletion forces occur between large colloidal particles suspended in a solution of non-adsorbing, smaller species (e.g. polymers or fine colloidal particles). The nature of the depletion (repulsive or attractive) depends on the distance between particles, and the oscillation of potential energy has a clear relation to the depletant diameter. Colloidal stability of the suspension is governed by the total interparticle potential energy (V_{total}), which can be expressed as Eq. 7.2:[7]

$$V_{total} = V_{vdW} + V_{elect} + V_{steric} + V_{struct} \qquad (7.2)$$

V_{vdW} is the attractive potential energy due to the van der Waals interaction, V_{elect} is the repulsive potential energy resulting from electrostatic interactions, V_{steric} is the repulsive potential energy resulting from steric interactions, and V_{struct} is the potential energy resulting from the presence of non-adsorbed molecules in the solution. Figure 7.10 shows the contribution of attractive
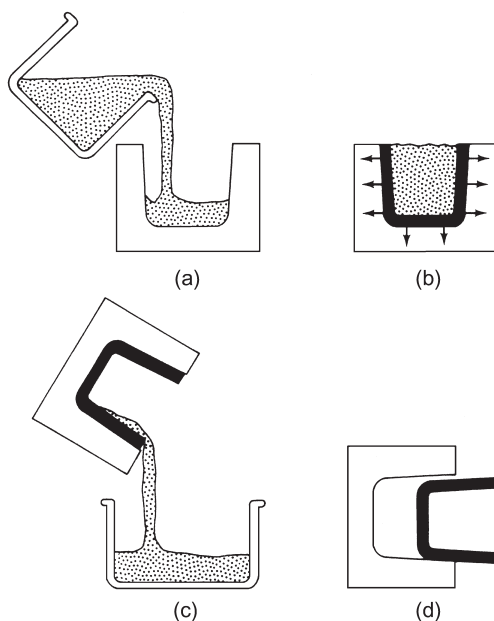
FIGURE 7.11 Schematic illustration of slip casting: (a) Fill mold with the slip; (b) Mold extracts liquid and forms compact along mold walls; (c) Excess slip is drained; and (d) Casting is removed after partial drying. *(From Richerson DW. Shape-forming processes. In: Modern ceramic engineering: properties, processing, and use in design, 2nd edition. New York: Marcel Dekker; 1992, p. 462, Fig. 10.34. Reproduced with permission of TAYLOR & FRANCIS GROUP LLC–BOOKS.)*

and repulsive potential energies to the total interparticle potential energy. This total interaction energy curve displays an energy barrier that prevents the particles from falling to the primary minimum and forming agglomerates. A shallow secondary minimum of the total interaction energy is also often present. Particles in this secondary minimum form isolated clusters (flocs) in suspension at a solid volume fraction below the gel point, or a particle network at higher volume fractions. Unlike the coagulated particles in the primary minimum, the structures in the secondary minimum can easily be dispersed by mixing or another intensive suspension treatment.

7.3.2.2 Slip Casting and Related Methods

In methods of this group, the shaping and consolidation of particles into green bodies occur by forced particle packing at the mold wall. In the case of slip casting, particle deposition is caused by fluid flow from the suspension (called slip) into the mold. The steps for forming the ceramic body by slip casting are shown in Figure 7.11. In slip casting, the dispersed ceramic suspension is poured into a microporous mold (usually made of gypsum). Due to capillary

forces the porous mold produces a suction pressure of up to 0.1 MPa[8] that draws the liquid from the suspension to the mold. The ceramic particles are too large to enter the mold pores and are deposited on the mold wall. After a sufficient thickness of the ceramic body has formed, the rest of the suspension is poured out and the body is allowed to dry prior to removal from the mold. Organic additives (0–2 vol.%) are dissolved in the suspension in order to improve the handling strength of the dried ceramic body. To increase the particle deposition rate, a mechanical load can be applied to the suspension. In pressure casting (also called pressure filtration) an external pressure is applied to the suspension in order to increase the fluid flow into the porous mold or filter. In centrifugal casting, the centrifugal force is applied to the suspension to increase the formation of a particle deposit.[8] The electrophoretic deposition method utilizes an electrostatically stabilized particle suspension.[9] Due to a unidirectional electric field (20–1000 V/cm) the charged particles move towards the oppositely charged electrode and deposit as a layer.

7.3.2.3 Direct Casting Methods

The most important feature in this group of methods is the capability to transfer the uniform particle dispersion from a stable suspension directly to the green body. The basic principle lies in a transformation of the liquid ceramic suspension into the solid body without removal of solvent. The stable suspension is poured into a nonporous mold where it is consolidated by gelation. The gelled body is strong enough to be de-molded and dried. Gelation of the suspension into a solid body can proceed in two ways. Either physical gels or chemical gels can be formed.[10] The physical particle gels rely on the formation of a physical bond between ceramic particles in dense suspensions and are mainly achieved by manipulating the interparticle forces to become attractive. Because the physical gels are based on vdW attractive forces, they are relatively weak and must be handled with care. Direct coagulation casting is the best known method based on this principle.[11] Strong chemical gels are formed by chemical reactions between either the particles or some species dissolved in the suspensions.[12] Gelcasting is a typical representative of these methods.[13,14] In gelcasting, a percolating polymer network is formed by polymerizing monomers dissolved in the suspension. All direct casting methods require suspensions with very high solid loading in order to produce applicable ceramic gels. Hence, tailoring the particle interactions in the suspension to maximize the solid concentration while keeping a reasonably low viscosity have become one of the most important issues in these shaping methods.

7.3.2.4 Tape Casting

Tape casting produces a thin layer of ceramic material by coating a carrier surface (thin organic film) with a ceramic suspension, usually by the doctor-blade process. The suspension for tape casting consists of ceramic particles in

a solvent that also contains dissolved binders and plasticizers that are incorporated to impart strength and flexibility to the cast tape. The suspension is spread into a thin layer by a doctor blade. During drying the volatile solvent is removed by evaporation and a flexible tape that consists of particle-filled polymer matrix is formed. Prior to sintering, the flexible sheets can be cut into desired shapes and dimensions and often the sheets are stacked to produce multilayer function blocks. This method can continuously produce thin ceramic sheets with thicknesses between 10 and 1000 μm.

7.3.3 Plastic Shaping Methods

Plastic shaping methods form the green body by deforming a ceramic–additive mixture that can flow plastically when stressed beyond a certain yield stress. However, the shaped body must be strong enough to be handled safely. There are two important methods for shaping the plastic ceramic mixtures, both derived from the plastics industry: injection molding and extrusion.

7.3.3.1 Injection Molding

To shape the ceramic mixture into a green body, the injection molding method utilizes a temperature-dependent transformation of the ceramic mixture from the liquid into the solid phase.[15] As noted in Figure 7.12, the injection molding process comprises several steps.[16] In the first step, the ceramic powder is mixed in a kneader with a thermoplastic binder (usually a mixture of thermoplastic polymers and waxes) and other additives that ensure the formation of a homogeneous ceramic mixture with suitable rheological properties. In the second step, the ceramic mixture is granulated/pelletized. In the next step, the heated barrel of an injection molding machine is filled with ceramic granules. After softening and plasticization of the granules in the barrel at elevated temperatures (50–250°C), the plastic mixture is injected into the mold. The mixture solidifies in the cold mold and the shaped green body can be ejected from the mold. The next steps, binder removal and sintering, are discussed in the following paragraphs. Injection molding is an optimal shaping method for the mass production of small and complex ceramic parts because the method can be automated and the extensive final machining of complex parts can be eliminated. However, the difficulties associated with binder removal from the fine-particle green body limit the use of injection molding to parts with wall thicknesses below 10 mm.[17]

7.3.3.2 Extrusion

In extrusion, the ceramic green body is shaped by forcing the ceramic paste through a nozzle. A straight extrudate with a controlled cross-section is then cut to an appropriate length to form the final green body. To obtain the desired plastic properties of the paste the ceramic powder is mixed with
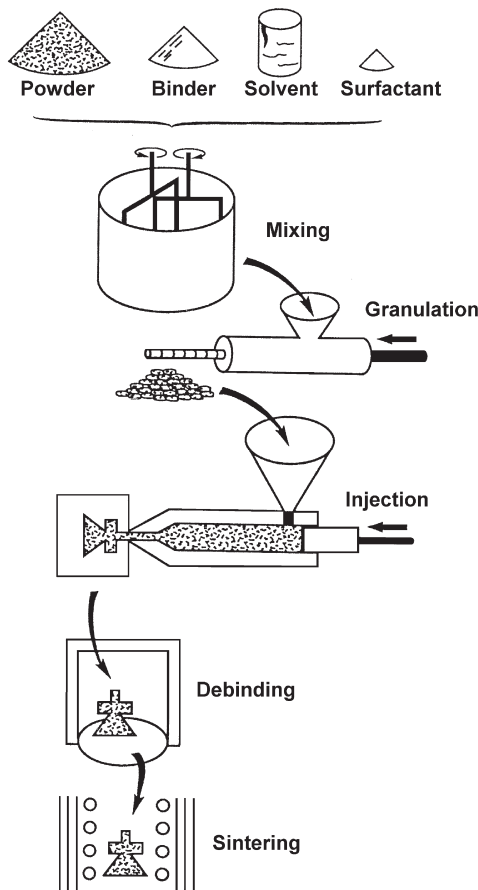
FIGURE 7.12   Schematic diagram of the steps in the injection molding method. *(From German RM, Hens KF, Lin STP. Key issues in powder injection molding. Ceram Bull 1991;70(8):1294–1302, Fig. 1. Reproduced with permission of The American Ceramic Society.)*

a solution containing an organic binder and other necessary additives. The solvent is commonly water, but non-aqueous solvents are also used. The extruded body must be stiff enough to prevent shape distortion and warpage. Therefore, the binder is selected such that it provides a high-viscosity ceramic mixture with pronounced yield stress (e.g. methylcellulose, polyvinyl acetate, polyvinyl glycol, etc.). The thermoplastic extrusion utilizing ceramic mixtures and forming steps similar to those used in injection molding has also been developed.[18] For the piston extruder, which consists of a barrel, a piston, and a die, the ceramic mixture must be prepared in advance in a kneader. The screw extruder, which is of more complex design than the piston extruder, can mix the powder and other additives into a homogeneous

paste by itself, and at the same time it can generate pressure to transport the mixture against the resistance of the die.

7.3.4   Solid Free-form Fabrication

Solid free-form fabrication (SFF) methods (often referred to as rapid proto-typing methods) are processes that allow ceramic bodies to be formed directly from computer-aided design (CAD) files, without the use of any forming tools such as molds or die. Although the principles of particular methods are totally different, a common feature of all SFF methods is the computer-controlled layer-wise deposition of material to build the ceramic body. The general SFF process begins with the virtual slicing of the CAD model. The slices are then created one on top of the other by a computer-controlled device to form the ceramic part. Even structures that are impossible to form by other shaping methods can often be prepared by SFF methods. The relevant SFF methods for ceramic processing include: 3D printing, direct ink-jet printing, stereolithography, fused deposition modeling, robocasting, and selective laser sintering. More details on these specific forming methods can be found in Chapter 18 of this book that is focused solely on this topic.

7.4   DRYING AND BINDER REMOVAL

All additives (solvents, binders, plasticizers, surfactants, dispersants, etc.) employed to shape and consolidate the green bodies must be removed from powder compacts prior to sintering. Drying the solvent from colloidal particle compacts after wet shaping, as well as binder removal from fine particle bodies after plastic shaping, are the critical steps in ceramic processing.

7.4.1   Drying of Porous Bodies

Drying the solvent from a porous particle compact can be divided into three stages[19]:

1. Constant-rate period (CRP).
2. First falling-rate period (FRP1).
3. Second falling-rate period (FRP2).

Figure 7.13 shows the stages of drying and the progress of powder compact shrinkage during drying. The first stage of drying is called the constant-rate period because the evaporation rate per unit area of the drying surface is independent of time. In CRP, the rate of drying (V_E) is controlled by external conditions and can be calculated according to Eq. 7.3:

$$V_E = k(p_v - p_a)$$

(7.3)
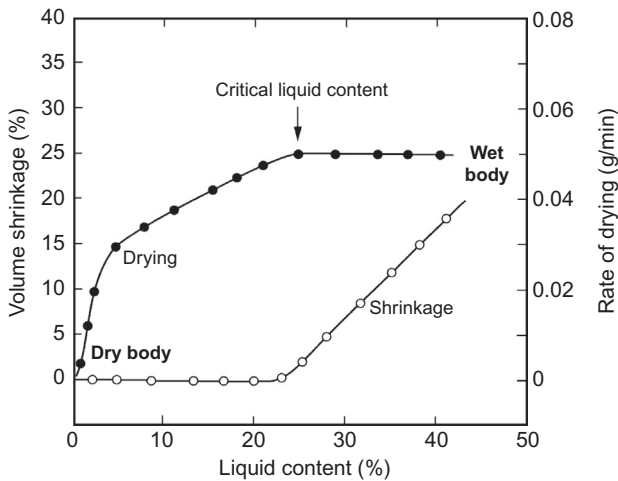
FIGURE 7.13 Rate of drying and volume changes during the uniform drying of porous body. *(From Kingery WD. Forming processes. In: Introduction to ceramics. New York: John Wiley & Sons; 1960, p. 57, Fig. 3.20. Reproduced with permission of John Wiley & Sons, Inc.)*

The saturated vapor pressure is p_v, p_a is the partial vapor pressure of the drying liquid in the surrounding atmosphere, and k is a factor dependent on temperature, body geometry, and ambient gas flow. In the CRP stage, liquid is transported by capillary forces to the body surface, where it evaporates. The evaporation occurs only from the body surface. Due to the gradual removal of the liquid, the particles come into mutual contact and the body becomes stiff. The moment the particles touch each other, the body stops shrinking and there is a critical liquid content in the body. Further evaporation drives the liquid–vapor interface from the body surface into the body interior and the first falling-rate period begins. During this stage the rate of drying decreases. The large pores are emptied first. The smaller pores with higher capillary tension remain fully saturated by liquid because they can draw liquid from larger pores, and as a result, an irregular drying front is established. The thickness of this region depends on the evaporation rate and the rate of redistribution of the liquid phase. With further evaporation the flow of the liquid to the surface is interrupted and the liquid is closed in isolated pockets. The liquid removal can now be realized by evaporation inside the body followed by vapor diffusion to the body surface. This stage is called the second falling-rate period.

In the case of thick-wall or fine-particle green bodies, the flow of liquid from the center to the surface during CRP and FRP1 stages is usually slower than the evaporation. Irregular redistribution of the liquid in the body generates a porous unsaturated surface layer and a saturated body center with a liquid content above the critical point. Such an inhomogeneous structure results in macroscopic stresses that are responsible for the distortion or even cracking

of dried bodies. Capillary stresses are also responsible for local defects around small, saturated pores surrounded by larger empty pores. These local defects can be combined with macroscopic stresses and result in severe cracking during the drying of fine-particle and thick-wall bodies.[19]

7.4.2   Binder Removal

The terms binder removal or debinding are usually used to refer to the removal of polymeric binders as well as other organic additives, such as plasticizers, lubricants, and dispersants. The binder removal step represents the most difficult step in ceramic injection molding, as well as in all other plastic shaping methods where all pores in the green body are fully saturated with the binder. In most of these methods, the binder removal limits the size and shape complexity of the green body because in bigger and more complex bodies it is not possible to remove the binder safely and in an acceptable time. The description of binder removal methods, including an overview of chemical and physical principles of the debinding processes was presented in several reviews.[20–23] It was clearly shown that besides new and advanced debinding methods such as supercritical, catalytic, or solvent binder removal, thermal debinding is still the most widely applied method due to its versatility and simplicity. Commonly used binders consist of more components with different molecular weights, and their thermal removal occurs via three mechanisms: evaporation, thermal degradation, and oxidative degradation. Unlike polymers, binder components with low molecular weights are not subject to scission of the molecular chain, and their removal is realized via diffusion to the body surface and evaporation. Binder components with high molecular weights (polymers) thermally degrade and form low-molecular-weight products. Thermal degradation of macromolecules proceeds uniformly throughout the volume of the polymer phase. The degradation products diffuse to the body surface or to the liquid–vapor interface where they can evaporate. The presence of oxygen in the ambient atmosphere during thermal debinding brings about the oxidative degradation of the polymeric binder at the body surface. Propagation of oxidative degradation into the interior is restricted by diffusion of oxygen into the binder as well as by diffusion of degradation products towards the surface and evaporation. Yet another debinding process can take place during thermal debinding when the body is surrounded by a porous medium (powder bed, porous pad). A capillary flow of the molten binder from the green body to the porous medium can occur, thus the binder content in the green body can be effectively decreased.[24,25]

Evaporation of low-molecular-weight binder components and the processes accompanying it are similar to those in drying a solvent in a particle body. However, diffusion of low-molecular-weight binder components and degradation products through the liquid binder to the body surface or liquid–vapor interface, where they can evaporate, is a slow process. Therefore, the heating

rate during thermal debinding must be carefully controlled to prevent exceeding the critical boiling temperature of these low-molecular-weight species.[26] The evolution of large amounts of gases inside the saturated pore structure results in the formation of defects such as bubbles, blisters, and cracks.

7.5 SINTERING

Sintering is an unavoidable step in the processing of advanced ceramic materials that significantly influences the microstructure of products, and thus their mechanical, optical, biological, electrical, or magnetic properties. It is therefore important to optimize the sintering process (e.g. by the choice of input powder material, by the choice of shaping and sintering techniques, by the choice of heating profile and sintering atmosphere, etc.). Although the sintering process has been known for thousands of years and systematically studied by physicists, chemists, and material engineers since the 1940s, a unified theory of sintering kinetics and its influence on final microstructure still does not exist, even in the case of pressure-less sintering. The reason for that is the complicated nature of mass transport in polycrystalline materials.

7.5.1 Fundamentals of Sintering: Thermodynamics and Kinetics

Several definitions of sintering can be found in the literature.[27–31] All of them express the fact that sintering is an irreversible process during which the surface energy of the system is decreased at elevated temperature. According to this, sintering is a thermal treatment for bonding particles into a coherent, predominantly solid structure via mass transport events that often occur on the atomic scale. Bonding leads to improved strength and lower system energy.[31] Sintering products are characterized by enhanced density and by improved properties, therefore sintering is used in a wide range of industries.

Although a complete description of the sintering process is not yet possible, the basic principles are known. The thermodynamic driving force for sintering is the reduction of surface energy, as the free surface of loose ceramic particles has more energy than that of grain boundaries in the sintered ceramics. The total surface energy change can be expressed by Eq. 7.4:

$$\Delta(\gamma^{sg} S) = \Delta\gamma^{sg \to ss} S + \gamma^{sg} \Delta S \qquad (7.4)$$

The symbol γ^{sg} is the interfacial energy of the solid/gas interface (loose powders), $\Delta\gamma^{sg \to ss}$ is the change of interfacial energy ($\gamma^{ss} - \gamma^{sg}$) of grain boundary formation (γ^{ss}) caused by sintering, S is the surface area of the initial powder, and ΔS is the lowering of the surface area caused by particle coarsening. Note that both members of the right-hand side of Eq. 7.4 are negative, therefore the decrease of the surface energy of the system can by caused by both sintering and coarsening (see also Figure 7.14).
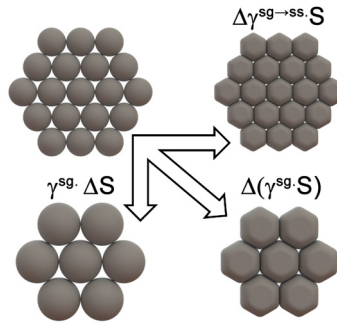
FIGURE 7.14 Schema of the decrease of surface energy $\Delta(\gamma^{sg}.S)$ during sintering and coarsening.

Unfortunately, coarsening and grain growth are undesirable in many applications because they degrade some important properties, such as hardness;[32] flexural strength;[33,34] resistance to mechanical[35,36] and biological wear;[37] electric conductance along grain boundaries;[38] or optical transparency.[39,40] Since the difference between γ^{sg} and γ^{ss} is of the order of $1\,J/m^2$, we can simply calculate that the change of surface energy during sintering of ceramic powder (e.g. alumina or zirconia as typical bioceramic materials) with a particle diameter of 100 nm (modern advanced ceramic powder materials for high-tech applications) is of the order of $1\,kJ/mol$. This value is relatively small, therefore it is very important to understand and control all variables involved in the sintering process in order to achieve the desired microstructure of the sintered body.[30]

Sintering stress (σ, pressure) is proportional to the ratio of the surface tension and the radius of the particle (pore), Eq. 7.5:[2]

$$\sigma \sim \gamma/r \qquad (7.5)$$

Therefore, the sintering stress in powder compacts with dimensions of the order of $1\,\mu m$ is in MPa, but in the case of particles of 10 nm the sintering stress is in the order of hundreds of MPa. Even so, the high driving force would have no meaning if there were no ways for mass transport to lead to energy reduction. In the case of sintering, such paths are viscous flow (applied especially for glasses and polymers) and the process of evaporation and condensation (applied especially for substances with ionic bonds). For advanced ceramics, it is mainly diffusion. According to the diffusion path, it can be divided into surface diffusion, volume diffusion (or lattice diffusion), and diffusion along grain boundaries (grain boundary diffusion). The most important for densification are bulk diffusion and diffusion along grain boundaries because only these mass transfers from the necks between particles into the pores cause contraction of the body and are accompanied by the gradual disappearance of the pores.
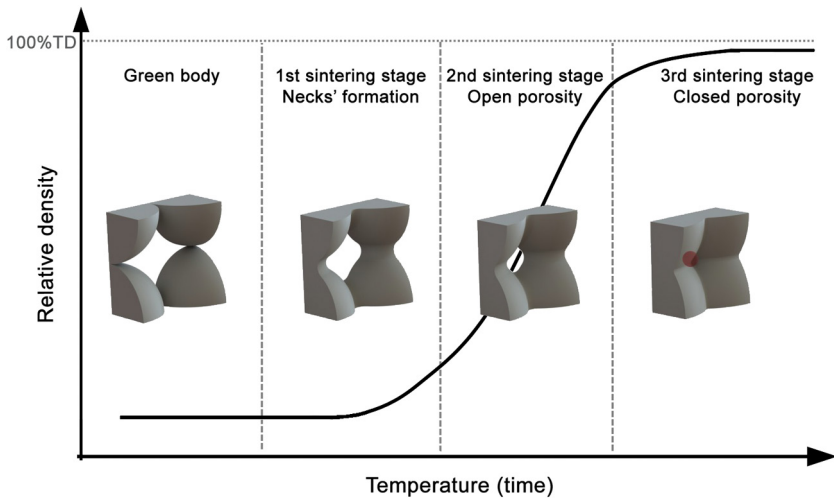
FIGURE 7.15   Three stages of sintering of ceramic materials.

Since diffusion is a thermally activated process, it is therefore necessary to sinter ceramics at elevated temperatures. During sintering, the green body goes through three sintering stages (Figure 7.15). In the first phase, necks are created among particles, thereby increasing the strength of the body; shrinkage is only a few percent. In the second phase, (the phase of open porosity) a continuous pore channel is formed and the body in this sintering stage can be compared to a porous sponge. These tubular pores shrink their radius and when the body reaches more than 92% of its theoretical density (i.e. the pores are only 8% of the body), the body enters the third sintering phase (the so-called closed porosity stage) when the pores are isolated from the outer surface of the ceramics.

7.5.2   Classification of Sintering Methods

The basic requirements for sintered parts are minimal defects; the required chemical and phase composition and microstructure (these determine the properties of the product); dimensional accuracy; reproducibility of production; low cost, etc. Although most of the properties are influenced by processing prior to sintering, there is still room to improve ceramic processing by the proper choice of sintering variables.

Depending on the application of external pressure, we divide the sintering process into pressure-less sintering and pressure-assisted sintering. If some of the components during sintering are in the liquid state, this is called liquid-phase sintering. Wettable liquid between particles (from capillary forces) increases sintering pressure.[27–31] This method is often used for sintering

non-oxide ceramics used as extremely hard cutting tools or for sintering metals (also dental amalgams, restorations, and appliances).[28] The liquid phase often chemically reacts with the surrounding solid phase or atmosphere, which leads to so-called reactive-based processing that in many cases exhibits low shrinkage and advanced shapability.[41] Advanced bioceramic materials are usually sintered without the presence of liquid phases (i.e. by solid-state sintering), but occasionally also by liquid-phase sintering (using bioglasses as reinforced phase).[42,43]

7.5.2.1 Pressure-less Sintering

The conventional pressure-less sintering technique is experimentally cheap and simple. In this method one can affect the heating regime (heating rate, sintering temperature, and dwell time) and the type of furnace atmosphere.

In the case of conventional pressure-less sintering, there is not yet a general opinion in the literature as to whether the final grain size of an individual body of defined final density can also be influenced by the choice of sintering regimes. Based on theoretical models of sintering, it has been suggested that the final density definitely determines the grain size of the sintered bodies.[44–46]

On the other hand, there are also reports that refined microstructures can be obtained by the correct choice of sintering profile. One of the most important is so-called two-step sintering (TSS) published by Chen and Wang.[47] In this method, the sample is heated in the first step to an elevated temperature to achieve a density higher than 75% t.d. (the point at which supercritical pores are removed from the sintered body), and then quickly cooled down in the second step and held at a lower temperature until full densification (without additional grain growth). This method is currently widely used for sintering different kinds of ceramic materials.[48–53] The significant decrease of grain size was reported mainly for materials with cubic crystal structures (Y_2O_3,[47] $BaTiO_3$,[51] $SrTiO_3$,[52] c-ZrO_2,[50,53] etc.).

Another kind of pressure-less sintering is microwave sintering. Microwaves are electromagnetic waves with a wavelength in the range of 1 mm to 1 m (and corresponding frequencies 300 GHz–300 MHz). Their interaction with ceramic materials leads to heat generation. This kind of heating differs from conventional sintering because it is not realized due to heat transfer, but by the energy conversion; therefore, microwave sintering can be very rapid (heating rates of ~1000°C/min can be achieved). On the other hand, microwave sintering is material dependent. The absorption of microwave energy depends on the material's dielectric loss (ceramic insulators such as Al_2O_3, ZrO_2, and MgO, and glasses have low response to microwave sintering at low temperatures, but enhanced at elevated temperatures); magnetic properties (metals); and microstructural properties (pore size distributions, grain size). More information about microwave sintering can be found in relevant books[28,30,31] and review papers.[54]

7.5.2.2   Pressure-assisted Sintering

For some high-tech ceramic applications (like transparent ceramics, bioceramics, structural ceramics, etc.) it is advantageous to use pressure-assisted sintering. The applied pressure contributes to the sintering driving force (see Eq. 7.5) and can considerably benefit densification. There are two principle ways to apply external pressure to the ceramic sample: isostatic (hot isostatic pressing) and uniaxial (hot pressing, sinter forging). A disadvantage of pressure-assisted sintering is the increased cost, therefore this method is applied only for components with high additional value.

7.5.2.3   Hot Isostatic Pressing

In hot isostatic pressing (HIP) the pre-consolidated powder is first tightly enclosed under vacuum in a glass or metal container, or alternatively, pre-sintered to the closed porosity stage. Then the ceramic component is placed into a furnace that can be pressurized (obviously by argon) up to hundreds of MPa and sintered at elevated temperature. The simultaneous effects of elevated temperature and increased pressure can heal some defects in ceramics and increase their final density so they can acquire additional properties (e.g. optical transparency[55] or higher mechanical properties[56]). The advantages of this method are the isostatic (and therefore homogeneous) pressure and the possibility of sintering the components with various shapes.

7.5.2.4   Hot Pressing

Hot pressing is the process where molding and sintering are performed in one step. Pressure is generated mechanically and is uniaxial. The sample obviously has the shape of a cylinder (or another planar geometry given by the shape of the piston). Graphite is the most common material for die construction because it is not expensive and shows excellent creep resistance at high temperatures. The advantage of this method lies in the possibility of particle rearrangement during the early stages of sintering.

7.5.2.5   Spark Plasma Sintering

Spark plasma sintering (SPS) is currently the most widely used method of plasma-activated sintering (e.g. in sintering of nanoceramics, transparent ceramics, etc.). In this method, sintering is the simultaneous action of mechanical pressure (similar to hot pressing) and the electric field pulse (Figure 7.16). Recently, some papers showed that the applied pressure is not necessary for rapid sintering in an SPS apparatus,[57,58] therefore rapid sintering of complex shaped ceramics is possible in SPS.

7.5.3   Influence of Sintering Atmosphere

The sintering atmosphere can also affect sintering. The first reason for this is technical: it is not possible to sinter ceramics in an oxidizing atmosphere, as
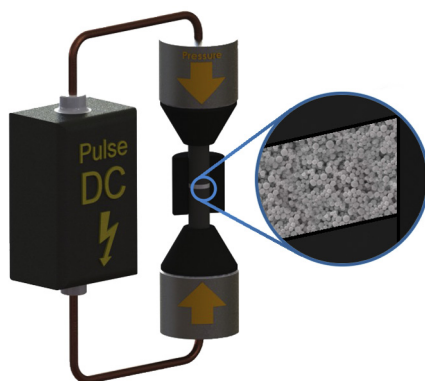
FIGURE 7.16   Schema of spark plasma sintering (SPS) method.

in the case of graphite heating elements (e.g. hot press, hot isostatic press, or SPS), or in high-temperature furnaces equipped with molybdenum or tungsten heating elements. The other reasons are physical (gases trapped in isolated pores) or chemical (oxidation prevention, volatility control, oxidation states, defect chemistry, reactive-based processing, etc.); therefore, sintering is implemented in vacuum,[59,60] inert,[61] hydrogen,[62] or nitrogen[63] atmospheres.

REFERENCES

1. Lange FF. Densification of powder compacts: an unfinished story. J Eur Ceram Soc 2008;28(7):1509–16.
2. Mayo MJ. Processing of nanocrystalline ceramics from ultrafine particles. Int Mater Rev 1996;41(3):85–115.
3. Butt H-J, Kappl M. Van der Waals forces. In: Surface and interfacial forces. Weinheim: Wiley-VCH; 2010. p. 5–53.
4. Kingery WD. Pressure forming of ceramics. In: Kingery WD, editor. Ceramic fabrication processes. Cambridge: Technology Press of Massachusetts Institute of Technology; 1958. p. 55–61.
5. Lange FF. Powder processing science and technology for increased reliability. J Am Ceram Soc 1989;72(1):3–15.
6. Horn RG. Surface forces and their action in ceramic materials. J Am Ceram Soc 1990;73(5):1117–35.
7. Lewis JA. Colloidal processing of ceramics. J Am Ceram Soc 2000;83(10):2341–59.
8. Schilling CH, Aksay IA. Slip casting. In: Schneider SJ, editor. Ceramics and glasses, (engineered materials handbook, vol 4. Metals Park, Ohio: ASM International; 1991. p. 153–60.
9. Corni I, Ryan MP, Boccaccini AR. Electrophoretic deposition: From traditional ceramics to nanotechnology. J Eur Ceram Soc 2008;28(7):1353–67.
10. Sigmund WM, Bell NS, Bergstrom L. Novel powder-processing methods for advanced ceramics. J Am Ceram Soc 2000;83(7):1557–74.
11. Gauckler LJ, Graule T, Baader F. Ceramic forming using enzyme catalyzed reactions. Mater Chem Phys 1999;61(1):78–102.
12. Tari G. Gelcasting ceramics: a review. Am Ceram Soc Bull 2003;82(4):43–6.

13. Young AC, Omatete OO, Janney MA, et al. Gelcasting of alumina. J Am Ceram Soc 1991;74(3):612–8.
14. Omatete OO, Janney MA, Strehlow RA. Gelcasting, a new ceramic forming process. Am Ceram Soc Bull 1991;70(10):1641–9.
15. Mutsuddy BC. Injection molding. In: Schneider SJ, editor. Ceramics and glasses, (engineered materials handbook, vol 4). Metals Park, Ohio: ASM International; 1991. p. 173–80.
16. German RM, Hens KF, Lin STP. Key issues in powder injection-molding. Ceram Bull 1991;70(8):1294–302.
17. Trunec M, Cihlar J. Thermal debinding of injection moulded ceramics. J Eur Ceram Soc 1997;17(2–3):203–9.
18. Trunec M. Fabrication of zirconia- and ceria-based thin-wall tubes by thermoplastic extrusion. J Eur Ceram Soc 2004;24(4):645–51.
19. Scherer GW. Theory of drying. J Am Ceram Soc 1990;73(1):3–14.
20. Trunec M, Cihlar J. Removal of thermoplastic binders from ceramic green bodies. Ceram-Silik 1997;41(2):67–80.
21. German RM. Theory of thermal debinding. Int J Powder Metall 1987;23(4):237–45.
22. Evans JRG, Edirisinghe MJ, Wright JK, et al. On the removal of organic vehicle from molded ceramic bodies. Proc R Soc A-Math Phys Eng Sci 1991;432(1885):321–40.
23. Calvert P, Cima M. Theoretical-models for binder burnout. J Am Ceram Soc 1990;73(3):575–9.
24. Lovro G, Dakskobler A, Kosmac T. Partial wick-debinding of low-pressure powder injection-moulded ceramic parts. J Eur Ceram Soc 2010;30(15):3013–21.
25. Lovro G, Dakskobler A, Kosmac T. Strength evolution of injecrion-molded ceramic parts during wick-debinding. J Am Ceram Soc 2012;95(1):188–93.
26. Trunec M, Cihlar J. Thermal removal of multicomponent binder from ceramic injection mouldings. J Eur Ceram Soc 2002;22(13):2231–41.
27. Kingery WD, Bowen HJ, Uhlmann DR. Introduction to ceramics. : John Wiley and Sons, Inc; 1960.
28. German RM. Sintering theory and practice. : John Wiley and Sons, Inc; 1996.
29. Kang SYL. Sintering. densification, grain growth, and microstructure. : Elsevier Butterworth and Heinemann; 2005.
30. Rahaman MN. Sintering of ceramics. : Taylor & Francis; 2008.
31. Fang ZZ. Sintering of advanced materials. Fundamentals and processes. : Woodhead Publishing Limited; 2010.
32. Krell A, Blank P. Grain-size dependence of hardness in dense submicrometer alumina. J Am Ceram Soc 1995;78(4):1118–20.
33. Krell A, Blank P. The influence of shaping method on the grain size dependence of strength in dense submicrometre alumina. J Eur Ceram Soc 1996;16(11):1189–200.
34. Koo OYT, Hong KJ, Park JS, Shin DC. Effect of grain size on transmittance and mechanical strength of sintered alumina. Mat Sci Eng A-Struct 2004;374(1-2):191–5.
35. Krell A, Klaffke D. Effects of grain size and humidity on fretting wear in fine-grained alumina, Al_2O_3/TiC, and zirconia. J Am Ceram Soc 1996;79(5):1139–46.
36. He YJ, Winnubst L, Burggraaf AJ, Verweij H, vander Varst PGT, deWith B. Grain-size dependence of sliding wear in tetragonal zirconia polycrystals. J Am Ceram Soc 1996;79(12):3090–6.
37. Lawson S. Environmental degradation of zirconia ceramics. J Eur Ceram Soc 1995;15(6):485–502.

38. Xu G, Zhang YW, Liao CS, Yan CH. Grain size-dependent electrical conductivity in scandia-stabilized zirconia prepared by a mild urea-based hydrothermal method. Solid State Ionics 2004;166(3-4):391–6.
39. Klimke J, Trunec M, Krell A. Transparent tetragonal yttria-stabilized zirconia ceramics: influence of scattering caused by birefringence. J Am Ceram Soc 2011;94(6):1850–8.
40. Apetz R, Van Bruggen MPB. Transparent alumina: a light-scattering model. J Am Ceram Soc 2003;86(3):480–6.
41. Janseen R, Scheppokat S, Classen N. Tailor-made pramic-based components-Advantages by reactive processing and advanced shaping techniques. J Eur Ceram Soc 2008;28:1369–79.
42. Santos C, Souza RC, Habibe AF, et al. Mechanical properties of Y-TPZ ceramics obtained by liquid phase sintering using bioglass as additive. Mater Sci Eng A Struct Mater 2008;478(1-2):257–63.
43. Oktar FN, Goller G. Sintering effects on mechanical properties of glass-reinforced hydroxyapatite composites. Ceram Int 2002;28(6):617–21.
44. Su HH, Johnson DL. Master sintering curve:a practical approach to sintering. J Am Ceram Soc 1996;79(12):3211–7.
45. Wang JD, Raj R. Estimate of the activation-energies for boundary diffusion from rate-controlled sintering of pure alumina, and alumina doped with zirconia or titania. J Am Ceram Soc 1990;73(5):1172–5.
46. Maca K, Simonikova S. Effect of sintering schedule on grain size of oxide ceramics. J Mat Sci 2005;40(21):5581–9.
47. Chen IW, Wang XH. Sintering dense nanocrystalline ceramics without final-stage grain growth. Nature 2000;404:168–71.
48. Balaya P, Ahrens M, Kienle L, et al. Synthesis and characterization of nanocrystalline $SrTiO_3$. J Am Ceram Soc 2006;89(9):2804–11.
49. Bodisova K, Sajgalik P, Galusek D, Svancarek P. Two-stage sintering of alumina with submicrometer grain size. J Am Ceram Soc 2007;90(1):330–2.
50. Mazaheri M, Valefi M, Hesabi ZR, Sadrnezhaad SK. Two-step sintering of nanocrystalline 8Y(2)O(3) stabilized ZrO2 synthesized by glycine nitrate process. Ceram Int 2007;35:13–20.
51. Wang XH, Chen PL, Chen IW. Two-step sintering of ceramics with constant grain-size, II: BaTiO3 and Ni-Cu-Zn ferrite. J Am Ceram Soc 2006;89:438–43.
52. Maca K, Pouchly V, Shen Z. Two-step sintering and spark plasma sintering of Al_2O_3, ZrO_2 and $SrTiO_3$ Ceramics. Integr Ferroelectr 2008;99(1):114–24.
53. Maca K, Pouchly V, Zalud P. Two-Step Sintering of oxide ceramics with various crystal structures. J Eur Ceram Soc 2010;30(2):583–9.
54. Oghbaei M, Mirzaee O. Microwave versus conventional sintering: A review of fundamentals, advantages and applications. J Alloys Comp 2010;494:175–89.
55. Maca K, Trunec M, Chmelik R. Processing and properties of fine-grained transparent $MgAl_2O_4$ ceramics. Ceram-Silik 2007;51(2):94–7.
56. Ruys AJ, Sorrel CC, Dickson MR, Brandwood A, Milthorpe BK. Sintering effects on the strength hydroxyapatite. Biomaterials 1995;16:409–15.
57. Salamon D, Shen Z. Pressure-less spark plasma sintering of alumina. Mater Sci Eng A Struct Mater 2008;A475(1–2):105–7.
58. Salamon D, Maca K, Shen Z. Rapid sintering of crack-free zirconia ceramics by pressure-less spark plasma sintering. Scr Mat 2012;66(11):899–902.
59. Srdic V, Winterer M, Hahn H. Sintering behavior of nanocrystalline zirconia prepared by chemical vapor synthesis. J Am Ceram Soc 2000;83(4):729–36.

60. Maca K, Dobsak P, Boccaccini AR. Fabrication of graded porous ceramics using alumina-carbon powder mixtures. Ceram Int 2001;27(5):577–84.
61. Xiong YY, Qian C, Sun J. Fabrication of porous titanium implants by three-dimensional printing sintering at different temperatures. Dent Mater J 2012;31(5):815–20.
62. Kachlik M, Maca K, Goina V, Kamba S. Processing of phase pure and dense bulk EuTiO3 ceramics and their infrared reflectivity spectra. Mater Lett 2012;74:16–18.
63. Atkinson A, Moulson AJ, Roberts EW. Nitridation of high-purity silicon. J Am Ceram Soc 1976;54(7/8):285–9.

Microstructure Characterization of Advanced Ceramics

Saso Sturm and Boštjan Jančar
Jožef Stefan Institute, Ljubljana, Slovenia

Contents

8.1 SURFACE TOPOGRAPHY

A surface in ceramics is defined as an interface between the solid bulk and the surrounding environment, which is liquid, gas, or vacuum. Understanding the surface structure becomes especially important when the surface structure and resulting electronic, chemical, and mechanical properties start to dominate the corresponding bulk. For example, the surface structure of the substrate material controls the adhesion of deposited thin film. Then, the final properties of materials characterized by the large surface-to-volume ratio, like nanostructures, are in many ways defined by the surface structure.

Ideally, the ceramic surface can be atomically flat, which is more the exception then the rule. In reality, the surface structure starts to deviate from its ideal configuration already at the nanometer region by forming atomic facets, steps, kinks, ledges, and point defects (Figure 8.1a).

In ceramic materials both the atom types and atom density between different crystallographic planes can vary significantly. Consequently, atomic-scale surface topography in ceramics depends on the surface terminating crystallographic plane, as shown in an $SrTiO_3$ crystal cube (Figure 8.1b). In contrast to metals, atomic bonds in ceramics are predominately ionic and covalent, which results in both local charge variations and the formation of dangling bonds at the ceramic surface. The surface atoms have a reduced number of nearest neighbors compared to their bulk counterparts. The non-equilibrium coordination of surface atoms can lead to a surface reconstruction involving
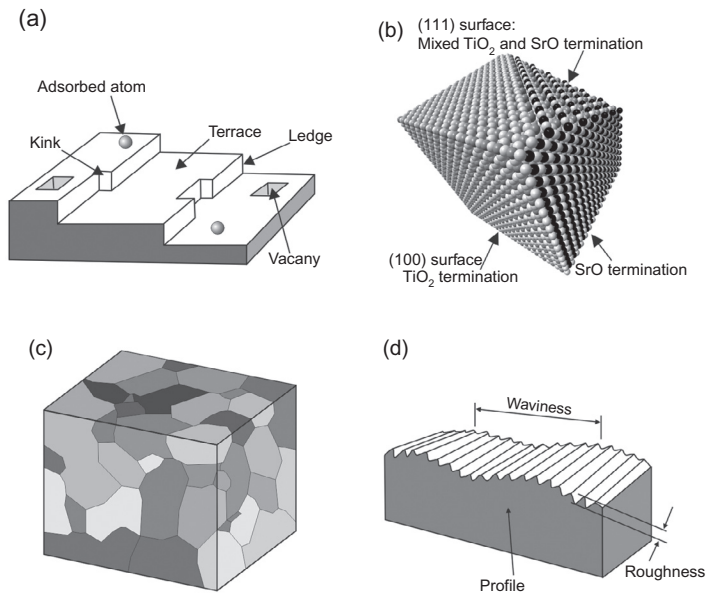
FIGURE 8.1 Schematic representation of ceramic surface topography at various length-scales: (a) Atomic-scale surface defects; (b) Atomic-scale surface topography of different crystallographic planes in SrTiO$_3$ crystal cube; (c) Ceramic microstructure at the surface of the bulk; and (d) Waviness and roughness produced by the unidirectional machining processing.

rearrangement of surface atoms. This is usually different from the bulk arrangement of atoms as it is driven by the tendency to reduce the excess of surface free energy relative to the bulk.[1]

When observing the surface of polycrystalline ceramic on the micrometer scale, a network of grains separated by the grain boundaries can be exposed. Various structural defects such as planar and point defects within individual grains are shown as straight lines and pits (Figure 8.1c). Material flaws like cracks and scratches are revealed as discrete irregularities, which often range over many grains. Understanding the overall surface topography can provide valuable information about the microstructure of the investigated ceramics. This can be further related to materials performance.[2]

At the macroscopic level, the surface topography is mainly characterized by roughness and waviness, with each other typical height and spacing often related to the specific machining process (e.g. grinding, polishing or sandblasting). Waviness is represented by the widely spaced irregularities that form a basis upon which roughness is superimposed. Roughness, probably the most important parameter for characterizing the texture of a surface, is represented by a shorter-wavelength component consisting of closely spaced irregularities (Figure 8.1d). It is quantified by the vertical deviations of a real surface from the mean line.[3]

For the characterization of ceramic surfaces, various investigative methods are used nowadays, depending on what scale is needed: macro-, micron- or nanoscale. Depending on the nature of the sampling, they can be divided into **optical** and **scanning probe** methods. Optical methods such as *conventional optical microscopy, confocal microscopy, optical profilometry*, and *scanning electron microscopy* (SEM) are noncontact methods that employ various specialized optical microscopy techniques in connection with different light sources. In contrast to optical methods, no lenses are required for scanning probe methods such as *stylus profilometery, scanning tunnelling microscopy (STM), and atomic force microscopy (AFM).* The working principle is based on the use of sharp-tip raster-scanning in contact or in very close proximity to the sample surface.

A **conventional optical microscope** is composed of a system of lenses that produce an enlarged image of an object that is placed in the focal plane of the objective lens. For observing the surface of ceramic materials, a reflected light source is commonly used (Figure 8.2a). Although quantitative data on surface topography is hard to obtain by this method, it is still widely used, mainly because it provides a quick check on sample quality during material processing. To expose the surface topography of ceramics, various contrast-enhancing microscopy modes can be applied, such as bright field, dark field, polarized light, phase contrast, and differential interference contrast.[4] The resolution of the optical microscope (i.e. the ability to distinguish two very small and laterally closely spaced objects as separate entities) is diffraction limited and is defined as follows (Eq. 8.1):

$$d = 0.61 \frac{\lambda}{NA} \qquad (8.1)$$

The symbol *d* signifies the smallest distance between two points observed by a light with given wavelength λ, and NA stands for numerical aperture and can reach the value of 1.4 in modern optics. For example, under blue light (~500 nm) the resolution limit would be 220 nm. The maximum usable magnification in the optical microscope is related to the resolution limit, which means that beyond certain magnification the image will look bigger but will show no more details. For a modern optical microscope the useful maximum magnification is around 1200x. Depth of field defines the resolving power parallel to the optical axis and decreases by both increasing the magnification and the value of numerical aperture. For example, at a magnification of 100x and an NA value of 0.95, the depth of field will be approximately 190 nm. Since the entire specimen is illuminated by the cone of light, the out-of-focus glare will severely limit the ability to focus sample features at various heights simultaneously, which makes the characterization of the ceramic's surface topography by this method difficult.

On the contrary, the use of **confocal microscopy** overcomes this problem, thus enabling the automated collection of three-dimensional data for
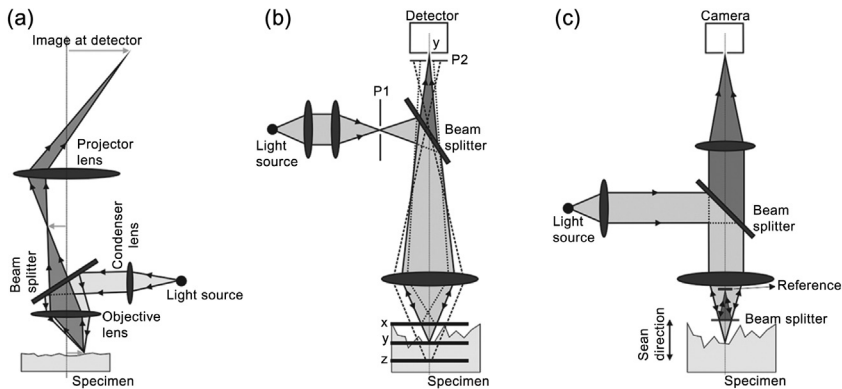
FIGURE 8.2   Schematics of (a) Reflected-light optical microscope; (b) Confocal microscope; and (c) Optical profiler with corresponding images and surface profiles.

surface topography. The working principle is based on focusing the laser beam through a small pinhole, which is confocal with a second pinhole positioned in front of a detector (Figure 8.2b). Whenever the surface is at the focus, the intense light will also focus through the detector pinhole and produce a high signal. An out-of-focus surface will scatter light over a wider area in the plane of the detector pinhole, resulting in a lower transmitted intensity. Three-dimensional surface topography is achieved by controlled vertical movements of the specimen and a raster scan of the light spot over the specimen with a vertical resolution of around 200 nm.[5]

Optical profilometry represents another noncontact surface metrology technique that uses an optical microscope in which light is split into two paths by a beam splitter placed between the sample and the objective lens (Figure 8.2c). One path directs the light onto the sample surface, while the other path directs the light to a reference mirror just below the objective lens. Reflections from the sample surface and the mirror are recombined, creating distinct interference fringes (shown as light and dark bands) that are projected to an array detector. From these interference images, the height differences across the surface are calculated, which forms the basis of the final three-dimensional surface topography image. The achieved vertical resolution is in the nanometer range, and lateral resolution is usually poorer since it is limited by the wavelength of the light.[6]

Scanning electron microscopy (SEM) signifies the major breakthrough in the characterization of ceramics. Nowadays, characterization techniques include many imaging and spectroscopic techniques that provide information about a specimen's topography, morphology, microstructure, crystallography, and composition, from the micron down to the nanoscale level.[7] SEM uses an electron source or gun that emits electrons with accelerating energies
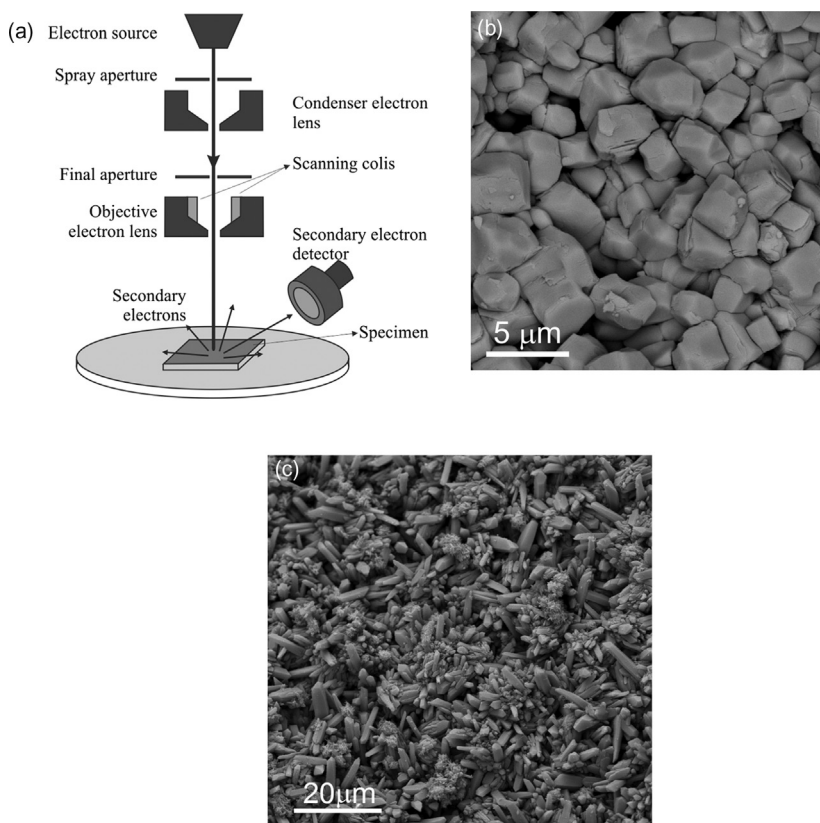
FIGURE 8.3   (a) Schematic of an SEM; and (b) SE image of BaTiO$_3$ polycrystalline ceramics and (c) quartz crystals fabricated by a hydrothermal synthesis. *(Courtesy of A. Lenart)*

of up to 30 keV (Figure 8.3a). The column consists of electromagnetic lenses and apertures that enable the formation of a fine electron probe focused on the specimen. The beam-deflection coils raster-scan the electron probe over the specimen, thus enabling scanning images to be produced. Samples in SEM are typically observed under high vacuum in order to avoid damage to the filament, as well as to prevent the incident electrons from scattering on residual gas molecules before reaching the specimen. SEM typically utilizes two imaging detectors for detecting secondary electrons (SE) and backscattered electrons (BEI). SE are low-energy electrons (<50 eV) that are emitted from very near the specimen's surface (<10 nm) and are sensitive to surface topography, as shown in Figure 8.3b. High-energy backscattered electrons (BE) are strongly dependent on atomic number (Z), with penetration depth much higher as compared to SE, and therefore less sensitive to surface topography. More often, BE images are used to reveal compositional variations in the polished sample. The nonconductive ceramic is coated with a thin conductive layer (carbon or

gold) to prevent charging in the SEM. Spatial resolution in the SEM is significantly higher compared to visible-light optical microscopes. This is due to the smaller wavelengths of electrons when compared to the wavelength of visible light. The wavelength for electrons of energy E_0 in SEM can be approximated with Eq. 8.2:

$$\lambda = \frac{1.24}{E_0^{1/2}} \tag{8.2}$$

The wavelength of electrons in an SEM at the accelerating voltage of 30 kV is 0.007 nm. Using Eq. 8.1, where NA is replaced by electron beam convergence (α~5 mrad), gives the theoretical resolution of around 0.8 nm. In reality, due to the nonideal nature of the gun and electromagnetic lenses, the actual spatial resolution of a modern SEM (SEI mode) is slightly above 1 nm with a useful magnification of up to 500,000x. The depth of field is more than 100 times better when compared to visible-light optical microscopes. This is due to the narrow electron beam (α). Although the resulting SEI images show a strong 'topological' contrast, the quantification of surface topography by SEM is not widely used since it requires the use of specialized techniques such as stereoscopic imaging.

Stylus profilometers are devices equipped with a mechanical stylus that consists of a diamond tip. By moving the surface being analyzed under the stylus, height variations as a function of the specimen's lateral position are measured by vertical movements of the stylus following the topography of the analyzed surface. Stylus instruments are based on a relatively simple operating principle, and are still widely used because they enable the investigation of ceramic surface areas of up to a few square centimetres. They can measure horizontal features down to a few nanometers, with vertical resolution of a few hundredths of a nanometer.

The invention of **scanning tunnelling microscopy (STM)** in 1982 marked the beginning of various high-resolution scanning probe methods for the characterization of specimen surface topography and chemistry down to an atomic-scale resolution.[8] STM requires an ultra-high vacuum and a clean atomically flat specimen surface. The principle of operation is based on detection of the tunnelling current between the atomically sharp tip and the sample surface. The tunnelling current is exponentially dependent on their separation. As the tip scans over the sample surface, sample features of different height will result in the exponential change in the tunnelling current (I), as represented by Eq. 8.3:

$$I \sim Ve^{-cd}, \tag{8.3}$$

where V stands for bias voltage between the tip and sample, d signifies the tip–sample separation, and c is a constant. The surface topography is obtained by scanning the tip over the sample. A constant tunnelling current is maintained at each horizontal (x,y) position, which is achieved by the vertical

adjustment of the tip through a feedback loop. Conductive or semiconductive samples are investigated in STM; this represents a severe limitation for the investigation of generally insulating ceramics.

A more appropriate technique for studying the surface features of noncon-ductive ceramics is **atomic force microscopy (AFM)**. AFM can operate under high-vacuum as well as under ambient and liquid environments. A sharp tip at the end of the cantilever is used for probing the sample surface. The change of the cantilever deflection is monitored by the laser beam reflected from the cantilever to the split photodiode detector.[9] For the detection of surface topog-raphy, a feedback loop regime is generally used. This maintains the tip–sample distance constant. During scanning, the vertical adjustment of the scanner at each horizontal position is recorded, which results in a fully quantitative three-dimensional map of surface topography with the typical nanometer-scale ver-tical and horizontal resolution. Surface topography maps can be achieved by scanning the tip over the sample surface either in *contact*, *tapping*, or *noncon-tact mode*. In contact mode, the tip is in contact with the sample surface. The tip follows the surface topography by keeping the force between the tip and the sample constant through a feedback loop (Figure 8.4). In tapping mode, the cantilever oscillates at its resonant frequency. During scanning, the oscil-lating tip is in contact with the sample only for a small fraction of time, which significantly reduces the overall lateral forces. The change of the tip oscillat-ing amplitude is used in a feedback loop for keeping the tip–sample distance constant. This method is convenient for investigation of delicate, soft sur-faces. In noncontact mode, the cantilever oscillates at a distance between 5 and 15 nm above the sample surface. The cantilever resonance frequency, and thus the oscillation amplitude, are decreased by the presence of capillary, van der Waals, electrostatic, or magnetic forces. These forces can extend a few nanom-eters above the sample surface. The amplitude signal is used for a feedback
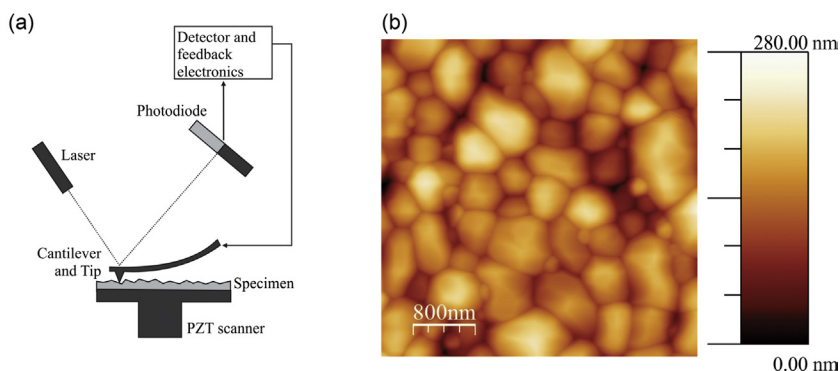
FIGURE 8.4   (a) Schematic of an AFM; and (b) AFM image of the $Bi_{12}SiO_{20}$ thin film heat treated at 700 °C for 30 min. *(Courtesy of A. Veber)*

loop. The spatial resolution of this method is a few orders of magnitude lower when compared to other AFM modes, and is therefore rarely used for studying surface topography.

8.2 POROSITY AND PORE STRUCTURE

Ceramic materials are mostly prepared by sintering compacted powders, which results in densification and development of a microstructure. The changes that occur within a compact due to mass transport during sintering proceed in several stages. In the initial stage, smoothening of the particle surface and formation of inter-particle neck structures take place, which results in the formation of a low-density structure with interconnected void channels. This is followed by the intermediate stage during which void channels shrink and eventually breakup forming isolated pores. In the final stage, densification proceeds by annihilation of pores through the diffusion processes. This is accompanied by grain growth and secondary recrystallization. The rate of annihilation of pores depends on the diffusion mechanism that takes part in the process and consequently on the location of the pore within the microstructure. Pores trapped within the grains can be annihilated only by lattice diffusion, whereas those at the grain boundary can also go by a much faster grain boundary diffusion.[10] For achieving high densities in a reasonable amount of time, it is therefore imperative that the least possible number of pores be trapped within the grains in the initial stages of sintering. Trapping the pores within grains depends on the relative mobility of the grain boundary to that of a pore, which further depends on the ratio of pore size to grain size. This defines a region in the grain size–pore size field where pores separate from the grain boundaries and become trapped within the grains.[11] The position of the pore separation field can be influenced by additions that affect grain boundary mobility (Figure 8.5). In general, low residual porosity (high density) in ceramic materials can be achieved by the addition of suitable dopants that simultaneously decrease the rate of grain growth and increase pore mobility.

Furthermore, the degree of elimination of porosity depends on the size of the pores that enter the final stage of sintering. The size of a pore within a matrix with a certain average grain size determines the number of grains around it, which determine the pore's interfacial energy and consequently whether it is prone to shrinkage or growth. This can also be interpreted in terms of surface curvature of grains surrounding the pore. The pores with less neighboring grains than determined by the dihedral angle exhibit concave boundaries, whereas those with more, exhibit convex boundaries (as viewed from the center of the pore). Thermodynamically material diffuses from under curved surfaces moving them towards the center of curvature[10]; pores with less than the equilibrium number of surrounding grains tend to shrink and those with more tend to grow (Figure 8.6). The presence of large pores in the final stage of sintering thus implies their presence in the microstructure of sintered ceramics,
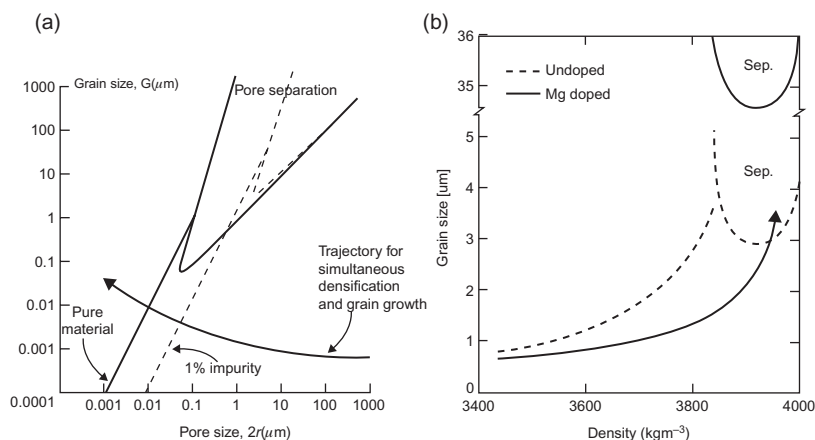
FIGURE 8.5   (a) Pore separation field in the grain size–pore size domain with a densification trajectory that does not intersect it[11]; and (b) Raise of pore separation field by doping.[12]
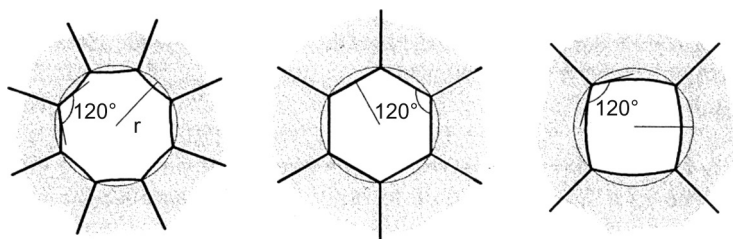
FIGURE 8.6   Pore surface curvature depending on the number of neighboring grains.[13] *Source: Kang SJL. Sintering. Elsevier Butterworth Heinemann.:2005. Page 141. Fig. 10.1*

which in many cases interferes with functional properties. Usually voids that become large pores form during powder compacting mostly due to the presence of agglomerates that can, to a certain extent, be avoided by optimizing the powder preparation process. Figure 8.7 shows SEM images of ceramics containing pores at the grain boundary and pores trapped within the grains.

In certain applications, such as bone fillers and scaffolds, however, materials with a high concentration of large pores are required. Taking into account the size of the pores present, materials are classified according to IUPAC as microporous (pore diameter $d < 2\,\text{nm}$), mesoporous ($2 < d < 50\,\text{nm}$), and macroporous ($d > 50\,\text{nm}$).

Pore structure of a material can be determined by utilizing microscopic techniques such as optical microscopy: SEM, AFM, and even TEM (see Sections 8.1 and 8.4 for details). These methods allow direct observation of pores from polished surfaces, cross sections, and fracture surfaces; however, quantitative information on pore size, shape, and size distribution can only be obtained by applying stereological analysis. Moreover, statistics are required to estimate the total porosity in an investigated material. A relatively simple
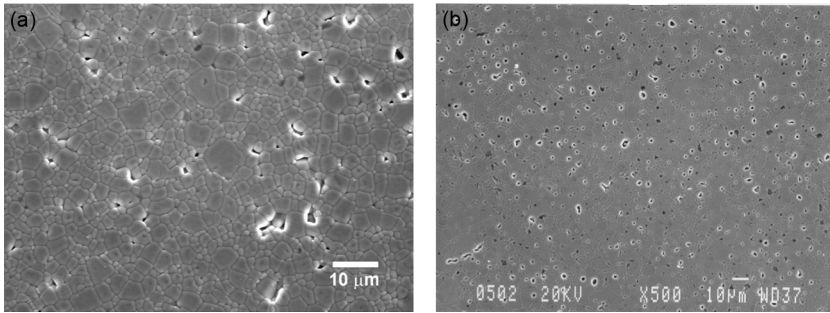
FIGURE 8.7 Secondary electron image SEM of an etched polished surface of $CaTiO_3$-based perovskite ceramics with (a) Pores at the grain boundaries; and (b) Some pores trapped within the grains. *(Courtesy of B. Jancar)*

approach that allows determination of the amount of porosity in a material is to measure the density, usually by Archimedes' principle. If the crystal structure of the investigated material is known, the theoretical density can be determined and the amount of residual porosity can be calculated. The material, however, needs to be single phase. A more complete analysis of the porosity can be performed by porosimetry, which utilizes intrusion of non-wetting liquid (usually mercury) into the pores. In this method, a sample is placed in a sealed sample cup connected to the capillary tube, and the system is evacuated and filled with mercury. Pressure is then applied to the top of the capillary, which forces mercury into the pores. The maximum diameter of the pores penetrated at a certain pressure is calculated using Washburn's equation (Eq. 8.4):

$$r = \frac{2\gamma}{p}\cos\phi \qquad (8.4)$$

The symbol r is the pore diameter; γ is the surface tension of mercury; ϕ is the contact angle between mercury and ceramics; and p is applied pressure. At every pressure change the amount of mercury that intrudes into the pores is measured and the final result is usually expressed by a cumulative percentage of volume up to certain pore diameter.

8.3 MICROSCOPIC DEFECTS

While functionality of a material depends on its electronic and crystal structure, it is most often the imperfections that govern the properties. In crystalline materials the imperfections are termed defects, which are either anomalies in the occupation of electronic energy states or disruptions of translational symmetry of the crystal structure with respect to the 'perfect' arrangement. The defects are often classified according to their spatial dimensionality ranging from 0D point defects, to extended defects, which can be 1D-line, 2D-area, or 3D-volume defects.
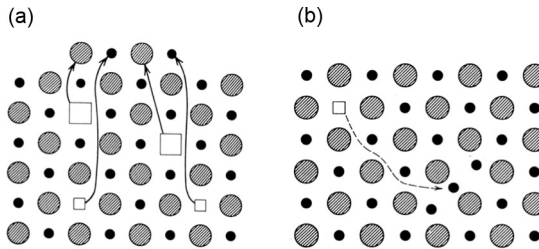
FIGURE 8.8   Schematics of (a) Schottky disorder; and (b) Frenkel disorder (Y-M. Chiang et al, Physical ceramics. New York: John Wiley and Sons; 1997).[14]

Point defects are either deviations from the perfect lattice associated with lattice points or excitations of electrons from the ground state. Atoms or ions can be missing from certain lattice points, they can be interstitially embedded, or they can be replaced by foreign species. The most common point defects in all crystalline materials are missing atoms or ions, which in terms of defect chemistry create vacancies. Formation of a vacancy is associated with breaking chemical bonds and the creation of local distortion in the crystal structure. This requires a certain amount of energy that is usually supplied from the thermal vibrations. The concentration of vacancies within the crystalline material is therefore thermodynamically a function of state, and consequently, the fraction of intrinsically vacant sites in a crystal strongly depends on the temperature. The most commonly encountered thermally activated intrinsic defects are Schottky and Frenkel disorders, which both involve creation of vacancies. Schottky disorder is associated with the formation of vacancies in ionic compounds where positive and negative ions simultaneously diffuse to the surface and leave regular crystallographic sites in the bulk of a crystal empty. Frenkel disorder is a migration of an atom or ion from its regular site into the interstitial (Figure 8.8).

In terms of standard Kroeger-Vink[14] notation, the disorders in a crystal of metallic salt MX, for example, are expressed as Eq. 8.5:

$$\text{Schottky disorder:} \quad MX \leftrightarrow V_M^x + V_X^x$$
$$\text{Frenkel disorder:} \quad MX \leftrightarrow M_i^x + V_M^x \tag{8.5}$$
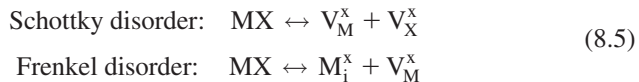
The symbol V denotes vacancy and the subscript denotes the site; M with subscript i denotes an interstitial metal ion.

The concentration of vacancies can also be extrinsically influenced by the introduction of aliovalent solutes into the host crystal structure. For example, substitution of Y_2O_3 into ZrO_2 creates two types of crystal defects, foreign atoms and oxygen vacancies (Eq. 8.6):

$$Y_2O_3 \xrightarrow{\;ZrO_2\;} 2Y_{Zr}' + 3O_O^x + V_O^{\infty} \tag{8.6}$$
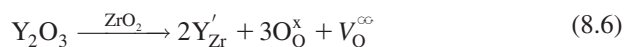
In accordance with Kroeger-Vink notation, the equation indicates that Y incorporates on the Zr site rendering its effective charge negative relative to the perfect lattice (denoted by a dash in the superscript) and causing the formation of an oxygen vacancy with a doubly positive charge relative to the perfect crystal lattice (denoted by dots in the superscript). Due to the presence of vacancies, the mobility on the oxygen sub-lattice increases, which results in an enhanced ionic conductivity in yttria-stabilized zirconia.

The formation of point defects in oxide systems is often associated with oxygen partial pressure in the surroundings that can also affect electronic conductivity. For instance, incorporation of Al_2O_3 into the crystal structure of semiconducting ZnO under high oxygen partial pressure causes formation of zinc vacancies, whereas lower concentration of oxygen in the surroundings results in liberation of gas from the oxygen sub-lattice and creation of electronic defects. In accordance with Kroeger-Vink notation this can be written as (Eq. 8.7):

$$
\begin{aligned}
Al_2O_3 &\xrightarrow{\text{ZnO}} 2Al_{Zn}^{\circ} + 3O_O^x + V_{Zn}'' - \text{high } p_{o_2} \\
Al_2O_3 &\xrightarrow{\text{ZnO}} 2Al_{Zn}^{\circ} + 2O_O^x + 2e' + \frac{1}{2}O_{2_{(g)}} - \text{low } p_{o_2}
\end{aligned}
\tag{8.7}
$$
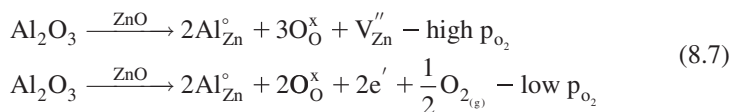
Presence of such electronic defects can increase electronic conductivity of a material by several orders of magnitude.

Apart from the electrical transport, point defects also considerably influence the mass transport in materials since the dominant diffusion mechanism in solids is the vacancy exchange mechanism.[15]

Among the extended defects, the simplest forms are 1D line defects called dislocations, which are local displacements of a crystal lattice that are commonly described by two borderline cases: edge and screw dislocations. The edge dislocation is usually interpreted as an extra half-lattice-plane and the screw dislocation is imagined to be a consequence of a virtual shear displacement of a perfect crystal (Figure 8.9). The distortion imposed on a perfect lattice by a dislocation is a vector quantity, and is generally quantified by the Burgers vector. The direction and the magnitude of the Burgers vector can simply be visualized as the distortion of the imaginary planar loop, with dimensions as multiples of the unit cell edges drawn around the dislocation.[10] The formation of dislocations is associated with the stress field that can either be induced by growth imperfections or external forces acting on a crystal. The external force can also cause glide of dislocations through the crystal by breaking and reestablishing chemical bonds between atoms in the neighboring planes. Such movement of dislocations results in a slip of lattice planes, which is manifested as plastic deformation of a material. In crystals, where bonding character is predominantly ionic, slip occurs more easily in certain directions as compared to others. A slip plane and a slip direction define a slip system.[17]
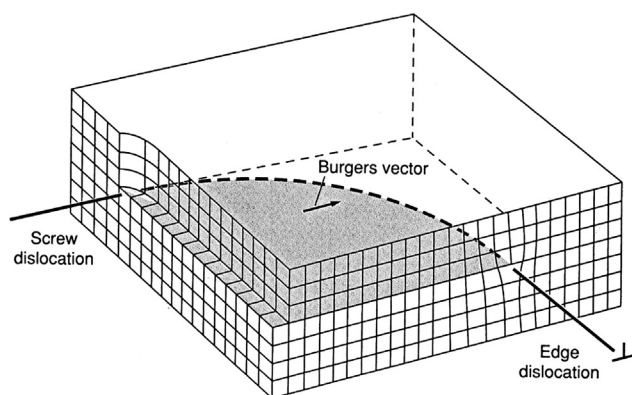
FIGURE 8.9   Schematics of Edge and Screw dislocation.[16]

The 2D planar defects that occur within the crystals are generally stacking faults, twin boundaries, and anti-phase boundaries. Stacking faults are anomalies in the stacking sequence of crystal planes that disrupt the continuity of a perfect lattice. For instance, in the cubic close-packed systems with the ABC-type stacking sequence, the missing C layer produces a stacking fault that is locally manifested as the hexagonal stacking sequence ABAB. Stacking faults are imperfections that are formed during crystal growth. Twin boundaries can be interpreted as boundaries between two intergrown crystals in different orientations related by a symmetry operation, most commonly reflection. Consequently, the twin boundary is a mirror plane also called a composition plane. Twinning in crystals can be a consequence of anomalies during the growth process or it can originate from a symmetry-breaking phase transition, which usually occurs due to temperature or pressure changes. In some crystals, twinning can also occur as a consequence of deformation. Anti-phase boundaries separate domains that exhibit opposite arrangements of atoms as compared to those in a perfect crystal. They form during a phase transition where translational symmetry is lost (e.g. ordering of atoms or ions on certain crystallographic sites). In some cases, anti-phase boundaries can also form during crystal growth as a mode of accommodation of local changes in chemistry.

The most common planar defects in polycrystalline materials are grain boundaries, which are interfaces between two crystals of the same material in different orientations. Grain boundaries are in principle interfacial structures (see Section 8.4).

The 3D volume defects found in materials are either precipitates or voids within or between individual grains. In polycrystalline ceramics, voids are commonly referred to as pores and their amount determines the density of a material and has a significant influence on functional properties (see Section 8.2).

In order to predict and control the properties, it is important to be able to analyze the defects in materials. While extended defects can be readily observed by means of different types of microscopy, the exact determination of point defects remains one of the most challenging tasks in materials science. Their size and usually low concentration renders even the most advanced microscopy techniques rather ineffective. The common methods of determination are by observing the properties that are directly dependent on the type and concentration of the point defects. In oxide systems measurement of electrical conductivity at different temperatures and different oxygen partial pressures enables determination of point defects present in the crystal structure. As discussed above, several types of charged defects can form in oxide materials as a result of impurities or dopants present in the structure. The dependence of the type of charged defects on oxygen partial pressure governs the amount and type of electrical conductivity.[18] The less common method used for determination of vacancies in semiconducting materials is positron annihilation spectroscopy (PAS).[19] The technique is based on observing the lifetime of a positron injected into a material. Upon interaction with electrons, positrons annihilate transforming energy into gamma photons that can be detected. The annihilation of a positron within a material proceeds very rapidly unless some trapping sites such as vacancies or voids are present in the structure. Based on the lifetime extension and with the aid of modeling, the concentration of vacancies can be deduced. By far the most common method in the case of oxide ceramics, especially for determination of foreign ions and cationic vacancies, is an accurate electron microprobe analysis. This is implemented either in a dedicated electron probe microanalyzer (EPMA), or nowadays, also in conventional SEMs. The principle is based on the detection of characteristic X-rays emitted from the specimen as a consequence of excitation by an electron beam. The characteristic X-ray photons are detected and counted by energy (ED) or wavelength-dispersive (WD) spectrometers from which the WD exhibits higher count rate and superior energy resolution. The operating principle of a WD spectrometer is in the selection of specific wavelengths of X-rays by a Bragg reflection on a single crystal and consequently counting them by a gas proportional counter. By applying correction methods, elements heavier than sodium can be quantitatively determined with an accuracy of 0.1 at.%[7]; application of a quasi-chemical approach[14] to defect equilibrium leads to the determination of point defect concentration.

Extended defects can be characterized by transmission electron microscopy (TEM), which allows atomically resolved imaging and analysis (see Section 8.4). Figures. 8.10 and 8.11 show examples of bright-field and high-resolution TEM images of planar defects in different ceramic materials.

8.4 INTERFACIAL BONDING STRUCTURES

In ceramics materials, an interface, which is defined as a common boundary between two solid bodies, can be geometrically described by six macroscopic
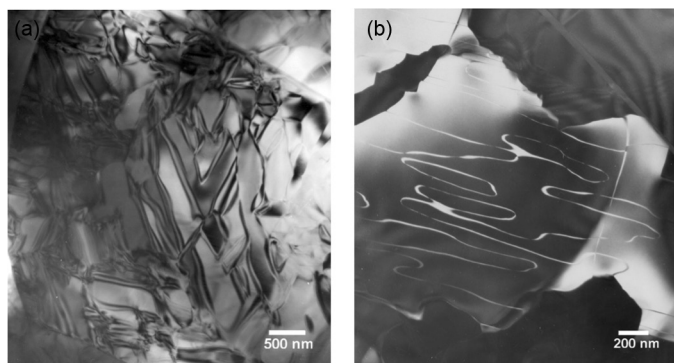
FIGURE 8.10   TEM-BF images of a symmetry-breaking phase transition induced by: (a) Twin domains separated by twin boundaries; and (b) Antiphase boundaries in CaTiO$_3$-based perovskite ceramics. *(Courtesy of B. Jancar)*
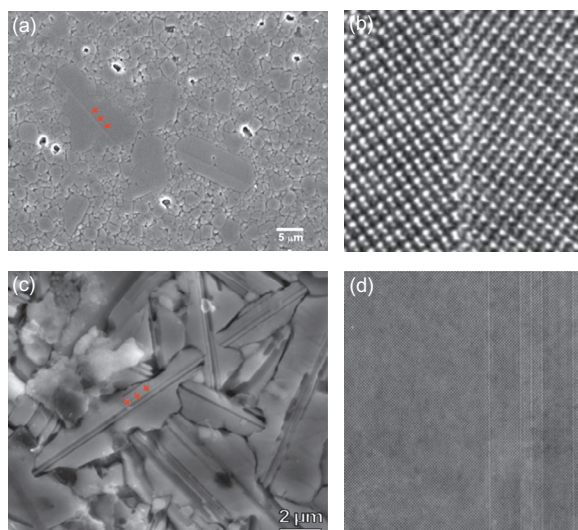
FIGURE 8.11   (a) Secondary electron SEM image of the microstructure of Ba(Zn$_{1/2}$W$_{1/2}$)O$_3$-based perovskite ceramics showing elongated grains containing parallel (111) growth twins; (b) HRTEM image of the twin boundary; and (c) Secondary electron SEM image of the microstructure of SrTiO$_3$-based perovskite ceramics showing elongated grains containing growth antiphase boundaries. *(Courtesy of B. Jancar and S. Sturm)*

and four microscopic degrees of freedom.[20] Within the macroscopic parameters, three are related and define the rotation of one crystal lattice with respect to the other, two describe the orientation of the interface, and one describes the handedness of either crystal. From the microscopic parameters, three describe the relative displacement of the crystals against each other. An additional

(a)   (b)   (c)   (d)
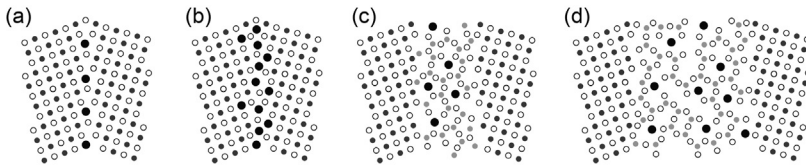
FIGURE 8.12 Illustration of GB structure evolution due to the preferential segregation of dopant atoms to the grain boundary from (a) Monolayer, to (b–c) Multilayer adsorption, and (d) Formation of an amorphous film.

parameter is needed to determine the position of the interface plane in case the basis of either crystal consists of more than one atom.

Besides the abovementioned crystallographic description, another very important parameter for describing the interfaces is their local chemistry. In this respect, interfaces can be either clean; decorated with segregated dopant atoms and precipitates; can show a disordered GB structure; or can contain amorphous films.[21,22] As a result, the interface structure and chemistry is often significantly different in relation to the neighboring bulk ceramics (Figure 8.12a). As such, interfaces may have a particularly strong impact on the ceramic properties and therefore need to be fully quantified in terms of their local crystal structure, chemistry, and electronic structure.

Most of the ceramic materials are polycrystalline. They are composed of randomly oriented crystal grains of the same or different phase that are separated from each other by internal interfaces. Grain boundaries (GB) represent one type of internal interface defined as homophase boundaries; these connect two crystal grains of the same crystal structure and composition. Based on the crystallographic orientation relationship between two neighboring grains, one can distinguish between special and general GBs. General GBs may be curved without any specific crystallographic orientation relationship between neighboring grains. Special GBs, on the contrary, can be constructed by a defined crystallographic relationship and are usually described by coincidence site lattice (CSL) theory. It represents a geometrical model of fitting two crystals at the interface by rotating one lattice with respect to another around a fixed coincident lattice point at the interface.[23] At specific orientations between the two lattices, a higher number of coincidence sites can occur. A new periodical structure, which is defined by the coincidence sites, has a unit cell size Σ that is equal to an integer number of unit cells of the initial lattices. It is assumed that GB has a low energy when the density of coincidence sites in both adjoining grains is high; therefore, the Σ value is low.

Heterophase boundaries are formed when two thermodynamically different phases are joined. For example, they are found in semiconductor multilayers, such as AlGaN/GaN superlattices.[24] These structures are composed of alternating layered phases of a different composition and same crystal structure which are grown in the same orientation. Another important group is metal–ceramic interfaces. These interfaces are about controlling the metal–ceramic

adhesion. Consequently, many technologically relevant applications, spanning from oxide ceramic coatings on metals as thermal barriers to medical implants in dentistry, depend on the quality of the metal–ceramic contact.[25] The metal–ceramic mechanical strength is ideally described by the work of separation (W_{sep}), which is defined as the reversible work needed to separate the interface into two free surfaces.[26] Depending on the state of coherency, interfaces can be further classified into coherent, semi-coherent, and incoherent interfaces.[27]

Transmission electron microscopy (TEM), which utilizes parallel electron beam illumination, has revolutionized the characterization and understanding of internal interfaces.[28] It presents the most powerful technique for studying interfaces, with a spatial resolution down to the atomic level. Conventional TEM comprises imaging techniques that use only one of the electron beams emitted from the specimen, either the primary beam or one of the diffracted beams. Respectively, so-called bright-field (BF) and dark-field (DF) images are formed that give information about, for example, general microstructure at high-spatial resolution, the presence of crystalline or amorphous phases, and planar and point defects and associated strain fields that can accumulate at interfaces. In addition, selected-area electron diffraction patterns (SAED) are obtained from defined nanometer-sized sample regions and provide extremely localized information about the crystallography. This is directly related to the observed image region (Figure 8.13).

High-resolution TEM (HRTEM), on the other hand, is an imaging technique that enables the formation of bright-field phase contrast images with a resolution below 0.1 nm. HRTEM, which employs several diffracted beams to construct the image, carries valuable information about the projected atomic structure. This makes the technique one of the most powerful for studying interface structure in real space.[30] Although HRTEM images precisely mirror the underlying crystal symmetry, the contrast variations in the image do not always match precisely with the atom position. For that purpose HRTEM image simulations combined with an iterative image-matching algorithm are required to retrieve the exact position of the atomic columns at the interface.[31] Another approach to studying local structure of interfaces is by applying the method of exit wave function reconstruction (WFR). WFR uses a focal series of experimental HRTEM images to reconstruct a complete wave function at the specimen exit surface. This method can ideally retrieve the structural features of the interface up to an information limit of the given microscope.[32]

In probe aberration-corrected scanning transmission electron microscopes (STEM), a focused electron probe with a diameter below 0.1 nm is raster-scanned across the specimen for acquistion of atomic-scale images. The intensity of each point during scanning is obtained by integrating the signal that reaches different circular or annular detectors placed in the optical axis below the specimen. Electrons that are scattered to high angles (>40 mrad) are detected by a high-angle annular dark-field detector (HAADF). In this way, the incoherent Rutherford scattered electrons are measured. Their intensity is roughly proportional to the square of the atomic number (Z) of the scattered
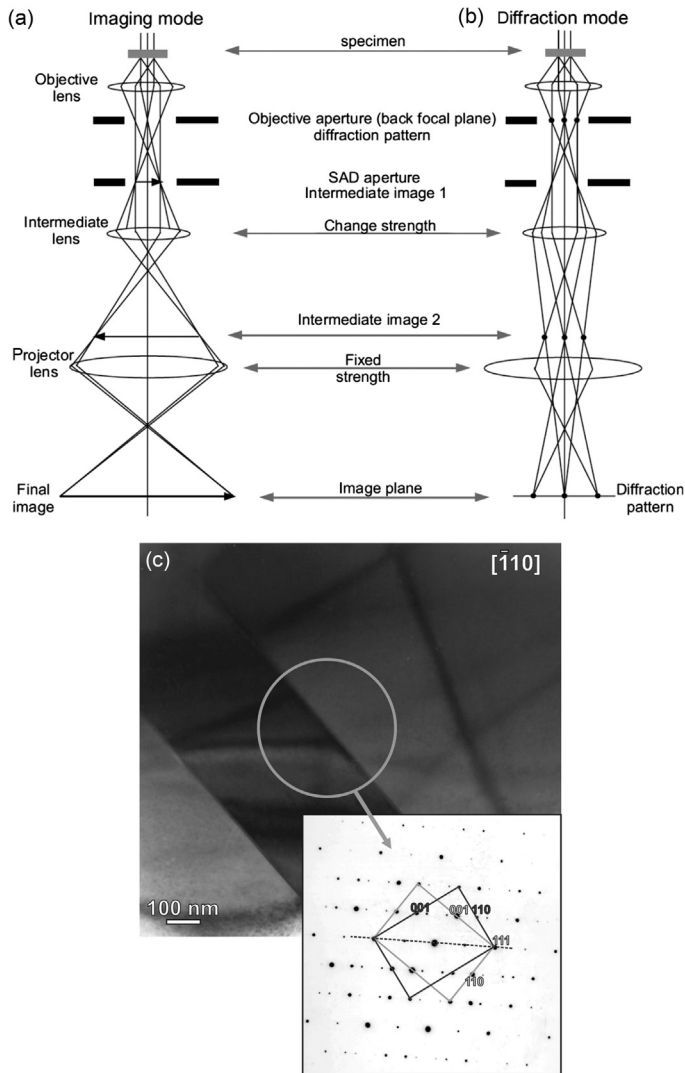
FIGURE 8.13 Schematic ray diagram of a conventional TEM: (a) Image mode; (b) Diffraction mode[28]; and (c) TEM image of a twin boundary in α-quartz and a corresponding SAED pattern.[29]

atom.[33,34] Consequently, the intensity of HAADF-STEM images reflects compositional variations at the atomic scale, which makes the reconstruction of both the atomic arrangement and atom types at the interface relatively straightforward. However, the light atoms are still difficult to detect mainly due to their low scattering power. This restricts the complete reconstruction of the interface structure. Typically, elements lighter than oxygen are extremely difficult to image. On the contrary, light elements, including hydrogen, can be
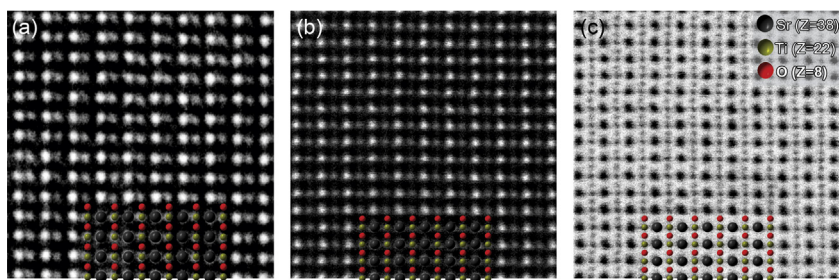
FIGURE 8.14 SrTiO$_3$ crystal structure imaged by (a) HRTEM; (b) HAADF-STEM; and (c) ABF-STEM with the superimposed corresponding structure model in <110> direction.

successfully imaged in the crystal structure by the use of a small-angle annulus detector. Since the small-angle scattering interaction takes place at the edges of atoms where the charge density is comparable for all atoms regardless of Z, the related scattering intensity is for both light and heavy atoms in the same order of magnitude.[35,36] The resulting annular bright-field STEM (ABF-STEM) images can therefore provide means for direct imaging of light and heavy atoms at the same time. In principle, by combining HRTEM, HAADF-STEM, and ABF-STEM imaging, a complete structural and compositional reconstruction of the interfaces can be performed (Figure 8.14).

The main experimental difficulty in extracting the interface-specific components, like concentration of dopant atoms segregated at GBs, is the overlap of interface signal with the adjacent bulk, which is often associated with a generally weak signal. Analytical electron microscopy (AEM), which combines TEM/STEM with various spectroscopic techniques, offers enough spatial resolution to reliably extract the useful information from the interfaces. The most widely used spectroscopic techniques associated with TEM are energy dispersive X-ray spectroscopy (EDXS) and electron energy-loss spectroscopy (EELS). While both EDXS and EELS are commonly used to detect compositional changes, EELS also provides information about the chemical states of ceramic interfaces. In this respect, EDXS and EELS are complementary techniques and are commonly available on the same microscope.

Several spectroscopic methods can be applied in order to extract the composition or chemistry of the analyzed interfaces. For example, quantitative EDXS or EELS mappings and line-profiles enable compositional determination of the sample at every analyzed spot. The reliable determination of interface composition mainly depends on the sampling quality, sample thickness, and electron probe size. In addition, various multivariate statistical analysis methods can be applied in order to further improve the quality of data.[37] The chemical composition of interfaces can then be obtained by applying a spatial-difference technique that is not limited by probe size.[38] With this technique the interface composition is computationally obtained from a spectrum acquired from a larger sample region containing the interface. For example,
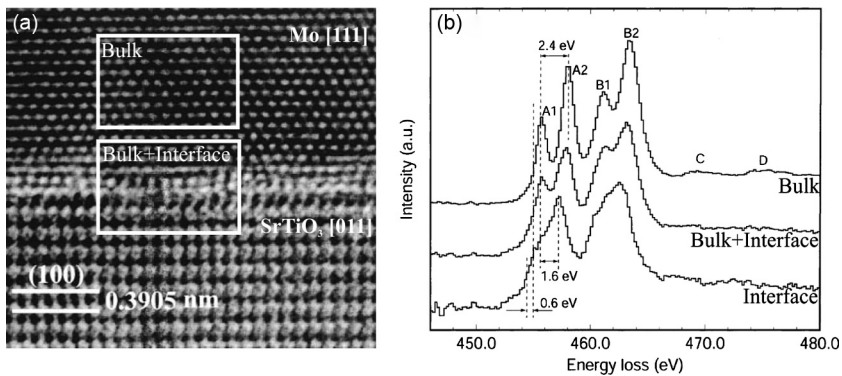
FIGURE 8.15 (a) HRTEM image of an Mo/SrTiO$_3$ interface. The superimposed boxes show the specimen region of EELS spectra acquisition. The interface-specific spectrum was obtained by subtracting the bulk spectrum from the bulk + interface spectrum (Gao, Scheu et al., 2003).[37]

in a yttrium-doped α-Al$_2$O$_3$ system, the GB yttrium concentration, quantified by a spatial-difference technique, amounts to between 3 and 6 atoms/nm^2.[39] The diameter of the round analyzed area containing both the GB and the adjacent alumina grains was 10 nm. Assuming that the concentration required to densely pack an atomic plane in α-alumina is on average 13 atoms/nm^2, the measured concentration of yttrium atoms at the interface is still well below one monolayer. This example clearly demonstrates the strength of these techniques for analyzing small concentrations of segregated atoms at the GBs.

Besides the composition of the interfaces, the related interfacial chemistry, which includes interfacial valence and bonding states, often offers a key for understanding the properties of interfaces and consequently the overall functional behavior of the ceramic bulk. The information about the bonding and valence is obtained from the fine structures superimposed on core-loss ionization edges in EELS. The interface-specific bonding structure was studied in metal/ceramic interfaces.[25] As an example, the local chemistry of the Mo/SrTiO$_3$ interface was successfully deduced by the spatial difference method combined with high-resolution EELS.[40] It was shown that in contrast to the SrTiO$_3$ bulk the Ti at the interface was in the reduced state and coordinated in disturbed TiO$_6$ octahedra (Figure 8.15). In addition, two-dimensional chemical maps revealing atomic-scale differences in bonding structure and valence were successfully acquired in various perovskite-based heterostructures.[41,42]

REFERENCES

1. Noguera C, editor. Physics and chemistry at oxide surfaces. Cambridge University Press; 1996.
2. Carter CB, Norton MG. Ceramic materials: science and engineering. Springer Science; 2007.
3. Basu B, Kalin M. Tribology of ceramics and composites: materials science perspective. John Wiley & Sons; 2011.

4. Leng Y. Materials characterization: introduction to microscopic and spectroscopic methods. John Wiley & Sons; 2008.
5. Ganesha U, Singaperumal M, Sirohi RS, et al. Characterization of surface topography by confocal microscopy: I. Principles and the measurement system. Meas Sci Technol 2000;11(3):305–14.
6. Leach R, editor. Optical measurement of surface topography. Springer-Verlag; 2011.
7. Goldstein J, Newbury DE, Joy D, et al. Scanning electron microscopy and X-ray microanalysis. Springer Science; 2003.
8. Chen CJ. Introduction to scanning tunneling microscopy, 2nd ed. Oxford Universtiy Press; 2008.
9. Eaton P, West P. Atomic force microscopy. Oxford University Press; 2010.
10. Kingery WD, Bowen HK, Uhlmann DR. Introduction to ceramics. John Wiley & Sons; 1976.
11. Brook RJ. Pore-grain boundary interactions and grain growth. J Am Ceram Soc 1969;52:56–7.
12. Bennison SJ, Harmer MP. Effect of magnesia solute on surface diffusion in sapphire and the role-of magnesia in the sintering of alumina. J Am Ceram Soc 1990;73(4):833–7.
13. Kang S-JL. Sintering. Oxford: Elsevier Butterworth-Heinemann; 2005.
14. Kroeger FA. Chemistry of imperfect crystals. North Holland; 1964.
15. Mehrer H. Diffusion in solids. Springer Verlag; 2007.
16. Ohring M. Engineering Materials Science. Academic Press Inc.; 1995.
17. Chiang Y-M, Birnie DP, Kingery WD. Physical ceramics. John Wiley & Sons, Inc.; 1997.
18. Eror NG, Smyth DM. Nonstoichiometric disorder in single-crystalline $BaTiO_3$ at elevated temperatures. J Solid State Chem 1978;24:235–44.
19. Krause-Rehberg R, Leipner HS. Positron anihilation in semiconductors defect studies. Springer-Verlag; 2003.
20. Sutton AP, Balluffi RW. Interfaces in crystalline materials. Oxford: Clarendon Press; 1995.
21. Subramaniam A, Koch CT, Cannon RM, et al. Intergranular glassy films: an overview. Mater Sci Eng A 2006;422(1–2):3–18.
22. Dillon SJ, Tang M, Carter WC, et al. Complexion: A new concept for kinetic engineering in materials science. Acta Mater 2007;55(18):6208–18.
23. Bollmann W. Crystal defects and crystalline interfaces. Springer-Verlag; 1970.
24. Shiojiri M, Ceh M, Sturm S, et al. Structural and compositional analyses of a strained AlGaN/GaN superlattice. J Appl Phys 2006;100(1):013110.
25. Scheu C, Dehm G, Ruhle M, et al. Electron-energy-loss spectroscopy studies of Cu-α-Al_2O_3 interfaces grown by molecular beam epitaxy. Philos Mag A 1998;78(2):439–65.
26. Finnis MW. The theory of metal - ceramic interfaces. J Phys Condens Mat 1996;8(32):5811–36.
27. Hull D, Bacon DJ. Introduction to dislocations, 3rd ed. Pergamon Press; 1984.
28. Williams DB, Carter CB. Transmission electron microscopy: a textbook for materials science, 2nd ed.: Springer Science + Business Media; 2009.
29. Lenart A, Samardžija Z, Godec M, et al. Twin-boundary formation in Japan-law twinned quartz crystals. Eur J Mineral 2012;24(3):509–17.
30. Reimer L. Transmission electron microscopy: physics of image formation and microanalysis, 4th ed.: Springer-Verlag; 1997.
31. Šturm S, Shiojiri M, Ceh M, et al. Atomic-scale structural and compositional analyses of Ruddlesden-Popper planar faults in AO-excess $SrTiO_3$ (A = Sr^{2+}, Ca^{2+}, Ba^{2+}) ceramics. J Mater Res 2009;24(08):2596–604.
32. Allen LJ, McBride W, O'Leary NL, et al. Exit wave reconstruction at atomic resolution. Ultramicroscopy 2004;100(1–2):91–104.
33. Pennycook SJ, Jesson DE. High-resolution Z-contrast imaging of crystals. Ultramicroscopy 1991;37(1–4):14–38.

34. Browning ND, Chisholm MF, Pennycook SJ, et al. Atomic-resolution chemical analysis using a scanning transmission electron microscope. Nature 2006;444(7116):235.

35. Batson PE. Electron microscopy: Hydrogen brightens up. Nat Mater 2011;10(4):270–1.

36. Ishikawa R, Okunishi E, Sawada H, et al. Direct imaging of hydrogen-atom columns in a crystal by annular bright-field electron microscopy. Nat Mater 2011;10(4):278–81.

37. Burke M, Watanabe M, Williams DB, et al. Quantitative characterization of nanoprecipitates in irradiated low-alloy steels: advances in the application of FEG-STEM quantitative microanalysis to real materials. J Mater Sci 2006;41(14):4512–22.

38. Sigle W. Analytical transmission electron microscopy. Annu Rev Mater Res 2005;35:239–314.

39. Gülgün MA, Sturm S, Cannon RM, et al. Transient dopant segregation and precipitation in yttrium-doped alumina. Int J Mater Res 2008;99(12):1324–9.

40. Gao M, Scheu C, Tchernychova E, et al. Successful application of spatial difference technique to electron energy-loss spectroscopy studies of Mo/SrTiO$_3$ interfaces. J Microsc 2003; 210(1):94–101.

41. Muller DA, Kourkoutis LF, Murfitt M, et al. Atomic-scale chemical imaging of composition and bonding by aberration-corrected microscopy. Science 2008;319(5866):1073–6.

42. Muller DA. Structure and bonding at the atomic scale by scanning transmission electron microscopy. Nat Mater 2009;8(4):263–70.

Mechanical Properties and Reliability of Advanced Ceramics

Tanja Lube and Robert Danzer

Institut für Struktur- und Funktionskeramik, Montanuniversität Leoben, Leoben, Austria

Contents

9.1   INTRODUCTION

Due to their special kind of chemical bonding, ceramic materials are stiff; hard; resistant to acidic and alkaline solutions; and biocompatible, all of which make them very well suited for applications in dentistry. Also, due to their chemical bonding, they are very brittle; their tensile strength has a large scatter and their total fracture strain is low (commonly less than a few parts per thousand). Their yield stress is a factor of 10 higher than the tensile strength.[1] Therefore, local stress concentrations cannot be relaxed by yield. These properties cause special needs with respect to design, manufacturing tolerances, and handling, both in production as well as in application. Proper design of ceramics aims at avoiding, or at least minimizing, tensile stresses but it has to be taken into consideration that stress even exists around compressive contact zones.

Mechanical testing of ceramics is more complicated than for ductile metals since geometric imperfections cannot be compensated for by small plastic deformations. Mechanical properties are strongly related to special processing details, and specimens should therefore be machined out of the processed ceramic products. Proper machining of specimens is complicated, expensive, and time consuming. Standardized procedures for testing are available for advanced ceramics[2–7] that use relatively large specimens. Appropriate testing procedures for very small specimens are far from being standardized.

Ceramic strength is limited by small flaws. These can be either discontinuities in the microstructure, or small cracks at the surface. They are either caused by processing of the material or are by the machining of surfaces of specimens and components. They cannot be avoided completely. Improvement of a certain material is often related to the reduction in the number and size of these flaws.

This chapter introduces the basic principles of linear elastic fracture mechanics as the basis for understanding brittle fracture, and then presents fracture statistics. These topics are followed by an example for designing with ceramics. In subsequent sections, several other damage mechanisms and their relevance in dental applications will be discussed. The chapter closes with sections that deal with mechanical testing of ceramics and fractography.

9.2   FRACTURE MECHANICS

9.2.1   Damage Mechanisms

For dental applications we can restrict our discussion to room temperature conditions. Here, **brittle fracture** is the most important failure mechanism. It occurs suddenly and without any significant prior plastic deformation, and the (elastic) failure strain is in the order of one to several per mill. At slightly smaller loads, cracks may grow steadily. This causes a loss of strength with time. Several crack-growth mechanisms are responsible for this phenomenon (e.g. **sub-critical crack growth**, SCCG; and **fatigue**). Corrosion due to body fluids is in principle possible, but will not be considered here.

Brittle fracture is inevitably the final active mechanism at failure. It is caused by the extension of a single crack around a flaw (the fracture origin), and almost reaches the speed of sound. It is nearly impossible to arrest this crack, and fracture of the part occurs immediately once a critical load is applied. Fracture origins can be cracks, which come into existence during inadequate handling of the green body, sintering, machining, corrosion, or by contact damage.

Failure after a period of time under load occurs if cracks grow to a critical size by SCCG, fatigue, creep, oxidation, or corrosion. Since this crack growth occurs without any visible deformation or without any detectable loss of stiffness of the parts, the delayed failure always occurs in a surprising and catastrophic manner. Many physical/chemical reasons for SCCG have been discussed, ranging from hydrolysis of silicon–oxygen bonds to ion exchange mechanisms and thermally activated bond breakage at the tip of a loaded crack, but this discussion is not yet finished. SCCG is accelerated by the action of some polar molecules (e.g. water or water vapor), and is thus related to stress corrosion cracking as observed in metals.[8–10] Some SCCG always precedes final catastrophic fracture in brittle materials, but if the load is applied very quickly, the contribution can be rather small.

Fatigue is considered here to be damage caused by the alternating (cyclical) application of loads. In ceramics, fatigue crack growth is caused by repeated (cyclical) damage to microstructural elements (e.g. by the breaking of crack bridges during the crack closure part of a loading cycle).[11,12] Like SCCG, fatigue can be a reason for delayed failure and may precede the sudden catastrophic failure of a component. Fatigue in ceramics has been observed under tension/compression cycling. It is much less pronounced under tension dwell loading. Under these conditions SCCG is, in general, dominant.

9.2.2   Basic Fracture Mechanics Principles and their Application to Brittle Fracture

It is assumed that under the action of tensile stresses, flaws behave like cracks. Fracture mechanics describe the behavior of cracks (length a) under the action of a mechanical load that pulls the crack borders apart.[13] In the simplest case (linear elastic fracture mechanics, LEFM), which applies to brittle ceramics, it is assumed that (1) a crack is a mathematical section through the material (i.e. the crack tip is infinitely sharp); (2) the material behaves like a linear elastic continuum; and (3) no forces can be transferred via the crack borders. It was shown in early work by Griffith[14] that a crack grows if the decrease in the Gibbs free energy associated with the crack growth is larger than the energy necessary to create the new crack surfaces. In general, two contributions to the change in the Gibbs free energy have to be considered: the work done by crack growth (∂W), and the changes in the elastic energy (∂U_{el}) associated with crack growth (Eq. 9.1):

$$\partial W - \partial U_{el} \geq G_c \partial A \qquad (9.1)$$

The energy necessary to create the new crack surfaces is proportional to the newly cracked area (∂a). The fracture energy (G_c) is the energy necessary to create a unit area crack surface.

It can be shown that for small cracks (crack length a) the work done by crack growth as well as the change in the elastic energy are also proportional to the newly formed cracked area. The left-hand side of Eq. 9.1 can be evaluated to give the fracture criterion:

$$\frac{(Y\sigma)^2}{E}\pi a = G \geq G_c \qquad (9.2)$$

In Eq. 9.2, the strain energy release rate (G) describes the total change of the Gibbs free energy of the unit area of the crack surface. Brittle fracture occurs if G reaches a critical value. The stress (σ) characterizes the amplitude of tensile stresses in the body (in a uniaxial and homogeneous stress field it is the stress), and Y is a geometric factor that accounts for the geometry of the specimen, the crack, and for the gradients of the stress field. For small cracks it is constant and in the order of one. For small scratch-like surface cracks, as can be caused by inadequate grinding, $Y = 1.12$, and for small penny-shaped cracks inside the body, $Y = 2/\pi$. Data for Y can be found in standard textbooks.[15,16] E is Young's modulus of the material. If all material-dependent properties are written on the right-hand side of the equation, and if we take the square root, we get the Irwin equation (Eq. 9.3).[17]

$$K \geq K_c, \text{where } K = \sigma Y\sqrt{\pi a} \text{ and } K_c = \sqrt{G_c E} \qquad (9.3)$$

K is the stress intensity factor (SIF) and K_c is the fracture toughness of the material. The SIF scales with the (local) stress field at the crack tip, which depends on a combination of crack length and the applied stress field. A crack extends spontaneously if the local stress intensity at the crack tip reaches a critical value, which is typical for the material. Eq. 9.3 is often used to analyze the tensile strength (brittle fracture) of brittle specimens. Eq. 9.4 describes brittle fracture in ceramics:

$$\sigma_f = \frac{K_c}{Y\sqrt{\pi a_c}} \qquad (9.4)$$

Strength depends on the toughness of the material. It is the higher, the smaller the size of the fracture origin $(\sigma_f \propto a^{-1/2})$. Since the size of the fracture origin differs from specimen to specimen, the strength of ceramics has a large scatter. It is not given by a simple number, but by a distribution function (the Weibull distribution[18,19]). Since the probability of finding a large flaw is higher in a large than in a small specimen, the mean strength of large specimens is

lower than the mean strength of small specimens. These probabilistic aspects of brittle fracture will be addressed in the following chapter.

If Eq. 9.3 is solved with respect to the crack size, we get the critical crack size (Griffith crack size, Eq. 9.5):

$$a_c = \frac{1}{\pi} \left(\frac{K_c}{Y\sigma_f} \right)^2 \tag{9.5}$$

In most strength tests, some SCCG happens before the final fracture occurs. This means that the cracks start to grow at stress intensity factors smaller than the fracture toughness. The Griffith crack size then corresponds to the size of the flaw plus the crack extension due to SCCG. This aspect will be considered in Chapter ?.

In the introduction, we claimed that fracture origins are flaws in the component or at its surface. We have shown that cracks extend spontaneously if the SIF reaches the fracture toughness. It is still a somewhat open question as to what causes a flaw to behave like a crack, but it is a matter of fact that flaws are origins of brittle fracture and that the flaw size roughly corresponds to the Griffith crack size. It is the experience of the authors that the Griffith crack size as calculated using Eq. 9.5 is in general a little larger (about 10%) than the flaw size determined on the fracture surface.

In many modern ceramics, the size of typical material flaws is around 30 μm, which reflects state-of-the-art materials processing. If fractures start from surface flaws, their stress intensity factor is higher than that of volume flaws. Due to the higher geometric factor of surface (compared to volume) cracks, Eq. 9.3 is fulfilled for much smaller cracks. Then surface cracks with a depth as small as 10 μm may become critical and have to be avoided. Figure 9.1 shows an example of a fracture origin (a) within (material flaw), and (b) at the surface of a (machining flaw) specimen.
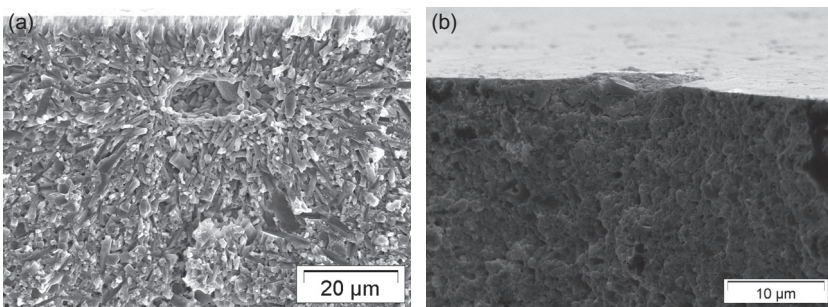
FIGURE 9.1   Fracture origins in silicon nitride bending specimens: (a) Volume flaw; and (b) Machining flaw.

9.2.3   Probabilistic Aspects of Brittle Fracture

For convenience, and without loss of generality, we only consider a uniaxial and homogeneous stress field, if not separately mentioned.

9.2.3.1   Weibull Distribution

In a set of fracture experiments on ceramic specimens, the strength data show, in general, a large scatter. In many materials the distribution of data can be described by the Weibull distribution (Eq. 9.6)[18,19]:

$$F(\sigma, V) = 1 - \exp\left[-\frac{V}{V_0} \left(\frac{\sigma}{\sigma_0} \right)^m \right] \qquad (9.6)$$

F is the cumulative probability of failure (in a specimen with volume V and at the stress σ). The volume V_0 is an arbitrary scaling volume. The Weibull modulus (m) describes the scatter of the strength data. The characteristic strength (σ_0) is the stress at which, for $V_0 = V$, $F(\sigma_0, V_0) = 1 - \exp(-1) \approx 63\%$ of the specimens fail. The sum of the probability of failure (F) and the reliability (R) is one ($F + R = 1$). Figure 9.2 shows a Weibull diagram of an alumina ceramic.

The Weibull distribution has only two independent parameters: m and $V_0\sigma_0^m$. Therefore, the choice of V_0 has an influence on the value of the characteristic
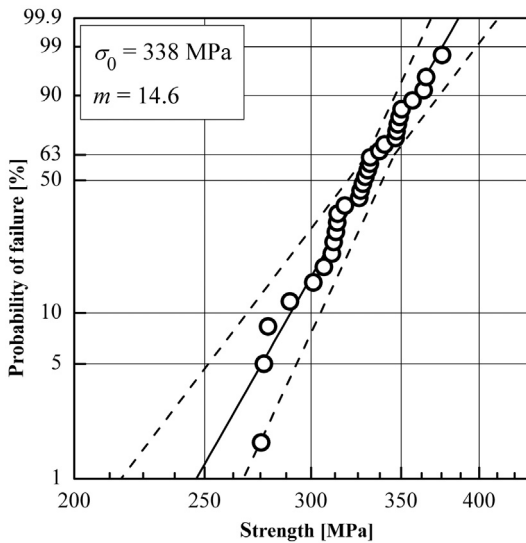
FIGURE 9.2   Cumulative probability of failure versus strength in a so-called Weibull diagram (data measured on commercial alumina). The axes are scaled to represent the Weibull distribution as a straight line (through line in the diagram). The slope of the line is the Weibull modulus. Dashed lines indicate the borders of the combined 90% confidence intervals.

strength (σ_0). Note that there is not always the same choice for the scaling volume, which can cause some confusion. When different data sets are compared, this aspect must be considered.

An important consequence of the Weibull distribution is that even at a very small stress, there remains some risk of failure. For $\sigma/\sigma_0 << 1$ it holds that $F \propto (\sigma/\sigma_0)^m$. Based on Weibull statistics it is not realistic to claim reliability of 100%.

9.2.3.2 Inhomogeneous Stress Fields

Strength testing of ceramics is often performed by flexural tests of rectangular beams, which cause an inhomogeneous uniaxial stress state, or by bending discs, which causes an inhomogeneous biaxial stress state. If only data that were measured using identical specimens were compared, the specimen's volume (Eq. 9.6) would in general be set equal to the scaling volume. Then the highest primary stress component in the specimen, at the moment of failure, could be defined to be the strength of the specimen. For a fair comparison of strength data measured on different specimens, or using different testing methods, a description of the influence of stress gradients is necessary.

Let us first analyze the situation for a uniaxial inhomogeneous stress state as it occurs, for example, in a 3-point bending test. High tensile stress only occurs in a small portion of the specimen, and half of the specimen is compressed. It is obvious that the volume V in (Eq. 9.6) has to be replaced by an 'effective' volume V_{eff}, which is roughly speaking, the volume under the high tensile stress. It is defined by Eq. 9.7:

$$V_{eff} = \int_{\sigma > 0} \left(\frac{\sigma(\vec{r})}{\sigma_r} \right)^m dV \qquad (9.7)$$

The position vector is $\vec{r}$, and σ_r is an arbitrary reference stress (in general the maximum of the first principal stress field). The effective volume is related to the reference stress by the equation: $\sigma_r^m V_{eff} = \sigma_0^m V_0$. For modern ceramics the Weibull modulus may be very high (e.g. $m = 10$–30). Then the effective volume can become very small. If a stress lower than the maximum stress is selected as the reference stress, the effective volume can become large, possibly even larger than the real volume of the component.

For standard bend bars, the effective volume can be calculated analytically by taking the maximum stress in the bar as the reference stress (Eq. 9.8):

$$V_{eff} = b \times h \times L \frac{k \times m + 1}{2(m + 1)^2} \qquad (9.8)$$

Here, b and h are the bar's width and height, respectively; L is the support roller distance; m is the Weibull modulus; and $k = l/L$ with the loading roller distance l. Of course, l is 0 for 3-point bending tests. Expressions for effective surfaces can be found in the literature.[20] For general loading situations, a numerical calculation is necessary (Eq. 9.7). For each loading case

the calculations have to be done only once because the integral scales with the load amplitude.

9.2.3.3 Multi-axial Stress Field

It is well known that the orientation of surface cracks can have a strong influence on the strength of specimens. Grinding may cause deep cracks in the grinding direction. Bending test bars ground in the longitudinal direction (i.e. in stress direction) have in general a much higher strength than bars ground perpendicular to that direction.[21] The reason is that in the first case the stress field does not tear the crack borders apart (mode I loading) but in the latter case it does. Biaxial (and multi-axial) stress states are more dangerous than uniaxial stress states since in the biaxial state any surface crack is mode I loaded and in the uniaxial field this only happens for cracks oriented perpendicular to the stress direction. Therefore, (for specimens with the same effective volume) the strength determined in a biaxial test is a little lower than in a uniaxial test. In the Weibull distribution this can be considered by replacing the stress with an equivalent stress: $\sigma \to \sigma_e$, which is the uniaxial tensile stress that would have the same damaging effect as an applied multi-axial stress state.

Several different definitions of the equivalent stress were proposed,[22] but the influence of the choice of the multi-axial failure criterion on the equivalent stress is, in general, small. The simplest criterion is the first principle stress criterion (FPS). Here it is assumed that the equivalent stress is equal to the first principle stress ($\sigma_{e.FPS} = \sigma_I$). Often used is the principle of independent action (PIA), where all tensile stress components (σ_I, σ_{II}, and σ_{III}) are assumed to act independently: $\sigma_{e.PIA} = (\sigma_I^m + \sigma_{II}^m + \sigma_{III}^m)^{1/m}$. The effect of compressive stresses is neglected in both cases. For a biaxial stress state, the FPS equivalent stress is $\sigma_{e,FPS} = \sigma_I$ and the PIA equivalent stress is $\sigma_{e,PIA} = 2^{1/m}\sigma_I$. For modern ceramic materials having a high Weibull modulus, the difference is only a few percent.

9.2.3.4 Size Effect on Strength

The strength of ceramic specimens strongly depends on their size. Since it is more likely to find a large flaw in a large specimen, the mean strength of a set of large specimens is smaller than that of a set of small specimens. This fact is addressed in Eq. 9.6 by the volume V. For the same probability of failure, but for specimens with different volumes V_1 and V_2, it holds (Eq. 9.9):

$$\sigma_1^m V_1 = \sigma_2^m V_2 \text{ or } \sigma_2 = \sigma_1 \left(\frac{V_1}{V_2}\right)^{1/m} \tag{9.9}$$

In other words, the strength scales with $\sigma \propto V^{1/m}$. The characteristic strength dependence on the effective specimen volume of an alumina ceramic is shown in Figure 9.3.

As mentioned earlier, flaws can exist in the volume and at the surface of a specimen. The relationships shown before relate to specimens failing from
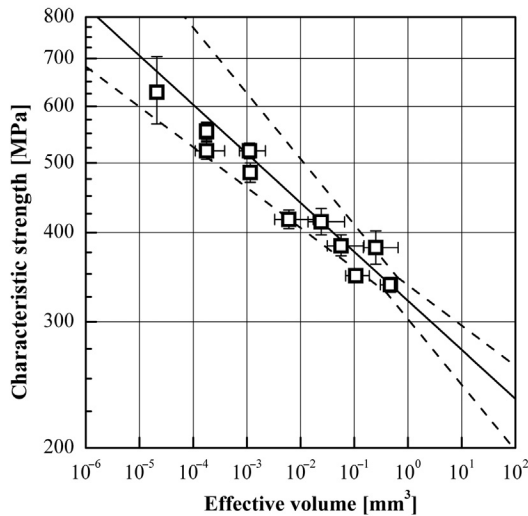
FIGURE 9.3   Strength test results of a commercial alumina ceramic. The plot is of the characteristic strength of sets of 15 to 30 specimens versus their effective volume on a log-log scale. The through line is the strength prediction on the basis of Eq. 9.9 from the value measured at the highest effective volume. The dashed lines indicate the combined 90% confidence intervals for the prediction.

volume flaws. If fracture origins are surface flaws, the volume in Eqs. 9.6–9.9 has to be replaced by the (effective) specimen surface.

9.2.3.5   Influence of Flaw Populations on Fracture Statistics

In many papers, the relationship between flaw populations and fracture statistics is analyzed. It is shown in the literature[23,24] that for volume flaws, which behave like non-interacting cracks and are stochastically distributed in the material, the fracture statistic is the Weibull statistic if the flaw size distribution follows an inverse power law: $g \propto a^{-p}$. In such a flaw size distribution, small flaws are much more frequent than large ones. Brittle fracture of the specimen occurs if the SIF at the most dangerous flaw reaches the fracture toughness of the material (the weakest link hypothesis applies). Then the Weibull modulus is strictly related to the parameter p of the power law: $m = 2\,(p-1)$. In that logic, the distribution of strength data simply describes the distribution of flaw sizes. A material with that behavior is called a Weibull material.[25]

However, other types of flaw distributions can also occur. Examples are bi- and multimodal flaw populations[26–28] or the simultaneous occurrence of volume and surface defects.[27] In these cases, a clear interpretation of fracture statistics and a precise determination of a design stress is only possible on the basis of very large data sets based on a high number of experiments coupled with a proper statistical analysis. This is difficult in technical practice. Furthermore, flaw

populations strongly depend on details of the materials processing and on the machining. Therefore, a simple transfer of laboratory data into a practical application can be totally misleading. In dentistry, the risk of inappropriate grinding, which may cause very large cracks and a significant loss of strength, is much higher than in industrial machining under much better defined conditions. Defects can also be introduced when different materials (i.e. veneers on a ceramic crown structure) are bonded to each other.[29]

9.2.3.6 A Simple Example for Designing with Ceramics

In this section we will give an example of designing with ceramics. We will determine the highest possible design stress (σ_{comp}) in a component that can be described as a bent beam. The beam is made of a fine-grained, high-strength alumina ceramic. It has an effective surface ($S_{eff,comp}$) of $1000\,mm^2$.

As stated earlier, failure in ceramics can occur at any stress, but at low stresses it is much less frequent than at high stresses. Therefore at the beginning of the design process, a probability of failure has to be defined, that can be tolerated in the analyzed application. If the damage associated with the failure of the component is high, the tolerable failure probability must be very low, and if the damage is negligible, it can be high. As an actual example, if the tolerable failure probability (F_{comp}) is 0.1% (0.001, meaning one in a thousand beams will fail), then the necessary reliability (R_{comp}) is 99.9% (or, $1 - F_{comp}$).

The strength of the ceramic has been measured with the punch on ring test (which is a biaxial strength test). The characteristic strength ($\sigma_{0,specimen}$) is $500\,MPa$ and the Weibull modulus ($m_{specimen}$) is 20. The fracture origins in the specimens were machining flaws. The effective surface of the specimens ($S_{eff,specimen}$) was $10\,mm^2$. The normalizing surface ($S_{0,specimen}$) was equal to the effective surface of the specimen.

To solve the problem we must consider the following:

a. *The fracture origins in the specimens were surface defects.* In Eqs. 9.6–9.9 the (effective) volume has to be replaced by the (effective) surface and it has to be checked that failures in the components are also caused by surface defects. In other words, it is assumed that $m_{specimen} = m_{comp} = m$.

b. *The effective surface of the specimens and the beam are different.* The effective surface of the specimens is only 1/100 of the effective surface of the components. Using Eq. 9.9 we get a reduction factor for the tolerable stress (Eq. 9.10):

$$f_{size} = \left(\frac{S_{eff,specimen}}{S_{eff,comp}} \right)^{1/m} \tag{9.10}$$

If volume flaws are relevant for failure in specimens and components, the effective surfaces in Eq. 9.10 have to be replaced by effective volumes. For the given numbers, Eq. 9.10 evaluates to $f_{size} = (10/1000)^m = (1/100)^{1/20} = 0.79$.

c. *The necessary reliability is higher than the reliability at the character-
istic strength.* A further reduction factor comes from the fact that the
characteristic strength of the specimens is determined for a reliability
of $(1-63\%) = 37\%$, and the claimed reliability of the beams is 99.9%.
Transforming Eq. 9.6 for components having the same effective surface we
get the factor (Eq. 9.11):

$$f_R = \frac{\sigma_{comp}(F_{comp})}{\sigma_{0,specimen}} = \left(\ln \frac{1}{R_{comp}} \right)^{1/m} \tag{9.11}$$

Inserting the numbers in Eq. 9.11 we get: $f_R = (\ln(1/0.999))^{1/20} = 0.71$.

d. *The stress state at strength testing was biaxial and in the component it is
uniaxial.* The stress state used for testing the specimens is more damaging
than the stress state in the components. To account for this we introduce
Eq. 9.12:

$$f_e = \begin{cases} 1 & \text{for the FPS criterion} \\ 2^{1/m} & \text{for the PIA criterion} \end{cases} \tag{9.12}$$

Inserting numbers into Eq. 9.12, we get $f_e = 2^{1/20} = 1.04$.

In summary, the design stress is the characteristic strength of the speci-
mens multiplied by the product of all correction factors (Eq. 9.13):

$$\sigma_{comp} = \sigma_{0,specimen} \ f_{size} \ f_R \ f_e \tag{9.13}$$

Eq. 9.13 gives $\sigma_{comp,FPS} = 500 \ 0.79 \ 0.71 \ 1 = 280$ MPa in the case of the
FPS criterion, and gives $\sigma_{comp,PIA} = 500 \ 0.79 \ 0.71 \ 1.04 = 290$ MPa in the case
of the PIA criterion, respectively.

In summary, one fracture in a sample of 1000 components or less can be
expected if the applied peak stress is 280 MPa or lower, and if failure is caused
by surface flaws. It should be kept in mind that many more failures may occur
if the machining of the components introduced more severe flaws than were
present in the specimens.

9.3   SUB-CRITICAL CRACK GROWTH

In the last section we focused on brittle fracture, in which a specimen fails
almost immediately after the application of a load, but ceramic components
also fail after some time under load. Like brittle failure, this behavior is also
related to flaws, which behave like cracks and grow to a critical size. This sub-
critical crack growth (SCCG) can also be described in the framework of linear
elastic fracture mechanics.

Early measurements of SCCG were made in glass by Wiederhorn.[8] In
the range of practical significance, he determined the crack growth rate to be

dependent on the SIF and recognized that the data follow a power law (Paris law for crack growth, Eq. 9.14):

$$v = v_0 \left(\frac{K}{K_c} \right)^n \tag{9.14}$$

The SCCG exponent n and the constant v_0 are temperature-dependent material parameters. The growth rate is higher in wet air or water than in dry air or vacuum. Other polar molecules in the environment of the specimens may also increase SCCG.[9]

SCCG is also observed in ceramic materials that contain a glassy silicate grain boundary phase. For such materials a typical room temperature value of the exponent is $n \approx 30$–50. For most dental ceramics n is approximately 20,[30] and in some cases even $n = 12$.[31] SCCG also occurs in glass-free ceramics; then n can be much higher (e.g. $n \approx 200$ for silicon carbide ceramics).[32]

Eq. 9.14 can be used to determine the lifetime (t_f) of a component under load. Note that the crack growth rate is $v = da/dt$, and thus $dt = (1/v)\, da$. Inserting Eq. 9.3, separating the time and crack length-dependent variables, and integrating we get Eq. 9.15:

$$\int_0^{t_f} \sigma(t)^n \, dt = \frac{2}{n-2} \frac{1}{v_0} \left(\frac{K_c}{Y\sqrt{\pi}} \right)^n a_i^{(2-n)/2} \left[1 - (a_c/a_i)^{(2-n)/2} \right] \tag{9.15}$$

The critical crack grows from its initial length (a_i) to the critical (final) length ($a_i = a_f$), then fast brittle failure occurs. In this calculation it has been assumed that the geometric factor (Y) is constant.

The value of n is a very high number ($n \gg 1$). Therefore, the second term in the square bracket can be neglected if any significant crack growth occurs.

9.3.1 Sub-critical Crack Growth Under Constant Load

Under load, the cracks in the specimen steadily grow and the strength decreases until it is equal to the applied stress. Then, without any warning, brittle fracture occurs. This behavior happens under all loading conditions, but in this instance, we are only considering the simple case of a test under constant load (with homogeneous and uniaxial stress, σ_{stat}). If not mentioned otherwise, the examples in this chapter are valid for a typical commercial alumina ceramic with a stress exponent of $n = 30$. In this case, the integral in Eq. 9.15 becomes trivial and we get Eq. 9.16:

$$t_f = \frac{2}{n-2} \frac{a_i}{v_i} \left[1 - \frac{a_c}{a_i} \frac{v_i}{v_f} \right], \tag{9.16}$$

where $\quad v_i = v(K_i), \qquad v_f = v(K_f) = v_0, \qquad K_i = \sigma_{stat} Y \sqrt{\pi a_i}, \qquad$ and $K_f = \sigma_{stat} Y \sqrt{\pi a_c} = K_c$, respectively.

Remember that the second term in the square bracket can (in general) be neglected. Then (Eq. 9.17):

$$t_f \approx \frac{2}{n-2} \frac{a_i}{v_i} \propto \sigma_{stat}^{-n} a_i^{-(n-2)/2} \tag{9.17}$$

The applied stress and the initial crack size have a significant influence on the lifetime of the specimen. For $n = 30$, a reduction of the initial size of the critical crack by 10% increases the lifetime 4.4-fold. A reduction of the applied stress by 10% leads to a 24-times longer lifetime. If the critical cracks are caused by grinding, the grinding process becomes the key procedure that determines the lifetime of the component.

It is interesting to note that the crack needs a large fraction of the lifetime to double in size, and less than a few percent for the final failure. Of course, the growth rate strongly depends on the initial size of the critical crack (Figure 9.4). As discussed earlier for geometrical identical specimens, the size of the critical defect scatters. In strength testing, this causes the scatter of strength; and in life-time testing, it causes a scatter of lifetime. If, for example, the strength data in a set of specimens scatters $\pm 20\%$, the span of the lifetimes (Eq. 9.16) would be from 1 s to 300,000 s (for $n = 30$).

For the lifetime of specimens determined under constant load, a Weibull distribution can be determined. Of course, this function is strongly related to
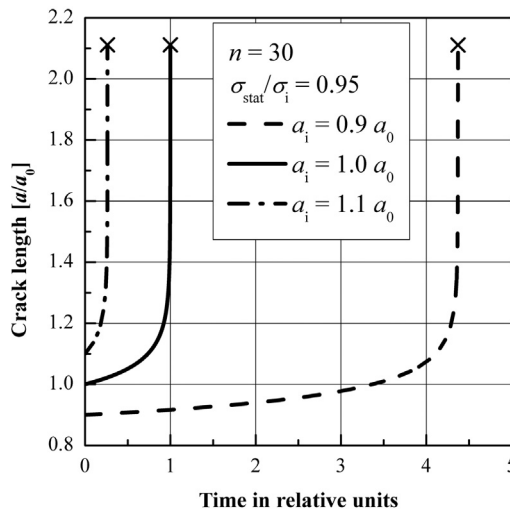
FIGURE 9.4   Crack length versus time for cracks of different initial size for a material with an SCCG exponent n = 30 and σ_{stat}/σ_t = 0.95). The time axis is normalized with the lifetime of a reference case (through line, relative lifetime 1). The influence of the initial crack length is visible: while a 10% decrease of the initial crack size increases the lifetime by a factor of~4.5 (dashed line), a 10% increase in initial crack length reduces the lifetime to approximately ¼ of the reference case (dash-dotted line).

the Weibull distribution of strength and the SCCG-behavior of the material. For example, the lifetime Weibull modulus is related to the strength modulus and the SCCG exponent: $m^* = m/(n-2)$. It is obvious that n can be determined by measuring m and m^*. For a typical ceramic with $m = 20$ and $n = 30$ the modulus of the lifetime Weibull distribution is: $m^* = 20/(30-2) = 0.71$.

9.3.2   Sub-critical Crack Growth Under Varying Load

The strong influence of crack size and load on the lifetime can be discussed in the simplest terms for a constant load, but in general the load is not constant but varying. Strength tests are often performed with a constant cross head speed of the testing machine, which translates to an (almost) constant stress rate ($\dot{\sigma}$) in the specimen. In this case, the left-hand side of Eq. 9.15 can be integrated analytically, and we get (Eq. 9.18):

$$\sigma_f^{n+1} = \frac{2(n+1)}{n-2} \frac{a_i}{v_0} \sigma_i^n \, \dot{\sigma} \left[1 - \left(\frac{\sigma_f}{\sigma_i} \right)^{n-2} \right], \text{ where } \sigma_i = K_c/(Y\sqrt{\pi a_i}) \qquad (9.18)$$

The inert strength is σ_i (i.e. the strength of the specimen without any SCCG), and the strength of the specimen after some SCCG is σ_f. In Figure 9.5, constant stress rate test results on a commercial alumina are shown. The plot is of the strength versus stress rate on a double logarithmic scale. At small stress rates the critical crack has time for growth. Then the square bracket in Eq. 9.18 can be neglected and it holds that $\sigma_f \propto \dot{\sigma}^{1/(n+1)}$. For stress rates
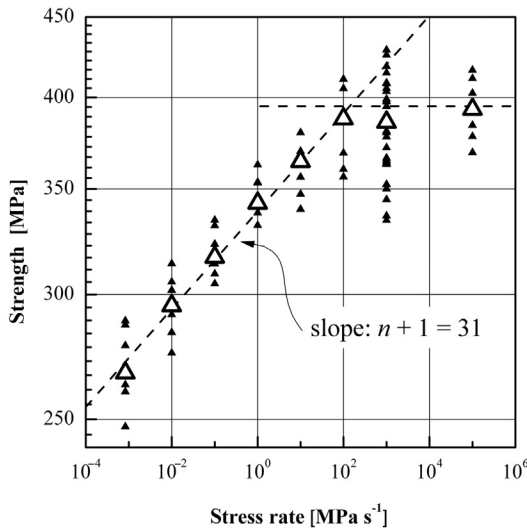
FIGURE 9.5   Strength versus stress rate for constant stress rate tests performed on a commercial alumina. The SCCG exponent determined using these data is n = 30.

higher than $\sim 10^2$ MPa s^{-1}, the testing time is too short for significant SCCG and the strength is equal to the inert strength.

In dental applications, stress fields, which vary in time, will occur. An important reduction of strength by SCCG can be expected and sudden failure of implants is possible in normal use. A lifetime assessment based on Eq. 9.15 is, in principle, possible.

9.3.3   Proof Testing

In industrial applications of ceramics, proof testing is often used to guarantee a component's minimum service life.[22,33–36] The intention of proof testing is to load the component with a stress field (amplitude σ_p), which is similar but a little higher than the stress field in service (amplitude $\sigma_s < \sigma_p$). All components which contain cracks larger or equal to $a_p = (1/\pi) \, (K_c/\sigma_p Y)^2$ will be destroyed. The critical crack size in service is $a_c = (1/\pi) \, (K_c/\sigma_s Y)^2$. The time the critical crack needs to grow from size a_p to a_c is the minimal lifetime of the component (if only SCCG is considered). In order to avoid sub-critical crack growth during the proof test procedure, the loading has to be applied with a high loading rate.

In reality, the stress fields in service are often very complex and cannot easily be simulated in a simple laboratory test. Then simpler loading scenarios are used for proof testing and a guarantee of the lifetime is no longer possible. In any case, such a proof test causes a significant increase in reliability.

9.4   FATIGUE

In the older literature, SCCG is sometimes called fatigue since a real cyclic fatigue effect caused by alternating loading, which overweighs the effect due to SCCG, had not been recognized at that time. Meanwhile, cyclic fatigue has been recognized as a possible damage mechanism in ceramics, and only minimal cyclic fatigue data exists for engineering ceramics.[11,37–40] From these data, however, it can be concluded that a Paris law for fatigue crack growth exists (Eq. 9.19):

$$\frac{da}{dN} = \left(\frac{\Delta a}{\Delta N}\right)_0 \left(\frac{\Delta K}{K_c}\right)^{\tilde{n}} \tag{9.19}$$

The material parameters, $(\Delta a/\Delta N)_0$, and the Paris exponent ($\tilde{n}$) are dependent on mean stress and temperature. N is the number of load cycles. It has been observed that the fatigue crack growth rate is, in some cases, much larger than the corresponding mean SCCG rate[22] if tension/compression cycles are applied, but it approaches the mean SCCG rate if testing is done with a high mean stress. In this case, the fatigue effect can be ignored.

Since fatigue, as well as SCCG, describe the extension of pre-existing cracks, and since in both cases a Paris-type law for the crack exists, the description of fatigue is very similar to that of SCCG. The fatigue lifetime strongly depends on

the applied stress amplitude and on the size of the initial cracks. All measures that can be taken to inhibit SCCG are also effective in reducing fatigue effects.

In summary, the significance of cyclic fatigue on the lifetime of ceramics in dentistry seems to be limited.

9.5   OTHER REASONS FOR DAMAGE

In previous chapters we described failure that started from crack-like flaws that are present in the finished products after their production. Sudden brittle fracture was the result of a sudden singular overload or of the stable growth of a crack under the applied load spectrum up to a critical size. The reader should also be aware that other loading modes exist. These seem to be harmless, but can produce cracks. These cracks can be the initial cracks for SCCG and fatigue crack growth. Examples of these modes of loading are thermal shock and contact loading. Other important reasons for unexpected failure can be internal stresses, which can come into existence during component processing.

9.5.1   Thermal Shock Damage

Products in dentistry do not in general suffer from great and sudden temperature changes. Thermal shock damage is thus not likely to occur in service of those parts. Therefore, this damage mechanism will not be treated in detail in this chapter, but it should be noted that thermal shock can be of high relevance during the processing of ceramic parts. Upon fast cooling, very large temperature changes or temperature differences can create high tensile stresses at the surface of the component and compressive stresses inside the component. These stresses (σ_{th}) scale with the temperature difference in the component, ΔT, the elastic modulus (E), and the coefficient of the thermal expansion of the ceramic material (α): $\sigma_{th} \propto E \, \alpha \, \Delta T$. For many ceramic materials the product αE is in the range of 2–3 MPa/K.[41] Temperature differences of 100 to 200°C can create stresses of several hundred MPa, which may exceed the strength of the material and cause severe cracking. Due to the compressive stresses in the bulk, these cracks may stop before final failure of the component. Figure 9.6 shows thermal shock cracks on the surface of a ceramic
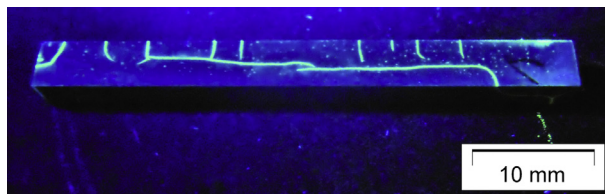
FIGURE 9.6   Ceramic specimen with thermal shock cracks. The specimen was quenched in cold water from several hundred degrees Celsius. The direction of the cracks is typical for the existence of a biaxial stress field.

specimen. The part was heated in a furnace and then quenched in water. Temperature gradients that cause thermal stresses can also be generated by local cooling (e.g. by manipulating a hot component using cold tweezers).

9.5.2   Contact Damage

Localized loading of surfaces (e.g. by static contact or dynamic impingement by small bodies) is of great significance in dentistry, since this is a typical loading for tooth and implants. Although the contact situation suggests that only compressive stresses occur, significant tensile stresses can also come into existence. Two typical cases can be distinguished: contact by a blunt body (indenter), and point loading by a sharp indenter.[42]

Blunt contact was investigated more than one hundred years ago by Hertz,[43] who analyzed the contact of a sphere and a flat surface. When the sphere touched the flat, the bodies deformed elastically and a circular contact area resulted. Underneath this contact area, compressive stresses arose. The contact zone was encircled by a narrow ring-shaped region where significant tensile stresses occurred; these had a maximum amplitude of about one-quarter of the mean contact pressure.[44] Since in stiff ceramic materials the contact zone can be very small and, consequently, compressive stresses can be very high, tensile stresses in that ring-shaped zone can also become very high. Ring-shaped cracks (Hertzian) or partially ring-shaped contact cracks can form at the surface (Figure 9.7a). These are not typically deep, but in any successive loading may act as a fracture origin.

Sharp contact is a (pseudo) point-loading situation and is used in indentation hardness testing (using a Vickers or Knoop indenter). Severe plastic deformation occurs under the contact point. This causes the formation of radial cracks and can even lead to chipping of surface fragments (Figure 9.7b). This type of damage is relevant in dentistry.

A variant occurs if the contact point is near an edge where the contact can cause the formation of an edge flake.[45–48] Such edge flakes can often be observed in ceramic tableware and tiles[49] (Figure 9.7c), and also in teeth.[50,51]

Finally, it should be noted that machining damage, as can be caused by grinding, is related to that form of damage. Several types of cracks can be caused by inappropriate machining; these resemble cracks caused by sharp indenters. An example sketch is shown in Figure 9.8.

9.6   MECHANICAL TESTING OF ADVANCED CERAMICS

Even though it was shown in Section 9.2.2 that fracture toughness (K_c) determines whether a pre-existing flaw in a component or specimen becomes critical (which leads to failure), the strength that determines the integrity of a component is the more easily accessible property. Like most mechanical properties of advanced ceramics, it is investigated using rectangular flexure bars,[2,3,6,52] discs, or plates under equibiaxial loading. Parallel to material development, substantial
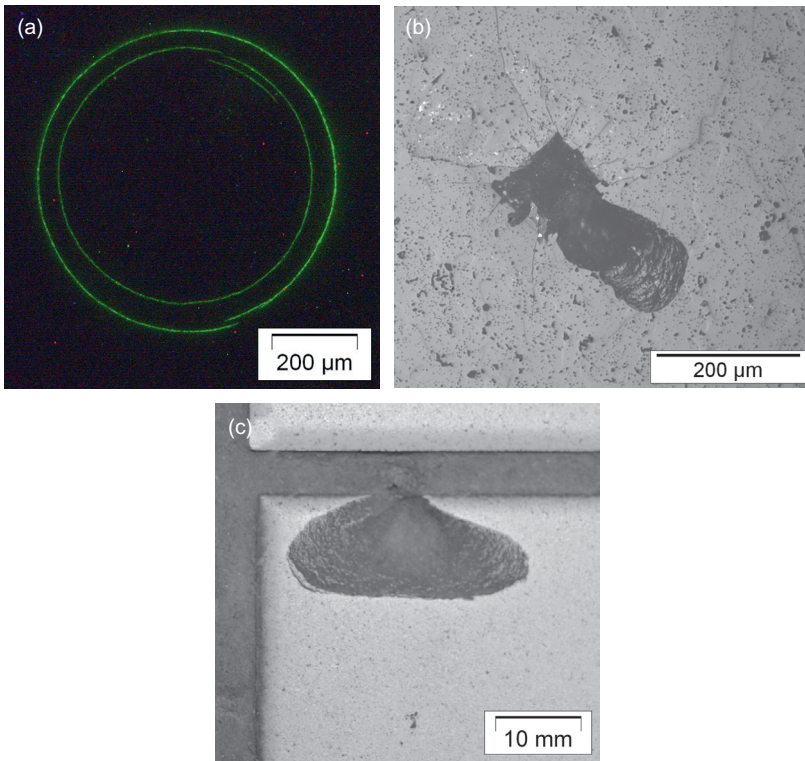
FIGURE 9.7   Contact damage caused by (a) A blunt (ball) indenter in silicon nitride; and (b) A sharp (pyramid) indenter in alumina. (c) If the contact site is close to an edge, flakes chip off.
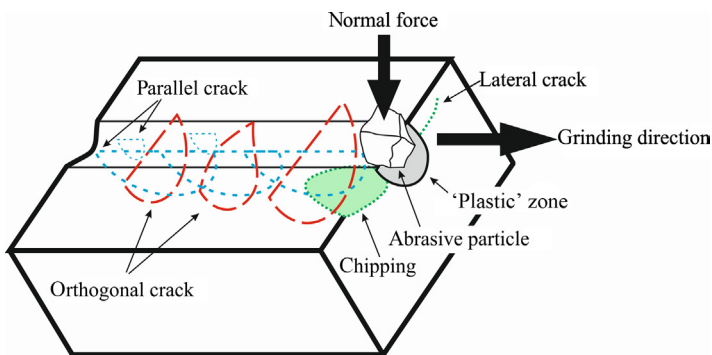
FIGURE 9.8   Illustration of cracks that can appear during grinding, after[21].

effort has been made to develop suitable and robust test procedures that are easy to perform, and that deliver adequately precise results.[53,54] In this section we will discuss the procedures adopted for testing dental ceramics with respect to their error budget, comparability, and significance.

9.6.1   Flexure Tests

Determination of the strength and fracture toughness of dental ceramics is standardized in ISO 6872.[55] According to this standard, flexural strength can be determined using prismatic bars with a wide range of allowable sizes, either in 3- or 4-point flexure. The error potential of bending tests has been exhaustively analyzed and is in the range of 5% for specimens tested on a 40 mm support span.[53,54,56] For smaller specimens, or for non-ideal loading arrangements, it can be even bigger. An important source of errors is established by fixing support and loading rollers, which promote friction effects during the test.[56] Contrary to the standard for advanced ceramics,[2] a wide range of specimen sizes is allowed in ISO 6872. While the width of the specimens is the same for all allowed test geometries, the thickness is limited to 0.1 times the support roller distance. This is an essential requirement for the validity of the linear elastic formulas that are used for the calculation of the strength from the fracture load. The variation in possible test geometries imposes a serious problem on the interpretation of strength values measured according to the ISO and on the use of its table 1, which defines minimum strength requirements for different classes of dental ceramics; the size effect on strength, as discussed in Section 9.2.3.4, is neglected. The requirements can be met more easily if small specimens are tested. With the biggest test geometry (4×3 mm bars broken in 4-point bending on a 40/20 mm span) a considerably lower strength (σ_{4PB}) will be measured than with the smallest possible geometry (σ_{3PB}, measured using 4×1.2 mm bars broken in 3-point bending on a 12 mm span). According to Eqs. 9.8 and 9.9, $\sigma_{4PB}/\sigma_{3PB}$ is 0.54 for a Weibull modulus (m) of 5, 0.70 for an m of 10, and 0.77 for an m of 15, respectively. It is therefore strongly recommended to report the test geometry together with the strength results.

9.6.2   Biaxial Tests

As an alternative to flexure tests, the strength may also be determined using a biaxial test, which is one of a variety of biaxial tests on discs.[57,58] The standard for dental materials[55] prescribes a piston-on-three-balls test with disc-shaped specimens with diameters from 12 to 16 mm and a thickness of 1.2 mm. A thin (thickness to support radius ratio ≈ 0.2) disc-shaped specimen is positioned on three small balls positioned along a circle and loaded by a small flat piston. The strength is calculated from the fracture load using a relation based on the simple linear elastic plate theory. This test holds sources for systematic measurement errors that shall be discussed subsequently. As long as the disc specimens are parallel and the test equipment is perfectly aligned, this calculation delivers sufficiently accurate strength results. Once the load application by the piston is not perfect (i.e. the piston does not touch the specimen with its entire circle-shaped end face but only along a small portion of its edge), the load distribution in the specimen is changed. The use of the suggested formula for strength calculation then gives erroneous strength values that differ from the true strength by more than 5%.

At the contact of the specimen and the support balls, tensile contact stresses arise which are (for a given load) the bigger the smaller the support balls are. These stresses may lead to localized failure at one of the support balls and not at the location of the maximum far-field stress in the center of the disc. The susceptibility for this kind of failure depends on the specimen's Young's modulus and strength, its geometry (ratio thickness t to support radius R; i.e. t/R), and the diameter of the balls. If high-strength materials are tested, t/R should be small and the ball diameter should be as big as possible to inhibit contact failure.[59]

In the test set-up the supporting balls are usually fixed to their prescribed positions along a 10 mm to 12 mm diameter circle. This fixation prevents any movement of the balls during the test and provokes friction effects between the disc and the balls that affect the stress distribution in the specimen. In the analytical evaluation formula these effects are neglected, and a systematic error is introduced to the strength value.[60]

ISO 6872 recommends placing a 0.05 mm thick polyethylene film between the specimen and the contact and loading devices, which reduces the contact stresses and/or the influence of any misalignment of the loading piston and influences the friction between specimen and support balls. This procedure is effective, but the effect of the film on the stress distribution is not evaluated. An additional uncertainty is added to the measured strength.

The evaluation of the biaxial test requires knowledge of Poisson's ratio (ν). This quantity is often not known for a specific material, and the standard prescribes a value of 0.25. The effect of an erroneous value for ν on the calculated strength can be substantial. An overestimation or underestimation of Poisson's ratio by 10% (i.e. the true, unknown Poisson's ratio is 0.225 or 0.275; 0.25 is used for the calculation) leads to an error of approximately $\pm 3.5\%$ in the calculated strength, which adds to the errors due to friction and misalignment.[60]

The piston-on-three-balls test is certainly an easy test to perform, but other biaxial strength tests like the ball-on-three-balls test are less prone to systematic errors due to friction, contact stresses, undefined specimen geometry, and misalignment, and deliver much more precise data without increased experimental effort.[57] For the ball-on-three-balls test, the total overall error is $\pm 1\%$ if Poisson's ratio is known to an approximate $\Delta \nu$ of 5%. It increases to a maximum of $\pm 5\%$ if $\Delta \nu$ is 25%.[57,60]

In addition to this procedure, the test set-up described in the ISO standard for implants for surgery,[61] which uses a ring-on-ring test and specimens with a diameter of 36 mm and a thickness of 2 mm, is also used for the characterization of dental materials.

9.6.3 Strength Statistics

Strength data measured according to ISO 6872 can be evaluated to determine the parameters of the strength distribution, if 15 or more specimens of one

material are tested. Knowledge of the strength distribution is the basis for a proper reliability analysis for ceramic components, as outlined in Section 9.2.3.6. The procedure described in the standard is a simplified version of what is standardized for advanced monolithic ceramics,[62–64] and gives different results due to a different fitting procedure. When strength statistics are evaluated, it should always be kept in mind that the Weibull modulus and the characteristic strength can only be determined within certain confidence bands. In the case of the Weibull modulus, these confidence bands can be quite wide if only a small number of specimens (15) is tested.[63,65] A detailed discussion of different evaluation methods for strength statistics can be found in the literature.[66]

Even though bending and biaxial strength tests apply different stress states to specimens, the measured strength (distributions) should be comparable in the framework of Weibull statistics (see Section 9.2.3). If strength results for the same materials from all methods (3-point bending, 4-point bending, and biaxial bending) are compared, they will have the same Weibull modulus (if the same defect population leads to failure), and can be ordered so that the test with the smallest effective volume (surface) gives the highest characteristic strength value and the one with the biggest effective volume (surface) gives the lowest characteristic strength value. The same has to be valid for a comparison of experiments performed on similar specimens but with different tests (i.e., the piston-on-three-balls test and the ball-on-three-balls test). There is, however, indication that this cannot be achieved in practical testing.[67]

To explain this discrepancy, it has to be considered that specimens are usually specifically produced for the test and that the production process (including firing and machining) is different for different tests and thus different typical flaws are present in the specimens. Additionally, one has to consider that the measurement uncertainty of a test has an influence on the determination of the Weibull modulus and the characteristic strength. If high measurement uncertainties are added to each measured strength datum, the error distribution may be wider than the inherent strength distribution (caused by the flaw distribution). High Weibull moduli ($m > 20$) can only be measured if the uncertainty is smaller than $\pm5\%$. A low Weibull modulus may thus be the consequence of imprecise tests.[68]

Additionally, one should always bear in mind that strength is measured on specimens that are specifically produced for the test using a production routine that differs from what is done in clinical practice. These strength values are useful for qualification procedures, for comparing materials, and for quality control purposes where the comparison is always done among such test specimens. For the reliability analysis of real components (crowns, etc.), however, these strength data may be inadequate because failure in service may occur due to another flaw type. If it can be assured that similar flaw types are responsible for failure in components and specimens, then the specimen strength distribution can also be designated as relevant for the components.

9.6.4   Fracture Toughness

A number of standardized procedures exist for the measurement of fracture toughness of advanced ceramics.[69–73] While the execution of one procedure[72] seems to be feasible for a standard mechanical testing laboratory, other methods[70,71,73] require specific skills that are only available at specialized testing facilities. Since some ceramic materials have a crack length-dependent fracture toughness (R-curve[1]), different methods also deliver different fracture toughness values for the same material.[22] Methods using the cracks associated with Vickers hardness indentations[74] do not give a fracture toughness value,[75] and should not be used. In summary, it can be stated that fracture toughness measurements, and the interpretation of the results of such measurements, should be left to specialists.

9.7   FRACTOGRAPHY

Fractography is a valuable discipline for learning from broken specimens or components. Since in ceramics almost no plastic deformation occurs, the pieces of a fractured body fit perfectly together, and in many cases the fracture origin and the direction of the crack growth can be read from the fracture surfaces. This can give information on critical (heavily loaded) areas in a component (i.e. weak microstructural features, material flaws, inappropriate machining, or inadequate use of components). Examples for successful application of fractography in dentistry are given in the literature.[76–78]

In general, the fracture origin is concentrically surrounded by a flat, featureless zone known as the fracture mirror. Such features are common in brittle fracture of ceramic materials. The fracture origin is a critical flaw that behaves like a crack. The crack path is perpendicular to the first principal stress (at least at the beginning of crack extension), and the fracture origin is surrounded by mirror, mist, and hackle. The size of the fracture origin, mirror, and mist, respectively, are found to be proportional to σ^{-2}, where σ is the stress in an uncracked body at the position of the origin of fracture.[79] Mirror constants can be found in the literature.[65,80–82]

This type of fracture can be found in both large and small systems (e.g. fractured natural rocks, tested specimens of advanced ceramic materials, and even broken ceramic fibers). Fracture mirror size measurements can be used for post-mortem determination of the failure stress in components (Figure 9.9).[83]

9.8   CONCLUDING REMARKS

The term 'dental ceramics' comprises a wide variety of materials that reaches from filled glasses to nearly dense sintered ceramics, from products that are shaped from powders and melts, to components milled from blanks before or after sintering. Their properties vary over a wide range: strength from 60 MPa to nearly 1000 MPa, fracture toughness from below 1 MPa m$^{0.5}$ to 10 MPa m$^{0.5}$, and Young's modulus from 70 GPa to 380 GPa.[84–88] The principles that describe their mechanical behavior are valid for all of these materials. On one
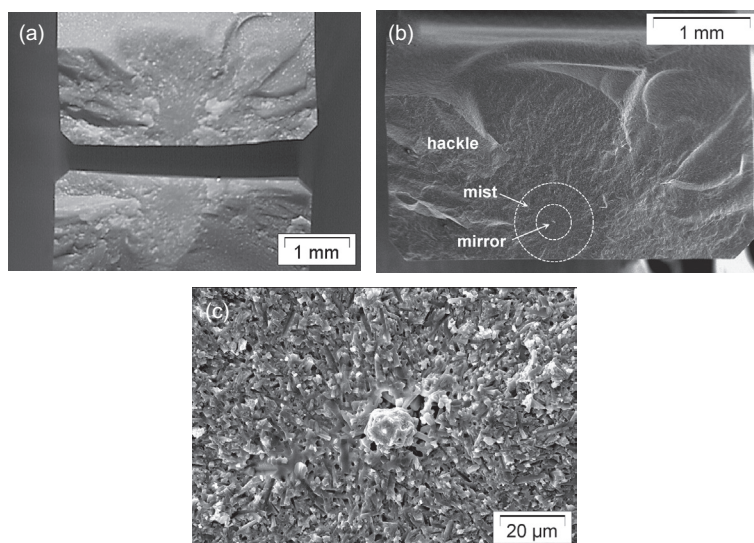
FIGURE 9.9   Fracture surface of a silicon nitride bending bar. (a) Macroscopic view of two mating fracture surfaces. The tensile stress was acting on the edges in the middle of the picture. The crack path is perpendicular to the loading direction. (b) Fracture surface of the upper piece from (a). Fracture mirror, mist, and hackle can be recognized on the fracture surface. (c) The fracture origin (agglomerate of sintering aids and inclusion) can be found in the center of the mirror. In the picture it spreads from the lower left-hand corner to the upper right-hand corner.

hand, the materials can be successfully used without an abundant risk of failure in low-stressed inlays and veneers, and on the other, they can be used to obtain structural parts like complex, highly loaded prostheses where the risk of failure should be minimized for the sake of the patients' well-being. A reliability analysis, as demonstrated in Section 9.2.3.6, can in principle be performed for any case, but this is not feasible in practice because each case is individual. In addition, there is always the discrepancy between data measured on specimens and the properties of the material finally present in the patient's denture.

The goals for further developments in the field of dental ceramics are thus not only material development (stronger, tougher, etc.), but also the development of reproducible machining and shaping procedures, as well as the establishment of robust, easy-to-apply design rules that take into account the specific properties of ceramics and incorporate the experience from the analyses of failures.

REFERENCES

1. Wachtman JB. Mechanical properties of ceramics. New York, Chichester: Wiley-Interscience; 1996.
2. EN 843-1: Advanced Technical Ceramics - Monolithic Ceramics - Mechanical Properties at Room Temperature: Part 1 - Determination of Flexural Strength, 1995.

3. ISO 14704: Fine Ceramics (Advanced Ceramics, Advanced Technical Ceramics) - Test Method for Flexural Strength of Monolithic Ceramics at Room Temperature, 2000.
4. ISO 24370: Fine Ceramics (Advanced Ceramics, Advanced Technical Ceramics)– Determination of Fracture Toughness of Monolithic Ceramics at Room Temperature by the Chevron-notched Beam (CNB) Method, 2005.
5. ISO 23146: Fine Ceramics (Advanced Ceramics, Advanced Technical Ceramics)– Determination of Fracture Toughness of Monolithic Ceramics at Room Temperature by the Single-edge Vee-notched Beam (SEVNB) Method, 2008.
6. ASTM C1161: Standard Test Methods for Flexural Strength of Advanced Ceramics at Ambient Temperature, 2002.
7. ASTM C1421: Standard Test Methods for Determination of Fracture Toughness of Advanced Ceramics at Ambient Temperature, 1999.
8. Wiederhorn SM. Influence of water vapour on crack propagation in soda-lime glass. J Am Ceram Soc 1967;50:407–14.
9. Michalske TA, Freiman SMA. Molecular interpretation of stress in silica. Nature 1982;95:511–2.
10. Schoeck G. Thermally activated crack propagation in brittle materials. Int J Fract 1990;44:1–14.
11. Gilbert CJ, Ritchie RO. Fatigue crack propagation in transformation toughened zirconia ceramic. J Am Ceram Soc 1987;70:C248–52.
12. Grathwohl G, Liu T. Crack resistance and fatigue of transforming ceramics; 1. materials in the $ZrO_2–Y_2O_3–Al_2O_3$ system. J Am Ceram Soc 1991;74:318–25.
13. Gross D, Seelig T. Fracture mechanics. Berlin: Springer; 2006.
14. Griffith AA. The phenomenon of rupture and flow in solids. Phil Trans Royal Soc Lond 1920;A221:163–98.
15. Murakami Y. The stress intensity factor handbook. New York: Pergamon Press; 1986.
16. Tada H, Paris P, Irwin GR. The stress analysis handbook. St. Louis: Del Research Corporation; 1985.
17. Irwin GR. Fracture Flügge S, editor. Handbuch der Physik. Berlin: Springer-Verlag; 1958. p. 551–89.
18. Weibull W. A Statistical theory of the strength of materials. Stockholm: Generalstabens Litografiska Anstalts Förlag; 1939.
19. Weibull W. A Statistical distribution function of wide applicability. J Appl Mech 1951;18:293–8.
20. Quinn GD. Weibull strength scaling for standardized rectangular flexure specimens. J Am Ceram Soc 2003;86(3):508–10.
21. Quinn GD, Ives LK, Jahanmir S. On the nature of machining cracks in ground ceramics. Part I: SRBSN strength and fractographic analysis. Mach Sci Technol 2005;9:169–210.
22. Munz D, Fett T. Ceramics. Berlin, Heidelberg: Springer; 1999.
23. Jayatilaka ADS, Trustrum K. Statistical approach to brittle fracture. J Mat Sci 1977;12:1426–30.
24. Danzer RA. General strength distribution function for brittle marterials. J Eur Ceram Soc 1992;10:461–72.
25. Danzer R, Lube T, Supancic P, et al. Fracture of ceramics. Adv Eng Mater 2008;10(4):275–98.
26. Danzer R, Reisner G, Schubert H. Der Einfluß von Gradienten in der Defektdichte und Festigkeit auf die Bruchstatistik von spröden Werkstoffen. Z Metallkde 1992;83:508–17.
27. Danzer R, Lube T, Supancic P. Monte-Carlo simulations of strength distributions of brittle materials - type of distribution, specimen- and sample size. Z Metallkde 2001;92(7):773–83.

28. Sigl L. Effects of the flaw distribution function on the failure probability of brittle materials. Z f Metallkd 1992;83:518–23.
29. Lohbauer U, Amberger G, Quinn GD, et al. Fractographic analysis of a dental zirconia framework: a case study on design issues. J Mech Behav Biomed Mater 2010;3(8):623–9.
30. Shirvandeh NS. Unterkritisches Risswachstum von Dentalkeramik am Beispiel von OPTEC OPC. Dissertation. Aachen: Rheinisch-Westfälischen Technischen Hochschule; 2000.
31. Taskonak B, Griggs JA, MJ J, et al. Analysis of subcritical cracl growth in dental ceramics using fracture mechanics and fractography. Dent Mat 2008;24:700–7.
32. Richter H, Kleer G, Heider W, et al. Comparative study of the strength properties of slip-cast and of extruded silicon-infiltrated SiC. Mater Sci Eng 1985;71:203–8.
33. Davidge RW. Mechanical behaviour of ceramics. Cambridge: Cambridge University Press; 1979.
34. Morrell R. Handbook of properties of technical & engineering ceramics, part 1: an introduction for the engineer and designer. London: Her Majesty's Stationary Office; 1989.
35. Soma T, Ishida Y, Matsui M, et al. Ceramic component design for assuring long-term durability. Adv Ceram Mat 1987;2:809–12.
36. Fischer H, Rentzsch W, Marx R. Elimination of low-quality ceramic posts by proof testing. Dent Mat 2002;18:570–5.
37. Kawakubo T, Komeya K. Static and cyclic fatigue behaviour of a sintered silicon nitride at room temperature. J Am Ceram Soc 1987;70(6):400–5.
38. Reece MJ, Guiu F, Sammur MFR. Cyclic fatigue crack propagation in alumina under direct tension-compression loading. J Am Ceram Soc 1989;72(2):348–52.
39. Gilbert CJ, Dauskardt RH, Ritchie RO. Behavior of cyclic fatigue cracks in monolithic silicon nitride. J Am Ceram Soc 1995;78(9):2291–300.
40. Gilbert CJ, Cao JJ, Moberlychan WJ, et al. Cyclic fatigue and resistance-curve behaviour of an *in situ* toughened silicon carbide with Al, B ,C additions. Acta Mat 1996;44(8):3199–214.
41. Ashby MF. Materials selection in mechanical design. Oxford: Butterworth-Heinemann; 2010.
42. Lawn BR. Fracture of brittle solids, 2nd ed. Cambridge: Cambridge University Press; 1993.
43. Hertz H. Über die Berührung fester elastischer Körper. J reine angew Math 1882;92:156–71.
44. Lawn BR. Indentation of ceramics with spheres: a century after Hertz. J Am Ceram Soc 1998;81(8):1977–94.
45. McCormick NJ, Almond EA. Edge flaking of brittle materials. Int J Hard Mat 1990;1(1):25–51.
46. Morrell R. Edge flaking similarity between quasistatic indentation and impact mechanisms for brittle materials. Key Eng Mat 2005;290:14–23.
47. Danzer R, Hangl M, Paar R. Edge chipping of brittle materials. In: Varner JR, Quinn GD, Frèchette VD, editors. Fractography of glasses and ceramics IV. Westerville: The American Ceramic Society; 2001. p. 43–55.
48. Chai H, Lawn BR. Edge chipping of brittle materials: effects of side-wall inclination and loadig angle. Int J Fract 2007;145:159–65.
49. Danzer R. Mechanical failure of advanced ceramics: the value of fractography. Key Eng Mat 2002;223:1–18.
50. Quinn GD, Hoffmann K, Scherrer SS, et al. Fractographic analysis of broken ceramic dental restorations. In: Varner JR, Wightman M, editors. Fractography of glasses and ceramics VI. Hoboken: Wiley; 2012. p. 161–74.
51. Kelly RJ. Fractography of dental ceramics. In: Varner JR, Quinn GD, editors. Fractography of glasses and ceramics IV. Westerville: ACS; 2000.
52. JIS R 1601: Testing method for flexural strength (modulus of rupture) of fine ceramics, 1995.

53. Baratta FI, MW T, Quinn GD. Errors associated with flexure testing of brittle materials. Watertown: U.S. Army Materials Technology Laboratory; 1997. p. 43.

54. Quinn GD, Morrell R. Design data for engineering ceramics: a review of the flexure test. J Am Ceram Soc 1991;74(9):2037–66.

55. ISO 6872: Dentistry - Ceramic Materials, 2008.

56. Lube T, Manner M, Danzer R. The Miniaturisation of the 4-Point Bend-Test. Fat. Fract. Engng. Mater Struct 1997;20(11):1605–16.

57. Börger A, Supancic P, Danzer R. The ball on three balls test for strength testing of brittle discs - stress distribution in the disc. J Eur Ceram Soc 2002;22(8):1425–36.

58. Fett T, Rizzi G, Ernst E, et al. A 3-balls-on-3-balls strength test for ceramic disks. J Eur Ceram Soc 2007;27(1):1–12.

59. Danzer R, Supancic P, Harrer W. Der 4-Kugelversuch zur Ermittlung der biaxialen Festigkeit spröder Werkstoffe. In: Kriegesmann J, editor. Technische Keramische Werkstoffe. Ellerau: HvB Verlag; 2009.

60. Börger A, Supancic P, Danzer R. The ball on three balls test for strength testing of brittle discs - part II: analysis of possible errors in the strength determination. J Eur Ceram Soc 2004;24(10-11):2917–28.

61. ISO 13356: Implants for surgery - Ceramic materials based on yttria-stabilized tetragonal zirconia (Y-TZP), 2008.

62. EN 843-5: Advanced Technical Ceramics - Mechanical properties of monolithic ceramics at room temperature: Part 5 - Statistical Evaluation, 2007.

63. ASTM C1239: Standard Practice for Reporting Uniaxial Strength Data and Estimating Weibull Distribution Parameters for Advanced Ceramics, 1995.

64. JIS R 1625: Weibull Statistics of Strength Data for Fine Ceramics, 1996

65. EN 843-6: Advanced Technical Ceramics - Monolithic Ceramics. Mechanical Properties at Room Temperature - Part 6: Guidance for Fractographic Investigation, 2009.

66. Quinn JB, Quinn GD. A practical and systmatic review of Weibull statistics for reporting strengts of dental materials. Dent Mater 2010;26:135–47.

67. Jin J, Takahashi H, Iwasaki N. Effect of test method on flexural strength of recent dental ceramics. Dent Mater J 2004;23(4):490–6.

68. Bermejo R, Supancic P, Danzer R. Influence of measurement uncertainties on the determination of the Weibull distribution. J Eur Ceram Soc 2012;32:251–5.

69. ASTM C 1421: Standard Test Methods for Determination of Fracture Toughness of Advanced Ceramics at Ambient Temperature, 2010.

70. ISO 15732: Fine Ceramics (Advanced Ceramics, Advanced Technical Ceramics)–Test method for fracture toughness of monolithic ceramics at room temperature by single edge precracked beam (SEPB) method, 2003.

71. ISO 18756: Fine Ceramics (Advanced Ceramics, Advanced Technical Ceramics)– Determination of fracture toughness of monolithic ceramics at room temperature by the surface crack in flexure (SCF) method, 2003.

72. ISO 23146: Fine Ceramics (Advanced Ceramics, Advanced Technical Ceramics)–Test methods for fracture toughness of monolithic ceramics–Single-edge V-notch beam (SEVNB) method, 2005.

73. ISO 24370: Fine Ceramics (Advanced Ceramics, Advanced Technical Ceramics)–Test method for fracture toughness of monolithic ceramics at room temperature by chevron-notched beam (CNB) method, 2005.

74. Anstis GR, Chantikul P, Lawn BR, et al. A critical evaluation of indentation techniques for measuring fracture toughness: i, direct crack measurements. J Am Ceram Soc 1981;64(9):533–8.
75. Quinn GD, Bradt RC. On the vickers indentation fracture test. J Am Ceram Soc 2007;90(3):673–80.
76. Quinn JB, Quinn GD, Kelly RJ, et al. Fractographic analyses of three ceramic whole crown restoration failures. Dent Mat 2005;21:920–9.
77. Quinn JB. The increasing role of fractography in the dental community. In: Varner JR, Quinn GD, Wightman M, editors. Fractography of glasses and ceramics V. Hoboken: Wiley-Interscience; 2007. p. 253–70.
78. Scherrer SS, Quinn GD, Quinn JB. Fractographic failure analysis of a Procera® AllCeram crown using strereo and scanning electron microscopy. Dent Mat 2008;4:1107–13.
79. Mecholsky JJ. Quantitative fractography: an assessment. Ceram Trans 1991;17:413–51.
80. Morrell R. Fractography of brittle materials. Teddington: National Physical Laboratory; 1999.
81. ASTM C1322: Standard Practice for Fractography and Characterization of Fracture Origins in Advanced Ceramics, 2005.
82. Quinn GD. Fractography of ceramics and glasses. Washington: National Institute of Standards and Technology; 2007.
83. Morrell R, Byrne L, Murray M. Fractography of ceramic femoral heads Varner JR, Quinn GD, Frèchette VD, editors. Fractography of glasses and ceramics IV. Westerville: The American Ceramic Society; 2001. p. 253–66.
84. Fischer H, Dautzenberg G, Marx R. Nondestructive estimation of the strength of dental ceramic materials. Dent Mat 2001;17:289–95.
85. Fischer H, Marx R. Fracture toughness of dental ceramics: comparison of bending and indentation method. Dent Mat 2002;18:12–19.
86. Guazzato M, Albakry M, Ringer SP, et al. Strength, fracture toughness and microstructure of a selection of all-ceramic materials. Part II. Zirconia-based dental ceramics. Dent Mat 2004;20:449–56.
87. Guazzato M, Albakry M, Ringer SP, et al. Strength, fracture toughness and microstructure of a selection of all-ceramic materials. Part I. Pressable and alumina glass-infiltrated ceramics. Dent Mat 2004;20:441–8.
88. Denry I, Holloway JA. Ceramics for dental applications: a review. Materials 2010;3:351–68.

Chapter 10

Interfaces Between Tissues and Ceramics

Peter Schüpbach

Schupbach Ltd, Service and Research Laboratory, Horgen, Switzerland

Contents

10.1 INTRODUCTION

The osseointegration of metallic implants correlates positively with moderately rough surfaces.[1,2] In addition, roughened surfaces have shorter healing times and maintenance of primary stability, thus creating conditions that make early or immediate loading possible. Contact and distance osteogenesis have been used to explain peri-implant bone healing with titanium-based surfaces. In contact osteogenesis, *de novo* bone forms on the implant surface, while in distance osteogenesis the bone grows from the old bone surface toward the implant surface in an appositional manner. Contact osteogenesis may lead to bone anchorage if the surface of the implant displays the appropriate surface topography. This chapter summarizes the available knowledge about whether ceramic implants offer the same patterns of bone formation as titanium-based implants.

Teeth develop simultaneously with periodontal tissues, remaining structurally contiguous with them, whereas implants and their transmucosal abutments are exogenously placed into the alveolar bone to become osseointegrated with the expectation that the peri-implant mucosa will adapt to the abutment surface and

fulfill the primary functions of the perigingiva (i.e. attachment and protection).[3] This requires that the structural framework of the peri-implant mucosa live up to the demands of gingival protection. Later in this chapter we will look at whether or not this requirement is fulfilled with titanium-based versus zirconia abutments.

10.2 METHODOLOGIES

The necessary methodologies for characterization of the interfaces for histology and imaging comprise the preparation of stained ground sections for light microscopy.[4] The same sections can be further prepared for backscatter scanning electron microscopy (B-SEM). Overviews and 3D reconstructions of specimens can be obtained by micro-computed tomography, whereas micro- and nanostructures of surfaces need high-resolution, field-emission scanning electron microscopes (FE-SEM).

10.3 INTERFACE BETWEEN CERAMIC IMPLANTS AND BONE

The way teeth are anchored in the alveolar bone is incredible.[3] The periodontal ligament, a dense connective tissue, is interposed between the root surface and bone. Strong collagen fiber bundles cross the space between them and are anchored in both the cementum and bone, respectively. Each single collagen fiber is composed of numerous, densely packed, single fibrils, and each single collagen fiber is deeply buried and anchored in the mineralized matrix of cementum (Figure 10.1). Thus the periodontal ligament serves as a flexible suspension system that resists displacing forces and protects the teeth against excessive occlusal load. Although it is a superb system, it is not quite perfect. Bacteria, with their endotoxins, may invade and destroy, first the junctional epithelium, and eventually the periodontal ligament. The resulting periodontal disease may gradually lead to the complete destruction of the periodontal ligament, and in turn, to the loss of a tooth.[5]

In 1952, Professor Per-Ingvar Brånemark[6,7] discovered the principles of osseointegration and initially met indignant resistance from his colleagues who argued: "How can a rather rigid ankylotic-like interface replace the sophisticated periodontal ligament that evolution has produced? Furthermore, how can a piece of metal become integrated in bone without fibrous encapsulation? And finally, how can the alveolar bone crest survive without the blood supply from the periodontal ligament?" All these questions were subsequently answered and thirty years later, in 1982, the discovery was acknowledged and his subsequent findings confirmed at an epic meeting of dental authorities organized by George Zarb and Ulf Lekholm in Toronto. The proceedings of this historic conference enabled dental implants to gain acceptance as a reliable treatment method in the global dental community.

Since the definition of the osseointegration concept, the properties of the interface between bone and implant, and the possibilities to improve it, have
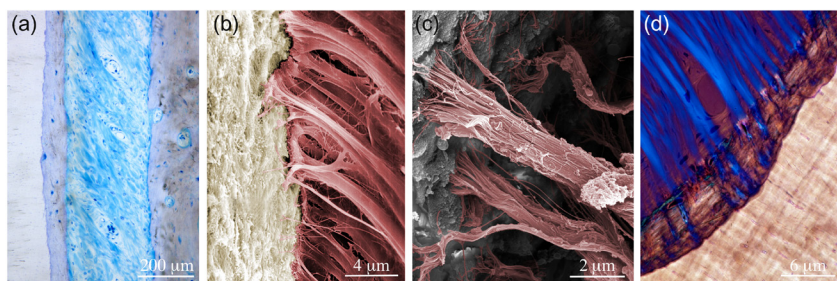
FIGURE 10.1   The periodontal ligament around human teeth. (a) Ground section; (b) Colorized SEM micrograph showing the attachment of collagen fiber bundles to the cementum; (c) Colorized SEM micrograph showing single fiber bundles composed of numerous single collagen fibrils; and (d) Anchorage of single fibers in cementum viewed under polarized light.
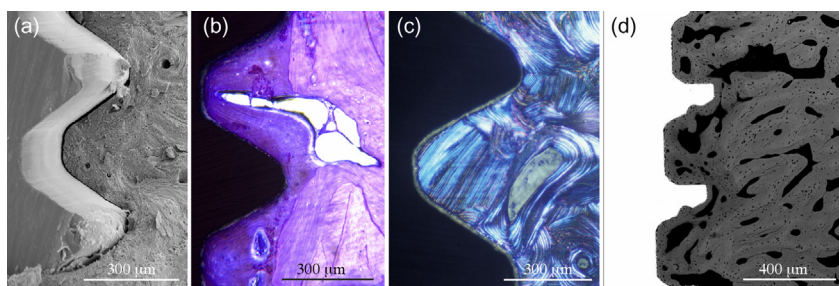
FIGURE 10.2   Successful osseointegration. (a) SEM micrograph of an osseointegrated machined implant; (b) Ground section; (c) Implant with anodized surface under polarized light; and (d) B-SEM view of implant with anodized surface.

been of great interest. The first dental implants were produced by machining titanium, and resulted in a minimally rough surface. There is general agreement[1] that new bone is formed on the old bone surface around machined implants, meaning that bone formation occurs outwards from the walls of the osteotomy and towards the implant surface. This phenomenon is called distance osteogenesis. With distance osteogensis, newly formed bone approximates the implant until the surface is reached (Figure 10.2).

In recent years, much effort has been devoted to enhancing bone formation by modifying the implant surface properties of titanium implants in order to roughen the surface texture.[8] Plasma-spraying, acid-etching, sandblasting, and electrochemical means have all been employed. A variety of articles have shown that the osseointegration of implants correlates positively with moderately rough surfaces. In addition, roughened surfaces have allowed for shorter healing times and the maintenance of primary stability, thus creating conditions that make early or immediate loading possible. The rough surfaces used nowadays allow for another type of bone formation, so-called contact
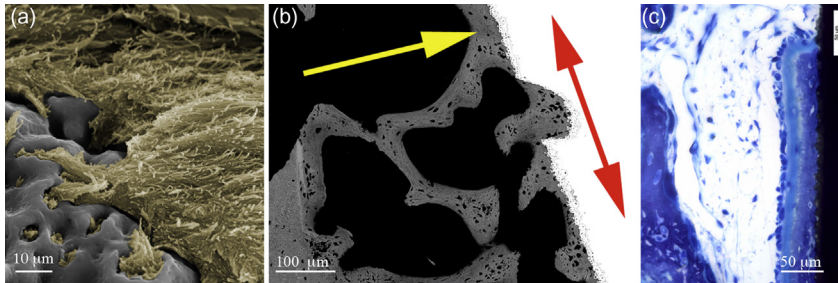
FIGURE 10.3 Osteoconductive bone formation. (a) Human histology 6 months after insertion shows bone anchored in the TiUnite pores; (b) In extraction sockets, newly formed bone crosses the gap between local bone (LB) and the implant surface by distance osteogenesis (yellow arrow); and (c) As soon as the implant surface is reached, new bone spreads over the surface by contact osteogenesis (red arrow) characterized by woven bone deposited directly on and along the surface.

osteogenesis, meaning that new bone is formed directly on and along an implant surface.[1] The interface between machined implants and bone is characterized by an intimate apposition of bone to the surface (Figure 10.3), while implants with a rough texture show a direct anchoring of bone to the surface as, for example, in the pores of an electrochemically anodized implant.[9]

As an alternative to titanium implants, ceramic materials such as alumina (Al_2O_3) and zirconia (ZrO_2) have been used in implantology. Various ceramic implant systems made of yttria-stabilized tetragonal zirconia polycrystals (Y-TZP) have become commercially available in recent years. Several studies assessed the clinical success of Y-TZP implants and whether the wound healing and osseointegration of Y-TZP is comparable to that of titanium implants.[10,11]

Wound healing comprises a cascade of events that the body brings into play to resolve injury. Nature's first priorities are to stop bleeding, restore function, and to prevent infection. Generally, wound healing events are grouped into four phases: hemostasis, inflammatory, proliferative/repair, and remodeling. Hemostasis starts immediately following the placement of an implant: blood proteins and platelets are attracted to the negatively charged ceramic surface of an anodized surface and become immediately activated (Figure 10.4). This first step is crucial for wound healing. Their activation is followed by the release of growth factors, such as platelet-derived growth factor (PDGF) and transforming growth factor beta (TGF-b). These factors play a crucial role in the regulation of wound healing.[12] During the first ten minutes, fibrin (the reaction product of thrombin and fibrinogen) is released at the wound site. The resulting stabilized blood clot reveals improved adherence to rough implant surfaces when compared to smooth implant surfaces, indicating that the surface chemical and physical properties of implant materials have a major influence on fibrin clot formation following the installation of an implant (Figure 10.5) Therefore, it is of interest to compare the outcome
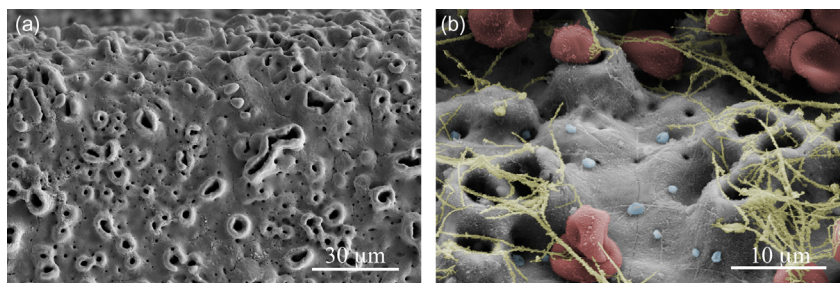
FIGURE 10.4   SEM micrograph of an anodized implant surface (a) and colorized SEM micrograph showing still-inactive platelets attracted to the implant surface and the initial formation of fibrin strands immediately following the contact of the surface with blood (b).
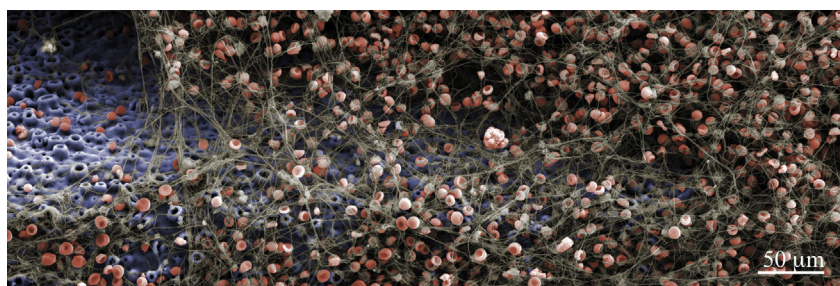
FIGURE 10.5   Colorized SEM micrograph showing the blood clot composed of blood cells, activated platelets, and fibrin attached to an anodized surface exposed to blood for 10 minutes in an in vitro experiment carried out by the author.

of blood clot formation on zirconia surfaces, to blood clot formation on titanium surfaces.

A recent study (Schüpbach et al., not yet published) compared the quality and the extension of the fibrin clot on machined zirconia abutments and on anodized implants. Human blood was applied to cover the specimens completely, and after 10 minutes the specimens were fixed and prepared for SEM. No differences were found in the quality of the blood clot. Both surfaces were covered by blood cells. The fibrin matrix, with entrapped thrombocytes and a meshwork of tiny fibrils in intimate contact with the surface, was firmly attached to both surfaces, but the blood clot extension was significantly less pronounced with the zirconia surface (Figure 10.6). This confirms a study by Traini et al.[13] that compared the blood clot extension associated with surface roughness on disk-shaped samples of sandblasted Y-TZP, machined titanium (m-Ti), and sandblasted acid-etched titanium (p-Ti). The Y-TZP demonstrated a significantly less amount of blood clot extension compared with the p-Ti specimens.
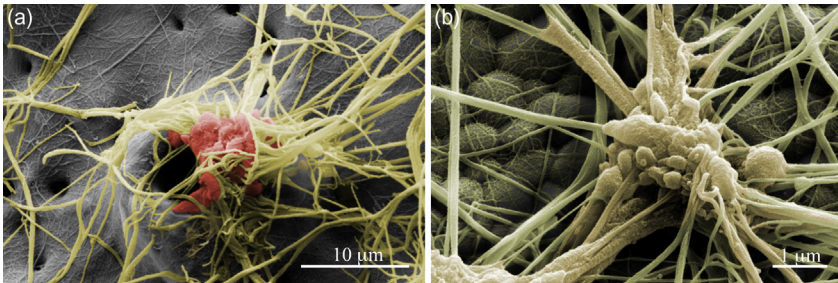
FIGURE 10.6 Hemostasis. Blood clots from the formation of the fibrin matrix and activated platelets embedded in the matrix. Colorized SEM micrographs of an anodized surface (a), and a zirconia surface (b).

The osseointegration of Y-TPZ implants was evaluated in different animal models and sites and under different loading conditions. In the experimental groups reported by Wenz et al.[10] the mean bone-to-implant contact ratio was above 60% in almost all experimental groups, which in accordance to criteria defined by Albrektsson et al.[14] indicates successful osseointegration. In studies that used titanium implants as a control, the outcome with zirconia implants was comparable to titanium implants.

Several studies reported a stronger bone response for zirconia implants with rough surfaces as compared to machine surfaces. A study in mini pigs by Gahlert et al.[15] that compared machined and sandblasted zirconia implants showed that surface characteristics had an important influence on bone integration. The zirconia implants were compared biomechanically and histomorphometrically with SLA titanium implants. The study showed higher bone stability values for the titanium SLA implants, followed by the rough zirconia and the machined zirconia. The findings suggest that rough zirconia implants can achieve higher stability in bone than machined zirconia implants. Roughening the machined zirconia implants enhances bone apposition and has a beneficial effect on the interfacial shear strength.

Another mini pig study conducted by Gahlert et al.[16] compared the bone tissue response of surface-modified zirconia and titanium implants. Cylindrical low-pressure injection-molded zirconia implants were produced with an acid-etched surface. Titanium implants of identical shape and sandblasted, acid-etched surface (SLA) served as controls. Histomorphometrical analysis with regard to bone density and bone-to-implant contact ratio showed no significant differences between the two types of implants. The interface between newly formed bone and both the zirconia and the titanium surfaces showed a thin band of bone following the contour of the threads, thus indicating osteoconductive bone formation.

In a rabbit study of early healing (two weeks and four weeks), Hoffman et al.[17] described a similar rate of bone apposition to four zirconia implants

with a roughened surface (Z-Look 3 implant) and four titanium implants with a sandblasted, acid-etched surface (Osseotite).

A pilot study in mini pigs compared one-piece Y-TZP implants with a sandblasted surface (Ra of 1.0 micron) to titanium implants with a sand-blasted, acid-etched surface (Ra of 2.75).[18] The zirconia implants were alternatively submerged and non-submerged. The titanium implants were all submerged. After a healing period of 4 weeks, both types of submerged implants achieved a bone-to-implant contact ratio of 53%. For the non-submerged implants, some epithelial downgrowth and crestal bone resorp-tion was reported, resulting in a BIC of 48%. The upper third of the implants showed bone formation by contact osteogenesis for both submerged and non-submerged implants. Apically, distance osteogenesis was observed.

An SEM study[19] compared zirconia implants with a modified ablative surface with acid-etched titanium implants at 1, 4 and 12 weeks. At 1 week, a remarkable attachment of bone was observed, which increased further to intimate bone contact after 4 weeks. At 12 weeks, osseointegration was com-plete. It is questionable whether the tissue observed after 1 week is indeed newly formed bone. Recent research shows that during the installation of implants with rough surfaces from various suppliers, the moderately rough surface texture acts like a micro-grained sandpaper: It scratches along the walls of the cortical and trabecular bone of the osteotomy and emerizes the bone surface. This results in a several-microns-thick smear layer composed of bone debris and blood that covers the implant surface (author's results; not yet published).

Human histologic evidence of successfully osseointegrated implants is extremely rare for titanium implants. The retrieval of histologic samples from successfully osseintegrated implants is the only irrefutable method of confirmation to generate valuable knowledge. Only one human study[20] evaluating the hard and soft tissue attachment to a two-piece zirconia dental implant is available. A healthy female patient requiring tooth replace-ment with dental implants received a two-piece zirconia implant together with conventional titanium implants implemented in a prosthesis. Clinical and radiographic evaluations at 6 months revealed stable osseointegrated zirco-nia and titanium implants. The zirconia implant tested was composed of a hot isostatic post compaction Y-TZP ceramic with a defined roughened sur-face (aluminium oxide-blasted). Light microscopic evaluation of the peri-implant soft tissues showed a healthy connective tissue and a firmly attached junctional epithelium. Histologic and B-SEM analyses revealed close bone apposition and bone marrow spaces at the zirconia interface (Figure 10.7). In some areas, however, bone was separated from the implant surface by a small band of connective tissue, which indicated fibrous encapsulation. The stabil-ity of the crestal bone level was excellent, and it was located coronal to the implant–abutment junction, thus eliminating the negative sequelae of the micro-gap.
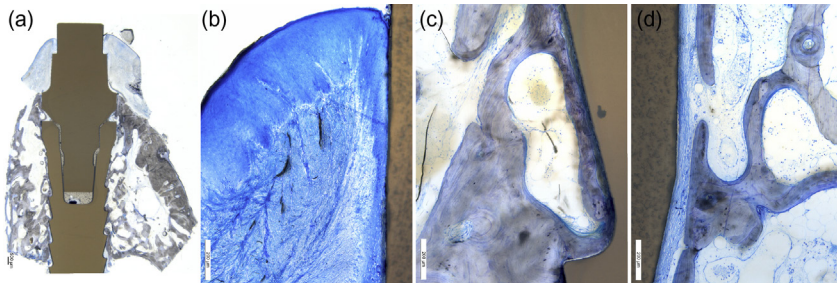
FIGURE 10.7 Human histologic evidence of a successfully osseointegrated, one-piece zirconia implant. (a) Overview; (b) Soft tissue attachment; (c) Osteoconductive bone formation; and (d) Fibrous encapsulation.
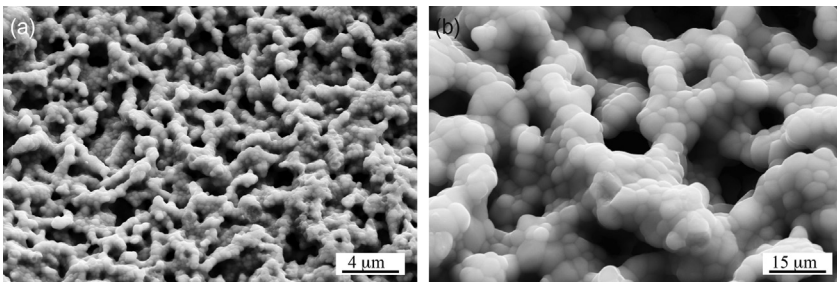
FIGURE 10.8 SEM micrographs of a modified porous zirconia surface at magnification 10,000x (a), and (b) at 30,000x.

10.4 INTERFACE BETWEEN POROUS CERAMIC IMPLANTS AND BONE

Sennerby et al.[21] compared topographically modified zirconia implants with electrochemically anodized, porous implants. Zirconia powder was cold isostatically pressed into rods and pre-sintered. A porous surface (Figure 10.8) was achieved by coating the implants with a slurry containing zirconia powder and a pore former. Subsequently, the implants were sintered. In the process, the pore former was burned off, which yielded a porous surface with a roughness (R_a) of 1.24, similar to an electrochemically anodized surface (R_a) of 1.3. Machined zirconia implants were used as a control.

Preparation of the electrochemically anodized surface by spark anodization in an electrolytic solution containing phosphoric acid promoted a ceramic, micrometer-scale thickening and an ionic impregnation of the TiO_2 layer, whereas the electric sparks led to a porous surface.[22,23] The oxidation modified the chemical composition and the degree of crystallinity of the TiO_2 layer, from amorphous, as with machined surfaces, to crystalline anatase and rutile forms. These characteristics, acting on their own, together or synergistically, resulted in faster and
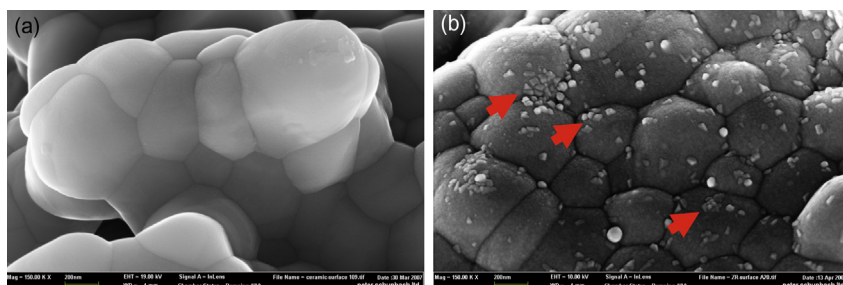
FIGURE 10.9 SEM micrographs. (a) A porous zirconia surface; and (b) An additional modification by dipping the implants into a stable solution containing crystalline nanoparticles of hydroxyapatite.[25]

stronger osseointegration for the anodized implants when compared to implants with machined surfaces.[24]

After 6 weeks, all implants achieved good stability and the healing period was uneventful. The machined implants showed bone in apposition to the implant surface and often a fibrous encapsulation, whereas the porous zirconia and the oxidized implants showed bone in intimate contact with the surface. The modified zirconia implants showed up to a four- to five-fold increase in resistance to torque forces compared with the machined implants, thus suggesting that porous modifications might increase stability in bone. No significant differences regarding stability and bone formation were observed between the modified zirconia and the oxidized surface.

Rocchietta et al.[25] evaluated whether or not the topographically altered porous zirconia surface can be further improved by an additional chemical modification to become highly osteoconductive, allowing for contact osteogenesis. The modified surfaces were again compared to an anodized implant surface. The latter showed fast bone formation at the level of HA and highly osteoconductive properties.[24,25] Hydroxyapatite coatings were obtained by either dipping the porous zirconia implants into a stable solution containing crystalline nanoparticles of hydroxyapatite with a CaP ratio of 1.67 (Figure 10.9), or by sputtering a thin layer of hydroxyapatite on the zirconia surface. This treatment resulted in a 150 nm thick hydroxyapatite layer on the zirconia surface.

The study showed bone formation by distance osteogenesis in cortical bone. No differences were observed between zirconia (Figure 10.10) and modified zirconia surfaces (Figure 10.11). Along the threads placed in the marrow chamber of the tibia bone, formation by distance osteogenesis took place. For all the examined surfaces, outward bone growth was observed to various degrees from the cortical bone layer along the implant surface embedded in bone marrow (Figure 10.12). A thin band of bone that formed directly on the various surfaces could be followed by both light microscopy and B-SEM spreading in an apical direction along the threads (Figure 10.13).
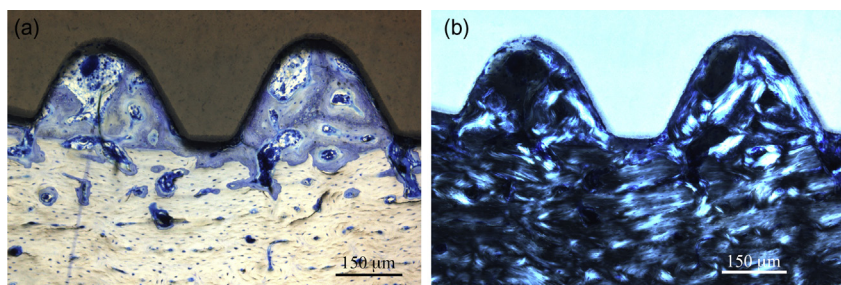
FIGURE 10.10 Ground sections showing the osseointegration of a porous zirconia implant in rabbit tibia cortical bone. (a) Stained ground section; and (b) Ground section in polarized light.
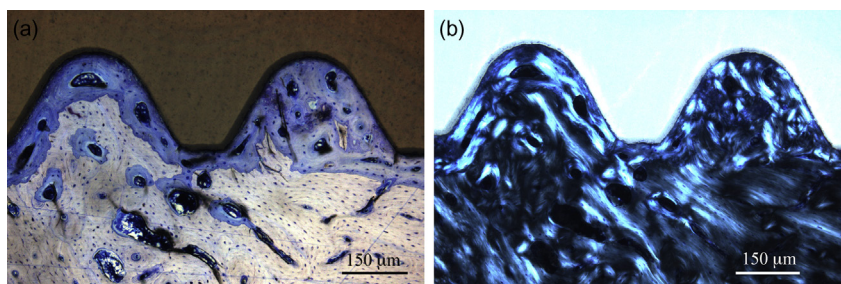
FIGURE 10.11 Ground sections showing osseointegration in rabbit cortical bone of a porous zirconia implant with an additional modification: dipping the implants into a stable solution containing crystalline nanoparticles of hydroxyapatite.[25] (a) Stained ground section; and (b) Ground section in polarized light.
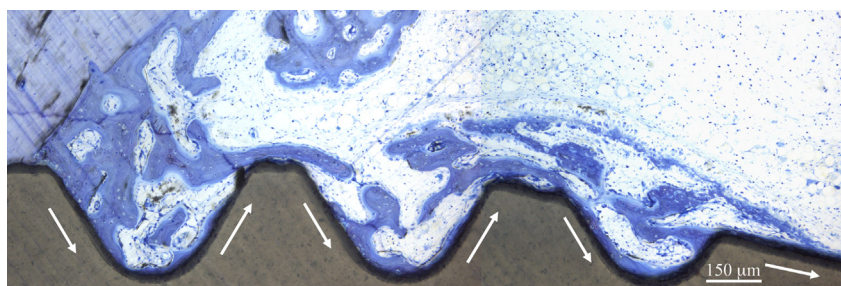
FIGURE 10.12 Osteoconductive bone formation outwards from cortical bone along the threads of a CaP-modified, porous zirconia surface.

B-SEM evaluations also showed interconnections between the pores through the up to 20-microns-thick modified surface and the ingrowth of bone into the pores (Figure 10.14). However, the additional chemical modification did not improve the final outcome for the zirconia implants in terms of speed of
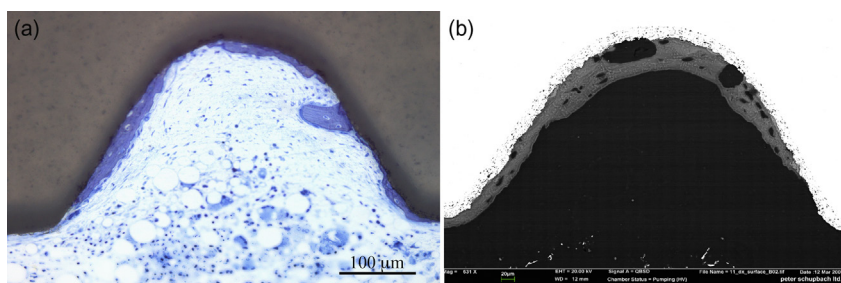
FIGURE 10.13 Higher magnifications of osteoconductive bone formation along a CaP-modified, porous zirconia surface. (a) In transmitted light; and (b) by backscatter SEM.
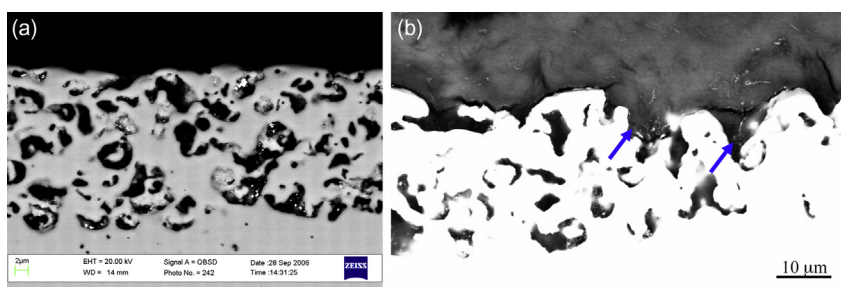
FIGURE 10.14 B-SEM micrographs showing interconnections between the pores through the up to 20-microns-thick modified surface (a); and the ingrowth of bone into the pores (arrows in b).

osteoconductivity and enhanced bone formation when compared to the electrochemically anodized surface.

Nanotechnology-modified zirconia oral implants were also evaluated by Lee et al.[26] and compared to the same anodized implant as in the study by Rocchietta et al.[25] Proprietary nanotechnology, surface-modified (calcium phosphate, CaP), microstructured zirconia implants (A and C), control porous zirconia implants, and electrochemically anodized porous oxide implants were implanted into the femoral condyle of rabbits. The anodized surface demonstrated significantly greater bone—implant contact compared with the A and C surfaces at 3 weeks ($p < 0.05$). Numerical differences between the porous zirconia surface, and A and C surfaces did not reach statistical significance ($p > 0.05$). Similarly, there were non-significant differences between the anodized and the porous zirconia surfaces ($p > 0.05$). At 6 weeks, there were no significant differences in BIC between any of the evaluated surfaces. It was concluded that the anodized and the porous zirconia implant surfaces exhibited high levels of osseointegration and confirmed their advanced osteoconductive properties. Addition of CaP nanotechnology to the zirconia surfaces did not enhance the already advanced high level of osteoconductivity displayed by the anodized surface and the porous zirconia surface.
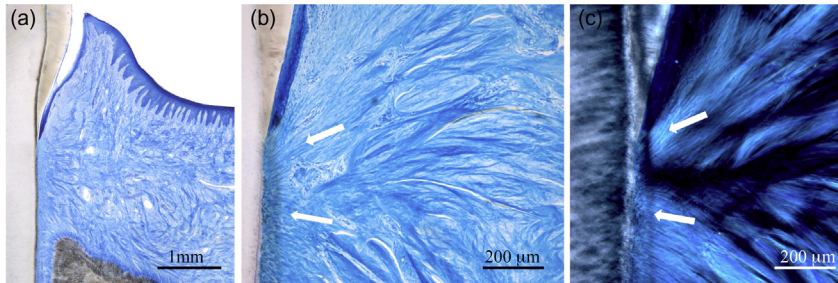
FIGURE 10.15 Ground sections through a tooth showing the periodontium (a); and its function-ally oriented collagen fibers anchored in root cementum in transmitted light (b); and in polarized light (c).

10.5   INTERFACE BETWEEN CERAMICS AND SOFT TISSUES

The primary function of the gingiva around our natural teeth, besides contrib-uting to the anchorage of the tooth in the jaw, is protection; that is, to provide a seal against the microbe-rich environment of the oral cavity, to stabilize the position of the tooth in the alveolar bone (in order to withstand the frictional forces of mastication), and to defend the interface between the teeth and the soft tissues against foreign invaders. The structural framework that fulfills these requirements offers a variety of amazing structures (Figure 10.15), among them the way the gingiva and the underlying periodontal ligament is protected and sealed by the junctional epithelium. Its anatomy and histology were first described by Schroeder and Listgarten[27] and further clarified in a great number of studies and reviews.[28] Apical to the cementoenamel junction, the connective tissue of the supra-alveolar fiber apparatus supports the junctional epithelium and provides stability for the mucosa. The attachment of the gingiva is specifi-cally assured by functionally oriented (towards the root cementum) collagen fibers firmly anchored in the mineralized cementum (Figure 10.15).

The peri-implant mucosa surrounding successful endosseous implants is in many ways analogous to that which surrounds natural dentition. Of the various tissues in contact with the implant/abutment unit, the junctional epi-thelium most closely matches the structures around a tooth (Figure 10.16). A direct biological attachment to the abutment surface via a basal lamina, and the formation of hemidesmosomes, has been described for several implant materials. Despite the similarities, significant differences exist in the way con-nective tissue in the absence of root cementum interfaces with the surfaces of abutments. It is generally agreed that in the absence of functionally oriented collagen fibers anchored in root cementum, the connective tissue fibers run in a direction more or less parallel to the abutment surface, either in the coronal-apical direction or circumferentially-oriented. Thus, the interface between connective tissue and the surface of the abutments looks rather smooth when
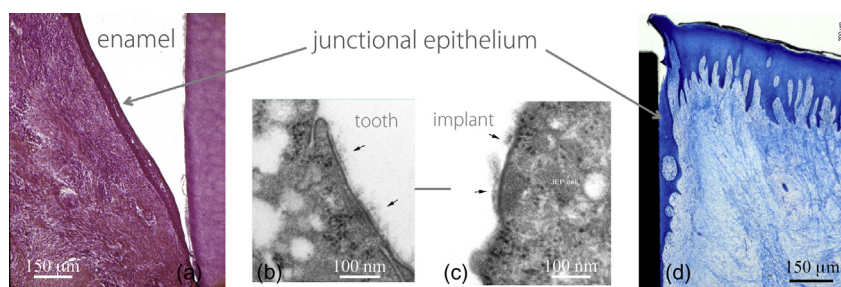
FIGURE 10.16 Ground sections showing the junctional epithelium next to enamel (a); a titanium surface (b); the corresponding hemidesmosomes (c); and basal lamina (d).
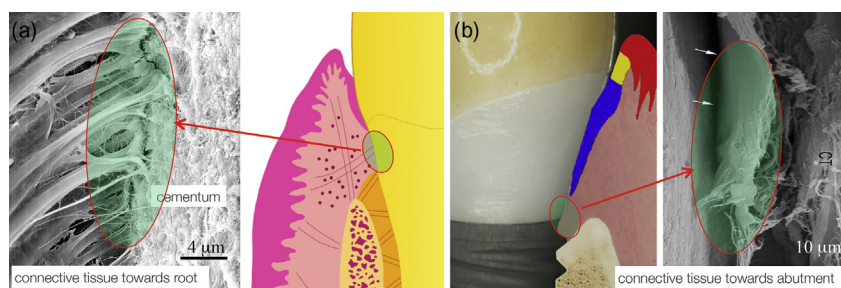
FIGURE 10.17 Attachment of the gingival connective tissue to root cementum by functionally oriented collagen fibers anchored in cementum (a); and adaptation only of connective tissue to a machined abutment (b).

evaluated by SEM (Figure 10.17). That means that the connective tissue is adapted only to the abutment surface and cannot support adherence of the junctional epithelium. Therefore, sealing of the peri-implant mucosa and protection of the underlying soft tissues and bone are based on the junctional epithelium only, which results in a much more vulnerable situation than around natural dentition.

Soft tissue shaped around implants made of alumina (Al_2O_3) and single-crystal sapphire demonstrated structures such as basal lamina, hemidesmosomes, and a connective tissue with collagen fibers that were mainly oriented parallel to the implant surface.[29] In an animal model, loaded zirconia and titanium implants revealed similar soft tissue dimensions.[30] Soft tissues at zirconia healing caps presented a lower inflammatory level in the tissues than at titanium healing caps.[31]

A recent study (Schüpbach et al., in preparation) compared the peri-implant soft tissues around both machined zirconia and titanium abutments in the dog model. In brief, buccal and lingual mucoperiosteal flaps were elevated. Then the periostea of the mucogingival flaps were fenestrated at the base of the flaps to allow tension-free flap apposition and transmucosal wound closure. Plaque
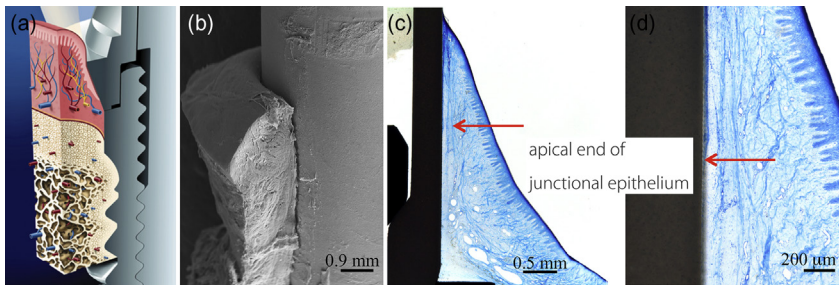
FIGURE 10.18 Schematic illustration of soft tissues and bone adjacent to an implant and abutment (a); the adaptation of the tissues to a zirconia abutment following cutting away parts of the peri-implant soft tissues (b); and ground sections through the peri-implant soft tissues adjacent to a machined zirconia abutment (c) and (d).
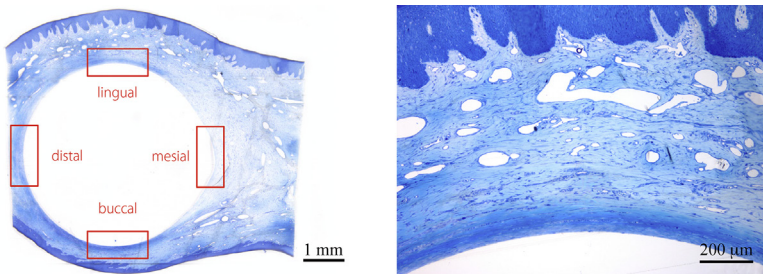
FIGURE 10.19 Semi-thin sections cut in a horizontal plane through soft tissues around a machined zirconia abutment.

control was maintained by a daily regimen until the completion of study. The animals were euthanized at Week 8 post-surgery. The specimens were prepared for light microscopy and histomorphometry either by ground section in the coronal-apical direction or by a series of semi-thin sections of the peri-implant mucosa on various horizontal levels. No differences were found in the architecture and the way the tissues adhered to both types of abutments via junctional epithelium (Figure 10.18). The presence of a basal lamina and hemidesmosome to titanium surfaces was described before[32] but has not yet been confirmed for zirconia abutments in this study. The ultrastructure evaluations are ongoing. The interface between connective tissue and both types of abutment surfaces was characterized by the presence of a dense ring of strong collagen fibers deposited directly on the abutment surface (Figures 10.19 and 10.20). Functionally oriented fibers were absent, meaning that the stability of the peri-implant mucosa is mainly based on fiber bundles arranged in a circular o-ring. Histomorphometric analysis comparing zirconia and titanium abutments revealed no statistically different values regarding percentage ratios of collagen, fibroblasts, blood vessels, and inflammatory cells.
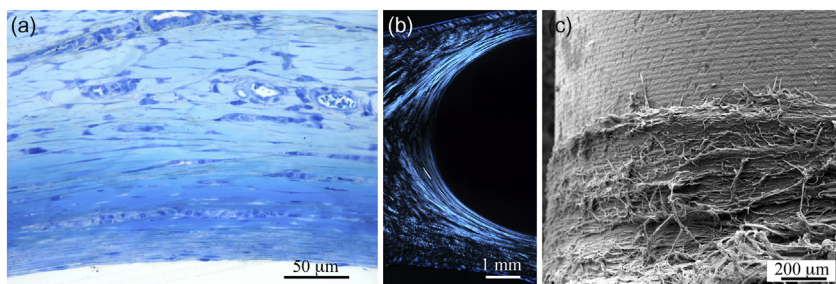
FIGURE 10.20 Semi-thin sections cut in a horizontal plane through soft tissues around a machined zirconia abutment at a higher magnification in transmitted light (a); in polarized light showing circular collagen fiber bundles (b); and in an SEM micrograph showing the o-ring of dense collagen fibers running circumferentially around a machined zirconia abutment (c).

CONCLUSIONS

In conclusion, distance and contact osteogenesis as described for machined and modified, moderately rough titanium implants are also present around machined and rough, modified zirconia implants. Very little information about the soft tissue outcome around zirconia abutments is available. However, present data suggest similar outcomes in terms of the architecture and function of the peri-implant soft tissues for zirconia abutments as compared to machined titanium ones.

ACKNOWLEDGMENTS

REFERENCES

1. Davies JE. Understanding peri-implant endosseous healing. J Dent Educ 2003;67(8):932–48.
2. Davies JE, Schüpbach P, Cooper L. The implant surface and biological response Osseointegration and dental implants. Iowa: Wiley-Blackwell; 2009. p. 213–23.
3. Lindhe J, Karring T, Araujo M. The anatomy of periodontal disease. In: Lindhe J, Lang NP, Karring T, editors. The anatomy of periodontal tissues, 5th ed. (Clinical periodontology and implant dentistry, vol 1) Blackwell Munksgaard; 2008. p. 3–48.
4. Donath K, Breuner G. A method for the study of undecalcified bones and teeth with attached soft tissues. The Säge-Schliff (sawing and grinding technique). J Oral Pathol 1982;11(4):318–26.
5. Kinane DF, Berglundh T, Lindhe J. Pathogenesis of periodontitis Lindhe J, Lang NP, Karring T, editors. Clinical periodontology and implant dentistry, vol 1 (5th ed.): Blackwell Munksgaard; 2008. p. 285–99.
6. Branemark P-I, Adell R, Breine U, et al. Intra-osseous anchorage of dental prosthesis. I. Experimental studies. Scand J Plast Reconstr Surg 1969;3(2):81–100.

7. Branemark P-I, Hansson BO, Adell R, et al. Osseointegrated implants in the treatment of the edentulous jaw. Experience from a 10-year period. Scand J Plast Reconstr Surg Suppl 1977;16:1–132.
8. Puleo DA, Thomas MV. Implant surfaces. Dent Clin North Am 2006;50(3):323–38.
9. Schüpbach P, Glauser R, Rocci A, et al. The human bone-oxidized titanium implant interface: A light microscopic, scanning electron microscopic, back-scatter scanning electron microscopic, and energy-dispersive x-ray study of clinically retrieved dental implants. Clin Implant Dent Relat Res 2005;7(Suppl. 1):S36–43.
10. Wenz HJ, Bartsch J, Wolfahrt S, et al. Osseointegration and clinical success of zirconia dental implants: a systematic review. Int J Prosthodont 2008;21(1):27–36.
11. Hisbergues M, Vendeville S, Vendeville P. Zirconia: established facts and perspectives for a biomaterial in dental implantology. J Biomed Mater Res B Appl Biomater 2009;88(2):519–29.
12. Park JY, Gemmell CH, Davies JE. Biomaterials 2001;22:2671–82.
13. Traini T, Caputi S, Gherlone E, et al. Fibrin clot extension on zirconia surface for dental implants: a quantitative in vitro study. Clin Implant Dent Relat Res 2013 http://dx.doi.org/10.1111/cid.12038. [Epub ahead of print].
14. Albrektsson T. On long-term maintenance of the osseointegrated response. Aust Prosthodont J 1993;7(Suppl: 15–24)
15. Gahlert M, Gudehus Z, Eichhorn S. Biomechanical and histomorphometric comparison between zirconia implants with varying surface textures and a titanium implant in the maxilla of miniature pigs. Clin Oral Implants Res 2007;8(5):662–8.
16. Gahlert M, Röhling S, Wieland M, et al. Osseointegration of zirconia and titanium dental implants: a histological and histomorphometrical study in the maxilla of pigs. Clin Oral Implants Res 2009;20(11):1247–53.
17. Hoffmann O, Angelov N, Gallez F, et al. The zirconia implant-bone interface: a preliminary histologic evaluation in rabbits. Int J Oral Maxillofac Implants 2008;23(4):691–5.
18. Stadlinger B, Hennig M, Eckelt U, et al. Comparison of zirconia and titanium implants after a short healing period. A pilot study in minipigs. Int J Oral Maxillofac Surg 2010;39(6):585–92.
19. Depprich R, Zipprich H, Ommerborn M, et al. Osseointegration of zirconia implants: an SEM observation of the bone-implant interface. Head Face Med 2008;4:30.
20. Nevins M, Camelo M, Nevins ML, et al. Pilot clinical and histologic evaluations of a two-piece implant. Int J Periodontics Restorative Dent 2011;31(2):157–63.
21. Sennerby L, Dasmah A, Larsson B, et al. Bone tissue responses to surface-modified zirconia implants: a histomorphometric and removal torque study in rabbits. Clin Implant Dent Relat Res 2005;7(Suppl. 1):S13–20.
22. Hall J, Lausmaa J. Properties of a new porous oxide surface on titanium implants. Appl Osseointegration Res 2000;1:5–8.
23. Larsson C. The interface between bone and implants with different surface oxide properties. Appl Osseointegration Res 2000;1:9–14.
24. Zechner W, Tangl S, Fürst G, et al. Osseous healing characteristics of three different implant types. Clin Oral Implants Res 2003;14(2):150–7.
25. Rocchietta I, Fontana F, Addis A, et al. Surface-modified zirconia implants: tissue response in rabbits. Int J Periodontics Restorative Dent 2009;29(3):245–55.
26. Lee J, Sieweke JH, Rodriguez NA, Schüpbach P, et al. Evaluation of nano-technology-modified zirconia oral implants: a study in rabbits. J Clin Periodontol 2009;36(7):610–7.
27. Schroeder HE, Listgarten MA. Fine structure of the developing epithelial attachment of human teeth. Basel: Karger; 1971. p. 91–120.

28. Schroeder HE, Listgarten MA. The gingival tissues: the architecture of periodontal protection. Periodontol 2000 1997;13:91–120.

29. McKinney Jr RV, Steflik DE, Koth DL. Evidence for a junctional epithelial attachment to ceramic dental implants. A transmission electron microscopic study. J Periodontol 1985;56(10):579–91.

30. Kohal RJ, Weng D, Bächle M, et al. Loaded custom-made zirconia and titanium implants show similar osseointegration: an animal experiment. J Periodontol 2004;75(9):1262–8.

31. Degidi M, Artese L, Scarano A, et al. Inflammatory infiltrate, microvessel density, nitric oxide synthase expression, vascular endothelial growth factor expression, and proliferative activity in peri-implant soft tissues around titanium and zirconium oxide healing caps. J Periodontol 2006;77(1):73–80.

32. Ikeda H, Yamaza T, Yoshinari M, et al. Ultrastructural and immunoelectron microscopic studies of the peri-implant epithelium-implant (Ti-6Al-4V) interface of rat maxilla. J Periodontol 2000;71(6):961–73.

Alumina- and Zirconia-based Ceramics for Load-bearing Applications

Corrado Piconi*, **Saverio Giovanni Condo†** and **Tomaž Kosmač****
*Orthopedics Institute, Sacred Heart Catholic University, Rome, Italy; †Dept. of Clinical Sciences and Translational Medicine, University of Rome Tor Vergata, Rome, Italy; **Jožef Stefan Institute, Ljubljana, Slovenia*

Contents

11.1 INTRODUCTION

In this chapter, a family of load-bearing bioinert oxide ceramics is described that is most commonly used in the construction of implantable medical devices. These materials, if properly designed, fabricated, and used in devices, must be able to withstand the stresses generated in the device by the patient's activity. If used in dentistry, these materials not only must withstand the stresses generated by masticatory loads, but they must also be aesthetic. There are only a few ceramic biomaterials that are suitable for this application (i.e. alumina (Al_2O_3), zirconia (ZrO_2; partially stabilized zirconium dioxide), and their composites.

Use of these ceramics as load-bearing biomaterials is based on their useful mechanical properties combined with excellent chemical stability and tissue compatibility. Being oxides, they are not subject to any oxidative reactions. This implies a complete inhibition of the release of cytotoxic ions due to corrosive attack in the body, thereby providing high biological safety.

Presently, alumina is mainly used as a load-bearing biomaterial in orthopedics, particularly in the bearings of total hip, shoulder, and knee replacements, whereas zirconia is favored in restorative dentistry. It is commonly used in the fabrication of crowns, bridges, abutments, root posts, implants, and orthodontic brackets. Most of these devices can nowadays be fabricated via soft CAD/CAM machining of green or partially sintered blanks, followed by sintering.[1] Ever since the early 2000s, when several hundred femoral heads made of zirconia failed shortly after implantation, zirconia was practically abandoned in orthopedics. At present, there are only two manufacturers still offering zirconia components for hip and knee replacements. Other manufacturers moved toward alumina-zirconia composites introduced in the biomaterials market in 2002 as load-bearing components for hip replacements.[2] They are used in a growing number of orthopedic devices and are now also gaining interest in dentistry.

11.2 ALUMINA IN DENTISTRY

Alumina was first mentioned as a biomaterial in a German patent entitled 'Artificial replacement for the interior and exterior of the human and animal body,' issued in 1933 by Max Rock.[3] The concept was too advanced for the technological level of the time, and was almost forgotten about until the mid-1960s when Degussa GmbH (Düsseldorf, Germany) released to market the highly sinter-active, low-soda alpha alumina powder Degussit Al23. Using this ceramic precursor, it was possible to sinter ceramic bodies to high density whilst maintaining adequate purity, stability in the physiologic environment, and mechanical properties suitable for the intended use. Thanks to this precursor, Dr. Sami Sandhaus, a Swiss dentist, developed and patented the medical device entirely made of polycrystalline high-purity alumina ceramic, the CBS® dental implant (Figure 11.1).[4]

FIGURE 11.1   Sandhaus dental implant, 1969. *(From Piconi C, Rimondini L, Cerroni L, Donati C, Mutone V. La zirconia in odontoiatria. Milano: Elsevier, 2008)*

FIGURE 11.2   Tübingen dental implants, 19. *(From Piconi C, Rimondini L, Cerroni L, Donati C, Mutone V. La zirconia in odontoiatria. Milano: Elsevier, 2008)*

Sandhaus's dental implant enjoyed good clinical success and led to the development of other devices made of sintered alumina. Heimke and Shulte[5] developed the so-called Tübingen dental implant manufactured by Friedrichsfeld (Mannheim, Germany) under the trademark Frialit®. The Tübingen dental implants were single-stage implants, designed in several shapes and sizes for replacing single teeth in either jaw (Figure 11.2).

The endoseous part of the implant was shaped in a series of cylindrical sections decreasing in diameter. The surface of the cylindrical sections had
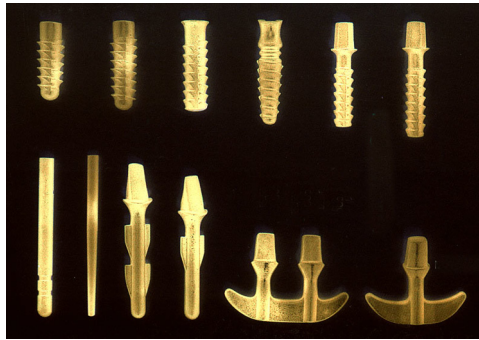
FIGURE 11.3   Feldmüle alumina dental implants. *(From Piconi C, Rimondini L, Cerroni L, Donati C, Mutone V. La zirconia in odontoiatria. Milano: Elsevier, 2008)*

circular grooves and dimples to allow bone ingrowth and thereby providing implant stability by bone interlock. The gingival part of the implant had a single circumferential groove to host the growth of gingival tissue. The clinical outcome reports were controversial: from very good in some (more than 90% success rate, 7 years postoperatively) to rather poor (less than 75%) in others.[6]

In the same period, Mutshelknaus and Dörre[7] developed anchor- and screw-shaped alumina dental implants, as well as endodotic dental posts, all of which were made of alumina ceramics manufactured by Feldmüle AG (now CeramTec GmbH, Plochingen, Germany; Figure 11.3).

In 1968, the US Army Medical Research and Development Command Dental Research Division funded a wide research program for alumina in medical devices. The dental wing of this program fostered the development of an implant for post-extractive sites, as well as a synthetic bone substitute. In this framework, T.A. Driskell developed the Synthodont® dental implant, an alumina osseointegrated single-tooth dental implant that gained significant clinical success.[8]

Another significant contribution from the United States came from research carried out by S.F. Hulbert and colleagues at Clemson University (Clemson, South Carolina) who investigated the biocompatibility of alumina.[9] Especially valuable was their contribution to a better understanding of the mechanism of bone ingrowth into porous ceramics, and to the determination of the characteristics of implant porosity necessary to allow mechanical interlocking with host bone.

During this same period, Japanese researchers were pursuing an entirely different approach. To overcome the mechanical limitations of the polycrystalline ceramic of that time, they concentrated their efforts on the development of devices obtained from alumina single crystals, a.k.a. synthetic sapphire. The clear and transparent gingival appearance of these implants offered significant aesthetic advantages over metallic implants in addition to high biological safety.[10]
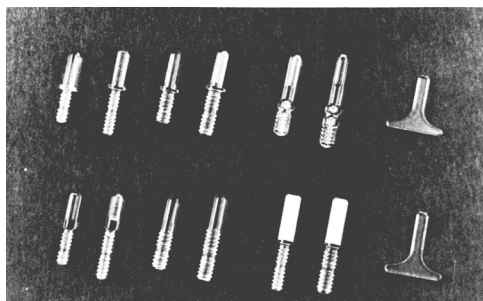
FIGURE 11.4   Bioceram® dental implants. *(From Piconi C, Rimondini L, Cerroni L, Donati C, Mutone V. La zirconia in odontoiatria. Milano: Elsevier, 2008)*

Kyocera Co. (Kyoto, Japan) started manufacturing blade-, tap-, and screw-type dental implants that were used in Japan from 1972 and penetrated the US market under the trade name Bioceram® (Figure 11.4). The long-term clinical outcomes were good. In a recently published report of a follow-up study encompassing a series of sixty-five tap-type porous sapphire dental implants it was reported that a few of them are still in place after 21 to 23 years.[11]

Besides the advantages in aesthetics and in biocompatibility, alumina dental implants had several shortcomings in terms of design, stiffness, and poor fracture toughness. The low flexural strength of the implants and defects introduced during surface grinding of the coronal part of the implants caused fractures in these types of devices that led to their demise in favor of titanium dental fixtures.[12]

Alumina also found application as a constituent of glass-ceramic composites used in the production of bridges and jacket crowns. Alumina and feldspathic glass powders (55 vol.% Al_2O_3) had been sintered on platinum foils previously shaped on prepared teeth.[13] Another approach was based on CAD/CAM milling of substructures for single crowns or fixed-partial dentures from blanks obtained by slip-casting and infiltration with a lanthanum aluminosilicate glass[14] or sintered as pure alumina cermics.[15] According to a summary of peer-reviewed clinical reports,[16] these devices show satisfactory outcomes in terms of longevity and aesthetics.

11.2.1   Structure of Alumina

Alumina (Al_2O_3) may occur in many metastable phases that irreversibly transform into alpha-alumina when heated to 1050–1200°C, depending on the crystal properties of the metastable precursors. In nature, alumina exists as corundum, or emery if it contains impurities. It occurs in the as gemstones with a color depending on the doping elements (e.g. ruby red due to the presence of chromium, or sapphire blue in different shades due to the presence of Ti^{3+} or Fe^{3+} ions in the lattice).

   The minerals commonly used to obtain high-purity alumina powders
(>99.5% Al_2O_3) are bauxite, a hydrated aluminum oxide, and native corun-
dum. Although the Bayer process is still most commonly used to convert
bauxite into alpha-alumina, several alternative routes have been developed
depending on the behavior of the starting raw materials and on their sources.
   The crystal structure of alpha-alumina is known to have a close-packed
hexagonal arrangement of oxygen ions. In its lattice, each aluminum cation
(Al^{3+}) is surrounded by oxygen anions O^{2-} that form two regular triangles on
both sides, twisted by 180° and lying on parallel planes. From the thermody-
namic point of view, alpha-alumina is the most stable aluminum oxide com-
pared to its transient, metastable counterparts. The strong ionic and covalent
chemical bonds between Al^{3+} and O^{2-} contribute to the characteristic materi-
als' properties, such as high melting point; low electric and thermal conductiv-
ity; high elastic modulus (stiffness) and hardness; and excellent resistance to
the attack of strong inorganic acids, such as orthophosphoric or hydrofluoric
acid (Table 11.1). However, when metal oxides such as alumina are immersed
in water or exposed to ambient air (which usually has at least 15% relative
humidity), their surfaces react with water to produce surface hydroxyl groups
(designated Me-OH). These in turn can further interact with proteins, which
results in wettability that is higher than that of several metallic alloys.
   Some of the above listed properties can be seen as drawbacks in den-
tistry. The high melting point especially makes it impossible to shape alumina
ceramics by casting. High hardness (20–30 GPa on the Mohs scale) makes
machining difficult and costly. High stiffness (10 times larger modulus than
that of dentine) contributes to high elastic mismatch between the natural tooth
structure and the prosthetic work.

TABLE 11.1 Physical Properties of Alumina

Property	Units	Value
Crystallography	–	Hexagonal
Lattice parameter a	nm	0.476
Lattice parameter c	nm	1.299
Property	K	2310
Density (theoretical)	g/cm^3	3.986
Thermal expansion coefficient	–	6.5
Thermal conductivity (298 K)>99.9% TD)	W/m K	30

Adapted from Greco et al. (1993).[28]

11.2.2   Mechanical Properties

Since their introduction into biomaterials in 1970,[17] sintered alumina ceramics have been subjected to a continuous development process. A key milestone in this development was a reference standard for medical-grade alumina. The first standard for alumina as a biomaterial was the German standard DIN 58835 that was the basis for the international standard ISO 6474[18] and the US standard ASTM F 603.[19] The current version of ISO 6474 released in 1994, is under revision and the revised version is circulating as a draft.

As a consequence of ever-tougher requirements imposed by clinicians, medical grade alumina has seen substantial improvements, especially with regards to mechanical properties and reliability. The increase in bending strength (from less than 400 MPa to more than 600 MPa in some medical-grade alumina used in orthopedics) is especially remarkable. It results from the many improvements introduced in materials processing (e.g. the selection of raw materials used as precursors, powder processing, sintering, quality control, etc.).[20]

In spite of improvements introduced in processing and the relevance of the results thus achieved, it should not be forgotten that alumina is a brittle material. This means that fracture energy cannot be dissipated by yielding at the crack tip (e.g. like in metals) such that alumina components may fail without any previous plastic deformation. Consequently, the mechanical properties of alumina are largely dependent on the presence of flaws acting as stress concentrators (e.g. notches and other surface defects; internal cracks; microstructure heterogeneities; and pores). Bending strength has a negative exponential dependence on porosity, the decrease with respect to the strength of fully dense material being remarkable even at low volume fractions of pores. The amount and connectivity of remnant pores are particularly crucial for the mechanical performance of devices operating in the human body where they are subjected to cyclic loading, then to fatigue, in a humid environment. The open porosity fraction that allows the penetration of liquids and gases into the bulk of the ceramic has an especially strong influence on the long-term strength of alumina and on the service life of a device.

The strength degradation of porous alumina in a wet environment has been discussed by several authors.[21–23] The reduction in strength is due to the growth of subcritical structural defects enhanced by the presence of water molecules. Permeating the material through open porosity, the water can interact with intrinsic microstructural defects (flaws) originating from the production technology. In a brittle material like alumina, subcritical cracks or flaws can grow at a speed much lower than the one leading to instantaneous failure. This behavior is known as subcritical crack growth (SCG). As discussed in Chapter 9, SCG is dependent on several variables (e.g. chemical species concentration, environment, and temperature).

The introduction of high-purity powders and the limit set for the content of calcia, alkali metal oxides, and silica impurities by standard ISO 6474 in

TABLE 11.2 Mechanical Properties of Polycrystalline Alumina

Property	Units	Alumina (1970s)	HIP Alumina	ISO 6474:80	ISO 6474:94
Al_2O_3 content	vol.%	99.1–99.6	>99.8	≥99.5	≥99.5
Density	g/cm^3	3.90–3.95	3.97	≥3.90	≥3.94
Avg. grain size	μm	≤4.5	1.75	≤7	≤4.5
Flexural strength	MPa	>300	650	>380	>400
Young modulus	GPa	380	400	380	N/A
Fracture toughness	MPa•m$^{1/2}$	3.5	4.5	N/A	N/A
Hardness	GPa	18	20–21	N/A	N/A

Adapted from Greco et al. (1993).[28]
ISO standard specifications are reported for reference.

1980, largely reduced the problem of strength degradation in alumina. Namely, CaO, NaO, and SiO_2 play an important role in the mechanical stability of alumina. CaO interactions with the aqueous environment, together with calcium migration and segregation, were found to be responsible for strength degradation,[24,25] while SiO_2 indirectly increased the risk of fatigue fracture by hindering densification and promoting grain growth during sintering.[22] Moreover, silica and alkalis (e.g. NaO) can segregate at grain boundaries, and their dissolution in physiologic liquids may lead to accelerated fatigue fracture.[26] For the same reason, the content in MgO added to alumina as a sintered additive to enhance densification while preventing discontinuous grain growth, has to be tuned to avoid deleterious excessive formation of Al_3MgO_4 spinel.

Since the population of flaws is characterized by a large scatter in size and by a random location within the solid body, the relationships between stress distribution, failure probability, and strength in alumina, as well as in other polycrystalline ceramics (see Table 11.2), need to be discussed on a statistical basis. The results of mechanical testing are commonly treated by the Weibull statistics that also help to identify the strength that grants each material the expected service life.[27]

11.2.3   Biocompatibility of Alumina

The biological safety of alumina has been well assessed, alumina as a ceramic biomaterial having more than forty years of clinical records. For a comprehensive review on this subject, the reader may refer to Piconi.[17]

Briefly, in vitro assays on alumina have been carried out with different cell lines (e.g. macrophages, lymphocytes, fibroblasts and osteoblasts) and

different cell conditions. The materials tested in direct or indirect contact had different physical forms (powders, granules, and dense ceramics) and different chemical/physical characteristics (e.g. reactive surface, chemical composition, impurity content, etc.) depending on their source. Assays performed using extracts did not show any release from alumina, and showed very low cellular reactivity. On the other hand, results of direct contact assays on powders were related to the concentration used. Dose-dependent cytotoxicity was observed on human lymphocytes,[28] on fibroblasts co-cultured with ceramic extracts,[29] and on macrophages during apoptosis.[30] Cytotoxic reactions in murine macrophages were reported to depend on particle size,[31] especially when entering into the nanometer range due to the high surface/volume ratio of nanoparticles.

The in vivo biocompatibility of alumina has been systematically explored since the early 1970s.[9] Implants of different physical form (powders, granules, dense or porous bars or pellets) inserted in different implantation sites (bone, muscles) in several animal models (rats, rabbits, mini-pigs) were used to assess adverse local reactions and/or systemic toxicity.

In soft tissue, a layer of connective tissue is transformed over time into a fibrous membrane surrounding dense alumina ceramics. In hard tissue, a thin proteoglycan layer at the bone-biomaterial interface is formed that is characteristic for a 'nearly inert' material. Stresses due to loading enhance bone apposition at the implant–tissue interface. Soft tissue reaction to the injection of alumina particles is characterized by less granulocytes and lymphocytes than after the injection of metals or polyethylene particles.[32] The absence of acute systemic adverse tissue reactions to ceramics was also reported after subcutaneous, intramuscular, or intraperitoneal and intra-articular injection of alumina and zirconia powders in rats and/or mice, as well as by implants made into the paraspinal muscles of rabbits, rats, or in rabbit bone.

11.3   ZIRCONIA IN DENTISTRY

Zirconia (ZrO_2) has been known about for a long time. Jacinth, a vermillion zirconia gemstone, was cited in The Apocalypse of St. John as being among the stones that form the walls of heavenly Jerusalem. The name 'zircon' comes from the old Persian word 'zar gun', or color of gold, for the aspect of some zircon ores. It was only in 1789 that Martin Heinrich Klaproth insulated zirconium dioxide after the heat treatment of some jacinth brought to him from the Far East.

Zirconia is a polymorphic material that occurs in three different forms depending on temperature: monoclinic (m) at room temperature, tetragonal (t) above 1170°C, and cubic (c) beyond 2370°C. The phase transitions are reversible, and in free crystals are associated with a volume expansion of about 0.5% in the case of the cubic to tetragonal (c→t) transition, and about 4% for the tetragonal to monoclinic (t→m) transition. On cooling, the t→m transformation is of special interest because sintered products of pure zirconia can break

into pieces due to stresses generated by the lattice expansion that accompanies the t→m transformation.

This feature limited the use of pure zirconia to refractories and pigments until 1929 when Ruff and coworkers[33] demonstrated that by adding a small quantity of calcium oxide to pure zirconia the cubic phase could be stabilized at room temperature. This ceramic, fully stabilized cubic zirconia, is still in use as an abrasive or refractory material, while cubic zirconia single crystals are replacing diamonds in jewelry for their similarly high refractive index and lower cost.

Interest in zirconia as a structural material for engineering applications came in 1972 when Garvie and Nicholson[34] reported on the structure and thermodynamic properties of a two-phase zirconia ceramic in the $CaO–ZrO_2$ system that consisted of large cubic grains that also contain tiny intragranular tetragonal precipitates. They named the material partially stabilized zirconia (CaO-PSZ) because of the lower concentration of stabilizing oxide than needed for complete stabilization of the cubic phase. Besides calcium oxide, there are some other oxides capable of partial stabilization of zirconia, notably magnesium oxide (Mg-PSZ) and yttrium oxide (Y-PSZ).

In 1975, Garvie, Hannink, and Pascoe[35] published their famous paper in *Nature* reporting on the stress-induced t→m transformation of the tetragonal precipitates in Mg-PSZ that lead to a substantial increase in strength and fracture toughness of the material. They entitled their paper 'Ceramic Steel?' because the microstructure and phase changes outlined above take place in a similar way as in 'martensitic' steels. Namely, the t→m phase transition (1) is not associated with any transport of matter (it is diffusion-less); (2) it is athermal (i.e. it takes place in a temperature interval rather than at a given temperature); and (3) it involves a structural change of the atoms in the lattice. This discovery was not only a real breakthrough in the development of zirconia-toughened ceramics, but also caused a deep change in the perception by engineers of ceramic components that exhibit extremely high strength and fracture toughness achieved by exploiting the martensitic phase transformation of thermodynamically metastable tetragonal zirconia.

A further advancement in zirconia ceramics was made in the second half of the 1970s thanks to Rieth et al.[36] and Gupta et al.[37] who developed the so-called yttria-tetragonal zirconia polycrystal (Y-TZP), an apparently monophase, fine-grained (0.3 to 0.5 μm in diameter) material, that nominally contained 2–3 mol.% yttria (Y_2O_3). Among all monolithic ceramics, Y-TZP exhibits the highest strength (exceeding 1000 MPa) when pressure-less sintered and reaches up to 2400 MPa when HIPed. Y-TZP is nowadays commonly called zirconia for its widespread use as a high-performance engineering and bioceramic material.[38]

Y-TZP was introduced into clinics in 1990 by the French company Ceramiques Techniques Desmarquest (St. Gobain). Thanks to work by a team led by Calés and Christel,[39] Y-TZP was added to the list of high-performance

TABLE 11.3 Manufacturers and Trade Names of Zirconia Blanks for CAD/CAM Machining

Manufacturer	Trade Name
VITA	In-Ceram YZ
Ivoclar	IPS ZirCAD
KaWo	Everest Z-block
Sirona	INcoris ZI
Nobel Biocare	Procera All-zircon
Degudent	CERCON
3M Espe	LAVA
Wieland	Zeno ZR
Noritake	Katana

bioceramic materials. It was notably used for manufacturing ball heads and cups as part of total hip replacements; that was also the first application of zirconia as a biomaterial in the construction of medical devices.

In dentistry, the first use of zirconia was in root posts, orthodontic brackets, and dental implants.[40] However, the real breakthrough came with the development of CAD/CAM technology that opened the path to the production of individually designed fixed-partial dentures (FPDs).[41] The replacement of traditional metal-based FPDs with all-ceramic prosthetic crowns, bridges, and full arch dentures has been driven mainly by the improved aesthetics and excellent tissue compatibility achieved using tooth-colored, metal-free systems (Table 11.3).

For the same reasons, there is a growing interest in Y-TZP-based all-ceramic dental implants. Bone apposition to zirconia is likely to take place without the interposition of fibrous tissues. This was demonstrated in 1993 by the research group of one of the present authors (CP)[42] who at that time was involved in experimental tap-type Y-TZP implants in post-extractive sites in the dog maxilla. The marking by orthotropic fluorochromes provided evidence for direct apposition of newly formed bone to the implant surface about 3 months post operatively (see Figure 11.5). Similar results have been reported by Akagawa, et al.[43] who tested PSZ screw-shaped dental implants in similar conditions and observed in histological sections direct bone apposition 3 months postoperatively. There was, however, some marginal bone loss observed in the early loaded implants.

Apart from bioactivity, the physical and chemical properties of dental implants made of zirconia (Figure 11.6) should comply with values specified
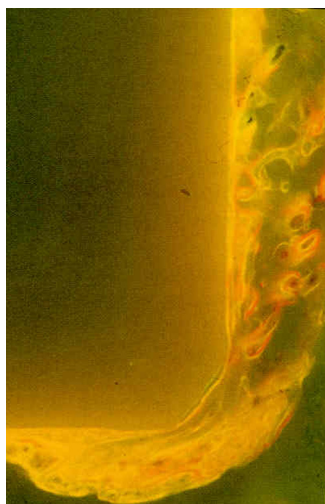
FIGURE 11.5 Bone apposition to experimental zirconia implant. *(From Piconi C, Rimondini L, Cerroni L, Donati C, Mutone V. La zirconia in odontoiatria. Milano: Elsevier, 2008)*

FIGURE 11.6 Zirconia dental implants. *(From Piconi C, Rimondini L, Cerroni L, Donati C, Mutone V. La zirconia in odontoiatria. Milano: Elsevier, 2008)*

in one of the following standards: ISO 13356[44] and the US standard ASTM F1873.[45] These apply to Y-TZP, while reference standard ASTM F2393 was issued for Mg-PSZ as a biomaterial.[46]

11.3.1 Structure of Zirconia

As already mentioned, zirconia exhibits three well-defined polymorphs: monoclinic, tetragonal, and cubic phases (Table 11.4). The high-temperature cubic phase has a face-centered structure in which the zirconium ion has an

TABLE 11.4 Physical Properties of Zirconia

Property	Units	Monoclinic	Tetragonal	Cubic
Lattice parameter a	nm	0.5156	0.5094	0.5124
Lattice parameter b	nm	0.5191	0.5177	N/A
Lattice parameter c	nm	0.5304	N/A	N/A
Density (theoretical)	g/cm^3	5.83	6.1	6.06
Melting point	K	2790		
Thermal expansion coefficient	N/A	5–10		
Thermal conductivity (298°K)>99.9% TD)	W/m K	2.5		

eight-fold coordination with the oxygen ions arranged in two equal tetrahedra. In the tetragonal form, the eight-fold coordinated zirconium ion is connecting two slightly distorted tetrahedra that are rotated through 90°. In the monoclinic form, the zirconium ion has seven-fold coordination with the oxygen ions arranged in a rather complex structure that resembles tetrahedral form.

By alloying pure zirconia with stabilizing oxides such as CaO, MgO, Y_2O_3, CeO_2, or La_2O_3, the stability range of the cubic phase can be extended to room temperature. In contrast, below about 700°C the tetragonal phase in bulk ceramics is thermodynamically unstable, but can be retained in its metastable form provided the tetragonal grains or precipitates are either constrained or the contribution of the surface energy is very high (i.e. their grains are very small). In such an instance, they can transform into the stable monoclinic form under an externally applied stress exerted by grinding, impact, or fracture. In the case of Y-TZP this can also occur under hydrothermal conditions. Retention of the t-phase allows the exploitation of the t→m phase transition as a toughening mechanism on a macroscopic scale. On a microscopic level, the relatively large volume expansion associated with the transformation leads to the development of internal stresses that oppose the opening of the crack and therefore act to increase the resistance of the material to crack propagation. For a detailed discussion of the transformation-toughening mechanisms in zirconia, the reader is referred to the original works of Lange,[47] Becher and Rose,[48] and Hannink et al.[49] that have also been summarized in a comprehensive review by Kelly and Denry.[50]

Briefly, the fracture in any polycrystalline ceramics takes place by the extension of an already existing defect in the material structure under an externally applied load. In zirconia-toughened ceramics with the tetragonal grain size and stabilizer content properly tuned, the stress concentration at the tip of the crack constitutes an energy source able to trigger the transformation of the tetragonal lattice into the monoclinic one. The t→m transformation that

takes place in the material zone ahead of the crack tip (the so-called 'process zone') dissipates part of the elastic energy that promotes progression of the crack. Moreover, the lattice expansion and the shear stresses due to the phase transformation generate a stress field in the lattice that increases the energy that opposes the propagating crack. The macroscopic effect of this mechanism is the increase in fracture toughness of the ceramic material.

11.3.1.1   Yttria-stabilized Tetragonal Zirconia Polycrystal (Y-TZP)

Y-TZP is a monolithic ceramic that consists of equiaxed partially stabilized tetragonal grains that typically contain 3 mol.% of yttria in the solid solution. Y-TZP ceramics are commonly pressure-less sintered at temperatures ranging from 1350 to 1550°C depending on the particle size in the starting powder. Very high fractional density (up to 99.5% of the theoretical value) and very fine and homogeneous grain size (0.3–0.5 μm) can be reached in this way. Since the ceramic is fired in the two-phase (c + t) region, the sintered material will eventually consist of predominantly (80–85%) tetragonal zirconia, with the minor fraction (about 15–20%) being cubic. However, due to a large similarity between the two crystal lattices, these two phases are barely discernible in the XRD pattern. The strength and fracture toughness of the sintered material are grain size-dependent and can be further influenced by the dopant concentration. A further contribution to transformability comes from the constraint exerted on the transforming grains by the stiffness of the matrix and by the residual stresses that originate either from inclusions, pores and other microstructural heterogeneities, or from the difference in shrinkage upon cooling between the crystal axes of the tetragonal unit cell.

11.3.1.2   Magnesia Partially-stabilized Zirconia (Mg-PSZ)

Mg-PSZ consists of relatively large cubic grains (e.g. 40 to 70 μm in diameter) containing a dispersion of rounded platelets of tetragonal phase 100 to 200 nm in diameter and 10 to 30 nm thick. A typical production route involves sintering of Mg-PSZ (8–10 mol.% MgO) powder compacts at about 1800°C (i.e. in the single-phase cubic region), and fast cooling to the two-phase c + t region at about 1400°C. The compact is then held at this temperature to allow nucleation and growth of the tetragonal precipitates within the cubic grains. The mechanical properties at room temperature can then be further improved by a second hold at about 1100°C.

The sintering temperature and dwell time, and the cooling rate and the annealing conditions, are the most critical process parameters because they control the size of the tetragonal precipitates that must not grow greater than about 200 nm. Above this threshold, they will spontaneously transform into the monoclinic structure, thereby decreasing the mechanical properties of the product.

So far, Mg-PSZ has never been a serious competitor to Y-TZP (Figure 11.7) as a biomaterial, one exception being Denzir-M material (Decim AB,
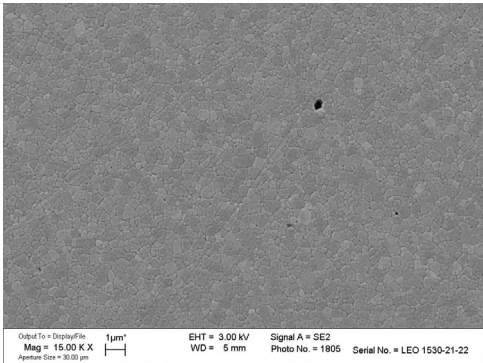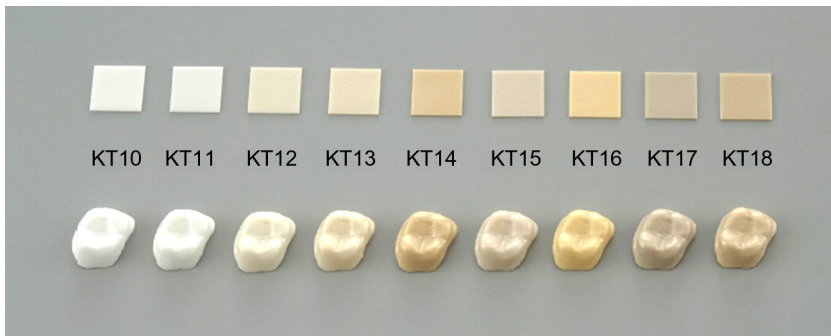
FIGURE 11.7   SEM image of Y-TZP microstructure. *(From Piconi C, Rimondini L, Cerroni L, Donati C, Mutone V. La zirconia in odontoiatria. Milano: Elsevier, 2008).*

TABLE 11.5 Mechanical Properties of Zirconia Ceramics

Property	Units	Y-TZP	Mg-PSZ
Density	g/cm^3	6	5.5
Grain size	μm	0.3–0.5	40–70
Flexural strength	MPa	900–1200	400–650
Young's modulus	GPa	210	210
Fracture toughness	MPa•m$^{1/2}$	7–9	8–11
Hardness	HV	12.5	12.5

Skellefteå, Sweden) that is used in dentistry. This may sound odd because Mg-PSZ was the first transformation-toughened ceramic ever made. Several critical points are likely to have decreased the interest in Mg-PSZ as biomaterial. The demanding and complex fabrication technology requires accurate temperature control and very high sintering temperatures. The latter are much higher than those used for Y-TZP, which also implies higher production costs that, together with the need of Si-free powders, forced the community to move toward Y-TZP.[51]

11.3.2   Mechanical Properties of Zirconia

The mechanical behavior of zirconia is strongly related to the polymorphism of its crystal structure (Table 11.5). In particular, the presence of the metastable t-phase and its transformability are of paramount importance. The presence of the t-zirconia in the material is prerequisite, while the transformability makes it effective. There is a strong grain- or particle size-dependence of the transformability
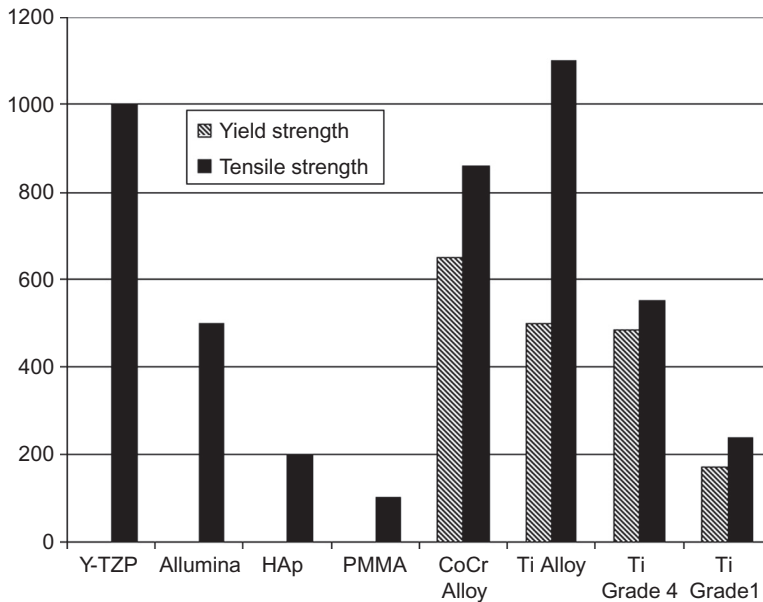
FIGURE 11.8   Comparison of tensile strength and yield strength among several dental ceramics and alloys. *(Adapted from Piconi C, Rimondini L, Cerroni L, Donati C, Mutone V. La zirconia in odontoiatria, Milano: Elsevier, 2008)*

that is further influenced by the amount and chemical nature of the dopant oxide as well as by the extent to which the neighboring grains (due to their stiffness or local stresses) oppose the expansion strain of the transforming ones.

The ability of a material to dissipate fracture energy around the tip of a propagating crack is called fracture toughness. In comparison to ductile metals, the fracture toughness of brittle ceramics is low, which is due to the absence of plastic deformation before fracture. Namely, plastic flow is a very efficient mechanism for dissipating fracture energy. There are several ceramics that exhibit very high strength, but they are barely used in practice due to their relatively low fracture toughness, which implies that the latter remains the major factor limiting the application of ceramics. The toughness of zirconia, although never attaining the level of metals, can reach values of about 10 MPa•m½, which is more than twice as high as for high-density alumina. The bending strength of Y-TZP (>900 MPa, 4-point bending) is superior as compared to other dental ceramics, and far above the yield strength of metallic alloys used in dentistry (Figures 11.8 and 11.9).

Not only bending strength and fracture toughness, but also hardness, elastic modulus, and thermal conductivity of zirconia are relevant characteristics for use in dentistry. While dense alumina has a hardness of about 20–22 GPa, the hardness of Y-TZP is about one half of this value (12–14 GPa), which is a clear advantage over alumina in the adaptation of coronal parts by grinding. Another advantage of zirconia in relation to alumina is that its elastic modulus is much lower than that of
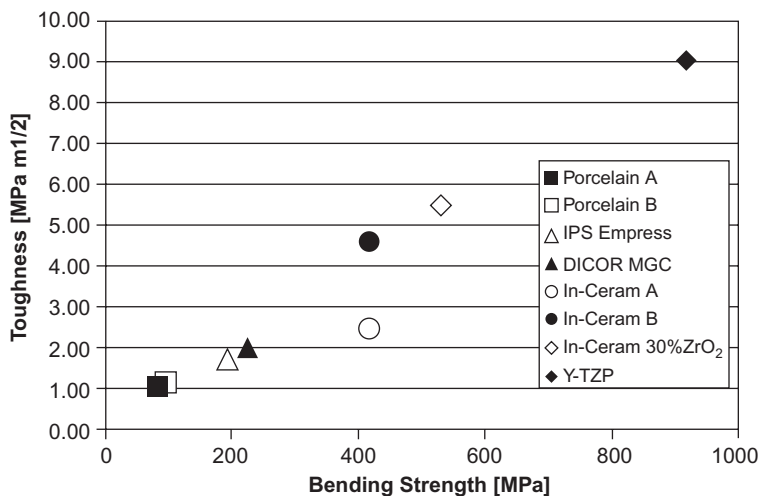
FIGURE 11.9 Toughness vs. bending strength in ceramics used in dentistry. *(Adapted from Piconi C, Rimondini L, Cerroni L, Donati C, Mutone V. La zirconia in odontoiatria, Milano: Elsevier, 2008)*

alumina (200 GPa vs. 380 GPa), which implies lower elastic stresses between the natural dentine and the prosthetic work. On the other hand, the elastic modulus of zirconia is twice as high as that of titanium alloys. This is a difference that must be considered while designing metal-to-zirconia connections because it may lead to microstrains under load. Because of the low thermal conductivity of zirconia (about one-tenth that of alumina) and its rather high thermal expansion coefficient, there can be stress accumulation during cooling in zirconia-based composites. This makes these materials very sensitive to thermal shock (see Section 11.3.2.1).

As a concluding remark on zirconia, it is worthwhile mentioning that the behavior of this material is strongly dependent on the selection of the ceramic powder, its processing, consolidation, and sintering, all of which are proprietary to each ceramic manufacturer (see Guazzato et al.[52], for example). Moreover, end users must keep in mind that zirconia is a metastable material that is susceptible not only to processing conditions, but also to the environment in which it is used.

11.3.2.1 Low-temperature Degradation

As already mentioned, the enhanced mechanical properties of zirconia-toughened ceramics are dependent on the existence of the metastable tetragonal phase and its ability to transform into a monoclinic structure under an externally applied stress. This transformability can be manipulated either by acting on the material's chemistry, or by altering the grain size and/or the constraint exerted by the matrix on the tetragonal grains. In cases of monolithic Y-TZP ceramics and particulate composites containing larger amounts (>15 vol.%) of dispersed yttria-doped zirconia particles, the transformation can further be initiated by energy coming from the external environment.

The hydrothermally induced spontaneous t→m transformation in Y-TZP ceramics was first reported by Kobayashi et al.[53] who also reported on severe degradation of the mechanical properties after prolonged exposure to water vapor in the temperature range 150–450°C. This behavior, known as low-temperature degradation (LTD), or aging, has been extensively investigated. However, the phenomenon is still not well understood. In the beginning, the work focused on aging at temperatures higher than 100°C. Later, the research was extended to conditions representative of the human body since Y-TZP is used as a biomaterial. The two most acknowledged models (developed by Sato and Shimada[54] and Yoshimura et al.[55]) are both based on localized chemical reactions between water and preferential sites on the grain boundaries that lead to annihilation of oxygen vacancies, thereby nucleating the transformation. The mechanism leading to nucleation of the t→m transformation is diffusion-controlled and hence temperature-dependent. Once nucleated, the transformation is martensitic in nature and is accompanied by extensive micro-cracking and surface grain pullout.[56] This ultimately leads to strength degradation. It has been demonstrated that LTD is a grain size and yttria content-dependent process that is further influenced by chemical, structural, and microstructural inhomogeneities, materials prehistory, and aging conditions. The role of the aqueous medium is not clear yet. The same holds true for the influence of the surface finish and residual stresses that result from cooling, phase partitioning, and/or mechanical surface treatment.[57–59] The activation energy of the phenomenon has been reported to be between 70 and 110 kcal/mol. All these aspects have to be taken into account while selecting the wet grinding conditions because, due to the very low thermal conductivity of zirconia (2.5 W/mK), the surface may locally reach very high temperatures that, although persisting for only a short time, can trigger the pernicious LTD on the ceramic surface.[60–62]

The remedies developed so far to control zirconia LTD are capable of slowing down the transformation kinetics, but they cannot prevent it. The most popular remedy consists of adding a small amount (typically 0.25 wt.%) of alumina (Al_2O_3) to zirconia during the co-precipitation process used in powder production. Provided that the grain size of sintered ceramic is kept below about 0.30 μm, the alumina-containing Y-TZP is nearly 'water resistant' when tested in an autoclave in distilled water at the sterilization temperature. Since alumina and zirconia are mutually insoluble, the added alumina will be found in the form of tiny inclusions in zirconia grain boundaries. Interestingly, there are only a few papers that attempt to explain the role of dispersed alumina in suppressing transformation kinetics. Thus, for example, Ross et al.[63] hypothesized that Al^{3+} ions act as stabilizers of the grain boundaries that are the reaction sites for the nucleation of LTD, while the model by Lu and Chen[57] hypothesized that alumina inclusions generate a stress field in grain boundaries that impeaches water molecules to react with the material.

Among equally effective (but more expensive) alternative remedies, the co-doping of zirconia and ceria (CeO_2),[64] and coating of the Y-TZP powder[65,66] with Y_2O_3 (the stabilizer oxide) prior to sintering, should be mentioned.
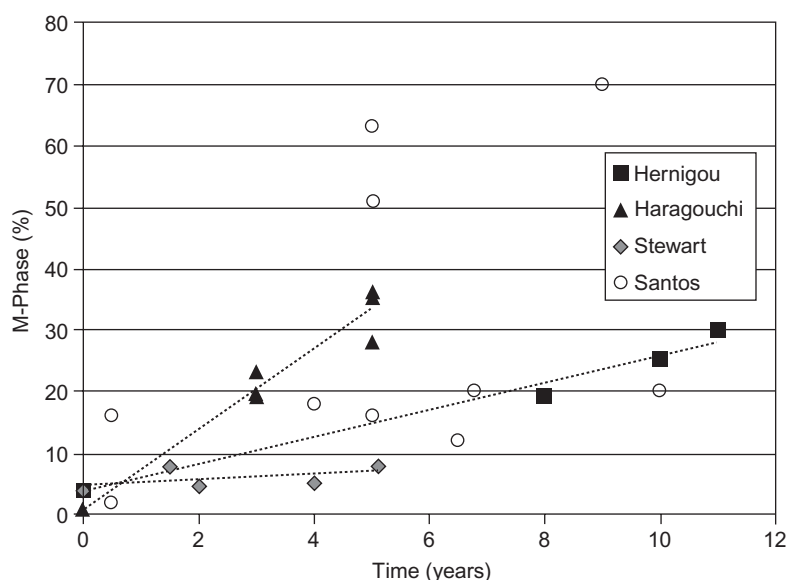
FIGURE 11.10   Difference in LTD kinetics among zirconia from different manufacturers. *(From Piconi C, Rimondini L, Cerroni L, Donati C, Mutone V. La zirconia in odontoiatria. Milano: Elsevier, 2008)*

Unlike Y-TZP, sintered Ce-TZP ceramics do not transform under hydrothermal conditions, which explains the reasoning behind co-doping with ceria and yttria. In contrast to homogeneously distributed stabilizers in co-doped Ce and Y-TZP grains, the distribution of yttria in ceramics produced from yttria-coated powders exhibits a radial gradient from the grain boundaries inwards toward the grains. When exposed to water vapor, the excess yttria forms hydroxides in the grain boundaries, thereby preventing yttria depletion on the grain surface. According to Sato's and Yoshimura's models, this triggers the transformation. As already mentioned, these two alternatives are effective but more expensive, and therefore not used in practice.

Also, the introduction of CuO or Fe_2O_3 allows the decrease of both the sintering temperature and the hydrothermal transformation by the formation of intermediate phases in zirconia.[63] It is noted that differences in LTD exist among the different materials on the market due to differences in the starting materials, process additives, and fabrication route that give different characteristics to the chemistry and microstructure (Figure 11.10).[66,67]

11.3.3   Zirconia Radioactivity

Emission of ionizing radiation (radioactivity) is a very common behavior in nature, much more than anticipated. It is noted that the human body

also contains radiation-emitting isotopes in variable concentrations. Among these isotopes, potassium 40 (^{40}K), which has a specific gamma activity of 32 Bq/g, is naturally present in the body in the range 110–140 g, depending on sex, age, and body mass. As a consequence, the body is a source that emits 3600–4500 Bq in gamma rays with energy of 1420 KeV. It is also noted that red meats, beans, bananas, nuts, and all food containing potassium, are natural gamma sources of variable intensity.

The source of zirconia radioactivity is in the ores that are used for production of the chemicals used in powder production. Uranium (^{238}U), thorium (^{232}Th), and the nuclides of their decay chains are contained in the centenary equilibrium in the ores; uranium and zirconia especially have a wide miscibility interval. This is why traces of radioactive nuclides can be found in many high-purity zirconia powders, including those used in the production of medical devices. It should be noted, however, that the ISO 13356 standard[60] sets limits to the specific activity of medical grade Y-TZPs to a maximum of 200 Bq/kg; all medical devices made of zirconia are strictly controlled for radioactivity.

The issue of zirconia radioactivity was raised in papers by Hopf et al.[68,69] Very high radioactive isotope content was observed in zirconia powders used as radiopacifiers in bone cements. Although obtained with different zirconia than used in clinical implants, these papers draw attention to the radioactivity of zirconia. Measurements performed on the ball heads for hip replacements[70] showed specific activities of about 10 Bq/kg, much less than for the human body (about 50 Bq/kg).

The gamma radiation of powders used in the production of Y-TZP ceramics was the object of extensive screening in view of their use as precursors for biomaterials. This work by Capannesi et al.[71] detailed the variability of the content in gamma emitters among different powders on the market (Figure 11.11), as well as the effectiveness of processes used for the purification of zirconium chemicals.[72] Namely, in high-purity materials, the specific activity may be lower than in the human body.[73] For instance, Postendorfer et al.[74] measured specific activities in zirconia demonstrating that doses of ionizing energy, due to the prolonged use of the zirconia components, are below the limits stated by the International Commission on Radiological Protection. Besides gamma radiation, a wide variability in wavelengths has also been observed in alpha emission among different zirconia precursors.[75]

Interestingly, up to the 1990s, dental porcelains may have contained uranium dioxide to mimic the fluorescence of natural teeth, and also ^{40}K due to the introduction of potassium (up to 10%) in the ceramic to decrease the metal–ceramic thermal expansion mismatch.[76–78] It is also noted that due to the content of potassium (then of ^{40}K), some feldspathic porcelains used in dentistry may reach specific radioactivities between 1950 and 3000 Bq/kg,[76] far higher than specified for zirconia for clinical implants in ISO standard 13356.
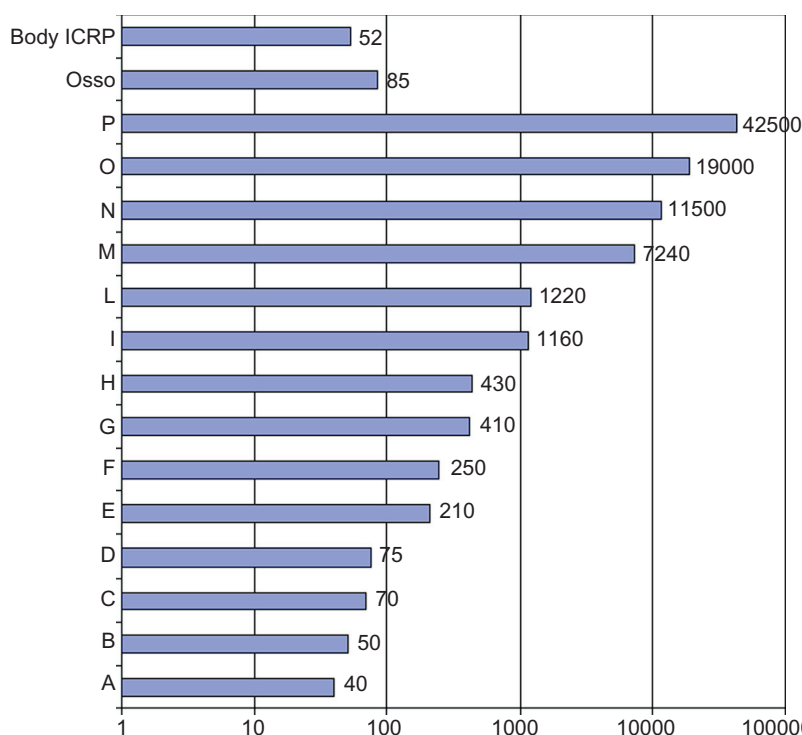
FIGURE 11.11   Specific gamma emission (Bq/k) of different zirconia powders.[71] Specific gamma emission of body and bone are reported for comparison.

11.3.4   Optical Properties

In restorative dentistry, the natural appearance of the prosthetic work is paramount. In this respect, silicate-based ceramics, in particular porcelains and glass-ceramics, are better at mimicking the radio-opacity of natural teeth than pressure-less sintered, biomedical grade Y-TZP. The remnant pores in 99–99.5% dense ceramics also containing 0.25% of dispersed alumina particles added to suppress aging, scatter light and therefore contribute to somewhat high opacity. The problem can be mitigated by using a finer powder with a lower amount of alumina that sinters to a high fractional density (>99.6% of the theoretical value) at moderate grain size, thereby also providing stability under hydrothermal conditions. The translucency of FPDs produced from this kind of powder was reported to almost match that for natural teeth.[79–81] Moreover, it is possible to give zirconia the shade of natural teeth by doping the ceramic with iron, titanium, cerium, and some other oxides (Figure 11.12).[82,83]

FIGURE 11.12 Noritake Y-TZP shades. *(From Piconi C, Rimondini L, Cerroni L, Donati C, Mutone V. La zirconia in odontoiatria. Milano: Elsevier, 2008.)*

11.3.5 Biocompatibility

Extensive reviews on biocompatibility tests performed in vitro and in vivo on zirconia have already been published elsewhere.[38] Briefly, zirconia has been tested in vitro under different physical forms (e.g. powders and dense ceramics). The results of these tests are usually influenced by the physical form, reactivity of the surface, chemical composition, impurity content, etc. as well as by cell conditions during the tests. Nevertheless, the absence of acute toxic effects has been reported by most of the authors; the materials were tested on different cell lines (e.g. macrophages, lymphocytes, fibroblasts, and osteoblasts) using direct and indirect contact tests. There is a general agreement on the absence of local or systemic toxic effects after the implantation of zirconia, regardless of its physical form. In the early post-operative phase, connective tissue was frequently observed at the bone–ceramic interface, a reaction typical of non-bioreactive ceramics. It was noted that the results of the tests were dependent upon the preparation of the implant site as well as on the surface properties of the implants (e.g. an increase in bone–implant contact has been reported after treatments that increased the surface roughness).[84]

In vitro mutagenic tests showed that in the absence of any such reactions on cells,[85,86] no tumors were observed after long-term implantation in rabbits.[38] The direct apposition of bone to zirconia implants as evidenced in earlier works[42,43] has been confirmed by several other authors (e.g. Cerroni[84] and Hisbergues).[87]

11.4 ALUMINA-ZIRCONIA COMPOSITES IN DENTISTRY

Besides PSZ and Y-TZP, zirconia toughening can be exploited to improve the mechanical properties of ceramics in several different ways. The classic work by Claussen enlists 15 zirconia-toughened ceramics (ZTCs), many of which never got past the development stage.[88] On the other hand, composites consisting of

zirconia and alumina found practical application as biomaterials due to their proven biocompatibility and superior mechanical properties as compared to monolithic constituents. These composites are known as zirconia-toughened alumina (ZTA) when alumina is the main phase, or as alumina-toughened zirconia (ATZ) when the main phase is zirconia. After the introduction of pink-colored alumina-zirconia hip joints (BIOLOX®delta, CeramTec GmbH, Plochingen, Germany) in 2000, this class of ceramic biomaterials has been the object of increased interest for a variety of load-bearing applications in orthopedics and dentistry.

An articulated research program was started in France during the 1980s to qualify ZTA as a biomaterial, with the main application in orthopedics. The research was focused on alumina that contained from 5 to 20 vol.% zirconia (stabilized by 2 mol.% Y_2O_3). Another material of interest was aluminum oxynitride (AlON).[89] In Italy, ZTA was investigated as a biomaterial in the late 1980s.[90] Most of the research was carried out in the framework of a Eureka 294 project ('Biomaterials') that aimed to develop ZTA and ATZ ball heads and cups for total hip replacements.[91] None of the results from these studies was transferable to clinics. On the other hand, the German BIOLOX®delta is already widely used in orthopedics. This ceramic contains 17 vol.% of dispersed Y-TZP particles in the alumina matrix, and strontium aluminate platelets that nucleate into the matrix during sintering as a third phase. For this feature, BIOLOX®delta is sometimes described[92] as a zirconia–platelet-toughened alumina (ZPTA). In contrast to orthopedics, ZTA has not yet found much application in dentistry. The main reason is probably that this material is opaque and thus not appreciated from an aesthetic point of view. There is an exception, however, porous alumina-Ce-TZP matrix infiltrated with glass. This glass-infiltrated material is known as the InCeram-Zirconia® system (Vita, Bad Sackingen, Germany), and is widely used in dentistry.

There are two more alumina-zirconia composites used in dentistry. They both belong to the ATZ class: Ziraldent® (Metoxit, Thayngen, Switzerland) and NANOZR® (Panasonic Electric Works, Osaka, Japan). Other alumina-zirconia composites are under development, including those that will be produced in a joint venture between ENEA (Faenza Technical Unit on Materials Technologies, Faenza, Italy) and GHIMAS S.p.A (Casalecchio di Reno, Italy).

11.4.1   Structure

The previous section outlined the transformation toughening mechanism in zirconia ceramics, and showed the role of chemical and mechanical energies in the stabilization to room temperature of the metastable tetragonal phase. In zirconia-alumina composites, the introduction of alumina into the material increases the energy threshold for the transformation because of the higher stiffness of the material. Namely, the elastic modulus of alumina is almost twice that of the zirconia (380 GPa vs. 200 GPa, respectively). ATZ may contain up to 40 wt.% of dispersed alumina. The constraint on tetragonal grains
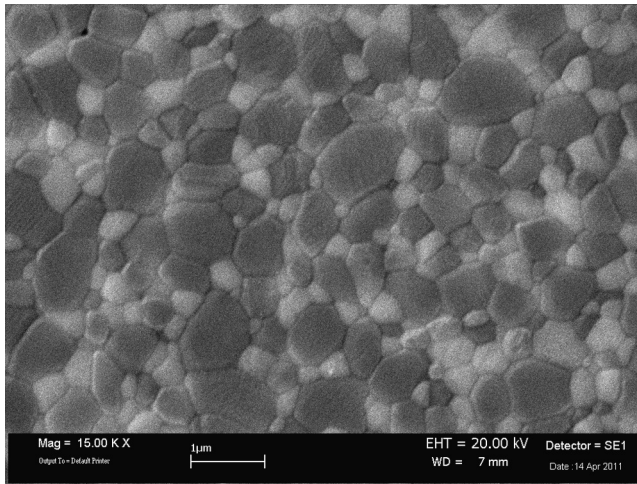
FIGURE 11.13   SEM image of the microstructure of the ENEA Z/A composite. Zirconia grains are in white. *(Courtesy of ENEA - Faenza Technical Unit on Material Technologies, Faenza, Italy and GHIMAS S.p.A., Casalecchio di Reno, Italy.)*

is exerted by the neighboring alumina grains as well as by the fraction of those zirconia grains that spontaneously undergo the t→m transformation during cooling from the sintering temperature.[93] In order to further increase the matrix constraint on the tetragonal zirconia grains, untransformable zirconia can also be introduced into the material. This is the case in ENEA material where a minor fraction of the 40 wt.% zirconia is in the monoclinic form.[93] The nominal composition of this ZTA shows the presence of two types of zirconia: metastable tetragonal (23.6 wt.%) and unstabilized monoclinic zirconia (16.4 wt.%), the balance being alumina and a blend of stabilizing oxides (0.5 wt.% Cr_2O_3+2 mol.% Y_2O_3). See Figure 11.13.

ZIRALDENT® is a homogenous blend of fine-grained alumina and zirconia with a nominal composition of 76 wt.% ZrO_2, 4 wt.% Y_2O_3, and 20 wt.% Al_2O_3, while NANOZR® (Panasonic Electric Works, Osaka, Japan) is a nanocomposite based on the research carried out by Nawa et al.[94] The optimized material is constituted by a 10 mol.% Ce-TZP matrix containing 30 vol.% of alumina, and characterized by an interpenetrating microstructure obtained by the introduction of a small amount of TiO_2 (0.2 mol.%) which promotes the grain growth of the matrix phase during sintering. In this way, nano-sized alumina grains become trapped within the zirconia grains, which results in the characteristic interpenetrated microstructure.

11.4.2   Mechanical Properties

Thanks to the enhancement in efficiency of transformation toughening, both dense ZTA and ATZ have mechanical properties that exceed those of alumina

TABLE 11.6 Mechanical Properties of Alumina-Zirconia Composites for Dental Devices

Material	Ref	Flexural Strength (MPa)	Fracture Toughness (MPa•m$^{1/2}$)	Hardness (GPa)	Notes
IN-CERAM®	Ban 2008	600	4,4	11	Glass-ceramic composite
ENEA ZTA	Maccauro 2009	1400	7	16	4-point bending
NANOZR®	Tanaka 2002	940	20	11.7	3-point bending
ZYRALDENT®	Metoxit 2011	2000	8	14	3-point bending

and zirconia that are their main components (see Table 11.6). The In-Ceram® composite, due to its high porosity fraction filled by glass, is an exception to this rule.

Specifically, the bending strength of the ZIRALDENT® (Metoxit AG, Tahingen, Switzerland) ATZ is remarkable. Dental implants made out of this composite have been submitted to an extensive testing program that uses as a reference point Zi-Unite Y-TZP dental implants (Nobel Biocare AG, Göteborg, Sweden).[95] The implants were tested to fracture both in the as-sintered state and after grinding by diamond burs. Before testing to fracture, the implant underwent hydrothermal treatment in simulated chewing conditions associated with thermal cycling between 5°C and 55°C (with a full cycle period of 132 s). The results show the significant influence of mechanical and thermal cycling, as well as of milling, on the mechanical strength of the implants. Although the mean fracture load of the ATZ implants was still very high (1098±97 N) in comparison to the one for Y-TZP implants (516±45 N), this load was only 64% of the initial value (1734±166 N) for this material. The bending strength of the NANOZR® ATZ did not show any improvement with respect to Y-TZP, but its fracture toughness was superior.[96,97] In the case of ENEA ZTA materials, the bending strength reflected a higher alumina content as compared to Y-TZP. It is expected that the redistribution of the stabilizers during sintering will lead to a higher transformability of the tetragonal phase, as well as to reduced residual tensile stresses, both resulting in the improvement of mechanical behavior (Figure 11.14).[93]

11.4.3   Biocompatibility

The absence of adverse tissue reactions to the implantation of either ZTA or ATZ was reported in the early 1990s during studies to investigate the potential
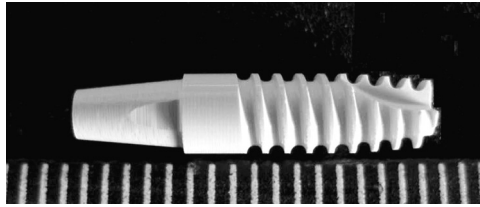
FIGURE 11.14 Experimental dental implant made out of ENEA Z/A composite. *(Courtesy of ENEA, Faenza Technical Unit on Material Technologies, Faenza, Italy, and GHIMAS S.p.A., Casalecchio di Reno, Italy.)*

of these composite ceramics as load-bearing biomaterials.[89,98] Yamashita et al. reported no significant differences in proliferation or in ALP activity of osteoblast-like cell (MC3T3-E1) co-cultures on CeTZP/Al$_2$O$_3$, Y-TZP, or CP titanium alloy.[99] Neither the expression of osteocalcin nor cell morphology was affected by the differences in chemistry and surface conditions of the materials tested. Similar results were reported by Setzer et al., who investigated the influence on the proliferation and differentiation of hFOB osteoblasts by titanium, Y-TZP, ATZ, and ZTA (Metoxit SA, Thayngen, Switzerland).[100] Notwithstanding the difference in nature and surface roughness among the materials tested, the behavior of hFOB cultured up to 28 days did not differ from the same cells co-cultured on either untreated titanium or Ti-Unite surfaces (Nobel Biocare, Göteborg, Sweden).

Maccauro et al. performed direct culture of CH310T½ mouse embryo-derived fibroblasts on disks of HIP-treated and sintered zirconia-alumina ENEA A/Z ceramic composite.[101] The tests results demonstrated the absence of any toxic effect of the ceramic composite on the cells in terms of mutagenicity or carcinogenicity, as well as the absence of DNA damage to the fibroblasts due to direct contact with composite ceramics. Tanaka et al.[96] carried out animal tests with experimental Ce-TZP/Alumina NANOZR® specimens in male Wistar rats, and observed no tumors, infections, or skin irritation after a maximum 24 weeks. Macrophages and lymphocytes, as well as eosinophils or foreign body giant cells, were seldom observed in the histologies. A fibrous membrane encapsulated the implants similar to the one observed in the implant made out alumina.

11.5 ADHESION

The problems related to adhesion of dental cements to the ceramic core are twofold. On one hand, strong bonding largely aggravates the disassembly of FPDs that need to be replaced (e.g. for major chipping or fracture); on the other hand, the interface bonding between the ceramic core and the luting agent (cement) tends to weaken steadily over time in the harsh environment of the oral cavity. This may ultimately lead to debonding. It has been reported that in certain
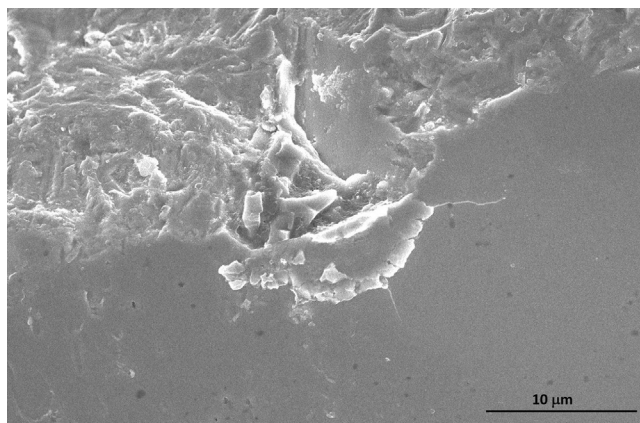
FIGURE 11.15   Impact-induced radial cracks in sandblasted zirconia. *(From T. Kosmac, unpublished work.)*

clinical situations, the long-term survival rate of zirconia-based dental restorations largely depends on the adhesive bond strength; a stronger bonding to the core is advantageous.[101,102] This especially holds true for the inlay-retained bridges that have become increasingly popular due to the conservative approach to prosthetic rehabilitation.[103] Missing single premolars and molars, as well as missing lateral incisors, where retentive wings are bonded to the palatal surface of adjacent teeth, represent main indications for this treatment modality.

In silica-based ceramics, a reliable bond can be achieved with hydrofluoric acid (HF) etching followed by silanization.[104] In contrast, chemically stable, silica-free Y-TZP ceramics are acid-etch resistant, and bonding protocols successfully used in silica-based ceramics cannot be implemented. Different mechanical and chemical conditioning methods have therefore been proposed to enhance the resin–ceramic bonding. In the case of zirconia, sandblasting, i.e. abrasion with airborne alumina particles has been commonly used to increase the surface roughness,[105] thereby creating micro-retentions. The process is not applicable to alumina ceramics because they are too hard and too brittle.

However, the effects of abrasion on zirconia are still controversial. Because Y-TZP materials exhibit a stress-induced transformation, the abraded Y-TZP surface will be transformed (i.e. constrained) as well as damaged. The residual surface compressive stresses due to the t→m phase transformation contribute to strengthening, whereas impact-induced surface flaws act as the stress concentrators; if their length greatly exceeds the depth of the impact-induced surface compressive layer, they will become strength determining.[60] The strength of abraded Y-TZP ceramics will therefore depend on the transformability and inherent mechanical properties of the material, as well as on the severity of the air-particle abrasion process (Figure 11.15).

As shown by Wang et al., the extent of the impact damage can be controlled by the abrasive particle size.[106] At a constant pressure, the abrasion of
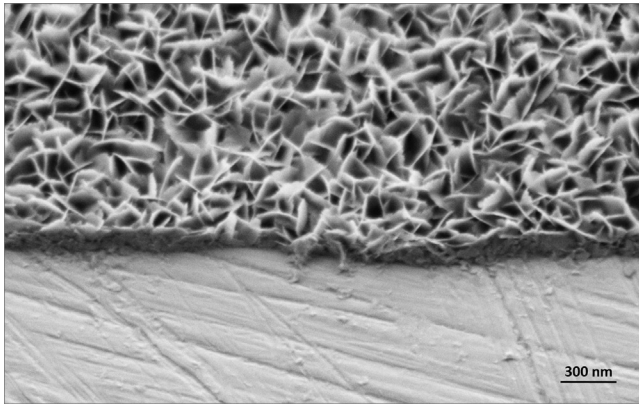
FIGURE 11.16 Nano-structured adhesive alumina coating deposited onto a sintered zirconia surface. *(From A. Kocjan's Ph.D. thesis, J. Stefan International Postgraduate School, Ljubljana, 2008)"*

the Y-TZP surface with the 50-μm alumina particles increased the strength of the material, while the abrasion of the very same material with the 120-μm particles resulted in strength degradation. A similar effect can be expected while abrading the Y-TZP ceramics at higher pressure, which should result in higher kinetic energy of the abrasive particles.[107]

As there is no clinical consensus on appropriate bonding procedures, considerable efforts are being made to develop alternative chemical and mechanical surface modifications of Y-TZP ceramics. New silane formulations,[108] hydroxylation of zirconia surfaces prior to silanization,[109] and vapor-phase deposition[110] have been reported to enhance chemical bonding. Efforts have also been made to develop a mechanical pre-treatment that would omit abrasion. Thus, for example, Derand et al.[111] applied a low-fusing porcelain pearl layer to increase roughness, while Phark et al.[112] modified the Y-TZP surface with a slurry containing zirconia powder (that was subsequently sintered). Aboushelib et al.[113] proposed so-called selective infiltration etching, which is based on inter-grain nano-porosities created during thermal pre-stressing of the surface grains using a specific temperature regime. However, the clinical performance of these alternative surface-preparation techniques remains to be tested.

More recently, a non-invasive process to promote resin bonding has been introduced that relies on a functionalization of the Y-TZP's surface; a nano-structured alumina coating is applied with a high surface area and good wetting ability. To fabricate the coating, a relatively simple process was developed that exploits dissolution/precipitation of aluminum hydroxides that originate from the hydrolysis of AlN powder in an aqueous suspension.[114] A uniformly thin nano-crystalline coating consisting of γ-AlOOH in the form of 6nm-thick and 250nm-long interconnected lamellae can be formed in this way. By heat treatment at 600–1200°C these lamellae can be transformed into a transient alumina without any noticeable change in the morphology, but their bonding to the substrate will be significantly improved. The coating shows a uniform thickness and a good surface coverage
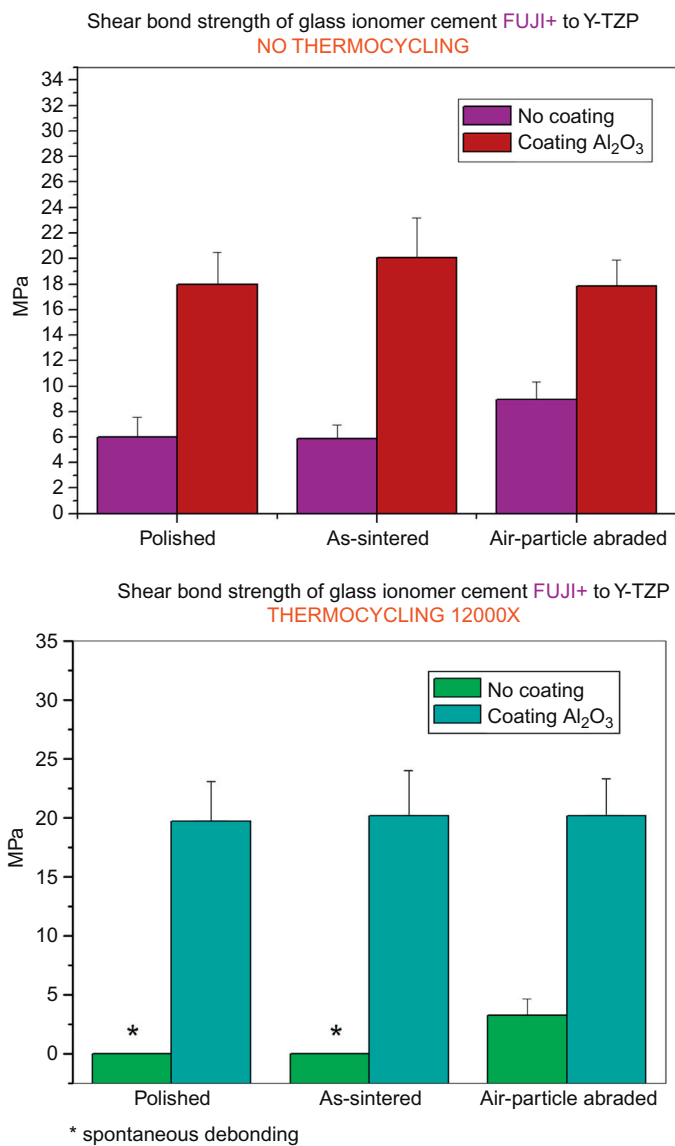
FIGURE 11.17   Shear bond strength of a glass-ionomer cement to sintered, polished, and sand-blasted Y-TZP ceramics (a) before; and (b) after thermocycling. *(From P. Jevnikar's Ph.D. thesis, Uni. Ljubljana, 2008.)*

(Figure 11.16). It is almost insensitive to thermocycling, and has the potential of durable improvement of the adhesive bond between the coated core material and the dental cements by a factor of 2–4, depending on the surface roughness of the substrate and the dental cement used (Figure 11.17).[115–117] The proposed method has already been used in experimental inlay-retained bridges to replace missing

single premolars and molars. Clinical examination after 12 months and encompassing 18 bridges revealed no debonding.

It is believed that primary telescopic crowns made of Y-TZP ceramics may also benefit from this coating. Telescopic dentures, where secondary telescopes are made using galvano-forming technology, must be removed from the oral cavity several times a day for hygiene and spontaneous debonding of the primary telescopes due to fatigue; this has been reported as a serious clinical problem. Furthermore, it is believed that the coating has the potential for durable improvement of bonded FPDs fabricated using the PRESS-on or CAD-on techniques developed to alleviate porcelain chipping, as well as of enhancing the adhesion of cements to zirconia implant abutments.

REFERENCES

1. Piconi C. Proprietà della zirconia. In: Piconi C, Rimondini L, Cerroni L, editors. La zirconia in odontoiatria. Milano: Elsevier Masson; 2008. p. 16–43.
2. Piconi C, Maccauro G, Muratori F. Alumina matrix composites in arthroplasty. Key Eng Mater 2005;284–6:979–82.
3. Rock, M. Künstliche Ersatzteile für das Innere und Aussere des menschliche und tierische Körpers, German Patent DRP 583.589:1933.
4. Sandhaus S. Noveaux aspects de l'implantologie. Paris: Julien Prelat; 1969.
5. Heimke G, Shulte W. Dental Implants having a Biocompatible Surface. US Patent 4.185.383: 1980.
6. Williams DF. The clinical applications of implants in oral and maxillofacial surgery. In: Cahn RW, Haasen P, Kramer EJ, editors. Material science and technology - Vol. 14: Medical and dental materials. Weinheim: VCH; 1992. p. 264–5.
7. Mutshelknaus E, Dörre E. Extensions -Implantate aus aluminiumoxid keramik. Quintessenz 1977;28:21–8.
8. Driskell TD, O'Hara MJ, Sheets HD, Green Jr GW, Natiella JR, Armitage J. Development and application of ceramics and ceramic composites for implant dentistry. In: Hall CW, Hulbert SF, Levine SN, Young FA, editors. Bioceramics–engineering in medicine (Part 2). New York: Interscience; 1972. p. 345–61.
9. Hulbert SF, Morrison SJ, Klawitter JJ. Tissue reaction to three ceramics of porous and non-porous structure. J Biomed Mater Res 1972;6:347–74.
10. Yamagami A, Kotera S, Kawahara H. Studies on a porous alumina dental implant reinforced with single-crystal alumina. In: Lemons JE, editor. Quantitative characterization and performace of porous implants for hard tissue applications–STP 953. Philadelphia: American Society for Testing and Materials; 1987. p. 399–408.
11. Takahashi T, Sato T, Hisanaga R, et al. Long-term observation of porous sapphire dental implants. Bull Tokyo Dent Coll 2008;49:23–7.
12. McKinney Jr RV, Koth DL, Steflik DE. The Bioceram implant system. In: McKinney Jr RV, editor. Endosteal dental implants. St Louis: Mosby Year Book; 1991. p. 215–30.
13. McLean JW. High-alumina ceramics for bridge pontic construction. Br Dent J 1967; 123:571–7.
14. Clause H. Vita In-Ceram, a new system for producing aluminum oxide crown and bridge substructures. Quint Zahntech 1990;16:35–46.

15. Andersson N, Odén A. A new all-ceramic crown. A dense-sintered, high purity alumina coping with porcelain. Acta Odont Scand 1993;51:59–64.
16. Della Bona A, Kelly RJ. The clinical success of all-ceramic restorations. J Am Dent Assoc 2008;139:8S–13S.
17. Piconi C. Alumina. In: Ducheyne P, Healey KE, Hutmacher DW, Grainger DW, Kirkpatrick CJ, editors. Comprehensive Biomaterials - Vol 1. Amsterdam: Elsevier; 2011. p. 73–94.
18. ISO TC150 Implants for Surgery - Ceramic materials based on high purity alumina, ISO 6474. Geneva: International Organization for Standardization.1981.
19. American Society for Testing and Materials, SC F04 on medical and surgical materials and devices. Standard Specification for High-Purity Dense Aluminum Oxide for Medical Application, ASTM F603. West Conshohoken, American Society for Testing and Materials. 1983.
20. Kuntz M, Masson B, Pandorf T. Current state of the art of ceramic composite material BIOLOX delta. In: Mendes G, Lago B, editors. Strength of materials. New York: Nova Science; 2009. p. 133–58.
21. Frakes JT, Brown SD, Kenner GH. Delayed fracture and aging of porous alumina in water and in physiological media. J Am Ceram Soc 1974;53:183–7.
22. Krainess FE, Knapp WJ. Strength of a dense alumina ceramic after aging in vitro. J Biomed Mater Res 1978;12:241–6.
23. Ferber MK, Brown SD. Subcritical crack growth in dense alumina exposed to physiological media. J Am Ceram Soc 1980;63:424–9.
24. Sinkaroy S, Levenson LL, Day DE. Influence of calcium migration on the strength reduction of alumina exposed to steam. Am Cer Soc Bull 1979;58:464–6.
25. Osterholm HH, Day DE. Dense alumina aged in vivo. J Biomed Mater Res 1981;15:279–88.
26. Dörre H, Hübner H. Alumina: processing properties and application. Heidelberg: Springer; 1984. p. 9–79.
27. Park J. Bioceramics. New York: Springer; 2008. p.120–132.
28. Greco F, Piantelli S, Maccauro G, Arena M, Piconi C. Risposta biologica ai materiali ceramici: risultati delle prove in vitro ed in vivo. Minerva Ortop Traumatol 1993;44:913–8.
29. Takami Y, Yamane S, Makinouchi K, et al. Protein adsorption onto ceramic surfaces. J Biomed Mater Res 1998;40:24–30.
30. Catelas I, Petit A, Zukor DJ, Marchand R, Yahia LH, Huk OL. Induction of macrophage apoptosis by ceramic and polyethylene particles in vitro. Biomaterials 1999;20:625–30.
31. Kranz I, Gonzalez JB, Dorfel I, et al. Biological response to micron- and nanometer-sized particles known as potential wear products from artificial hip joints: part II: reaction of murine macrophages to corundum particles of different size distribution. J Biomed Mater Res 2009;89-A:390–401.
32. Christel P, Meunier A, Dorlot J-M, et al. Biomechanical compatibility and design of ceramic implants for othopedic surgery. In: Ducheyne P, Lemons JE, editors. Bioceramics: material characteristics versus in vivo behavior (Ann New York Academy of Sciences, vol. 523). New York: The New York Academy of Sciences; 1988. p. 234–56.
33. Ruff O, Ebert F, Stephen E. Contributions to the ceramics of highly refractory materials: II, System Zirconia-Lime. Z Anorg Allg Chem 1929;180:215–24.
34. Garvie RC, Nicholson PS. Structure and thermodynamical properties of Partially Stabilized Zirconia in the CaO-ZrO$_2$ System. J Am Ceram Soc 1972;55:152–7.
35. Garvie RC, Hannink RHJ, Pascoe RT. Ceramic Steel?. Nature 1975;258:703–4.
36. Rieth PH, Reed JS, Naumann AW. Fabrication and flexural strength of ultra-fine grained yttria-stabilised zirconia. Bull Am Ceram Soc 1976;55:717.

37. Gupta TK, Bechtold JH, Kuznickie RC, Cadoff LH, Rossing BR. Stabilization of tetragonal phase in polycrystalline zirconia. J Mater Sci 1978;13:1464.

38. Piconi C, Maccauro G. Zirconia as a ceramic biomaterial. Biomaterials 1999;20:1–25.

39. Christel P, Meunier A, Heller M, Torre JP, Cales B, Peille CN. Mechanical Properties and short-term in-vivo evaluation of Yttrium-Oxide-Partially-Stabilized Zirconia. J Biomed Mater Res 1989;23:45–61.

40. Sandhaus S, Pasche H. Tenon radiculaire en zircone pour la realisation d'inlay-cores tout ceramiques. Tribune dentaire 1994;2:2–17.

41. Piconi C. Proprietà della zirconia. In: Piconi C, Rimondini L, Cerroni L, editors. La Zirconia in Odontoiatria. Milano: Elsevier Masson; 2008. p. 16–43.

42. Miani C, Piconi C, Piselli D, Ponti M. Prove sperimentali in vivo della zirconia in implantologia orale. Riv Ital Osseoint 1994;106:605–14.

43. Akagawa Y, Ychigawa Y, Nikai H, Tsuru H. Interface histology of unloaded and early loaded partially stabilized zirconia endosseous implants in initial bone healing. J Prosthet Dent 1993;69:599–604.

44. ISO TC150 Implants for Surgery - Ceramic materials based on yttria-stabilized tetragonal zirconia (Y-TZP), ISO 13356. Geneva: International Organization for Standardization. 1997.

45. American Society for Testing and Materials, SC F04 on medical and surgical materials and devices. Standard specification for high-purity dense yttria tetragonal zirconium oxide polycrystal (Y-TZP) for surgical implant applications, ASTM F-1873. West Conshohoken, American Society for Testing and Materials. 1998.

46. American Society for Testing and Materials, SC F04 on medical and surgical materials and devices. Standard specification for high-purity dense magnesia partially stabilized zirconia (Mg-PSZ) for surgical implant applications, ASTM F-2393. West Conshohoken, American Society for Testing and Materials. 2004.

47. Lange FF. Transformation toughening. J Mater Sci 1982;17:225–63.

48. Becher BF, Francis Rose LR. Toughening mechanisms in ceramic systems. In: Swain MV, editor. Structure and properties of ceramics, Material science and technology, Vol 11. New York: VCH; 1998. p. 410–61.

49. Hannink RHJ, Kelly PM, Muddle BC. Transformation toughening in zirconia containing ceramics. J Am Ceram Soc 2000;83:461–87.

50. Kelly JR, Denry IL. Stabilized zirconia as a structural ceramic: an overview. Dent Mater 2008;24:289–98.

51. Hannink RJH, Howard CJ, Kisi EH, Swain RW. Relationship between fracture toughness and phase assemblage in Mg-PSZ. J Am Ceram Soc 1994;77:571–9.

52. Guazzato M, Albakry M, Ringer SP, Swain MV. Strength, fracture toughness and microstructure of a selection of all-ceramic materials. Part II – zirconia based dental ceramics. Dent Mater 2004;20:449–56.

53. Kobayashi K, Kuwajima H, Masaki T. Phase change and mechanical properties of ZrO_2-Y_2O_3 solid electrolyte after aging. Solid State Ionics 1981;3–4:461–87.

54. Sato T, Shimada M. Transformation of yttia-doped tetragonal ZrO_2 polycrystals by annealing in water. J Am Ceram Soc 1985;68:356–9.

55. Yoshimura M, Noma T, Kawabata K, Somiya S. Role of H_2O on the degradation process of Y-TZP. J Mater Sci Lett 1987;6:465.

56. Chevalier J, Cales B, Drouin JM. Low temperature aging of Y-TZP ceramics. J Am Ceram Soc 1999;82:2150–4.

57. Lu HG, Chen S-Y. Low temperature aging of t-ZrO_2 polycrystals with 3 mol.% Y2O3. J Am Ceram Soc 1987;70:537–41.

58. Tsubakino T, Sonoda K, Nozato R. Martensite transformation behavior during isothermal ageing in partially stabilized zirconia polycrystals by annealing in water. J Mater Sci Lett 1993;12:193–6.

59. Deville S, Chevalier J, Gremillard L. Influence of surface finish and residual stress on the ageing sensitivity of biomedical grade zirconia. Biomaterials 2006;27:2186–92.

60. Kosmać T, Oblak Č, Jevnikar P, Funduk N, Marion L. Strength and reliability of surface treated Y-TZP dental ceramics. J Biomed Mater Res (Appl. Biomater.) 2000;53:304–13.

61. Rekow DE, Thompson VP. Near surface damage–a persistent problem in crowns obtained by computer-aided design and manufacturing. Proc Inst Mech Eng [H] 2005;219:233–43.

62. Kosmać T, Oblak Č, Marion L. The effect of dental grinding and sandblasting on ageing and fatigue behavior of dental zirconia (Y-TZP) ceramics. J Eur Ceram Soc 2008;28:1085–90.

63. Ross IM, Rainforth WM, McComb DW, Scott AJ, Brydson R. The role of trace addition of alumina to yttria-tetragonal zirconia polycrystals (Y-TZP). Scripta Mater 2001;45:653–60.

64. Boutz NMR, Winnubst AJA, Van Langerak B, et al. The effect of ceria co-doping on chemical stability and fracture toughness of Y-TZP. J Mater Sci 1995;30:1854–62.

65. Lawson S, Gill M, Smith JM, Dransfield GP, Egerton TA, McColgan P. Ageing studies of novel Y-TZPs. In: Duran P, Fernandez JF, editors. Third Euro-Ceramics - Vol 3, Bioceramics. Proc of the 3rd intl. Symp of the European Ceramic Society. Faenza: Faenza Editrice; 1993. p. 507–12.

66. Piconi C, Burger W, Richter HG, Vatteroni R, Cittadini A, Boccalari M. New Y-TZP powders for biomedical applications. J Mater Sci Mater Med 1997;8:113–8.

67. Eide R, Tvinnerheim HM, Höl PJ. Different yttrium stabilized zirconium oxide core have different element contents. International Association for Dental Research–Pan European Federation Meeting. Sept 13–16, 2006 , Dublin: Ireland. Dental Material Poster Session I, poster 13, <http://iadr.confex.com/iadr/pef06/preliminaryprogram/index.html>.

68. Hopf Th, Hopf Ch, Glöbel B. About radioactivity of some PMMA bone cements. Acta Orthop Bel 1990;56:443–4.

69. Hopf Th, Sherr O, Glöbel B, Hopf Ch. Vergleichende tierexperimentelle Untersuchung zur Gewebsveträglichkeit und Messungen der radioaktiviät vershiedener Rötgenkontrastmittel. Z Orthop 1989;127:620–4.

70. Calès B, Peille CN. Radioactive properties of ceramic hip joint heads. In: Heimke G, editor. Bioceramics 2: Proc of the 2nd Intl. Symp. on Ceramics in Medicine. Köln: Deutsche Keramische Gesellschaft; 1990. p. 152–9.

71. Capannesi G, Piconi C, Sedda AF, Greco F. Radioactivity measurements of zirconia powders. In: Ravaglioli A, Krajewski A, editors. Bioceramics and the human body. Amsterdam: Elsevier; 1992. p. 211–6.

72. Burger W, Cittadini A, Bossi D, Boccalari M, Piconi C, Vatteroni R. The relevance of zirconia purity in biomedical applications. In: Abstracts & transactions of 11th European Conf. on Biomaterials, Pisa, Italy, 10–14 September 1994. European Society for Biomaterials, p.177–9.

73. Piconi C, Casarci M. Purification of chemicals for the production of biomedical grade Y-TZP ceramics. In: Rammlair D, Mederer J, Oberthur RB, Petinghaus H, editors. Applied mineralogy. Rotterdam: Balkema; 2000. p. 205–7.

74. Porstendörfer J, Reineking A, Willert H-G. Radiation risk estimation based on activity measurements on zirconium oxide implants. J Biomed Mater Res 1996;32:663–7.

75. Fischer-Brandies E, Pratzel H, Wendt T. Zur Radioaktivitaten Belastung durch Implantate aus Zirkonoxid. Dtsch Zahnärztl 1991;46:688–90.

76. Mackert JR. Side-effects of dental ceramics. Adv Dent Res 1992;6:90–3.

77. Caropreso S, Cerroni L, Piconi C, Condò SG. Porcellane dentali: radiattività degli agenti luminofore dei rinforzanti strutturali. Odontostomatologia 1996;22:396–403.

78. Veronese I, Guzzi G, Giussani A, Cantone MC, Ripamonti D. Determination of dose rates from natural radionuclides in dental materials. J Environ Radioactivity 2006;91:15–26.

79. Heffernan MJ, Aquilino SA, Diaz-Arnold A, Haselton DR, Stanford CM, Vargas MA. Relative translucency of six all-ceramic systems. Part I: Core materials. J Prost Dent 2002;1:4–9.

80. Mutone V. Estetica su zirconia–proprietà ottiche. In: Piconi C, Rimondini L, Cerroni L, editors. La Zirconia in Odontoiatria. Milano: Elsevier Masson; 2008. p. 182–3.

81. Baldissara P, Liukacej A, Ciocca L, Valandro FL, Scotti R. Translucency of zirconia copings made with different CAD/CAM systems. J Prost Dent 2010;104:6–12.

82. Calés B. Colored zirconia ceramics for dental applications. In: LeGeros RZ, LeGeros JP, editors. Bioceramics 11: Proc of the 11th Intl. Symp. on Ceramics in Medicine. New York: World Scientific Publ; 1998. p. 591–4.

83. Shah K, Holloway J, Denry IL. Effect of coloring with various metal oxides on the microstructure, color, and flexural strength of 3Y-TZP. J Biomed Mater Res: Appl Biomater 2008;87B:327–37.

84. Cerroni L. Biocompatibilità. In: Piconi C, Rimondini L, Cerroni L, editors. La Zirconia in Odontoiatria. Milano: Elsevier Masson; 2008. p. 46–61.

85. Satoh Y, Niwa S. Tissue-biomaterial interface characteristics of zirconia ceramics. In: Hulbert JE, Hulbert SF, editors. Bioceramics 3: Proc of the 3rd Intl. Symp. on ceramics in medicine. Terre Haute: Rose–Hulman Inst. of Technology; 1990. p. 101–8.

86. Covacci V, Bruzzese N, Maccauro G, et al. In vitro evaluation of the mutagenic and carcinogenic power of high purity zirconia ceramics. Biomaterials 1999;20:371–6.

87. Hisbergues M, Vendeville S, Vendeville S. Zirconia: established facts and perspectives for a biomaterial in dental implantology.

88. Claussen N. Microstructural desin of zirconia toughened cramics (ZTC). In: Claussen N, Ruhle M, Heuer AH, editors. Science and technology of zirconia II (Advances in ceramics, Vol.12). Columbus: The American Ceramic Society; 1994. p. 325–51.

89. Rieu J, Goeuriot P. Ceramic composites for biomedical applications. Clin Mater 1993;12:211–7.

90. Fassina P, Zaghini N, Bukat A, Piconi C, Greco F. Bioceramics by gel precipitation (GSP) process. In: Vincenzini P, editor. ceramics in substitutive and reconstructive surgery (Materials Science Monographs, 69). Amsterdam: Elsevier; 1991. p. 3–14.

91. Salomoni A, Tucci A, Esposito L, Stamenkovich I. Forming and sintering of multiphase bioceramics. J Mater Sci Mater Med 1994;5:651–3.

92. Burger W, Richter HG. High strength and toughness alumina matrix composites by transformation toughening and "in situ" platelet reinforcement (ZPTA). Key Eng Mater 2001;192–195:545–8.

93. Magnani G, Brillante A. Effect of the composition and sintering process on mechanical properties and residual stresses in zirconia-alumina composites. J Eur Ceram Soc 2005;25:3383–92.

94. Nawa M, Bamba N, Sekino T, Niihara K. The effect of TiO_2 aadition on Strengthening and toughening in intragranular type of 12Ce-TZP/Al_2O_3 nanocomposites. J Eur Ceram Soc 1998;18:2–219.

95. Kohal RJ, Wolkewitz M, Müller C. Alumina-reinforced zirconia implants: survival rate and fracture strength in a masticatory simulation trial. Clin Oral Implants Res 2010;21:1345–52.

96. Tanaka K, Tamura J, Kawanabe K, Nawa M, Oka M, Uchida M, et al. Ce-TZP/Al_2O_3 nanocomposite as a bearing material in total joint replacement. Biomed Mat Res Part B: Appl Biomater 2002;53B 2622–270.

97. Ban S, Sato H, Suehiro Y, Nakanishi H, Nawa M. Biaxial flexure strength and low temperaturae degradation of Ce-TZp/Al$_2$O$_3$ nanocomposite and Y-TZP as dental restoratives. Biomed Mat Res Part B: Appl Biomater 2008;87B:492–8.

98. Nordlund A, Zetterqvist L, Oden A. A comparative experimental investigation in monkeys between three different implant materials. Int J Oral Maxillofac Surg 1989;18:373–7.

99. Yamashita D, Machigashira M, Miyamoto M, et al. Biocompatibility of zirconia with osteoblast-like cells. In: Kim S, editor. Bioceramics 22. Seoul: The Korean Society for Biomaterials; 2009. p. 337–40.

100. Setzer B, Bächle M, Metzger MC, Kohal RJ. The gene-expression and phenotypic response of hFOB 1.19 osteoblasts to surface modified titanium and zirconia. Biomaterials 2009;30:979–90.

101. Maccauro G, Bianchino G, Sangiorgi S, et al. Development of a New zirconia-toughened alumina: promising mechanical properties and absence of in vitro carcinogenicity. Int J Immunipathol Pharmacol 2009;22:773–9.

102. Wegner SM, Kern M. Long-term bond strength to zirconia ceramic. J Adhesive Dent 2000;2:139–47.

103. Kern M. Clinical long term survival of two-retainer and single-retainer all-ceramic resin bonded fexed partial dentures. Quintessence Int 2005;36:141–7.

104. Della Bona A, Anusavice KJ. Microstructure, composition, and etching topography of dental ceramics. Int J Prosthodont 2002;15:159–67.

105. Blatz M, Sadan A, Kern M. Resin-ceramic bonding: a review of the literature. J Prosthet Dent 2003;89:268–74.

106. Wang H, Aboushelib MN, Feilzer AJ. Strength influencing variables on CAD/CAM zirconia frameworks. Dent Mater 2008;24:633–8.

107. Wegner SM, Kern M. Long-term bond strength to zirconia ceramic. J Adhesive Dent 2000;2:139–47.

108. Matinlinna JP, Lassila LVJ, Vallittu P. Pilot evaluation of resin composite cement adhesion to zirconia using a novel silane system. Acta Odontol Scand 2007:44–51.

109. Lohbauer U, Zipperle M, Rischka K, Petschelt A, Muller FA. Hydroxylation of dental zirconia surfaces: Characterization and bonding potential. J Biomed Mater Res Part B: Appl Biomater 2008;87B:461–7.

110. Piascik JR, Swift EJ, Thompson JY, Grego S, Stoner BR. Surface modification for enhanced silanation of zirconia bonding. Dent Mater 2009;25:1116–21.

111. Derand T, Molin M, Kvam K. Bond strength of composite luting cement to zirconia ceramic surfaces. Dent Mater 2005:1158–62.

112. Phark JH, Duarte S, Blatz M, Sadan A. An in vitro evaluation of the long-term resin bond to a new densely sintered high-purity zirconium-oxide ceramic surface. J Prosthet Dent 2009;101:29–38.

113. Aboushelib MN, Kleverlaan CJ, Feilzer AJ. Selective infiltration etching technique for a strong and durable bond of resin cements to zirconia based materials. J Prosthet Dent 2007;98:379–88.

114. Krnel K, Kocjan A, Kosmač T. A simple method for the preparation of nanostructured aluminate coatings. J Am Ceram Soc 2009;92:2451–4.

115. Jevnikar P, Krnel K, Kocjan A, Funduk N, Kosmac T. The effect of nano-structured alumina coating on resin-bond strength to zirconia ceramics. Dent Mater 2010;26:688–96.

116. Zhang SC, Kocjan A, Lehmann F, Kosmac T, Kern M. Influence of contam-ination on resin bond strength to nano-structured alumina-coated zirconia ceramic. Eur J Oral Sci 2010;118:396–403.

117. Jevnikar P, Golobic M, Kocjan A, Kosmac T. The effect of nano-structured alumina coating on the bond strength of resin-modified glass ionomer cements to zirconia ceramics. J Eur Ceram Soc: 2641–2645.

Dental Glasses and Glass-ceramics

Simon Jegou Saint-Jean

Contents

12.1 INTRODUCTION

Glasses and glass-ceramics are important materials used in restorative dentistry thanks to their biocompatibility, excellent aesthetic properties, good mechanical strength, and relative ease of use. Depending on their chemical, physical, and optical properties, these ceramics can be used as inlays; onlays; veneers; partial or full crowns and bridges bonded to natural teeth or to implant abutments. In addition to biocompatibility, dental glass-ceramics must match or exceed the properties of natural teeth in terms of aesthetics, mechanical strength, wear, and chemical durability in the oral environment.

Modern aesthetic restorative dentistry owes a lot to the unraveling of centuries old secrets of the Chinese potters. Although a porcelain type similar to translucent Chinese porcelain was already produced in some European countries (e.g. in Dresden at the Meissen factory), historically, it was the French

Jesuit missionary Father d'Entrecolles, who in 1717 discovered the secrets of porcelain handcrafting during a mission in King-te-Tching, at that time the porcelain center of China. This led to identification of the components and proportions used by the Chinese potters, namely the common minerals kaolin (50%), feldspar (25–30%), and silica (20–25%). The first dental application was made in 1774 by the French pharmacist Alexis Duchateau and the French dentist Nicolas Dubois de Chemant, with the help of porcelain manufacturers at the Guerhard factory in Saint-Germain-en-Laye. Duchateau, who wanted to replace his ivory denture and who had noticed the particular hardness and chemical resistance of the porcelain utensils he was using, succeeded in making himself the first porcelain denture. Since then, the composition of denture porcelain has been modified by substituting kaolin for feldspar in order to increase translucency. Porcelain dentures are still used today, although the denture base and the whole denture are progressively being replaced with poly(methyl methacrylate) (PMMA).

Seventy years or so later, in 1837, Stockton was the first to manufacture a porcelain tooth. He was followed in 1889 by Charles H. Land, who developed and patented the all-porcelain jacket crown that was further developed and used until the 1950s. To improve the fracture strength, in the 1950s porcelain restorations were reinforced with a metal substructure on which the porcelain was fused (Abraham Weinstein). These porcelain-fused-to-metal restorations (PFM) have been extensively used since then with continuously improved aesthetics and quality, and have demonstrated excellent clinical performance. Although there are some obvious aesthetic disadvantages with using metal frameworks (such as opacity, unaesthetic metal rings at the tooth margin, and grayish appearance of the gums), PFMs are still considered to be the gold standard in terms of reliability and still account today for about 80% of the total crown restorative market.

The resurgence of all-ceramic restorations came in 1965 with McLean & Hugues, who reinforced feldspathic porcelain with a large volume fraction (up to 50%) of fine alumina crystals that allowed its use as a dental core material further veneered with an aesthetic porcelain.[1] Additional efforts in the direction of polycrystalline ceramics led to the development by Sadoun[2] of a slip-casted porous alumina core infiltrated with an aesthetic lanthanum glass (In-Ceram®; 1987, Vita, Bad Säckingen, Germany) and later on to the introduction by Andersson & Odén in 1993 (Procera®; Nobel Biocare, Kloten, Switzerland) of pure polycrystalline alumina as a dental core further veneered with an aesthetic porcelain.[3] On the front of purely glass-ceramic materials, the first introduction of strong monolithic dental cores had to wait until 1984 and the introduction of the castable (and later the machinable) mica glass-ceramic Dicor® (Dentsply International, York, PA, USA),[4] which was the result of considerable effort by Corning Glass Works (Corning Inc., NY, USA) in the 1950s to develop glass-ceramics. This castable glass-ceramic was abandoned because it was associated with complicated and timely manufacturing

procedures in the dental lab. This left it open to heat-pressable ceramics that were not only easier to process, but were also more reliable. Such important pressable ceramics are the leucite glass-ceramics (e.g. IPS Empress®; Ivoclar, Schaan, Liechtenstein),[5] and the lithium disilicate glass-ceramics (IPS Empress® II, IPS e.max®; Ivoclar, Schaan, Liechtenstein).[6]

In Section 12.2 of this chapter, the different types of glasses and glass-ceramics will be presented and classified as a function of their microstructure and physical and chemical properties from which the clinical applications are derived. Only the most commonly used dental ceramics and those of historical interest will be described. These ceramics consist of the feldspathic porcelains, the reinforced feldspathic porcelains, the fluormica glass-ceramics, the leucite glass-ceramics, the lithium disilicate glass-ceramics, and the apatite glass-ceramics. Glass-infiltrated oxide ceramics of the In-Ceram® type will only be briefly described because they don't really fit into this classification, although they still represent important glass-based materials used in restorative dentistry. The properties and clinical applications of the different glass-ceramics will be summarized in a table at the end of this section (Table 12.1). In Section 12.3, the limits and challenges experienced with glass-ceramic restorations will be addressed and discussed. Finally, in Section 12.4, current and possible future developments will be presented and proposed before drawing general conclusions at the end of the chapter.

12.2   CLASSES OF DENTAL GLASS-CERAMICS

12.2.1   Feldspathic Porcelains

Feldspathic porcelain is an aluminosilicate glass derived from the ternary system $K_2O–Al_2O_3–SiO_2$ (see Figure 12.1). It is made from melting mixtures of pure natural feldspars (orthoclase $K_2O.Al_2O_3.6SiO_2$ and albite $Na_2O.Al_2O_3.6SiO_2$), kaolin $(Al_2O_3.SiO_2.2H_2O)$, quartz (SiO_2), and metal oxide additives. A typical composition of a feldspathic porcelain is 52–62 wt.% SiO_2, 11–16 wt.% Al_2O_3, 9–11 wt.% K_2O, 5–7 wt.% Na_2O, and additives.[7] Feldspathic porcelain gets its glassy structure from the melting of feldspar. Its amorphous structure consists of a disordered network of polymer-like chains made of silica tetrahedra linked together by sharing common oxygen atoms. The length of the chains is dependent on the chemical composition of the glass. These chains can be tuned by varying the proportions of starting minerals and by adding metal oxide modifiers that help break down the silica chains during melting. Shortening of the Si-O chains has the effect of increasing the fluidity of the melt, and of reducing its fusing temperature.

Traditional porcelain is a high- to medium-fusing porcelain (above 1300°C). The emergence in the 1950s of PFM crowns triggered the development of low-fusing porcelain formulations (850–1100°C) that permitted their fusion onto metal alloy substructures. This was achieved by introducing into the glass mixture, oxides of alkali and alkaline earth metals, such as potassium,

TABLE 12.1 Types of Dental Ceramics

Material	Crystalline Phase	Processing Method	Physical Properties	Clinical Indication
Feldspathic porcelain	Amorphous glass	Powder slurries for the layering and firing technique	σ: 60–70 MPa; K_{Ic}: 0.92–1.26 MPa.m$^{1/2}$; E: 70 GPa; H: 6 GPa; CTE: varying depending on application	Resin-bonded laminate veneers and veneering of metallic and ceramic cores
Reinforced feldspathic porcelain (aluminous, leucite, fibers)	Alumina, leucite, fibers	Powder slurries for the layering and firing technique Hot press	σ: 120–150 MPa; K_{Ic}: 1.5 MPa.m$^{1/2}$; CTE: 16.0–17.3 $\times$ 10^{-6}K^{-1} (multi-indication alloys); CTE: 13.8–15.2 $\times$ 10^{-6}K^{-1} (high gold content, reduced precious metal content, palladium-based and non-precious metal alloys); CTE: 16.0–17.5 $\times$ 10^{-6}K^{-1} (gold-palladium-silver alloys); CTE: 7.2–7.9 $\times$ 10^{-6}K^{-1} (alumina, spinell, and zirconia glass-infiltrated ceramics); CTE: 9.0–10.5 $\times$ 10^{-6}K^{-1} (zirconia)	Resin-bonded laminate veneers and crowns, veneering of multi-unit bridges
Fluormica glass-ceramic (tetrasilicic mica) (Dicor®) (Dicor® MGC (light/dark))	$K_2Mg_5Si_8O_{20}F_4$	Castable CAD/CAM	σ: 150 MPa, K_{Ic}: 1.4–1.5 MPa.m$^{1/2}$; H: 362 MPa (Knoop), E: 70.3 GPa; CTE: 7.2 $\times$ 10^{-6}K^{-1}; S: 127/147 MPa; K_{Ic}: 1.4–1.5 MPa.m$^{1/2}$; H: 3.3–3.5 GPa (Knoop); E: 68 GPa; CTE: 6.4 $\times$ 10^{-6}K^{-1}	Resin-bonded laminate veneers, anterior crowns, posterior inlays
Leucite glass-ceramic (IPS Empress® Esthetic and IPS Empress® CAD)	KAlSi2O6 (tetragonal phase)	Hot press CAD/CAM	σ: 160 MPa; K_{Ic}: 1.3 MPa.m$^{1/2}$; H: 6.2 GPa (Vickers), E: 65 GPa; CTE: 16.6 $\times$ 10^{-6}K^{-1} (100–400°C); CTE: 17.5 $\times$ 10^{-6}K^{-1} (100–500°C)	Resin-bonded laminate veneers, inlays, onlays, and crowns

(Continued)

TABLE 12.1 (Continued)

Material	Crystalline Phase	Processing Method	Physical Properties	Clinical Indication
Lithium disilicate glass-ceramic (IPS emax®)	$Li_2Si_2O_5$	Hot press CAD/CAM	σ: 360/400 MPa; K_{Ic}: 2.25/2.75 MPa. $m^{1/2}$; H: 5.8 GPa (Vickers); E: 95 GPa; CTE: $10.2 \times 10^{-6} K^{-1}$ (100–400°C). CTE: $10.5 \times 10^{-6} K^{-1}$ (100–500°C)	Resin-bonded laminate veneers, inlays and onlays, crowns, bridges in the anterior region up to premolars
Fluorapatite glass-ceramic (IPS e.max® Ceram)	$Ca_5(PO_4)_3F$	Powder slurries for the layering and firing technique	σ: 90 MPa; H: 5.4 GPa Vickers; CTE: $9.5 \times 10^{-6} K^{-1}$ (100–400°C)	Resin-bonded laminate veneers, veneering of lithium disilicate glass-ceramic and zirconia frameworks
Glass-infiltrated spinell (Vita In-Ceram® Spinell)	$MgAl_2O_4$	Slip casting CAD/CAM	σ: 400 MPa; K_{Ic}: 2.7 MPa.$m^{1/2}$; E: 185 GPa; CTE: $7.7 \times 10^{-6} K^{-1}$	Inlays and anterior crowns
Glass-infiltrated alumina (Vita In-Ceram® Alumina)	Al_2O_3 (hexagonal phase)	Slip casting CAD/CAM	σ: 500 MPa; K_{Ic}: 3.9 MPa.$m^{1/2}$; E: 280 GPa; CTE: $7.4.10^{-6} K^{-1}$	Laminate cores, crowns, abutments, anterior bridges
Glass-infiltrated zirconia (Vita In-Ceram® Zirconia)	ZrO_2 (yttria-stabilized tetragonal phase)	Slip casting CAD/CAM	σ: 600 MPa; K_{Ic}: 4.4 MPa.$m^{1/2}$; E: 258 GPa; CTE: $7.8.10^{-6} K^{-1}$	Anterior and posterior crowns and bridges
Pure alumina (corundum)	Al_2O_3 (hexagonal phase)	CAD/CAM	σ: 500–700 MPa; K_{Ic}: 4.5 MPa.$m^{1/2}$; E: 270–380 GPa; H: 12 GPa; CTE: $7.10^{-6} K^{-1}$	Laminate cores, crowns, 4-unit bridges
Yttria-stabilized tetragonal zirconia polycrystals (3Y-TZP)	ZrO_2 (yttria-stabilized tetragonal phase)	CAD/CAM	σ: 900–1400 MPa; K_{Ic}: 6-10 MPa.$m^{1/2}$; E: 205–210 GPa; H: 13.9 GPa; CTE: $10.5.10^{-6} K^{-1}$	Laminate cores, anterior and posterior crowns and bridges, abutments and implant bridges

(Continued)

TABLE 12.1 (Continued)

Material	Crystalline Phase	Processing Method	Physical Properties	Clinical Indication
Enamel	≈ 90% $Ca_5(PO_4)_3OH$ (hydroxyapatite)		σ: 261–288 MPa (10 MPa if not supported by dentin); K_{Ic}: 0.6–1.5 MPa. $m^{1/2}$; E: 70–100 GPa; H: 3–5 GPa.	
Dentin	≈ 70% $Ca_5(PO_4)_3OH$ (hydroxyapatite)		σ: 232–305 MPa; K_{Ic}: 3.1 MPa.$m^{1/2}$; E: 15–30 GPa; H: 0.6 GPa.	

Abbreviations: σ, flexural strength; K_{Ic}, fracture toughness; H, hardness; E, Young's modulus; CTE, coefficient of thermal expansion.
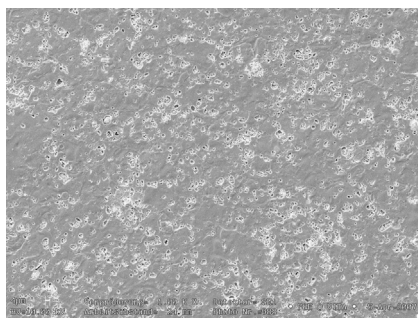
FIGURE 12.1   SEM micrograph of an etched commercial feldspathic porcelain showing the fine distribution of leucite crystals in the glass phase (VITA VM® 9). *(Courtesy of Michael Tholey, Vita, Bad Säckingen, Germany)*

sodium, lithium, calcium, magnesium, and barium, that disrupt the cross-link-ages of the Si-O 3D network and also act as fluxing agents that increase the flowability of the melted glass. Furthermore, the coefficient of thermal expansion (CTE) of the glass can be adjusted by varying the proportions of metal oxide additives in order to match the CTE of the underlying substructure. It is actually desirable that the veneering porcelain has a slightly lower CTE than the substructure, in order to put the glass under little compression and the substructure into tension, which is beneficial for the strength of the veneer bonding. In the case of veneering of metal substructures, the CTE of the glass has to be increased. To achieve a higher CTE of the glass, components with high CTE have to be chosen in large quantitities. Such components are the metal oxides Na_2O, K_2O, Al_2O_3. In contrast, glasses that contain a high con-tent of alkaline earth oxides (MgO, Li_2O, ZnO, and CaO) have a lower CTE.[8]

Another efficient way to increase the CTE of the feldspathic glass is to add crystals of tetragonal leucite, which has a high CTE ($22 \times 10^{-6}\,K^{-1}$). The leucite-containing feldspathic porcelains are used as veneering materials for metal and ceramic frameworks or as reinforced resin-bonded glass-ceramic cores (see Sections 12.2.2 and 12.2.4). Typical CTE values of veneering porcelains for the metallic and ceramic substructures are given in Table 12.1.

Feldspathic glass is produced by melting at high temperature (1200–1600°C) a mixture of finely grained raw materials and quenching the molten glass in cold water to break it up into small fragments called frit. This operation can be repeated several times in order to obtain a homogeneous frit. The frit is subsequently ground into fine glass particles, typically around 25 μm, to be further blended with an aqueous or organic liquid and polymeric binders to form a powder slurry. The powder slurry is applied on a refractory die coated beforehand with a thin platinum foil, or applied directly on a dental core and placed in a dental furnace for the first densification by careful evaporation of the liquid. The porcelain layer is subsequently heated slowly to burn out the binder, fired at temperatures from 750 to 950°C (at which point the glass particles soften and coalesce to form a dense part), and finally cooled slowly to avoid cracking and crazing. The heating process is normally performed under vacuum to remove pores and entrapped air bubbles that can reduce the strength of the restoration. After construction of the dental restoration, a glaze is further fused onto its outer surface at low temperature to produce an impervious, smooth and shiny surface.

These porcelains can be made in various tooth shades according to the widely used Vitapan Classical system (Vita, Bad Säckingen, Germany), and in different levels of opacity and translucency to mimic the optical properties of tooth dentine and enamel structures. This is achieved by adding metal oxide pigments to the starting glass powder or to the glass frit, typically, for example, TiO_2 for yellow-brown shades; MnO for lavender; Fe_2O_3 for brown and red; CoO for blue; and CuO or Cr_2O_3 for green. The opacity is achieved by the addition of very fine and homogeneously dispersed particles of CeO, TiO_2, ZrO_2, and SnO. Such opaque porcelains are conventionally used as a first opaque layer to mask the underlying metallic framework or discolored tooth, and are subsequently layered with dentine and enamel porcelains to give the final restoration a natural tooth color.

Unfortunately, feldspathic glasses are brittle. Also, their flexural strength is low (about 60–70 MPa). For that reason their clinical application is limited to low load-bearing anterior applications such as veneers resin-bonded to enamel and dentin, and veneering aesthetic porcelains fused onto stronger dental cores. There is an increasing variety of commercial aesthetic feldspathic porcelains, too many to list here.

12.2.2   Reinforced Feldspathic Porcelain

Several attempts have been made over the past few decades to improve the strength of feldspathic porcelains in order to expand their clinical use to dental

cores for anterior and posterior restorations. Typical methods for reinforcing porcelain ceramics are the creation of residual compressive stresses within the surface of the restoration–which are introduced, for instance, by thermal tempering (rapid cooling) or ionic exchange–or the addition of fine crystals that deflect and arrest crack propagation in the material.

In 1965, MacLean and Hugues were the first to develop stronger feldspathic porcelains by reinforcing the porcelain core with up to 50% alumina, thus yielding a dental core with a flexural strength of 120–150 MPa.[1] This core, further veneered with an aesthetic feldspathic porcelain, was commercialized by Vita under the brand name Vitadur® (Vita, Bad Säckingen, Germany), and was later (in 1976) improved by using a platinum metal foil as a substructure to further reinforce the restoration.[9,10] Since then, further developments have been carried out that incorporate, for instance, partly molten, fine-grained feldspars. Controlled heating is used for increased homogeneity (Vitablocs® Mark II; 1991, Vita, Bad Säckingen, Germany).[11] Also important has been reinforcing the porcelain materials with leucite crystals either added as a synthetic powder or grown through the incongruent melting of feldspar (e.g. Optec® HSP; 1989, Jeneric/Pentron Inc., Wallingford, CT, USA), and reinforcing the porcelain with fibers (Mirage™; 1989, Mirage™ Dental Systems, Chameleon Dental Products, KS, USA).[12] These last techniques have yielded feldspathic porcelains with strength of up to 150 MPa. Such porcelains exhibit sufficient strength to be used as resin-bonded veneers, inlays, onlays, crowns, and veneering materials with leucite-reinforced feldspathic porcelains being the most widely used (e.g. Vita VM series; Vita, Bad Säckingen, Germany).

The most remarkable addition to the field in stronger aesthetic dental ceramics came along with the development of glass-ceramics in the late 1950s by Corning Glass Works. Glass-ceramics materials represent a good compromise as they combine the aesthetic properties of glasses and the mechanical properties of crystalline ceramics. Glass-ceramics differ from feldspathic porcelains in that they contain more than 50 vol.% of fine and uniformly distributed crystals grown directly from the glass through a controlled crystallization process. This controlled nucleation and crystallization process involves a 2-stage heat treatment called 'ceraming.' A first heat treatment is carried out at a temperature slightly above the glass transition temperature (Tg) at which it is maintained for a sufficient period of time to nucleate a maximum number of crystals from the starting glass frit. In the second step, the nucleated glass is heated at a higher temperature and held for a certain time to allow for the growth of crystals of optimal size. The type of crystals; their microstructure and distribution in the glass; their nucleation and growth rates; the crystal volume fraction in the glass; as well as the physico-chemical properties of both the crystals and the remaining glass, influence critical properties of the restoration such as translucency; strength and toughness; machinability; and chemical durability. These properties can be controlled by proper adjustments of the chemical composition of the starting glass, and by careful study of each

step of the heat treatment schedule. Indeed, as the nucleation and crystallization process is time- and temperature-related, a careful evaluation of the DTA and thermal expansion curves; the X-ray diffraction data; and the SEM data, is critical to determining the most appropriate heat treatment for maximized crystal nucleation and growth.

The first dental glass-ceramic derived from the research of Corning Glass Works was a fluormica glass-ceramic with a flexural strength of 150 MPa (Dicor®; 1984, Dentsply International, York, PA, USA).[4] Dicor® was first available as a castable glass-ceramic ingot for manufacture in the lab using the lost wax technique, and later also as a machinable block (Dicor® MGC). Difficulties encountered in the lab with castable glass-ceramics led to the further development of heat-pressable glass-ceramics. The most important glass-ceramics, namely, mica glass-ceramics, leucite glass-ceramics, lithium disilicate glass-ceramics, and apatite glass-ceramics, will be presented in the next sections.

12.2.3 Fluormica Glass-ceramics

The very first dental glass-ceramic was developed by Grossman in 1972[13] and commercialized in 1984 by Dentsply International under the trademark Dicor® for the fabrication of resin-bonded anterior crowns, veneers, inlays, and onlays. Fluormica glass-ceramic consists of a 55% volume fraction of small block-like tetrasilicic fluormica platelets (1–2 µm large, 0.5 um thick) of the type $K_2Mg_5Si_8O_{20}F_4$ (Figure 12.2), and is characterized by high translucency, high chemical resistance, hardness similar to natural teeth, moderate thermal expansion, good machinability, and good flexural strength (ca 150 MPa).
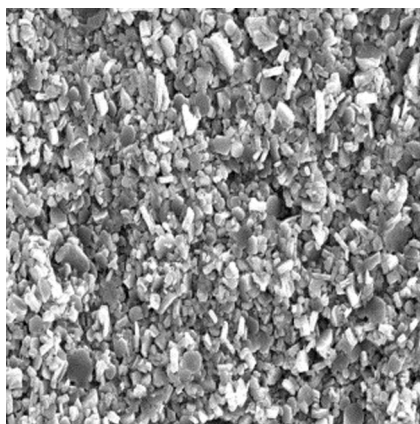
FIGURE 12.2   SEM micrograph of tetrasilicic fluormica glass-ceramic etched with ammonium bifluoride (Dicor® MGC-light, magnification ×2000 and field of view: 60 µm×60 µm). *(N.M. Jedynakiewicz, N. Martin, The effect of surface coating on the bond strength of machinable ceramics, Biomaterials, Volume 22, Issue 7, April 2001, Fig. 4, Pages 749–752.)*

Tetrasilicic mica glass-ceramic is produced from the base glass system K_2O–MgF_2–MgO–SiO_2. It is composed of 56–64 wt.% SiO_2, 15–20 wt.% MgO, 12–18 wt.% K_2O, 4–9 wt.% F, 0–2 wt.% Al_2O_3, 0–5 wt.% ZrO_2, and small amounts of CeO_2 to simulate the fluorescent character of natural teeth.[14] The high translucency is obtained thanks to a very fine crystallite size ($\approx 1\,\mu m$) and to a refractive index of the crystals matching that of the glass. Tetrasilicic mica is formed through a two-stage crystallization process that involves a glass-in-glass phase-separation mechanism. A first heating of the parent glass at 625°C for 1–6 hours induces a fine-scaled glass phase separation and formation of fine quasi-spherical mica grains. Upon further heating at 1000–1150°C for 1–8 hours, the mica grains recrystallize by grouping the fine-scale spherical mica grains into larger sizes of about 1–2 μm. Choice of the appropriate heating temperature, heating rate, and annealing time is critical for the development of fine crystals uniformly dispersed in the glassy matrix. Such fine microstructure is beneficial to the machinability, translucency, and strength of the mica glass-ceramic.

Dicor® was available in the form of both castable glass ingots and machinable CAD/CAM blocks for the Cerec® chairside system (Sirona Dental Systems Inc. NY, USA), and was recommended for inlays, onlays, and crowns. Restorations made of castable Dicor® were manufactured at the dental lab in a specially designed machine by melting the glass block at 1370°C for 6 minutes and subsequently centrifugally casting the melt for 4 minutes into a dental mold formed using the lost wax technique. Once divested, the cooled glass restoration was again invested and ceramed at 1075°C for 6 hours following a slow 1.5-hour temperature ramp-up to form the final glass-ceramic restoration. This was further glazed with a colored glass. The machinable version of Dicor® (Dicor® MGC) consisted of pre-ceramed blocks containing a higher volume fraction of the mica crystals (70%) but exhibiting the same properties as the castable version, although its translucency was slightly reduced. The good machinability of Dicor® MGC is due to its mica sheet structure along which the glass-ceramic fractures upon machining. Several competing materials were developed at the same time: Cera Pearl® apatite glass-ceramic (Kyocera Corp, Kyoto, Japan),[15,16] and Olympus Castable Ceramic OCC® (Olympus Optical Co, Tokyo, Japan)[17] lithia-containing fluorphlogopite $NaMg_3(Si_2AlO_{10})F_2$ and beta spodumene crystals of $LiOAl_2O_{34}SiO_2$.

These castable glass-ceramics presented the disadvantage of shrinking during the ceraming procedure and had to be prepared in the dental lab, which resulted in a time-consuming work flow, high risk of product inhomogeneity, and poor margin fit as compared to PFMs. This led to their discontinuation. Instead, new heat-pressable glass-ceramics were developed that exhibited higher strength and were easier to process in the dental lab. The first developed pressable glass-ceramic was the high leucite-containing glass-ceramic IPS Empress I® (1986-1987, Ivoclar, Schaan, Liechtenstein), which was rapidly followed by a number of equivalent systems. For example: Optimum Pressable Ceramic OPC® (Jeneric/Pentron Inc., Wallingford, CT, USA); Finesse®

(Dentsply Inc., NY, USA); Authentic® (Jensen Dental, CT, USA); and PM™9 (Vita, Bad Säckingen, Germany). In 1998, stronger lithium disilicate glass-ceramics (IPS Empress II®, now IPS e.max®; Ivoclar, Schaan, Liechtenstein) entered the dental market as both pressable and machinable blocks.

12.2.4   Leucite Glass-ceramics

Leucite glass-ceramics are made by the controlled crystallization of leucite in the same ternary phase system (SiO_2–Al_2O_3–K_2O) as the conventional felds-pathic porcelains, but with a greater content K_2O of at least 12 wt.%. Leucite glass-ceramics consist of a 35–45% volume fraction of randomly shaped 1–5 μm crystals evenly and densely distributed in the glassy matrix and arranged like strings of beads along the glass grain boundaries (Figure 12.3). A typical composition of the commercial leucite glass-ceramic IPS Empress® is disclosed by Höland[7] as follows: 59–63 wt.% SiO_2, 19–23.5 wt,% Al_2O_3, 10–14 wt.% K_2O, 3.5–6.5 wt.% Na_2O, 0–1 wt.% B_2O_3, 0–1 wt.% CeO_2, 0.5–3 wt.% CaO, 0–1.5 wt.% BaO, and 0–0.5 wt.% TiO_2.

Tetragonal leucite ($KAlSi_2O_6$) nucleates and grows in the parent glass by a surface crystallization mechanism initiated at the surface of the glass construct and propagating inward toward the bulk. Therefore, to increase the density of the nuclei and insure a greater crystallization and homogeneous dispersion of the crystals throughout the glass-ceramic body, a finely grained starting glass powder needs to be used and compacted. In this manner, the crystals can nucleate and grow from each of the fine glass particles that further coalesce upon firing at 950°C to form an almost fully dense and homogeneous glass-ceramic block. To maximize the crystal growth rate, a second heat treatment is required at 1050°C, which yields a glass-ceramic with a flexural strength of 160 MPa. The quantity of crystals and the crystallization kinetics are determined by the chemical composition of the precursor glass and the heat treatment.
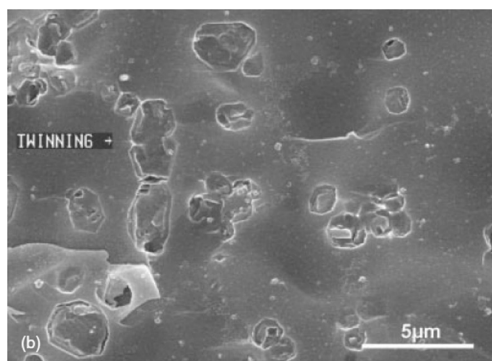
FIGURE 12.3   SEM micrograph of leucite glass-ceramic (IPS Empress®, etched in 2.5% hydrofluoric acid for 3 seconds). *(W. Höland, G.H. Beall, Glass-Ceramic Technology 2nd edition, John Wiley & Sons, Fig. 2.34b, Page 129)*
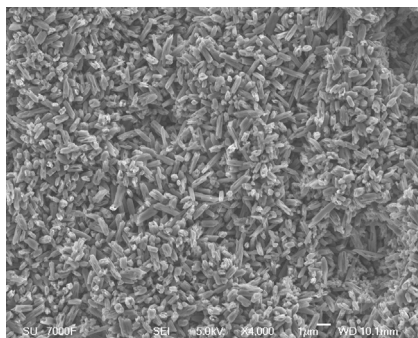
FIGURE 12.4   SEM micrograph of lithium disilicate glass-ceramic (etched in hydrofluoric acid for 15 seconds).

Adding components such as Na_2O, Li_2O, or LiF to the SiO_2-Al_2O_3-K_2O system lowers the fusion temperature of the glass and increases the rate of leucite crystallization. A large quantity of leucite crystals reinforces the glass by defecting and arresting the propagation of cracks. The residual glass with a CTE slightly lower than the leucite crystals are put in compression, which further enhances the strength of the glass-ceramic.

Leucite glass-ceramics present excellent aesthetics thanks to a high and adjustable translucency (crystals and glass have a similar index of refraction) and the possibility of coloring the glass in natural tooth shades through addition of metal oxide pigments. Although the strength of leucite glass-ceramics is as much as twice the strength of conventional feldspathic porcelains, it is still insufficient for posterior fixed dental prosthetics (bridges). Their applications span from resin-bonded laminate veneers; to inlays and onlays; and to anterior and posterior crowns.

12.2.5   Lithium Disilicate Glass-ceramics

Lithium disilicate glass-ceramics are derived from the SiO_2–Li_2O system that was first investigated by Stookey at Corning Glass Works in the 1950s. They consist of a large volume fraction of up to 70% fine rod-like entangled $Li_2Si_2O_5$ crystals, and a minor amount of lithium orthophosphate (Li_3PO_4) crystals that are randomly oriented and uniformly dispersed in the glassy matrix (Figure 12.4). A typical composition as disclosed by Ivoclar contains 57.0–80.0 wt.% SiO_2, 11.0–19.0 wt.% Li_2O, 0.0–13.0 wt.% K_2O, 0.0–11.0 wt.% P_2O_5, 0.0–8.0 wt.% ZrO_2, 0.0–8.0 wt.% ZnO, 0.0–5.0 wt.% Al_2O_3, 0.0–5.0 wt.% MgO, and 0.0–8.0 wt.% coloring oxides. P_2O_5 is a key component as it acts as a heterogeneous nucleating agent that promotes volume nucleation of the lithium silicate phases.

The mechanism of crystallization, as compared to leucite glass-ceramics, is a volume crystallization where the crystals nucleate and grow throughout

the glass. Crystallization of lithium disilicate is heterogeneous and can be achieved through two different processing routes, a two-stage or three-stage process, depending on whether the glass-ceramic is intended to be used as a machinable block for the CAD/CAM milling technique or as a pressable ingot for the lost wax hot pressing technique. In both cases, the parent glass is formed into glass blocks or ingots by pressure-casting into a steel mold, a glass melt of synthetic raw materials that contains quartz, lithium oxide, phosphor oxide, alumina, potassium oxide, and color-imparting oxides. Before cooling down to room temperature, the poured melt is transferred into a pre-heated furnace at 450–550°C to relax the glass block and avoid stress build-ups in the glass. At this stage, the glass block can be kept in the furnace at the same temperature for about 1 hour to initiate nucleation of the lithium silicate phases prior to carrying out the subsequent crystallization heat treatments. Alternatively, the glass blocks can also be prepared by compacting glass powder ground from the glass frit.

For the manufacture of restorations from machinable blocks (IPS e.max CAD) a three-stage crystallization process is used to precipitate lithium disilicate. In the first stage, a glass block is heated at 450–550°C for 5 min to 1 hour to form a maximum number of nuclei to ensure efficient crystal growth of metasilicate crystals. This first treatment can also be carried out during the cooling step as already mentioned. In the second stage, the glass block is heated at a temperature of 690–710°C for 10–30 min to form lithium metasilicate (Li_2SiO_3) crystals grown epitaxially from the nano-lithium orthophosphate nuclei and cooled down to room temperature. This intermediate metasilicate phase is present in a volume fraction of 40% and consists of evenly dispersed small platelet-shaped crystals of 0.2–1.0 μm that strengthen the glass to a flexural strength of about 130 MPa. This material (blue block) is still weak, but thanks to its microstructure it can be milled to form the desired dental part. In the third stage, after milling of the restoration into the desired shape, the material is heated at 850°C for 20–31 min in a dental porcelain furnace to precipitate the final strong lithium disilicate phase and some minor amounts of lithium orthophosphate crystals. This sintering step is associated with a 0.2% shrinkage accounted for in the CAD software. During this stage, the lithium metasilicate crystals fully react with the surrounding glass silica through a solid-state reaction to form small rod-like and interlocked 1.5 μm-long crystals of lithium disilicate in a volume fraction of up to 70%, which gives the glass-ceramic its high strength (360 MPa) and high fracture toughness (2.25 MPa.m½).[7,18,19]

For the manufacture of restorations using the lost wax hot pressing technique, a two-stage crystallization process is used to crystallize lithium disilicate. In the first stage, the glass ingot containing nuclei formed during the cooling step or pre-heating step is nucleated and crystallized to lithium disilicate in one single heat treatment at 750–850°C for about 2 hours. In the second stage, carried out in the dental lab, the crystallized ingot is hot pressed at

920°C to flow viscously into the dental mold made by the lost wax technique to form the desired restoration, and is held at this temperature for 5–15 min. This last hot pressing step yields 3 to 6 μm-long needle-like crystals of lithium disilicate in a volume fraction of about 70%. These elongated crystals, compared to the rod-like crystals formed in the sintered CAD/CAM material, are responsible for the slightly higher strength and fracture toughness of the pressable ceramic, 400 MPa and 2.75 MPa.m½, respectively.[20]

Thanks to a high flexural strength, relatively high fracture toughness, and a good and adjustable translucency, lithium disilicate glass-ceramics can be used as resin-bonded veneers, inlays, onlays, crowns, and 3-unit bridges up to the second premolar. The hot-press ingots and the CAD/CAM blocks are available in various colors (5 to 16 A-D Vita shades and 4 bleach shades) and four levels of translucency, namely high translucency (HT), medium translucency (MT), low translucency (LT), and high opacity (OH) that are controlled by the nanostructure of the crystals. Coloration is achieved by addition of metal oxides directly to the raw powder that is later dissolved in the glassy matrix. Such metal ions are V^{3+} (yellow), Ce^{4+} (yellow), and Mn^{3+} (brownish). The restoration can be further characterized with stains and glazed or veneered with a specific apatite aesthetic glass-ceramic using the cut-back technique.

To adapt to the specific chemistry and CTE of lithium disilicate glass-ceramics, a new type of glass-ceramic was developed by Ivoclar that contains fluorapatite crystals. This glass-ceramic is described in the following section.

12.2.6   Fluorapatite Glass-Ceramics

Nano-fluorapatite glass-ceramic IPS e.max® Ceram is a low-fusing aluminosilicate glass-ceramic especially designed to veneer IPS e.max® lithium disilicate IPS e.max Press® and CAD zirconia frameworks (Figure 12.5). It crystallizes through a mechanism of controlled volume crystallization resulting in different concentrations of nano-fluorapatite crystals with a diameter of 100 nm and a length of less than 300 nm; and micro-fluorapatite crystals with a diameter of 300 nm and a lengths of 2–5 μm.[7,21] The adjustable volume fraction in each of the two crystal types (the total amount of fluorapatite in the glass-ceramic is between 19 and 23 wt.%) allows for the control of translucency (amount of micro-crystals), brightness, and opalescence (amount of nano-crystals). A typical composition as disclosed by Ivoclar contains 60.0–65.0 wt.% SiO_2, 8.0–12.0 wt.% Al_2O_3, 6.0–9.0 wt.% Na_2O, 6.0-8.0 wt.% K_2O, 2.0–3.0 wt.% ZnO; and additions of CaO, P_2O_5, and F (2.0–6.0 wt.%), other oxides (2.0–8.5%); and pigments (0.1–1.5 wt.%).

IPS e.max® Ceram is available in the form of powdered bottles for the layering technique and comes in all classical Vita A-D shades, Chromascop® (Ivoclar's own shade system) and bleach shades. It is fired at 750–760°C without changing the morphology of the apatite crystals yielding a final strength of 90 MPa.
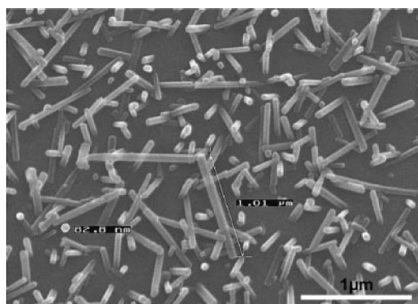
FIGURE 12.5   SEM micrograph of fluorapatite glass-ceramic (etched in 2.5% hydrofluoric acid for 10 seconds). *(W. Höland, G.H. Beall, Glass-Ceramic Technology 2nd edition, John Wiley & Sons, Fig. 3.23, Page 237)*
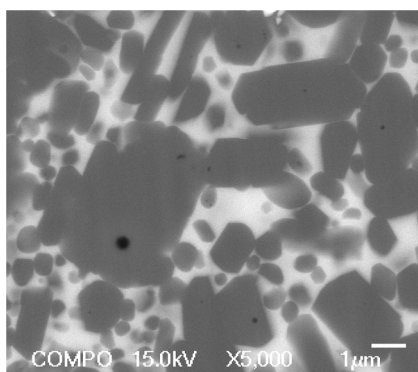
FIGURE 12.6   SEM micrograph of glass-infiltrated alumina (In-Ceram® Alumina).

12.2.7   Glass-infiltrated Oxide Ceramics

The glass-infiltrated oxide ceramic frameworks consist of a porous pre-sintered ceramic core that is subsequently infiltrated with a low-viscosity lanthanum aluminosilicate glass fired at 1100°C for 4–6 h (Figure 12.6). The ceramic core can be fabricated in the dental lab either by slip casting a ceramic powder slurry on a porous refractory die, or by milling out from a pre-fabricated CAD/CAM ceramic block made by powder dry-pressing. The latter fabrication method provides a more homogeneous framework after glass infiltration and consequently a higher strength. The In-Ceram® material is available in three variations subsequently veneered with an esthetic porcelain: a spinell core, an alumina core, or an alumina–zirconia core resulting in dental restorations with successively increasing bending strength and decreasing translucency, respectively (Table 12.1).

   Vita In-Ceram® Spinell consists of 78 vol.% magnesium aluminum oxide ($MgAl_2O_4$) and 22 vol.% infiltration glass. It exhibits the highest aesthetics of

the In-Ceram® range (most translucent), but also the lowest flexural strength and fracture toughness, 350 MPa and 2.7 MPa.m½, respectively. For that reason, Vita In-Ceram® Spinell is only recommended for inlays and anterior crowns.

Vita In-Ceram® Alumina was the first system launched on the market (1989). It consists of 75 vol.% polycrystalline alumina and 25% infiltration glass. It achieves a high strength of 400–500 MPa and a medium translucency that makes it suitable for anterior and posterior crowns, and bridges in the anterior area.

Vita In-Ceram® Zirconia is based on In-Ceram® Alumina (67 wt.%), with the addition of ceria-stabilized zirconia (33 wt.%). It consists of 56 vol.% polycrystalline alumina, 24 vol.% polycrystalline zirconia, and 20 vol.% infiltration glass. It is the strongest material of the In-Ceram® range, and exhibits a high strength of 700 MPa. Because it is opaque, it is recommended for crowns and 3-unit posterior bridges and offers the possibility of masking discolored teeth.

12.2.8   Summary Table

Table 12.1 summarizes all of this data.

12.3   LIMITATIONS AND CHALLENGES

Feldspathic porcelains are the materials of choice for the production of vivid dental restorations. Extensive research in this field has permitted the development of porcelain and glass-ceramic restorations with translucency, color, fluorescence, and opalescence that allow for a tooth-like appearance with natural shade and natural diffusion and reflection of light. Although PFMs and all-ceramic restorations do not last as long as full gold restorations, their undisputed aesthetics and acceptable lifespan (from 10 years up to the life of the patient, ~50 years) make them the gold standard in modern dentistry.

However, the main limitation with feldspathic porcelains and glass-ceramics is their relatively poor bending strength and fracture toughness, at least for applications in the posterior region. For that reason, several attempts have been made over the past decades to improve the fracture resistance. These methods have ranged from the use of finer-grained raw materials, improved glass manufacturing processes, improved heat treatment schedules, and reinforcement of the porcelain ceramics with crystals of alumina, fluormica, leucite, and lithium disilicate yielding ceramics with flexural strengths as high as 350 MPa. Although these improvements have contributed to expanding their range of indications to resin-bonded anterior and posterior crowns, the strength achieved by glass-ceramics is still not sufficient for their use as anterior multiple-unit bridges and posterior bridges (>3 units) for which a metal or ceramic core is needed. Additionally, a direct consequence of the limited strength of feldspathic porcelains and glass-ceramics is the necessity to prepare

all-ceramic crown restorations with a wall thickness that allows for sufficient fracture resistance to normal cycling loads (100–700 N at a frequency of about 1.5 Hz). Conventional practice dictates that feldspathic porcelain has to be applied with a minimum thickness of 1.0 mm on a metal, or a ceramic core of at least 0.5 mm to avoid fracture and chipping. This implies a total tooth reduction minimum of 1.5 mm in the occlusal region and 1.0 mm in the circular and marginal regions. This might not always be clinically possible if the vitality of the tooth must be preserved or if limited vertical space is available. Moreover, in the case of molars, the complex geometry of the occlusal surface imposes lower wall thicknesses in regions subjected to the highest loads, in particular, the central occlusal area. For these clinical cases, a full gold crown would be the best option, although it would not offer the expected aesthetics. A compromise can be found, for instance, by applying an aesthetic porcelain only in the circular region, if the clinical situation is favorable.

Another particular setback of feldspathic porcelains, which is also related to their limited strength, is their delamination, fracture, and surface chipping when veneered on stronger frameworks, in particular, zirconia frameworks. A systematic review performed by E. Pjeturson[22] on the performance of single crowns after an observation period of at least 3 years estimates a 5-year survival rate of 93.3% (i.e. the restoration remains in situ with or without modifications) for the all-ceramic restorations, and 95.6% for metal-ceramic crowns. Among the all-ceramic crowns, dense alumina crowns showed the highest survival rate with 96.4%. This was followed by reinforced glass-ceramics (various materials) with 95.4%, glass-infiltrated crowns (In-Ceram® types) with 94.5%, and finally, glass-ceramics (various materials) with 87.5%. For anterior crowns, the performance of all-ceramic crowns was equivalent to PFMs, whereas for posterior teeth, only the alumina and reinforced glass-ceramic crowns showed similar results to PFMs. The majority of the fractures reported with these all-ceramics crowns were actually fractures of the core, which accounted for 85% of the reported complications. The cumulative complication rate due to porcelain chipping was 3.7% as compared to 5.7% for PFMs. For veneered zirconia crowns, the published clinical data is limited since the use of zirconia in dentistry is relatively new. In another systematic review performed by E. Pjeturson[23] on all-ceramic FDPs (lithium disilicate glass-ceramic; glass-infiltrated alumina and zirconia; and zirconia) and metal-ceramic FDPs, no framework fracture was reported for the zirconia restorations, but chipping and extended fracture of the veneering porcelain was reported with a yearly incidence of 1.98% to 12.2% according to two different studies included in the review. This translates to an estimated 5-year cumulative rate of 10–60%. The 5-year incidence of porcelain chipping for the whole all-ceramic group was 13.6% with 4–8% for the lithium disilicate glass-ceramic FDPs (rate not reported for the In-Ceram® types). In comparison, the PFMs had the lowest cumulative chipping with 2.9%. With regard to

the survival rate, a 5-year rate of 88.6% was estimated for the all-ceramic FDP group compared to 94.4% for metal-ceramic FDPs with a higher incidence of framework and veneer fracture (6.5% and 13.6%) for all-ceramic than for metal-ceramic FDPs (1.6% and 2.9%).

Several explanations for porcelain chipping in PFMs and all-ceramic restorations have been given in the literature, ranging from a mismatch in CTE between the veneering porcelain and the framework; defects in the porcelain material; improper design of the supporting framework; improper porcelain thickness; improper firing and cooling rates; and improper handling, both in the dental lab and by the dentist. The porcelain firing process seems to be the main root cause for the observed failures, especially in the case of zirconia frameworks since zirconia is a very poor thermal conductor. Differences in cooling rates between the thin core and the thick veneering porcelain, and between the outer part of the veneering porcelain and its inner part close to the framework, create a temperature gradient within the porcelain layer that results in an uneven solidification and contraction of the porcelain upon cooling.[24] This contraction mismatch creates important residual stresses at the surface and within the bulk of the porcelain that may lead to formation of cracks. The formation of compressive or tensile stresses in the porcelain veneer is directly dependent on the cooling mode, fast or slow, and on the thickness ratio between the core and the porcelain. In metal-ceramic restorations, tempering by fast cooling is proven to increase the strength of the restoration by creating compressive stresses at the surface of the porcelain. In all-ceramic zirconia restorations compressive forces are also measured at the surface of the porcelain upon cooling (an increase with fast cooling), but it seems that the stress-depth profile changes from compressive at the surface to tensile, and back to compressive in a direction toward the framework. This might explain the porcelain chipping and delamination observed in the clinic.[25] Although it is established that faster cooling rates increase surface compressive stresses, it is not clear whether slow cooling or fast cooling is beneficial for the long-term performance of veneered zirconia restorations. Indeed, manufacturers generally recommend allowing for a slow cooling of 20°C/min below the Tg temperature of the porcelain before allowing for bench cooling in air.

As a general good clinical practice rule, the choice of material should be dictated by the specific clinical situation and not the opposite. The choice of material depends on the space available to build the aesthetic and functional restoration, but also on the nature of the underlying structure. Depending on whether the underlying structure is a natural tooth or an aesthetic ceramic abutment, or contrarily, a discolored tooth or a metallic abutment, ceramics may be chosen as semi- to highly translucent to permit the color of the underlying substructure to shine through, or as semi-opaque or opaque to mask its color. As an indication of the different optical properties of various all-ceramic systems, Figure 12.7 summarizes the translucency level of feldspathic porcelains, glass
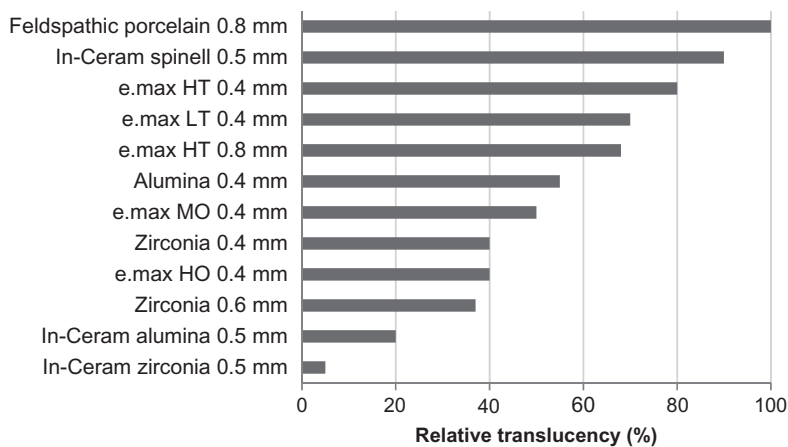
FIGURE 12.7   Translucency of dental ceramics. *(Courtesy of P. Margossian)*

ceramics, and polycrystalline ceramics as a function of the material thickness. At equivalent thicknesses, feldspathic porcelain is the most translucent ceramic, followed by In-Ceram® Spinell, lithium disilicate IPS e.max® glass-ceramic, alumina, zirconia, In-Ceram® Alumina and In-Ceram® Zirconia.[26]

A particular example of interest is the comparison of the IPS e.max® and zirconia dental ceramics. At a thickness of 0.4 mm, the translucency of IPS e.max® HT is higher than that of zirconia, but when translated to clinically relevant thicknesses (i.e. 0.8 mm for IPS e.max® and 0.4 mm for zirconia) both materials exhibit equivalent translucency. This clearly indicates that it is possible to achieve satisfying aesthetic results with semi-translucent ceramics while keeping the amount of tooth preparation minimal.

As an illustration of possible aesthetic outcomes with different restorative materials, see the clinical case presented in Figure 12.8. This case features a smile composed of two different types of restorations: a veneered zirconia coping on Tooth 12, and a PFM restoration on Tooth 21 surrounding a Natural Tooth 11. Although the evidence shows that both types of restorations (especially the metal-ceramic 21) show lower diffusion of light under LED illumination as compared to the natural tooth, these restorations achieved aesthetics close to Natural Tooth 11 that are difficult to differentiate with an untrained eye.

Feldspathic porcelains, reinforced feldspathic porcelains, and glass-ceramics have shown good to excellent clinical results during their use over the past few decades as ceramic materials for single tooth restorations. However, for bridge applications, their use is limited today to 3-unit bridges in the anterior and premolar region unless veneered on a strong metal or ceramic framework. This leaves an important gap that today is only filled by polycrystalline ceramic materials, with zirconia by far the most utilized framework material
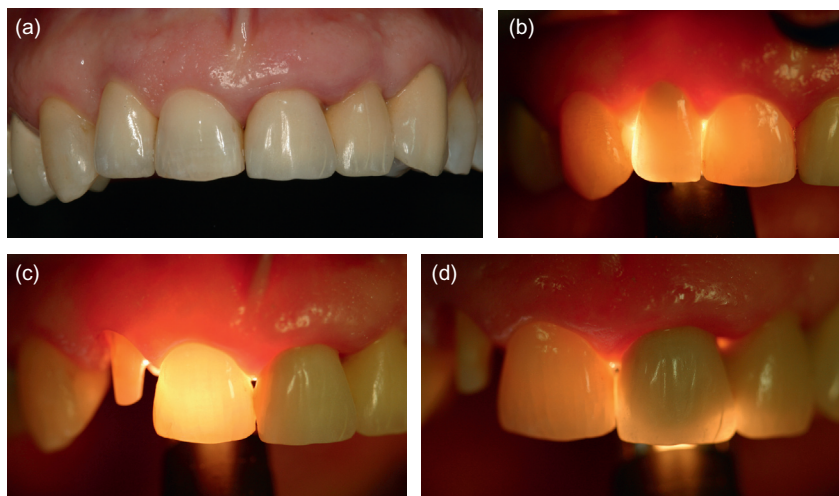
FIGURE 12.8 Smile featuring (a) A veneered zirconia Procera® coping on Tooth 12 (2nd tooth on the left from the midline), natural tooth 11 (1st tooth on the left from the midline), and a PFM restoration on tooth 21 (1st tooth on the right from midline). Respective restorations are illuminated with an LED: (b) Procera® zirconia crown; (c) Natural tooth; and (d) PFM restoration. *(Courtesy of P. Margossian)*

even though it presents limited aesthetics compared to glass-ceramics and shows important porcelain chipping rates as mentioned earlier.

To obtain aesthetically pleasing and long-term performing single- and multi-unit posterior restorations, there seem to be three obvious development routes. First, the bending strength and fracture toughness of the current glass-ceramic materials must be improved. Second, the translucency of strong polycrystalline ceramics, particularly zirconia, has to be improved. As a third route, new materials and product concepts must be developed. In the next section, we will see some of the recent developments in these directions, and suggestions for potential future developments.

12.4　FUTURE DEVELOPMENT

With clear advantageous aesthetics and a continuously growing market of digital treatment workflows; and CAD/CAM manufacturing allowing virtually one treatment in one visit, all-ceramic restorations have a bright future. As seen in the previous sections, the main challenge with dental glasses and glass-ceramics is insufficient flexural strength and fracture toughness for use in the posterior region. Currently, there are not many means to counter this problem. Either the aesthetic porcelain has to be bonded directly to tooth enamel and dentine, or it has to be supported by a strong but less aesthetic

ceramic substructure. The obvious and ideal solution would be to develop a ceramic that combines both high aesthetics and high strength to permit its use as a monolithic dental restoration. A few examples of the latest developments in the field from both academia and industry will be described in detail in Chapter 16. These encompass the new translucent zirconia grades for full-contour applications, stronger glass-ceramics, the composite glass-ceramic-glass materials, and the hybrid polymer-ceramic materials.

CONCLUSION

In this chapter, an historical review of the development of all-ceramic restorations, as well as a presentation of state-of-the-art restoration possibilities were given with particular emphasis on glasses and glass-ceramics. Current limitations and challenges were also exposed, and some possible directions for future developments were proposed. As can be seen, there is no single material perfectly suited for all clinical situations. Instead, the choice of material must be dictated by specific clinical requirements and not the opposite (i.e. by choice of treatment). Today there is a multitude of ceramic materials that are well-suited to solving different clinical challenges, and knowledge of these materials and their properties is therefore critical for long-term treatment success.

It is the hope of the author that this chapter has provided dental professionals and ceramists with a better understanding of the dental glass-ceramics in use today, including both their potential and limitations. Nevertheless, many efforts involving materials scientists, biologists, clinicians, and engineers are still needed, to develop more reliable materials and innovative product and treatment concepts that will help treat patients in a less invasive, less painful, and more comfortable and rapid manner. It is a great and fascinating challenge for a materials scientist to participate in such developments, and it will be very exciting to follow the innovations to come in the next decade.

ACKNOWLEDGMENTS

REFERENCES

1. McLean JW, Hughes TH. The reinforcement of dental porcelain with ceramic oxides. Br Dent J 1965;119:251–67.
2. Decrange M, Sadoun M, Heim N. Les céramiques dentaires: 2ᵉ partie. Les nouvelles céramiques. J Biomat Dentaire 1987;3:61–9.
3. Andersson M, Odén A. A new all-ceramic crown. A dense-sintered, high-purity alumina coping with porcelain. Acta Odontol Scand 1993;51(1):59–64.

4. Adair PJ, Grossman DG. The castable ceramic crown. Int J Periodonthics Restorative Dent 1984;4(2):32–46.
5. Wohlwend A, Schärrer P. Die Empress-Technik. Ein neues Verfahren zur Herstellung von volkeramischen Kronen. Inlays und Facetten. Quintessenz Zahntech 1990;16:966–78.
6. Schweiger M, Höland W, Frank M, Drescher H, Rheinberger V. IPS Empress® 2: A new pressable high strength glass-ceramic for esthetic all ceramic restoration. Quintessence Dent Technol 1999;22:143–52.
7. Höland W, Beall GH. Chap. 2: Composition systems for glass-ceramics, Chap. 4: Applications of glass-ceramics. Glass-ceramic technology, 1st ed. Westerville: The American Ceramic Society, Wiley; 2002. p. 119–24. p. 291–300.
8. El-Meliegy E, van Noort R. Theoretical estimation of glass properties. Glasses and glass ceramics for medical applications. New York: Springer New York Inc; 2011. p. 88–93.
9. McLean JW, Sced IR. The bonded alumina crown. 1. The bonding of platinum to aluminous dental porcelain using tin oxide coatings. Aust Dent J 1976;21:119–27.
10. McLean JW, Kedge MI, Hubbard JR. The bonded alumina crown. 2. Construction using the twin foil technique. Aust Dent J 1976;21:262–7.
11. Vitablocs® Mark II for Cerec. Material Science and Clinical Studies. Vident™ Scientific Brochure; 2000.
12. Katz S. High strength feldspathic dental porcelains containing crystalline leucite. US Patent 4,798,536 Jan 17, 1989.
13. Grossman DG. Tetrasilicic Mica Glass-ceramic Method. US Patent 3,732,087 May 8, 1973.
14. Beall GH. Design and properties of glass-ceramics. Annu Rev Mater Sci 1992;22:91–119.
15. Hobo S, Iwata T. Castable apatite ceramics as a new biocompatible restorative material: I. Theoretical considerations. Quintessence Int 1985;16:135–41.
16. Hobo S, Iwata T. Castable apatite ceramics as a new biocompatible restorative material: II. Fabrication of the restoration. Quintessence Int 1985;16:207–16.
17. Uryu Y, Suzuki H, Ijima H, Kurokawa H, Watanabe F, Hata Y, et al. Clinical use of castable ceramics (OGC) crown. Shikagu 1989;77:1485–95.
18. Höland W, et al. Principles and phenomena of bioengineering with glass-ceramics for dental restoration. J Eur Ceram Soc 2007;27:1521–6.
19. Schweiger M, Rheinberger V, Burke H, Höland W. Lithium silicate materials. US patent 2008/0125303A1.
20. Schweiger M, Frank M, Rheinberger V, Höland W. Lithium disilicate glass ceramics dental products. US Patent 6,342,458 B1, Jan 29, 2002.
21. Höland W, Rheinberger V. Nucleation and crystallization phenomena in glass-ceramics. Adv Eng Mater 2001;3(10):768–74.
22. Pjetursson BE, Sailer I, Zwahlen M, Hämmerle CHF. A systematic review of the survival and complication rates of all-ceramic and metal-ceramic reconstructions after an observation period of at least 3 years. Part I: single crowns. Clin Oral Impl Res 2007;18:73–85.
23. Sailer I, Pjetursson BE, Zwahlen M, Hämmerle CHF. A systematic review of the survival and complication rates of all-ceramic and metal-ceramic reconstructions after an observation period of at least 3 years. Part II: fixed dental prostheses. Clin Oral Impl Res 2007;18:86–96.
24. Mainjot AK, Schajer GS, Vanheusden AJ, Sadoun MJ. Influence of cooling rate on residual stress profile in veneering ceramic: Measurement by hole drilling. Dent Mater 2011;27:906–14.

25. Mainjot AK, Schajer GS, Vanheusden AJ, Sadoun MJ. Influence of veneer thickness on residual stress profile in veneering ceramic: Measurement by hole drilling. Dent Mater 2012;28:160–7.
26. Margossian P, Laborde G, Koubi S, Couderc G, Maille G, Botti S, et al. Propriétés optiques des systèmes céramocéramiques : implications cliniques. Réalités cliniques 2010;21(3):45–51.

Requirements of Bioactive Ceramics for Dental Implants and Scaffolds

James Zhijian Shen* and **Jenny Fäldt†**

Berzelii Center EXSELENT on Porous Materials, and Department of Materials and Environmental Chemistry, Arrhenius Laboratory, Stockholm University, Stockholm, Sweden; †Nobel Biocare AB, Göteborg, Sweden

Contents

13.1   INTRODUCTION

The most common material used in dental implants today is titanium metal, which was introduced by P-I Brånemark four decades ago.[1,2] Full ceramic implants were proposed as an alternative in the 1970s, but are still under development today.[3,4] Implant fixation, its stability, and load transfer from implant to surrounding tissues are achieved by the direct structural and functional connection between a load-bearing implant and the surrounding living bone, or, in other words, by interaction/interference between bone and a foreign material. This process is described as osseointegration and is strongly dependent on the material and surface properties of the implants.[2] Bone scaffolds are artificial structures capable of supporting 3D tissue formation to replace conventionally used bone graft for structural restoration.[5] As an alternative, titanium or bioactive ceramics was selected to make porous bone scaffold. The basic challenge in developing a suitable scaffold for bone tissue engineering is to mimic the complex physiological environment in which bone cells grow and differentiate to yield bone formation and vascularization.

In the development of materials for dental implants and scaffolds it is essential to understand how is new bone formed on foreign surfaces and how does the material integrate with autologous bone through complex biological processes as well as in which way do cells interact with the material. The healing process after inserting dental implants and scaffolds into the jawbone is initiated by the surgical trauma that takes place during the opening of soft tissue and drilling in the host bone. Blood immediately comes into contact with the surface, followed by different cells involved in the inflammatory response. Proteins secreted by the cells can affect inflammation, bone healing, and immune reactions, as well as alter the structure and physiochemical properties of the foreign surface. Bone tissue formation then continues with a series of complex processes involving, for example, angiogenesis, formation of new blood vessels from pre-existing vasculature, and bone cell differentiation. Old bone tissue damaged by drilling undergoes a remodeling process in which osteoclasts resorb bone and then osteoblasts form new bone. As the osseointegration process proceeds, the space between the inserted material and the old bone is filled with woven bone, which grows fast but has a random collagen structure. The woven bone is gradually replaced with lamellar bone that has a regular (lamellar) collagen structure. This improves the mechanical properties.

Development of a new implant or scaffold material is a long journey that moves stepwise from an idea to a final and launched product. During the early stage, in vitro models play an important role. These studies give information about positive and negative effects that a structure has on the different cells, as well as any risk of toxicity. However, the healing process of a dental implant or scaffold in the jaw is a complex interplay between different cell types in a 3D environment. This cannot be achieved with in vitro models. It is therefore important to evaluate the response of a new material, structure, or geometry in

an in vivo situation using a suitable animal model, or, if possible, by directly entering combined in vitro and clinical studies. In this chapter, the bone growth mechanisms will thus always be discussed based on the characterization and quantification methods used.

13.2 OSSEOINTEGRATION

Osseointegration is not a precisely defined biological term, but rather an empirical concept and process that was initially suggested by P-I Brånemark based on his histomorphometrical observation that stable anchorage of a titanium implant was achieved by direct bone-to-implant contact. He refined his definition in 1985, as a direct structural and functional connection between ordered living bone and the surface of a load-carrying implant.[6] Yet, the term itself has provided no insight into the mechanisms by which bone becomes juxtaposed to an endosseous implant surface.[7] It is a term that has eluded satisfactory scientific definition.[8]

Nevertheless, it is commonly accepted that osseointegration is signified by a direct and intimate contact between bone and implant surface without any visible intermediate tissue layer. Osseointegration can thus be quantitatively characterized by histomorphometric analysis, especially the measurement of the bone-to-implant contact (BIC).[6] Figure 13.1 shows a state-of-the-art SEM micrograph of an interface between bone and implant with a high degree of BIC and coherence. From a microstructural point of view, the new definition and the BIC measurement do not, however, resolve the old puzzle of what resolution level the direct structural connection can be measured at and how is it possible to characterize whether a true functional connection exists or not.[9] By microstructural characterization of the implant–bone interface after in vivo tests, it is feasible to verify whether there is any interfacial fibrous tissue formed. However, it is not straightforward to justify how the peri-implantal gap is filled by the newly formed bone, even though many terms with vague definitions (e.g. bone precipitation, bone deposition, bone apposition, and bone integration) are used in the literature to interpret the very same phenomenon. For guiding the material development process it is crucial to determine the bone growth mechanism (i.e. to understand how does the physicochemical interaction between living bone tissue and the implant gradually develop on a microscopic scale).

It has been known for more than a century that a cement line is formed during the bone remodeling phase.[10] The cement line is a distinct anatomical boundary between new and old bone at remodeling sites. As shown in SEM, it appears clear that this cement line divides newly formed bone with lower density from the existing old bone with higher density (Figure 13.2). Interestingly, a layer similar to the cement line has also been observed at the implant surface. Davies suggested in 1998, that the cement-like line at the implant surface is part of *de novo* bone formation. It provided a cell biological view of the
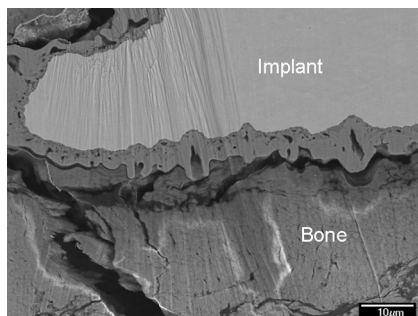
FIGURE 13.1 SEM micrograph taken on an ion-beam polished section that reveals a microscopic level of osseointegration. On the Ti implant there is a porous layer of titania about 5–10 thick. The fact that bone follows the implant surface, and bone fragments stick to the titania layer above the gap (an artifact introduced during sample preparation due to the dehydration of bone) indicates a strong bond between bone and implant in this region.
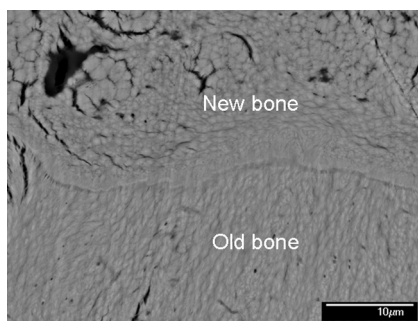
FIGURE 13.2 SEM micrograph taken on an ion-beam polished section that reveals the high-resolution microscopic view of a cement line between old and new bone with different density. EDS analysis indicated that the Ca/P ratio of the new bone is 1.349, which is lower than that of the old bone (1.526).

phenomenon known as contact osteogenesis that was first reported by Osborn and Newesley in 1980 in their histological study of bone contacts with different types of implants.[7,11] With this bone growth mechanism, new bone forms first on the implant surface. It implies that bone formation does not only proceed towards the implant from existing bone (distant osteogenesis). Similar to normal appositional bone growth, the existent bone surfaces provide a population of osteogenic cells that lay down new matrix, which, as osteogenesis continues, encroaches on the implant itself.

Davies suggested that the cement-like layer observed on the implant surface is formed when osteogenic cells reach the implant surface and secrete collagen-free proteins that later turn into a mineralized interfacial matrix. In front of the cement line a series of events will form a calcified collagen

compartment. Thus, there is a collagen-free calcified tissue layer that separates the implant from the collagen compartment of bone. Several studies have found osteoblasts, osteoids, and mineralized matrix adjacent to the layer on the implant's surface.[7] This suggests that bone is deposited on, and extends outward from, the implant. There are even findings in the literature that claim 30% faster bone growth extending away from the implant than moving towards the implant.

Biological understanding of these different healing reactions and sequences is essential for elucidating the mechanism underlying the osseointegration process; and for establishing criteria for materials selection; and hierarchical structure design of future dental implants and scaffolds.

13.3 PHENOMENOLOGICAL VIEW OF BIOACTIVITY

Perhaps, terms such as 'bioactive' and 'bioactivity' are ones that we use frequently but whose precise definitions are forgotten. This may be true, because in general, bioactivity can describe any beneficial or adverse effect that artificial matter has on living matter. In this section, bioactivity is defined much more narrowly as any beneficial effect of an inserted material on bone formation that can be characterized by experimental quantification methods. Even on this basis, bioactivity is a much more complex property than one would expect. It is influenced by many materials parameters (physical and chemical properties as well as the hierarchical structure of the surfaces) and biological considerations (interactions with cells and proteins, and the influence of inserted material on differentiation-induced activities).

13.3.1 Bioactivity and Simulated Body Fluid Test

According to Kokubo et al. a bioactive material is defined as a material on which bone-like hydroxyapatite (HA) forms selectively when it is immersed in a serum-like solution (i.e. a material that accelerates heterogeneous HA crystallization on its surface in a solution supersaturated towards HA).[12] This is a phenomenological definition of bioactivity that is oversimplified to a solitary chemical process by bypassing the possible contribution of biological reactions. Since this test has been standardized as an in vitro characterized method, this definition and a way of characterizing the bioactivity has been widely spread in the community. However, one has to be aware of the fact that surface morphology of the materials, and many experimental parameters such as ion concentration and CO_2 partial pressure, may severely influence the HA nucleation and crystallization processes and thus the bioactivity of the tested materials.

In a recent review, Bohner et al.[13] addressed this issue and introduced a new recipe (SBF-JL2 solution; Table 13.1) as an alternative to the one suggested by Kokubo et al. This solution is simple in its ionic composition and

TABLE 13.1 Compositions of the Simulated Body Fluids

Ion (reagent, purity)	Ion Concentrations (mol/L)		
	Blood Plasma	c-SBF2	SBF-JL2
Na^+ (NaCl, 99.5%)	142.00	142.00	142.00
K^+ (KCl, 99.5%)	5.00	5.00	N/A
Mg^{2+} ($MgCl_2.6H_2O$, 98.0%)	1.50	1.50	N/A
Ca^{2+} ($CaCl_2$, 95.0%)	2.50	2.50	2.31
Cl^- (1.0 M-HCl)	103.00	147.96	109.90
HCO_3^- ($NaHCO_3$, 99.5%)	27.0	4.20	34.88
HPO_4^{2-} ($K_2HPO_4.3H_2O$, 99.0%)	1.00	1.00	1.39
SO_4^{2-} (Na_2SO_4, 99.0%)	0.50	0.50	N/A
pH, temperature	7.2–7.4, 37°C	6.25–7.40, 37°C	7.40, 37°C
$p(CO_2)$ (atm)	N/A	Not controlled	0.05

Note: c-SBF2 was recommended by Kokubo et al. and SBF-JL2 was recommended by Bohner et al.

is in equilibrium with dicalcium phosphate dihydrate (DCPD). The suggested experimental conditions are close to the physiological conditions (i.e. ionic strength of 140 mM, initial Ca^{2+} concentration around 2.5 mM, pH 7.4, 37°C, and CO_2 partial pressure of 0.05 atm). Our own experiments revealed, however, that the SBF-JL2 solution is oversaturated towards HA precipitation, which implies that HA may precipitate on any rough surface independently of the chemical composition of the surfaces.

On the microscopic level, the heterogeneous crystallization of HA on existing surfaces is a process that involves electrostatic interactions of the surface with the calcium and the phosphate ions in SBF via sequential formation of metastable intermediates (i.e. Ca-rich and Ca-deficient phases of amorphous calcium phosphate, ACP).[14] Ceramics made of HA, or ones that already contain HA in their compositions, reveal a desirable negative surface charge when they expose hydroxyl and phosphate units in their crystal structures. This negative surface is maintained when the HA is immersed in a basic solution, whereas it may be partially or totally balanced by attracting positively charged protons in an acidic solution. This implies that the pH value of the SBF is a critical parameter for the heterogeneous crystallization of HA. A drop in pH value below 7 will also facilitate the dissolution of the early formed HA nuclei and thus retard the crystallization of HA. The formation of HA can be experimentally approved by direct SEM observation (Figure 13.3) or by analyzing the change of surface chemical compositions.
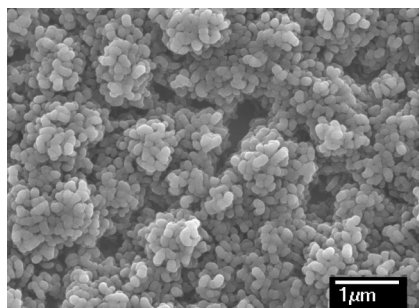
FIGURE 13.3 SEM micrograph that reveals that an HA layer formed on the surface of an HA-doped zirconia nanocomposite in c-SBF2 within one week, but not on a reference sample monophasic zirconia (3Y-TZP) that is regarded as not bioactive according to definition.

When the two SBF compositions listed in Table 13.1 were tested, there was a different time evolution of the pH value. The SBF-JL2 is used under a controlled $p(CO_2)$ of 5%. The CO_2 acts as a buffer that keeps the pH constant at 7.4 during the entire experiment. When c-SBF2 is used, however, the $p(CO_2)$ is not controlled. As a consequence, the pH drops to 6.25 and $p(CO_2)$ immediately increases to 5.8% when the sample is immersed in the solution.[13] Such a difference in the initial pH value of the two different types of SBFs explains the experimental observation that the HA layer formed on an HA-doped zirconia nanocomposite in SBF-JL2 is denser than the one formed in c-SBF2. It appears that a slightly basic environment (pH 7.4) favors the heterogeneous crystallization of HA on existing HA, whereas a slightly acidic environment (pH 6.25) obstructs HA formation. Theoretical analysis carried out by Lu et al. indicates that the kinetics of HA precipitation can be considerably affected by the presence of carbonate ions or by the formation of Ca-deficient HA. Their calculations showed that in general, precipitation of carbonate-containing and/or Ca-deficient HA, is kinetically more favorable than that of stoichiometric HA.[15]

13.3.2 Bone Formation by Distant and Contact Osteogenesis

As described in Section 13.2, two-bone growth mechanisms have been proposed in the literature, namely distant osteogenesis and contact osteogenesis. Phenomenologically, in the former case new bone is formed on the surface of existing bone and grows towards the implant surface (also called ingrowth, a term often found in the literature); in the latter case, new bone is formed directly on the implant surface as a cement-like layer. With the advance of characterization technologies, more detailed microstructure features of the cement-like layer have been exposed that indicate the necessity of searching further for its biological origin.

As illustrated in Figure 13.4, with a detailed analysis of the bone–implant interfaces by a recently developed technique of taking SEM images on argon
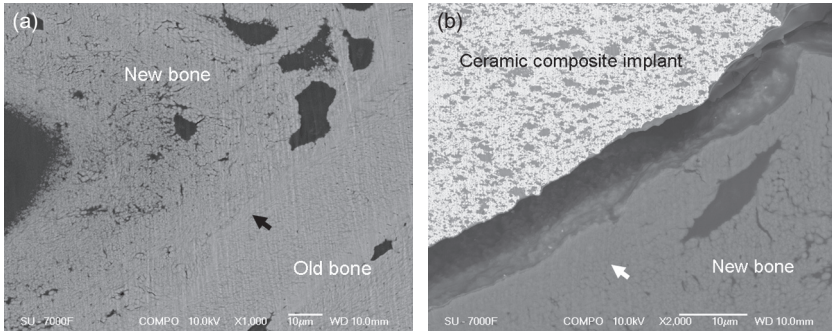
FIGURE 13.4 Two SEM micrographs taken on an argon ion-polished cross-section of an HA-doped zirconia nanocomposite containing 40 vol.% HA after in vivo test that reveals the density difference of the bones formed by distant and contact osteogenesis, respectively. (a) New bone formed by distant osteogenesis from the old bone, where the black arrow indicates the location of the cement line; and (b) Contact osteogenesis occurs at the implant surface and yields the formation of a layer of new bone with higher density, as indicated by the white arrow. The gap between implant and bone is an artifact introduced during sample preparation due to the dehydration of bone.

ion beam-polished cross-sections, additional information on the microstructural features of osseointegration can be obtained.[16] First of all, this gentle sample preparation route facilitates the distinction of new and existing bone in BSE images because the as-prepared surfaces are free from scratches and other artifacts often introduced by mechanical polishing. Therefore, a small density difference becomes clearly visible in similar micrographs. Secondly, and more importantly, argon ion polishing allows for a detailed analysis of the thin bone layer at the surface of the implants. In the case of the implant made of an HA-doped zirconia nanocomposite, a dense layer of bone is found to form on the surface of the implant (Figure 13.4). This is distinct from the remainder of the bone with lower density and resembling the cement line formed on existing bone, as shown in Figure 13.2.

This observation supports the idea that there are two bone growth mechanisms: distant osteogenesis that yields bone with lower density, and contact osteogenesis that yields bone with higher density. In the former case, newly formed bone grows on the surface of existing bone and in-grows towards the implant surface, implying that a rough and/or porous surface will increase the bone–implant contact area after healing is complete. In the latter, newly formed bone, in addition to in-growth, precipitates directly on the implant surface, where mineralization occurs via kinetically favored heterogeneous nucleation of HA. It grows outwards from the implant and towards the existing and in-growing bone.

13.3.3 Bioactive Versus Osseoconductive

Apparently, bone formed by contact osteogenesis is denser than bone formed by distant osteogenesis (Figure 13.4). When the distant osteogenesis

mechanism dominates, a strong chemical connection may be established at the interface between newly formed bone and existing bone, but is not as likely between the newly formed bone and the implant surface. Here, a physical or mechanical connection is more probable instead. In contrast, when the contact osteogenesis mechanism is active together with a distant osteogenesis mechanism, the same type of interaction may be established at both the interface between newly formed bone and the implant surface, and the interface between newly formed bone and existing bone. In this regard, one can classify a material that is able to facilitate contact osteogenesis during in vivo tests as an in vivo bioactive material in a similar way as in vitro bioactivity is defined.

In the literature, dental implant materials that are able to establish osseointegration with surrounding bone are often regarded as osseoconductive.[6,17] Based on the definition and discussion above, it appears that an osseoconductive material does not necessarily resemble in vitro bioactivity, whereas an in vitro bioactive material is most probably also osseoconductive. For example, the HA-embedded zirconia ceramic nanocomposite is proven to be both in vitro bioactive and osseoconductive based on the in vitro and in vivo tests performed (see Figures 13.3 and 13.4). It is thus more advantageous than monophasic zirconia for enhancing osseointegration. On the other hand, although monophasic zirconia ceramic is not in vitro bioactive, it can be osseoconductive, and should therefore not be excluded as a potential dental implant material. When osseointegration is established around a non-bioactive material such as zirconia, the gap between the implant and existing bone is filled by new bone formed via a distant osteogenesis mechanism only. In such a case, avoiding inflammatory reactions and the formation of fibrous tissue during the entire healing phase become crucial issues in order to ensure strong osseointegration. As bone and implant are bound merely by physical coherence, increasing the accessible surface area for in-growing bone is expected to enhance osseointegration. This is exactly what has been indicated by previous studies that revealed that roughening the surface of zirconia implants increases the resistance to shear stress and torque forces.[18,19]

13.4 BIOLOGICAL VIEW OF BIOACTIVITY

13.4.1 *De Novo* Bone Formation at Foreign Surfaces

From a biological point of view, bone formation on non-biological substrates is a consequence of a sequence of osteogenic cell differentiation and biological reactions influenced by the hierarchical structures of implants. Immediately after implantation, initial blood contact with the implant surface creates a dynamic state of cellular activity that starts with the activation of platelets and leukocytes in the peri-implant hematoma and the attachment of transitory structural proteins (such as fibrin) to the implant surface. Retention of these proteins by the implant surface is dependent upon the surface

topography of the latter, and it is through this 3D biological architecture that putative osteogenic cells migrate to the implant surface. The differentiating osteogenic cells then secrete a collagen-free organic matrix that provides nucleation sites for calcium phosphate mineralization. Calcium phosphate crystal growth follows nucleation, and concomitant with crystal growth at the developing interface where collagen fibers assemble, is initiated afterwards. Thereafter, the calcification of the collagen compartment will occur both in association with the individual collagen fibers and in the inter-fiber compartments. This is a mechanism known as *de novo* bone formation suggested by Davids et al. to give a cellular provenance of contact osteogenesis.[20,21]

Davids et al. disclosed that the *de novo* bone formation during contact osteogenesis takes place in the exact same manner as the formation of the cement line in normal bone remodeling sites. In both cases, the *de novo* bone formation process can be experimentally evaluated either by in vitro or in vivo methods.[20,21] One distinct feature of the early phase of *de novo* bone formation is the separation of the collagen compartment of bone from the underlying substratum by a collagen-free calcified tissue layer containing non-collagenous bone proteins with a thickness of~0.5 μm.

13.4.2   Balance Between Osteoblast and Osteoclast Cells

As indicated by Müller et al. in their recent series of work, bone formation at a deep level is a complex process controlled by morphogenetically active signaling molecules.[22–26] These molecules or growth factors display a spatially and temporally precise pattern of expression during differentiation of osteoblast and osteoclast cells. In addition, a homeostatic cross-talk between these cell lineages via signaling molecules occurs. Osteoblast differentiation starts from the mesenchymal stem cells. This lineage ends with the osteocytes. The major transcription factor Runx2, which is under the control of BMP2, is synthesized in chondrocytes and causes a stage-dependent increase in structural and functional proteins (e.g. b-ALP, COLI, OP, ASP, and also RANKL, BSP, and OC) in osteoblasts. The osteocytes either become embedded in the HA deposits and release sclerostin, an inhibitable PTH hormone glycoprotein that inhibits BMP2, or the osteoblasts undergo apoptosis.

Osteoclasts are multinucleated cells that originate from the hematopoietic lineage. Those stem cells undergo differentiation and maturation in the presence of the macrophage colony-stimulating factor (M-CSF) and RANKL. As markers for the multinucleated osteoclasts, a high expression level of the tartrate-resistant acid phosphatase (TRAP), as well as calcitonin receptor (CTR) binding and expression of integrin avb3, have been used (see Figure 13.5). The osteoblasts direct the pre-osteoclasts to the osteoclast through RANK/RANKL, an interaction that is blocked by OPG. The osteoclasts start to differentiate from hematopoietic stem cells (circulating mononuclear cells) through activation of the PU.1 transcription factor and inflammatory signals. The CD34+
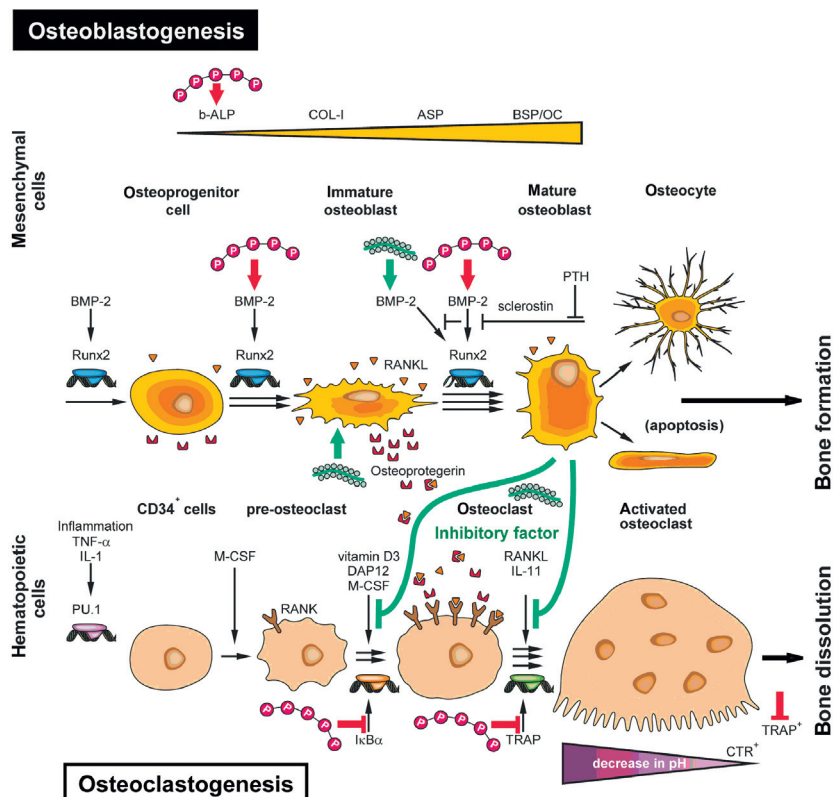
FIGURE 13.5   Differentiation of the progenitor cells of the bone (HA) forming osteoblasts (osteoblastogenesis) and the bone (HA) resorbing osteoclasts (osteoclastogenesis). *(Courtesy of Werner Müller.)*

osteoclast precursor cells, after entering the circulation system, and in the presence of macrophage-colony stimulating factor (M-CSF) and 1,25-dihydroxy-vitamin D3 [1,25(OH)2D3], become recruited onto the surface of bone. The pre-osteoclasts, after the stimulation of the DAP12 adapter protein/receptor, undergo multi-nucleation to the osteoclasts. Those cells express in the presence of dihydroxy-vitamin D3 the receptor RANK. After binding of RANKL to RANK the osteoclasts dissolved HA by lowering the pH. Markers for the activated osteoclasts are TRAP, CTR, and integrin avb3.

A cytokine/receptor triad is crucial in the control of bone formation and bone remodeling: RANKL with its receptor (RANK) and the endogenous decoy receptor osteoprotegerin (OPG). RANKL is synthesized by the osteoblastic lineage cells and is essential for the differentiation of those cells that are involved in bone resorption, the osteoclasts. RANKL is expressed on osteoblasts, T cells, dendritic cells, and their precursors, from where it can be
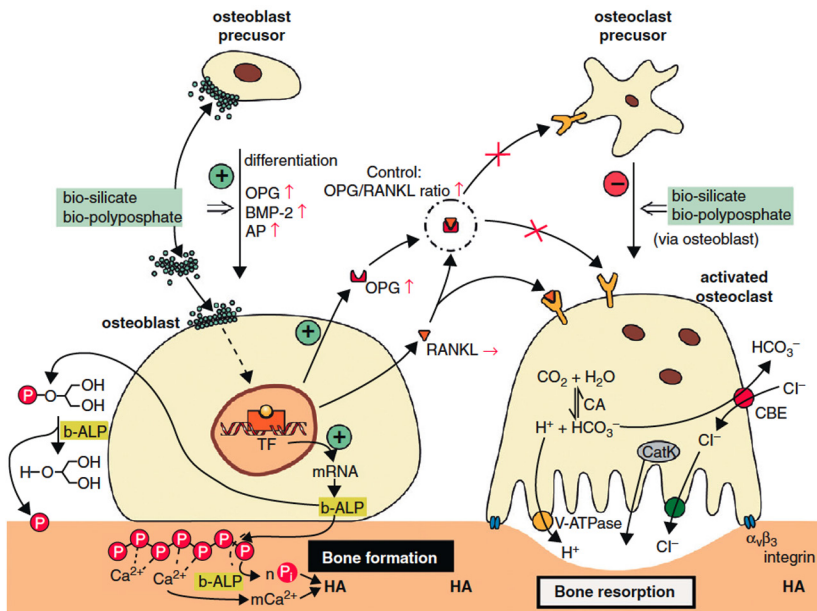
FIGURE 13.6 Schematic outline of the tuned interaction of the cytokine/receptor triad RANKL–RANK–OPG and BMP2 that controls the terminal differentiation steps of the osteoblasts and osteoclasts. *(Courtesy of Werner Müller.)*

released by specific proteases. This ligand binds to the cell surface receptor RANK, which is located on precursor and mature osteoclasts. After binding of RANKL to RANK, the osteoclasts become activated and resorb bone mineral; during this process the cells have close contact with the bone surface. At this interphase to the bone vesicles are formed (via integrin, avb3) that contain proton pumps and acid hydrolases (cathepsin K). Those enzymes and vesicles are inserted into the cells at the bone-apposed area under formation of a 'ruffled border.' A resorptive hemivacuole is formed between cell and bone, which allows the protons to dissolve HA of the bone (see Figure 13.6). Intracellular pH is thought to be maintained at a near-neutral level by chloride/bicarbonate exchange and the help of carbonic anhydrase. The activity and function of RANKL is under control of OPG that is secreted by stromal cells and osteoblasts. OPG scavenges RANKL by binding to it, and neutralizes its function.

Through cell culture studies it has been revealed that adding artificial materials, such as the inorganic polymers bio-silica and bio-polyphosphate, can increase the level of bone growth factors thus stimulate the synthesis of hydroxyapatite in vitro.[22,23,25] Exposing SaOS-2 cells, a non-transformed osteogenic sarcoma cell line originating from primary osteosarcoma cells, to bio-silica, for instance, induces transcription of the *osteoprotegerin* (OPG) gene; no effect is seen on the steady-state expression of the receptor activator for

NF-κB ligand [RANKL]. Furthermore, bio-silica increases the steady-state level of transcripts for *BMP-2*, which is a known inducer of bone formation and of bone regeneration, while triggering the release of an osteoclast inhibitory factor that prevents growth and differentiation of osteoclast-like RAW 264.7 cells in in vitro assays. The targets of bio-silica and bio-polyphosphate in the last step of differentiation of osteoblasts and osteoclasts are marked in Figure 13.6. They cause an increased OPG/RANKL ratio as a result of osteoblast activation, a process that is paralleled by an impairment of osteoclast maturation. Bio-polyphosphate induces the expression/activation of bone-specific alkaline phosphatase (b-ALP), which results in an increased supply of inorganic phosphate (Pi). In addition, this biopolymer increases the intracellular level of Ca^{2+} and hence provides the second component of HA crystallite formation.

13.5   LOAD-BEARING DENTAL IMPLANTS

Base on the current fundamental understanding described above, it appears more crucial to generate a proper surface than to optimize the bulk properties in the design of ceramic implants. An in vitro bioinert (not bioactive) ceramic may be turned into an in vivo bioactive ceramic through proper modification of its surface chemistry and architecture. It is known that contact bone growth is promoted by surface nanostructure features, and that bone anchorage is secured by surface micropores. In addition, bone formation is competitive with the fibrous encapsulation and bacteria accumulation during the healing phase. As long as the fibrous encapsulation and bacteria accumulation can be prohibited, osseointegration may well be established between bone and any ceramic surface. Compared with bone formation, the studies performed so far on fibrous encapsulation are limited, though it has been revealed that there seems to be a threshold of micromotion above which fibrous encapsulation prevails over osseointegration.[27] Better understanding of the mechanism of fibrous encapsulation may open up alternative solutions for achieving better osseointegration.

13.5.1   Anti-infection and Antimicrobial Effect

The oral cavity is a severe environment with variations in pH, wear, and exposure to different types of bacteria. Dental implants, as with natural teeth, provide surfaces on which bacteria try to colonize. This increases the risk of infection, which is followed by inflammation, and in severe cases, even bone retraction. Accumulation of bacteria can yield the formation of biofilms composed of organized bacterial assemblies on the surface of dental implants. Biofilms are highly resistant to antibiotics and host defenses, which results in persistent infections that are difficult to treat. This can lead to further health complications.

To preserve a healthy situation and prolong survival of the treatment, it is necessary to inhibit the formation and growth of biofilms. Prevention of biofilm formation can be achieved through three strategies: (1) impairment of bacterial adhesion; (2) destruction of bacteria by radicals; and (3) avoidance of bacteria accumulation by controlled release of antibiotics and other antimicrobial therapies. It indicates the critical roles that surface chemistry and architecture play in the design of implants.

The ability to impair bacterial adhesion represents an ideal strategy for combating bacterial pathogenesis and preventing infection. Specific proteins expressed on the surface of bacterial cells (adhesins) mediate the adhesive interactions between the pathogen and implant surface. The bacterial species prevalent in implant colonization include the Staphylococcus genus (70%). Staphylococci strongly adhere to metal surfaces, particularly titanium, but scarcely colonize glass surfaces. Anti-adhesion molecules can be used to functionalize implant surface coatings. This impairs the adhesive interactions between the pathogen and implant surface.

The body reacts to the implant, as to any other invader, by recruiting inflammatory cells. Cells from the immune system leave the blood vessels and rapidly migrate towards the implant site. Since the implant is too large to be phagocytosed, the outcome might be a so-called frustrated phagocytosis, where the immune cells release toxic substances, including reactive oxygen species (radicals), into surrounding tissue. If such radicals become entrapped on the implant's surface, they can destroy bacteria there.

Material like titania, particularly in its anatase form, demonstrates photocatalytic behavior. It generates radicals when exposed to UV light. Certain commercial titanium implants, such as the TiUnite®, have a titania surface layer with a high content of titanium in the anatase phase as compared to naturally formed titania on turned titanium surfaces. The methylene blue assay has been used to detect photocatalytic activity of the surfaces. The blue color degrades over time due to radicals produced from the surface during UV irradiation. Apparently, the TiUnite® discs demonstrated the highest photocatalytic activity, while the turned titanium discs gave rise to an increased photocatalytic effect as compared to a blank control (see Figure 13.7). A simple treatment of exposing such implants to UV light immediately before implantation to generate radicals on their surface can sufficiently improve their antimicrobial properties for a limited amount of time. This can be used as an alternative to UV exposure for cleaning colonized surfaces.

In a recent study carried out by the authors, the antibacterial properties of the turned titanium and titanium discs with a commercial TiUnite® surface were investigated through evaluation of the biofilm formation on the surfaces after incubation in a mixed culture of four oral bacteria, namely, *Streptococcus sanguis*, *Actinomyces graevenitzii*, *Actinobacillus actinomycetemcomitans*, and *Neisseria subflava*. As was revealed by the confocal laser scanning microscope images shown in Figure 13.8, the TiUnite® surface had a prohibitive
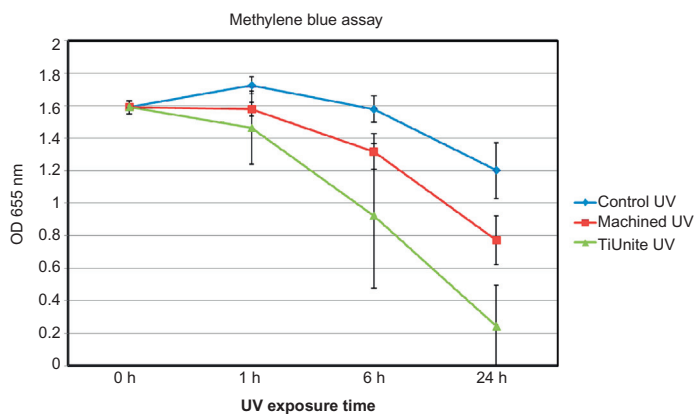
FIGURE 13.7 Graph illustrating the breakdown of methylene blue by different UV-irradiated surfaces. The decrease of color corresponds to the photocatalytic activity of the surface.
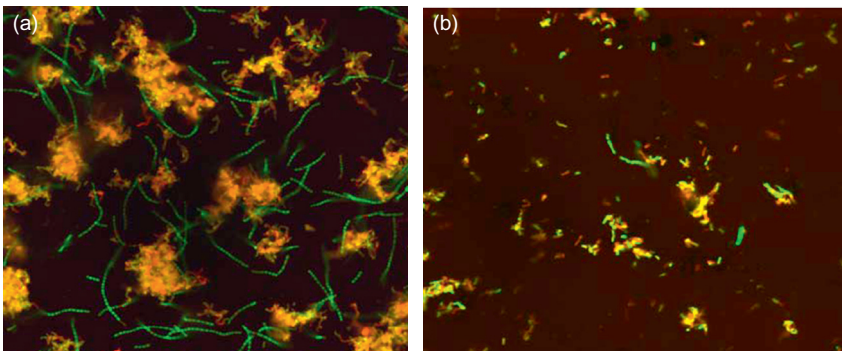
FIGURE 13.8 CLSM images of (a) Non-UV-irradiated, turned titanium; and (b) TiUnite® discs. Live bacteria stain green, and dead bacteria stain red.

effect on biofilm formation on its own as compared to the turned titanium surface with regards to the area of bacterial coverage.

Alternatively, anti-virulence drugs could be used in combination therapy in which bacterial clearance is mediated by standard antibiotics, and the symptoms of virulence are suppressed. For this purpose, surfaces with nanostructured architecture need to be developed that host and allow a controlled release of antibiotics and/or other anti-inflammatory drugs.

13.5.2 Surface-induced Calcium Phosphate Crystallization

As discussed in Section 13.3, the in vitro HA formation from SBF occurs exclusively through heterogeneous nucleation at the surface. Recent studies have further demonstrated that the crystal nucleation in SBF starts with the

generation of aggregates of calcium phosphate pre-nucleation clusters that densify at a templating surface. In the next step, the densification of these clusters leads to the formation of an amorphous calcium phosphate (ACP) precursor phase which ultimately transforms into the crystalline HA.[28] This is also true for HA formation in enamel that seems never to occur directly by the association of ions from solution, but proceeds through an ACP precursor phase.[29] Such fundamental understanding of the early bone-formation process again addresses the importance of surface chemistry and architecture on determining the process of contact bone formation, particularly now that surface architecture can be tailored down to the nanoscale level.

13.5.3 Choosing the Material

For load-bearing purposes, sufficient mechanical strength and fracture toughness are prerequisites that limit the choice of possible candidates for ceramic materials. Alumina, zirconia, and their composites are the first choice, as these ceramics are abundant, easy to prepare, and have a positive aesthetic appearance. Another candidate is silicon nitride, which is strong enough for implant purposes, is biocompatible, and can become bioactive through surface modification; however, its dark gray color does not meet aesthetic requirements, as with titanium metal.

Early alumina ceramic was studied with very limited success.[3,30–32] Later, the potential of yttria partially stabilized tetragonal zirconia ceramic (Y-TZP, commonly referred to as zirconia ceramic) was explored. This resulted in the launch of several commercial brands of zirconia ceramic implants.[18,32–39] Ceramics attracted attention owing to the following advantages:

1. Bioinert or chemical inertness. Ceramics, as opposed to titanium metal, are chemically more inert, which implies a very low allergic risk. They are therefore ideal for patients who don't want metal in their mouths, and for patients with hypersensitive reactions to titanium.[40,41]
2. Aesthetics. Ceramic implants are more aesthetic since they can be made white or tooth-colored, and even translucent. This is particularly advantageous in the anterior region where gray titanium implants sometimes show through the gums.
3. Soft-tissue friendly. It has been demonstrated that adhesion of plaque and bacteria on zirconia implants is lower than on titanium implants, which reduces the risk of inflammatory reactions in the adjacent soft tissue.[42–44]
4. One-piece implants. These avoid bacterial colonization in the microgap. Conventional screw-retained two-piece implants unavoidably form an interface between the implant and abutment (commonly referred to as a microgap), with a width of up to 50 μm. It has been reported that this microgap is a critical factor that increases the risk of bone retraction caused by bacterial colonization.[44–48]

The use of ceramic materials opens up the possibility of eliminating the above problems by producing customized one-piece implants that integrate the implant root and abutment into a single unit.

In the orthopedic field it is well known that alumina and zirconia ceramics cannot osseointegrate as good as titanium metal does.[49] In dentistry, published preclinical and clinical investigations, however, seem to indicate that both alumina and zirconia ceramic implants have a high level of bone-to-implant contact that is also regarded as a high level of osseointegration (in most of the cases). Nevertheless, a recent review concluded that the scientific clinical data for ceramic implants in general, and for zirconia implants in particular, is not yet sufficient to recommend ceramic implants for routine clinical use.[3]

Obviously, further investigations of the impact of implant materials, designs, and surface modifications on mechanical and biological performance are required. In a recent study, we demonstrated that a family of in vitro bioactive ceramic nanocomposites composed of micron-sized hydroxyapatite (HA) grains embedded in a zirconia or alumina matrix of nanograins provoke osseointegration by involving both distant and contact bone growth mechanisms; certain in vivo non-bioactive ceramics may still establish osseointegration with the surrounding bone merely by the distant bone growth mechanism, provided that the possible inflammatory reactions and formation of fibrous tissues are avoided during the entire healing procedure.

13.6 MORPHOGENETICALLY ACTIVE SCAFFOLDS FOR BONE TISSUE ENGINEERING

13.6.1 3D Matrices Mimicking the Natural Cellular Environment

Bone is a natural composite with a functional gradient, structural, and compositional hierarchy composed of three major structural components: hydroxycarbonate apatite (HA), collagen, and pores. It has a hard and dense outer layer, known as cortical bone, with 10–30% porosity, and a porous interior (i.e. cancellous bone with a higher porosity level of 30–90% and large pores). The mechanical properties of bone vary widely from cancellous to cortical bone. Bone scaffolds are porous frameworks with tailored chemical composition and porous architecture intended for inducing cartilage and bone tissue regeneration. They may also be referred to as 3D matrices that mimic the natural cellular environment for cells to grow, differentiate, and deposit biomimetic HA.

Bone tissue engineering is a complex and dynamic process that initiates with migration and recruitment of osteoprogenitor cells. This is followed by their proliferation, differentiation, and matrix formation, along with remodeling of the bone. The scaffold designed to mimic the natural organic 3D bone structure must follow the nano-fibrous architecture, being highly porous to allow an ingrowth of cells and an efficient transport of morphogens, cytokines,

growth factors, nutrients, oxygen, and waste products. A further prerequisite for an efficient and functional scaffold is the ability to allow vascularization of the inserted material. Besides being mechanically suitable, the material must be osteoconductive. Synthetic bone scaffolds have advantages over bone grafts because they are not fraught with uncertainties (e.g. disease transmission, risk of infection, or immunogenicity). In a physiological framework, the bone cells find a suitable scaffold with an appropriate porosity that allows cell in-growth, and where they can differentiate and communicate with neighboring cells.

13.6.2 Bone Scaffold Materials and Their Fabrication Techniques

So far, bioactive ceramic scaffolds have been made from three families of ceramics (i.e. calcium phosphates, CaP; bioglasses; and composites).[50] CaPs are the major constituents of bone. CaP-based scaffolds allow new bone formation and biomineralization by surface-induced CaP crystallization (see Section 13.5.2) and contact osteogenesis (see Section 13.3.2). By adjusting the content of β-tricalcium phosphate (β-TCP), CaP-based scaffolds can be made partially degradable. Bioglass scaffolds release calcium and phosphate ions from their surface after implantation; this promotes formation of a hydroxycarbonate apatite (HCA) layer on them, most probably by a surface-induced CaP crystallization mechanism (see Section 13.5.2). This HCA layer can significantly enhance osteoblast activity,[35] and also adsorb proteins and growth factors that facilitate new bone formation in vivo.[35] One common drawback of the CaP- and bioglass-based ceramic scaffolds is that they are all very fragile.

Sufficient improvement in their mechanical performance can be achieved by employing a composite strategy, while limited improvement can be achieved by optimizing their pore architecture. Sealing surface defects with a biodegradable polymer coating, or developing an interconnected CaP-polymer scaffold, for instance, also takes advantage of both CaPs and polymers to meet the mechanical and physiological requirements of the host tissue. Adding polymer into CaPs increases the toughness and compressive strength of scaffolds to that of natural bone, which improves the biological and mechanical integrity between bone and scaffolds.

The bioactive ceramic scaffolds mentioned above were engineered to enhance bone formation and growth. They may be regarded as osseoconductive (see Section 13.3.3). However, they are biologically inactive due to the lack of ligands for the bone cell surface receptors to induce cell-specific differentiation processes. This limitation may be removed by seeding the scaffolds with bone marrow stem cells and/or by introducing and harboring drugs, genes, and different growth factors into the scaffolds. Indeed, this is the current trend in scaffold development. An even smarter approach is to use those morphogenetically active materials such as bio-silica and bio-polyphosphate to prepare novel, functionally active scaffolds with self-regulatory activities that stimulate HA formation (see Section 13.4.2).
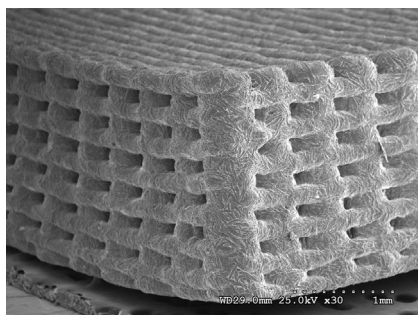
FIGURE 13.9   A β-tricalcium phosphate scaffold prepared by robocasting. *(Courtesy of Pedro Miranda González.)*

Porous scaffolds for bone regeneration require well-defined pore architectures with pore size in the microporous region (i.e. around a few hundred microns to facilitate tissue in-growth), which can hardly be achieved by traditional ceramic-shaping techniques (see Chapter 7). Accordingly, new processing concepts of free-form fabrication (see Chapter 18), such as robocasting, have been developed to prepare scaffolds with tailor-made interconnected macroporosity. Bioactive ceramic scaffolds based on HA, β-TCP, and bioactive glasses, have been prepared in this manner.[51–53] One such example is shown in Figure 13.9. Use of these novel techniques allows both the size and the shape of the macropores to be controlled, as well as the pore volume. Scaffolds with customized external geometry may also be prepared on an industrial scale.

ACKNOWLEDGMENTS

REFERENCES

1. Brånemark PI, Adell R, Breine U, Hansson BO, Lindström J, Ohlsson A. Intraosseous anchorage of dental prostheses. I. Experimental studies. Scand J Plast Reconstr Surg 1969;3:81–100.
2. Brånemark PI, Hansson BO, Adell R, Breine U, Lindstrom J, Hallen O, et al. Osseointegrated implants in the treatment of the edentulous jaw. Experience from a 10-year period. Scand J Plast Reconstr Surgery 1977;16:1–132.

3. Andreiotelli M, Wenz HJ, Kohal R-J. Are ceramic implants a viable alternative to titanium implants? A systematic literature review. Clin Oral Impl Res 2009;20 (Suppl. 4):32–47.

4. Hayashi K, Matsuguchi N, Uenoyama K, Sugioka Y. Re-evaluation of the biocompatibility of bioinert ceramics in vivo. Biomaterials 1992;13:195–200.

5. Bose S, Roy M, Bandyopadhyay A. Recent advances in bone tissue engineering scaffolds. Trends Biotechnol 2012;30(10):546–54.

6. Brånemark PI. Introduction to osseointegration. In: Brånemark PI, Zarb G, Albrektsson T, editors. Tissue integrated prostheses. Osseointegration in clinical dentistry. Berlin, Chicago, Tokyo: Quintessence; 1985. p. 1–76.

7. Davies JE. Mechanisms of endosseous integration. Bone Bond Nat biomater surf 1998;11(5):391–400.

8. Albrektsson T, Johansson C. Quantified bone tissue reactions to various metallic materials with reference to the so-called osseointegration concept. In: Davies JE, editor. The bone-biomaterial Interface. Toronto: Univ of Toronto Press; 1991. p. 357–63.

9. Albrektsson T, Albrektsson B. Osseointegration of bone implants: a review of an alternative mode of fixation. Acta Orthop Scand 1987;58:567–77.

10. Kölliker A. Die normale résorption des Knochengewebes und ihre Bedeutung für die Enstehung der typschen Knochenformen. Leipzig, Germany: FCW Vogel; 1873.

11. Osborn JF, Newesley H. Dynamics aspects of the implant bone interface. In: Heimke G, editor. Dental implants—materials and systems. Munich: Carl Hanser; 1980. p. 111–23.

12. Kokubo T, Takadam H. How useful is SBF in predicting in vivo bone bioactivity?. Biomaterials 2006;27(15):2907–15.

13. Bohner M, Lemaitre J. Can bioactivity be tested in vivo with SBF solution?. Biomaterials 2009;30(12):2175–9.

14. Kim HM, Himeno T, Kawashita M, Kokubo T, Nakamura T. The mechanism of biomineralization of bone-like apatite on synthetic hydroxyapatite: an in vitro assessment. J R Soc Interface 2004;1:17–22.

15. Lu X, Leng Y. Theoretical analysis of calcium phosphate precipitation in simulated body fluid. Biomaterials 2005;26:1097–108.

16. Gruner D, Faldt J, Jansson K, Shen ZJ. Argon ion beam polishing: a preparation technique for evaluating the interface of osseointegrated implants with high resolution. Int J Oral Maxillofac Implants 2011;26(3):547–52.

17. Albrektsson T, Brånemark PI, Hansson HA, Lindstrom J. Osseointegrated titanium implants. Requirements for ensuring a long-lasting, direct bone-to-implant anchorage in man. Acta Orthop Scand 1981;52:155–70.

18. Gahlert M, Röhling S, Wieland M, Sprecher CM, Kniha H, Milz S. Osseointegration of zirconia and titanium dental implants: a histological and histomorphometrical study in the maxilla of pigs. Clin Oral Impl Res 2009;20:1247–53.

19. Sennerby L, Dasmah A, Larsson B, Iverhed M. Bone tissue responses to surface modified zirconia implants: a histomorphometric and removal torque study in the rabbit. Clin Implantol Dental Relative Res 2005;7:S13–20.

20. Davies JE, Chernecky R, Lowenberg B, Shiga A. Deposition and resorption of calcified matrix in vitro by rat bone marrow cells. Cells Mater 1991;1:3–15.

21. Davies JE, Ottensmeyer P, Shen X, Hashimoto M, Peel SF. Early extracellular matrix synthesis. In: Davies JE, editor. The bone-biomaterial interface. Toronto: Univ of Toronto Press; 1991. p. 214–28.

22. Müller WEG, Boreiko A, Wang X, Krasko A, Geurtsen W, Custódio MR, et al. Morphogenetic activity of silica and bio-silica on the expression of genes controlling biomineralization using SaOS-2 cells. Calcif Tissue Int 2007;81:382–93.

23. Wiens M, Wang XH, Schröder HC, Kolb U, Schloßmacher U, Ushijima H, et al. Biomaterials 2010;31:7716–25.
24. Müller WEG, Wang XH, Diehl-Seifert B, Kropf K, Schloßmacher U, Lieberwirth I, et al. Inorganic polymeric phosphate/polyphosphate as an inducer of alkaline phosphatase and a modulator of intracellular Ca2+ level in osteoblasts (SaOS-2 cells) *in vitro*. Acta Biomater 2011;7:2661–71.
25. Wang XH, Schröder HC, Wiens M, Schloßmacher U, Müller WEG. Bio-silica: molecular biology, bochemistry and function in demosponges as well as its applied aspects for tissue engineering. Adv Mar Biol 2012;62:231–71.
26. Schröder HC, Wang XH, Wiens M, Diehl-Seifert B, Kropf K, Schloßmacher U, et al. Silicate modulates the cross-talk between osteoblasts (SaOS-2) and osteoclasts (RAW 264.7 cells): inhibition of osteoclast growth and differentiation. J Cell Biochem 2012;113:3197–206.
27. Szmukler-Moncler S, Salama H, Reingewirtz Y, Dubruille JH. Institut Straumann, Waldenburg, Switz, Timing of loading and effect of micromotion on bone- dental implant interface: review of experimental literature. J Biomed Mater Res 1998;43(2):192–203.
28. Dey A, Bomans PHH, Müller FA, Will J, Frederik PM, deWith G, et al. The role of pre-nucleation clusters in surface-induced calcium phosphate crystallization. Nat Mater 2010;9:1010–4.
29. Beniash E, Metzler RA, Lam RSK, Gilbert PUPA. Transient amorphous calcium phosphate in forming enamel. J Struct Biol 2009;166:133–43.
30. Driskell TD, Heller AL. Clinical use of aluminum oxide endosseous implants. J Oral Implantol 1977;7:53–76.
31. Chang YS, Oka M, Nakamura T, Gu HO. Bone remodeling around implanted ceramics. J Biomed Mater Res 1996;30:117–24.
32. Dubruille JH, Viguier E, Le Naour G, Dubruille MT, Auriol M, Le Charpentier Y. Evaluation of combinations of titanium, zirconia, and alumina implants with 2 bone fillers in the dog. Int J Oral Maxillofac Implants 1999;14:271–7.
33. Nagai N, Takeshita N, Kiniwa S. Basic and clinical-study on the dental endosseous implant of zirconia ceramic. J Dental Res 1987;66:928.
34. Schultze-Mosgau S, Schliephake H, Radespiel-Troger M, Neukam FW. Osseointegration of endodontic endosseous cones: zirconium oxide vs titanium. Oral Surg Oral Med Oral Pathol Oral Radiol Endod 2000;89:91–8.
35. Gahlert M, Gudehus T, Eichhorn S, Steinhauser E, Kniha H, Erhardt W. Biomechanical and histomorphometric comparison between zirconia implants with varying surface textures and a titanium implant in the maxilla of miniature pigs. Clin Oral Implants Res 2007;18:662–8.
36. Wenz HJ, Bartsch J, Wolfart S, Kern M. Osseointegration and clinical success of zirconia dental implants: a systematic review. Int J Prosthodont 2008;21:27–36.
37. Silva NR, Coelho PG, Fernandes CA, Navarro JM, Dias RA, Thompson VP. Reliability of one-piece ceramic implant. J Biomed Mater Res Part B 2009;88:419–26.
38. Koch FP, Weng D, Kra¨mer S, Biesterfeld S, Jahn-Eimermacher A, Wagner W. Osseointegration of one piece zirconia implants compared with a titanium implant of identical design: a histomorphometric study in the dog. Clin Oral Impl Res 2010;21:350–6.
39. Rocchietta I, Fontana F, Addis A, Schupbach P, Simion M. Surface-modified zirconia implants: tissue response in rabbits. Clin Oral Impl Res 2009;20:844–50.
40. Lalor PA, Revell PA, Gray AB, Wright S, Railton GT, Freeman MA. Sensitivity to titanium. A cause of implant failure?. J Bone Joint Surg Br 1991;73:25–8.
41. Sicilia A, Cuesta S, Coma G, Arregui I, Guisasola C, Ruiz E, et al. Titanium allergy in dental implant patients: a clinical study on 1500 consecutive patients. Clin Oral Implants Res 2008;19:823–35.

42. Akagawa Y, Hosokawa R, Sato Y, Kamayama K. Comparison between freestanding and tooth-connected partially stabilized zirconia implants after two years' function in monkeys: a clinical and histologic study. J Prosthet Dent 1998;80:551–8.

43. Scarano A, Di Carlo F, Quaranta M, Piattelli A. Bone response to zirconia ceramic implants: an experimental study in rabbits. J Oral Implantol 2003;29:8–12.

44. Covani U, Marconcini S, Crespi R, Barone A. Bacterial plaque colonization around dental implant surfaces. Implant Dent 2006;15(3):298–304.

45. Piattelli A, Vrespa G, Petrone G, Iezzi G, Annibali S, Scarano A. Role of the micro-gap between implant and abutment: a retrospective histologic evaluation in monkeys. J Periodontol 2003;74:346–52.

46. Broggini N, McManus LM, Hermann JS, Medina RU, Oates TW, Schenk RK, et al. Persistent acute inflammation at the implant-abutment interface. J Dent Res 2003;82(No. 3):232–7.

47. Scarano A, Assenza B, Piattelli M, Iezzi G, Leghissa GC, Quaranta A, et al. A 16–year study of the microgap between 272 human titanium implants and their abutments. J Oral Implantol 2005;31(6):269–75.

48. Tesmer M, Wallet S, Koutouzis T, Lundgren T. Bacterial colonization of the dental implant fixture–abutment interface: an in vitro study. J Periodontol 2009;80(12):1991–7.

49. Chevalier J, Gremillard L. Ceramics for medical applications: a picture for the next 20 years. J Eur Ceram Soc 2009;29:1245–55.

50. Bose S, Roy M, Bandyopadhyay A. Recent advances in bone tissue engineering scaffolds. Trends Biotechnol 2012;30(No. 10):546–54.

51. Michna S, Wu W, Lewis JA. Concentrated hydroxyapatite inks for direct-write assembly of 3-D periodic scaffolds. Biomaterials 2005;26:5632–9.

52. Miranda P, Saiz E, Gryn K, Tomsia AP. Sintering and robocasting of β-tricalcium phosphate scaffolds for orthopaedic applications. Acta Biomater 2006;2:457–66.

53. Deliormanli AM, Rahaman MN. Direct-write assembly of silicate and borate bioactive glass scaffolds for bone repair. J Eur Ceram Soc 2012;32:3637–46.

Chapter 14

Surface Modifications of Load-Bearing Ceramics for Improved Osseointegration

Martin Stefanic and Tomaž Kosmač
Jožef Stefan Institute, Ljubljana, Slovenia

Contents

14.1 INTRODUCTION

Nowadays, titanium is mostly used for the fabrication of dental and orthopedic implants. Although titanium and its alloys are still considered to have appropriate mechanical and biological properties, years of clinical experience have raised several concerns related to its usage; for example, bio-corrosion and negative aesthetic impact. Due to continuous advances in health treatments and public expectations, there is a demand for biocompatible, corrosion-resistant materials that also meet aesthetic criteria. Several high-performance engineering ceramics, such as zirconia, alumina, zirconia-toughened alumina (ZTA), alumina-toughened zirconia (ATZ), and silicon nitride, meet these criteria, and are appealing materials for the fabrication of load-bearing bone

implants due to their outstanding mechanical properties, biocompatibility, corrosion resistance, and aesthetic properties. However, much work is still needed b reach their full potential as biomaterials.

One intrinsic property of these high-performance engineering ceramics is that they provide a biologically inert surface, which makes them biocompatible so that they do not trigger unwanted reactions in the immune system. This makes ceramics an ideal candidate in situations where no interactions with surrounding tissues is desired, as in the case of dental abutments, crowns, and bridges. In contrast, surface inertness of ceramics is a drawback in situations where strong interaction with tissue is desirable, as is the case with bone implants. As a result of surface inertness a soft and non-adherent fibrous layer develops around the implant and at the bone–implant interface. In some cases, the fibrous capsule can become several hundred micrometers thick, which quickly loosens the implant. Loosening invariably leads to clinical failure for a variety of reasons, including fracture of the implant or the bone adjacent to the implant.[1]

Various studies have clearly correlated the clinical success of bone implants to their surface properties, i.e. surface topography and chemical composition.[2] Surface topography relates to the degree of surface roughness and the orientation of surface irregularities.[3] Regardless of implant composition, surface topography is considered a critical component for achieving implant stability for sufficient osseointegration. For this reason, surface topography has been one of the main focuses of the scientific community working in the field of bone implants.[2] Surface topography has an influence on the adhesion, proliferation, and differentiation of cells; their expression of local factors, and on the biomechanical stability of the implant in the bone. The smooth or machined implant surfaces used in the past have been replaced by modified rough surfaces, including topographic features in the millimeter-nanometer range, that are all believed to be relevant to the biological response of the host. In addition to surface topography, the quality of the bone–implant interface has also been strongly associated with the surface chemistry, including surface chemical composition, crystallinity, free energy, charge, wettability, and presence of impurities.[4] Surface chemistry strongly affects the adsorption of proteins and their conformation, and consequently influences cell and tissue responses. As a result of specific surface chemistry, some materials can form chemical bonds with the bone. Such a phenomenon is particularly desirable for bone implants since it enables rapid and strong anchorage to bone. Materials with bone-bonding ability are known as bioactive materials. Typical representatives of bioactive materials are bioactive glasses and calcium phosphates.[1] Numerous studies have focused on the modification of surface chemistry of high-performance ceramics in order to prepare bioactive load-bearing ceramics with improved stability in bone. An important advantage of implants with bioactive surfaces is that the biochemical attachment is more rapid compared to biomechanical fixation, and it functions at a time when proper

biomechanical bonding has not yet been developed. It takes weeks before bone starts growing into surface irregularities, and the bioactive surface can stabilize the implant before this event.[3] Various authors have investigated the phenomenon of bioactivity and which materials can bond to living bone.[5] A common feature found at the interface between bioactive materials and bone after in vivo tests was a thin hydroxyapatite layer. Kokubo's group made a significant contribution to the understanding of bioactivity. They proposed an in vitro experiment to reproduce the formation of biological hydroxyapatite on bioactive materials in vivo by immersing the material in simulated body fluid (SBF) with a composition similar to the inorganic portion of the human blood plasma.[5] Despite the fact that experiments with SBF represent a big simplification of a real in vivo situation, and that many authors expressed concerns regarding the method,[6,7] it has been frequently used and has become a widely accepted approach for testing the bioactivity of materials.

Since surface properties of load-bearing bone implants are of key importance for their long-term stability, numerous studies have focused on their surface modifications in order to improve osseointegration. Optimal surface treatment of the implant could lead to faster and stronger bone formation around the implant, which could confer better stability during the healing process and thus allow more rapid loading of the implant.[2] Studies on surface modifications of load-bearing bone implants have been mainly performed on metals[8]; much less work has been done on high-performance bioceramics. Surface modification techniques that have been applied to bioceramics can be divided into two types: (1) modifications of surface topography; and (2) modifications of surface chemistry. These two approaches are commonly interrelated. For example, modifications of surface chemistry can alter surface topography and vice versa. Hence, for a correct interpretation of results, surface properties should be characterized in detail with appropriate and precise methods when studying the influence of various surface treatments on biological responses.

14.2 MODIFICATIONS OF SURFACE TOPOGRAPHY

Numerous studies have shown marked differences in the in vitro and in vivo responses to implants with different surface topographies. This demonstrates that the ability of the implants to support bone formation can be enhanced by modifying the surface topography.[9] Surface topography can be divided into three levels according to the scale of the features: macro-, micro- and nano-sized. The macro level is meant here as topographical features in the range of millimeters to tens of microns. This scale is directly related to implant geometry. The micro level determines the surface roughness in the range of $1-10\,\mu m$. This range of roughness maximizes the interlocking between mineralized bone and the surface of the implant. The nanometer range is considered to be below $100\,nm$. Surface profiles in the nanometer range play an important

role in the adsorption of proteins, adhesion of cells, and thus on the rate of implant osseointegration.[10] Numerous reports have shown that both the early fixation and long-term mechanical stability of the prosthesis is better in the case of rough surfaces as compared to smooth surfaces. A rough surface enables bone ingrowth into small surface irregularities and enables biomechanical bonding. Thus, osseointegration strongly depends on the strength of biomechanical bonding.[3] At a more fundamental level, surface topography affects protein adsorption and cell behavior by inducing specific cell signals, and consequently regulates the formation of extracellular matrix and bone apposition.[9] Animal trials with titanium implants have shown that a moderately rough surface with an average surface roughness (S_a) of about 1.5 μm and a developed surface area (S_{dr}) of about 50% promotes better bone response as compared to rougher or smoother surfaces.[2] Implants with higher roughness (i.e. more than 2 μm) have also shown good results, however, risks related to higher roughness include increased incidence of peri-implantitis, increase in ionic leakage.[3] Also, excessive roughness can make it harder to remove an implant, and can be detrimental to implant strength.[9] Texturing an implant's surfaces at the nano-scale offers new possibilities for the manipulation of the biological response. It is believed that the biological response to an implant's surface could be improved by mimicking the nano-scale components of the extracellular matrix components of natural tissue. Various studies have shown that nano-structured materials affect protein adsorption and conformation; improve cell attachment; decrease inflammation; and accelerate wound-healing and angiogenesis.[11] Furthermore, novel titanium implants supplied by world-leading manufacturers indeed exhibit nano-roughness as a common property, which is absent in their commercial predecessors. Hence, a possible common mechanism behind the strong bone response to many new implants is a nano-roughness pattern. However, the optimal surface nano-topography for selective adsorption of proteins that can lead to the adhesion of osteoblasts and rapid bone apposition is still unknown.[2]

Various methods have been developed to modify the topography of titanium implants, such as machining, sandblasting, titanium plasma spraying, and chemical/electrochemical etching. Some of these surface modification techniques, in particular sandblasting and acid etching, have been applied on high-performance ceramics and clearly demonstrated that surface topography has a strong influence on the biological response to ceramics.[12–20] While abrasion and etching can be easily applied to metals, the comparatively high hardness and chemical stability of high-performance ceramics renders this more difficult to achieve than in the case of metals. For this reason, alternative techniques are being developed for the surface modification of ceramic surface topography.

One such innovative technique for preparation of rough and porous zirconia surfaces includes dipping a pre-sintered zirconia implant into a zirconia slurry that contains a pore-former.[21] During subsequent sintering the pore-former

is burned off and leaves a rough porous structure on the surface, while the core implant becomes fully dense. Using the above described procedure, Sennerby et al. prepared zirconia implants with three different topographies and compared their osseointegration in rabbit bone.[22] The average roughness of implants with modified topography was $R_a = 1.24\,\mu m$ and $R_a = 0.93\,\mu m$, while the untreated machined implants had an R_a of $0.75\,\mu m$. Modified surfaces showed much stronger bone tissue response and a 5-fold increase in resistance to removal torque as compared to untreated machined surfaces after six weeks' of healing in rabbit bone. In addition, bone integration of the modified implants was similar to commercial titanium implants. Results of the study suggest that surface-modified zirconia implants can reach a firm stability in bone. Gahlert et al. did an animal study aimed at evaluating bone anchorage to machined ($R_a = 0.13\,\mu m$) and sandblasted ($R_a = 0.56\,\mu m$) implants in a pig model.[16] After 4, 8, and 12 weeks of bone healing, removal torque testing was performed to evaluate the interfacial shear strength of each surface type. The results showed significantly higher removal torque values and quantity of bone apposition on rough zirconia as compared to machined zirconia. This study confirmed the findings of Sennerby et al., that a rougher zirconia surface is preferential for bone anchorage.[22] A novel method for roughening the surface of zirconia was presented.[23] The method comprises different combinations of sandblasting and acid-etching treatments. Alumina or silicon carbide particles were used for sandblasting, while acid-etching treatments were performed using combinations of HNO_3, H_2O_2, and HF solutions at different concentrations and temperatures; and for different treatment times. By varying these parameters, different topographies can be obtained on zirconia at the nanometer-, submicrometer-, and micrometer-scales. In addition, by applying different treatments, the wettability of the zirconia could also be controlled. Recently, Hoffman et al. compared bone healing and apposition around zirconia implants (in rabbits) with different surface characteristics.[17] Zirconia implants with (a) untreated, (b) sandblasted, and (c) laser-treated surfaces were examined. After 6 and 12 weeks' of healing, the trend of higher bone apposition on laser-modified surfaces was observed. However, compared to the differences from other experimental groups, there was no statistical significance. Oliva et al. reported a one-year follow-up of zirconia implants in humans.[24] The osseointegration of implants with two different surface topographies was compared: one group of implants had a surface roughness of $R_a = 0.3\,\mu m$, while the second group was coated with bioactive glass with the composition $Na_2O–K_2O–MgO–Al_2O_3–CaO–SiO_2–P_2O_5–F$ and the surface roughness $R_a = 0.43\,\mu m$. One year after implantation, both implants showed firm stability, and no significant difference was observed between the two implant groups. The overall success rate of implants was 98%, which is comparable with the success rate reported for titanium implants. Nevertheless, this study focused only on differences in surface topography. When comparing

the two surfaces, differences in surface chemical composition should be taken into an account since bioactive glass coatings could considerably affect the bone response solely on the basis of chemical composition. Park et al. presented an innovative procedure for controlling the surface topography of zirconia implants using powder injection molding (PIM) technique.[25] In the PIM process a suspension of ceramic particles and organic binders is used. The suspension is injected under low or high pressure into a mold that has a shape of the final product (negative, a dental implant). Prior to sintering, the organic binders embedded in the molded parts must be removed via thermal pyrolysis or solvent detracting. It was shown that zirconia implants with controlled surface roughness can be prepared in a reproducible manner if the ceramic suspension is injected into the mold with a textured wall. Using such a procedure, two different ceramic implants with surface roughness of $R_a = 0.5 \mu m$ and $2 \mu m$ were prepared and tested, respectively. The implants were inserted into the rabbit bone, and after a short period of healing, their osseointegration was investigated. While implants with roughness of $R_a = 2 \mu m$ showed much higher RTQ values as compared to implants with smoother surfaces, there were no significant differences in bone-to-implant contacts between the two implants. The study showed that PIM is an efficient technique for the reproducible fabrication of implants with controllable surface topography. In addition, it is a cheap process and has the potential to be translated into mass production.

Laser treatments have also been applied to ceramics to modify the surface topography. For example, femtosecond laser treatment has been found to be an efficient approach for microstructuring and nanostructuring of zirconia.[26,27] Delgado-Ruiz et al. first demonstrated that rapid femtosecond laser treatment can successfully modify the commercially available zirconia implants at micro- and nano-scales.[26] Laser pulses could generate different surface patterns in a controlled manner, such as big conical-shaped holes of a few micrometers and pyramidal grooves and nanometric polycrystal structures of less than 100 nm. The R_a of dental implants could be enhanced from an initial $1.58 \mu m$ for control implants to $2.43 \mu m$ for surfaces with holes, and up to $9.5 \mu m$ for surfaces with grooves. Moreover, laser ablation removed surface layers, which resulted in decreased concentration of contaminants, such as carbon and aluminium, and decreased the portion of the monoclinic zirconia phase. Both of these could significantly improve the performance of zirconia implants in vivo since it is known that surface impurities can affect biocompatibility and that the monoclinic zirconia phase on the surface significantly decreases the mechanical properties and reliability of zirconia implants.[28,29] Despite the encouraging results from the material point of view, there have not been any biological tests conducted so far to assess the influence of described topographical and chemical changes of the surface on the biological response. Another laser treatment that was found to successfully roughen the surface of zirconia was CO_2 irradiation.[30,31] Surface roughness was increased linearly by

increasing the laser power from the initial average roughness $R_a = 0.295\,\mu m$ of untreated samples to $R_a = 0.305\,\mu m$ $(0.6\,kW/cm^2)$, $0.333\,\mu m$ $(0.9\,kW/cm^2)$, $0.717\,\mu m$ $(1.6\,kW/cm^2)$, $1.882\,\mu m$ $(1.9\,kW/cm^2)$, and $3.854\,\mu m$ $(2.5\,kW/cm^2)$. Laser power also influenced the surface microstructure of zirconia substrates. In addition, besides changing the surface topography, laser treatment also changed the surface chemistry by increasing the number of OH functional groups on the surface, which rendered the surface bioactive according to the SBF test. However, after 14 days of immersion, only a few apatite islands were observed on the surface, which could indicate that laser treatment produced only certain areas with apatite-nucleating capacity. Aboushelib et al. developed a new method for the preparation of a highly retentive nano-porous zirconia surface, the so-called selective infiltration etching (SIE).[32] In this technique, the zirconia surface is coated with a special infiltration glass and heated above its glass transition temperature. The molten glass diffuses between the grain boundaries of zirconia, and exerts surface tension and capillary forces that result in sliding, splitting, and rearrangement of the surface grains. After cooling to room temperature, the glass is dissolved in an acidic bath, exposing the newly created nano-scale, inter-grain surface porosity. While this technique was initially developed to improve the zirconia-resin bond strength for prosthetic applications, the authors later investigated whether SIE could improve the osseointegration of zirconia implants. In vivo tests in rabbits[32] and rats[33] showed that zirconia treated with SIE had good osseointegration and did not elicit any neurotoxic effects. In addition, bone-to-implant contact of SIE-treated zirconia implants was significantly higher as compared to sintered zirconia implants and titanium implants.

Several studies utilized in vitro cell culture tests and protein adhesion tests to evaluate the biological response at a more fundamental level and predict the clinical performance of materials. Although more reliable results can be expected from the in vivo investigations, in vitro tests clearly indicate some benefits, such as faster and more convenient analysis, lower price, and an ability to evaluate the biological response at a more fundamental level. This approach is also less ethically questionable than in vivo animal tests. Bachle et al. studied how different zirconia surface topographies influence the response of CAL72 osteoblast-like cells.[15] Zirconia substrates with three different surface treatments were used: machined surfaces $(R_a = 0.15\,\mu m)$, sandblasted surfaces $(R_a = 0.85\,\mu m)$, and sandblasted and HF acid-etched surfaces $(R_a = 0.93\,\mu m)$. Other than the determination of surface topography, other physicochemical properties of the surface were not evaluated. The study revealed no significant difference in the behavior of osteoblast-like cells on different surfaces. The initial adhesion and spreading of cells was good on all surfaces examined and the cells showed similar vitality and proliferation rates on all surfaces. Even the non-treated machined substrates supported fixation of cells. The authors concluded that cell attachment, morphology and proliferation, were not affected by the topography of the substrate. Wang et al. studied the response of osteoblasts

to zirconia surfaces with different surface topographies (i.e. micro-rough surfaces with nanosized grains, micro-rough surfaces without nanosized grains, and polished surfaces).[19] The SBF test of bioactivity showed that only the surface with nano-features had apatite forming ability, suggesting that nano-features are essential for bioactive property. Similarly, the adhesion and proliferation rate of osteoblasts was significantly higher on those surfaces as compared to micro-rough surface without nano-grains and polished surfaces. The authors concluded that combined macro- and nano-topography is favorable for implant osseointegration. In contrast to the results of Bachle et al., this study showed differences in cell response, indicating that surface nano-features on zirconia have a significant impact on cell behavior.[15] Webster et al. studied protein adhesion and cell interactions with nano-phase alumina ceramics.[34] They prepared alumina substrates with 24, 45, and 167 nm-sized grains. Ceramics with smaller grains and hence more grain boundaries exhibited higher roughness at the nano-scale and more hydrophilic character. Significantly higher amounts of serum proteins, collagen, and vitronectin were adsorbed on nano-phased alumina as compared to conventional alumina. In addition, osteoblast adhesion was also statistically higher on alumina with smaller grains as compared to coarser grained alumina. The results of higher vitronectin adsorption and higher osteoblasts adhesion on nano-phase ceramics support earlier findings showing that vitronectin stimulates osteoblast adhesion. In contrast to osteoblasts, the adhesion of fibroblasts and endothelial cells rose with increasing the grain size, presumably due to a greater surface roughness at the nano-scale, a higher number of grain boundaries, and higher hydrophilicity of the nano-phased ceramics. The ion beam-assisted deposition (IBAD) technique was utilized for preparation of transparent and nanocrystalline cubic and mixed-phase zirconia films.[35] The coatings displayed ultra-hydrophilic character and in vitro cell tests showed that the growth and proliferation of bone marrow stromal cells on nanostructured zirconia coatings was enhanced as compared with the conventional orthopedic metallic and ceramic smooth surfaces. It was also demonstrated that such coatings were superior even to bulk hydroxyapatite in terms of cell adhesion and growth. The same group also carried out computational analysis of the initial immobilization of one known structural fragment of the adhesive protein fibronectin and found out that the initial immobilization of the protein fragment on the nanostructured zirconia surface is achieved with much larger adsorption energy as compared to the smooth surface. This difference is due to the strong attractive electrostatic interactions between the protein fragment and the nanostructured surface. In contrast, in the case of adsorption on the flat, uncharged surface, this factor is negligible.[36] In another study,[20] the response of SaOS-2 osteosarcoma cells on zirconia with two different surface topographies (sandblasted vs. sandblasted/acid-etched) and acid-etched titanium surfaces was investigated. Both of the ceramics studied had surface roughness of about 1.1 μm. Cell behavior on both surfaces was similar. While the adhesion rate was slightly higher on sandblasted surface, the differentiation rate

was higher on sandblasted and acid-etched zirconia. Both surfaces showed an improved osteoblast response as compared to titanium.

14.3   MODIFICATIONS OF SURFACE CHEMISTRY

Methods aimed at the alteration of surface chemistry of bioceramics can be divided into three groups: chemical treatments, physical treatments, and deposition of bioactive coatings.

14.3.1   Chemical Treatments

Chemical treatments are aimed at applying functional groups on the surface of biomaterials for the optimization of surface chemistry. Studies on metal oxide gels and self-assembled monolayers (SAM) have shown that certain functional groups, such as –OH, –COOH, PO_4H_2, and –NH_2 have the apatite nucleation ability in SBF.[37] Chemical treatments, that have been so far applied to functionalize high-performance ceramics include immersion in acidic and alkaline baths.[38]

Hydroxylation of the surface was found to be a very successful approach for the bioactivation of ceramics.[30,31,38–40] During the hydroxylation treatments, additional –OH groups are attached on the ceramic surface which increase hydrophilicity, act as centers for apatite nucleation in SBF,[38,41] and promote cell attachment.[30,40,42] Uchida et al. prepared bioinert, nano-sized ATZ composite with high strength and high fracture toughness, and studied the possibilities of modifying the surface chemistry to induce apatite nucleation in SBF by soaking the materials in different concentrated and diluted alkaline and acidic solutions at 90°C for four days.[38] The solutions include H_3PO_4 (5 M and concentrated), H_2SO_4 (5 M and concentrated), HCl (concentrated), and NaOH (5 M and concentrated). All treatments applied were found successful and promoted apatite nucleation on the ATZ in SBF. The authors suggested that apatite nucleation occurred as a result of an increased number of Al-OH and Zr-OH groups attached on the surface. In addition, the highest rate of apatite nucleation was observed for the substrates treated with 5 M H_3PO_4. This observation was explained by the hypothesis that the H_3PO_4 treatment resulted in an increased Zr/Al ratio on the surface as detected with XPS. This in turn resulted in an increased number of surface Zr-OH groups, which are supposed to be more favorable for apatite nucleation than Al-OH (as observed earlier in the study with metal-oxide gels).[41] A similar observation was made by Faga et al. who studied the bioactive potential of chemically treated ATZ and ZTA composites.[39] They adopted the procedure of Uchida et al. and applied various treatments with H_3PO_4 or NaOH with different concentrations at 80–100°C for different times in an autoclave or under atmospheric pressure. The prepared samples were tested for bioactivity by immersing them in more supersaturated SBF (1.5X SBF) for four weeks. Only

in the case of H_3PO_4 treatment of ATZ (80 wt.% zirconia) in an autoclave for 4 hours were the ATZ specimens able to induce apatite nucleation in concentrated SBF. XPS surface analysis of these samples did not detect any phosphate phase, and the only observed difference was an increased concentration of –OH groups. Another interesting observation was that apatite crystals preferably grew on zirconia grains. This assumption agrees with the findings of Uchida et al.[38] which gives support to the suggested existence of threshold percentages for zirconia in the alumina-zirconia composites for promoting apatite nucleation. Also worth mentioning here is that H_3PO_4 treatment did not cause any strength degradation due to low-temperature degradation of the ATZ composite. In another study, hydroxylation of alumina was achieved by soaking the substrate into 1 M NaOH solution at 100°C for 24 hours, according to the following equation (Eq.14.1)[40]:

$$Al_2O_3 + 2NaOH + 3H_2O \rightarrow 2Na^+ + 2\left[Al(OH)_4\right]^- \qquad (14.1)$$
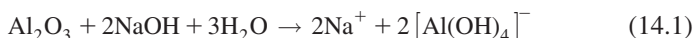
The as-treated alumina surfaces showed a pronounced effect on the activity of osteoblast-like cells. Cell proliferation, attachment, and osteocalcin expression were significantly higher on the treated alumina as compared to the non-treated one. Mechanical tests showed that aggressive treatments with NaOH had no deteriorating effect on the short- and long-term mechanical behavior of the ceramic material. Heat treatment in NaOH solution was also found to be successful in the case of porous ZTA ceramics.[42] NaOH treatment resulted in increased proliferation of MG63 osteoblasts and alkaline phosphatase (ALP) activity. Both studies showed that subjecting ceramics to a hot alkaline bath results in hydroxylation of the surface, which elicits a favorable cell response.[40,42] Nevertheless, it is not known whether the as-treated surface has apatite nucleation ability in SBF. Besides –OH groups also other functional groups have been conjugated to ceramics by utilizing chemical treatments. Bertazzo et al. did studies on the carboxylation of alpha-[43] and gamma-alumina surfaces.[44,45] Treatments included different carboxylic acids. When the alumina substrate was immersed in the dicarboxylic acid, carboxylate-aluminoxane was formed on the surface.[43,44] Such treatment resulted in a very reactive surface which was able to induce nucleation of large, elongated, sharp-edged crystals in SBF after 6 hours. In contrast, no crystal precipitation occurred on the non-treated specimens. The authors explained that bioactivity was achieved through the formation of free carboxyl groups on the surface of alumina, which complexed calcium ions from the SBF solution and formed nucleation sites on the surface of the sample. In addition, in vitro cell culture tests showed that the viability of pre-osteoblasts was significantly higher on alumina substrates treated with carboxylic acid as compared to non-treated ones. Nevertheless, it is worth mentioning that the shape of the deposited large crystals on the treated alumina was very different from the nanocrystalline biological-like deposits that are usually observed on bioactive materials when immersed in SBF. Although the

EDS analysis confirmed the presence of Ca and P elements on the treated alumina surface, the obtained Ca/P ratio of these crystals was much higher than in the case of biological-like CaP crystals that usually precipitate from the SBF, and have a Ca/P ratio between 1.33–1.67. Unfortunately, the authors did not perform any analysis in order to obtain information about the phase composition of the deposits on alumina.

14.3.2   Physical Treatments

Physical deposition methods, such as ion implantation, UV treatment, CO_2 irradiation, and laser treatment have been applied for the modification of the surface chemistry of bioceramics in order to improve its biological properties.

CO$_2$ irradiation has been used as a method for the bioactivation of magnesium partially-stabilized zirconia (Mg-PSZ). The CO_2 laser caused surface melting of Mg-PSZ and exposed Zr^+ and OH^- ions that created Zr-OH groups on the surface. As a consequence, surface wettability was improved. Laser treatment improved the bioactivity of Mg-PSZ, and in contrast to non-treated ceramics, apatite crystals formed on Mg-PSZ after 14 days of immersion in SBF. In addition, cell tests showed that osteoblasts had improved adhesion on the laser-treated samples as compared to untreated samples. Laser treatment also changed the topography of zirconia, which could also have a major influence on the cell behavior.

Ion implantation, which has been studied in several works, resulted in the significant improvement of the biological response to alumina, zirconia, and hydroxyapatite ceramics.[46–49] Zreiqat et al. studied the implantation of magnesium ions in alumina ceramics by using a metal vapor vacuum arc (MVVA) ion source. In vitro tests with human bone-derived cells revealed that Mg incorporation in alumina ceramics significantly improved the initial adhesion and differentiation of cells by increasing the expression of bone-related proteins, such as integrin receptors, focal adhesion kinase, collagen type I, and intracellular signaling molecules.[48,49] In another study, Mg^{2+} implantation in ZrO_2 ceramics resulted in the apatite forming ability of zirconia after immersion in the SBF.[46,50] Zhao et al. demonstrated that ion implantation can also be applied to graft–NH$_2$ groups on the surface of alumina. In further in vivo tests they compared the healing and osseointegration of NH_2^+ treated; and bare, non-treated, alumina implants in the jaw bones of dogs.[47] Results showed that NH$_2$ groups on the surface of alumina can clearly accelerate the healing time and enhance the bone deposition around the implant, making the Al_2O_3 ceramic implants more biocompatible to surrounding tissue.

Att and coworkers examined the effect of UV light treatment of zirconia on the biological response of osteoblasts.[51] Inspired by previous studies which demonstrated the ability of UV treatment to prepare a super-hydrophilic TiO_2 surface[52] and to significantly improve the osseointegration of titanium implants,[53] the authors hypothesized that UV treatment would have a similar

effect on zirconia and would promote a cell's bioactivity. UV light treatment transformed the zirconia surface from hydrophobic to hydrophilic and reduced the atomic percentage of surface carbon in a UV light dose-dependent manner. These photo-generated surface changes increased the capacity of zirconia for attachment, spread, proliferation, and ALP activity of rat bone marrow-derived osteoblasts and enhanced their mineralization capability.

14.3.3   Bioactive Coatings

Bioactive materials, such as calcium phosphates (CaP) with compositional resemblance to bone mineral, as well as certain formulations of glasses or glass-ceramics, show excellent biological properties. After implantation in bone tissue they can elicit specific biological responses that can result in strong bonding between the bone and the material. These bioactive materials can be applied as coatings on the surface of stronger but bioinert ceramics and can act as an intermediary layer that enables better fixation of the implant in the bone.[1] Essential requirements for the bioactive coatings on load-bearing bone implants are: the formation of a firm interface with bone tissue, and sufficient mechanical stability to withstand the mechanical forces present during implantation in the bone. In addition, coatings should present controlled dissolution rates in body fluids and possibly act as a drug delivery system.

14.3.3.1   Calcium Phosphate Coatings

Various techniques for the deposition of CaP coatings have been developed. Among them, plasma-sprayed hydroxyapatite coatings on the stems of metallic hip implants have already found great success in clinics. Besides plasma spraying, other techniques have also been extensively investigated.[54] A biomimetic wet-chemical approach that utilizes immersion of an implant in SBF is one of the most studied procedures for the deposition of CaP coatings on ceramics. While the SBF was originally proposed for testing the bioactivity of materials, it was later used by SBF inventors to coat bioinert organic, ceramic, and metallic materials with bone-like apatite crystals.[55] Advantages of the method are low price, preparation of uniform coatings on substrates with complex shapes, and good control over the thickness, morphology, and phases present. Also, coatings can be applied to different substrates, such as metals, polymers, and ceramics. Moreover, low temperatures enable incorporation of drugs into the coatings, which makes them potential drug delivery systems at the site of implantation. However, the original biomimetic coating method suffers from several drawbacks related to the relatively slow process, poor reproducibility, complex preparation of reaction solution, etc. In order to circumvent these problems, various modified biomimetic procedures and reaction solutions have been proposed.[56–58] Parameters that affect the properties of CaP coatings (e.g. phases present, morphology, thickness and adhesion of coating) are composition of

the reaction solution, concentration of salts present in the solution, volume of the solution, agitation, renovation, temperature, and time of the synthesis.

Since time is an important parameter to consider when looking at applicability of the method, many studies have focused on the synthesis of CaP coatings in as short a time as possible while still preserving satisfactory properties of the coatings. Different tensile strengths of the biomimetic coatings on substrates were reported, ranging from 3 MPa to 30 MPa.[59,60]

Cortes et al. studied the formation of a biomimetic hydroxyapatite coating on Mg-PSZ/Al$_2$O$_3$ composite in SBF and 1.4 SBF.[61] The study revealed that apatite nuclei form on zirconia composite after 21 days of immersion, however, when the solution was not renewed, the apatite coating did not form. In contrast, if the substrate was re-immersed into the fresh 1.4 SBF, a 20 µm thick apatite coating precipitated on the Mg-PSZ/Al$_2$O$_3$ after 7 days of immersion. Rambo et al. prepared a highly porous Al$_2$O$_3$ scaffold from natural cellulosic sponges via pyrolysis and Al-vapor-phase infiltration.[62] Afterwards they applied a two-step procedure and used two 5X-SBF solutions for deposition of a hydroxyapatite coating on an Al$_2$O$_3$ porous scaffold. In the first step, the Al$_2$O$_3$ samples were immersed in 5X-SBF for 24 hours in order to trigger precipitation of the CaP coating. These pre-coated porous bodies were then soaked for 72 hours in the second 5X-SBF solution; this solution had a lower concentration of Mg^{2+} and HCO$_3^-$ ions and consequently enabled faster precipitation of a biomimetic hydroxyapatite coating. Klopcic et al., who adopted a modified biomimetic procedure developed by Bigi et al. for titanium substrates,[56] studied the deposition of CaP on alumina and zirconia ceramics.[63,64] The procedure was effective for depositing a thin hydroxyapatite[63] or octacalcium phosphate[64] coating on alumina and zirconia ceramics. The coatings were able to induce apatite nucleation in SBF in a short period of time. However, the prepared coatings had very poor mechanical strength and were easily removed from the substrate using the Scotch-Tape test. When the OCP coatings were subjected to heating at 1050°C, adhesion of the coating was improved and was accompanied by the transformation of the OCP phase to the HA. Stefanic et al. from the same research group proposed a simple two-step wet-chemical procedure for the rapid deposition of biomimetic octacalcium phosphate coatings on zirconia ceramics.[65] The procedure included two steps where two highly supersaturated reaction solutions with simple composition were used. In the first step of the synthesis, the zirconia substrate was immersed into the highly supersaturated CaP solution with pH 7.4. A thin apatite layer precipitated on the zirconia through an amorphous and OCP precursor and uniformly covered the surface after 1 hour of immersion. This layer later served as a seeding layer for the secondary nucleation of CaP crystals in the second step of the synthesis when the substrate was immersed into the CaP solution with a lower degree of supersaturation, and enabled rapid growth of the OCP coating with a lamellar morphology (Figure 14.1).
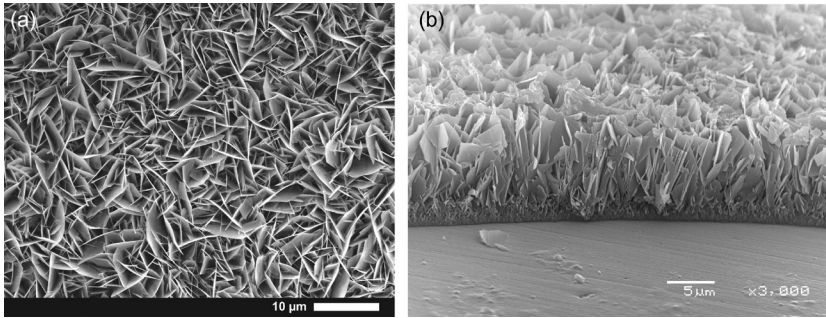
FIGURE. 14.1   SEM image showing upper view (a), and side view (b) of the biomimetic CaP coating on zirconia ceramic substrate.[66]
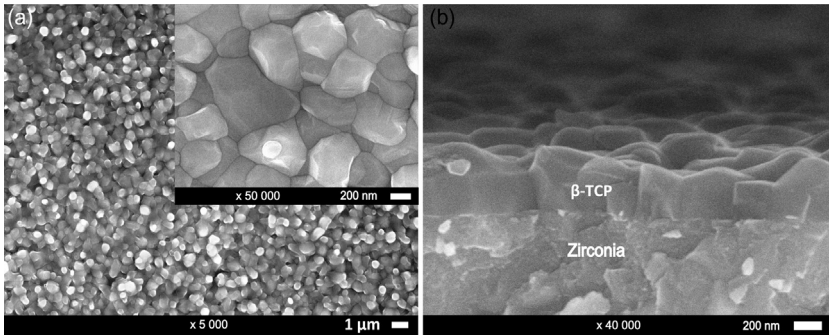
FIGURE. 14.2   SEM images of the β-TCP coating on the zirconia substrate. The β-TCP coating was obtained by applying a further post-deposition processing to the biomimetic CaP coating. Upper view (a) and side view (b) of the β-TCP coating on zirconia are shown.

Despite the several advantages of biomimetic CaP coatings, a major drawback that limits their application in clinics is their poor mechanical strength.[66] Therefore, heat treatment of the biomimetic CaP coatings has been studied as a way of improving the coating adhesion.[66] Stefanic et al.[66] developed a novel method for deposition of a thin β-TCP coating on zirconia substrate. The developed procedure involved two-steps: (i) the rapid wet-chemical deposition of a biomimetic CaP coating and (ii) subsequent post-deposition processing of the deposited biomimetic CaP coating, which included a heat treatment at 900 °C, followed by a short sonication (≈1 min) in a water bath. The obtained β-TCP coating were dense and uniform, had a thickness of ≈500 nm and displayed a roughness in the nanometre range (Figure 14.2). The β-TCP coating possessed excellent adhesion to the substrate and demonstrated an apatite-mineralization ability in a simulated body fluid and enhanced the adsorption of serum proteins on the zirconia.

Jiang et al. prepared an HA coating on a porous alumina scaffold using a thermal decomposition method.[67,68] They first deposited a hydroxyapatite precursor layer on alumina by utilizing a precursor solution[67] or suspension route.[68] This was followed by a thermal treatment to remove organic parts and obtain a thin and nanocrystalline layer of stoichiometric hydroxyapatite. Using such a procedure they were able to obtain a homogenous coating over the entire surface and also in the pores of the alumina scaffold. In addition, the coatings induced apatite nucleation in SBF and a simple tape test indicated good adhesion of the coating to the alumina substrate.

The sol-gel method was used to deposit flour-hydroxyapatite (FHA) coatings on zirconia.[69] The coating procedure included spin-coating of the FHA sol on zirconia with heating between 400 and 800°C. The prepared FHA coatings had uniform and dense morphology and the coatings heated above 500°C had a very strong adhesion strength of around 70 MPa. In addition, proliferation of MG63 cells was similar to the plastic control. When the CaP coatings on substrates were exposed to higher temperatures, it led to poor mechanical stability of the coating due to thermal stress caused by the difference in thermal expansion coefficients between the CaP coating and the substrate. Therefore, the idea of applying a gradient hydroxyapatite-glass coating was introduced to circumvent this problem. The coating was prepared on α-Al_2O_3 ceramic substrate by a multilayer slurry-dipping and sintering at 1100°C.[70] The coating composition varied gradually; hydroxyapatite content increased and glass content decreased gradually from the interface to the surface layer. Prepared coatings showed good biological response in rats, had very good tensile strength, and there was no cracking at the substrate-coating interface or within the coating. However, the procedure for the preparation of the coating was rather time-consuming since sintering of the substrate was needed after each slurry dipping.

An interesting approach was suggested by Suzuki et al., who deposited a Ti-HA composite coating onto a zirconia femoral component used for the cementless type of total knee arthroplasty.[71] The composite coating was prepared by first arc spraying a 500 μm thick macroporous titanium layer on zirconia; then a 50 μm HA layer was flame-sprayed on. In vivo tests performed on beagles showed improved osseointegration of the coated zirconia implants as compared to non-coated ones. Improved osseointegration was achieved by the macroporous structure of Ti, which enabled mechanical interlocking of the implant in the bone, and osteoconductive behavior of HA. This enhanced bone ingrowth into the pores and grooves of the implant.

Rochietta et al. evaluated whether CaP coatings on zirconia could improve osseointegration of topographically altered zirconia implants when implanted in rabbits.[72] They applied two different CaP coatings. One type was composed of a 20 nm thick layer of nanostructured HA crystals that were prepared by dipping the zirconia implants into a solution that contained HA nanoparticles. This was followed by drying and heat treatment at 700°C. The second type was composed of a 150 nm thick and dense CaP coating that was obtained by

sputtering. To assess the osseointegration of different surfaces, they measured RTQ and bone-to-implant contacts in rabbit femora and tibiae. Results showed that CaP coatings did not significantly improve the final outcome in terms of strength or the speed of osteoconductivity. In a similar study, Lee et al. compared the osseointegration of microstructured CaP-coated zirconia implants and commercially available titanium implants TiUnite™, in a rabbit trabecular bone model.[73] Microstructured surfaces on zirconia were prepared according to the previously described procedure,[21] which included spraying a slurry of zirconia powder and a pore-former onto a pre-sintered zirconia ceramic implant. Afterwards, the slurry-coated implant was sintered to full density. During sintering the pore-former was burned away, leaving a porous coating on the core implant. In addition, two different kinds of CaP coatings were applied onto a ceramic implant (coatings A and C), both composed of nanocrystalline hydroxyapatite particles. In fact, coating C was prepared in the same manner as in the study by Rocchietta et al.[73] After 3 weeks of healing, the CaP-coated ceramic implants showed statistically lower osseointegration as compared to titanium implants. There were no statistically significant differences in osseointegration following a 6-week healing period. The study showed that thin nanocrystalline CaP coatings on zirconia implants do not enhance the bioactivity of zirconia implants.

Available results for the in vivo trials did not indicate the superior osseointegration of CaP-coated ceramic implants as compared to non-coated. Nevertheless, due to the limited number of in vivo studies performed and the types of CaP coatings tested, it is not possible to draw any conclusions about the usefulness of CaP coatings on high-performance ceramics. In addition, since positive effects of CaP ceramics on in vivo bone formation and healing have already been well-reported, CaP coatings remain a promising approach for bioactivation of inert bioceramics. For this purpose, future studies will need to focus on the development of techniques for preparation of novel CaP coatings that will improve the osseointegration of inert bioceramic implants, and also on the precise and detailed biological evaluation of the prepared CaP coatings.

14.3.3.2   Bioactive Glass and Glass-Ceramic Coatings

Bioactive glasses and glass ceramics have been extensively studied since the early 1970s when Hench et al. discovered that some glasses in the system SiO_2–CaO–Na_2O–P_2O_5 form direct contact with bones and soft tissues without being rejected by the body. They proposed a 12-step model to describe interfacial reactions between bioactive glasses and bone that lead to the formation of bonds and a tight contact. Their findings led to the development of a second-generation of biomaterials.[1] Later, various bioactive glass and glass-ceramic formulations were developed and studied in order to tune their bioactivity and adjust their properties for specific applications. Nevertheless, nowadays commercially available bioactive glasses are still based on mixtures from the SiO_2–CaO–Na_2O–P_2O_5 system.

While in the past bioactive glasses have been mainly produced by means of standard melting techniques, recently, great attention has been focused on glasses obtained by sol-gel methods. The sol-gel procedure makes it possible to produce glasses with compositions unobtainable via conventional melting, and which are bioactive in a wider range of compositions. In addition, sol-gel glasses can be produced with a strictly controlled porosity, which makes them very promising for specific biomedical applications.[74]

Bioactive glasses and glass-ceramics have been clinically employed mainly in non-load-bearing applications, such as middle ear implants, endosseous ridge maintenance implants, as particulates for bone regeneration, and as active agents in toothpastes for reduction of tooth sensitivity.[75] Due to their favorable biological properties, they also show a great potential to act as coatings on inert, load-bearing ceramic implants to improve their osseointegration. However, despite their potential, bioactive glass coatings are not used in clinics. The most studied techniques for fabrication of glass coatings are enameling and thermal spraying.[1] Besides these techniques, there are other methods under investigation, such as rapid-immersion coating;[1] electrophoretic[76] and sol-gel[75] deposition; grit blasting;[76] laser cladding;[77] pulsed laser deposition;[78] and particle vacuum infiltration.[79] However, only a few of them, such as enameling[1,80–87] and dip-coating,[67,88] have been applied to coating ceramic substrates with bioactive glass and glass-ceramics.

Enameling is a traditional technique for the production of glass coatings. This process is relatively simple and cheap and enables good control over the thickness of coatings. During the enameling procedure, a thin piece of glass or a suspension containing the glass powder is deposited onto the substrate. Subsequently, the glass is glazed by a proper heat treatment. The temperature of the glazing process must be carefully set in order to avoid crystallization of the glass and cracking of the coating.[72] Most of the bioactive glasses have a thermal expansion coefficient much higher than that of high-performance ceramics, such as alumina or zirconia. For this reason, a considerable residual tensile stress is induced in the glass coating upon cooling, which results in crack formation and insufficient adhesion at the interface. This problem can be avoided by increasing the silica content in the glass and reducing the thermal expansion coefficient. However, this can lead to two drawbacks. Firstly, the window of glass composition is markedly reduced. It is known that glass with too high a silica concentration has reduced bioactive capacity. Secondly, increased silica content requires higher heating temperatures, which can result in ion exchange between the glass and the ceramic substrate, and consequently this can lead to undesirable changes in the glass composition. This, in turn, can adversely affect its bioactivity. For example, in the case of bioactive glass coating an alumina ceramic, only a small amount of alumina (1.5 wt.%) in a glass can result in a bioinert character of the glass.[85] In addition, a high processing temperature can result in the formation of chemical by-products at the ceramic-glass interface, which may reduce the coating adhesion.[89]

Enameling was used to coat zirconia and alumina with bioactive phosphosilicate glass and glass ceramics AP40 and RKKP with composition in the system SiO_2–β-$Ca_3(PO_4)_2$–CaO–Na_2O–K_2O–MgO–CaF_2.[80,83–85] In order to prevent coating cracking due to the thermal coefficient mismatch between the glass coating and the ceramic substrate, additional zirconia-glass composite layer was introduced at the interface.[84,85] By finding the optimal heating regime, they could prepare homogenous and crack-free coatings with good adhesion and without residual porosity. In vitro and in vivo biological tests on AP40 and RKKP coatings revealed that the coatings induced apatite nucleation in SBF; increased serum protein adsorption; enhanced adhesion, spreading and growth of fibroblasts and osteoblast-like cells,[82,90] improved the metabolic activity of both healthy and osteopenic primary osteoblasts; and induced higher bone apposition in rats as compared to non-coated ceramics. Rahaman et al. used the enameling approach to coat Mg-PSZ with silicate-based glass (designated as 13–93 and 6P68) and borate-based glass (designated as H12), which have similar thermal expansion coefficients to the Mg-PSZ substrate.[81] Thus, they could obtain crack-free glass coatings without the need for application of an additional intervening layer on the substrate. The 6P68 glass provided the highest adhesive strength (40 ± 2 MPa), but the in vitro test showed that it had limited bioactivity; the H12 glass had lower adhesive strength (18 ± 2 MPa) but the highest bioactivity. In order to prepare the coating with optimum adhesion strength and bioactive properties, they successfully developed a functionally graded coating that consisted of a 6P68 interfacial layer and an H12 surface layer.

Kim et al. deposited composite coatings of a CaO–Na_2O–P_2O_5 glass and HA particles on zirconia disks.[67] This coating procedure included dip-coating of substrate in the HA-glass slurry, drying, and heat treatment. They investigated the effects of glass compositions, mixing ratios of glass to HA, and heat-treatment temperatures (800°C, 900°C, 1000°C) on the coating properties. Coatings with the highest amount of glass phase (50 wt.%, Figure 14.3), reached the highest values of tensile strength of 40 MPa, which was 80% higher than the adhesion of pure HA coatings (22 MPa). The osteoblast-like cells grew and spread actively on the composite coating samples. The proliferation numbers and ALP activities of the cells on the composite coatings were improved by 30–40% when compared to bare zirconia substrates.

Dip-coating was also found to be successful for coating alumina disks with sol-gel-derived 58S bioglass, with a composition of 58 mol.% SiO_2, 38 mol.% CaO, and 4 mol.% P_2O_5.[88] The alumina specimen was dipped into a 50 wt.% 58S bioglass suspension for 5 min. After drying and firing at 1200 °C for 1 h, a bioglass coating with a thickness of 200–300 μm was formed on the alumina specimen. Although the thermal expansion coefficient of bioglass was lower compared to alumina substrate (0.73 $10^{-6°}C^{-1}$ vs. 9.47 $10^{-6°}C^{-1}$), the resultant thermal stresses could be relaxed due to softening of the glass, and the obtained bioglass coating was adherent and crack-free.
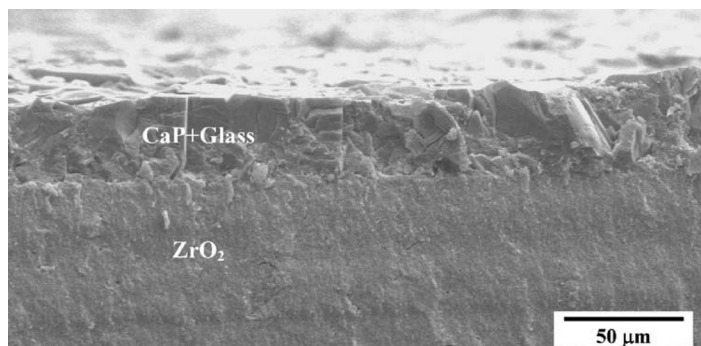
FIGURE. 14.3 SEM micrograph of the cross-section of a CaP-glass composite coating on ZrO_2.[67] The glass amount and composition used were 50 wt.% and 30 mol.% CaO, respectively, and the HT temperature was 800°C.

Concerning the biological tests on glass and glass-ceramic coatings on bioceramics, there have not been many in vitro and in vivo tests performed. Besides the above mentioned in vitro[82,83] and in vivo[91] tests there have been two case reports on the in vivo performance of apatite-mullite glass-ceramic-coated zirconia implants as compared to untreated and acid-etched commercial zirconia implants in humans.[24,92] The prepared surfaces had different surface roughness: uncoated zirconia ($R_a = 0.62\,\mu m$), apatite-mullite glass-ceramics coating ($R_a = 0.92\,\mu m$), and acid-etched surface ($R_a = 1.16\,\mu m$). The highest implant success rate was observed for acid-etched implants (97.5%), while there have not been any statistical differences in the success rate of glass-ceramics-coated (93.6%) and uncoated (92.8%) zirconia implants. The authors proposed that higher surface roughness of acid-etched implants was the main reason for their superior success.

Although bioactive glass and glass-ceramics coatings show great potential for the improvement of osseointegration of bioinert high-performance ceramics, more research will need to be conducted on the optimization of coating technologies that already exist, or on the development of new coating methods. This is particularly true for the correlation of the physicochemical properties of prepared coatings to biological response.

14.3.4   Other Approaches for Modification of Surface Chemistry

Schickle et al. reported an innovative method for the introduction of different functional groups onto alumina ceramics using a tailored, self-assembled monolayer (SAM) technique.[93] The method is comprised of three steps. First, silane groups were attached to the surface by PVD or spray pyrolysis. In the second step, these reacted with octenyltrichlorosilane (OTS) SAM with $CH = CH_2$ functional groups that were introduced by immersing the samples in a 5% ethanol solution of OTS. And in the final step, –OH or –COOH

groups were coupled with the–CH = CH2 groups by further chemical treatment. Unfortunately, no biological tests have been conducted to evaluate the prepared surfaces.

Vargas et al. fabricated thin silica coatings with micropatterned pillars on zirconia.[94] Their fabrication strategy combined sol-gel synthesis of silica coatings and subsequent patterning of the coatings using soft lithography. The alamar blue assay showed that the viability of MG63 osteoblast-like cells was higher on zirconia with flat or micropatterned silica coatings as compared to bare zirconia substrates. Higher viability of cells was explained with higher silicon content since the topography of silica had no influence on the biological response.

Leivvo et al. produced different $3Al_2O_3$–$2SiO_2$ coatings on α-alumina substrates using sol-gel synthesis. Prepared sol-gel coatings were either amorphous or contained nano-sized mullite crystals. In addition, coatings of thermally sprayed aluminosilicate and diphasic γ-alumina-silica nano-sized colloids were prepared. Despite the differences in physical and chemical structures among individual alumina-silicate coatings, cell culture testing with rat osteoblasts showed good biocompatibility for all tested coatings.

Recently, Liu et al. reported the possibility of improving the biocompatibility of zirconia by coating it with 3,4-dihydroxy-L-phenylalanine (L-DOPA) film.[95] Previous studies showed that L-DOPA is an important molecule secreted by marine mussels for the formation of adhesive pads. The bio-inspired L-DOPA film significantly altered the chemical properties of the zirconia surface without affecting its topography. Moreover, the L-DOPA coating also outperformed uncoated zirconia in osteoblast responses, including cell adhesion, cytoskeleton development, and cell number increase.

REFERENCES

1. Hench LL, Wilson. J. An introduction to bioceramics. London: World Scientific; 1999.
2. Wennerberg A, Albrektsson T. Effects of titanium surface topography on bone integration: a systematic review. Clin Oral Implan Res 2009;20:172–84.
3. Albrektsson T, Wennerberg A. Oral implant surfaces: Part 1–review focusing on topographic and chemical properties of different surfaces and in vivo responses to them. Int J Prosthodont 2004;17:536–43.
4. Anil S, Anand PS, Alghamdi H, Jansen JA. Dental implant surface enhancement and osseointegration. In: Turkyilmaz I, editor. Implant dentistry – a rapidly evolving practice InTech; 2011. p. 83–108.
5. Kokubo T. In vitro evaluation of bone bioactivity. In: Kokubo T, editor. Bioceramics and their clinical applications Woodhead Publishing; 2008.
6. Bohner M, Lemaitre J. Can bioactivity be tested in vitro with SBF solution? Biomaterials 2009;30:2175–79.
7. Pan HB, Zhao XL, Darvell BW, Lu WW. Apatite-formation ability – Predictor of 'bioactivity'?. Acta Biomater 2010;6:4181–88.

8. Kim, K.-h.; Narayanan, R.; Rautray, T. R. Surface Modification of Titanium for Biomaterial Applications (Biomaterials – Properties, Production and Devices); Nova Science Pub Inc, New York, 2010.

9. Tomsia AP, Launey ME, Lee JS, Mankani MH, Wegst UG, Saiz E. Nanotechnology approaches to improve dental implants. Int J Oral Maxillofac Implants 2011;26 (Suppl 25–44) discussion 45–29.

10. Le Guehennec L, Soueidan A, Layrolle P, Amouriq Y. Surface treatments of titanium dental implants for rapid osseointegration. Dent Mater 2007;23:844–54.

11. Ainslie KM, Thakar RG, Bernards DA, Desai TA. Inflammatory response to implanted nano-structured materials: understanding and controlling protein, cell, and tissue responses. In: Puleo DA, Bizios R, editors. Biological interactions on materials surfaces: Springer; 2009. p. 356–72.

12. Blaschke C, Volz U. Soft and hard tissue response to zirconium dioxide dental implants - A clinical study in man. Neuroendocrinol Lett 2006;27:69–72.

13. Kohal RJ, Weng D, Bachle M, Strub JR. Loaded custom-made zirconia and titanium implants show similar osseointegration: an animal experiment. J Periodontol 2004;75:1262–68.

14. Kohal RJ, Baechle M, Han JS, Hueren D, Huebner U, Butz F. In vitro reaction of human osteoblasts on alumina-toughened zirconia. Clin Oral Implan Res 2009;20:1265–71.

15. Bachle M, Butz F, Hubner U, Bakalinis E, Kohal RJ. Behavior of CAL72 osteoblast-like cells cultured on zirconia ceramics with different surface topographies. Clin Oral Implants Res 2007;18:53–59.

16. Gahlert M, Gudehus T, Eichhorn S, Steinhauser E, Kniha H, Erhardt W. Biomechanical and histomorphometric comparison between zirconia implants with varying surface textures and a titanium implant in the maxilla of miniature pigs. Clin Oral Implan Res 2007;18:658–62.

17. Hoffmann O, Angelov N, Zafiropoulos GG, Andreana S. Osseointegration of zirconia implants with different surface characteristics: an evaluation in rabbits. Int J Oral Implantol 2012;27:352–58.

18. Schliephake H, Hefti T, Schlottig F, Gedet P, Staedt H. Mechanical anchorage and peri-implant bone formation of surface-modified zirconia in minipigs. J Clin Periodontol 2010;37:818–28.

19. Wang GC, Liu XY, Zreiqat H, Ding CX. Enhanced effects of nano-scale topography on the bioactivity and osteoblast behaviors of micron rough ZrO_2 coatings. Colloid Surface B 2011;86:267–74.

20. Hempel U, Hefti T, Kalbacova M, Wolf-Brandstetter C, Dieter P, Schlottig F. Response of osteoblast-like SAOS-2 cells to zirconia ceramics with different surface topographies. Clin Oral Implants Res 2010;21:174–81.

21. Adilstam F, I. M., Patent SE032539-2., in, 2003.

22. Sennerby L, Dasmah A, Larsson B, Iverhed M. Bone tissue responses to surface-modified zirconia implants: A histomorphometric and removal torque study in the rabbit. Clin Implant Dent R 2005;7:S13–20.

23. Scharnweber D, Kurort G, Ritter M. EP2522301A2 Method for treating ceramic surfaces and ceramic implants on the basis of zirconium oxide, in, 2009.

24. Oliva J, Oliva XV, Oliva JD. One-year follow-up of first consecutive 100 zirconia dental implants in humans: A comparison of 2 different rough surfaces. Int J Oral Max Impl 2007;22:430–35.

25. Park YS, Cung SH, Shon WJ. Peri-implant bone formation and surface characteristics of rough surface zirconia implants manufactured by powder injection molding technique in rabbit tibiae. Clin Oral Implants Res 2012.

26. Delgado-Ruiz RA, Calvo-Guirado JL, Moreno P, Guardia J, Gomez-Moreno G, Mate-Sanchez JE, et al. Femtosecond laser microstructuring of zirconia dental implants. J Biomed Mater Res B 2011;96B:91–100.

27. Barsch N, Werelius K, Barcikowski S, Liebana F, Stute U, Ostendorf A. Femtosecond laser microstructuring of hot-isostatically pressed zirconia ceramic. J Laser Appl 2007;19:107–15.

28. Kosmac T, Oblak C, Jevnikar P, Funduk N, Marion L. Strength and reliability of surface treated Y-TZP dental ceramics. J Biomed Mater Res 2000;53:304–13.

29. Piconi C, Maccauro G. Zirconia as a ceramic biomaterial. Biomaterials 1999;20:1–25.

30. Hao L, Lawrence J, Chian KS, Low DKY, Lim GC, Zheng HY. The formation of a hydroxyl bond and the effects thereof on bone-like apatite formation on a magnesia partially stabilized zirconia (MgO-PSZ) bioceramic following CO_2 laser irradiation. J Mater Sci-Mater M 2004;15:967–75.

31. Hao L, Lawrence J, Chian KS. Osteoblast cell adhesion on a laser modified zirconia based bioceramic. J Mater Sci Mater Med 2005;16:719–26.

32. Aboushelib M, Salem N, Abotaleb A, Abd El Moniem N. Influence of surface nano-roughness on osseointegration of zirconia implants in rabbit femur heads using selective infiltration etching technique. J Oral Implantol 2011.

33. Ertan AA, Celebi N, Bayolken M, Onur MA, Aboushelib MN, Feilzer A, et al. Surface topography of zirconia implants does not alter action potentials of isolated rat sciatic nerves. J Biomed Mater Res Part B, J Biomed Mater Res B Appl Biomater 2009;88:182–90.

34. Webster TJ, Ergun C, Doremus RH, Siegel RW, Bizios R. Enhanced functions of osteoblasts on nanophase ceramics. Biomaterials 2000;21:1803–10.

35. Namavar F, Cheung CL, Sabirianov RF, Mei WN, Zeng XC, Wang G, et al. Lotus effect in engineered zirconia. Nano lett 2008;8:988–96.

36. Sabirianov RF, Rubinstein A, Namavar F. Enhanced initial protein adsorption on engineered nanostructured cubic zirconia. Phys Chem Chem Phys 2011;13:6597–609.

37. Tanahashi M, Matsuda T. Surface functional group dependence on apatite formation on self-assembled monolayers in a simulated body fluid. J Biomed Mater Res 1997;34:305–15.

38. Uchida M, Kim HM, Kokubo T, Nawa M, Asano T, Tanaka K, et al. Apatite-forming ability of a zirconia/alumina nano-composite induced by chemical treatment. J Biomed Mater Res 2002;60:277–82.

39. Faga MG, Vallee A, Bellosi A, Mazzocchi M, Thinh NN, Martra G, et al. Chemical treatment on alumina-zirconia composites inducing apatite formation with maintained mechanical properties. J Eur Ceram Soc 2012;32:2113–20.

40. Fischer H, Niedhart C, Kaltenborn N, Prange A, Marx R, Niethard FU, et al. Bioactivation of inert alumina ceramics by hydroxylation. Biomaterials 2005;26:6151–57.

41. Li PJ, Ohtsuki C, Kokubo T, Nakanishi K, Soga N, Degroot K. The Role of hydrated silica, titania, and alumina in inducing apatite on implants. J Biomed Mater Res 1994;28:7–15.

42. He X, Zhang YZ, Mansell JP, Su B. Zirconia toughened alumina ceramic foams for potential bone graft applications: fabrication, bioactivation, and cellular responses. J Mater Sci Mater Med 2008;19:2743–49.

43. Bertazzo S, Rezwan K. Control of alpha-alumina surface charge with carboxylic acids. Langmuir 2009;26:3364–71.

44. Bertran S, Bertazzo Hydroxyapatite formation on alumina surface modified by aluminoxane. Key Eng Mat 2007:330–2. 753–756. 2007.

45. Bertazzo S, Zambuzzi WF, da Silva HA, Ferreira CV, Bertran CA. Bioactivation of alumina by surface modification: a possibility for improving the applicability of alumina in bone and oral repair. Clin Oral Implan Res 2009;20:288–93.

46. Liang H, Wan YZ, He F, Huang Y, Xu JD, Li JM, et al. Bioactivity of Mg-ion-implanted zirconia and titanium. Appl Surf Sci 2007;253:3326–33.

47. Zhao Q, Zhai GJ, Ng DHL, Zhang XZ, Chen ZQ. Surface modification of Al2O3 bioceramic by NH^{2+} ion implantation. Biomaterials 1999;20:595–99.

48. Zreiqat H, Evans P, Howlett CR. Effect of surface chemical modification of bioceramic on phenotype of human bone-derived cells. J Biomed Mater Res 1999;44:389–96.
49. Zreiqat H, Howlett CR, Zannettino A, Evans P, Schulze-Tanzil G, Knabe C, et al. Mechanisms of magnesium-stimulated adhesion of osteoblastic cells to commonly used orthopaedic implants. J Biomed Mater Res 2002;62:175–84.
50. Liang H, Huang Y, He F, Ding HF, Wan YZ. Enhanced calcium phosphate precipitation on the surface of mg-ion-implanted ZrO_2 bioceramic. Surf Rev Lett 2007;14:71–77.
51. Att W, Takeuchi M, Suzuki T, Kubo K, Anpo M, Ogawa T. Enhanced osteoblast function on ultraviolet light-treated zirconia. Biomaterials 2009;30:1273–80.
52. Wang R, Hashimoto K, Fujishima A, Chikuni M, Kojima E, Kitamura A, et al. Light-induced amphiphilic surfaces. Nature 1997;388:431–32.
53. Aita H, Hori N, Takeuchi M, Suzuki T, Yamada M, Anpo M, et al. The effect of ultraviolet functionalization of titanium on integration with bone. Biomaterials 2009;30:1015–25.
54. León B, Jansen J. Thin calcium phosphate coatings for medical implants 2009.
55. Abe Y, Kokubo T, Yamamuro T. Apatite coating on ceramics, metals and polymers utilizing a biological process. J Mater Sci Mater Med 1990;1:233–38.
56. Bigi A, Boanini E, Bracci B, Facchini A, Panzavolta S, Segatti F, et al. Nanocrystalline hydroxy-apatite coatings on titanium: a new fast biomimetic method. Biomaterials 2005;26:4085–89.
57. Tas AC. Synthesis of biomimetic Ca-hydroxyapatite powders at 37 degrees C in synthetic body fluids. Biomaterials 2000;21:1429–38.
58. Habibovic P, Barrere F, van Blitterswijk CA, de Groot K, Layrolle P. Biomimetic hydroxy-apatite coating on metal implants. J Am Ceram Soc 2002;85:517–22.
59. Qu HB, Wei M. Improvement of bonding strength between biomimetic apatite coating and substrate. J Biomed Mater Res B 2008;84B:436–43.
60. Kim HM, Miyaji F, Kokubo T, Nakamura T. Bonding strength of bonelike apatite layer to Ti metal substrate. J Biomed Mater Res 1997;38:121–27.
61. Rambo CR, Muller FA, Muller L, Sieber H, Hofmann I, Greil P. Biomimetic apatite coating on biomorphous alumina scaffolds. Mat Sci Eng C-Bio S 2006;26:92–99.
62. Klopcic SB, Kovac J, Kosmac T. Apatite-forming ability of alumina and zirconia ceramics in a supersaturated Ca/P solution. Biomol Eng 2007;24:467–71.
63. Pribosic I, Klopcic SB, Kosmac T. Biomimetic preparation and characterization of bioactive coatings on alumina and zirconia ceramics. J Am Ceram Soc 2010;93:288–94.
64. Stefanic M, Krnel K, Pribosic I, Kosmac T. Rapid biomimetic deposition of octacalcium phosphate coatings on zirconia ceramics (Y-TZP) for dental implant applications. Appl Surf Sci 2012;258:4649–56.
65. Jiang GW, Shi DL. Coating of hydroxyapatite on porous alumina substrate through a thermal decomposition method. J Biomed Mater Res 1999;48:117–20.
66. Jiang GW, Shi DG. Coating of hydroxyapatite on highly porous Al_2O_3 substrate for bone sub-stitutes. J Biomed Mater Res 1998;43:77–81.
67. Kim HW, Georgiou G, Knowles JC, Koh YH, Kim HE. Calcium phosphates and glass com-posite coatings on zirconia for enhanced biocompatibility. Biomaterials 2004;25:4203–13.
68. Wang ZQ, Xue DF, Chen XX, Lu BL, Ratajczak H. Mechanical and biomedical properties of hydroxyapatite-based gradient coating on alpha-Al_2O_3 ceramic substrate. J Non-Cryst Solids 2005;351:1675–81.
69. Suzuki T, Fujibayashi S, Nakagawa Y, Noda I, Nakamura T. Ability of zirconia double coated with titanium and hydroxyapatite to bond to bone under load-bearing conditions. Biomaterials 2006;27:996–1002.
70. Rocchietta I, Fontana F, Addis A, Schupbach P, Simion M. Surface-modified zirconia implants: tissue response in rabbits. Clin Oral Implants Res 2009;20:844–50.

71. Lee J, Sieweke JH, Rodriguez NA, Schupbach P, Lindstrom H, Susin C, et al. Evaluation of nano-technology-modified zirconia oral implants: a study in rabbits. J Clin Periodontol 2009;36:610–17.

72. Sola A, V.C.a.A.C.D. Bellucci, Bioactive glass coatings: a review. 2011.

73. Jones JR. Review of bioactive glass: from hench to hybrids. Acta Biomater 2013;9:4457–86.

74. Stojanovic D, Jokic B, Veljovic D, Petrovic R, Uskokovic PS, Janackovic D. Bioactive glass-apatite composite coating for titanium implant synthesized by electrophoretic deposition. J Eur Ceram Soc 2007;27:1595–99.

75. Braem A, Neirinck B, Schrooten J, Van der Biest O, Vleugels J. Biofunctionalization of porous titanium coatings through sol-gel impregnation with a bioactive glass-ceramic. Mat Sci Eng C-Mater 2012;32:2292–98.

76. Koller G, Cook RJ, Thompson ID, Watson TF, Di Silvio L. Surface modification of titanium implants using bioactive glasses with air abrasion technologies. J Mater Sci-Mater M 2007;18:2291–96.

77. Comesana R, Quintero F, Lusquinos F, Pascual MJ, Boutinguiza M, Duran A, et al. Laser cladding of bioactive glass coatings. Acta Biomater 2010;6:953–61.

78. Borrajo JP, Serra J, Gonzalez P, Leon B, Munoz FM, Lopez M. In vivo evaluation of titanium implants coated with bioactive glass by pulsed laser deposition. J Mater Sci-Mater M 2007;18:2371–76.

79. Drnovsek N, Novak S, Dragin U, Ceh M, Gorensek M, Gradisar M. Bioactive glass enhances bone ingrowth into the porous titanium coating on orthopaedic implants. Int Orthop 2012;36:1739–45.

80. Krajewski A, Ravaglioli A, Mazzocchi M, Fini M. Coating of ZrO_2 supports with a biological glass. J Mater Sci Mater Med 1998;9:309–16.

81. Rahaman MN, Li Y, Bal BS, Huang W. Functionally graded bioactive glass coating on magnesia partially stabilized zirconia (Mg-PSZ) for enhanced biocompatibility. J Mater Sci Mater Med 2008;19:2325–33.

82. Bosetti M, Verne E, Ferraris M, Ravaglioli A, Cannas M. In vitro characterisation of zirconia coated by bioactive glass. Biomaterials 2001;22:987–94.

83. Torricelli P, Verne E, Brovarone CV, Appendino P, Rustichelli F, Krajewski A, et al. Biological glass coating on ceramic materials: in vitro evaluation using primary osteoblast cultures from healthy and osteopenic rat bone. Biomaterials 2001;22:2535–43.

84. Ferraris M, Verne E, Appendino P, Moisescu C, Krajewski A, Ravaglioli A, et al. Coatings on zirconia for medical applications. Biomaterials 2000;21:765–73.

85. Brovarone CV, Verne E, Krajewski A, Ravaglioli A. Graded coatings on ceramic substrates for biomedical applications. J Eur Ceram Soc 2001;21:2855–62.

86. Martorana S, Fedele A, Mazzocchi M, Bellosi A. Surface coatings of bioactive glasses on high strength ceramic composites. Appl Surf Sci 2009;255:6679–85.

87. Kim CY, Jee SS. Hydroxyapatite formation on bioactive-glazed alumina. J Eur Ceram Soc 2003;23:1803–11.

88. Liu JL, Miao XG. Sol-gel derived bioglass as a coating material for porous alumina scaffolds. Ceram Int 2004;30:1781–85.

89. Sola A, Bellucci D, Cannillo V, Cattini A. Bioactive glass coatings: a review. Surf Eng 2011;27:560–72.

90. Rosengren A, Oscarsson S, Mazzocchi M, Krajewski A, Ravaglioli A. Protein adsorption onto two bioactive glass-ceramics. Biomaterials 2003;24:147–55.

91. Stanic V, Aldini NN, Fini M, Giavaresi G, Giardino R, Krajewski A, et al. Osteointegration of bioactive glass-coated zirconia in healthy bone: an in vivo evaluation. Biomaterials 2002;23:3833–41.
92. Oliva J, Oliva X, Oliva J. Five-year success rate of 831 consecutively placed zirconia dental implants in humans: a comparison of three different rough surfaces. Int J Oral Maxillofac Implants 2010;25(2):336–44.
93. Schickle K, Kaufmann R, Campos DFD, Weber M, Fischer H. Towards osseointegration of bioinert ceramics: introducing functional groups to alumina surface by tailored self assembled monolayer technique. J Eur Ceram Soc 2012;32:3063–71.
94. Pelaez-Vargas A, Gallego-Perez D, Magallanes-Perdomo M, Fernandes MH, Hansford DJ, De Aza AH, et al. Isotropic micropatterned silica coatings on zirconia induce guided cell growth for dental implants. Dent Mater 2011;27:581–89.
95. Liu Y-T, Tzer-Min Lee T-SL. Enhanced osteoblastic cell response on zirconia by bio-inspired surface modification. Colloids Surf B Biointerfaces 2013.

Industrial-scale Production of Customized Ceramic Prostheses

Dag Henrik Bergsjö*, Matts Andersson*, Rikard Söderberg* and Johan Carlson†

*Chalmers University of Technology, Göteborg, Sweden; †Fraunhofer-Chalmers Research Centre for Industrial Mathematics, Göteborg, Sweden

Contents

15.1 INTRODUCTION

Today, there are many solutions for dental rehabilitation. A damaged tooth can be replaced with a dental crown, and a toothless patient can be rehabilitated with implants and a corresponding bridge set-up. Traditionally, a dental crown is manufactured by veneering porcelain to a metal surface that is obtained through the use of casting principles. Implant rehabilitations used to rely on a high degree of handcraft by the dentist, where freehand drilling into the jaw-bone was supported by X-ray pictures and was done before implant insertion.

Crown and implant rehabilitations can be provided at a much higher degree of industrialization by means of mass customization. The most common dental rehabilitations are crown restorations for single teeth, while full-arch implant rehabilitations are the most comprehensive treatments. Trends in industry lean toward a higher degree of automation in production and manufacturing where key characteristics of a well-functioning ceramic prosthesis are cost reduction, patient satisfaction, and quality in both function and perception.

State-of-the-art manufacturing of ceramic prostheses follows an overall generic process that consists of five major steps:

1. Creation of 3D data from the patient.
2. Creation of standard transformation language (STL) data by computer-aided design (CAD).
3. Computer-aided manufacturing (CAM) of the customized dental product.
4. Veneering.
5. Placing of the final product in the patient's mouth.

Depending on the manufacturer and medical device supplier, this process follows different paths and requires different amounts of automation and hand-crafting. The major difference is how the data for the CAD model is generated (e.g., directly by an intraoral scanner or on a mold) and where the customized product is manufactured. Three types of production concepts exist today, namely the following:

1. Chair-side production: All components of the design and manufacturing system are located in the clinic.
2. Laboratory production: The traditional production method in which the dentist ships an impression or digital scan to the local lab, where it is then used to produce the products.
3. Centralized production: This is a larger facility than the local lab. The products are manufactured in an industrialized manner. Data from either the lab or the dentist are collected and sent to central manufacturing, most often using proprietary instruments and data protocols.

In general, there are four different types of prosthetics in use today, and these are manufactured in different ways. The main alternatives are as follow:

1. Removable prosthetics: Partial and full dentures.
2. Fixed prosthetics: Cemented crown, bridge, post, and core.
3. Combined prosthetics: Cemented attachment and removable prosthesis.
4. Implant prosthetics: Bone-anchoring system for fixed and removable restorations.

This chapter is organized as follows: Firstly, the history of customized production is given, including how the Procera system was invented and designed in the early 1980s, up until the introduction of 3D-CAD in the mid-1990s. After this historical perspective, we go into further detail concerning

the materials that are used in modern dentistry. Then the reader will be introduced to the current practice of the digital rehabilitation process, focusing on CAI/CAD/CAM procedures and processes. In this chapter, generic processes and state-of-the-art practices will be explained both from a dental lab perspective and a central production perspective. It is the authors' intention to keep this chapter as free as possible from branding and specific proprietary products. This is a difficult task to achieve, however, since the central production concept consists of so-called closed or proprietary systems. There is a focus on implants and ceramics as the most interesting path for the future. After the CAI/CAD/CAM section, the four different types of prosthetics that are in use today are presented. This section also covers how they are manufactured and introduces both metal-based products and ceramic materials. Following, there is a passage that presents novel approaches for introducing real-time simulation into the planning of oral surgery. There is a focus on placement accuracy for implants and the simulation of geometrical aspects of teeth and dental products. The final section presents quality issues encountered in dental replacement and discusses stacking of different sources of variation and how to eliminate variation from the process.

15.2   THE HISTORY OF CUSTOMIZED PRODUCTION FROM THE PROCERA PERSPECTIVE

In recent decades, predictable dental implants have been introduced that have revolutionized dentistry. As described already in Chapter 4, the introduction of the modern dental implant in the 1970s by Professor Per-Ingvar Brånemark led to increasing interest in biocompatibility in dentistry.[1] The mechanism behind osseointegration is still not fully understood, but the realization that living tissue can exist in close contact with certain materials with specific surface properties made a dramatic change in dentistry. The rehabilitation process prescribed by Brånemark was the two-stage or conventional approach. Quite early on it was found to be both time-consuming and costly as it required a second surgical procedure as well as the design of an interim removable prosthodontics device. Due to this, the immediate, or one-stage implant was invented and is now common. It is preferably prescribed when the implant positioning and osseointegration forecast is relatively uncomplicated.

The reason for starting development of the Procera system was the need to introduce titanium as a material for artificial dental crowns. The normal crown in the dental society at the time was based on a metal crown veneered with feldspathic porcelain (PFM). The material for the crown was usually an alloy with at least 70% precious metals. However, this is not a biocompatible material and often caused reactions in patients with sensitive gums. Titanium was used to replace gold alloy with the objective of avoiding gum reactions. Titanium copings could not, however, be produced using the existing methods available to dental technicians.

FIGURE 15.1   The first version of the Procera copy-milling system.

In 1982, a group led by Dr. Matts Andersson started work on industrializing the production of individualized crowns by using copy-milling and spark erosion methods. The process was developed from 1982–1985 and was clinically tested in several trials. The process came into commercial production in the late 1980s. Commercially, the system supplied a limited market, and in 1989 further development of the system was initiated and focused on alumina as a replacement for titanium in crowns. Alumina was accepted as a highly biocompatible material. It had earlier been used as an implant material for tooth replacement. Some attempts to use it for individual crowns had been made, but not in its full, densely sintered form (see Chapter 12 for more details on alumina-reinforced feldspathic porcelain and glass-infiltrated alumina). By modifying the copy-milling machines already developed for the production of titanium crowns, it was now possible to manufacture crowns in fully sintered alumina. The process was based on copy-milling and ceramic powder processing (Figure 15.1).

The entire process was at that time purely mechanical, and no computers were attached to the system. However, in the patent for the Procera process, it was mentioned that computers could be used instead of a physical master for copying a virtual master.

In early 1990, work was started on computerizing the order-to-manufacturing process. From a system point of view, this was achieved by dividing the copy-milling machine into two machines: a scanner and a computer-controlled milling machine. The scanning machine used a touch probe to define the geometry and transferred the information by an electronic protocol to the milling machine. That made it possible to minimize the amount of information that had to be exchanged between the two units. This architecture made it further

FIGURE 15.2   An early process description (1994) of the Procera system supported by 2D CAD/CAM.

possible to use public telephone landlines to connect the system (Figure 15.2). This allowed a dental clinic to transmit customer orders directly to a centralized manufacturing location without any loss of data. The Procera system was launched in 1994, and in 1996, the yearly production rate reached 1 million copings.

The early CAD system used was based on two-dimensional drawings, and this limited the types of products that could be manufactured compared to the original mechanical Procera system. This naturally led to the introduction of 3D CAD technology in the Procera system, which made it possible to manufacture more products with a higher degree of geometrical complexity, including all individualized ceramic products used in dentistry at the time. This was made possible with a new touch probe scanner working in a volume $100 \times 100 \times 100$ mm, which, for example, allowed the production to include bridges, implant-supported bridges, and surgical guides within the system. Recently, the system was upgraded with a new scanner based on optical technology and second-generation 3D software.

15.3   CERAMIC VERSUS METALLIC MATERIALS

Materials currently used in the production of dental products are mainly cobolt-chrome, titanium, and zirconia. Historically, alumina has also been a popular material and can still be used for applications with high aesthetical requirements (e.g. front teeth). There are also some new branded materials that have better aesthetic properties than zirconia, for example.

Three types of dental alloy categories are applicable: high-precious, semi-precious, and non-precious metals. High-precious alloy is composed of at least 60% noble metal (gold, palladium, or platinum) of which at least 40% must be gold. Semi-precious alloy must have a noble metal content over 25%, and in non-precious or base alloys, noble metals make up less than 25%. These materials often contain a large percentage of nickel, chromium, beryllium, cobalt, or pure titanium. Today the most widely used alloy is cobalt-chromium. Cobalt-chrome crowns and bridges are produced by casting, milling, or laser sintering. Laser sintering is growing as a manufacturing method due to better cost, less grinding, and excellent fit. There are still some issues regarding porosity, where the porcelain veneering can fracture if there is open porosity in the surface layer of the cobalt-chrome product (refer to Chapter 18 for more details). Titanium is considered the most biocompatible metallic material approved so far. Casting of titanium requires special equipment, and the veneering is different compared to the noble and non-precious metals. This has limited the use of titanium. However, for implants, titanium is widely used due to its great osseointegration characteristics.

Alumina was introduced with Nobel Biocare's Procera system and has been considered the most aesthetic core ceramic material. Today, some technicians prefer to use alumina coping in the front region of the mouth if there are high aesthetic demands. Customized zirconia (Y-TZP) prostheses are most commonly produced by milling pre-sintered porous blanks, but they are also created by grinding hot isostatic pressed (HIPed) fully dense blocks. The pre-sintered material is available in different shades, and more translucent material has also become available in recent years. Zirconia is well known for its excellent strength, which can support 14-unit bridges produced with the material. Lithium disilicate base glass ceramics are another family of ceramic materials that have been widely used for producing monolithic single crowns. They have become very popular due to their good aesthetic characteristics and their ease-of-use in the lab. They are produced either by casting or by milling out blanks by CAD/CAM processing (refer to Chapters 11 and 12 for more details).

15.4   CAI/CAD/CAM

The first step in the digital process of tooth rehabilitation is to collect digital data from the patient that will serve as a basis for manufacturing a customized prosthesis. This first step is called computer-aided impressioning (CAI). In general, either a mechanical system or an optical system can be used to import the digital data. Optical scanners are more common today and are considered to be both cheaper and faster than a mechanical system. Optical scanners use a type of light beam (either white light or a laser beam). The difference in wavelength of the reflected light is measured to calculate the distance to the point measured. These measured points are then combined to form a computer model of the scanned object. The mechanical scanner performs the same type

of measures and calculations but utilizes a mechanical touch probe to measure the distance to the scanned object.

There are three main types of process to import the current structure of a patient's mouth and remaining teeth in the beginning of a rehabilitation process. The baseline process can be called the conventional half-digital process, and involves an impression followed by a dental cast, which is then scanned into the system. This baseline can be improved by eliminating the dental casting step, making it faster than its predecessor. The process is called the conventional full-digital process. It implies that a dental impression is brought directly to the 3D scanner. The newest and fastest way to perform a scan is with an intraoral scanner, where both the impression and dental cast process steps can be eliminated. This is known as the fully digital process without dental impression. One major advantage, apart from the obvious reduction of steps, is the increased accuracy tied to the intraoral scanners. Precision of the scanners is in the range of ±20 microns, which is well within the accepted range for a final assembly, and should not be off by more than 70 microns. Quality issues and tolerances will be further addressed in the quality section.

For CAD, there exists a multitude of software that is continuously updated and refined to support design of dental products and planning of surgical procedures. Positioning and orientation of implants can be made in the planning systems after importing the anatomically correct information from the patient. In the planning phase of a surgery, the crown or bridge is designed to work with a suitable implant or abutment. Some of the software supports direct ordering of the most suitable chair-side and customized products. There are many proprietary data formats that are supported by different manufacturers; however, the STL format is becoming widely accepted as a standard for storage of CAD data. There are proprietary closed systems (e.g. Lava, Etkon, and NobelGuide) and 'open systems' (e.g. 3shape and Dental Wing). Open systems are the most popular today in lab production environments because the lab is free to buy machinery and upgrades from any producer.

One commercially available software package used for planning surgical and prosthetic phases is NobelGuide. This software enables the clinician to transfer planned implant information and positions in advance of the actual implant placement. While implant selection and placement has always been based on radiological judgments, usually determined by using 2D radiographic images, this method provides the clinician with radiological data for all three dimensions. After completing the surgical planning in a virtual environment, the data specifying the positions of the implants are used to order the components required for the surgery and to manufacture the surgical template by rapid prototyping (Figure 15.3).

In the CAM procedure, data from CAD tools are used to manufacture the different products needed. In general, CAM is associated with different types of milling devices, but the use of rapid-prototyping devices is growing

FIGURE 15.3   Overview of a surgical procedure (from Left to Right): patient examination; radiographic guide and index; CT/CBCT scan; virtual planning; surgical template and index; and clinical procedures.

(see Chapter 18). However, rapid prototyping of ceramic devices is still in its infancy. Milling can be done with either 3-, 4-, or 5-axis machines; both wet and dry milling are available.[2] The simplest 3-axis machines can work in three spatial directions, generally called the X, Y, and Z dimensions. The 3-axis machines are easier to work with than the more complex 4- and 5-axis machines, and therefore offer less costly products. By introducing a fourth axis, a tension bridge, it is possible to make more complex shapes, such as bridges with large vertical height displacement, and save both materials and time in the production process. Introducing yet another axis, the rotation of the milling spindle, the 5-axis milling device makes it possible to produce even more complex products such as lower jaw frameworks on converging abutment teeth.

Metallic Ti and dense glass ceramic glass-infiltrated ceramics and highly sintered alumina and zirconia need cooling during machining. This is called wet milling, or precision hard milling, and means that a water jet is used to cool the surface of the processing material. Dry milling, or oversize soft milling, is available for low, pre-sintered zirconia and offers a couple of benefits over wet milling, such as shorter milling times, cheaper tools, and less damage.

15.5   PRODUCTION OF DENTAL PROSTHETICS

The production chain varies depending on the different types of prosthetics that are manufactured. The principles of the centralized manufacturing system are still based on an order-to manufacturing process similar to the early Procera system, but with improved quality, time, and cost parameters. In the competing lab-based approach, manufacturing is performed on a smaller scale

and is potentially able to offer a higher degree of flexibility and craftsman-ship that is appreciated by some dentists. This section mainly focuses on how the different types of prosthetics are manufactured, with a natural focus on implant prosthetics and the use of ceramic materials.

15.5.1   Removable Prosthetics

When considering removable prosthetics, it is possible to do either a partial or full denture. When there are teeth remaining in the jaw, a partial denture is used to replace only the missing teeth. In this case, the denture is attached and fixed to the existing teeth using clasps, and normally rests on the patient mucosa (soft tissue). A partial denture is a dental prosthesis construction of artificial teeth and soft tissue in acrylic attached to a metal skeleton. The metal skeleton that is not covered with acrylic is polished to prevent the accumulation of bacteria.

Full dentures are made completely of acrylic and rest on the mucosa. In the upper jaw (maxilla), the prosthesis is held in place by suction, which normally provides enough stability. In the lower jaw (mandibula), stability is often quite limited, and to improve stability, the denture is held in position by ball attach-ments on, typically, 2–4 mini implants.

Removable prosthetics are predominantly manufactured in a lab environ-ment and require a high degree of fitting to the patient. The first step by the technician is to design and sculpt a wax skeleton based on a stone model, as imprinted from the patient. This skeleton is tested against the patient's mouth to ensure a proper fit. After adjustments are made to the wax frame, the wax is embedded in a cuvette, and cast in cobalt-chrome (i.e. Vitallium) through the lost-wax principal. After divesting, the cobalt-chrome skeleton is ground and polished. Artificial teeth and soft tissue wax are attached to the skeleton and examined in the patient. A mold is produced, and the wax is removed through boiling. An acrylic pink resin is then pressed into the cavity left by the wax.

The removable prosthetics can also be developed by CAD/CAM methods. From the CAD file a wax-up frame can be printed or a cobalt-chrome skeleton directly sintered. From that point, the conventional procedure is followed to finalize the denture.

15.5.2   Fixed Prosthetics

Fixed prosthetics are crowns or bridges cemented on prepared teeth or implants. The main difference to removable prosthetics is that these can only be removed by a dentist. Historically, crowns and bridges were made com-pletely from metal, and later with a combination of metal and porcelain. Today most crowns and bridges are still made of a metal core and porcelain fused on top (PFM), even though the use of ceramics is increasing rapidly.

There are two methods used to produce a frame for fixed prosthetics. The first method is the traditional manual wax-up of the frame, where the wax

frame is embedded in a cuvette, and cast using the lost-wax principle. The second (and increasingly popular) way is by computerized CAD/CAM scanning and design of the framework, where a CAD file is created and used as a basis for digital manufacturing. The product is milled and ground and then laser sintered in the final dental frame material. It is also possible to print a wax frame for casting using rapid prototyping (i.e. a 3D printer).

Theoretically, it is possible to achieve a cementation gap of 2040 microns at the margin, and an overall cementation gap of 50 microns. In practice, accuracy below 100 microns is acceptable in most cases.

15.5.3   Combined Prosthetics

Within combined prosthetics, existing teeth are incorporated in the prosthesis construction to improve the stability of a removable prosthesis. There are different types of designs applicable to combined prosthesis. The first is telescopic denture, where inner metal crowns are attached to the remaining natural teeth and a secondary set of crowns is added as part of the denture prosthesis. The second is called dental attachment, and involves a connector containing two or more parts. One part is connected to a tooth, root, or implant, and the other part is connected to a prosthesis (skeleton). There are generally two ways of making this, either with precision attachments that are machined, or with semi-precision attachments that are directly cast from plastics or wax.

When telescopic dentures, crowns, or bridges are used, primary copings are cemented on natural teeth. Secondary copings are incorporated into the prosthesis framework. The fixation of the prosthesis is enabled through the steep wall design of the primary and secondary copings. The materials used for this prosthesis are precious or non-precious metals in both the primary and secondary copings. Crowns and gingiva are mostly produced in acrylic.

15.5.4   Implant Prosthetics

The last types of prosthetic we will look at is implant prosthetics. A dental implant fixture is a bone-anchoring system for a fixed or detachable dental prosthesis. Due to osseointegration of titanium in human bone, the implant is very rigid in construction and able to withstand large forces.

There are a few different restorative options with implants depicted in Figure 15.4. The first option (a) is the implant-level cement-retained restoration, which means that an abutment with the shape of a tooth preparation is attached to the implant and the crown is cemented on top of the abutment. The second option (b) is the implant-level screw-retained restoration, which means that a crown is retained with a screw through the occlusal surface of the crown and threads into the implant threads. The third option (c) is the abutment level screw-retained restoration, which means that an over denture bar or implant bridge is utilized to fixate the prosthesis.

FIGURE 15.4   Different types of implant prosthetics.
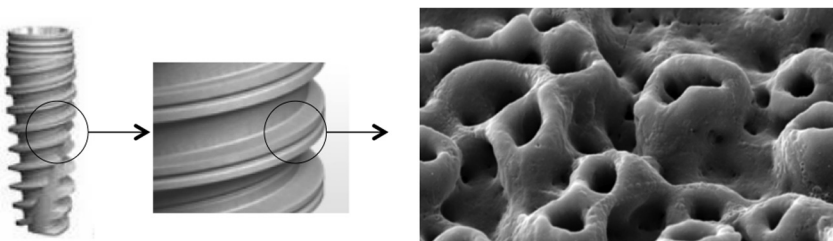
FIGURE 15.5   Nobel Active implant with the TiUnite surface.

There exist a large number of different implants specialized for different tasks. The fixture screws are designed to fit all kinds of treatment indications and hence come in all different dimensions, such as short, long, narrow, thick, parallel, and conical profiles. The fixture screws also vary in thread type; for example, double-threaded fixture screws speed up insertion. The introduction of grooves on the implant's threads increases the surface of the implant and attracts bone cells (Figure 15.5). The implant surface has long been a subject of discussion regarding the healing success rate of an implant. In the early years of dental implant treatments, the implants were all machined. Later it was found that roughened, modified surfaces speed up osseointegration. Nowadays, all producers have some kind of surface modification, and they all seem to work well. The connection between the fixture screw and the abutment varies and is supplier dependent. There is no commonly agreed upon standard. Today it is more common with internal connections as compared to external connections that where common on older fixture screws. Tolerances of the interface feature geometries are typically within 0.03 mm.

Considering implant abutments, crowns can be cemented on top of an abutment in the same way as on a natural tooth abutment. For screw-retained crowns, it is possible to make the porcelain veneering directly on the abutment if the implant is ideally placed. After tightening the abutment screw, the screw hole is filled with acrylic resin. Chair-side standard abutments are normally mass-produced by implant providers. However, dentists often prefer to order a lab-produced customized abutment or veneered full-contoured, screw-retained

crowns. In such cases, the lab technician can either wax-up or use CAD software to design the abutment.

Implant bridges are seated on several implants. This ensures stability of the design. The subgingival surfaces are machined or polished to prevent bacteria accumulation. For the frame, both non-precious metals can be used, as well as zirconia. Implant bridges are produced from both a traditional wax-up technique and CAD/CAM. It is important that implant interfaces be tightly seated on implants, as a bad fit can lead to loosening of an implant due to high load from tightening of the implant screw. Accuracy on implant interface positions should be within 0.02 mm.

An implant bar provides support to a denture via clips, balls, or other retention devices. Accuracy requirements are similar to those of an implant bridge. The implant interface positions should be within 0.02 mm. Implant bar overdentures are manufactured either by casting of wax-up or by welding bars on tering/EBM using titanium or cobalt-chrome. Some manufacturing methods require a second milling of the implant interface in order to reach the accuracy requirements and surface smoothness.

15.6   SIMULATION TOOLS

The introduction of CAI/CAD/CAM in the healthcare industry has been gradual. In some areas, healthcare has been at the leading edge of development, such as in the field of computer imaging, but in others it has lagged, especially where cost efficiency and optimization are of great importance. For example, many aerospace and automotive companies have used IT to cut costs significantly by transitioning from simple IT and data management to advanced 3D modelling and digital analysis of their product design and manufacturing systems. Today, virtual development in these industries is improving product quality and eliminating the need to build physical prototypes. This suggests that the medical device industry and healthcare in general will possibly see an IT revolution where real-time simulation and analysis can offer great improvements for patients and for the healthcare sector as a whole.

Simulation of surgical outcomes in real-time using 3D models of the human body is a new approach to planning surgery. Traditionally, this has been left to the individual surgeon or dentist, and relies on their individual skills, experience, and handcraft. In cases where there exist a variety of possible procedures, the surgeon can base his or her decision on accurate simulations and 3D models. The surgeon is thus better informed and aware of possible risks and alternatives regarding the specific patient. The introduction of optimization and simulation is shown in a flow chart diagram for a dental surgery (Figure 15.6). The dashed boxes show the potential added steps.

15.6.1   Simulation to Prevent the Effect of Variation in Implants

The objective in Figure 15.7 is to simulate implant positioning in order to predict the risk associated with positioning. Poor positioning of implants leads
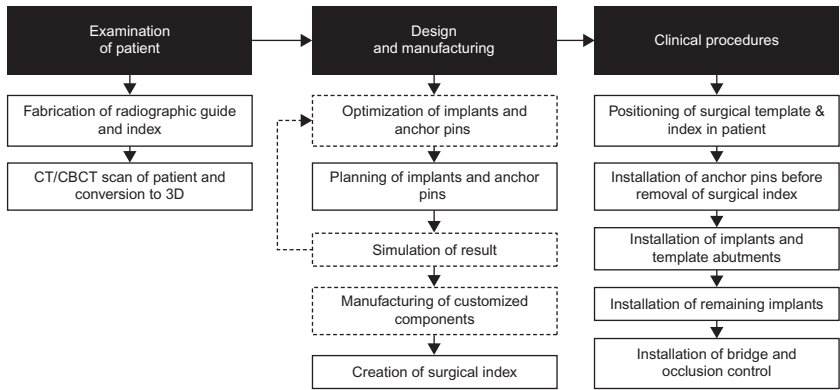
FIGURE 15.6   Impacted process (dashed boxes show potential added steps).
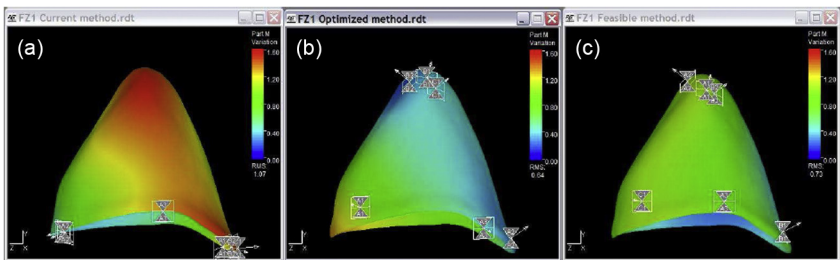
FIGURE 15.7   Surface areas of dental preparations (red areas indicate high variation): (a) Tooth before optimization; (b) Optimal; and (c) Practical compromise.

to longer healing times and more patient suffering. At the same time, simulation models can help increase the ability of the implant to function when the positioning is not optimal, that is, to position the implant to be insensitive to variation (i.e. robustness). Prior research in dental implants has shown that the design of the tooth preparation has a large impact on the function and durability of the implanted artificial tooth. Simulation models have shown the potential to reduce variation by up to 50% by using optimization software for positioning of dental crowns during tooth preparation.[3] Application of these principles can be extended to other types of implant surgery, thereby improving patient outcomes through variability reduction.

15.6.2   Optimizing the Geometry and Preparation Process for Dental Abutments

Mathematical rules of how to design an optimal tooth preparation exist. However, there is still a big gap between theory and practice. Simulation software and scanning tools can be improved by introducing a simulation step that utilizes the mathematical algorithms to calculate optimal abutments (Figure 15.8). This can
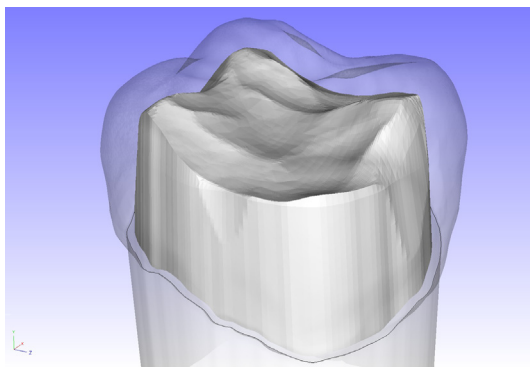
FIGURE 15.8   Optimal calculated preparation and exterior of original tooth.
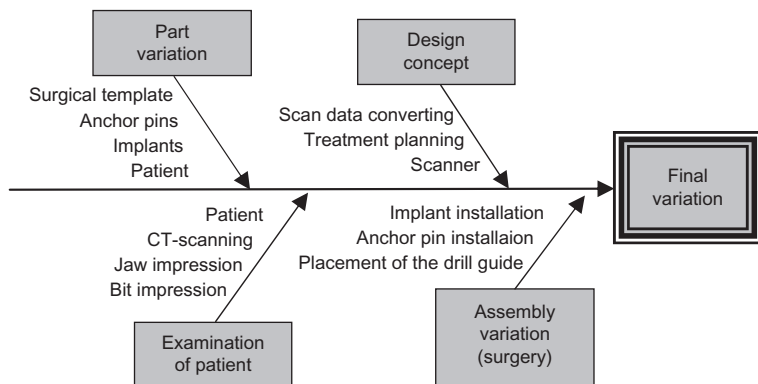
FIGURE 15.9   Sources of variation.

then assist the dentist in designing the optimal preparation and calculating an optimal path for the cutting tool, to avoid sensitive areas, and to minimize unnecessary tissue removal or damage.

15.7   QUALITY CONTROL

The core quality attributes of dental prostheses are strength, marginal fit, and aesthetics.[4] This section will mainly focus on the marginal fit and how variation affects the marginal fit. During the digital manufacturing process, each step leads to variation, and therefore it is essential to eliminate variation in all steps of the process. It has been shown that closed CAD/CAM systems consistently deliver solutions that vary less than 70 microns, and that (CAD/CAM) fabrication shows the same accuracy of fit as conventional techniques.[5]

Sources of variation for implant rehabilitation are shown in Figure 15.9. The impact of the different sources of variation differs with the type of treatment and with the machinery used in the process.

REFERENCES

1. Adell R, Lekholm U, et al. A 15-year study of osseointegrated implants in the treatment of the edentulous jaw. Int J Oral Surg 1981;10(6):387–416.
2. Beuer F, Schweiger J, Edelhoff D. Digital dentistry: an overview of recent developments for CAD/CAM generated restorations. Br Dent J 2008;204(9):505–11.
3. Kero T, Söderberg R, et al. A method for improving dental crown fit - increasing the robustness. World Acad Sci Eng Technol 2010:39.
4. Raigrodski AJ. Contemporary materials and technologies for all-ceramic fixed partial dentures: a review of the literature. J Prosthet Dent 2004;92(6):557–62.
5. Bindl A, Mörmann WH. Marginal and internal fit of all-ceramic CAD/CAM crown-copings on chamfer preparations. J Oral Rehabil 2005;32(6):441–7.

Advanced Dental-restoration Materials: Concepts for the Future

James Zhijian Shen[*] **and Tomaž Kosmač**[†]

[*]*Berzelii Center EXSELENT on Porous Materials, and Department of Materials and Environmental Chemistry, Arrhenius Laboratory, Stockholm University, Stockholm, Sweden;*
[†]*Jožef Stefan Institute, Ljubljana, Slovenia*

Contents

16.1 INTRODUCTION

The development of ceramics for restorative dentistry is strongly driven by patient needs and clinical indications. The aim is to replace or restore missing or damaged teeth with a high long-term survival rate. Besides the demands of materials with integrated and balanced functions that can be achieved and retained through a multi-step approach involving materials process and clinical operations, process constraints and compatibilities are always concerns during materials development. This chapter discusses the material demands for solving the problems encountered in current restorative dentistry that indicate the direction of future developments.

So far, the main driving force for the replacement of traditional metal-based, fixed-partial dentures (FPDs) and porcelain-fused on metals (PFMs)

with all-ceramic prosthetic crowns and bridges is the improved aesthetics and excellent tissue compatibility achieved by using metal-free systems that enable tooth-like colors. For the same reasons, full-ceramic post-and-core systems and implant superstructures were introduced to replace traditionally used metals. Ceramic materials are currently applied to two categories of applications in restorative dentistry: all-ceramic FPDs and implantable components. While the former demands mainly integrated and balanced properties of mechanical and aesthetic origins, the latter relies strongly on material's bio-oriented properties.

In past decades, there have been major advances in the application of sintered yttria partially stabilized zirconia (Y-TZP) ceramics for load-bearing FPDs. The superior mechanical properties of Y-TZP allow them to be used for the fabrication of multi-unit posterior bridges. Additionally, they enable a substantial thickness reduction of FPDs in the visible part of the dental arch that are subjected to lower mechanical stresses.

The clinical follow-up studies performed so far are very promising. Among the problems associated with the durability and reliability of zirconia-based all-ceramic FPDs, porcelain chipping is usually mentioned first. Chipping of porcelain veneered to ceramics occurs much more frequently than chipping of porcelain bonded to metal-ceramic FPDs. As described in detail in Chapter 5, it has been found that porcelain chipping is likely to start from a surface flaw in the veneer that is needed because of its aesthetic appearance, low hardness, and elastic modulus. Unfortunately, its strength and fracture toughness are low, such that the veneer represents the weakest link of the prosthetic work. In addition to poor mechanical properties, porcelain chipping is also affected by its poor wetting ability to the ceramic core in the melt state during fusing at high temperature. Also, properties of the ceramic core (i.e. high chemical stability, low thermal conductivity and high elastic modulus) are less favorable compared to a metallic core. Minor chipping damages can be temporarily repaired, but in most cases the whole prosthetic work must be replaced. Other causes for failure of all-ceramic FPDs are debonding (i.e. loss of coherence between the prosthetic work and the prepared tooth structure ensured by the luting cement), fracture of the framework, and delamination of the veneering porcelain. Fracture is due to the locally exceeded stress concentration in the framework, while debonding and delamination are associated with the chemical inertness of the core material, as well as with the stresses in the bi-layered structures due to thermal and elastic mismatch.

There are several concepts pursued worldwide for overcoming the chipping problem. For example, instead of handmade porcelain techniques, PRESS-ON and CAD-ON have been introduced (refer to Chapter 12 for more details). The former involves hot-pressing of a softened glass-ceramic onto the prefabricated ceramic framework, followed by hard-milling, diamond grinding, and polishing until the desired shape is obtained. After cooling to room temperature, the glass-ceramic exhibits less porosity, favorable aesthetics,

and better mechanical properties as compared to conventional porcelain, and should be less susceptible to chipping. The CAD-ON variant differs from the PRESS-ON technique in that the porcelain veneer is produced by precise hard-milling using CAD/CAM techniques. The two parts are then joined together before cementation.

When In-Ceram™ glass-infiltrated ceramic is used as the core material, the same low-melting glass is used in infiltration and in hot-joining, whereas any of the conventional luting cements can be used in the bonding of the two dissimilar materials at room temperature. The reasoning behind these two routes is straightforward, with clearly recognizable proprietary attributes exploited in each variant. Attempts are also being made to develop functionally graded Y-TZP ceramics with a dense core and a glass-infiltrated surface skin with a continuously decreasing content of zirconia.

In contrast to these interfacial engineering approaches, part of the community is gearing toward a rather radical solution (i.e. porcelain-free crowns and bridges), despite the increased risk of erosion on the juxtapose opposite tooth enamel, which begs ethical concerns and discussions. By eliminating the veneering layer, the aging-susceptible core ceramic is likely to become the weakest link, as it will be directly exposed to the aggressive wet environment of the oral cavity. Therefore, in the instance that this concept will see implementation in clinical practice, aging, friction, and enamel wear of the antagonist teeth may become very serious issues that result in a growing interest in alternative thin coatings and new core ceramic materials. Among them, ceramic matrix composites (CMCs) based on zirconia–alumina (refer to Chapter 11) and ceramic matrix hybrids (CMHs) based on a bio-mimetic polymer-infiltrated ceramic concept are particularly worth mentioning.

The success rate of dental implants is very high today. What the community is looking for in general is to preserve a healthy situation to secure a prolonged survival of the treatment. Full ceramic implants are attractive for improving aesthetics, particularly the part linked to soft tissue. Despite the fact that the use of full ceramic implants in the clinic is still controversial, ceramics are routinely used nowadays as a surface layer on titanium-based implants, as bioactive fillers, and as morphogenetically active scaffolds. For such applications, the integration and balancing of mechanical and bio-oriented properties of ceramics with tailored hierarchical pore structures is essential for further enhancement and securing of the healing process. Biomimetic materials and their processing concepts is another topic of general interest.

16.2   STRONG GLASSES AND GLASS-CERAMICS

As seen in previous chapters, the main challenge with glasses and glass-ceramics is the insufficient flexural strength and fracture toughness for their use in the posterior region. Otherwise, glasses and glass-ceramics represent the most aesthetic category of materials used in restorative dentistry. Currently,

there are fewer ways to bypass this drawback; for instance, by bonding the aesthetic porcelain directly to tooth enamel and dentin or by supporting the aesthetic porcelain layer with a strong, but less aesthetic, ceramic substructure.

Development of stronger glasses and glass-ceramics is an obvious and straightforward solution. When such materials become strong enough, they may be used as monolithic dental restoration even in the posterior region. One direction for this development effort is to optimize the microstructure of current silicate-based glasses and glass-ceramics by implementing the ceramic nanocomposite concept. One such example worth mentioning here is a new nanocrystalline glass-ceramic material based on Mg–Al–Si–O (but not on the commonly used Li–Si–O system) developed by a research group in Jena, Germany. By using zirconia as a nucleation agent and modifying the glass composition by doping ZnO or P_2O_5, glass-ceramics with high-strength can be prepared. A bending strength of 475 MPa has been reported by annealing at 1000 °C for three hours. This glass-ceramic has a micro-hardness of up to 13.3 GPa and a fracture toughness of up to 2.7 MPa m½.[1]

From a more general perspective, glass and glass-ceramics based on alumina-rich or silica-free aluminate systems are worth exploring. It has been reported that glasses comprising continuously linked $[AlO_x]$ (instead of $[SiO_x]$) polyhedrals can be prepared in Re–Zr–Al–O systems; 'Re' represents yttrium or any rare-earth metal. Glass-ceramics can then be prepared by further annealing. Replacing $[SiO_x]$ by $[AlO_x]$ polyhedrals increases the cross-link strength of the glass network. It also generates new possibilities for the preparation of glass-ceramics with alumina and other stronger crystals as major constitutional phases.[2] These glass-ceramics have the potential to provide integrated mechanical, chemical, and aesthetic properties that are required for restorative dentistry. The technical challenge right now is that the formation of this family of glasses requires extremely high cooling rates that cannot be met by the currently applied process for the preparation of silicate-based glasses. New processing concepts thus have to be developed in order to take the advantage of these materials. Figure 16.1 shows the SEM micrograph of a novel material of this type composed of nano-sized zirconia grains embedded in a glass matrix.

When the currently available processing sequence is no longer a technical restriction, the family of ceramic materials based on aluminate or zirconate eutectic compositions will become an alternative option. These materials can't be regarded as glass-ceramics by established definitions since they do not pass through a glass state during cooling from a melt state towards a ceramics consisting of crystalline phases and a residual glass phase. The unique interlocking microstructure among eutectic constitutions (by rapid, and preferably, directional solidification) is very different from the type of microstructures commonly observed in conventional ceramics. In principle, such microstructures ought to have the potential to provide the materials with improved fracture toughness.[3] Over the past few decades, rapidly solidified oxide eutectic
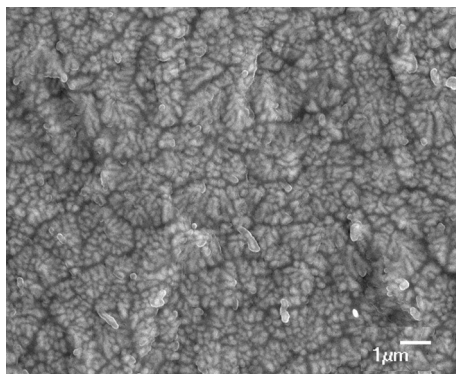
FIGURE 16.1   SEM micrograph taken on glass-ceramics composed of nano-sized zirconia grains embedded in a glass matrix.

ceramic composites have been intensively explored outside restorative dentistry. For instance, it has been reported that the $Al_2O_3/Y_3Al_5O_{12}/ZrO_2$ ternary eutectic composites prepared by rapid solidification techniques have demonstrated remarkable toughness in the region of ~8–9.0 MPa · m½.[4,5]

16.3   FUNCTIONAL GRADIENT MATERIALS

Another approach to overcoming the drawback of veneer chipping is to implement the functional gradient materials (FGMs) concept that has proven effective for preventing cracks in thermal barrier coatings (TBC).[6] It has been suggested that, based on a similar principle, veneer chipping may be substantially mitigated by an appropriate grading of the elastic modulus at the ceramic surface.[7] A family of graded zirconia ceramics (GZCs) have been accordingly prepared.[8] In the first step, these new composite materials were prepared in such a way that a porous skin with graded pore structure was formed on a dense core made of zirconia. Figure 16.2 illustrates this materials design concept. In principle, besides zirconia, other ceramics may also be used as core materials. The pores existing in the skin were then filled with a glass in a similar way as when making In-Ceram™ materials. By these means, a gradient of elasticity is generated from the outer surface of the material inward the bulk. The influence of the elastic modulus profile on the flexural damage resistance of such GZCs has been elucidated. It may provide a theoretical guideline for future development of functional gradient materials with improved load-bearing properties.

The advantages of this concept are three-fold:

1. A higher resistance to flexural damage is achieved compared to monolithic Y-TZP ceramics.
2. A higher resistance to occlusal surface contact damage than veneered monolithic Y-TZP ceramics. A 30° angulated fatigue sliding contact test
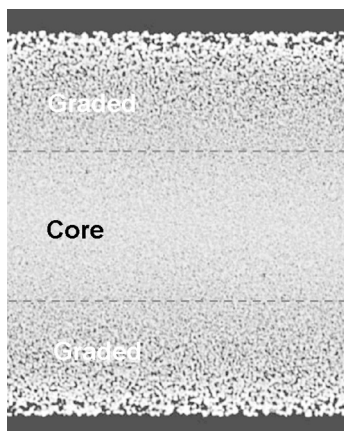
FIGURE 16.2 Illustration of the GZC concept.

performed at 200 N in water with a WC indenter revealed the formation of fine lateral cracks after 10 million cycles for the glass-zirconia-glass composite material with 50 μm residual glass, whereas cracks propagating through the entire veneer were observed after 100,000 cycles with 0.5 mm thick monolithic zirconia veneered with 1 mm porcelain.[7]

3. The residual glass on the outer surface acts as an aesthetic glaze whereas the inner glass surface acts as an etchable cementation surface.

No doubt the FGM concept represents one of the solutions for currently encountered veneer chipping problems. However, further innovation on the process side is needed in order to take full advantage of this concept. Otherwise, the application of this concept in the scale-up production of real components with complicated and individualized geometry would be hard to accomplish.

16.4   THIN AND MULTILAYERED COATINGS

The preparation of thin and preferably multilayered coatings has been an established approach outside the field of restorative dentistry for changing or modifying the surface properties of a material in order to improve its corrosion and wear resistance; to change its color; and to increase its functionality. Application of this concept has the potential for modifying the surface properties that are of importance in restorative dentistry; for instance, to modify the color of aesthetic ceramics; to change the surface roughness and wear behavior of full contour crowns; and to reduce bacterial adhesion on abutments.

Thin coating requires techniques that are be incompatible with the current lab-based CAD/CAM processing approach. These techniques are closely product-related, and often have to be included in the material fabrication process. The currently available coating processes for ceramics can be divided
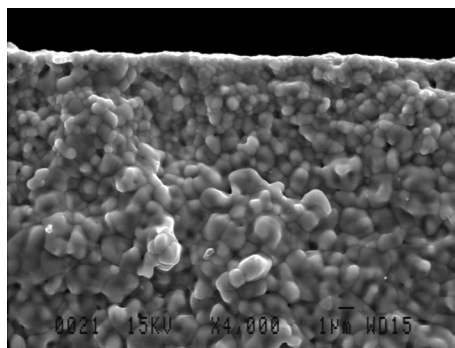
FIGURE 16.3   SEM of a thin ceramic coating applied on a ceramic substrate.

into two groups, namely, coatings applied before sintering, and coatings applied on a sintered material. When the coating is applied before sintering with methods like dip-coating or painting, it is desirable that the coating and the substrate materials be compatible with respect to both the sintering process and thermal expansion. If not, undesired chemical reactions and an uneven sintering shrinkage may occur at the interface, as well as the formation of thermal stresses. On the other hand, when the coating is applied on a sintered material by thermal spraying, sputtering, or sol-gel methods, it is in many cases sufficient to gain coherence by an additional heat treatment step. Figure 16.3 shows the microstructure of a ceramic sample with a thin layer of ceramic coating that consists of much finer grains than those in the matrix.

Ceramic coatings were introduced into dentistry by thermally spraying hydroxyapatite on titanium implants in the 1980s. The coating had a thickness of 50–100 microns and the bone attached to the coating, while the coating in some cases was lost from the titanium implant due to poor adhesion. The reason for this was to a large extent related to the fact that the hydroxyapatite structure was destroyed at the high temperatures used, in combination with thermal stresses at the interface of the coating and the implant. These problems introduced a general concern regarding implant coatings and changed the direction of the research towards thinner coatings applied by methods where the process temperature was reduced, such as sputtering. To further address the adherence of the coating to the substrate issue, particles or a surface patterning consisting of small spots has been applied. The results from some recent biological evaluations on the tissue response to implants coated with hydroxyapatite nanoparticles have not been consistent.

Most of the development of ceramic coatings in dentistry has so far focused on calcium phosphates and hydroxyapatite on titanium implants. With the spread of the full contour crown concept, and when the ceramic implants of inert materials such as zirconia are on the way to being introduced, there is an increased need to modify the surface with respect to both chemistry

and surface topography (refer to Chapter 14). With a ceramic substrate and a ceramic coating it would be possible to combine conventional ceramic shaping processes and coating techniques in the fabrication process. The thickness of the coating can then be varied and controlled on a microscopic level. The composition at the surface can also be changed from one material to another (even gradually). In some cases, the applied material will merge with the substrate and may not be treated as a coating at the end. It might instead be regarded as a surface modification due to its similarity with the substrate, or as a gradient material.

Current technical developments have made it possible to produce a thin ceramic coating from gaseous phases by, for instance, laser chemical vapor deposition (CVD) at low temperature with sufficiently high deposition rates. The CVD process is generally not considered suitable for preparing dense oxide ceramics at high deposition rates because the precursors for synthesizing oxides are commonly too reactive under an oxidizing atmosphere. Recent achievements with laser CVD, however, have convincingly demonstrated that high deposition rates ranging from several hundreds of μm/h to several tens of mm/h are achievable in practice.[9,10] This success has been ascribed to the fact that lasers can ionize precursor gases, thus forming plasma that alters the kinetics of chemical reactions. The photon-controlled chemical reactions of precursors are able to run much faster and at substantially lower deposition temperatures. Due to the high deposition rate achieved at low temperature, this technique has the potential to be implemented in the current CAD/CAM-based central production-processing set-up. Figure 16.4 shows a layer of alumina coated by the laser CVD process.
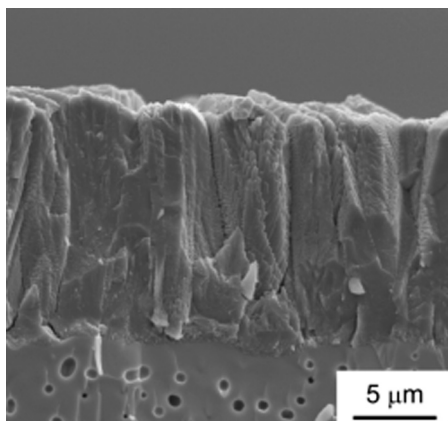
FIGURE 16.4   SEM micrograph that reveals the cross section of a sample coated with a layer of alumina by laser CVD.

16.5 TRANSLUCENT LOAD-BEARING CERAMICS

To improve the optical translucency of load-bearing ceramics is another obvious and straightforward solution to the challenge of veneer chipping. Readers may have already noticed the emergence of monolithic restorations made of new translucent zirconia grades that can be pre-colored or colored by infiltration with coloring liquids. The relatively high translucency of these new zirconia grades makes possible the manufacturing of (fully) anatomic restorations without the need for aesthetic veneering porcelain. Instead, the restoration can be simply characterized with stains, and glazed with a very thin glass layer. This concept is spreading quickly nowadays despite the fact that the available clinical data on this new type of monolithic restoration is limited. Concerns are also being raised about possible excessive abrasion of the opposite dentition and an excessive stiffness of the restoration. This is especially true in the case of implant-supported FDPs and full-arch restorations, which may impair the implants or the jawbone and articulations.

The loss of optical transparency of polycrystalline materials consisting of optically transparent grains is mainly due to light scattering by pores, inclusion, and/or grain boundaries.[11] In principle, ceramics consisting of optically transparent crystals, such as zirconia and alumina, all have the potential to gain optical translucency, or even transparency, provided that they do not contain second-phase inclusions and the porosity is eliminated below a certain degree (typically 0.01%). Technically, this is not always easy to achieve, as less than 0.1 vol.% residual porosity is often hard to remove; this is high enough to scatter the light and turns the otherwise translucent ceramics opaque.[12]

Besides eliminating pores, there are two common approaches to further improve the optical translucency of ceramics. These are either to increase the grain size well above the wavelength of the visible light, or to reduce the grain size well below it, in order to reduce the light scatter and birefringence caused by grain boundaries. The latter approach is more favorable for producing aesthetic ceramic dental prostheses since the nanoceramic structure obtained in this way also concurrently increases the mechanical strength of the ceramics. In the case of zirconia, caution has to be taken, however, that the stability of the tetragonal zirconia phase is strongly influenced by its grain size. The doping level of the stabilizer must therefore be optimized in order to obtain balanced mechanical and optical properties.

In practice, besides assuring full densification, effort has to be made to improve the homogeneity of the ceramic compact. As it will be described in more detail in Chapter 17, the inhomogeneous packing of ceramic powders and the inclusion of hard agglomerates and impurity particles will lead to pore coarsening instead of pore elimination. High translucency can only be preserved under the processing conditions when care is also taken to avoid contamination during milling and sintering. For that reason, dry milling,

careful cleaning after milling, and sintering in a clean atmosphere are highly recommended.

It is expected that the translucency of zirconia ceramics has the potential to be further improved with the achievement of more careful optimization of each step in the entire processing chain, starting from powder synthesis. Yet, in the end, zirconia prostheses may still not be able to satisfy the high aesthetic demands in the anterior region. The pearl-like optical appearance of polished zirconia ceramics is determined by the high refractive index of its constitutional crystals, which is an intrinsic physical property of zirconia and cannot be altered by microstructure manipulation. Coloring of zirconia ceramics is another challenge. Most coloring elements have very low or no dissolution concentration in the zirconia crystal lattice. Their segregation in grain boundaries has a negative influence on mechanical properties.

Today, lithium disilicate glass-ceramics are the most popular choice for dental prostheses in the anterior region. In the future, translucent alumina could be another option. It was already demonstrated in the beginning of the 1960s that alumina ceramics could be made translucent. Alumina is easy to color by alloying coloring elements into its crystal lattice. In comparison with zirconia, alumina is chemically very stable and has no aging problems. It has a lower refractive index that warrants its potential for improved aesthetics. Some obvious drawbacks of alumina that restrict its current application in dentistry are its lower damage tolerance, its high hardness, and its high Young's modulus. The damage tolerance of alumina can be improved by minimizing processing defects (see details in Chapter 17). In the literature it has been reported that carefully prepared alumina ceramics can achieve a bending strength well above 1000 MPa (i.e. two times higher than that of lithium disilicate glass-ceramics).[13] High hardness and a high Young's modulus are intrinsic physical properties of corundum crystal that can not be altered. The corresponding drawbacks may, however, be offset by a thin and preferably multilayer coating with a reduced hardness and Young's modulus. Figure 16.5 shows the copings made of translucent and non-translucent alumina ceramics, respectively.

FIGURE 16.5 Photo of three copings made of no-translucent (Middle) and translucent (Left and Right) alumina ceramics.

16.6   POLYMER CERAMIC HYBRIDS

Ceramic fracture toughness can be drastically increased by adding an organic polymer phase. Such hybrid toughening principles were demonstrated by an example of hybrids formed in an alumina-PMMA system. It was reported that by combining two ordinary compounds (alumina and polymethyl methacrylate) into ice-templated structures, hybrids with high toughness of more than 300 times (in energy terms) that of their constituents were formed. The hybrid material also retained a reasonable yield strength of ~200 MPa.[14]

Two dental hybrid materials have been developed recently by exploring this concept: a hybrid system consisting of nano-ceramic particles embedded in a polymer matrix,[15] and a hybrid system consisting of a porous ceramic core infiltrated with a polymer.[16] The former consists of a highly crossed-linked polymer matrix reinforced with 79% ceramic particles. These particles are of three different types: 20 nm non-agglomerated silica particles, 4–11 nm non-aggregated zirconia particles, and 0.6 to 1 μm-aggregated zirconia/silica clusters. All the particles are treated with a silane-coupling agent that allows them to bond to the resin matrix. The SEM micrograph shown in Figure 16.6 reveals the microstructure of this hybrid material. The benefits as claimed by the manufacturer are: (1) a faster manufacturing procedure as firing is not required and milling, polishing, and adjustment are easier; (2) high durability and shock absorption; and (3) intra-oral adjustability with light-cured restoratives. This material launched at the end of 2011 is available as CAD/CAM blocks in 8 shades based on the VITAPAN Classic system and at two levels of translucency. Thanks to its strength of 200 MPa and fracture toughness of 2.0 MPa · m½ it is offered by the manufacturer for permanent veneers, inlays, onlays, and tooth and implant-supported single crowns.

The latest hybrid material consists of a porous ceramic framework that is further infiltrated with a mixture of polymers (15–20% of total volume). It
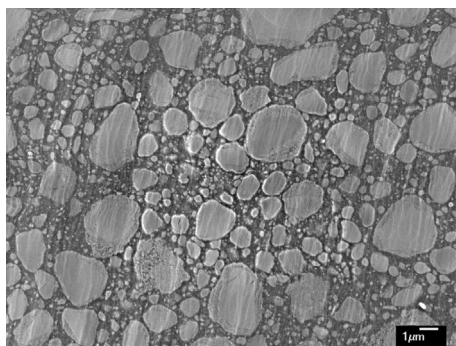
FIGURE 16.6   SEM micrograph taken of a well-polished section that reveals the microstructure of a polymer ceramic hybrid material consisting of a highly cross-linked polymer matrix reinforced with 79% ceramic particles. (Lava Ultimate, 3 M.)

is a new material that was launched in 2013 as CAD/CAM blocks available in five shades and two levels of translucency (3D Master shades 0M1, 1M1, 1M2, 2M2, 3M2). Thanks to a favorable combination of mechanical properties of both ceramics and polymers it is expected to exhibit a higher fracture resistance than conventional reinforced feldspathic porcelains. A recent study reported elastic modulus, hardness, and fracture toughness values of 30 GPa, 2.6 GPa, and 1.7 MPa · m½, respectively. Long-term stability of these hybrid materials in an erosive oral environment is a concern that requires further follow-up studies.

16.7 STRONG POROUS CERAMICS

The high elastic modulus of Y-TZP ceramics relative to that of dentin appears to be an emerging problem in restorative dentistry as it may lead to the development of stresses at the interface of the zirconia frameworks and tooth preparations. This can in turn cause a marginal seal failure due to fracture, which leads to periodontal disease and secondary caries. Moreover, the higher rigidity of Y-TZP posts can be a predisposing factor for vertical root fractures. Therefore, Y-TZP is not recommended for patients with bruxism. Besides, it is almost impossible to retreat teeth restored with zirconia posts because it is too difficult to grind away the Y-TZP post and remove it from the root canal.[17] To prevent root fractures, a post should have an elastic modulus similar to that of dentin, a property which enables a more uniform distribution of stress by distributing the occlusal load.[18]

Introducing porosity into the Y-TZP is a way of meeting the conflicting demands of lowering the elastic modulus while retaining sufficiently high strength and fracture toughness. This not only proves beneficial in terms of stress development/distribution in the dentin-ceramic interface, but also lowers the susceptibility to low-temperature degradation (LTD). It may even open up the possibility of increased bioactivity when bioactive ingredients and growth factors are immobilized inside pores with tailored structures. It is believed that a compromise between the elastic and mechanical properties can be obtained in this way, whereas additional porcelain veneering is expected to 'seal' the surface of the core material and to re-establish the aesthetic appearance. The targeted values of elastic modulus and flexural strength are 80 GPa and 800 MPa, respectively, with the Weibull modulus m > 15 (m is the measure of the reliability of the material; refer to Chapter 9). These are expected by the development of proper processing techniques.

In general, brittle ceramic materials become even more fragile when large concentrations of pores/voids are accommodated in their structure. It is thus challenging to prepare porous ceramic bodies that combine high porosity with high mechanical strength. In currently established techniques, pores are formed in the green body stage (e.g. by freeze-casting,[19,20] replication,[21,22] sacrificial/emulsion templates,[23,24] or direct-foaming methods[25,26])
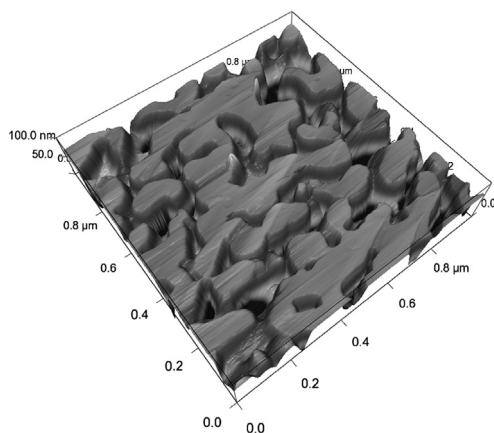
FIGURE 16.7   AFM image of porous alumina ceramics that reveals the strong necking between individual grains.

where mechanical rigidity of the porous ceramics is achieved by growth of the inter-particle contacts via surface atomic diffusion in the initial stages of subsequent sintering. In order to prepare strong macroporous ceramics, the potential advantages of addition or in situ formation of nano-particles and new consolidation principles such as coalescence-mediated necking of nano-grains need to be further explored.[27,28] Figure 16.7 shows an AFM image of a strong porous alumina ceramic sample prepared by a coalescence-mediated necking principle.[28]

16.8   BIOMIMETIC MATERIALS

The application of biomimetic principles represents another direction for future development of materials for restorative dentistry. On one side it covers the mimicking of natural materials structures, and on the other side the natural materials processes.

Bone and teeth as natural materials are characterized by their microstructures that combine complex architectures with well-organized heterogeneities.[29,30] Tooth enamel, for example, is well known for both its iridescent beauty and its amazing toughness (refer to Chapter 2). The hierarchical integrations of structural heterogeneities that span multiple-length scales (from nano- to macroscopic) strengthen these natural materials consisting of otherwise very weak minerals. Man-made materials can so far barely achieve the types of smart structures found in natural materials. Sophisticated operations are often necessary to introduce very simple structural hierarchy in polycrystalline materials. With the development of novel processing technologies (see Chapter 18), it appears that in the near future it will be possible to produce, in limited processing steps, materials with tailor-made chemical and/or
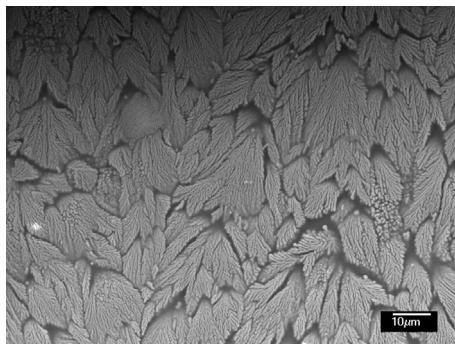
FIGURE 16.8　SEM image taken on a laser-sintered ceramic material based on zirconia that reveals the type of biomimetic structure formed.

microstructural heterogeneities. Improved performances and/or multifunctions are expected to emerge in these materials with engineered structural hierarchies in multiple-length scales, from nanometers and micrometers to above centimeters. The SEM image shown in Figure 16.8 is taken on a laser-sintered ceramic material based on zirconia.[31] It reveals the type of biomimetic structural hierarchies formed.

Biogenic bone formation is accomplished at body temperatures, while the production of synthetic hydroxyapatite (HA) requires high temperature. Nature's energy efficient approach is controlled by morphogenetically active signaling molecules. These molecules or growth factors display a spatially and temporally precise pattern of expression during differentiation of osteoblasts as compared to their mesenchymal progenitor stem cells and osteoclasts from their hemopoietic precursor cells. In addition, a homeostatic crosstalk between these cell lineages via signaling molecules occurs. It is a challenging task to develop materials that are able to mimic the inductive stimuli role of the physiological extracellular matrix (ECR). In the last few years, naturally occurring polymers, polyphosphate (bio-polyP) and bio-silica, have been identified to cause morphogenetic activity on both osteoblasts and osteoclasts.[32–34] The biomimetic processes mediated by these natural inorganic polymers may point the way toward the development of next-generation implantable materials.

ACKNOWLEDGMENTS

Jegou Saint-Jean, Dr. Erik Adolfsson, Dr. Andraž Kocjan, Prof. Matts Andersson, and Prof. Dr. Werner E.G. Müller and his colleagues.

REFERENCES

1. Dittmer M, Rüssel C. Colorless and high strength MgO/Al$_2$O$_3$/SiO$_2$ glass-ceramic dental material using zirconia as nucleating agent. J Biomed Mater Res B Appl Biomater 2012;100B(2):463–70.
2. Rosenflanz A, Frey M, Endres B, Anderson T, Richards E, Schardt C. Bulk glasses and ultra-hard nanoceramics based on alumina and rare-earth oxides. Nature 2004;430:761.
3. Waku Y, Nakagawa N, Wakamoto T, Ohtsubo H, Shimizu K, Kohtoku. Y. A ductile ceramic eutectic composite with high strength at 1,873 K. Nature 1997;389:49–52.
4. Oliete PB, Pena JI, Larrea A, Orera VML, Lorca J, Pastor JY. Ultra-high strengthnanofibrillarAl2O3–YAG–YSZ eutectics. Adv Mater 2007;19:2313–8.
5. Su HJ, Zhang J, Cui CJ, Liu L, Fu HZ. Rapid solidification of Al2O3/Y3Al5O12/ZrO2 eutectic *in situ* composites by laser zone remelting. J Cryst Growth 2007;307:448–56.
6. Sasaki M, Wang Y, Hirano T, Hirai T. Design of SiC/C functionally gradient material and its preparation by chemical vapor deposition. J Ceram Soc Jpn 1989;97:539–43.
7. Zhang Y, Chai H, Lee JJ-W. Chipping resistance of graded zirconia ceramics for dental crowns. J Dent Res 2012;91(3):311–5.
8. Zhang Y, Kim JW. Graded structures for damage resistant and aesthetic all-ceramic restorations. Dent Mater 2009;25:781–90.
9. Goto T. High-speed deposition of zirconia films by laser-induced plasma CVD. Solid State Ionics 2004;172:225–9.
10. You Y, Ito A, Tu R, Goto T. Low-temperature deposition of α-Al2O3 films by laser chemical vapor deposition using a diode laser. Appl Surf Sci 2010;256:3906–11.
11. Apetz R, Van Bruggen MPB. Transparent alumina: a light scattering model. J Am Ceram Soc 2003;86(3):480–6.
12. Krell A, Hutzler T, Klimke J. Transmission physics and consequences for materials selection, manufacturing, and applications. J Eur Ceram Soc 2009;29:207–21.
13. Yeh TS, Sacks MD. Low-temperature sintering of aluminum oxide. J Am Ceram Soc 1988;71(10):841–4.
14. Munch E, Launey ME, Alsem DH, Saiz E, Tomsia AP, Ritchie RO. Tough, Bio-Inspired Hybrid Materials. Science 2008;322:1516–20.
15. Koller M, Arnetzl GV, Holly L, Arnetzl G. Lava ultimate resin nano ceramic for CAD/CAM: customization case study. Int J Comput Dent 2012;15:159–64.
16. He LH, Swain M. A novel polymer infiltrated ceramic dental material. Dent Mater 2011;27:527–34.
17. Akkayan B, Gulmez T. Resistance to fracture of endodontically treated teeth restored with different post systems. J Prosthet Dent 2002;87:431–7.
18. Özkurt Zeynep, işeri Ufuk, Kazazoğlu Ender. Zirconia ceramic post systems: a literature review and a case report. Dent Mater J 2010;29(3):233–45.
19. Scheffler M, Colombo P. Cellular ceramics: structure, manufacturing, properties and applications. Weinheim: Wiley-VCH; 2005.
20. Gibson LJ, Ashby MF., 2nd ed. Cellular solids: structure and properties, 510 Cambridge: Cambridge University Press; 1997.
21. Roy DM, Linnehan SK. Hydroxyapatite formed from coral skeletal carbonate by hydrothermal exchange. Nature 1974;247:220–2.

22. Sandhage KH, et al. Novel, bioclastic route to self-assembled, 3D, chemically tailored meso/nanostructures: shape-preserving reactive conversion of biosilica (diatom) microshells. Adv Mater 2002;14:429–33.

23. Yang D, Qi LM, Ma JM. Eggshell membrane templating of hierarchically ordered macroporous networks composed of TiO_2 tubes. Adv Mater 2002;14:1543–6.

24. Imhof A, Pine DJ. Ordered macroporous materials by emulsion templating. Nature 1997;389:948–51.

25. Gonzenbach UT, Studart AR, Tervoort E, Gauckler LJ. Ultrastable particle-stabilized foams. Angewandte Chemie—Int Ed 2006; 21:3603–10.

26. Chandrappa GT, Steunou N, Livage J. Materials chemistry-macroporous crystalline vanadium oxide foam. Nature 2002;416:702–5.

27. Dakskobler A, Kocjan A, Kosmač T. Porous alumina ceramics prepared by the hydrolysis-assisted solidification method. J Am Ceram Soc 2011;94(5):1374–9.

28. Shen Z-J, Xiong Y, Höche T, Salamon D, Fu Z, Belova L. Ordered coalescence of nanocrystal: a path to strong macroporous nanoceramics. Nanotechnology 2010;21:205602.

29. Aizenberg J, Weaver JC, Thanawala MS. Skeleton of Euplectella sp.: structural hierarchy from the nanoscale to the macroscale. Science 2005;309:275.

30. Lee LP, Szema R. Inspirations from biological optics for advanced photonic systems. Science 2005;310:1148–50.

31. Gruner D, Shen Z-J. Ordered coalescence of nano-crystals during rapid solidification of ceramic melts. Cryst Eng Comm 2011;13(17):5303–5.

32. Müller WEG, Wang XH, Diehl-Seifert B, Kropf K, Schloßmacher U, Lieberwirth I, et al. Inorganic polymeric phosphate/polyphosphate as an inducer of alkaline phosphatase and a modulator of intracellular Ca^{2+} level in osteoblasts (SaOS-2 cells) *in vitro*. Acta Biomater 2011;7:2661–71.

33. Wang XH, Schröder HC, Wiens M, Schloßmacher U, Müller WEG. Bio-silica: molecular biology, bochemistry and function in demosponges as well as its applied aspects for tissue engineering. Adv Mar Biol 2012;62:231–71.

34. Schröder HC, Wang XH, Wiens M, Diehl-Seifert B, Kropf K, Schloßmacher U, et al. Silicate modulates the cross-talk between osteoblasts (SaOS-2) and osteoclasts (RAW 264.7 cells): inhibition of osteoclast growth and differentiation. J Cell Biochem 2012;113:3197–206.

Defect Minimization in Prosthetic Ceramics

Erik Adolfsson[*] **and James Zhijian Shen**[†]

[*]*Ceramic Materials, Swerea IVFAB, Mölndal, Sweden;* [†]*Department of Materials and Environmental Chemistry, Arrhenius Laboratory, Stockholm University, Stockholm, Sweden*

Contents

17.1 INTRODUCTION

An optimized combination of aesthetics, reliability, and durability of ceramics will become more important in the future when thinner structures are desired and new concepts such as full contour crowns are introduced. To meet these requirements, materials with properties beyond those of ceramics used today must be developed.[1] The general approach to achieve this has mainly been focused on the development of new advanced ceramics and ceramic composites with a drastic reduction in grain sizes, which results in powder processing that is more challenging.[2] This approach has so far been of limited success and few of the developed materials have shown properties that are significantly improved as compared to conventional materials in use. A major reason for this is that properties such as strength and reliability are not only controlled by

the composition or grain size of the material, but are also determined by the defects present within the materials.

From a process point of view, bulk defects can be introduced from raw materials, contaminations, and the fabrication processes.[3,4] In addition to these bulk defects, surface-related defects are introduced by shaping processes such as grinding of sintered materials,[5] machining of green or pre-sintered materials,[6–8] surface treatments by blasting,[9,10] or adjustments by grinding and polishing performed by the dentist. The defects from each processing step accumulate and determine the evolution of the microstructure and the final performance of the ceramic material. Therefore, it appears obvious that ceramics with an improved mechanical performance will not be obtained by the introduction of new advanced materials only. Optimization and development of suitable fabrication processes that are adjusted for these materials are equally necessary, if not even more urgent, especially if the full potential of the materials developed are to be reached.

17.2   THE DECISIVE ROLE OF DEFECTS

When a material is exposed to a load, stress concentrations are formed around discontinuities in the material such as defects, which makes them a critical strength-determining factor. Once the stress reaches a critical value, a propagating crack that reaches terminal velocity will cause the material to fracture in a detrimental fashion, as described in Chapter 9. The stress concentration is further dependent on the size, shape, and orientation of the defects, where a larger defect size and reduced crack tip radius contribute to an increased stress concentration. With the assumption of a random orientation and a shape that depends on the nature of the defect, the strength of ceramic materials is often limited by the largest defects present. However, the defects do not have to be large in order to influence the mechanical performance. A defect size of a few microns can be sufficient to influence the performance of a high-strength ceramic, and if the size of the strength-limiting defects were increased four times, approximately half of the strength would be lost.

In addition to the defect size, the frequency or number of defects per volume in the material will also contribute to how the defects influence the strength. A large number of equal-sized strength-limiting defects (high frequency) give a narrow strength distribution and high reliability since the fractures are likely to be initiated from defects of similar size. If there are only a few large defects present (low frequency), the possibility that these are exposed to high stress is reduced. As a result, some fractures are induced by large defects and some by small defects. This gives a large variation in strength and makes it difficult to predict the material strength, implying low reliability.

Once formed, the bulk and subsurface defects are difficult to remove and the final product will thus contain an accumulated defect population formed
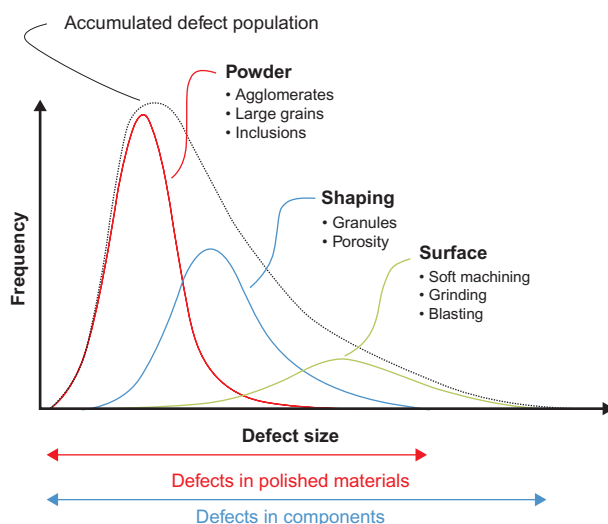
FIGURE 17.1   An illustration of the size and frequency of various defects formed during the fabrication of a ceramic material. Material performance is determined by the accumulated defect populations, which depend on the raw material and the fabrication process used.

by the size and frequency of each defect population present as illustrated in Figure 17.1. The reason for the formation of the largest defects is, however, not possible to predict. In one case, hard agglomerates in the raw material can be responsible for the largest defect population, while grinding marks on the surface can be found to be the largest defects in another case. Therefore, in real practice, the ceramic's performance is strongly dependent on the process history of the materials. This implies that properties such as strength and translucency will not necessarily be the same when the ceramics are prepared through different processes or by different producers, even if the same raw materials are used.

17.3   MINIMIZING DEFECTS IN POWDERS

Defects can be introduced either from the ceramic raw material or from the processed granules that are used to facilitate handling of the raw material.[11] The presence of defects such as hard agglomerates, impurities, organic inclusions, etc. in the raw material, was previously a common problem that often reduced the material performance. These defects related to the raw material can to a large extent be avoided through improved powder production processes, careful control of the production, and processing in a clean environment. However, even in well-known and frequently used powders, dense fragments (Figure 17.2) are present and may cause inhomogeneities in the green body with respect to particle packing and density[12]; It was found that
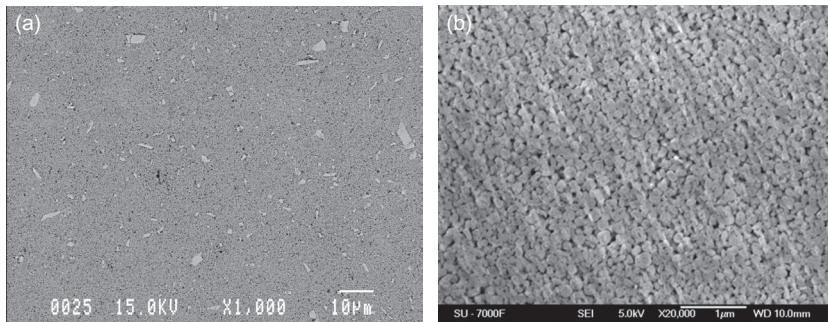
FIGURE 17.2 Microstructure of a CIPed and pre-sintered zirconia material with dense fragments (a) as compared to a more processed zirconia powder (b).

such inhomogeneities in green density that originated from inhomogeneous packing of particles yielded the formation of locally interconnected pores that coalesced to form larger pores during the final stage of sintering. This phenomenon, known as pore enlargement, harms the optical translucence of the formed ceramics.[13] As long as these fragments are small in size they may not influence the mechanical performance or the overall sintering shrinkage of the material. While on the microscopic level the initial variation of the green density caused by dense fragments may influence the sintering.[14] To further improve the homogeneity of a green body made from such powder would require additional processing of the powder in order to remove agglomerates. The most common techniques for removing agglomerates, as opposed to milling,[15] are sedimentation/decantation, filtration, and sieving.[2,16]

17.4 MINIMIZING DEFECTS IN MATERIALS PROCESSES

Shaping processes are often responsible for a large number of defects in ceramic materials. As detailed in Chapter 7, these processes involve both the consolidation of ceramic particles to form a green body, and additional steps to obtain the desired shape before and/or after sintering. The defects can then be present either as bulk defects that originate from the particle packing during consolidation of the green body, or as surface defects that originate from the interaction between materials and the pressing or machining tools.

17.4.1 Green Bodies

The formation of green bodies can be done through either a dry compaction process of granulated powder[17] or through a wet process[4,16,18] where a ceramic suspension is used and casted by various techniques (see Chapter 7 for more details). Most of the ceramics used nowadays in dentistry are made through the dry process where granules with a size in the range between several tens

to several hundreds of microns, consisting of submicron- or even nano-sized particles, are poured into a die or mold. An external uni-axial and/or isostatic pressure is applied to the mold or die to deform the granules and increase the particle packing within the green compact. In an ideal case, the compaction process gives a homogenous green body with no trace of the boundaries from adjacent granules. This requires that the granules be evenly distributed and that the granule characteristics (e.g. hardness, deformability, size distribution, granule density) are favorable for the granules to merge during compaction.[12,19–21] However, this is not always the case; both unsuitable granule characteristics and random packing of granules are potential sources of defects.[22]

Even though some general principles regarding granule characteristics are known, such as the fact that hard elastic granules tend to form larger defects compared to softer granules.[23] The knowledge to select suitable granule characteristics with the aim to minimize their influence on the final material is still far from sufficient despite the efforts made to reduce the defects caused by granules in sintered materials.[11,19,24,25] One reason for this might be found in the complexity of the fabrication process of ceramics materials prepared from granules, that includes granule formation, compaction and the burnout of organic additives. The granules do not only deform during compaction, their characteristics change continuously as their density increases, and may thus vary both between different granules in the compact as well as within a single granule. A better understanding of suitable granule characteristics for the compaction process is thus required, and might be one of the most important topics in avoiding additional granule-related defects. As long as these problems remain unsolved, it will be difficult to enhance the reliability and reach the full potential of the ceramic materials developed.

Granules are prepared through two main routes. Spray drying is the dominant process where a powder suspension is sprayed into warm air and each droplet is allowed to dry and form a granule. When water is removed from the surface of the droplet during drying, a mass transport occurs from the interior towards the surface. This material transport within the droplet can result in an uneven particle or binder distribution within the granule, which is an undesirable situation since it can give unpredictable granule characteristics. To avoid some of these problems, freeze granulation was developed and used on a much smaller scale as compared to spray drying. Instead of removing water from the droplets by air-drying, the suspension is sprayed into liquid nitrogen to rapidly solidify the droplets by freezing. The water is then removed from the frozen granules in a second step by sublimation in a freeze-drying procedure without any mass transport in the liquid state. The granules are thus assumed to obtain a higher degree of homogeneity and have been suggested for use in the preparation of granules that facilitate the formation of green compacts with a reduced defect concentration.[23–28] However, from investigations of granule microstructure, various inhomogeneities, such as pores and particle segregations, can be characterized and quantified in granules prepared either by spray-drying, or by

freeze granulation. Voids can be formed by entrapment of air in the droplets during spraying and segregation of particles in the granules can be found in spray-dried as well as freeze-granulated materials. The freeze-granulated materials are thus not as homogeneous as often claimed. The particle segregation within the granule is caused by the formation of ice crystals during freezing and the segregation is found to increase with the granule size and the water content in the suspension.[12]

The interparticle porosity within individual granules can, however, be assumed to be less crucial for the formation of larger defects since these pores are significantly smaller as compared to the cavities formed in-between the granules. In an ideal case where equal-sized granules are closely packed, the pore volume in-between the granules corresponds to around 30 vol.% of the mold. In a real case, the granules poured into a mold would not be closely packed. A large number of stacking faults are likely formed and result in cavities with a size similar to the size of the granules. The intergranular voids might increase even further in both size and number if non-spherical granules are introduced, such as hollow and donut-shaped types. Even if the size of the initial voids is significantly reduced during compaction, narrow intergranular defects can still present in the green body if the granules were not able to deform sufficiently to merge with the adjacent granules during compaction. An example of this is shown in Figure 17.3, where the round shape of a granule was found at the fracture surface of a bending bar and the polished cross section with typical crack-like defects between granules that were not merged during compaction. The length of these defects can be large in one direction and small in another, which results in a small defect volume that is not necessarily found by density measurements (see Chapter 8 for more details). On the other hand, the shape of these defects easily results in the formation of higher stress concentrations around the sharp crack tip as compared to spherical inclusions. These types of defects can thus have a significant impact on strength. To some extent, the size of the granule-related defects can be reduced by the use of smaller granules. However, a certain granule size is still needed in order to obtain a sufficient fluidity of the powder granules in order to facilitate the mold filling.[3]

17.4.2   Colloidal Processing

Producing ceramics through colloidal processing is not a new concept. The term ceramics has a Greek origin: objects formed by casting. Pottery and porcelain are traditionally formed by colloidal processes. More details of colloidal processes can be found in Chapter 7. Despite the lower production rate compared to dry-pressing, colloid processes appear to be crucial for the success of certain approaches that have potential for future production of individualized ceramic dental prostheses as described in detail in Chapters 7 and 18.

One obvious advantage of colloidal processes as compared to dry-pressing is the possibility of achieving much higher levels of homogeneity
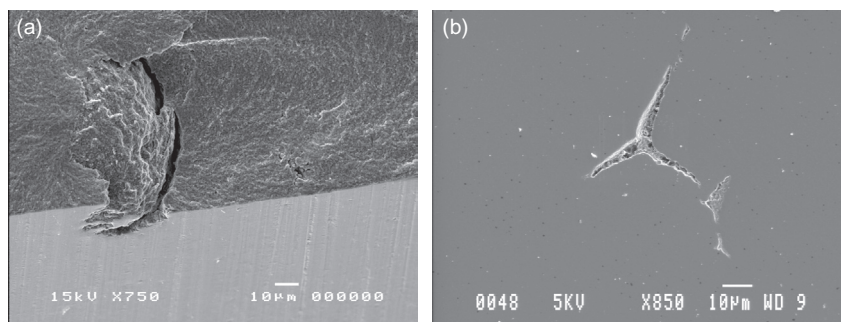
FIGURE 17.3   An SEM fractograph of the fracture surface of a bending bar prepared from a granulated powder (a), which reveals the presence of a granule-related defect. (b) An SEM image taken on a polished cross section of a material CIPed at 300 MPa that reveals defects formed between granules that were not completely merged during compaction.

with improved packing of individual particles, which contributes to higher green densities and reduced sintering temperatures.[4] Furthermore, the use of colloidal methods allows the intergranular voids that are often formed during dry-pressing to be eliminated. The positive contributions of such advantages to the improvement of mechanical and optical properties would not be recognized if the accompanying drawbacks of the process were not overcome. These are density gradients and drying, which can cause deformation or even crack formation if the drying process is not properly controlled.[29] One such example is shown in Figure 17.4.

17.4.3   Sintering

The process involves heating and can be divided into three stages, an initial (usually slow) heating of the green body to burn off organic additives, sintering at high temperatures, and finally, cooling. All these stages can contribute to the formation of defects such as cracks, pores, or large grains. These can be either directly temperature-related or associated with the green body characteristics.

To facilitate handling and compaction of ceramic powders, various organic processing additives are usually added. Even if the amount is small by weight (usually in the range of 3–5 wt.%), the corresponding volume of the additives in a zirconia material would be in the range of 15–25 vol.%. When such a volume of material is burned off, a low heating rate is normally applied during the initial stage to avoid the formation of high internal gas pressures that can cause fracture in the green body.

An important consideration during densification is the adjustment of the sintering process to obtain an even temperature distribution within the green body. This allows the porosity to be removed from the internal volume during
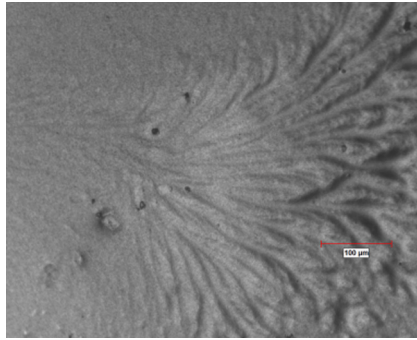
FIGURE 17.4   A microscopic image taken on the dried surface of a cast sample that reveals the density gradients associated with the water diffusion paths.

densification, and minimization of the remaining porosity. Modifications of the heating rate, geometrical shape, composition, or furnace type can then influence the temperature distribution in the sample and cause an uneven densification of the remaining porosity. This means that a sintering procedure found to be suitable for the densification of a specific material may not be directly applicable if the geometrical shape is significantly changed. Higher heating rates can usually be used for thin structures as compared to thicker parts where more time is needed for the heat to transfer through the material and reduce the temperature gradients during sintering. Also, dense materials can be influenced by heating or cooling rates, as are often used in veneering procedures. The temperature difference between the surface and internal structure can induce thermal stresses that are large enough to induce the formation of surface cracks or interfacial cracks, as in the case of laminated composites such as veneered ceramic crowns.[30] Large differences in the thermal expansion coefficient and thermal conductivity between different phases further enhances such thermal stresses. Figure 17.5 shows the micro-cracks formed at the alumina side of the interface between alumina and veneered porcelain.

The inorganic additives used for various purposes, such as to influence the color of dental ceramics, can interact with the main material and significantly enhance material mobility during sintering and cause abnormal grain growth. Independent of the method used to incorporate the additive, it is important that the additive be evenly distributed within the green body to avoid locally high concentrations that may contribute to uneven densification. Figure 17.6 shows one such example for sintered alumina ceramics.

17.4.4   Machining and Surface Texturing

The defect populations from earlier stages in the fabrication chain are often randomly distributed within the bulk material and determine the level for the
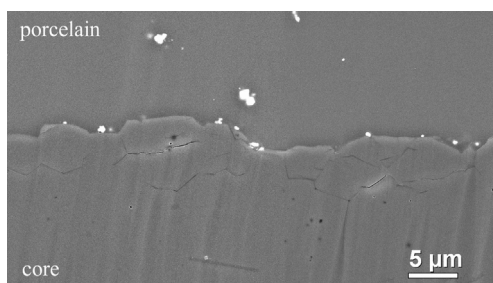
FIGURE 17.5   An SEM image taken on an ion beam-polished cross-section of a veneered alumina crown that reveals the micro-cracks formed at the alumina side of the interface between alumina and veneered porcelain.
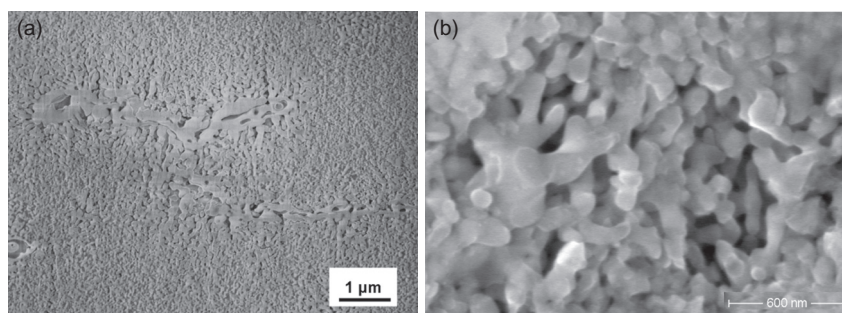
FIGURE 17.6   SEM images that reveal the abnormal grain growth of alumina (a) and the inhomogeneous necking of grains during sintering of alumina caused by uneven particle packing in thea green body, which yields the formation of hardly aggregated grains that become difficult to completely densify (b).

mechanical properties that can be reached. All the following processes used to change the shape or the surface structure of the ceramic, such as milling, grinding, or sandblasting, induce surface structures and cracks. These may act as defects and can have a large impact on the mechanical performance, especially when located at the surface where the tensile stresses are formed. As soon as these surface defects are of a size that is comparable to or larger than the bulk defects, the mechanical performance is influenced and the strength decreased. For all surface changes it is thus important to adjust the process parameters to the material used in order to minimize formation of undesired defects and an unnecessary reduction in strength.

There has been a desire to find a versatile shaping process that can be used for both standardized and individualized ceramic dental prostheses. One solution was to prepare a powder compact, also called blank, and use it either, in the green state, or as pre-sintered (i.e. sintered at a low temperature to burn

off the organic additives and to form necks between the particles to increase the rigidity of the blank). From these blanks, material can be removed by machining with conventional hard metal cutting tools. In combination with CNC machines and CAD/CAM systems adapted from other industries, it has been possible to increase the productivity of both standardized as well as individualized dental components. For more details of such processes refer to Chapter 15.

When cutting tools are used to machine a pre-sintered ceramic blank, the material removal process is different compared to when a deformable material is machined. When the cutting edge of the tools passes through the pre-sintered ceramic blank, the material in front of the edge is crushed into small fragments. The new surface then consists mainly of a large number of small fractured surfaces. In addition to these, the surface may also have some chippings and scratches from the interaction between the tool edge and the machined surface (Figure 17.7). The scratches are a result of the interaction between the tool and material, while chippings are a result of an unsuitable choice of machining parameters. With a suitable combination of material and machining parameters, the defects induced by machining can be minimized and the strength can reach almost the same level as can be obtained for a polished surface. On the other hand, with unsuitable machining parameters, the defects induced at the machined surface can easily reduce the strength by 30% compared to a material machined with suitable parameters. It is thus important to select a combination of material and cutting parameters that minimize the formation of surface defects formed in the machining process. Even though the strength of ceramic materials is strongly influenced by the machined surface, the relationship between the surface characteristics and the machining parameters have received limited attention so far. Development of these
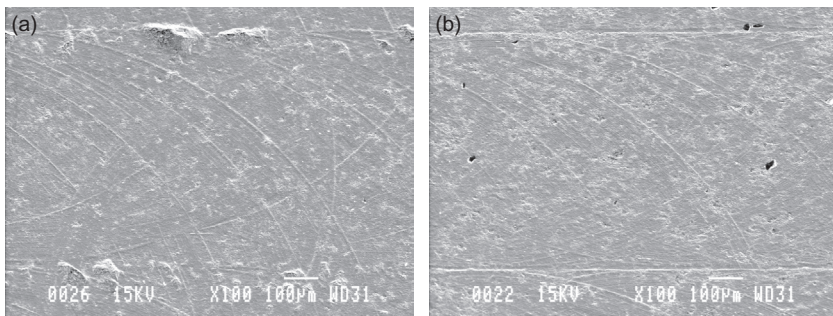
FIGURE 17.7　The surfaces in (a) and (b) were prepared from the same materials and with the same tools; while different machining procedures were used. The machining procedure used for material (a) was found to be responsible for chippings, which reduced the strength of the by one-third as compared to material (b). This indicates how important it is to use a suitable machining procedure in order to avoid additional defects and strength reductions.

production methods is mainly based on empirical experience[7] with the intention of increasing productivity.

Grinding with an abrasive tool is the traditional way to change the shape of a sintered ceramic and is used both industrially and clinically where adjustments of crowns and bridges are needed. In contrast to conventional cutting tools which often have two or three edges that interact with the machined material, a grinding tool consists of diamond particles embedded in a resin or metal matrix. The grinding tool then has a large number of cutting edges that interact with the ceramic and allow a small amount of material to be removed by each edge. The use of a coarser grinding tool allows a higher material removal rate and is often initially used when the shape of a sintered component needs to be adjusted. As a result, the surface may not only have scratches from the grinding tool, but small fractures and micro-cracks may also form. The depth of the scratches and micro-cracks formed by the grinding tool depends on the size of the abrasives and the pressure applied. When sufficient material has been removed and the desired shape has been obtained, it is important that the surface structure and damages from the grinding procedure are removed. This is usually done by another grinding tool with smaller abrasives. The procedure is usually repeated several times in industrial grinding and sample preparation of ceramics to minimize the damage from grinding and avoid strength reductions (Figure 17.8).

Sandblasting, where an abrasive is fed into a high air flow directed to a surface at a pressure of a few bars, is a common method to clean or increase the surface roughness in many industrial applications. The method has also been introduced to the field of restorative dentistry where alumina particles with a size of 50–250 microns are used in both productions and dental labs to increase the surface roughness of dental implants or crowns in order to enhance the ability to bond with luting cements.[31] Both grinding and blasting will influence the surface roughness and induce defects at the material surface. As soon as these defects induced by the surface treatments is comparable to or
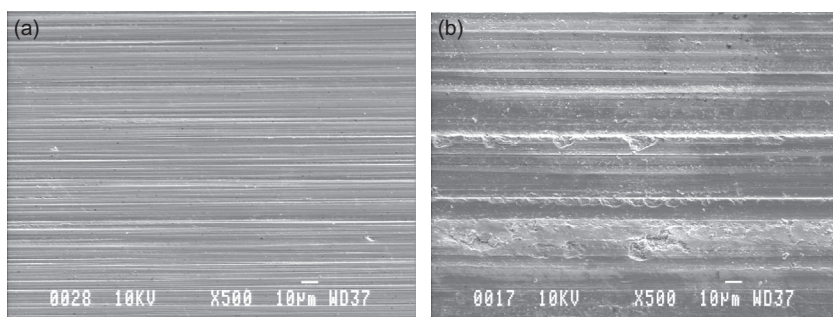
FIGURE 17.8   Surface grinded with a 25 μm (a), and a 180 μm (b) grinding wheel. The coarser grinding shows fractures, in addition to the grinding scratches.
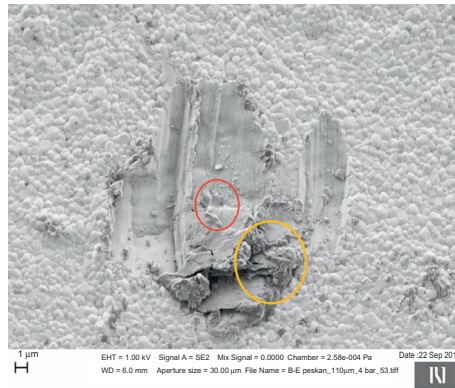
FIGURE 17.9   Surface of zirconia blasted with alumina particles. *(Courtesy of Tomaž Kosmač)*

larger than the other defect populations present, the additional surface defects will cause the material strength to decrease. This is however not always the case for ceramics containing tetragonal zirconia, where an increased strength instead can be obtained. This has been explained by two competing factors that influence the strength of surface treated zirconia ceramics. The compressive stress formed at the surface (caused by the phase transformation induced by grinding or blasting procedures), which contribute to strengthening, and mechanically induced surface flaws, which cause strength degradation.[32,33] However, the impact of hard particles does not only have positive influences. There are also risks of crack formation, especially when particle size and air pressure are increased. The SME micrograph shown in Figure 17.9 reveals the damage (i.e. plastic deformation and cracks in the red circle, and welded alumina in the yellow circle) to the surface of Y-TZP ceramics after being hit by an impacting alumina particle of 110 microns in size (when a sandblasting pressure of 4 bars and a distance of 20 mm are applied).

17.5   EVALUATION OF THE PRESENCE OF DEFECTS

Evaluating the presence of defects in ceramic materials is not an easy task. Microscopy and X-rays can be used to study defects on the surface and within the material, but the most crucial defects are not always found. One of the few reliable methods is strength measurement accompanied by fractography. When a load is applied to the material, stress concentrations are formed around all defects exposed to the stress. As the load is increased, a critical stress is eventually reached around the defects most critical for the strength. A crack then propagates and causes the material to fracture. Through a mechanical evaluation, the defects most crucial for the strength can be found that are present at the tensile surface or slightly below.
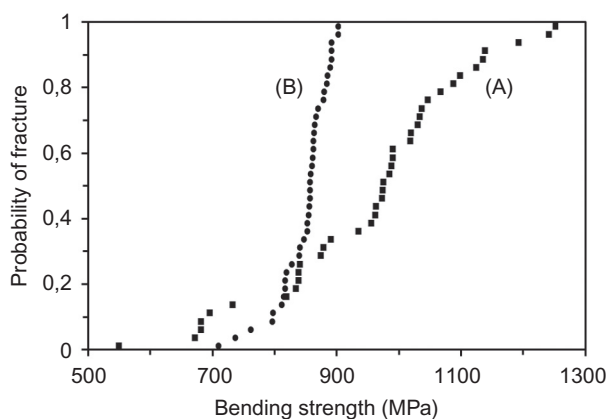
FIGURE 17.10   Four point bending strength of two ceramic materials used in dentistry. To reduce the influence from surface defects, the tensile surfaces of the bars were polished.

The probability of fracture when exposed to a given stress of two different ceramic materials used in dentistry is shown in Figure 17.10. In order to evaluate material performance and to avoid the influence from surface defects caused by various shaping processes used in production, the mechanical evaluation was performed on bending bars with a polished surface. Material (A) showed a large spread of strength values from around 600 to 1200 MPa. This indicated that the fractures were initiated from a large variation of defect sizes. It further means that the largest defects, which correspond to the lowest strength, were not sufficiently frequent to be present and responsible for the fracture in all samples, but were still sufficient to reduce both the strength and reliability of the material. A significant improvement of material (A) would then be possible if the larger defect populations could be avoided (by improved material fabrication processes). If such improvement of the material process was successful, an average strength close to 1200 MPa would be possible to reach, as indicated by the highest strength values obtained. On the other hand, material (B) showed a lower average strength, but also a significantly lower spread of strength values as compared to material (A), which indicated that the strength-limiting defect population present was very narrow in size. If the strength-limiting defect in material (B) turned out to be small, further optimization of the process would not result in an increased strength.

17.6   SUMMARY

The mechanical performance of a ceramic material is to a large extent determined by the defects present. Strength measurements are thus usually performed on samples with carefully prepared surfaces that exclude the defects

normally introduced by various fabrication processes used in production. The strength of products that contain defects from both the material and fabrication process is usually reduced compared to the materials with carefully treated surfaces. This means that the material's strength data, as given in the literature or from producers, is only valid for the material and the processes used in the evaluation. Since defects are to a large extent process-related, strength is not necessarily the same for identical raw material if the processing is done by different producers.

If a component fractures, the material usually takes the blame for the result and is deemed to be unsuitable for the application. This could be true, but another possible explanation might be that the fabrication process was not adjusted to the material. Without using a suitable combination of materials and processes, additional defects are unnecessarily introduced from the process and will cause the strength of the component to be reduced. It is thus important to optimize the fabrication process in order to minimize additional defects. If this is done successfully, the strength of the ceramic component can then be maintained at a level close to the strength obtained from a mechanical evaluation of the material where the surface was carefully prepared to remove surface defects.

REFERENCES

1. Luthy H, Filser F, Loeffel O, Schumacher M, Gauckler LJ, Hammerle. CHF. Strength and reliability of four-unit all-ceramic posterior bridges. Dent Mat 2005;21:930–7.
2. Bowen P, Carry C. From powders to sintered pieces: forming, transformations and sintering of nanostructured ceramic oxides. Powder Technol 2002;128(2–3):248–55.
3. Reed JS. Principles of ceramic processing. New York, USA: John Wiley & Sons; 1995. p418–p445.
4. Lang FF. Powder processing science and technology for increased reliability. J Am Ceram Soc 1989;72:3–15.
5. Handbook of ceramic grinding and polishing, Edited by Marinescu ID, Hans K, Tonshoff, Inasaki I: Noyes publications, Willam Andrew Publishing, Norwich, New York, USA.
6. Song JH, Evans JRG. On the machinability of ceramic compacts. J Eur Ceram Soc 1997;17:1665–73.
7. Desfontaines M, Jorand Y, Gonon M, Fantozzi G. Characterisation of the green machinability of AlN powder compacts. J Eur Ceram Soc 2005;25:781–91.
8. Kondo N, Hyuga H, Kita H. Effect of green machining on strength of silicon nitride with as-sintered surface. J Ceram Soc Jap 2007;115(8):504–6.
9. Kosmac T, Oblak C, Jevnikar P, Funduk N, Marion L. Strength and reliability of surface treated Y-TZP dental ceramics. J Biomed Mater Res (Appl Biomater) 2000;53:304–13.
10. Sato H, Yamada K, Pezzotti G, Nawa M, Ban S. Mechanical properties of dental zirconia ceramics changed with sandblasting and heat treatment. Dental Mater J 2008;27(3):408–14.
11. Kendall K. Influence of powder structure on processing and properties of advanced ceramics. Powder Technol 1989;58:151–61.

12. Adolfsson E, Shen Z. Effects of granule density on strength and granule related defects in zirconia. J Eur Ceram Soc 2012;32(11):2653–9.
13. Xiong Y, Hu J, Shen Z, Pouchly V, Maca K. Preparation of transparent nanoceramics by suppressing pore coalescence. J Am Ceram Soc 2011;94(12):4269–73.
14. Lange FF. Densification of powder compacts: An unfinished story. J Eur Ceram Soc 2008;28:1509–16.
15. Bowen P, Carry C, Luxembourg D, Hofmann H. Colloidal processing and sintering of nanosized transition aluminas. Powder Technol 2005;157(1–3):100–7.
16. Lewis J. Colloidal processing of ceramics. J Am Ceram Soc 2000;83(10):2341–59.
17. Baklouti S, Chartier T, Franc J. Mechanical properties of dry-pressed ceramic green products: the effect of the binder. J Am Ceram Soc 1997;80(8):1992–6.
18. Sigmund W, Bell N, Bergstrom L. Novel powder-processing methods for advanced ceramics. J Am Ceram Soc 2000;83(7):1557–74.
19. Walker W, Reed J, Verma S. Influence of granule character on strength and Weibull modulus of sintered alumina. J Am Ceram Soc 2004;56:50–6.
20. Frey RG, Halloran JW. Compaction behavior of spray-dried alumina. J Am Ceram Soc 1984;67:199–203.
21. Shinohara N, Okumiya M, Hotta T. Formation mechanisms of processing defects and their relevance to the strength in alumina ceramics made by powder compaction process. J Mater Sci 1999;34:4271–7.
22. Tanaka S, Chia-Pin C, Kato Z, Umeatsu K. Effect of internal binder on microstructure in compacts made from granules. J Eur Ceram Soc 2007;27:873–7.
23. Moritz T, Nagy A. Preparation of super soft granules from nanosized ceramic powders by spray freezing. J Nanoparticle Res 2002:439–48.
24. Baklouti S, Coupelle P, Chartier T, Baumard JF. Uniaxial pressing of spray-dried alumina agglomerates. Ceram. Trans 1994;51:271–5.
25. Baklouti S, Chartier T, Baumard JF. Mechanical properties of dry-pressed ceramic green products: the effect of the binder. J Am Ceram 1997;80(8):1992–6.
26. Uchida N, Hiranami T, Tanaka S, Uematsu K. Spray-freeze-dried granules for ceramics fabrication. Am Ceram Soc Bull 2002;81(2):57–60.
27. Raghupathy BPC, Binner JGP. Spray granulation of nanometric zirconia particles. J Am Ceram Soc 2011;94(1):42–8.
28. Stuer M, Zhao Z, Bowen P. Freeze granulation: Powder processing for transparent alumina applications. J Eur Ceram Soc 2012;32(11):2899–908.
29. Scherer GW. Theory of drying. J Am Ceram Soc 1990;73(1):3–14.
30. Swain MV. Unstable cracking (chipping) of veneering porcelain on all-ceramic dental crowns and fixed partial dentures. Acta Biomater 2009;5(5):1668–77.
31. Kern M, Wegner SM. Bonding to zirconia ceramic: adhesion methods and their durability. Dent Mater 1998;14:64–71.
32. Kosmac T, Oblak C, Jevnikar P, Funduk N, Marion L. The effect of surface grinding and sandblasting on flexural strength and reliability of Y-TZP zirconia ceramic. Dent Mater 1999;15:426–33.
33. Kosmac T, Oblak C, Jevnikar P, Funduk N, Marion L. Strength and reliability of surface treated Y-TZP dental ceramics. J Biomed Mater Res 2000;53:304–13.

Advanced Direct Forming Processes for the Future

Danjela Kuscer* and **James Zhijian Shen†**
Jožef Stefan Institute, Ljubljana, Slovenia; †Berzelii Center EXSELENT on Porous Materials, and Department of Materials and Environmental Chemistry, Arrhenius Laboratory, Stockholm University, Stockholm, Sweden

Contents

18.1 INTRODUCTION

The manufacturing approach currently applied to produce customized ceramic parts in restorative dentistry includes milling of dry-pressed green bodies or pre-sintered ceramic blanks and in rare cases even fully densified blocks. This operation wastes a tremendous amount of materials. For example, to make a four-unit dental bridge from a cylindrical blank as illustrated in Figure 18.1, less than 5% of the material is retained in the product. More than 95% of the material ends up as scrap that cannot be recycled. As a consequence, the spread of this technique has made dentistry the second-largest consumer of zirconia in the world. Therefore, there is a strong desire for alternative processes for the sustainable development of materials solutions in restorative dentistry.

Additive manufacturing (AM) techniques have attracted attention to meet such demands for the production of customized components directly through bottom-up processing approaches, as illustrated in Figure 18.1. It is defined by
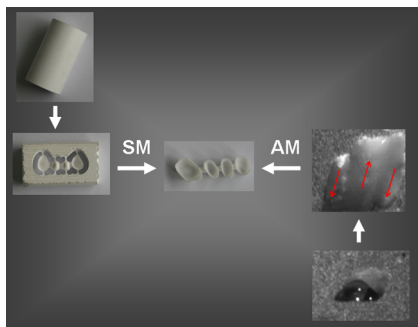
FIGURE 18.1   Additive manufacturing versus subtractive manufacturing.

the American Society for Testing and Materials (ASTM) as the process of join-ing materials to make objects from 3D digital data, usually layer upon layer, as opposed *to subtractive manufacturing* (SM) methods such as *computer numerical control* (CNC) milling (ASTM F2792-10 Standard Terminology for Additive Manufacturing Technologies). Addition of material means that units of material feedstock are brought together and fused or bonded to a larger unit. The feature of stacking layer-by-layer naturally implies the possibility of build-ing up three-dimensional (3D) net-shaped structures by direct writing of liquid suspensions or even by directly fusing dry powders.

Based on the selective delivery of materials and/or energy, the AM family of techniques can be classified into two categories, namely, printer- or noz-zle/extrusion-based systems; and beam-based systems. The former is usually referred to in the literature as *lithograph based ceramic manufacturing, ink-jet printing* or *robocasting*, whereas the latter covers (in general) *laser sintering* and *electron beam sintering*. The printer-based techniques consist of the robotic deposition of highly concentrated colloidal suspensions (i.e. inks capable of fully supporting their own weight during assembly thanks to their carefully tai-lored composition and viscoelastic properties). After the assembly is finished, the structures are dried and then sintered to achieve the required density during which the dimensional tolerance of the components is often strafed. The beam-based systems expose thin layers of powder to a rapid scanning laser beam or electron beam. The beams induce the formation of melt droplets and fuse them together to form, upon cooling, rigid 3D objects with the desired dimensional accuracy in one single processing step. In this way, the sintered parts can be put into immediate use without requiring any post-sintering machining.

The AM family of techniques has become an elegant tool for the produc-tion of bone scaffolds with the purpose of cell seeding and/or cell encapsula-tion, or for direct tissue repair/regeneration. They have already been applied to the manufacture of metal-based dental implants, crowns, and bridges. Their potential for the preparation of customized ceramic components is cur-rently being investigated in both academia and in industry. It is worthwhile

mentioning that while both laser beam and electron beam techniques can be applied to melt metals, only the laser beam is applicable for melting ceramics. Furthermore, the process of successively adding material to a final product makes the final material properties of the products made by the AM family of techniques highly dependent on the machine type and the process parameters in the additive operation. Therefore, it becomes very hard to accurately predict the properties of these materials without coupling them to a specific type of machine and to a fixed set of process parameters. In this chapter, we will only introduce basic principles of the AM family of techniques. The feasible application of these techniques in future production will be determined by the progress in control of dimensional tolerance, the residual stress, and their characteristic heterogeneous microstructures.

18.2   INK-JET PRINTING TECHNOLOGIES

Ink-jet printing is an attractive technique for realizing high-quality structures with a micrometer-sized resolution. The technique is based on the jettability of fluid through nozzles and the subsequent formulation of drops due to the surface-tension effect. The drops land on the substrate at the desired position by applying precise digital control of the jetting where they form two- or three-dimensional structures. The principles of continuous and drop-on-demand ink-jet printing are described. Piezoelectric ink-jet printing is considered in more detail, including a discussion of fluid properties, drop formation, and behavior of the drop on the substrate. Finally, drying and firing of ink-jet printing structures are reviewed.

In many fields of high technology an essential step is the deposition of functional layers with the desired architecture and thickness on various substrates. Ink-jet printing, which has traditionally been used as a printing and marking technique, is being explored as a viable method for processing coatings and three-dimensional structures in various fields, including electronics, ceramics, the life sciences, and in biological applications. Ink-jet printing involves the direct deposition of a fluid in a desired pattern via a layer-by-layer build sequence. The fluid (ink) is either a suspension or a solution based on inorganic, organic, polymer, or biological materials. By controlling the amount and location of the ink deposit, the energy consumption and production of undesirable waste during the manufacturing step are radically reduced. Additional attractive characteristics of this method are its simplicity, accurate control of structures, and high level of reproducibility based on CAD/CAM principles. Inkjet printing has emerged as an attractive technology that bridges the gap between the high-resolution structures realized by conventional lithography (~1 μm and below) and the ~100-μm resolution achieved by screen-printing technology. Furthermore, printing information is created directly from a computer and is stored digitally. It is a non-contact, additive method that allows the mask-less deposition of various materials, and it is therefore a very
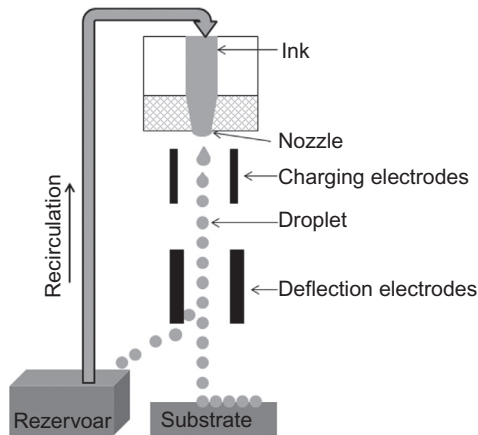
FIGURE 18.2   Principle of continuous ink-jet printing technology.

flexible process compatible with many substrate materials, including ceramics, metals, polymers, and textiles. It is equally well suited to mass production and to small development batches.

Ink-jet technology is classified as either continuous or as the drop-on-demand ejection of droplets. In *continuous ink-jet printing technology* (Figure 18.2), a continuous stream of ink is emitted from a nozzle. The device consists of a multi-nozzle print head, a charging electrode, a deflection electrode, and an ink shield to drain off the unused ink. The drops, ejected from nozzles by way of a vibrating piezo-crystal, are subjected to an electrostatic field in order to electrically charge them. The charged drops pass through the deflection electrode that controls their direction. Depending on the nature of the imposed electric field, the charged droplets are either directed to the substrate, or they are diverted to a recirculation system. Since the droplets are generated continuously, they are directed to the substrate only when and where a dot is desired. Continuous ink-jet printing technology is characterized by its high-speed printing capability and its ability to use volatile solvents that enable rapid drying of printing structures. Limitations of the technology are the relatively low printing resolution, the high maintenance, the requirement that the ink must be electrically charged, and the possibility of ink contamination during the recirculation process.

In drop-on-demand ink-jet printing technology, droplets are ejected only when required and are generated by a pressure pulse. In *thermal ink-jet printing technology*, a pressure pulse is produced by heating the ink. The ink in the pressure chamber is heated by a resistive element, and the temperature of the ink located near the heater surface increases to several hundred degrees Celsius. As a consequence, the ink vaporizes. The bubble produces an expansion-induced outwards pressure that forces a controlled amount of
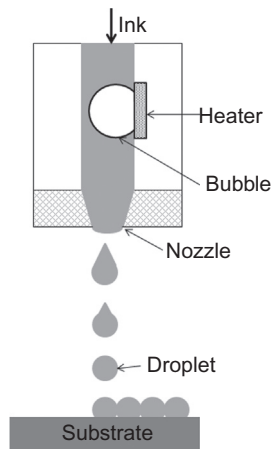
FIGURE 18.3   Principle of thermal ink-jet printing technology.

ink out of the nozzle as a droplet. After the heater is switched off, the bubble is vented to the atmosphere and the chamber refills with ink. The process is shown in Figure 18.3. Low-cost, replaceable printing heads and minimal maintenance make this technology attractive, and therefore it is widely used in personal desktop printers. However, the ink, which is required to be a low-boiling-point fluid able to withstand high temperatures, presents some limitations, especially when damaged by high temperatures.

Piezoelectric ink-jet printing technology is based on the formation of droplets using a mechanically created pressure pulse. The printing head consists of an array of chambers, each of which is linked to an individual nozzle that is filled with a fluid. The piezoelectric element, an actuator that is located in a chamber, changes its dimensions under an applied voltage. This generates a pressure pulse that ejects the fluid from the nozzle. Under optimal electrical conditions, the ejected fluid develops into a single droplet that lands on the substrate. The operating principle of piezoelectric ink-jet printing is shown in Figure 18.4.

This technology has many advantages, the most important being long printing-head life and low maintenance costs. It enables printing of many types of fluids, including solvent-based, water-based, phase-change and UV-curable liquids, and the processing of two- and three-dimensional structures with a high resolution. Even though the high cost of the printing head and associated hardware limits the use of this technology for low-cost end products, piezoelectric ink-jet printing technology is widely used for the deposition of functional materials, especially in the fields of electronics and the life sciences. It is this technology that is considered to be more feasible for ink-jet printing of customized ceramic parts.
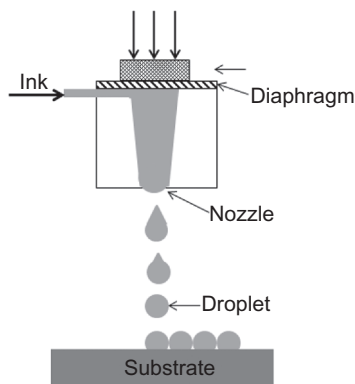
FIGURE 18.4   Principle of piezoelectric ink-jet printing technology.

18.2.1   Fluid Properties

Ink-jet printing technology requires a fluid that is ejected from a nozzle. The size of the ejected droplet depends ultimately on the type of printing technology, the nozzle geometry, the jetting conditions, and the properties of the ink. For piezoelectric ink-jet printers the typical nozzle diameter ranges from 10 to 150 μm. The size of the nozzle depends mostly on the final application. With a small nozzle size, high-resolution structures can be realized; however, the machining of the nozzle involves more complicated processes, which is reflected in the high cost of the printing head. Also, particulate ink tends to clog in the printing head with small nozzles and therefore reduces the reliability and repeatability of the printing process. With respect to the piezoelectric ink-jet printing of a suspension of inorganic functional particles, the key requirement is the formulation of the inks with a high degree of colloidal stability and the physical properties required for the particular inkjet printer.

The size of the particles is an important parameter in the ink-jet printing of suspensions. The maximum size is limited by the diameter of the nozzle. According to the literature, the ratio between the nozzle diameter and the d_{100} value (which represents the particle size where all the particles are smaller than this value) has to be 50:1 to avoid any clogging of the nozzle. In other words, all the particles have to be 50-times smaller than the diameter of the nozzle. Powder with a particle size below 1 μm, typically a few tens or hundreds of nanometers, dispersed in a certain solvent is generally needed for printing. However, sub-micrometer-sized particles tend to agglomerate in the solvent due to their high surface energy, which makes it more difficult to prepare a highly concentrated, stable dispersion for ink-jet printing.

Ink-jet printing of commercially available nano-sized particles, such as silver,[1] copper,[2] ZrO_2,[3] Al_2O_3,[4] and yttria-stabilized zirconia[5] has been reported. The powder is dispersed in water or an organic solvent (e.g. acetone, isopropyl
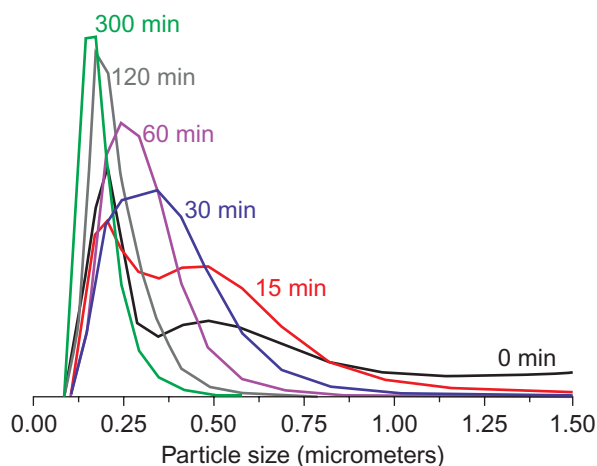
FIGURE 18.5   The particle size distribution as a function of milling time for a suspension containing 5 vol.% of TiO_2 in water at pH 10.

alcohol, paraffin wax, α-terpineol), using various additives that enable steric or electrostatic stabilization of the particles. The ink-jet printing was realized using 21- or 50-μm-sized nozzles.

Ultrafine particles can be processed using the top-down approach, especially for materials with a complex chemical composition.[5,6,7] In the top-down approach the micrometer-sized particles, usually processed by solid-state synthesis, are comminuted to nano-size dimensions. Milling is widely used in ceramic processing to reduce the average particle size of a material; to modify the particle size distribution; to disperse agglomerates and aggregates; and in some cases, it provides effective dispersion.[8] The ball milling of micrometer-sized, agglomerated TiO_2 powder in water at pH 10 has been used to process aqueous TiO_2 ink for piezoelectric ink-jet printing.[9] For successful ink-jet printing using a nozzle size of 21 μm, all the particles/agglomerates have to be smaller than 420 nm. By carefully controlling both the milling parameters (e.g. milling time, TiO_2/milling-ball ratio, and rotation speed), and the dispersion parameters (e.g. pH and solid load), nano-sized TiO_2 particles were well dispersed in water. Particle size distribution as a function of milling time is shown in Figure 18.5. It is clear that after 300 minutes of intensive milling of TiO_2 particles in water, sub-micrometer particles with a narrow particle size distribution were obtained. All the TiO_2 particles/agglomerates were smaller than 480 nm and the zeta-potential of −45 mV illustrated the high stability of this suspension. The suspension was easily applicable for printing with a conventional print head with nozzle sizes of around 20 μm.

In piezoelectric ink-jet printing the drop formation is initiated by a pressure pulse applied to the fluid that enables the propagation of a fluid through the nozzle. The fluid is ejected from the nozzle as a jet at a relatively high
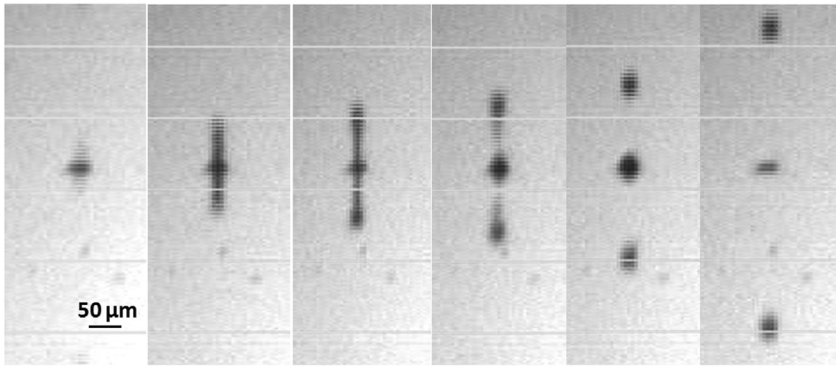
FIGURE 18.6 Stroboscopic image showing a continuous jet, a drop with a ligament, and an individual drop.

speed. However, it is in an unstable state and transforms into the energetically more stable, spherical shape. First, the jet breaks and an individual drop forms a ligament or tail that is connected to the drop (Figure 18.6). The ligament stretches the main drop and in the next stage it joins the main drop. Sometimes the ligament does not join the main drop but forms a small satellite drop that lands on the substrate in the vicinity of the main drop. During these processes the velocity of the drop decreases due to dissipative energy loss from viscous forces, the energy required to create a new liquid surface, and air drag. Since the radius of the nozzles in a typical ink-jet printer is of the order of 20 μm, the gravitational effect is negligible.

The most important forces that control the behavior of drops during ink-jet printing are those originating from viscosity and surface tension. To determine the possibility of drop formation during the ink-jet printing of Newtonian liquids, the Reynolds (Re), the Weber (We), and the inverse Ohnesorge (Z) numbers are used. The dimensionless Reynolds number is defined as the ratio of the inertial forces to the viscous stress within the drop (Eq. 18.1):

$$Re = \frac{\rho dv}{\eta} \qquad (18.1)$$

The symbol ρ is the density of the fluid (kg/m^3), d is the diameter of the nozzle (m), v is the travel velocity of the fluid (m/s), and η is the dynamic viscosity of the fluid (Pa s).

The Weber number is a dimensionless number that represents the ratio of the inertial forces and the interfacial stresses (Eq. 18.2):

$$We = \frac{\rho dv^2}{\gamma} \qquad (18.2)$$

where ρ is the density of the fluid (kg/m^3), d is the diameter of the nozzle (m), v is the travel velocity of the fluid (m/s), and γ is the surface tension of the fluid (N/m).

The printability range of the ink can be estimated based on an approximate solution to the Navier-Stokes equation as the inverse Ohnesorge number Z that is independent of the fluid velocity.[10] Therefore, the Z number is commonly used to describe the printability of a fluid (Eq. 18.3):

$$Z = \frac{(d\rho\gamma)^{\frac{1}{2}}}{\eta} \tag{18.3}$$

The symbol d is the nozzle diameter (m), ρ is the density of the ink (kg/m^3), γ is the surface tension of the ink (N/m), and η is the dynamic viscosity of the ink (Pa s).

One can see that the density, surface tension, and viscosity of the ink are the most important parameters for ink formation. Their absolute values depend on the specific print head, and in most cases on the geometry of the nozzle. The usual ranges of the viscosity and surface tension of the ink that is suitable for piezoelectric ink-jet printing ranges from between 5 and 20 mPa.s and 25 and 35 mN/m, respectively. In the case of suspensions, the particle properties and effective volume fraction of the solids in the ink play important roles, as already discussed.

Based on numerical analysis, stable drop formation is reported to occur at $Z > 2$ for drop-on-demand ink-jet printing technologies.[10] Experimentally determined printable ranges of $1 \leq Z \leq 10$[9,11] were reported for non-Newtonian liquids such as TiO$_2$ and lead-zirconate titanate inks. Based on different solvent mixtures of ethylene-glycol, ethanol, and water the printable range of $4 \leq Z \leq 14$ was determined.[12] It was reported that printing an ink with too low of a Z value resulted in low-resolution structures due to the formation of droplets with a long drop tail; it also took a long time to generate a single droplet.[12] In this case, the viscous forces are dominant and a large pressure is required for ejection of the drop. When the Z value was below 1, the formation of drops was not possible.[13] Ink with too high a Z value resulted in low-quality printed structures as well. During printing, drop formation can be accompanied by undesired satellites that often do not recombine with the main drop. It was reported that the volume of the drop increases as the value of Z increases.[1] Both phenomena reduce printing accuracy and lower the resolution of printed structures.

18.2.2 Impact of the Drop on a Substrate

Ink-jet-printed structures are formed by the precise positioning of the drop of fluid on the substrate. The behavior of the drop on the substrate is of fundamental importance in order to tailor the architecture of the printed features. When a liquid drop hits the planar substrate, it will deform on the substrate prior to reaching an equilibrium configuration. The impact process can

(a)

(b)

(c)

(d)
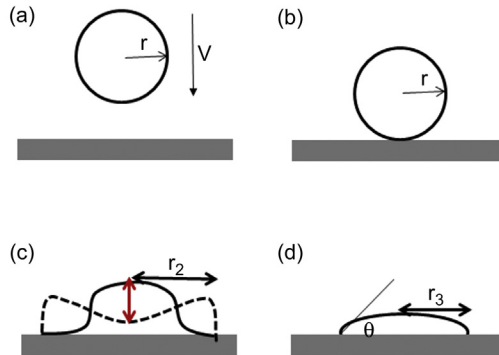
FIGURE 18.7   Schematic representation of drop-on-substrate behavior.

be divided into the three phases shown in Figure 18.7: the drop with diameter r that is ejected from the nozzle (a) makes contact with the substrate in the first phase (b). In the second phase the drop deforms, flattens, and spreads on the substrate to form a thin layer with diameter r_1. The diameter of the drop in this phase depends on wetting and impact conditions, and is in general different from the diameter of the drop in free flight (r). A rapid radial fluid flow regularly followed by interfacial oscillations is characteristic for this phase (c). In the third phase of impact, the thin fluid layer stays at rest or recoils and finally forms a drop with diameter r_3, which has an equilibrium shape and position on the substrate (d).[14] All these processes occur over a time scale of milliseconds.[13]

Factors that influence drop behavior on the substrate include the velocity of the drop at impact, the viscosity and the density of the ink, and also the wettability of the ink on the substrate (i.e. surface tension and contact angle). Drop spreading for an ink on a selected substrate can be estimated with Eq. 18.4[15]:

$$\frac{r_{max}}{r} = \sqrt{\left(\frac{We^2 + 12}{3(1 - [\cos\theta] +)\dfrac{4We^2}{\sqrt{Re}}} \right)} \tag{18.4}$$

The symbol r_{max} is the maximum drop radius, r is the in-flight drop radius, θ is the contact angle, We is the Weber number, and Re is the Reynolds number.

18.2.3   Ink-jet Printed Lines and Layers

For many applications, a continuous and homogeneous distribution of material on the substrate is needed. This requires good contact between the individual
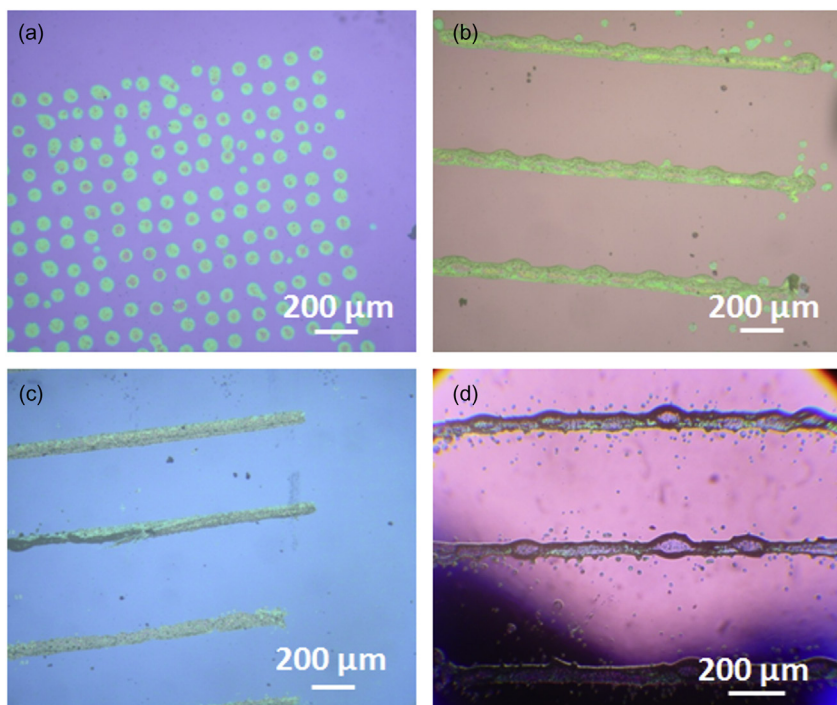
FIGURE 18.8   (a) Isolated drops; (b) Scalloped pattern; (c) Smooth pattern; and (d) Bulging pattern.

drops to form the desired two- or three-dimensional features. Thus, adjusting printing conditions such as drop volume, printing speed, drop spacing, drop frequency, height of the print head above the substrate, as well as the properties of the substrate, must be addressed. Some of these conditions are defined by the printing system (e.g. diameter of the nozzle), but others can by varied (e.g. drop spacing and drop frequency).

Drop spacing represents the distance between the centers of two neighboring drops. A few typical patterns emerge when varying the drop spacing. Isolated drops (Figure 18.8a) appear on the substrate when drops are printed at a drop spacing larger than twice the drop's radius. In this case, the isolated drop lands and dries on the substrate. If we decrease the drop spacing, the drops partly overlap, merge together, and then the resulting line is narrower than the one with isolated drops. Here, the rounded contact lines are clearly visible and the pattern is commonly referred to as a scalloped pattern (Figure 18.8b). A line with a smooth, straight edge and uniform thickness is the narrowest, and is produced at the optimal drop spacing (Figure 18.8c). A further decrease in the drop spacing leads to smooth lines with discreet bulging along the lines (Figure 18.8d). The bulging that occurred at the

minimum drop spacing is a dynamic function of the transverse velocity of the printing head relative to the substrate.[16] It was reported that unstable lines are formed when the drops are placed too close together, but the line stability increases when the transverse velocity increases.[14]

18.2.4 Drying and Densification

The drops, lines, or layers deposited on the substrate by ink-jet printing transform into a solid phase either through the drying (evaporation of the solvent), phase-change (solidification), and polymerization of the monomer using ultraviolet light (UV), or by other mechanisms that ultimately depend on the chemical composition of the ink. In the following example, we confine our discussion to the drying of a drop that represents an important step in producing thick films ready for firing.

The drops after ink-jet printing and drying must be uniform in order to realize structures with a smooth surface, sharp edges, desired thickness, and required architecture. For the drops that contain particles dispersed in a certain solvent, it is common to observe a non-uniform, ring-like deposit on the substrate.[17] This shape of the drop is related to the evaporation of the solvent. When the drop hits the substrate, it spreads onto the substrate and the solvent evaporates. The drop then tends to shrink during drying as the liquid between the particles is removed and the interparticle separation decreases. However, the drop edges are pinned at the substrate and therefore the drop cannot shrink. To keep the contact line fixed and to preserve the spherical shape of the drop that is dictated by the surface tension, the liquid that evaporates from the edge of the drop must be replaced by liquid from the center of the drop. This radial flow transports material from the center of the drop towards its edge, which results in a ring-like drop shape. The process and the ring-like shape of the TiO_2 drop are shown in Figure 18.9.

This phenomenon, known as the coffee-ring effect, can be minimized by controlling the evaporation rate of the solvent. In ink-jet printing technology, evaporation of the solvent is frequently controlled by heating or cooling of the
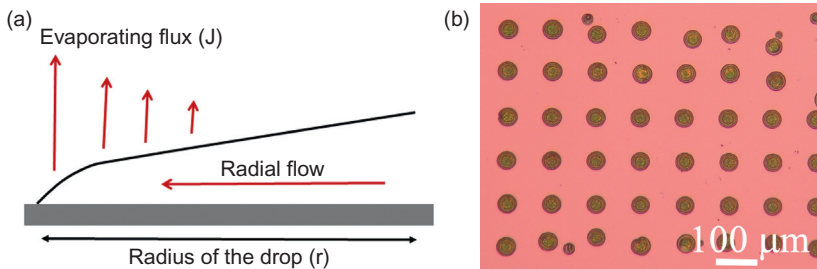
FIGURE 18.9 (a) Schematic representation of flows during evaporation of solvent from the drop; and (b) TiO_2 drops on Si substrate with ring-like shape.

substrate. It has been shown that increasing the substrate temperature accelerates the radial flow toward the edge of the drop and consequently promotes the coffee-ring effect.[18] Cooling of the substrate has the opposite effect due to the lower evaporation rate at the edge of the drop. After drying, the deposit must be consolidated to develop the desired microstructure and properties by sintering.

In the case of ink-jet printing, the layer is deposited on a certain substrate, and therefore the densification is different than for a bulk ceramic. Since the bulk ceramic shrinks isotropically in all three directions, the layer shrinks exclusively in the direction perpendicular to the substrate. The as-deposited layer is clamped to the substrate and therefore it densifies in constrained conditions. The sintering behavior of the thick-film structure under constrained sintering conditions is widely discussed in the literature.[19–22] Under constrained conditions a slower densification rate and generation of processing defects have been observed in thick-film structures. This may originate from the stresses that are present in the thick-film structure during sintering. The in-plane tensile stresses reduce the driving force for sintering and promote the formation of cracks in the structure. The magnitude of the tensile stress depends on the shear rates and the densification rate of the film. When the thick-film structure responds in an appropriate way to the stresses, the quantity of defects is reduced and the density is improved. In addition, during processing, the thick film is in direct contact with chemically different materials. Therefore, the main difficulty with thick-film processing is ensuring good adhesion as well as avoiding chemical reactions between the active layer and the substrate.

18.3   LASER SINTERING

Laser sintering is an empirical term that refers to a method belonging to the AM family of techniques, initially established as a rapid prototyping tool.[23] It uses a high-energy laser beam to fuse particle granules directly into complex, net-shaped, 3D components in a layer-by-layer manner by repeating a scanning of the laser beam over a single layer of the powder granules, thereby consolidating them via full or partial melting. The process scheme is established by CAD and CAM. These unique processing conditions result in characteristic advantages (i.e. high geometrical design freedom, high flexibility, and near net shape production). Due to these advantages, laser sintering has rapidly developed over the last decades.[24–26]

Laser waves have two fluctuating physical components characterized by electric (E) and magnetic (H) field vectors. The absorbed radiation energy in solid materials results in kinetic energy of free electrons, excitation energy of bound electrons, or excess kinetic energy of charged particles. The typical overall energy relaxation times are of the order 10^{-12}–10^{-6} s for ceramics.[27] The conversion of radiation energy into heat, and its subsequent conduction within the material gives a temperature distribution profile. The optical

penetration depth of radiation into the bulk of a ceramic sample is determined by both the intrinsic properties of the ceramic and its grain-size distribution. The interaction depth of the radiation within the constituent single grains is determined by the optical properties or the heat diffusion length.[28] Most ceramics are poor absorbers of heat and are much less reflective than metals for long infrared wavelengths; hence, radiation energy tends to penetrate more effectively in ceramics than in metals.[29] The absorption length of a CO_2 laser in Al_2O_3-based ceramics is, for instance, $345 \pm 22\,\mu m$, as compared to less than $0.1\,\mu m$ for most metallic materials.[30]

One factor that must be taken into consideration is that laser sintering of ceramics uses polycrystalline spherical granules as precursors. Light absorption of such granules is enhanced by scattering of the laser beam at impurity, pore, and grain boundaries.[31] Optical transparent spherical granules may trap light to form an optical cavity by continuous surface reflections.[32] Owing to this multiple scattering and reflection at the interfacial regions, lasers can even heat materials with low intrinsic optical absorption coefficients. On the other hand, the optical absorption coefficient of a ceramic is dependent on temperature, and is sensitive to the formation of a color center (F-Center) and to doping. F-Centers often strongly increase the light absorption at visible and infrared regions. Depending on the size of scattering sources, there are two kinds of light scattering that are of importance for laser sintering, namely, Rayleigh and Mie scatterings. Rayleigh scattering is predominant when the particle size is much smaller than the wavelength of the laser used (typically less than one tenth of the wavelength, corresponding to $\sim$100 nm for an Nd:YAG laser, for example). Mie scattering dominates when the particle size is roughly comparable to the wavelength of the laser used.

The laser sintering process is characterized by high energy densities and short interaction times, which result in very high temperature gradients and cooling rates (>104 K/s). Therefore, the process leads to the formation of unique microstructures that essentially influence the mechanical properties of the sintered ceramics. Since the mid-1980s when the selective laser sintering concept was developed and patented by Dr. Carl Deckard at the University of Texas at Austin,[23] several laser sintering systems have been commercialized and applied for industrial-scale production of individually designed components made of organic polymers and metallic alloys. The effort to apply this family of technologies for sintering ceramics was initiated in the early 1990s in academia; this effort, however, has not yet yielded any promising results. Ceramists are facing an obvious challenge here as to how to handle the rapid melting and solidification processes that they never encounter in common ceramic sintering. The potential for using laser sintering to produce novel or improved materials with tailored microstructures is still awaiting exploration.

ACKNOWLEDGMENTS

REFERENCES

1. Kosmala A, Zhang Q, Wright R, Kirby P. Development of high concentrated aqueous silver nanofluid and ink-jet printing on ceramic substrate. Mat Chem Phys 2012;132:788–95.
2. Kumashiro Y, Nakako H, Inada M, Yamamoto K, Izumi A, Ishihara M. Novel materials for electronic device fabrication using ink-jet printing technology. Appl Surf Sci 2009;256:1019–22.
3. Zhao X, Evans JRG, Edirisinghe MJ. Direct ink-jet printing of vertical walls. J Am Ceram Soc 2002;85(8):2113–5.
4. Seerden KAM, Reis N, Evans JRG, Grant PS, Halloran JW, Derby B. Ink-jet printing of wax-based alumina suspensions. J Am Ceram Soc 2001;84(11):2514–20.
5. Sukeshini MA, Cummins R, Reitz TL, Miller RM. Ink-jet printing: A versatile method for multilayer solid oxide fuel cells fabrication. J Am Ceram Soc 2009;92(12):2913–9.
6. Tseng WY, Lin SY, Wang SR. Particulate dispersion and freeform fabrication of BaTiO3 thick films via direct ink-jet printing. J Electroceram 2006;16:537–40.
7. Lee DH, Derby B. Preparation of PZT suspensions for direct ink-jet printing. J Eur Ceram Soc 2004;24:1069–72.
8. Hotta H, Yilmaz T, Shirai K, Ohta K, Sato K, Watari K. State of the dispersant and particle surface during wet-jet milling for preparation of a stable slurry. J Am Ceram Soc 2008;91(4):1095–101.
9. Kuscer D, Stavber G, Trefalt G, Kosec M. Formulation of an aqueous titania suspension and its patterning with ink-jet printing technology. J Am Ceram Soc 2012;95(2):487–93.
10. Fromm JE. Numerical calculation of the fluid dynamics of drop-on-demand jets. IBM J Res Dev 1984;28:322–33.
11. Noguera R, Lejeune M, Chartier T. 3D fine scale ceramic components formed by ink-jet prototyping process. J Eur Ceram Soc 2005;25:2055–9.
12. Jang D, Kim D, Moon J. Influence of fluid physical properties on ink-jet printability. Langmuir 2009;25:2629–35.
13. Derby B. Ink-jet printing of ceramics: From drops to solid. J Eur Ceram Soc 2011;31:2543–50.
14. Stringer J, Derby B. Formation and stability of lines produced by ink-jet printing. Langmuir 2010;26(12):10356–72.
15. Lewis JA. Direct-write assembly of ceramics from colloidal inks. Curr Opin Silid State Mar Sci 2002;6:245–50.
16. Duinevald PC. The stability of ink-jet printed lines of liquid with zero receding contact angle on a homogeneous substrate. J Flid Mech 2003;477:175–200.
17. Deegan RD, Bakajin O, Dupont TF, Huber G, Nagel SR, Witten TA. Capillary flow as the cause of ring stains from dried liquid drops. Nature 1997;389:827–9.
18. Siltman D, Subramanina V. Ink-jet printed line morphologies and temperature control of the coffee ring effect. Langmuir 2008;24:2224–31.
19. Bordia RK, Raj R. Sintering behavior of ceramic films constrained by a rigid substrate. J Am Ceram Soc 1985;68:287–92.
20. Li F, Pan J, Cocks A. Defect healing and cracking in ceramic films during constrained sintering. J Am Ceram Soc 2012:1–7. doi:10.1111/j.1551-2916.2012.05420.x.
21. Mohanram A, Lee S, Messing GL, Green DJ. Constrained sintering of low-temperature co-fired ceramics. J Am Ceram Soc 2006;89:1923–9.
22. Tzeng SY, Jean JH. Stress development during constrained sintering of alumina/glass/alumina sandwich structure. J Am Ceram Soc 2002;85:335–40.
23. Deckard C. Method and apparatus for producing parts by selective sintering. U.S. Patent 4,863,538. 1989.

24. Chuna CK, Leong KF, Lim CS. Rapid prototyping: principles and applications, 2nd ed. Singapore: World Scientific; 2003.

25. Stotko CM. Laser sintering layer by layer. Nat Photonics 2009;3:265.

26. Murr E, et al. Metal fabrication by additive manufacturing using laser and electron beam melting technologies. J Mater Sci Technol 2012;28(1):1–14.

27. Dahotre NB, Harimkar SP. Laser fabrication and machining of materials.: Springer press; 2007.

28. Fischer P, Karapatis N, Romano V, Glardon R, Weber HP. A model for the interaction of near-infrared laser pulses with metal powders in selective laser sintering. Appl Phys A: Mater Sci Process 2002;74:467–74.

29. Li JF, Li L, Stott FH. Comparison of volumetric and surface heating sources in the modeling of laser melting of ceramic materials. Int J Heat Mass Tran 2004;47:1159–74.

30. Lawrence J, Minami K, Li L, Edwards RE, Gale AW. Determination of the absorption length of CO_2, Nd:YAG and high power diode laser radiation for a selected grouting material. Appl Surf Sci 2002;186:162–5.

31. Apetz R, van Bruggen MPB. Transparent alumina: a light-scattering model. J Am Ceram Soc 2003;86(3):480–6.

32. Elliott GR, Murugan GS, Wilkinson JS. Chalcogenide glass microsphere laser, Opt Express, 182010, 26720–7.

Index

Note: Page numbers followed by "*f*" and "*t*" refer to figures and tables, respectively.